Macroevolution, thermal ecology and extinction in terrestrial Mesozoic tetrapods

By

Scott Hartman

A dissertation submitted in partial fulfillment of

the requirements for the degree of

Doctor of Philosophy

(Geoscience)

at the

UNIVERSITY OF WISCONSIN–MADISON

2020

Date of final oral examination: 6/30/2020

The dissertation is approved by the following members of the Final Oral Committee:

Shanan E. Peters, Professor, Geoscience (primary advisor)
Stephen R. Meyers, Professor, Geoscience
D. Clay Kelly, Professor, Geoscience
David M. Lovelace, Museum Scientist, UW Geology Museum
Warren Porter, Retired Professor, Integrative Biology
Douglas Rouse, Professor, Plant Pathology

Dedicated to Jen and Alex.

Table of Contents

Acknowledgments

I would not have made it to this stage without significant fortune of opportunity and enthusiastic assistance from a small army of collaborators, mentors, family and friends. To that end I want to thank my advisor, Shanan Peters, whose emphasis on physical processes driving biological processes, and the use of databases to ask questions that cannot otherwise be addressed has permanently altered the way I look at research problems. He is also to be commended for putting up with my interest in vertebrates, rather than the bugs he would probably have preferred. Thanks to my committee members Clay Kelly, Dave Lovelace, Stephen Meyers, Doug Rouse & Warren Porter, you have been patient with my timeline, provided excellent feedback, and have been a pleasure to work with. A special thanks to Doug for stepping in on short notice to resolve a last-minute administrative requirement.

As science has become more collaborative, I have been fortunate to work with excellent coauthors. For Chapter 3 I want to thank Mickey Mortimer, David Lovelace, Dean Lomax, Bill Wahl, and Jessica Lippincott. I particularly wish to thank Mickey, whose ongoing work on theropod phylogenetics underlies much of the paper. For Supplemental Paper A I want to thank Dave Lovelace, Paul Mathewson, Ben Linzmeier and Warren Porter. Paul's ability to fix code when it was broken, and to fix my understanding of the code when it was not was invaluable. Without Warren's decades of work on Niche Mapper and the research behind it Chapter 1 would not have been possible. For Supplemental Paper B I would like to thank Christophe Hendrickx and Octávio Mateus for allowing me to contribute to the project, and for the excellent background provided in theropod publication history, just as I was gearing up to publish a new theropod. And finally, for Supplemental Paper C I want to thank Mike Pittman, Tom Kaye, Xiaoli Wang, Xiaoting Zheng, Amanda Falk, and Xing Xu. Tom has been an indefatigable

advocate of laser-stimulated fluorescence imaging, convincing many doubters, including myself. Mike's knowledge of paravian anatomy and willingness to share data and observations made the skeletal reconstruction process for the paper one of my favorites to date.

I want to thank the Jurassic Foundation, the Western Interior Paleontological Society, and donors on Experiment.com for funding research on Chapter 3. I also want to thank the Department of Geoscience for providing financial support via the George J. Verville Award in Geology and Geophysics, and a C.F. Schiesser Outstanding Student Research Paper Award for Chapter 3, as well as a summer TA appointment. I would also like to thank the department for the experience of taking my daughter to a Geoscience awards banquet, which she adored.

I am indebted to (and not in debt, due to) the Department of Integrative Biology for financial support as both a TA and a lecturer, and for making me a L&S Teaching Fellow and a Comm-B Teaching Assistant Fellow. A heartfelt thanks to Jean Heitz for giving me a chance to TA Intro Bio 151/152, and for Nazan Gillie for providing me the opportunity to lecture courses for iBio. Nazan is one of the kindest and most generous individuals I know, and Jean's leadership of the Intro Bio program and commitment to producing the best learning experience possible for undergraduate biology students continues to inspire me. Thanks are also (over) due to the talented and long-suffering 151/152 coordinators: Jon Breschak, Kerry Martin, Carlos Peralta, Jeremiah Yahn, Brian Parks, and Julie Collins, whose unwavering belief in the goodness of our students' intentions continues to underpin how I approach my students. Every one of you has helped shape my pedagogical views, and I would not be where I am today without you. Sadly, I am forced to note that Jean and Carlos recently passed away. This is a crushing emotional blow to all who knew them, but it makes me more determined than ever to improve myself as an instructor and mentor.

The community of graduate students and researchers at UW-Madison is wonderful, whether supplying insight into the process of navigating grad school, exchanging ideas, or just supplying camaraderie. I want to thank Ben Linzmeier (who is rightly getting thanked in several places), Mike Johnson, Marshal Tofte, Andrew Zaffos, Jon Husson, Sharon McMullen, Deborah Rook, Brittany Hupp, Daniel Segessenman, Shan Ye, Daven Quinn, and Aaron Kufner. I also need to extend a special thanks to Aaron Kufner, Jacki Whisenant, Stef Buxel-Florenzen and James Burnham, who were indispensable TAs for the courses I instructed.

My interests in paleontology were nurtured by several teachers and mentors before graduate school, including Brent Breithaupt and Jay Lillegraven at the University of Wyoming. I gained valuable research and leadership skills, and field experience all over the western US while working at the Wyoming Dinosaur Center, The Tate Geological Museum, and the Dinamation Society. I want to thank Bob Bakker and Jim Kirkland for their early encouragement in the field, which helped an undergrad believe paleontology was something he could pursue. Although not actually sentient, I should probably thank the photocopy machine in the University of Wyoming's Geology Library, as in a pre-PDF world with my first access to scientific journals I spent as much time with it as anyone else my freshman year.

I must thank my parents, Robert and Barbara Hartman, and my brother Robbie Hartman for their continual support and encouragement. I should specifically thank and/or blame my mother, who encouraged me to go on my first paleontology field digs in the summer before my senior year of high school, because she was afraid I might not go to college otherwise – surprise, now I've gone to *all* the college! And finally, thanks to my wonderful wife Jennifer and my incredible daughter Alex, whose love, support, and quiet suffering while I learned to balance teaching, research, writing, parenting and husbanding can never be fully repaid.

Publication References

Eventually all chapters will be published, but Chapter 3 has already been submitted and published in a peer-reviewed scientific journal. I also coauthored several non-chapter publications connected to my dissertation research which are referenced below and included as supplementary appendices.

Chapter 3:

Hartman, Scott, Mickey Mortimer, William R. Wahl, Dean R. Lomax, Jessica Lippincott, and David M. Lovelace. (2019) A new paravian dinosaur from the Late Jurassic of North America supports a late acquisition of avian flight. *PeerJ* 7: e7247. https://doi.org/10.7717/peerj.7247

Supplemental Appendix A (Related to Chapter 1):

Lovelace, D., Hartman, S., Mathewson, P., Linzmeier, B., & Porter, W. (2020). Modeling Dragons: Using linked mechanistic physiological and microclimate models to explore environmental, physiological, and morphological constraints on the early evolution of dinosaurs. PLoS ONE 15(5): e0223872. https://doi.org/10.1371/journal.pone.0223872

Supplemental Appendices B&C (Related to Chapter 3):

Hendrickx, C., Hartman, S., & Mateus, O. (2015). An overview of non-avian theropod discoveries and classification. *PalArch's Journal of Vertebrate Palaeontology*, *12*(1).

Wang, X., Pittman, M., Zheng, X., Kaye, T., Falk, A., Hartman, S., & Xu, X. (2017). Basal paravian functional anatomy illuminated by high-detail body outline. *Nature communications*, *8*, 14576.

Catalog Numbers

The following specimens used in Chapter 2 were measured at, and are curated by the University of Wisconsin Zoological Museum:

Museum catalog number	Species	Described in
UWZ S22273	*Taparius indicus*	Chapter 2
UWZ CA608	*Sphenodon punctatus*	Chapter 2
UWZ S29952	*Iguana iguana*	Chapter 2
UWZ 24757	*Chelydra serpentina*	Chapter 2
UWZ S29953	*Alligator mississippiensis*	Chapter 2
UWZ 26427	*Alligator mississippiensis*	Chapter 2
UWZ 23344	*Alligator mississippiensis*	Chapter 2
UWZ 32201	*Alligator mississippiensis*	Chapter 2
UWZS 22261	*Rhea americana*	Chapter 2
UWZS 23946	*Rhea americana*	Chapter 2
UWZ S22272	*Rhea americana*	Chapter 2
UWZS 23342	*Dromaius novaehallandiae*	Chapter 2
UWZS 23823	*Aptenodytes forsteri*	Chapter 2
UWZS 23786	*Pelecanus erythrorhynchos*	Chapter 2
UWZS 25230	*Gyps africanus*	Chapter 2

The following specimen, which forms the basis of the description in Chapter 3, is curated at the Wyoming Dinosaur Museum, Inc.

Museum Catalog number	Species	Described in
WYDICE-DML-001	*Hesperornithoides miessleri*	Chapter 3

Data Repository Information

Chapter 1

All Chapter 1 supplemental data is hosted on FigShare.

S.1-1 Microclimate models input dataset:

https://figshare.com/articles/Microclimate_Biophysical_input_filee_-_Dissertation/12455825

S.1-2 Biophysical models input dataset:

https://figshare.com/articles/Biophysical_model_inputs_-_Dissertation/12455828

S.1-3 All Niche Mapper output plots (no burrowing):

https://figshare.com/articles/Raw_Niche_Mapper_output_plots_no_burrowing_/12480155

S.1-4 All Niche Mapper output plots (burrowing enabled):

https://figshare.com/articles/Raw_Niche_Mapper_plots_with_burrowing_allowed/12480158

S.1-5 Raw output files from Niche Mapper simulation:

https://figshare.com/articles/Niche_Mapper_Output_Files/12485894

Chapter 2

All Chapter 2 supplemental files are hosted on FigShare.

S.2-1 Anteroposterior centrum length measurements, in mm:

https://figshare.com/articles/Vertebral_length_database/12525872

S.2-2 Vertebral length vs estimate correlation statistics – simple model:

https://figshare.com/articles/Simple_vertebral_length_estimate_correlation_statistics/12526205

S.2-3 Estimated and real vertebral lengths collated by biological group:

https://figshare.com/articles/Estimated_and_real_vertebral_lengths_collated_by_testing_group/12526247

S.2-4 Mass calculations spreadsheet:

https://figshare.com/articles/Mass_Estimate_Calculation_Spreadsheet/12552134

Chapter 3

S.3-1 DatasetS1.nex which was used to run the phylogenetic analysis, is hosted by PeerJ:10.7717/peerj.7247/supp-2

S.3-2 DatasetS2.nex which contains character and state definitions is hosted by PeerJ: 10.7717/peerj.7247/supp-3

S.3-3 3D data file of the skull is available on Figshare: https://figshare.com/articles/Skull_block_pdf/7029284/1

S.3-4 3d data file of the body block is available on Figshare: https://figshare.com/articles/Body_Block_pdf/7029299/1

Supplementary Appendix A

SA.1-1 Appendix. Niche mapper variables:

https://doi.org/10.1371/journal.pone.0223872.s001

SA.1-2 Appendix. Model test using Varanus komodoensis on Komodo Island:

https://doi.org/10.1371/journal.pone.0223872.s002

SA.1-3 Appendix. Parameterizing biophysical model dimensions for fossil vertebrates:

https://doi.org/10.1371/journal.pone.0223872.s003

SA.1-4 Appendix. Sensitivity analyses and additional figures:

https://doi.org/10.1371/journal.pone.0223872.s004

SA.1-5 Table of target resting metabolic rates for classes of animals:

https://doi.org/10.1371/journal.pone.0223872.s005

Supplementary Appendix C

SC. 1-1 Supplementary Figures, Supplementary Tables, Supplementary Notes and Supplementary References:

https://static-content.springer.com/esm/art%3A10.1038%2Fncomms14576/MediaObjects/41467_2017_BFncomms14576_MOESM2137_ESM.pdf

Table of Figures

Table of Tables

Introduction

Historically, the study of ancient life has occurred in myriad cultures and places prior to the 1859 publication of Darwin's *The Origin of Species* (Simpson, 1942; Needham, 1959; Mayor, 2001 & 2007; Rudwick, 2008). Even viewed solely within the Western scientific tradition, systematic fossil collection began a century and a half before *Origin*, and paleontology as a formal science began in the last decade of the 18th century, as Georges Cuvier used detailed comparisons of extinct proboscideans to establish the factuality of extinction (Cuvier, 1800; cf. McGowan, 2001).

Despite collecting the fossil remains of giant sloths in South America while voyaging on the HMS Beagle, Darwin was ultimately not impressed with the value of fossils for understanding the patterns and processes of evolution, nor for their utility in understanding major transitions in lifestyle or locomotion owing to the incompleteness of the fossil record in the mid-late 19th century (Darwin, 1900 Chapters X-II; Fernicola, et al., 2009; Gawne, 2015). Vertebrate fossil taxa were more thoroughly utilized as evidence for evolution by Darwin's supporters (Huxley, 1870; Gawne, 2015), and as fossil collection and documentation expanded it has become commonplace to utilize fossils to interpret evolutionary patterns (e.g. Cope, 1896c; Simpson, 1944; Valentine, 2014). The vertebrate fossil record has since become a primary source of data for investigations into major transitions in modes of life and/or locomotion (e.g. Marsh 1880, Seeley, 1901; Gingrich et al., 2001; Clack, 2006).

For almost a century after the publication of *The Origin of Species* most investigations into the mode and tempo of evolutionary radiations and extinction emphasized the role of biotic interactions (cf. Gould, 2002). The last several decades have seen a shift towards increased

quantification of data (Sepkoski 2012 & 2013) as well as an emphasis on how physical systems interact with and drive evolutionary patterns (e.g. Alvarez, 1983; Gould, 1987; Bennett, 1990; Peters, 2005; Schaltegger et al., 2008). The threat of anthropocentric climate change in the modern has added urgency to attempts at understanding how changes in prevailing thermal regimes impact organisms and ecosystems.

In my attempt to stand on the shoulders of these giants I have investigated both the role of physical changes in driving mass extinctions (modeling thermal ecology and stress during the End Triassic Extinction, Chapter 1) and a major evolutionary transition in locomotion (the origin of avian flight, Chapter 3). In between these bookends I attempt to improve the precision with which volumetric analyses are done on extinct vertebrates (constraining archosaur torso dimensions, Chapter 2). Reconstructed proportional data has seen frequent use as 3D scanning and analysis tools become more affordable and accessible (e.g. Hutchinson, et al., 2011; Mallison, 2012; Clauss, et al., 2017). It also provides a more robust starting point for modeling thermal ecology. In addition to the research found in Chapters 1-3, I contributed to several papers directly tied to my dissertation research, which can be found in Supplemental Appendices A-C.

The End Triassic Extinction

The End Triassic Extinction (ETE) is recognized as one of the five mass extinction events in Earth history (Raup & Sepkoski, 1982). Initially some workers disputed the severity and cause of the ETE, as well as the synchroneity of the terrestrial and marine extinctions (e.g. Hallam, 2002; Olsen, et al., 2002) but over the last two decades converging lines of evidence from high resolution isotopic climate proxies (Schaller et al., 2011), pCO_2 curves derived from plant

stomatal indices and long-chain N-alkanes (Whiteside et al., 2010; Ruhl et al. 2011), and high resolution geochronology (Blackburn et al., 2013) have resulted in a consensus that significant volcanogenic atmospheric carbon input (perhaps 12k-38k gigatons, cf. Ruhl et al. 2011; Heimdal, et al. 2020) resulted in a geologically rapid series of global warming events at the Triassic/Jurassic boundary (e.g. Fig. I-1).

High resolution U-Pb dating, palynology, and magnetostratigraphy were used to tie the onset of extrusive Central Atlantic magmatic province (CAMP) emplacement in Morocco with the ETE. Blackburn et al. (2013) utilized high-precision U-PB dating from CAMP extrusives to test and refine a floating astrochronology framework for the Newark Basin. Using U-Pb dates to anchor the floating chronology, they utilized a least-squares optimization to refine the date of the ETE to 201.564 Ma +/- 0.015 Ma (analytical uncertainty) and 0.22 Ma (decay constant uncertainty). Correlating the Newark basin to the Moroccan Argana basin via palynology and the E23r normal magnetic polarity chron suggests the first recorded magmatic pulse of CAMP emplacement coincides with a simultaneous terrestrial and marine ETE. In contrast, Davies, et al. (2017) recently argued that the first CIE and best estimate for initiation of biotic extinction began ~100,000 years before the first extrusive eruptions. They instead attributed the initial pulse of atmospheric CO_2 to intrusive sills deposited in an organic-rich deposition basin in Brazil (Davies, et al., 2017).

Either way, the initial pulse of atmospheric CO_2 resulted in ocean acidification, a collapse of coral reef communities, and the loss of several clades of marine life including all conodonts (Hautman, 2004; Van de Schootbrugge, et al., 2007). Terrestrial ecosystems saw a global fern spike (Whiteside, et al., 2010) followed by significant loss of floral and faunal clades by the time Early Jurassic ecosystems recovered (Benton,1994; Fowell, et al., 1994; Brusatte, et al., 2008).

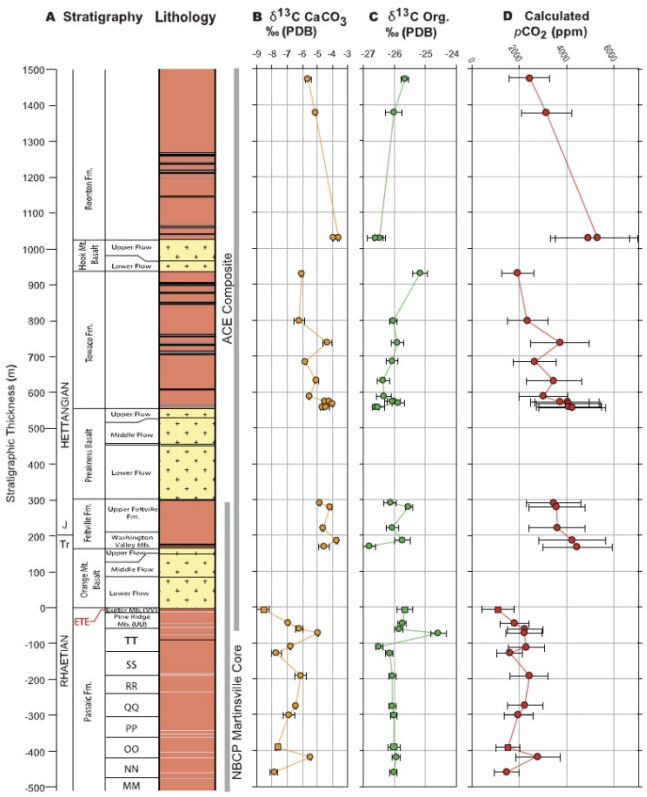

Fig I-1. Stratigraphy of the upper Newark Basin. *Stratigraphic correlation of δ13C values pedogenic carbonate (B) and direct paleosols surface measurements (C) and calculated atmospheric CO_2 (Schaller et al., 2011).*

Most workers have accepted a series of four pulses over 620,000 years, although disagreement about the potential role of intrusive vs extrusive activity (e.g. Heimdal, et al., 2018; Capriolo, et al., 2020) and the possibility of only three main pulses threaten to complicate modeling (Whiteside, et al., 2010; Schaller, et al., 2011; Blackburn et al., 2013; Heimdal, et al., 2020). The disruptive potential of these disagreements is alleviated, however, as carbon isotopic excursions (CIEs) record pulses of atmospheric CO_2 regardless of source, and models of atmospheric carbon input to match CIEs are in agreement that the first pulse had the largest impact on global temperatures (Huynh & Poulsen, 2005; Heimdal, et al., 2020; Landwehrs, et al., 2020). This coincides with the fossil record, as the fern spike and biotic collapse of the marine

and terrestrial systems are similarly tied to the first recorded CIE (Whiteside, et al., 2010, Blackburn, et al., 2013; Davies, et al., 2017).

A separate potential problem arises from conflicting estimates of atmospheric CO_2 before and during the first pulse of the ETE, and the resulting degree of warming. Schaller et al. (2011) attempted to estimate atmospheric CO_2 using pedogenic carbonate nodules collected from paleosols interbedded directly with CAMP extrusives in the Newark Basins. Starting from a mean pre-CAMP atmospheric pCO_2 of ~2,000 ppm it was estimated pCO_2 levels would rise to 4,000-5,000 ppm (Fig 1.2). Working in the same basin, Whiteside et al. (2010) came to similar values analyzing sediment $\delta^{13}C_{toc}$ and $\delta^{13}C_{alk}$ of wood.

Analyzing long-chain plant cuticle *n*-alkanes in Austria, Ruhl et al. (2011) found a negative $\delta^{13}C_{alk}$ (their $\delta^{13}C_{n\text{-alkane}}$) of 8.5‰, more than twice the CIE found by previous studies (Whiteside el al., 2010; Schaller, et al., 2011). They suggested lower $\delta^{13}C_{alk}$ results in previous studies may stem from thermal degradation or mixing of organic C sources, invoking variance between the $\delta^{13}C_{alk}$, $\delta^{13}C_{wood}$, and $\delta^{13}C_{toc}$ samples of Whiteside et al. (2010) as potentially favoring thermal damage. Ruhl, et al. did note that their own results could have been confounded by a change in floral composition (seen as a major influx of coniferous *Classopollis meyeriana* pollen) but noted that during the Paleocene-Eocene thermal maximum a similarly dramatic shift from mixed conifer/angiosperm floras to pure angiosperm floras only accounted for a negative 1-2‰ shift. Assuming a 6.5-8.5‰ CIE value Ruhl, et al. calculated a pulse of ~38,000 gigatons (Gt) of carbon would need to be released, a significantly higher value than other studies.

Estimates of pCO_2 derived from fossil leaf stomata provide an important independent line of evidence for atmospheric CO_2 levels. Since the density of plant stomata is directly related to

the efficiency of gas exchange through leaf stomata, the stomatal index (SI) is relatively free of confounding diagenetic processes once controlled for plant species and surface sample size (Retallack, 2001). Sampling across the Triassic/Jurassic boundary suggest a peak atmospheric pCO_2 of 4,000-5,000 ppm at the ETE (Retallack 2002 & 2013), similar to values calculated from carbonate and wood isotopes, and lower than those suggested by Ruhl, et al. (2011).

The need to improve global warming models due to anthropogenic climate change in the modern (e.g. Anderson, et al., 2016) has resulted in more robust methods for modeling ETE climates. Heimdal, et al., (2020) were able to replicate ocean and terrestrial CIEs using a long-term ocean–atmosphere–sediment carbon cycle reservoir (LOSCAR) model. Their ETE pulse required the input of 8,800 Gt of carbon which raised atmospheric pCO_2 levels to 3,800 ppm. Heat stress may not have been the only thermal stressor experienced during the ETE. Landwehrs, et al. (2020) modeled the climatic impact of up to 500 Gt of aerosolized sulfur emitted alongside pulses of 7,500 Gt carbon released over 1-6 kyr. This resulted in a period of strong transient cooling that gave way to sustained warming of up to 4.4 °C over initial temperatures. They used lower values of carbon emissions and subsequent atmospheric pCO_2 levels than prior attempts (e.g. Schaller, et al. 2011, Retallack, 2013; Heimdal, et al., 2020), but Landwerhrs, et al., demonstrated a logistic relationship between increased CO_2 emissions and peak temperature increase across the ~6 kyr pulses that make it a straightforward process to generate an “extra hot” climate to compare model organism performance in competing ETE scenarios.

The Origin of Birds

The origin of powered flight has, to date, occurred three times in vertebrates: Among the ancestors of pterosaurs, bats, and birds (Dudley & Yanoviak, 2011). While the vicissitudes of fossilization and discovery have been unkind with regard to the origins of bat and pterosaur flight, stem-avians have a remarkable fossil record represented by thousands of fossils from hundreds of species spanning all continents across a period of more than 100 million years (Brusatte, et al., 2014; Cau, 2018). Among vertebrates the abundance of avian and stem-avian fossils may provide the best current dataset for understanding a major evolutionary transition in locomotion and subsequent radiation (cf. Mayr, 2016).

An abundance of data does not necessarily result in consensus. As long ago as 1880 dueling hypotheses were introduced over whether bird ancestors had acquired flight in a terrestrial or arboreal context (Williston, 1879; Marsh, 1880), a dichotomy that would frame origin of flight debates for over a century (e.g. Heilmann, 1926; Ostrom, 1979; Martin, 1991; Paul, 2002). Though little scientific debate about the factuality of the dinosaurian ancestry of birds has existed since the late 1980s (Gauthier, 1986; Padian, et al., 1999; Norell, et al., 2001, Prum, 2003) the dramatic increase in collection and description rate combined with the growing incidence of soft-tissue preservation among fossil stem-avians beginning in the late 1990s has allowed for much higher taxonomic sampling in phylogenetic analyses, narrowing the search for avialan sister taxa to a handful of clades of paravian maniraptoran theropods (Clark, et al., 2002; Brusatte, et al., 2014; Angolin, et al., 2018).

An increase in taxonomic sampling brought a concurrent broadening in models of potential selective pressures leading to the origin of avian flight. Wing assisted incline running

(WAIR), a model wherein living birds at an ontogenetic stage prior to flight are still able to utilize their wings to generate aerodynamic forces sufficient for walking up steep inclines otherwise untraversable, was proposed as a possible driver of pre-flight wing adaptation in theropods (Dial, 2003; Tobalske & Dial, 2007). While the WAIR model is now thought to have played at best a late role in shaping pre-flight wings (Dececchi, et al., 2016), the expansion beyond a strict "trees down vs. ground up" dichotomy was a welcome heuristic advance. Additional lines of inquiry into pre-flight wing use includes the importance of wings to brooding (Hopp & Orsen, 2004) and the potential role of display or sexual selection (Dimond, et al., 2011; Persons & Currie, 2019).

The expansion of available stem-avian taxa resulted in a concurrent increase in knowledge of transformational anatomical series between stem and crown avians (Figure I-2). But our ability to utilize high-resolution sequences of morphologic change are challenged by ongoing disagreements about fine-grain phylogenetic position. Part of this debate stems from taxonomic sampling in theropod phylogenetics not keeping pace with the rate of discovery. Rather than ever-increasing taxonomic sample sizes, the past two decades has often seen the expansion of character sampling without concomitant increases in taxonomic sampling (Hartman, et al., 2019). The selection of taxa has also been biased in favor of well-known or well-preserved specimens, which can impact the types of topologies found in phylogenetic analyses (Jenner, 2004). Finally, there has often been an uncritical re-use of previous characters and scorings (Sereno, 2007; Hartman et al., 2019).

This has resulted in several ongoing debates about the order in which flight-related features were acquired. One example is the "neoflightless" model, wherein flight is inferred to

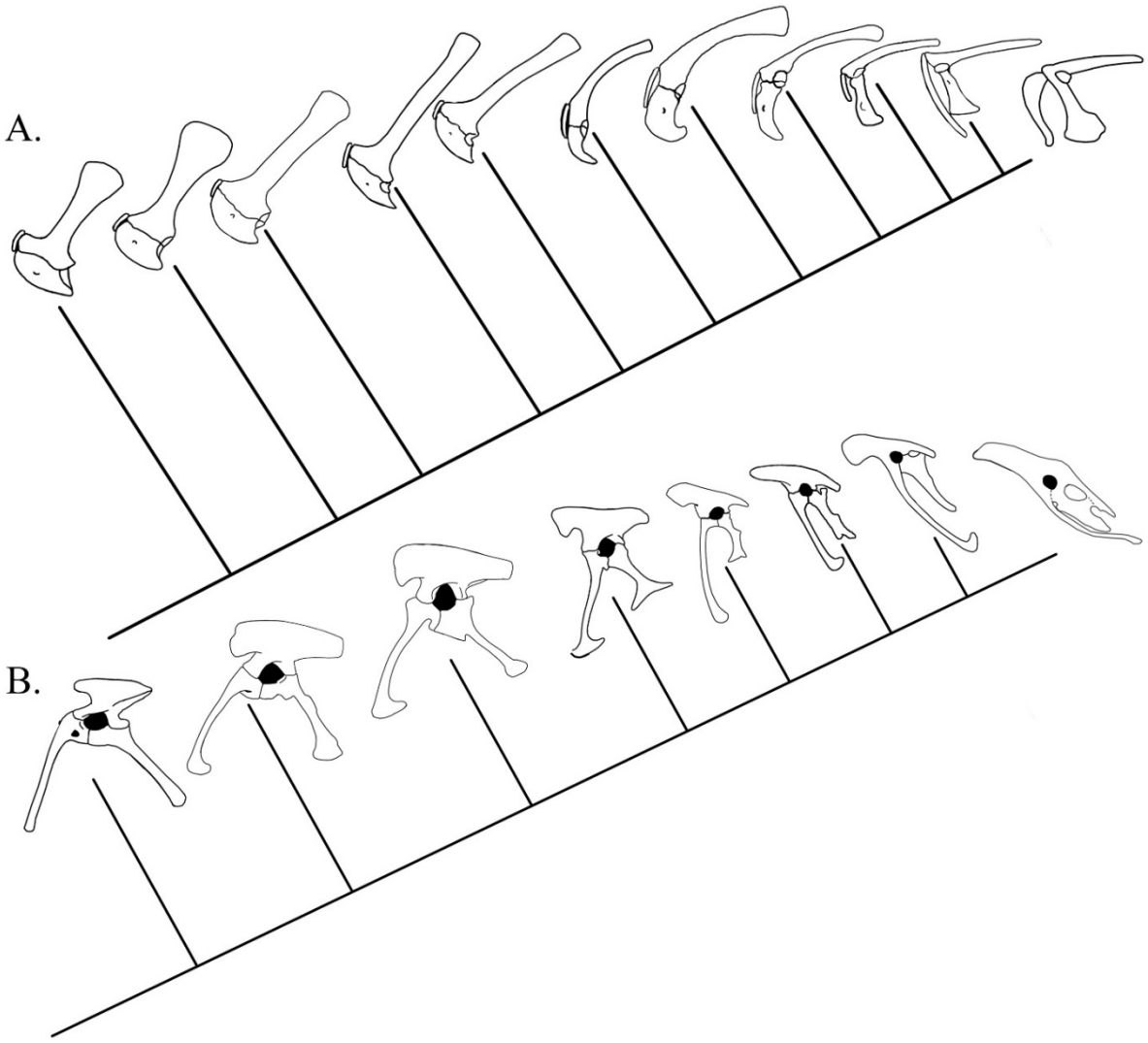

Fig I-2. Two examples of a series of anatomical states seen the pelvic (A) and pectoral (B) girdles between stem- and crown-group avians. *From left to right the genera are (A) Eoraptor, Cryolophosaurus, Marshosaurus, Sinocalliopteryx, Falcarius, Anzu, Archaeopteryx, Jeholornis, Cathayornis & Teratornis; (B) Eoraptor, Cryolophosaurus, Marshosaurus, Falcarius, Archaeopteryx, Jeholornis, Cathayornis & Messelornis.*

have evolved more stemward, and so most flightless winged theropods are interpreted as having descended from volant ancestors (Paul, 2002, Agnolin, et al., 2018). At the same time, numerous papers have found little evidence of arboreal adaptations in theropods historically considered to be candidates for either tree-climbing or flight (e.g. Dececchi & Larsson, 2011; Dececchi, et al., 2016), but instead evidence for a drawn-out terrestrial acquisition of characters later exapted for

flight (Dececchi & Larsson, 2011; Cau, 2018) and the potential for more than one origin of powered aerial behavior in the ancestors of birds (Pei, et al., 2020). These competing hypotheses will require additional phylogenetic testing with expanded taxonomic samples to disentangle.

Overview of Chapters

In chapter one the mechanistic thermal modeling program Niche Mapper is used to explore the thermal ecology of thirteen Late Triassic amniotes according to the principles of Kearney & Porter (2009), analyzed according to protocols developed for using Niche Mapper on vertebrates in deep time by Lovelace, et al. (2020). Thermal constraints are examined in hot-house monsoon and desert conditions typical of the Late Triassic (Prochnow, et al., 2006; Preto, et al., 2010) to evaluate initial pre-ETE thermal stress, and then tested against several competing interpretations of ETE climatic changes.

In chapter two I explore the problem of estimating torso dimensions and volume in extinct vertebrates. I test two models of estimating missing data in vertebral columns, to varying degrees of success. I also look at extant and extinct exemplars of rib orientation and quantify the impact using incorrect rib angulation inferences have on modeling and mass estimates.

In chapter three a new species of small theropod from the Late Jurassic of western North America is described, *Hesperornithoides miessleri*. A phylogenetic analysis with greatly-expanded taxonomic sampling recovers *Hesperornithoides* as a clear paravian, with weaker support for it belonging specifically to troodontids. The phylogenetic results strongly refute the neoflightless model of avian origins but do support multiple independent origins of aerial behavior within stem-avians. This paper has been published in the journal PeerJ (Hartman, et al., 2019).

References

Alvarez, L. 1983. Experimental evidence that an asteroid impact led to the extinction of many species 65 million years ago. Proceedings of the National Academy of Sciences of the United States of America, 80(2), p.627.

Agnolin, F., Motta, M.J., Brisson, F., Lo Coco, G. and Novas, F.E., 2018. Paravian phylogeny and the dinosaur-bird transition: An Overview. Frontiers in Earth Science, 6, p.252.

Anderson, T.R., Hawkins, E. and Jones, P.D., 2016. CO_2, the greenhouse effect and global warming: from the pioneering work of Arrhenius and Callendar to today's Earth System Models. Endeavour, 40(3), pp.178-187.

Bennett, K.D., 1990. Milankovitch cycles and their effects on species in ecological and evolutionary time. Paleobiology, 16(1), pp.11-21.

Benton, M. J. 1994. Late Triassic to Middle Jurassic extinctions among continental tetrapods: testing the pattern. In the Shadow of the Dinosaurs: Early Mesozoic Tetrapods, 366-397.

Blackburn, T. J., Olsen, P. E., Bowring, S. A., McLean, N. M., Kent, D. V., Puffer, J., & Et-Touhami, M. 2013. Zircon U-Pb geochronology links the end-Triassic extinction with the Central Atlantic Magmatic Province. science,340(6135), 941-945.

Brusatte, S. L., Lloyd, G. T., Wang, S. C., & Norell, M. A. 2014. Gradual assembly of avian body plan culminated in rapid rates of evolution across the dinosaur-bird transition. Current Biology, 24, 2386-2392. DOI: 10.1016/j.cub.2014.08.034

Brusatte, S. L., Benton, M. J., Ruta, M., & Lloyd, G. T. 2008. Superiority, competition, and opportunism in the evolutionary radiation of dinosaurs. Science, 321(5895), 1485-1488.

Capriolo, M., Marzoli, A., Aradi, L.E., Callegaro, S., Dal Corso, J., Newton, R.J., Mills, B.J., Wignall, P.B., Bartoli, O., Baker, D.R. and Youbi, N., 2020. Deep CO 2 in the end-Triassic Central Atlantic Magmatic Province. *Nature communications*, *11*(1), pp.1-11.

Cau, A. 2018. The assembly of the avian body plan: A 160-million-year long process. Bollettino della Società Paleontologica Italiana. 57(1), 1-25. DOI: 10.4435/BSPI.2018.01

Clark, J., Norell, M. and Makovicky, P., 2002. Cladistic approaches to the relationships of birds to other theropod dinosaurs. Mesozoic birds: above the heads of dinosaurs, pp.31-61.

Clauss, M., Nurutdinova, I., Meloro, C., Gunga, H.C., Jiang, D., Koller, J., Herkner, B., Sander, P.M. and Hellwich, O., 2017. Reconstruction of body cavity volume in terrestrial tetrapods. Journal of anatomy, 230(2), pp.325-336.

Cope, E. 1896. The primary factors of organic evolution. Open Court.

Cuvier, G. 1800. Extrait d'un ouvrage sur les espèces de quadrupèdes dont on a trouvé les ossemens dans l'intérieur de la terre, adressé aux savans et aux amateurs des sciences.

Darwin, C. 1900. On the Origin of Species by Natural Selection or, The Preservation of Favored Races in the Struggle for Survival in 2 Volumes. Werner Company International Science Library. Akron, Ohio. Reprint of 6th edition.

Dececchi, T. A., Larsson, H. C., & Habib, M. B. 2016. The wings before the bird: an evaluation of flapping-based locomotory hypotheses in bird antecedents. PeerJ, 4, e2159.

Dececchi, T.A. and Larsson, H.C., 2011. Assessing arboreal adaptations of bird antecedents: testing the ecological setting of the origin of the avian flight stroke. PloS one, 6(8).

Dimond, C.C., Cabin, R.J. and Brooks, J.S., 2011. Feathers, dinosaurs, and behavioral cues: defining the visual display hypothesis for the adaptive function of feathers in non-avian theropods. Bios, 82(3), pp.58-63.

Dudley, R. and Yanoviak, S.P., 2011. Animal aloft: the origins of aerial behavior and flight. *Integrative and comparative biology*, *51*(6), pp.926-936.

Fernicola, J.C., Vizcaíno, S.F. and De Iuliis, G. 2009. The fossil mammals collected by Charles Darwin in South America during his travels on board the HMS Beagle. Revista de la Asociación Geológica Argentina, 64(1), pp.147-159.

Fowell, S.J., Cornet, B. and Olsen, P.E., 1994. Geologically rapid Late Triassic extinctions: palynological evidence from the Newark Supergroup. Pangaea: Paleoclimate, Tectonics and Sedimentation During Accretion, Zenith and Break-up of a Supercontinent. Geological Society of America Special Paper, 288, pp.197-206.

Gauthier, J. A. 1986. Saurischian monophyly and the origin of birds. Memoirs of the California Academy of Sciences, 8, 1-55.

Gawne, R. 2015. Fossil evidence in the Origin of Species. BioScience, 65(11), pp.1077-1083.

Gingerich, P.D., ul Haq, M., Zalmout, I.S., Khan, I.H. and Malkani, M.S., 2001. Origin of whales from early artiodactyls: hands and feet of Eocene Protocetidae from Pakistan. Science, 293(5538), pp.2239-2242.

Gould, S.J. 2002. The structure of evolutionary theory. Harvard University Press.

Gould, S.J. 1987. Time's arrow, time's cycle: Myth and metaphor in the discovery of geological time (Vol. 2). Harvard University Press.

Hallam, A. (2002). How catastrophic was the end-Triassic mass extinction?. Lethaia, 35(2), 147-157.

Hartman, S., Mortimer, M., Wahl, W.R., Lomax, D.R., Lippincott, J. and Lovelace, D.M., 2019. A new paravian dinosaur from the Late Jurassic of North America supports a late acquisition of avian flight. PeerJ, 7, p.e7247.

Hautmann, M., 2004. Effect of end-Triassic CO 2 maximum on carbonate sedimentation and marine mass extinction. Facies, 50(2), pp.257-261.

Heilmann, G., 1926. The Origin of Birds (Appleton, New York).

Heimdal, T.H., Jones, M.T. and Svensen, H.H., 2020. Thermogenic carbon release from the Central Atlantic magmatic province caused major end-Triassic carbon cycle perturbations. Proceedings of the National Academy of Sciences, 117(22), pp.11968-11974.

Hopp, T.P. and Orsen, M.J., 2004. 11. Dinosaur Brooding Behavior and the Origin of Flight Feathers. Feathered dragons: studies on the transition from dinosaurs to birds, p.234.

Huynh, T. T., & Poulsen, C. J. (2005). Rising atmospheric CO_2 as a possible trigger for the end-Triassic mass extinction. Palaeogeography, Palaeoclimatology, Palaeoecology, 217(3), 223-242.

Hutchinson, J.R., Bates, K.T., Molnar, J., Allen, V. and Makovicky, P.J., 2011. A computational analysis of limb and body dimensions in Tyrannosaurus rex with implications for locomotion, ontogeny, and growth. PLoS One, 6(10).

Huxley, T. 1870. Further evidence of the affinity between the dinosaurian reptiles and birds. Quarterly Journal of the Geological Society of London 26: 12–31.

Jenner, 2004. The scientific status of metazoan cladistics: Why current research practice must change. Zoologica Scripta. 33, 293-310.

Kearney, M., & Porter, W. (2009). Mechanistic niche modelling: combining physiological and spatial data to predict species' ranges. Ecology letters, 12(4), 334-350.

Lovelace, D.M., Hartman, S.A., Mathewson, P.D., Linzmeier, B.J. and Porter, W.P., 2020. Modeling Dragons: Using linked mechanistic physiological and microclimate models to

explore environmental, physiological, and morphological constraints on the early evolution of dinosaurs. Plos one, 15(5), p.e0223872.
Mallison, H. 2010. The digital Plateosaurus I: body mass, mass distribution, and posture assessed using CAD and CAE on a digitally mounted complete skeleton. Palaeontologia Electronica, 13(2), 8A.
Marsh, O. 1880. Odontornithes: a monograph on the extinct toothed birds of North America (Vol. 1). Museum.
Martin, L.D., 1991. the Origin of Birds. Origins of the higher groups of tetrapods: controversy and consensus, p.485.
Mayor, A. 2007. Fossil legends of the first Americans. Princeton University Press.
Mayor, A. 2001. The first fossil hunters: paleontology in Greek and Roman times. Princeton University Press.
Mayr, G., 2016. Avian evolution: the fossil record of birds and its paleobiological significance. John Wiley & Sons.
McGowan, C. 2001. Dragon Seekers: How an Extraordinary Circle of Fossilists Discovered the Dinosaurs and Paved the Way for Darwin. Perseus Publishers.
Needham, J. 1959. Science and Civilization in China: Volume 3, Mathematics and the Sciences of the Heavens and the Earth. Cambridge University Press.
Norell, M.A., Clark, J.M. and Makovicky, P.J., 2001. Phylogenetic relationships among coelurosaurian theropods. New perspectives on the origin and early evolution of birds, pp.49-68.
Olsen, P. E., Kent, D. V., Sues, H. D., Koeberl, C., Huber, H., Montanari, A., ... & Hartline, B. W. 2002. Ascent of dinosaurs linked to an iridium anomaly at the Triassic-Jurassic boundary. Science, 296(5571), 1305-1307.
Ostrom, J.H., 1979. Bird Flight: How Did It Begin? Did birds begin to fly “from the trees down” or “from the ground up”? Reexamination of Archaeopteryx adds plausibility to an" up from the ground" origin of avian flight. American Scientist, 67(1), pp.46-56.
Padian, K., Hutchinson, J.R. and Holtz, T.R., 1999. Phylogenetic definitions and nomenclature of the major taxonomic categories of the carnivorous Dinosauria (Theropoda). Journal of Vertebrate Paleontology, 19(1), pp.69-80.
Paul, 2002. Dinosaurs of the Air. The Johns Hopkins University Press, Baltimore. 460 pp.
Pei, R., Pittman, M., Goloboff, P.A., Dececchi, T.A., Habib, M.B., Kaye, T.G., Larsson, H.C., Norell, M.A., Brusatte, S.L. and Xu, X., 2020. Powered flight potential approached by wide range of close avian relatives but achieved selectively. bioRxiv.
Persons, W.S. and Currie, P.J., 2019. Feather evolution exemplifies sexually selected bridges across the adaptive landscape. Evolution, 73(9), pp.1686-1694.
Preto, N., Kustatscher, E., & Wignall, P. B. 2010. Triassic climates—State of the art and perspectives. Palaeogeography, Palaeoclimatology, Palaeoecology, 290(1), 1-10.
Prochnow, S. J., Nordt, L. C., Atchley, S. C., & Hudec, M. R. 2006. Multi-proxy paleosol evidence for middle and late Triassic climate trends in eastern Utah. Palaeogeography, Palaeoclimatology, Palaeoecology, 232(1), 53-72.
Prum, R.O., 2003. Are Current Critiques of the Theropod Origin of Birds Science? Rebuttal to. The Auk, 120(2), pp.550-561.
Raup, D. M., & Sepkoski Jr, J. J. 1982. Mass extinctions in the marine fossil record. Science, 215(4539), 1501-1503.

Retallack, G. J. 2001. A 300-million-year record of atmospheric carbon dioxide from fossil plant cuticles. Nature, 411(6835), 287-290.

Retallack, G. J. 2002. Carbon dioxide and climate over the past 300 Myr.Philosophical Transactions of the Royal Society of London. Series A: Mathematical, Physical and Engineering Sciences, 360(1793), 659-673.

Retallack, G.J., 2013. Permian and Triassic greenhouse crises. Gondwana Research, 24(1), pp.90-103.

Rudwick, M. 2008. The meaning of fossils: episodes in the history of palaeontology. University of Chicago Press.

Ruhl, M., Bonis, N. R., Reichart, G. J., Damsté, J. S. S., & Kürschner, W. M. 2011. Atmospheric carbon injection linked to end-Triassic mass extinction. Science, 333(6041), 430-434.

Schaller, M. F., Wright, J. D., & Kent, D. V. 2011. Atmospheric pCO_2 perturbations associated with the Central Atlantic Magmatic Province. Science,331(6023), 1404-1409.

Schaltegger, U., Guex, J., Bartolini, A., Schoene, B. and Ovtcharova, M. 2008. Precise U–Pb age constraints for end-Triassic mass extinction, its correlation to volcanism and Hettangian post-extinction recovery. Earth and Planetary Science Letters, 267(1-2), pp.266-275.

Seeley, H.G., 1901. Dragons of the air: an account of extinct flying reptiles. Methuen & Company.

Sepkoski, D. 2013. Towards "A Natural History of Data": Evolving practices and epistemologies of data in paleontology, 1800–2000. Journal of the History of Biology, 46(3), pp.401-444.

Sepkoski, D. 2012. Rereading the fossil record: the growth of paleobiology as an evolutionary discipline. University of Chicago Press.

Sereno, 2007. Logical basis for morphological characters in phylogenetics. Cladistics. 23, 565-587. DOI: 10.1111/j.1096-0031.2007.00161.x

Simpson, G. 1942. The beginnings of vertebrate paleontology in North America. Proceedings of the American Philosophical Society, pp.130-188.

Simpson, G.G., 1944. Tempo and mode in evolution (No. 15). Columbia University Press.

Tobalske, B. W., & Dial, K. P. 2007. Aerodynamics of wing-assisted incline running in birds. Journal of Experimental Biology, 210, 1742-1751. DOI: 10.1242/jeb.001701

Van de Schootbrugge, B., Tremolada, F., Rosenthal, Y., Bailey, T. R., Feist-Burkhardt, S., Brinkhuis, H., ... & Falkowski, P. G. 2007. End-Triassic calcification crisis and blooms of organic-walled 'disaster species'. Palaeogeography, Palaeoclimatology, Palaeoecology, 244(1), 126-141.

Valentine, J., 2014. Phanerozoic diversity patterns: profiles in macroevolution. Princeton University Press.

Whiteside, J. H., Olsen, P. E., Eglinton, T., Brookfield, M. E., & Sambrotto, R. N. 2010. Compound-specific carbon isotopes from Earth's largest flood basalt eruptions directly linked to the end-Triassic mass extinction. Proceedings of the National Academy of Sciences, 107(15), 6721-6725.

Williston, S.W., 1879. Are birds derived from dinosaurs. Kansas City Review of Science, 3, pp.457-460.

Chapter 1

Thermal ecology of terrestrial amniotes during the End Triassic Extinction

Abstract

It is broadly accepted that the End Triassic Extinction was due to a global warming event triggered by volcanically mediated increase in atmospheric CO_2. Prior modeling based on carbon isotope excursions suggest an input of volcanogenic sulfur and 7,500 to 12,500 GT of CO_2 resulted in a strong transient cold phase followed by prolonged warming over a period of 1-10 kyr. Terrestrially this coincides with major faunal and floral upheaval, but the causal relationship between environmental change and selectivity in extinction have not been mechanistically tested. I employed the mechanistic modeling program Niche Mapper on thirteen Late Triassic amniotes to test how changes in thermal conditions before and during the End Triassic Extinction would alter available foraging time, core body temperature, and metabolic costs of thermoregulation. Surprisingly, the proposed transient cold phase of the ETE better explains the selectivity of terrestrial extinctions than the global warming phase, although reinforcing selection during cooling and warming phases likely explains terrestrial ETE extinction and survivorship.

Introduction

All organisms, living or extinct, exist within the physical constraints placed on them by their environments. The derivation of heat-balance equations from experimental data and first principles make it possible to model the thermal response of organisms, and establish the climate space they can potentially occupy (Barlett & Gates, 1967; Levy, et al., 2012; Dudley, et al., 2013). In extant organisms mechanistic niche modelling has demonstrated efficacy at predicting temperature preference, habitat selection, range extension, and food requirements of animals across a wide range of size and phylogenetic diversity (e.g. Kearney & Porter, 2009; Levy, et al., 2012; Mathewson & Porter, 2013; Fitzpatrick, et al., 2015; Dudley, et al., 2016).

Anticipating future work on extinct organisms, Porter & Gates (1969) explored the role of size and insulation in modulating temperature fluctuations in hypothetical tetrapods from a few grams up to 100 kg. Using a modified form of their heat-transfer equations, Spotila, et al. (1973) further investigated the role size plays in damping the impact of external temperature change on thermoregulation in ectotherms. Spotila, et al. claimed their results demonstrated that large non-avian dinosaurs could have exploited 'gigantism', achieving a functionally homeothermic core temperature as long as they lived in the warm, stable climatic regimes historically hypothesized for the Mesozoic (Skoczylas, 1981).

Dunham, et al. (1989) applied a more sophisticated microclimate model to the Late Cretaceous dinosaur *Maiasaura* while investigating the role of size and life history strategy in dinosaur thermoregulation. While confirming the importance increasing mass plays in insulating an organism from temperature change, their whole-body heat generation and counter-current heat exchange model demonstrated that average body temperatures in ~5 tonne poikilotherms would have been lower than those calculated by Spotila, et al. (1973) and would not have resulted in high homeothermic temperatures.

Though the use of mechanistic modeling to investigate thermal ecology in extant ecosystems has steadily made advancements with extant taxa (e.g. Kearney & Porter, 2009; Long, et al., 2014; Lin, et al., 2019), attempts to apply it to Mesozoic faunas largely stopped after Dunham, et al. (1989). Recent advances in multi-proxy reconstruction of local paleoclimates and improved global climate modeling (GCMs) now allow a robust basis to utilize mechanistic modeling to once again investigate competing hypotheses of extinction and survivorship in ancient ecosystems (Hartman, et al., 2015 & 2016; Lovelace, et al., 2020).

The End Triassic Extinction (ETE) has been causally linked to a geologically rapid series of global warming events driven by outgassing and contact metamorphism during the emplacement of Central Atlantic magmatic provinces (CAMP) during rifting of the proto-Atlantic and initial breakup of Pangea at the end of the Triassic (Huynh & Poulsen, 2005; Blackburn et al., 2013; Davies, et al., 2017; Capriolo, et al., 2020). Heimdal, et al. (2020) provided a robust quantitative framework for the amount and duration of carbon injected into the atmosphere to explain observed carbon isotope excursions in the geologic record. Additionally, GCMs based on aerosolized sulfur and elevated atmospheric CO_2 levels during isotopic excursion events can serve as the basis for mechanistic microclimate models (Landwehrs, et al., 2020).

Here I utilized a series of microclimate models to investigate the thermal ecology of thirteen representative Late Triassic species before the ETE, as well as the transient cold and global warming stages of the ETE. While both stages contribute significant thermal stress, the transient cold phase appears to have played a large role in extinction selectivity during the ETE.

Methods

I employed the mechanistic thermal modeling program Niche Mapper™ (Porter & Mitchell, 2006). Developed at UW-Madison, Niche Mapper combines user inputted microclimate models with biophysical organismal models to calculate heat and mass balance solutions for an organism within its environment hourly, for up to a year. To increase the rate of inputting data for model runs, I employed an R script developed in conjunction with Benjamin Linzmeier and David Lovelace to automate the process of running thousands of climate and physiological states through Niche Mapper.

Selection of taxa, as well as comparisons with pre-ETE geographic ranges were evaluated using the Paleobiology Database (paleobiodb.org). Outcrop data was obtained from the Macrostratigraphy Database (macrostrat.org). Paleogeographic reconstruction and rotation of fossil occurrences and outcrop area utilized Gplates (gplates.org), and maps were plotted using QGIS (QGIS, 2019).

Microclimate Models

Niche Mapper's microclimate model uses 49 user inputted fields to define maximum and minimum wind speed, air temperature, humidity, cloud cover, shade, insolation, and soil properties, plus seasonal variation thereof (See Appendix S1 of Lovelace, et al., 2020 for the complete list). During model runs Niche Mapper fits a sinusoidal curve to inputted minimum and maximum seasonal values to calculate hourly profiles for air, ground, and ground cover temperatures, relative humidity, convective cooling due to wind, and solar and thermal radiation between emissive and reflective surfaces and the biophysical model (Fig. 1-1). Maximum air temperature and wind speed as well as minimum relative humidity and cloud cover were set to happen an hour after solar noon (cf. Geiger, et al., 2009). Solar radiation reaching the biophysical model is varied according to day of year, hour of day, latitude, cloud cover, and the potential to seek shade and/or burrows (McCullough & Porter, 1971; Porter, et al., 1973; Kearney, et al., 2014).

To test the thermal ecology of organisms prior to the ETE, two baseline microclimates were utilized. These were derived from the baseline Late Triassic microclimate model of Lovelace, et al. (2020) and include a seasonally wet monsoon-based microclimate model

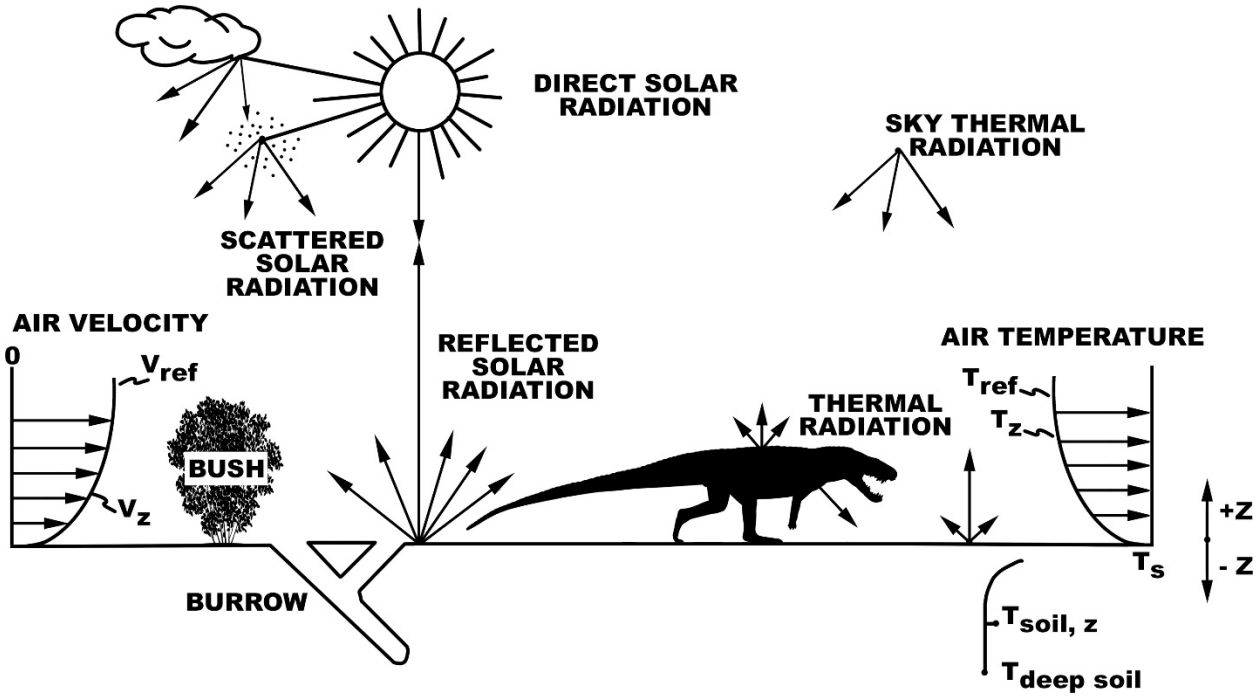

Fig 1-1. Organism-environment heat balance interactions. *The organism's heat and mass balances that influence body temperature are determined by where it chooses to be each hour to remain within its preferred body temperature range. Niche Mapper allows it to find a location each hour where it can remain active, or not, if necessary, to optimize body temperature, energy demands and/or water balance.*

Parameter	Model	Source	Input Range
Air Temperature	Microclimate	1,2	21-31C LowLat; 14-24C HiLat
Relative Humidity	Microclimate	2,3,4	Dry: 13-65%; Monsoon: 48-96%
Cloud Cover	Microclimate	2,4	50-90%
Wind Speeds	Microclimate	2,5,6	1-4 m/s
Atmospheric % O_2	Biophysical	2,7	18%
Atmospheric % CO_2	Biophysical	2,8,9	0.13%

Table 1-1. Inputs for baseline Late Triassic microclimate models. *References: [1] Prochnow, et al., 2006 [2] Lovelace, et al., 2020 [3] Sellwood & Valdes, 2006 [4] Parish, 1993 [5] Weather Spark data 1 [6] Weather Spark data 2 [7] Berner, et al., 2003 [8] Cleveland, et al., 2008 [9] Berner & Kothavala, 2001.*

(Dubiel, et al., 1991; Prochnow, et al., 2006; Preto et al., 2010), as well as a more arid "desert" microclimate model to simulate continental interiors at 12º latitude. To expand the range of geographic testing, a higher latitude (55º) microclimate based on pre-ETE temperatures of Landwehrs, et al. (2020) were also run (Table 1-1). To simulate scenarios during the ETE both transient cold and prolonged global warming phase microclimates were created based on environmental models of Landwehrs, et al. (Table 1-2). An additional, higher temperature "extra hot" microclimate model was also created to reflect the higher pCO_2 values suggested by previous authors (Whiteside, et al. 2011; Retallack, 2013; Heimdel, et al., 2020; Table 1-2).

Parameter	Model	Source	Input Range
Air Temperature	Microclimate	10,11,12,13	Cold: 14-23C, Hot: 29-39C, XHot: 41-31C
Relative Humidity	Microclimate	2,3,4	Dry: 13-65%; Monsoon: 48-96%
Cloud Cover	Microclimate	2,4	50-90%
Wind Speeds	Microclimate	2,5,6	1-4 m/s
Atmospheric % O_2	Biophysical	7,11,12	17.3%
Atmospheric % CO_2	Biophysical	8,9,11,12	0.4%

Table 1-2. Inputs for ETE microclimate models. *[10] Whiteside, et al. 2011 [11] Retallack, 2013 [12] Heimdal, et al., 2020 [13] Landwehrs et al., 2020. Other references are the same as Table 1-1.*

Biophysical Models

Dimensional measurements obtained direct directly from specimens and/or published data (see supplemental file S.1-1) are converted in Niche Mapper into simplified geometric shapes (e.g. cylinders, spheres, truncated cones, and ellipsoids) to represent the head, neck, limbs, torso, and tail (Fig. 1-2). The simplified organismal model is therefore made up of

geometric subunits whose heat transfer properties can be more rapidly calculated (Kowalski & Mitchell, 1976; Porter, et al., 2006). In addition to the heat generated within each model subunit, user inputs can specify the presence or absence of a subcutaneous fat layer and its thickness, as well as the presence and characteristics of a layer of epidermal insulation such as fur or feathers. Heat generated within the body must pass through either or both layers (as specified) before being shed into the environment via radiation and convection. Radiant or reflected heat must also pass through the epidermal and/or subcutaneous fat layer (if present) before being absorbed by the body.

Animals can be flagged to adopt specific behavioral configurations, such as laying down or sitting, in which case direct heat conductance to or from the ground is also modeled. Provided with environmental conditions specified in the microclimate model, Niche Mapper solves a heat balance equation over time, calculating heat lost to the environment via radiation (Q_{rad}), convection (Q_{conv}), cutaneous evaporation (Q_{evap}) and respiration (Q_{resp}), plus heat gained from the environment from direct and reflected solar input (Q_{sol}), heat generated internally (Q_{met}), and the amount of heat that can be transiently stored within the flesh (Q_{st}). This is calculated as follows:

$$Q_{met} - Q_{resp} - Q_{st} - Q_{evap} = Q_{rad} + Q_{conv} - Q_{sol}$$

If the animal is modeled as possessing an epidermal covering of fur or feathers, the additional layer slowing down heat transfer is accounted for by (Q_{fur}):

$$Q_{met} - Q_{resp} - Q_{st} - Q_{evap} = Q_{fur} = Q_{rad} + Q_{conv} - Q_{sol}$$

Mass is calculated by Niche Mapper from resulting model volumes and assigned densities. Calculated mass was checked against Graphic Double Integration and previously

published mass estimates (e.g. Peczkis, 1995; Paul, 1997; Seebacher, 2001). Diet composition was inferred from dental morphology. Skin transpiration and breathing efficiency were estimated from extant analogs. For more detailed explanations of heat exchange across fur or feathers see Porter, et al. (2006), Porter & Kearney (2009) and Matthewson & Porter (2013).

Niche Mapper solves the heat balance equation for individual body parts every hour of every day, which are then summed to provide the total metabolic rate necessary to maintain an organism's specified target core temperature. If the model is unable to maintain the target core temperature range within its allowed active metabolic rate within a given hour it will attempt to regain homeostasis by triggering a series of physiological and then behavioral modifiers to gain or shed heat as necessary.

Physiological solutions (when enabled) occur in the following order: 1) Increase fur or feather layer depth to increase insulation (similar to the piloerect response in extant mammals and fluffing feathers in extant birds); 2) Increase or decrease thermal conductivity of the outer "flesh" layer (to simulate vasodilation and vasoconstriction of peripheral blood vessels); 3) Allow core body temperature to rise or fall (simulating temporary toleration of heat storage or loss) within a user defined range; 4) Increase the rate of surface evaporation (to simulate heat loss via sweating); 5) Increase respiratory heat loss (to simulate panting).

If user-allowed physiological changes fail to maintain thermal homeostasis, user-enabled behavioral options are then triggered, including shade seeking, climbing, entering a burrow, wading, swimming, or adopting postures that reduce surface area (e.g. curling up). The heat

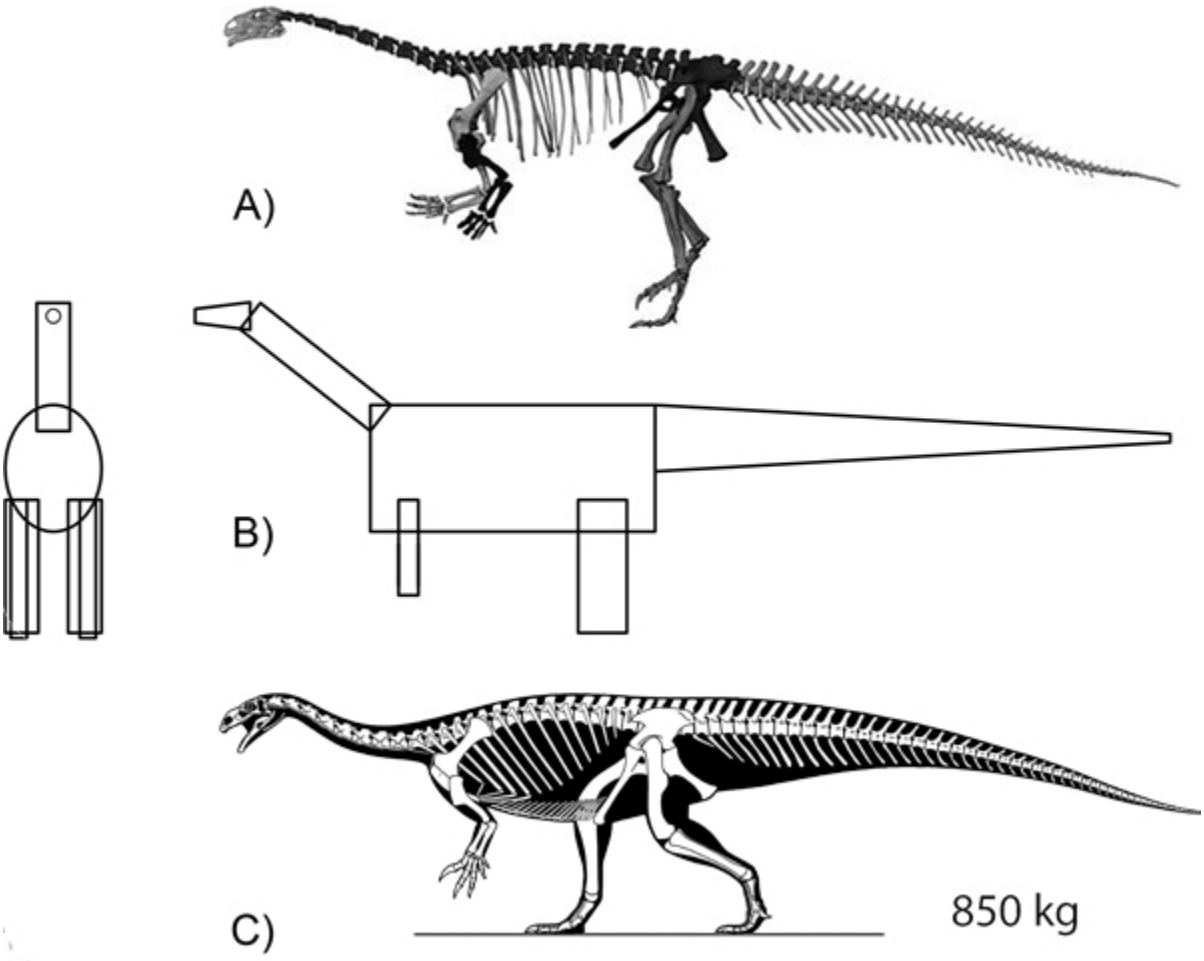

Figure 1-2. Creating proportional models for biophysical input. *Linear dimensions are taken from fossil data (A) e.g. this surface scan of GPIT1. That data can be input to create a geometrically simplified (B) Niche Mapper model. A rigorous reconstruction of the skeletal anatomy can also be used to solve anatomical problems in 3D data (C) or to create silhouettes used to make independent GDI mass estimates.*

balance equation is resolved after each incremental attempt either until thermal homeostasis is regained, or until all options are exhausted. In the latter case the thermoregulatory solution closest to the target metabolic rate is adopted for the hour.

Hourly energy consumption and water loss are summed for the day, allowing for a mass balance equation to be calculated to establish daily food, water, and oxygen budgets. Q_{met}

establishes the necessary daily energy budget, which when adjusted for user-inputted caloric density of available food and digestive efficiency of the organism determines the food budget. Q_{met} also specifies the respiratory budget. Metabolic energy is directly tied to oxygen consumption (Bennet, 1978; McKechnie & Wolf, 2004), and with user specified values for atmospheric oxygen percentage and the efficiency of extraction in the respiratory system the frequency of ventilation can be calculated.

For a detailed overview of all inputs for the biophysical model see Supplemental file S1, and Lovelace, et al., 2020. When modeling extant organisms, the requisite physiological values can be measured directly or taken from values reported in the literature. With extinct species these values must be inferred, but the majority of inputs are either constrained by the physical properties of materials (e.g. fur, feathers, flesh conductivity) that are unlikely to have varied in the past, are relatively straightforward to infer from fossils (e.g. herbivory, carnivory, or omnivory), or turn out to have a minimal impact on modeled results (e.g. skin reflectivity and respiratory efficiency; see Lovelace, et al., 2020). Some values such as digestive efficiency impact food budget but are otherwise immaterial to daily heat calculations (Lovelace, et al., 2020). Some behavioral responses can be ruled out by size or gross anatomy (e.g. 500+ kg archosaurs are unlikely to have climbed trees or burrowed to avoid heat).

Other biophysical model inputs have a large influence on results and require more detailed inference. These include basal metabolic rate, target core body temperature, the presence or absence of epidermal insulation and the presence or absence of subcutaneous fat deposits. These are addressed by clade or genus as appropriate, along with the rationale for taxa selection in the following section.

Modeled Late Triassic Taxa

Representative taxa were selected to represent all major large bodied and most small-medium bodied clades of Norian amniotes (Fig. 1-3). In addition to taxonomic and mass variation, they fill different ecological niches, and exhibited a variety of reconstructed metabolic and thermoregulatory strategies.

Synapsids

The clade made up of mammals and stem-mammals is represented in this study by a dicynodont and a basal mammaliaforme. Dicynodonts were a group of herbivorous therapsids that were geographically widespread and diverse in the Late Permian and Early Triassic but had steadily declined in diversity during the Middle and Late Triassic. By the Norian remaining dicynodonts were restricted to a handful of large species (Sulej & Niedźwiedzki, 2019). Despite prior claims of late-surviving Gondwanan dicynodonts, recent work clarifies that no known dicynodonts survived the ETE (Knutsen & Oerlemans, 2020). For the purposes of this investigation the Norian taxa *Placerias* was modeled.

While molecular clocks suggest an origin of crown-mammals in the Middle or early Late Triassic (Liu, et al. 2018), to date the Late Triassic fossil record consists of closely-related non-mammalian mammaliaforme clades Docodonta and Morganucodonta (Luo, et al., 2015). These mammal-like species were small-bodied and insulated with fur (Ji, et al., 2006), and survived the ETE occupying diverse small tetrapod niches alongside their more derived mammalian relatives until the Early Cretaceous (Ji, et al., 2006; Meng, et al. 2015). Given the size and metabolic similarity within the clade only one representative was modeled for this study.

***Placerias* –** *Placerias* was a large (~800 kg) Late Triassic dicynodont that lived in North America (Lucas, 2002). Proportional measurements were taken from a cast of a large specimen on display at the New Mexico Museum of Natural History, which is based on specimens from the type quarry (Fiorillo, et al., 2000). Given the widespread use of subcutaneous adipose tissue in extant mammals regardless of habitat (Pond, 1992), an adipose layer was modeled in Niche Mapper. Dicynodonts exhibit elevated rates of growth (Botha-Brink & Angielczyk, 2010) and oxygen isotopes indicating a higher degree of homeothermy than found in more basal tetrapods occurring in the same habitat (Rey, et al., 2017). In contrast, coprolites convincingly assigned to a large Late Triassic dicynodont in Poland suggest a relatively simple digestive tract with long gut retention time (Bajdek, et al., 2014). Together with the phylogenetic position of dicynodonts this suggests an incipient level of endothermy, perhaps on par with extant basal mammals such as monotremes. Based on this a target core temperature of 32C was used, and a monotreme-level BMR was calculated for use in the biophysical model based on McNab (2008).

The final variable to consider is the potential for fur-like epidermal structures. Fur-like structures were described in carnivorous coprolites from the Permian (Bajdek, et al., 2016). Since bones from dicynodonts were also common in the coprolites it was inferred that the fur could potentially be linked to them. Given that other, more crownward synapsids were also potential prey in the Permian, it is unclear how strong this association is. The lack of more direct evidence is less problematic for *Placerias*, as using extant mammals as analogs the mass and habitat suggest that fur would be strongly reduced or absent, even if having epidermal insulation was plesiomorphic in smaller, more basal dicynodonts. As such the skin was modeled without a fur layer, with evaporative cooling rates similar to extant naked-skinned mammals.

Mammaliaforme (cf. *Morganucodon*) – The only body fossil of a Triassic mammaliaforme is from the poorly-known docudont *Tikitherium* (Datta, 2005). But ghost lineage and molecular clock data demonstrate that mammaliaformes were a common part of Late Triassic ecosystems (Luo, 2007; Liu, et al., 2018). Since no complete Late Triassic mammaliaforme skeleton is known, the proportional data was taken from Early Jurassic *Morganucodon* (Kielan-Jaworowska, et al., 2005). Direct evidence of epidermal insulation in mammaliaformes (Ji, et al., 2006) required a small mammal-like fur layer in the biophysical model, as well as evaporative values similar to extant mammals. Mammaliaformes are fairly crownward and close to the position of monotremes, so they were modeled with monotreme BMRs (McNab, 2008) and a similar 32C target core temperature. Given the small size and similar ability in extant ecomorphs, the model was also allowed to seek shelter in burrows for thermoregulation. Tooth morphology suggests an insectivorous lifestyle (Kielan-Jaworowska, et al., 2005), which in Niche Mapper was modeled as an omnivorous diet with food and nutritional levels intermediate to that of herbivores and carnivores (Lovelace, et al., 2020).

Archosaurormorpha

Archosauromorphs represent a large and diverse clade that includes all diapsids closer to birds and crocodiles than to lizards (Ezcurra, 2016). In addition to the more familiar derived archosaurs (a clade composed of the common ancestor of birds and crocodiles and all its descendants) basal archosauromorphs were represented in the Triassic by a range of sprawling aquatic, arboreal, and herbivorous clades (Ezcurra, 2016). Basal archosauromorphs were diverse throughout most of the Triassic but become rare in terrestrial ecosystems by the Late Triassic. They are represented in this study only by the beaked herbivorous rhynchosaurs, which made

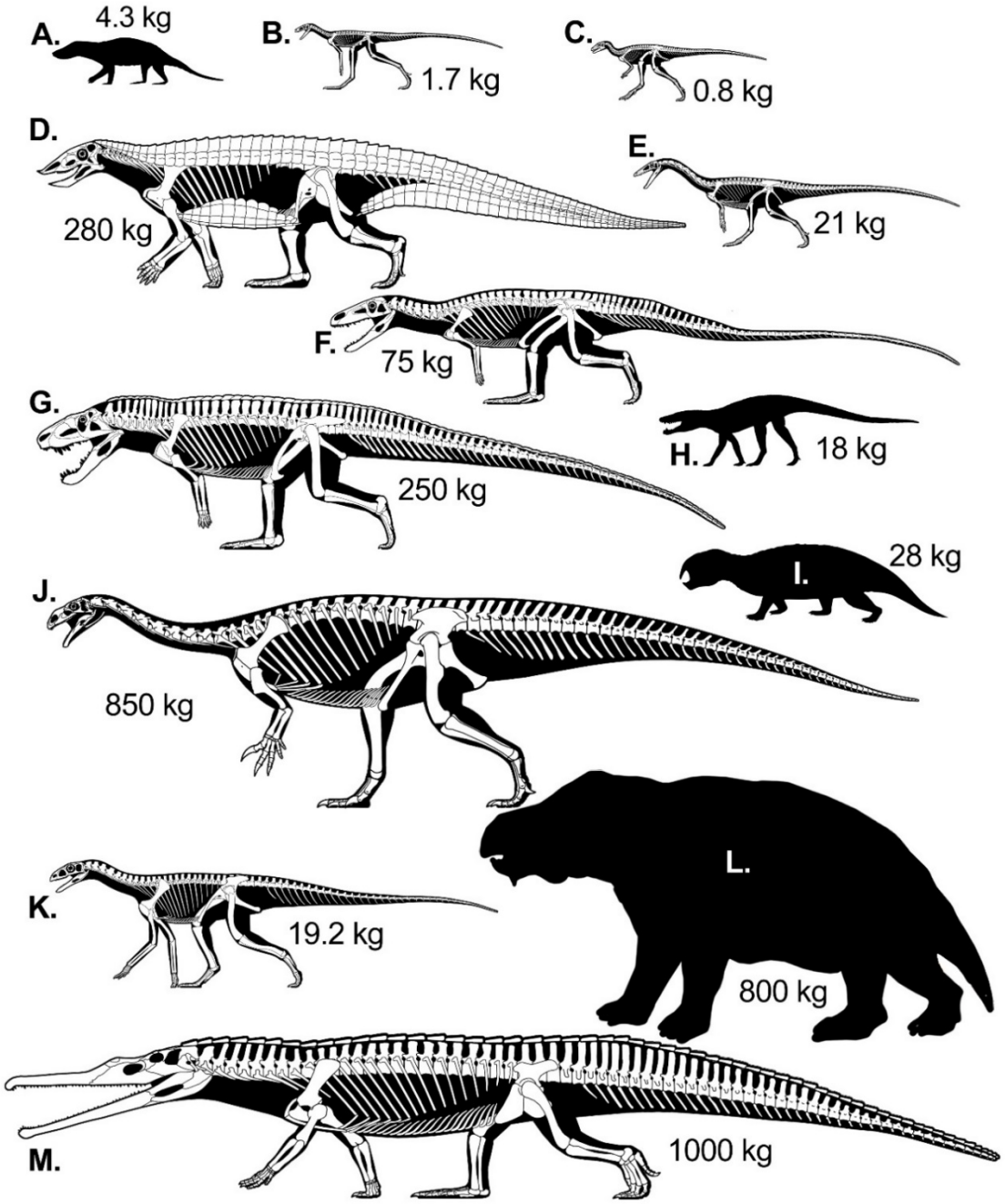

Figure 1-3. Representative skeletals and/or silhouettes with mass estimates of taxa used in this study. *A) Mammaliaforme (cf. Morganucodon), B) Dromomeron, C) hypothetical small ornithischian (cf. Cursor), D) Desmatosuchus, E) Coelophysis, F) Poposaurus, G) Postosuchus, H) Hesperosuchus, I) rhynchosaur (cf. Hyperodapedon), J) Plateosaurus, K) silesaurid (cf. Eucoelophysis), L) Placerias and M) Rutiodon. Silhouettes A, I & H are modified Public Domain images from Phylopic.org (A & I), and Wikimedia Commons. L. provided by David Lovelace, all others are copyright Scott Hartman. Silhouettes are only loosely to scale, to provide visibility for smaller taxa. Rigorous skeletal reconstructions were made to help clarify proportional data, black silhouettes are schematic representations of taxa where proportional data was derived from literature or mount data.*

it until the Late Triassic (Ezcurra, et al., 2016; Andrews & Pough, 1985).

Rhynchosaur (cf. *Hyperodapedon*) - Rhynchosaurs largely died out at the end of the Carnian, but specimens have been reported from the Norian (Spielmann, et al., 2013). Norian specimens are diagnostic but fragmentary, so Niche Mapper proportions were based on the well-known Carnian *Hyperodapedon* (Mukherjee & Ray, 2014). Rhynchosaur growth as determined by osteohistology generally exhibits low, squamate-like growth rates (Ricqlès et al., 2008; Botha-Brink & Smith, 2011) but does occasionally show elevated growth rates early in ontogeny (Veiga, et al., 2014). Given their phylogenetic position, low growth rates, and lack of locomotory, respiratory, or food processing adaptations associated with higher basal metabolic rates, the rhynchosaur biophysical model was inputted with a squamate BMR, and a 30C target core temperature.

With no evidence of epidermal insulation outside of Archosauria, the rhynchosaur model used literature values for scaly skin dermal reflectivity and heat transmission (Lovelace, et al., 2020). Substantial subcutaneous fat layers are not widespread outside of synapsids (Pond, 1992), so only a minimal value was input for the rhynchosaur model. Although a 28 kg animal would require a relatively large burrow, burrowing lizards exist at a similar sizes (e.g. Træholt, 1995) and has been found in Komodo dragons that reach up to 70kg (Lutz & Lutz, 1997). Moreover, burrowing is widespread among sprawling, ectothermic species when thermally stressed (Stevenson, 1985).

Crocodile-line archosaurs

Pseuodsuchians are archosaurs closer to crocodiles than to birds. Among extant ecosystems this group only includes eusuchians such as alligators and crocodiles, but Middle and

Late Triassic ecosystems were filled with a diverse array of pseudosuchians. The reason most pseudosuchian clades went extinct at the ETE while dinosaurs and the ancestors of modern eusuchians did not is subject to substantial debate ongoing (e.g. Olsen, et al., 1987; Stubbs, et al., 2013; Hudgins, et al., 2020). To test the role of thermal ecology in pseudosuchian extinction five taxa were modeled.

***Rutiodon* –** Although phytosaurs like *Rutiodon* superficially resembled living crocodilians (Fig. 1-3M) they are distant relatives, being recovered as either the most primitive members of Pseudosuchia (e.g. Brusatte, et al., 2010) or sometimes recovered outside of Pseudosuchia altogether (Nesbitt, 2011). The skull and teeth of phytosaurus suggest a similar ecological role to modern crocodilians, one based largely around fish and supplemented by the occasional terrestrial vertebrate. Despite their superficial similarity, trackways attributed to phytosaurs suggest they used a more upright stance, akin to the "high walk" that modern eusuchians only use on occasion (Padian, et al., 2010). Bone histology exhibits a growth pattern similar to living eusuchians (Ricqlès, et al., 2003; Scheyer, et al., 2013), so an ectothermic BMR and a target core temperature of 30C has been utilized in Niche Mapper.

Rutiodon is well known from several complete specimens, reaching lengths of up to 8 meters, and a mass of 1,000 kg (Huene, 1913; Hurlburt, 2003). Crocodile-like osteoderms are found in phytosaurs, so skin was modeled after extant eusuchian skin reflective and transmissive properties, with no epidermal insulation and minimal subcutaneous fat insulation. Phytosaurs do not seem to have survived the ETE (Lucas & Tanner, 2007)

***Desmatosuchus* –** Aetosaurs were heavily armored, herbivorous pseudosuchians found only in the Late Triassic (Desojo, 2012). Histologically determined growth rates generally match those

of phytosaurs and extant eusuchians (Ricqlès, et al., 2003; Scheyer, et al., 2013). Modern crocodilian values were therefore used for skin, insulation, BMR, target core temperature (30C) and evaporative cooling inputs, similar to *Rutiodon*. *Desmatosuchus* grew up to 4.5 meters in length and perhaps 300 kg (Small, 1985). Some anatomical proportions were filled in from better described remains of other aetosaurs (Fig. 1-3D; e.g. Walker, 1961).

Poposaurus – *Poposaurus* is the eponymous member of Poposauridae, a more crownward clade of carnivorous Late Triassic loricatan pseudosuchians (Nesbitt, 2011). Despite being a croc-line archosaur that is closer to extant crocodilians that phytosaurs and aetosaurs, poposaurids were obligate bipeds, converging on the condition seen in theropod dinosaurs (Gauthier, et al., 2011). *Poposaurus* is known from a virtually complete and well-described postcranial specimen, YPM 57100 which formed the basis of the proportional inputs for the biophysical model (Fig. 1-3F; Schachner, et al., 2020).

Poposaurid BMR is more challenging to infer. The expanded pelvic musculature suggests a shift to increased scope in locomotion (Clarke & Pörtner, 2010; Schachner, et al., 2020). Histological analysis of *Poposaurus* shows a pattern of rapid growth more similar to dinosauriforms, but with bone vascularization levels overlapping the range of extant eusuchians (Schachner, et al., 2020); smaller-bodied poposaurids show evidence of slower growth rates (Nesbitt, 2007). Although poposaurids show a reduction in dermal armor, there is no evidence for epidermal insulatory structures or other heat-retaining adaptions in the group. Taken as a whole, poposaurids show evidence of elevated metabolic activity compared to extant crocodilians, but below the level seen in dinosaurs. To square this circle the biophysical model used the lowest level endothermic BMR calculater (“monotreme”, McNab, 2008) and a target core temperature intermediate to that of extant ectotherms and endotherms (35C). Other dermal

values were adopted from extant relatives (Lovelace, et al., 2020). Poposaurids did not survive the ETE.

***Postosuchus* –** Moving more crownward, rauisuchians are a group of large, exclusively carnivorous loricatans from the Middle and Late Triassic. *Postosuchus* reached 4.5 meters in length and an estimated mass of 250+ kg (Chatterjee, 1985; Weinbaum, 2013). The type and paratype specimens of *Postosuchus* were used as the basis of the proportional inputs (Fig. 1-3G; Weinbaum, 2013). *Postosuchus* is also primarily bidpedal, though given the number of quadrupedal intermediates between it and poposaurids it is clear this was another independent origin of bipedal locomotion in the Late Triassic (Nesbitt, 2011; Weinbaum, 2013). *Postosuchus* appears somewhat less committed to bipedalism, in that the slightly-built forelimbs could probably bear weight at low speeds, and there appears to be an ontogenetic shift to shorter arms as individuals age (cf. specimens in Weinbaum, 2013) suggesting the possibility of a more quadrupedal hatchling or juvenile stage.

Postosuchus runs into a similar metabolic inference scenario as discussed for *Poposaurus.* Histology shows an elevated rate of growth compared to modern crocodilians, but less so than seen in dinosauriforms or even the fastest growing loricatans (Legendre, et al., 2013; Klein, et al., 2017). Similar strategies for calculating BMR and specifying target core temperature (35C) were used as for *Poposaurus*. Osteoderms are known for *Postosuchus*, so it can be unambiguously assigned to a skin type similar to living crocodilians (Weinbaum, 2013). Like most croc-line archosaur clades, rauisuchians did not survive the ETE.

***Hesperosuchus* –** Moving one final step crownward, crocodylomorphs are the loricatan clade that contains living crocodilians. Despite their phylogenetical proximity, Late Triassic

crocodylomorphs were in many ways the least visually similar to living crocodilians in ecology and gross anatomy, consisting of small-to-medium sized gracile, terrestrial carnivores (Nesbitt, 2011). The upright, quadrupedal stance of basal Late Triassic crocodylopmorphs like *Hesperosuchus* included limbs with cursorial proportions (Clark, et al., 2001; Lecuona & Desojo, 2012). Proportional data was taken primarily from AMNH 6758 (Colbert, 1952).

Hesperosuchus has challenges when inferring metabolic rates. Despite being the most cursorial pseudosuchian in the model dataset, its bones exhibit degrees of vascularization and growth rates almost identical to that seen in living crocodilians (Ricqlès, et al., 2008). While faster growth requires more energy and a concomitant increase in metabolic rate, the opposite is not necessarily true (cf. Myhrvold, 2016), with *Homo sapiens* being a notable example of an endothermic amniote with a slow growth rate (Leigh, 2001). Since the return to a secondarily reduced ectothermic BMR in living crocodilians is theoretically tied to their reinvading aquatic habitats (Seymour, et al., 2004; Ricqlès, et al., 2008; Legendre, 2014), and *Hesperosuchus* shows no evidence of aquatic adaptations, incipient endothermic BMR levels and an intermediate target core temperature or 35C like other loricatans was used in this study. The presence of unambiguous osteoderms in basal crocodylomorphs allows for the use of extant crocodilian literature values for skin reflectance and flesh conductivity (Molnar, et al., 2015).

Bird-line archosaurs

Ornithodirans are the clade made up of the most recent common ancestor of birds and pterosaurs, and all its descendants (Gauthier, 1986). Given the emphasis on terrestrial amniotes, modeled ornithodirans were restricted to dinosauromorph taxa. Ichnological data suggests an Early Triassic origin for dinosauromorphs (Brusatte, et al., 2011), though body fossils do not show up until the Middle Triassic and dinosauromorphs do not become a common part of

Triassic ecosystems until the Late Triassic. Basal dinosauromorphs were quite small, but by the end of the Triassic prosauropod dinosaurs had reached a ton or more in mass (Mallison, 2010). Due to a combination of growth rates, isotopic paleothermometry, and enhanced aerobic scope all dinosauromorphs appear to have been at least incipiently endothermic (Pontzer, et al., 2009; Eagle, et al., 2011; Werner & Griebeler, 2014).

***Dromomeron* –** A basal lagerpetid dinosauromorph, *Dromomeron* was a ~1m long, bipedal omnivore of the Late Triassic (Irmis, et al., 2007; Griffin, et al., 2019). *Dromomeron* is mostly known from hind limb elements, so other lagerpetids contributed to a composite reconstruction (Fig. 1-3B) to achieve proportional inputs (Sereno & Arcucci, 1994; Cabreira, et al., 2016). Histological analysis of the femur of *Dromomeron* demonstrastes an elevated growth rate similar to those seen in croc-line archosaurs showing incipient endothermy (Ricqlès, et al., 2008; Griffin, et al., 2019), so a similar BMR and target core temperature (35C) were assigned.

The presence or absence of epidermal insulation in basal dinosauromorphs is more contentious. There is extensive evidence for epidermal coverings in small-medium sized theropod (Xu, et al., 2009; McKellar, et al., 2011; Xing, et al., 2016) and small ornithischian dinosaurs (Zheng, et al., 2009; Godefroit, et al., 2014) as far back as the Early Jurassic (Kundrát, 2004). Detailed morphological similarity to epidermal structures in pterosaurs has been used to argue that some form of epidermal insulation is primitive to all ornithodirans (Yang, et al., 2019). But many large dinosaur clades only exhibit reticulate scales and/or osteoderms, and in the absence of direct evidence Triassic taxa character optimization studies do not favor epidermal filaments plesiomorphic to Ornithodira (Campione, et al., 2020). Despite their opposition to fully homologous filaments across Ornithodira, Campione, et al. postulate a scenario wherein similar genes are co-opted repeatedly in ornithodirans of small size. The

absence of direct epidermal data at the base of Ornithodira and the small number species for which character states can be confidently specified risks systematic bias in the results (Heath, et al., 2008; Müller & Dias-da-Silva, 2019). Given *Dromomeron*'s small size (1.7 kg) the biophysical input model was specified with a reduced layer of epidermal filaments. Lagerpetids did not survive the ETE.

Silesaurid (cf. *Eucoelophysis*) – Silesaurids were a group of omnivorous or insectivorous small-medium sized, facultatively quadrupedal herbivorous dinosauromorphs generally recovered as the sister group to Dinosauria (Kammerer, et al., 2012; Qvarnström et al., 2019). Silesaurids were a common part of Middle Triassic and early Late Triassic ecosystems (Ezcurra, 2006; Kammerer, et al., 2012). They became less common during the Late Triassic and ultimately did not survive the ETE. Late Triassic silesaurid remains are largely incomplete, so the Middle Triassic *Asilisaurus* was scaled to the appropriate size to provide proportional data (Fig. 1-3K). Silesaurid histology exhibits growth rates and bone texture intermediate between *Dromomeron* and early dinosaurs (Griffin, et al., 2019), so an incipient endothermic BMR was inputted along with a target core temperature of 37C, intermediate between *Dromomeron* and dinosaurs.

Small ornithischian (cf. *Eocursor*) – Substantial taxonomic revision of fragmentary specimens eliminated nearly all putative ornithischians from the Triassic (Irmis, et al., 2007b; Agnolín & Rozadilla, 2018). One possible exception is *Eocursor*, which is clearly an ornithischian (Butler, 2010) but whose Late Triassic/Early Jurassic status depends on stratigraphic resolution within the Elliot Formation (McPhee, et al., 2017). Regardless, ghost lineages suggest the presence of small ornithischians by the Late Triassic, so modeling a representative taxon is informative about the clade's ability to avoid extinction during the ETE.

Within Dinosauria more derived endothermy is supported by multiple lines of evidence including circulatory pressure (Seymour & Lillywhite, 2000), isotopic paleothermometry (Eagle, et al., 2011), osteological correlates for increased respiratory performance (Wedel, 2009), power generation during locomotion (Pontzer, et al., 2009; Seymour, 2013) and the majority of dinosaurian growth rates (Myhrvold, 2016). A ratite level of BMR was calculated (McNab, 2009), and a target core temperature of 38C was used (Maloney, 2008; Lovelace, et al., 2020). Jurassic small-bodied ornithischians with evidence for dermal impressions show several types of filamentous structures (Zheng, et al., 2009; Godefroit, et al. 2014), so an epidermal layer was modeled. Taphonomy supports burrowing in small taxa (e.g.Varricchio, et al., 2007).

***Plateosaurus* –** Basal sauropodomorphs appeared in the Late Triassic as small, omnivorous bipeds (cf. Martinez & Alcober, 2009), but by the end of the Late Triassic they were medium to large sized bipedal herbivores, with some reaching a tonne or more in mass (Mallison, 2010; Otero, et al., 2019). Proportional data was taken from GPIT1 (Figures 1-2; 1-3J; Mallison, 2010). In addition to arguments supporting an elevated metabolism made above for all dinosaurs, Lovelace, et al. (2020) modeled and tested *Plateosaurus* in a Niche Mapper virtual metabolic chamber and concluded that a ratite-like BMR was the most plausible condition, so a 38C target core temperature and a ratite-level BMR was used. Other biophysical inputs were adopted from the vetted model of Lovelace, et al. (2020).

***Coelophysis* –** Theropod dinosaurs are the clade that includes birds. Body fossils are first found in the Late Triassic, and by the end of the Triassic theropod-bearing ecosystems are dominated by coelophysids (Hendrickx, et al., 2015). While no direct evidence is present for or against epidermal filaments, they are so far ubiquitous in small theropods preserved with skin impressions. As with *Plateosaurus* above, *Coelophysis* was extensively modeled and vetted in

Niche Mapper previously (Lovelace, et al., 2020), from which all biophysical input values were adopted, including a ratite-level BMR and a target core temperature of 38C.

Niche Mapper Plots

All biophysical input values can be found in supplemental dataset S2. Niche Mapper output files were collated in R (R Core Team, 2013) and converted into plots using ggplot2 (Wickman, 2016). After solving heat and mass balance equations allowing all 13 model organisms to successfully thermoregulate withing a given microclimate model for a year Niche Mapper outputs massive amounts of data. Compiling hourly values after a running 13 taxa in 13 environments results in 50,700 entries for 64 different categories (n=3,244,800 data points). Removing the seasonal pattern of changing thermal values over time also removes crucial daily and seasonal context. To convey the data without losing temporal context three of the most useful indicators of thermal performance were plotted for the entire model year: Each organism's core temperature ($T_{core)}$, metabolic energy use (ME), and percent shade seeking behavior necessary to thermoregulate within a microenvironment (cf. Lovelace, et al., 2020; all raw data is available in supplemental database S.1-5).

Figure 1-4 shows example T_{core} plots of a 280 kg *Desmatosuchus* in two different microclimates: The pre-ETE monsoon microclimate modeled on geochemical proxies representative of low-latitude pre-ETE environments in North America (Prochnow, et a., 2006; Lovelace, et al., 2020) and a more arid, ETE "hot" microclimate' representative of an ETE global warming climate as modeled by Landwehrs, et al (2020). Comparing both environments at mid-September, most of the day in the monsoon baseline microclimate *Desmatosuchus* was able to maintain T_{core} within a +/-3C range of its target core temperature value. Within that range

enzymes are operating at their maximal efficiency (Peterson, et al., 2007). Beyond that range conformational changes reduce enzymatic efficiency, and at higher temperatures it eventually leads to denaturing of enzyme proteins (Angilletta, et al., 2010). For an hour in the early afternoon the T_{core} of *Desmatosuchus* rises above 38C. During this time, the animal would experience a form of heat stress as non-optimal enzymatic activity resulted in a slowing down of metabolic processes.

During the same mid-September day in the ETE dry microclimate, T_{core} of *Desmatosuchus* rises above optimal body temperature range for a more significant 8 hours during midday. If the change between the baseline monsoon environment and the desert hot environment occurred in a geologically rapid timeframe, such as during the ETE (e.g. Heimdal, et al., 2020; Landwehrs, et al., 2020) the result would be reductions in metabolic efficiency of 20-30% for a third of the day (Angilletta, et al., 2010). For herbivores like *Desmatosuchus*, where the need for lengthened gut retention time results in digestion throughout the day (Farlow, 1987; (Franz, et al., 2011), this metabolic stress would reduce survival margins even if ME and available foraging time remained equal.

Looking at ME (Fig. 1-5) a 280 kg *Desmatosuchus* in the pre-ETE monsoon microclimate can be active all day, but morning and evening hours required an increase in metabolic rate from ~2 times BMR to 3-4 times BMR. This results in an increase in daily energy expenditure (DEE), which is presumably non-optimal, but research shows DEE is only tightly linked to BMR in placental mammals (Koteja, 1991; Ricklefs, et al., 1996), and with sufficient foraging time ME increases are not inherently a problem until extreme multiples (5x or more)

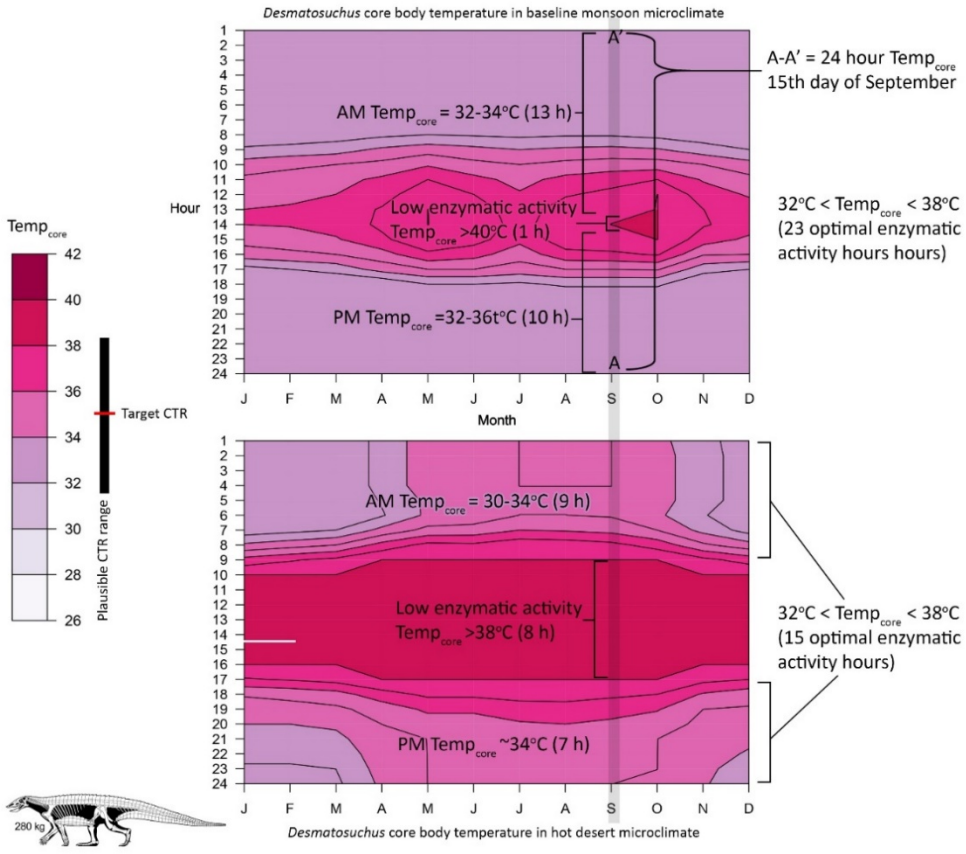

Fig 1-4. Daily fluctuations in core temperature and enzymatic efficiency. *Enzymatic reaction rates are temperature dependent, only working efficiently around a narrow core temperature range. Outside of that range digestion and other metabolic activity slows down significantly (see text).*

of BMR are necessary (Lovelace, et al., 2020). Heat buildup, on the other hand can only be offset by lowering metabolic activity to a point, as an organism cannot reduce ME much below the basic metabolic processes necessary to keep the animal alive (i.e. BMR), and when active ME cannot be reduced even that far. So while DEE would be somewhat higher in the baseline monsoon environment compared to the desert hot ETE environment, in the latter there would be several hours in midday when the animal would simply have to forgo all activity to avoid dangerous heat buildup (cf. Mole, et al., 2016).

Shade seeking behavior is undertaken as an energetically inexpensive way to thermoregulate. Shade seeking may occur during daylight hours when T_{core} is too high to reduce

incoming solar radiation and to shelter in a microenvironment with lower than ambient temperature. Shade seeking can also occur at night to maintain heat, as vegetative cover slows the loss of radiant ground heat (Lovelace, et al., 2020). In the baseline microenvironment the modeled *Desmatosuchus* seeks 'night shade' for warmth during overnight hours, but otherwise enjoys a solid 15 hours of foraging time without need to seek shade (Fig. 1-6). In the desert hot microclimate, the *Desmatosuchus* spends a similar amount of time seeking shade at night, but also retreats to the shade for 8 hours during midday, resulting in just 7 hours of foraging time without the constraint of seeking shade. How devastating this is depends on resource density within the environment, and the necessary foraging hours required to meet an organism's DEE. In a heavily forested area, seeking shade is not necessarily a problem, but in the Late Triassic continental interiors were very dry, and in wetter areas megamonsoon conditions and seasonal aridity kept stands of trees spaced out and restricted to year-round sources of water (Dubiel, et al., 1991).

As an herbivore, finding a shaded grove near water with appropriate foliage for consumption would ameliorate foraging/shade problems in the short term, but on longer timescales losing this much foraging time would potentially be devastating, especially for larger herbivores, which spend 50-70% of each day foraging (e.g. Owen-Smith, 1979, Plumb & Dodd, 1993). If we assume these changes occurred in 6,000 years or less, the strong reduction in foraging time and efficient enzymatic activity would probably be enough to cause extirpation, and with widespread climatic conditions eventual extinction.

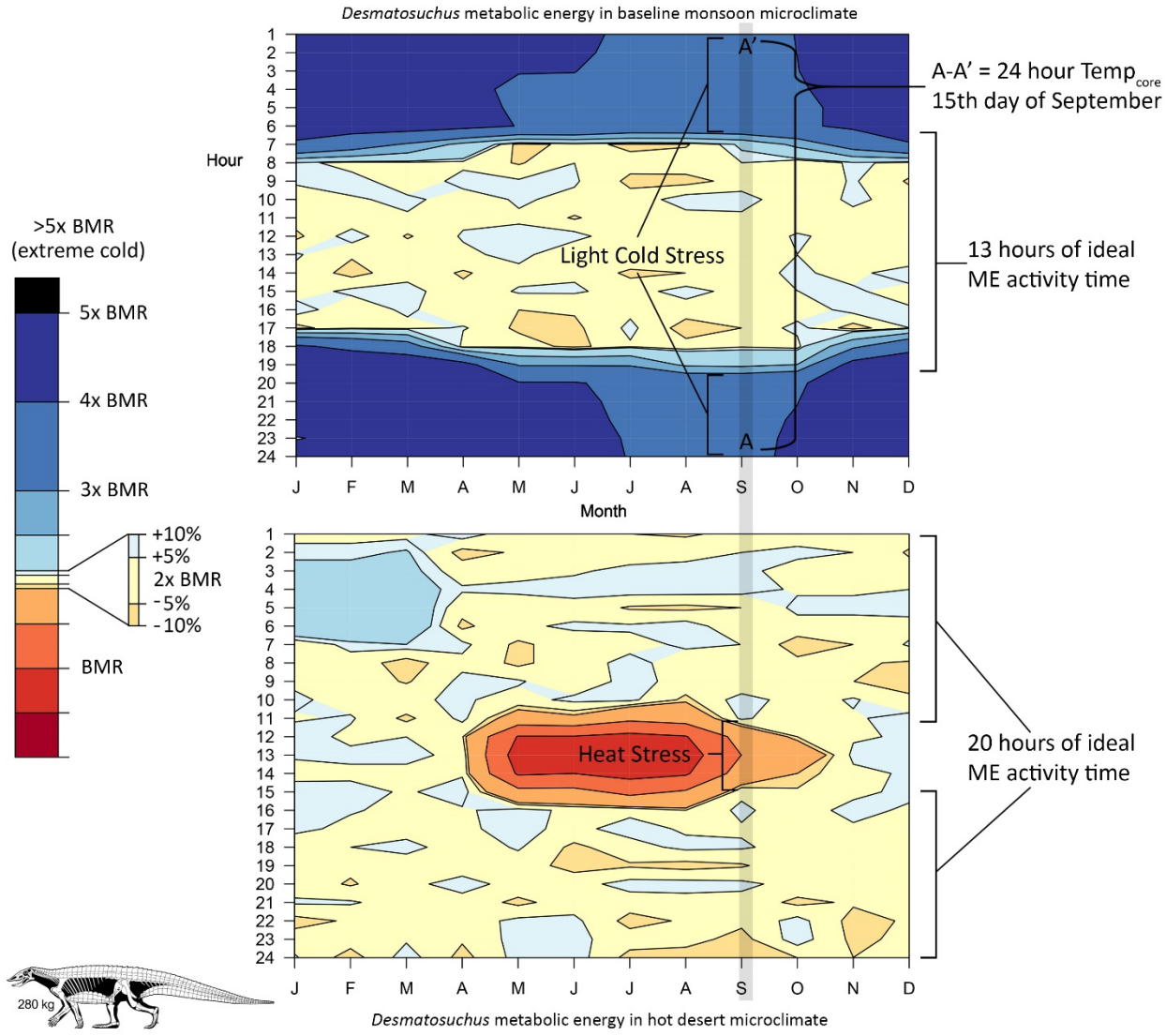

Fig 1-5. Daily fluctuations in metabolic energy. *In the absence of specialized physiological adaptations, amniotes generally attempt to thermoregulate without their energy expenditure exceeding 2x basal metabolic rate (see text), though overheating is a greater problem until extreme (5x BMR) levels are reached.*

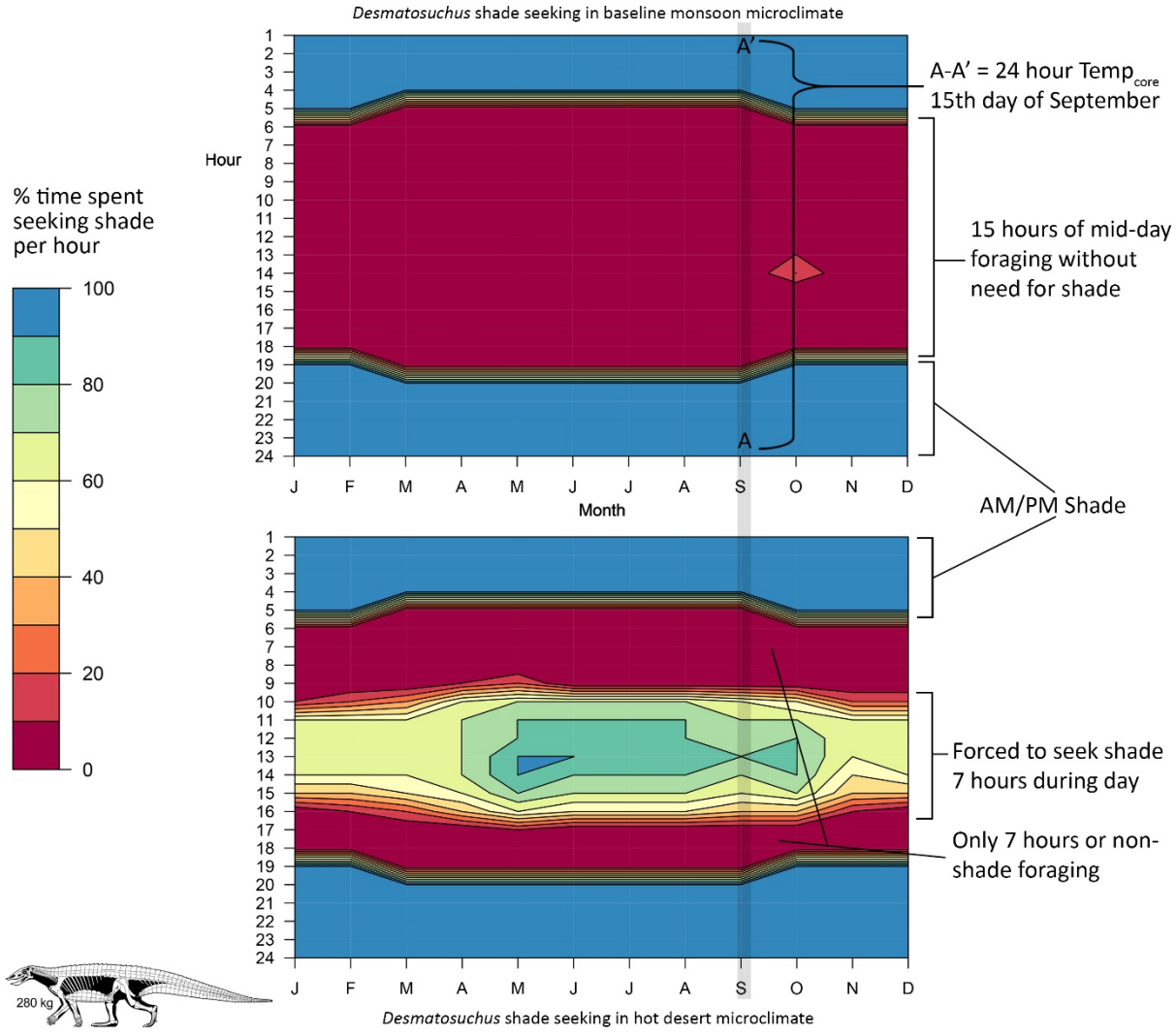

Fig 1-6. Daily fluctuations in shade seeking behavior*. Shade can be used to cool off during daylight hours, but since plants slow down the radiation of heat when it is dark, "night shade" seekingf can help warm an animal at night.*

Burrowing vs non-burrowing

For burrowing taxa such as *Dromomeron*, a heuristic challenge with interpreting plots arises (Fig. 1-7). Since burrows insulate occupants from the external environment, the metabolic costs of thermoregulation drop to near-BMRs levels while they are inside, dipping into the orange-to-red part of ME plots. Because this is also what is seen, albeit for very different reasons

when non-burrowing animals overheat (that is, where they are trying to reduce ME as low as possible due to excess heat load), an unintended consequence is portions of the day spent in a burrow - the easiest and safest thermoregulation available – appear the same as excess heat buildup, which is one of the most dangerous thermoregulatory challenges a modeled animal can encounter (compare *Dromomeron* in Fig. 1-7 to *Desmatosuchus* in Fig. 1-5). Burrowing taxa (small ornithischian, *Dromomeron,* mammaliaform, *Hesperosuchus,* and rhynchosaur) were run with burrowing both enabled and disabled (plots for both can be found in supplementary files S.1-4 and S.1-5). Running simulations without burrowing is informative about the ability of small taxa to function without a burrow (e.g. if forced to leave due to changing climatic conditions). For consistency, aggregate microclimate results will be figured without burrowing enabled, but additional figures of the thermal performance of burrowers with burrowing enabled will be presented separately and explicitly labeled as such.

Results for environmental simulations

Three plots are produced for each of the 13 taxa in each of the 13 microclimate models, resulting in 507 full resolution plots. Since much of the value of the plots come from comparing results between taxa within the same microclimate, results are presented with reduced scale images of 39 plots (e.g. Fig. 1-8). Collated pdfs of individual full-resolution plots are available in supplemental files S.1-3 & S.1-3). Thermal ecology will first be examined in pre-ETE microclimates, as a self-check to see to see how taxa perform in environments known to be viable before the end Triassic extinction. From there we will move on to the thermal ecology of taxa within the aerosolized sulfur-induced transient cold periods predicted by Landwehrs, et al. (2020), before examining two different atmospheric pCO_2 scenarios for the subsequent global warming phase.

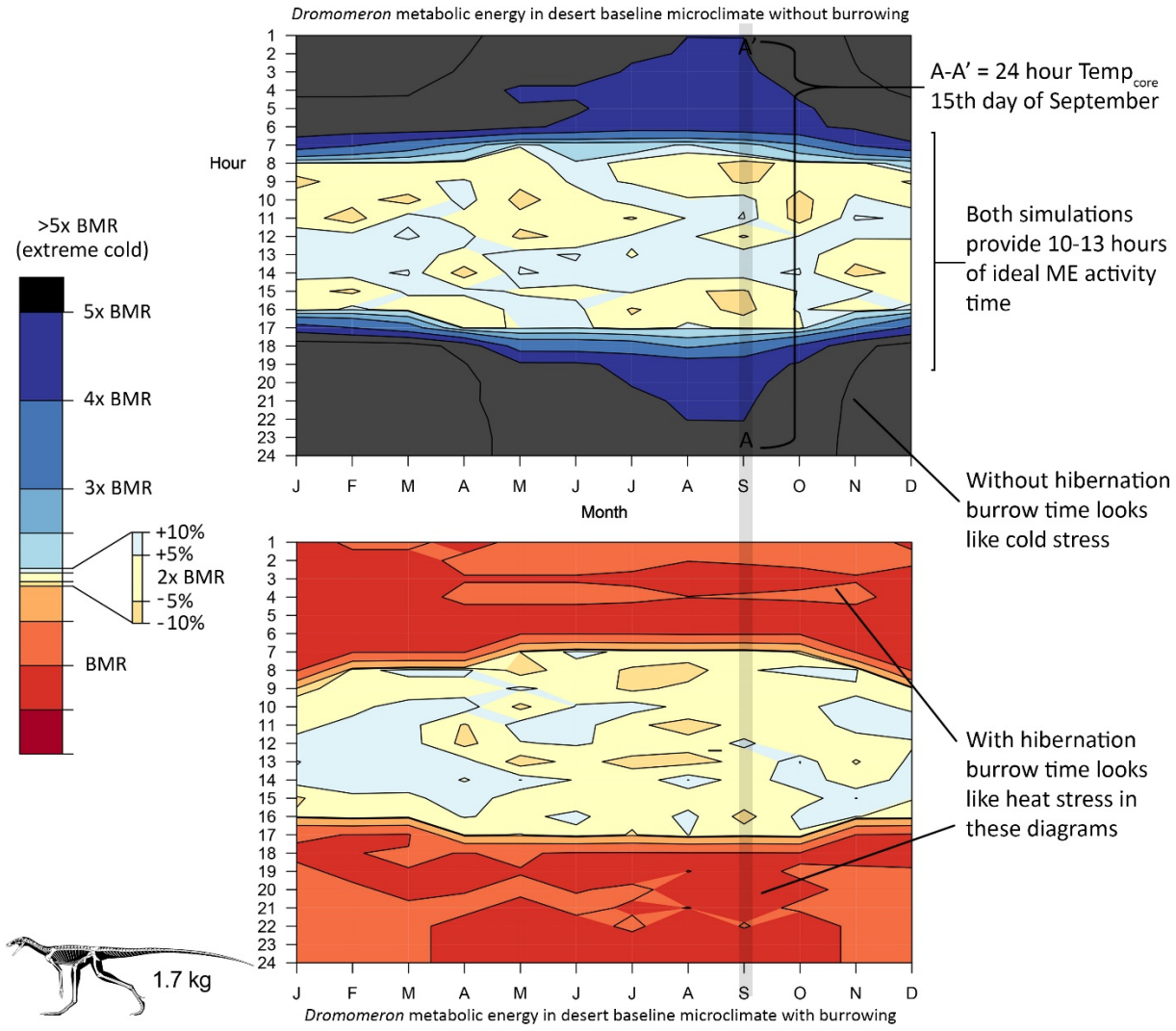

Fig 1-7. Impact of modeling hibernation on ME plots. *Daily fluctuations in shade seeking behavior with without hibernation (top) and with hibernation enabled (bottom).*

Results

Looking at the results of low latitude Late Triassic microclimates based on Lovelace, et al. (2020) and Landwehrs, et al. (2020) there is little difference in thermal performance between the monsoon and arid environments (Figs. 1-8 to 1-10). The arid environment shows a slight increase shade seeking behavior at midday for most taxa, with *Placerias* the most impacted with a 1.5% increase in shade seeking behavior during a simulated year. Conversely, the small

terrestrial crocodilian *Hesperosuchus* need to seek 0.4% less shade in the more arid environment. The theropod *Coelophysis* needed to seek more midday shade in the monsoon microclimate but required less night shade for a net gain of 1.9% foraging time. Given daily variation in foraging efficiency, annual variations in climate and longer variations due to orbital forcing (Bahr, et al., 2020) it seems unlikely that these small changes to foraging time would have impacted survival. Indeed, with similar temperatures shared between the monsoon and arid microclimates thermal variation between them is too small to directly impact habitat preference; instead, non-thermal factors like water availability and food resource density would have been more important in habitat selection (Noy-Meir, 1974). Based on sedimentological and geochemical proxies, seasonal monsoon conditions would have dominated low latitude portions of Pangea due to the Late Triassic mega-monsoon (Preto et al., 2010), but exceptionally arid, desert-like conditions were common in the continental interiors (Whiteside, 2011).

The small ornithischian dinosaur was modeled as a potential burrower, but pre-ETE it would have been able to thermoregulate at night most of the year by raising its ME to 3-4.5x BMR. Enabling burrowing (Fig. 1-9) for the small ornithischian resulted in a warmer T_{core} and lower ME overnight in the burrow, but in pre-ETE microclimates burrowing is not strictly necessary on thermal ecology grounds. In contrast, *Dromomeron* is non-viable without burrowing enabled (Fig. 1-8 & Fig. 1-10). When allowed to use a burrow overnight (Fig. 1-9) *Dromomeron* maintains an elevated T_{core} at little ME cost, and can use thermal inertia and potential trips back to the burrow as necessary to forage successfully throughout the day. Based on these results it appears *Dromomeron* was an obligate burrower and almost certainly diurnal,

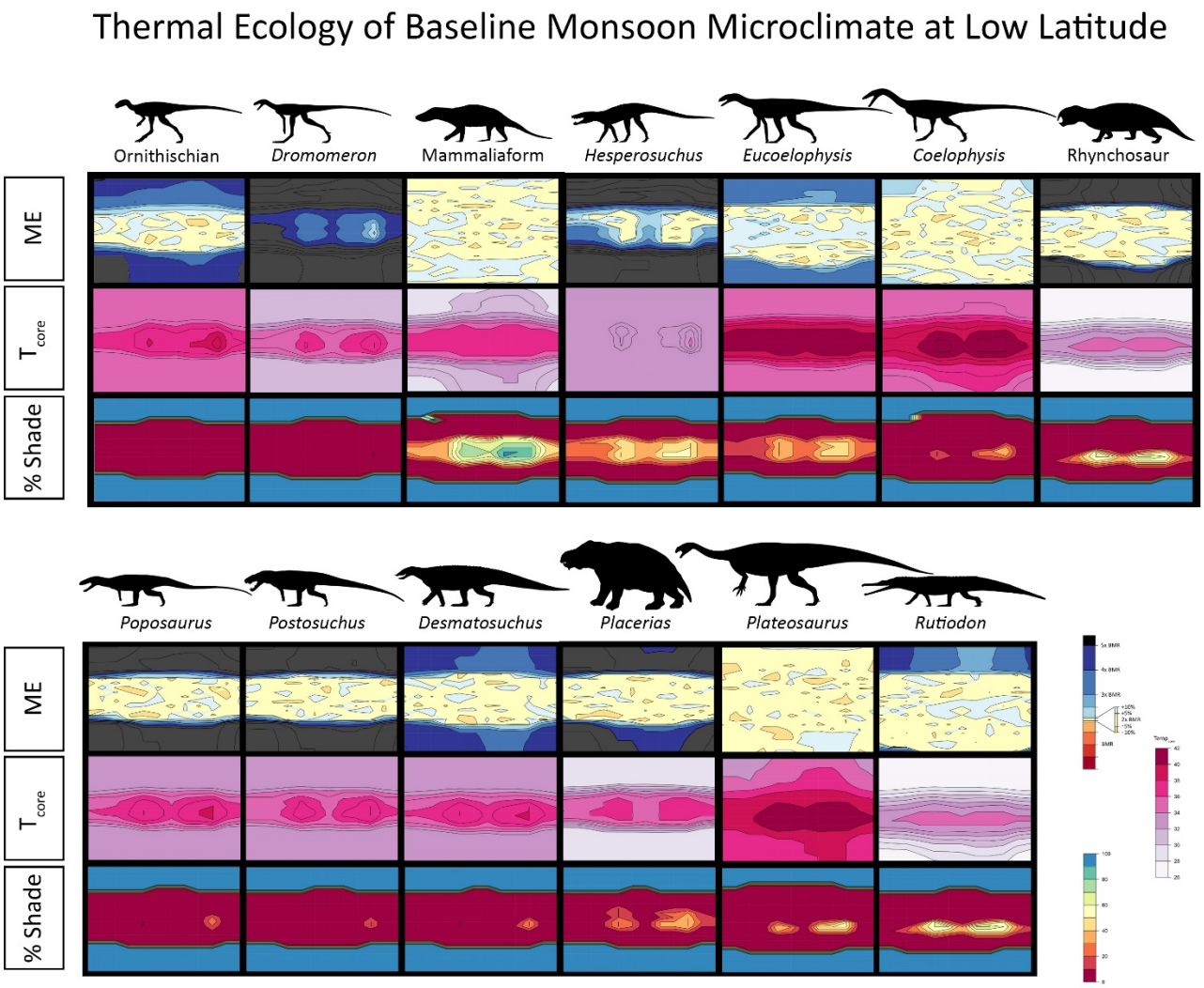

Fig. 1-8. Thermal ecology in a typical Late Triassic seasonal monsoon environment at 12 degrees latitude. *Species are arranged from smallest to largest left to right and top to bottom. Burrowing enabled plots can be seen in Fig. 1-9. Full size color keys can be found in Figs. 1-4 through 1-7. Abbreviations: ME, metabolic energy; T_{core}, core temperature; %Shade, amount of time per hour an animal must seek out shade to thermoregulate.*

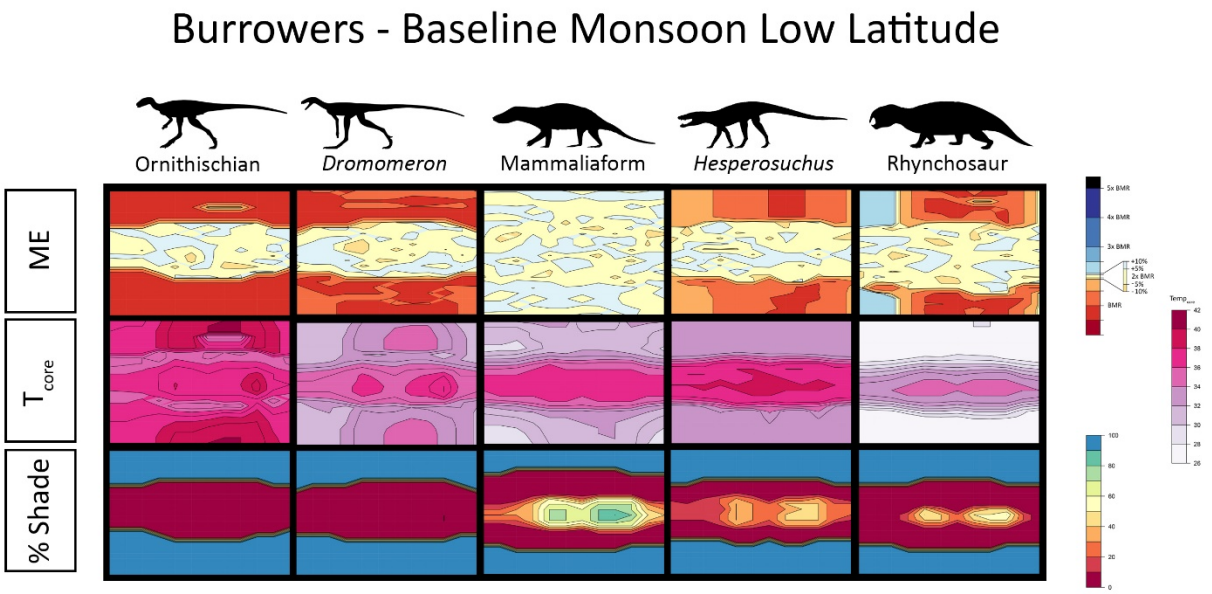

Fig. 1-9. Thermal ecology with burrowing enabled in the baseline monsoon environment at 12 degrees latitude. *Species are arranged from smallest to largest left to right. Red areas in the metabolic energy plots are due to lowered thermoregulation costs while in a burrow, not from heat stress. Full size color keys can be found in Figs. 1-4 through 1-7. Abbreviations: ME, metabolic energy; T_{core}, core temperature; %Shade, amount of time per hour an animal must seek out shade to thermoregulate.*

whereas the small ornithischian could engage in crepuscular or cathemeral activity patterns without encountering strong thermal constraints, though the elevated ME costs at night outside the burrow suggest that being nocturnal was less likely.

The 4.3 kg mammaliaform could thermoregulate at night year round with or without burrowing enabled (Figs. 1-8 & 1-9). Aside from being larger than either the small ornithischian or *Dromomeron*, the mammliaform's denser mammal-based epidermal insulation and a reduced surface area to mass ratio owing to its more compact build account for these differences. During the day the mammaliaform core temperature regularly rose above 36C (from a T_{core} of 32C), so foraging would have been more thermally favorable at night, especially since its small size (4.3 kg) would allow it to forage under foliage cover to provide night shade. This result is congruous

with well-developed olfactory and acoustic anatomy in mammaliaformes, which have been interpreted as evidence for subterranean and nocturnal habitats being widespread within the clade (Luo, 2011).

The other burrowing taxa, *Hesperosuchus* and rhynchosaur would have been immediately under significant cold stress if they left their dens at night in either ecosystem, year-round (Figs. 1-8 & 1-10). With burrowing enabled (Fig. 1-9) both taxa function effectively as diurnal animals, though the rhynchosaur would be forced to expend additional ME to warm itself even in a burrow during the winter months.

The 19.2 kg *Eucoelophysis* was not modeled as a burrower and maintained its core temperature over night without excessive ME costs. At midday during much of the year T_{core} would rise above the target of 37C enough to result in shade seeking behavior. In summer months that could elevate to 40-42C, resulting not only in reduced foraging time but the potential for reduced enzymatic function and a risk of heat stroke for hours at a time. Given this pattern of thermal constraints and the insectivorous/omnivorous diets inferred for silesaurids (Qvarnström et al., 2019) a crepuscular activity pattern would make the most sense in these environments.

The 21 kg theropod *Coelophysis* was able to thermoregulate at night with minimal ME expenditure (Figs. 1-8 & 1-10), supporting its referral to non-burrowing status. During the summer half of the year its T_{core} would rise from a targeted 38C to 42C, resulting in extensive shade seeking behavior. Despite the longstanding assumption that Mesozoic dinosaurs were largely diurnal (e.g. Crompton, et al., 1978), a nocturnal, crepuscular, or cathemeral sleep cycle all seem more likely. The congeneric Early Jurassic *Coelophysis rhodesiensis* from South Africa

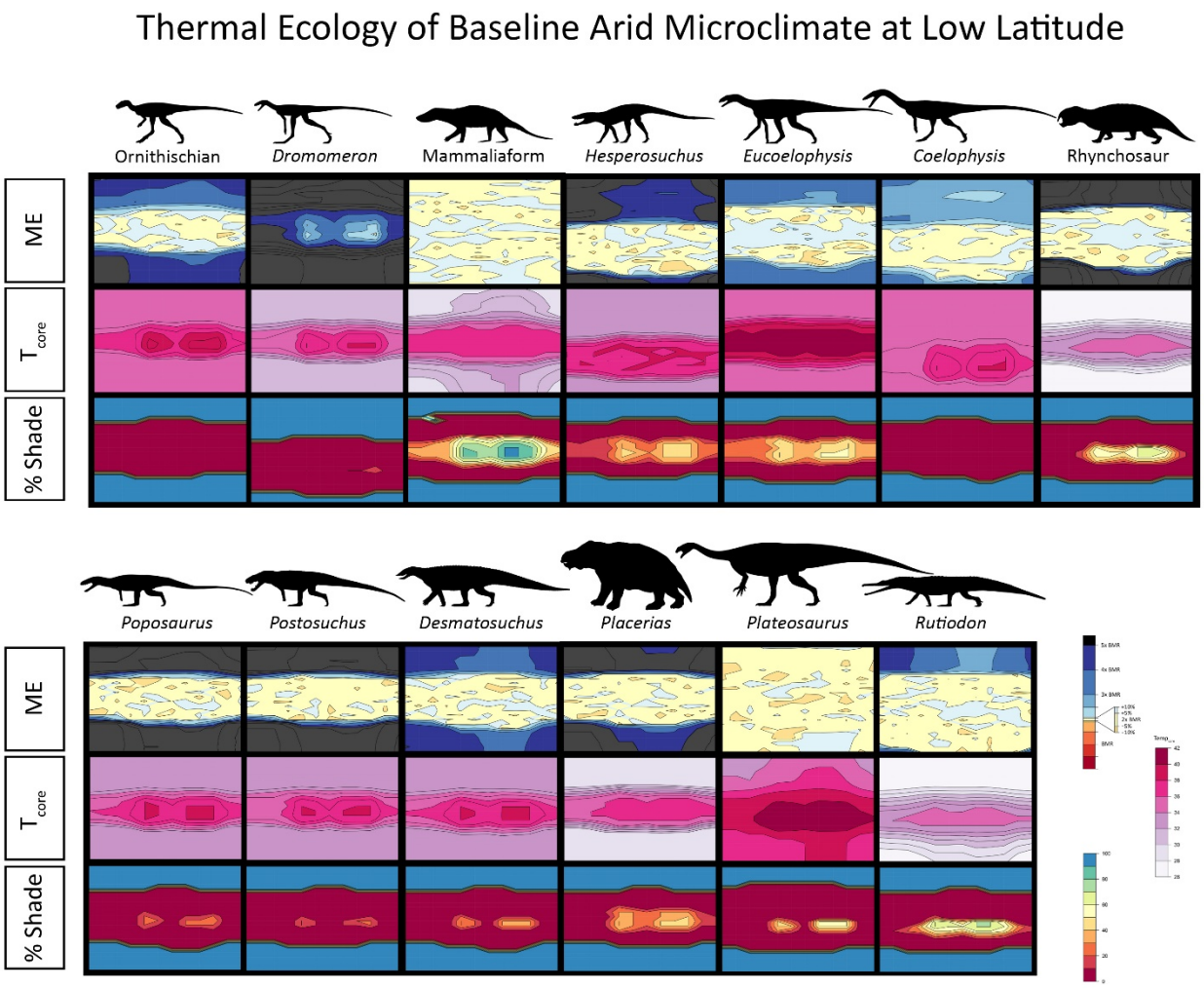

Fig. 1-10. Thermal ecology in a more arid Late Triassic environment*. Species are arranged from smallest to largest left to right and top to bottom. Full size color keys can be found in Figs. 1-4 through 1-7. Abbreviations: ME, metabolic energy; T_{core}, core temperature; %Shade, amount of time per hour an animal must seek out shade to thermoregulate.*

was previously found to be nocturnal based on sclerotic ring morphology (Schmitz & Motani, 2011), further reinforcing how unlikely a diurnal lifestyle was for Late Triassic *Coelophysis*.

The two bipedal pseudosuchians *Poposaurus* and *Postosuchus* fare remarkably alike in the baseline conditions, despite the latter at 250 kg out massing the former (75 kg) several times over. Both thermoregulate effectively during the day but face excessive cold stress at night.

While traditionally not thought of as burrowing animals due to their size and lack of obvious digging adaptations, Komodo dragons (up to 70 kg) and American alligators (up to 450 kg) burrow, though it's not clear if there is a size limit to when individual alligators stop burrowing (Wolfe, et al., 1987; Lutz & Lutz, 1997).

The armored, 280 kg *Desmatosuchus* performs better, maintaining a viable T_{core} without expending excessive amounts of ME. *Desmatosuchus* also avoids shade seeking behavior for all but a couple of hours a day during the hottest months of the year. The much larger but similarly low BMR pseudosuchian *Rutiodon* follows a similar pattern, although its larger thermal inertia allows it to stay warmer overnight (Figs. 1-8 & 1-10).

The 800kg herbivorous stem-mammal *Placerias* appears to experience an unfavorable combination of cold stress at night year-round, and up to 6 hours daily of 20-40% shade seeking behavior at midday. It is possible that the current consensus view of dicynodonts is wrong, and they had more derived endothermy and/or better developed epidermal insulation. Alternatively, dicynodonts have long been inferred to spend part of the year in and around water, like stem-mammalian hippos (Ramezani, et al., 2014), and multiple species (including *Placerias*) have been found in social groupings in autochthonous quarries (Fiorillo et al., 2000; Ugalde, et al., 2018). The type quarry for *Placerias* (Fiorillo et al., 2000) is a low-energy, high water table environment containing a multi-generational bone bed with a minimum of 40 individuals; there is no evidence of hydrologic transport or sorting (Fiorillo et al., 2000). If *Placerias* were using standing water to cool off during summer days and grouping up as a herd to conserve heat at night it would solve the apparent paradox of these results. Modeling grouped individuals would be a worthy topic for future analyses.

The 850 kg herbivorous dinosaur *Plateosaurus* was able to thermoregulate at night with low ME expenditure, but encounters up to 9 hours of daylight where its T_{core} is between 40 and 42C. While 40C is only 2º warmer than the *Plateosaurus* target T_{core} of 38C, once vertebrates pass 40C ME can quickly spiral out of control as cell membrane permeability starts to increase exponentially, requiring extensive active transport to maintain ion gradients necessary to mitochondrial function and homeostasis (Huynh & Poulsen, 2005). This means *Plateosaurus* would have had have regularly risked critical heat loading during summer months. It is tempting to ascribe a nocturnal activity cycle to *Plateosaurus*, but large herbivores are rarely nocturnal, and without the ability to burrow to reduce its midday heat load *Plateosaurus* would have become dangerously hot even while sleeping during the day. Indeed, the best solution would to simply be absent from these environments, and as noted by Lovelace, et al. (2020) that is consistent with paleobiogeography, with *Plateosaurus* and other larger sauropodomorphs absent from low latitude habitats in the Late Triassic.

Turning to higher latitude (55º) pre-ETE microclimate models, we see the impact of cooler temperatures (Landwehrs, et al., 2020) and stronger seasonality on modeled taxa (Figs. 1-11 to 1-13), with colder winters that limit activity for some taxa. The amount of precipitation (F. 1-11 & 1-12) makes an even smaller difference at high latitudes than it did in the low latitude microclimates. Without burrowing enabled, burrowing taxa except the mammaliaform are non-viable, requiring too much ME year-round to maintain T_{core}. With burrowing enabled (Fig. 1-13), the small ornithischian, *Dromomeron*, and *Hesperosuchus* maintain viable T_{core} year-round, albeit with very different foraging strategies. The ornithischian with its elevated BMR and epidermal insulation displays monotonic conditions across the modeled year, able to maintain ideal T_{core} at reduced ME levels, while spending up to 30% of each hour in its burrow. Being

agnostic regarding daily thermal patterns suggests a cathemeral behavioral pattern, although any behavioral pattern would be plausible, allowing for behavioral flexibility to adapt to changing

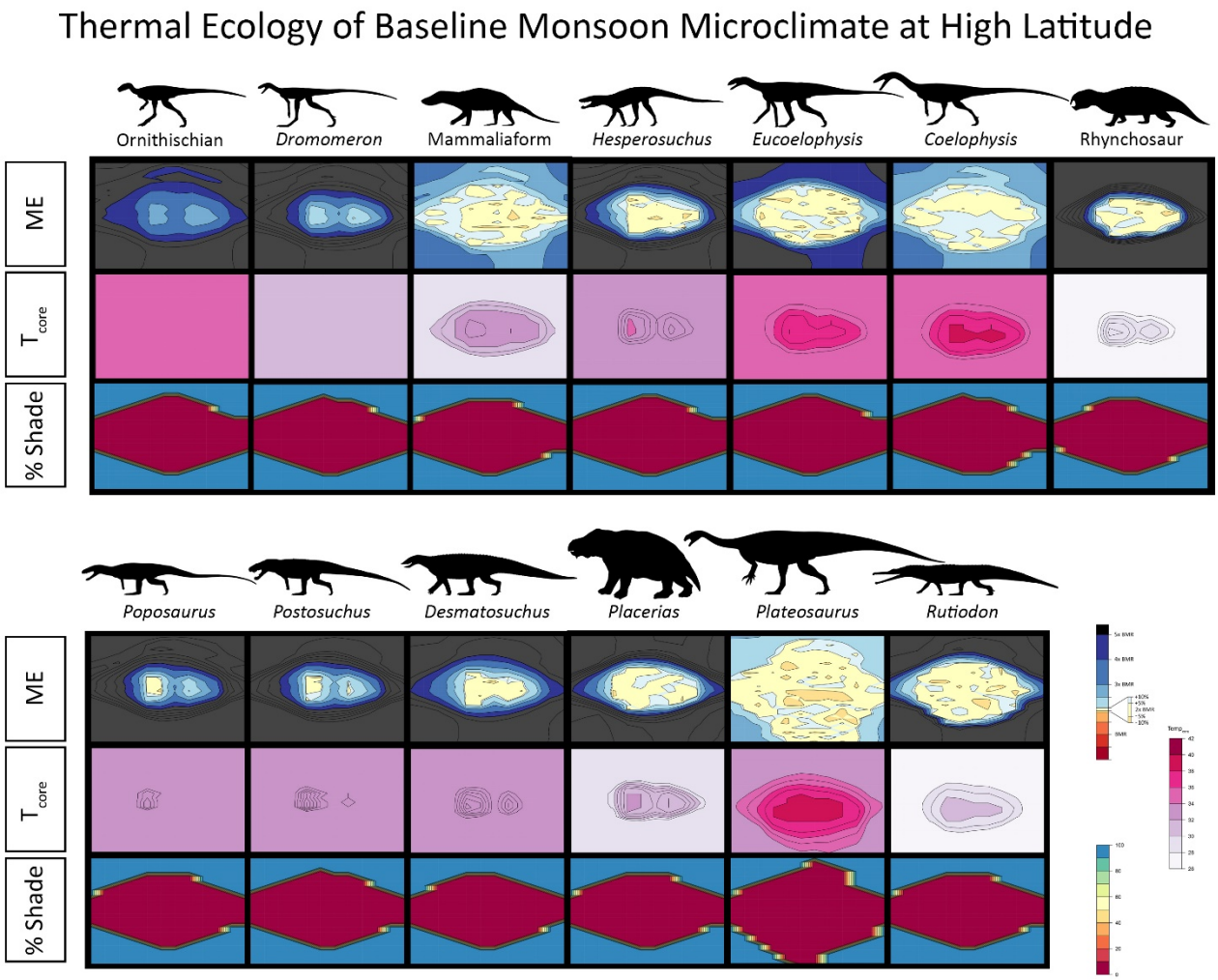

Fig. 1-11. Thermal ecology in a typical Late Triassic seasonal monsoon ecosystem at 55º latitude. *Species are arranged from smallest to largest left to right and top to bottom. Full size color keys can be found in Figs. 1-4 through 1-7. Abbreviations: ME, metabolic energy; T_{core}, core temperature; % Shade, amount of time per hour an animal must seek out shade to thermoregulate.*

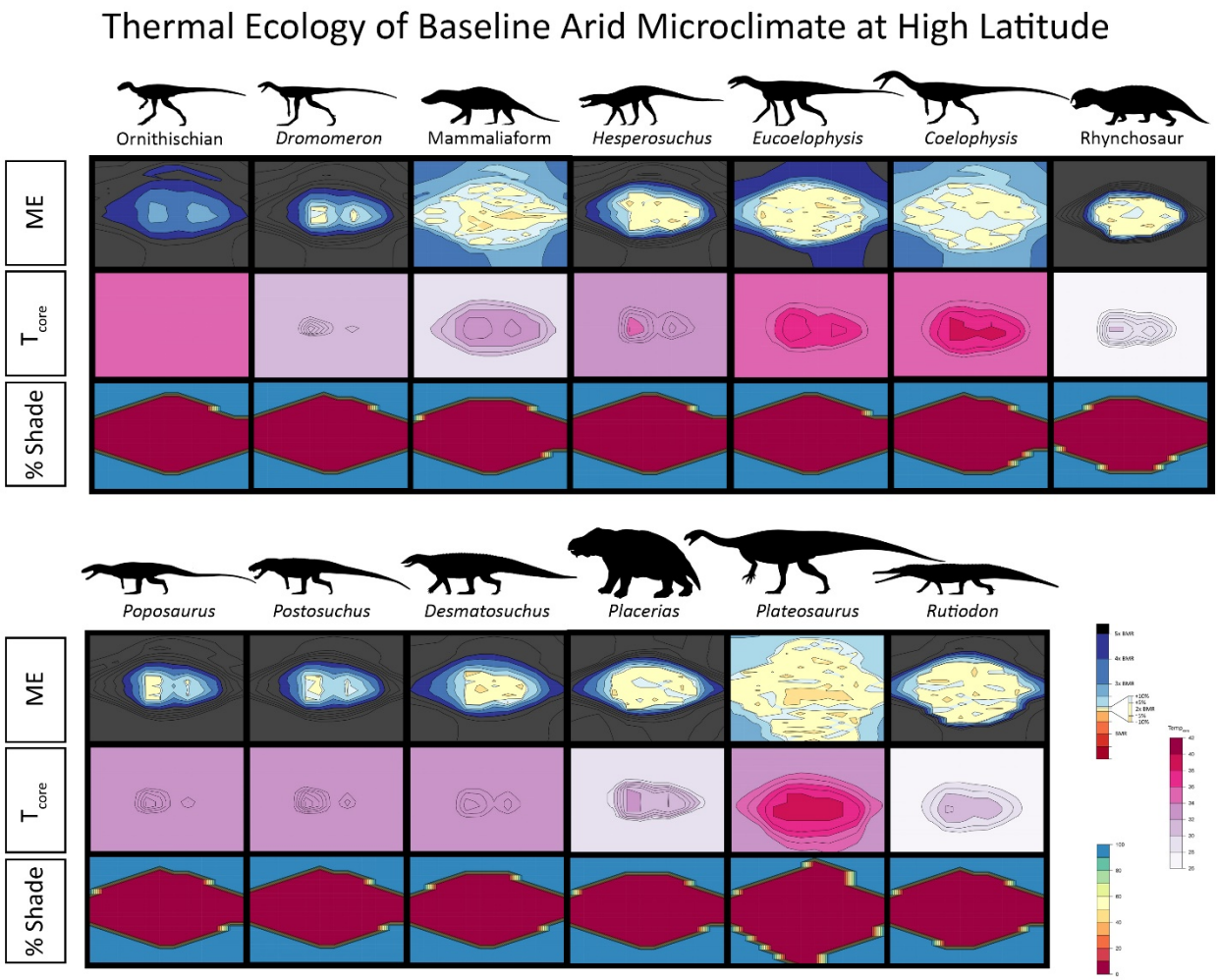

Fig. 1-12. Thermal performance in a Late Triassic arid ecosystem at 55º latitude. *Species are arranged from smallest to largest left to right and top to bottom. Full size color keys can be found in Figs. 1-4 through 1-7. Abbreviations: ME, metabolic energy; T_{core}, core temperature; % Shade, amount of time per hour an animal must seek out shade to thermoregulate.*

circumstances (including seasonal amounts of daylight, local weather patterns, etc.). *Dromomeron* was more constrained by the need to seek shade most of the year to thermoregulate (Fig. 1-13). At less than a meter in length and under 2 kg, *Dromomeron* is still small enough to forage under cover of foliage, but it suggests that it and other small dinosauromorphs may have been restricted at high latitudes to areas of dense vegetation. *Hesperosuchus* is also restricted to

100% shade seeking behavior from November through April. At 18 kg, foraging under cover of foliage would be more difficult raising the possibility of seasonal dormancy, as seen in brumating extant crocodilians (e.g. Hale, et al., 2020).

With burrowing enabled the mammaliaform can effectively thermoregulate year-round. From November through March time spent in burrow or under shade increases, and in December and January non-shaded foraging time shrinks to as low as two hours a day. With hibernation potentially playing an important role in the origin of mammalian endothermy (Grigg & Beard, 2000; Rial, et al., 2010) a period of seasonal dormancy cannot be ruled out and should perhaps be expected.

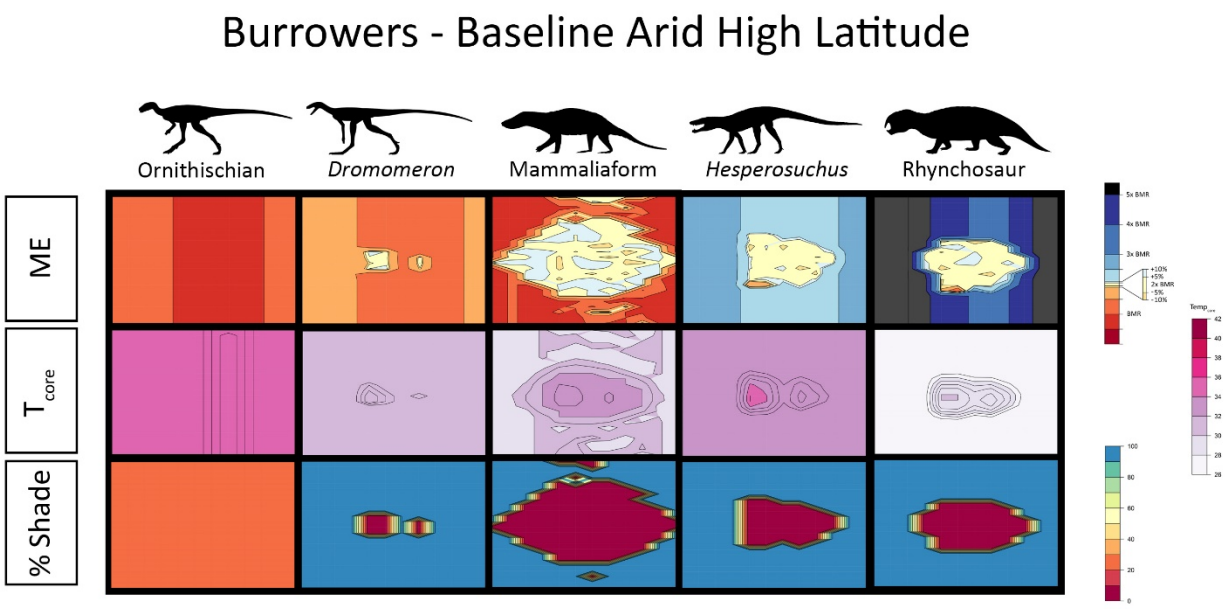

Fig. 1-13. Thermal ecology with burrowing enabled in the baseline monsoon environment at 12 degrees latitude. *Species are arranged from smallest to largest left to right. Red areas in the metabolic energy plots are due to lowered thermoregulation costs while in a burrow, not from heat stress. Full size color keys can be found in Figs. 1-4 through 1-7. Abbreviations: ME, metabolic energy; T_{core}, core temperature; % Shade, amount of time per hour an animal must seek out shade to thermoregulate.*

The last burrowing taxa, the rhynchosaur, performs much worse at high latitude. While able to maintain a reduced T_{core} (down to 26C from a target of 30C) from April to mid-October, the remaining four months require an implausible amount of ME to maintain even the lower T_{core} range, without leaving its burrow. Some form of brumation would be necessary during these months to reduced metabolic energy costs when foraging became impossible.

Coelophysis effectively thermoregulates 24 hours a day year-round. The lack of heat stress at high latitudes during the day in summer months raises the intriguing possibility that closely related species might vary drastically in circadian rhythm, something seen in congeneric lizards today (Arad, et al., 1989). The other non-burrowing dinosaur, *Plateosaurus* also demonstrates the ability to effectively thermoregulate year-round. *Plateosaurus* at high latitude performs significantly better than at low latitude, since heat stress inducing midday temperatures are gone. As noted by Lovelace, et al. (2020), this matches the Late Triassic distribution of dinosaurs, with small-medium sized theropods like *Coelophysis* found in low and high latitude environments, while large sauropodomorph body fossils are only found at higher latitudes (Fig. 1-14).

Both *Poposaurus* and *Postosuchus* expend more than 5x their BMRs to maintain T_{core} at high latitudes year-round, with implausibly high levels of ME being required 24 hours a day from October through March. This would be non-viable unless they could effectively utilize both burrowing and seasonal dormancy. This explanation may also be unnecessary, as *Postosuchus* and *Poposaurus* are currently only known from low latitude environments in the Late Triassic (Weinbaum, 2013; Schachner, et al., 2020). While the relatives of both are known from higher

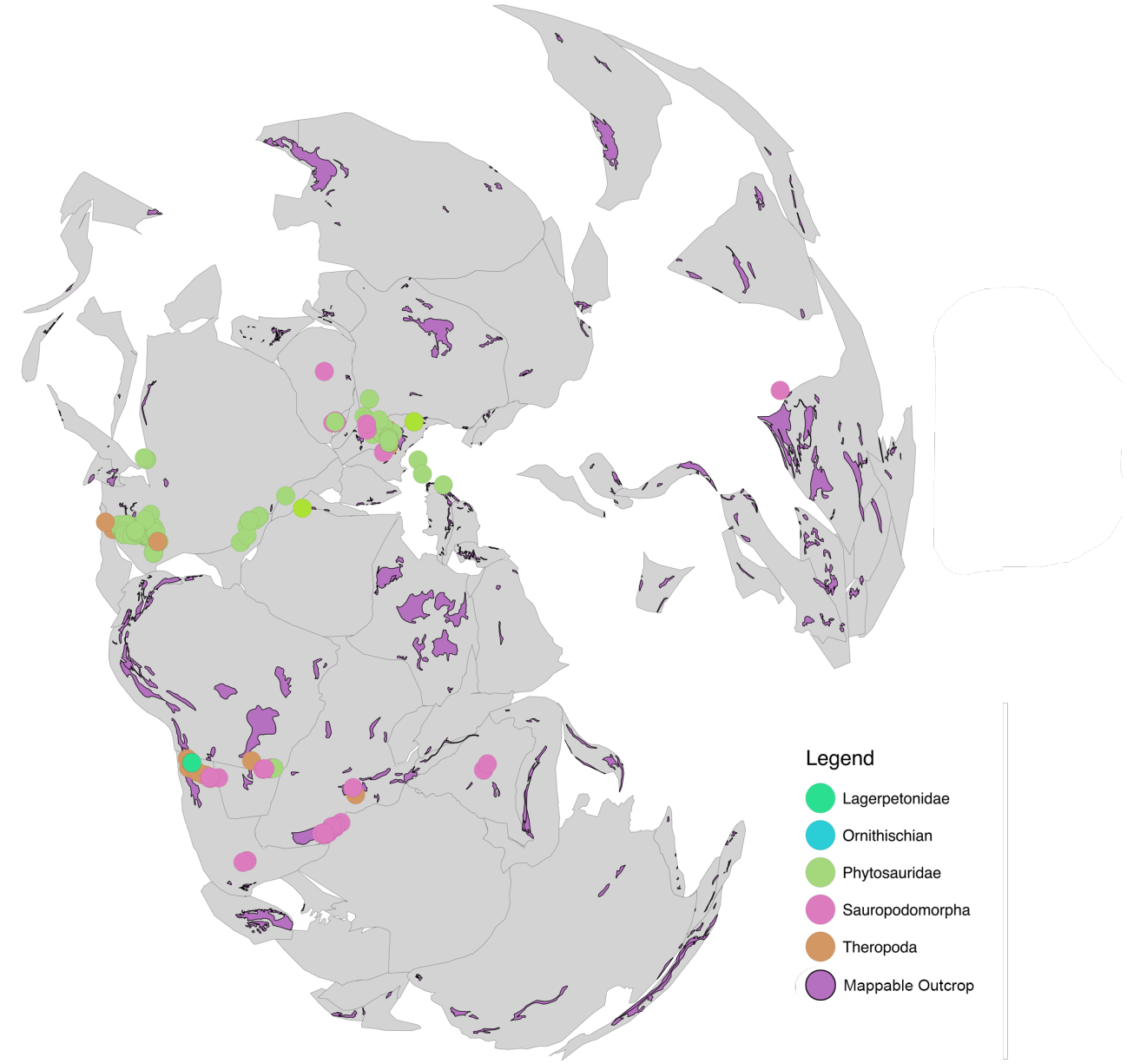

Figure 1-14. Global distribution of archosauromorph body fossils in the Norian. *Occurrence data from paleobiodb.org, outcrop data from Macrostrat.org.*

latitudes earlier in the Triassic, it is notable that the more biogeographically diverse relatives of *Poposaurus* were either smaller (Li, et al., 2006; Nesbit, 2011) or had elaborated sails that could have raised T_{core} without expending as much ME (e.g. Butler, et al., 2011).

Desmatosuchus was able to thermoregulate during the day year-round, though from mid-December to mid-January the number of hours of reasonable ME expenditure drop from 6 to 3 hours a day. While the year-round foraging ability of *Desmatosuchus* makes it a more plausible inhabitant of high latitudes than *Poposaurus* or *Postosuchus*, it seems likely that some form of bromation would have been necessary during winter months. The extensively armored exterior of aetosaurs would make this a safer proposition, though *Desmatosuchus* itself is only known from low latitudes. Other aetosaurs that lived at higher latitudes such as *Steganolepis* were smaller and would have been more amenable to burrowing (Walker, 1961). Adaptations for scratch-digging (cf. Dróżdż, 2018) reinforce the idea that smaller, high latitude aetosaurs would have used burrowing and seasonal dormancy to survive winters at reasonable ME levels.

A similar scenario plays out with *Placerias*, where like *Desmatosuchus* it could thermoregulate effectively during midday hours year-round, but experienced cold-stressed ME levels at night, which expand to several hours of morning and evening in December and January. *Placerias* itself is only known from low latitude deposits, and other dicynodonts that are found at high latitudes follow a bimodal mass distribution. Permian and early Triassic dicynodonts are smaller animals that show extensive adaptations to burrowing (Ray & Chinsamy, 2003; Botha-Brink, 2017), while high latitude Middle and Late Triassic dicynodonts are huge – reaching 4-5 tonnes in size (Romano & Manucci, 2019). Although beyond the scope of this project, future work should investigate whether this dichotomy in mass and locomotor adaptation could be tied to disparate strategies to survive at high latitudes.

Rutiodon performs similarly to *Placerias*, though it exhibits more favorable ME rates and non-shade foraging time compared to *Placerias*. *Rutiodon* appears unable to raise T_{core} above 27C from October through March. Being too large to burrow, it is unclear whether this would be

a viable climate for *Rutiodon. Rutiodon* itself is only known from deposits at low paleolatitude, and as the Late Triassic progressed phytosaur remains became progressively more concentrated around low to mid-latitude ecosystems (Fig. 1-14) suggesting that higher latitude cold stress contributed to excluding phytosaurs at high latitudes over time.

Thermal Ecology of the ETE Transient Cold Phase

Modeling both vulcanogenic aerosolized sulfur as well carbon emissions, Landwehrs, et al., (2020) found up to 500 Gt of sulfur emitted would result in a strong transient cold phase, with temperatures falling by as much as 10C approximately 2,000 years after initiation of the first major ETE pulse. This was used to model transient cold ETE monsoon and arid low latitude microclimates. There turned out to be almost no difference in thermal performance during the transient ETE cold phase between the monsoon and arid microclimates (Figs. 1-15 & 1-16), so taxa thermal performance will be reported at as if they are a single climate unless explicitly noted. Since Landwehrs, et al. model showed high latitude and interior drying during the cold phase, only an arid ETE cold phase microclimate for high latitudes was run.

Of the burrowing taxa, with burrowing not enabled only the mammaliaform could thermoregulate at reasonable T_{core} and ME rates all day year-round, although T_{core} did fall to 30C regularly at night. *Hesperosuchus* was able to maintain reasonable T_{core} and ME rates for 8-9 hours a day year-round, but without a burrow was exposed to significant ME cold stress for the remainder of each day.

With burrowing enabled the small ornithischian had almost identical thermal performance to the pre-ETE baseline climates, demonstrating that its combination of size, BMR, epidermal insulation, and burrowing allowed it to thermoregulated effectively in a wide range of

climatological scenarios. *Dromomeron* was able to get by with a reasonable ME year-round, although its body temperature falls into the range of 30-31C and it is unable to warm up further even within a burrow. This was compounded by not being able to forage without cover essentially the entire year. Especially under geologically rapid climate change these shifts from

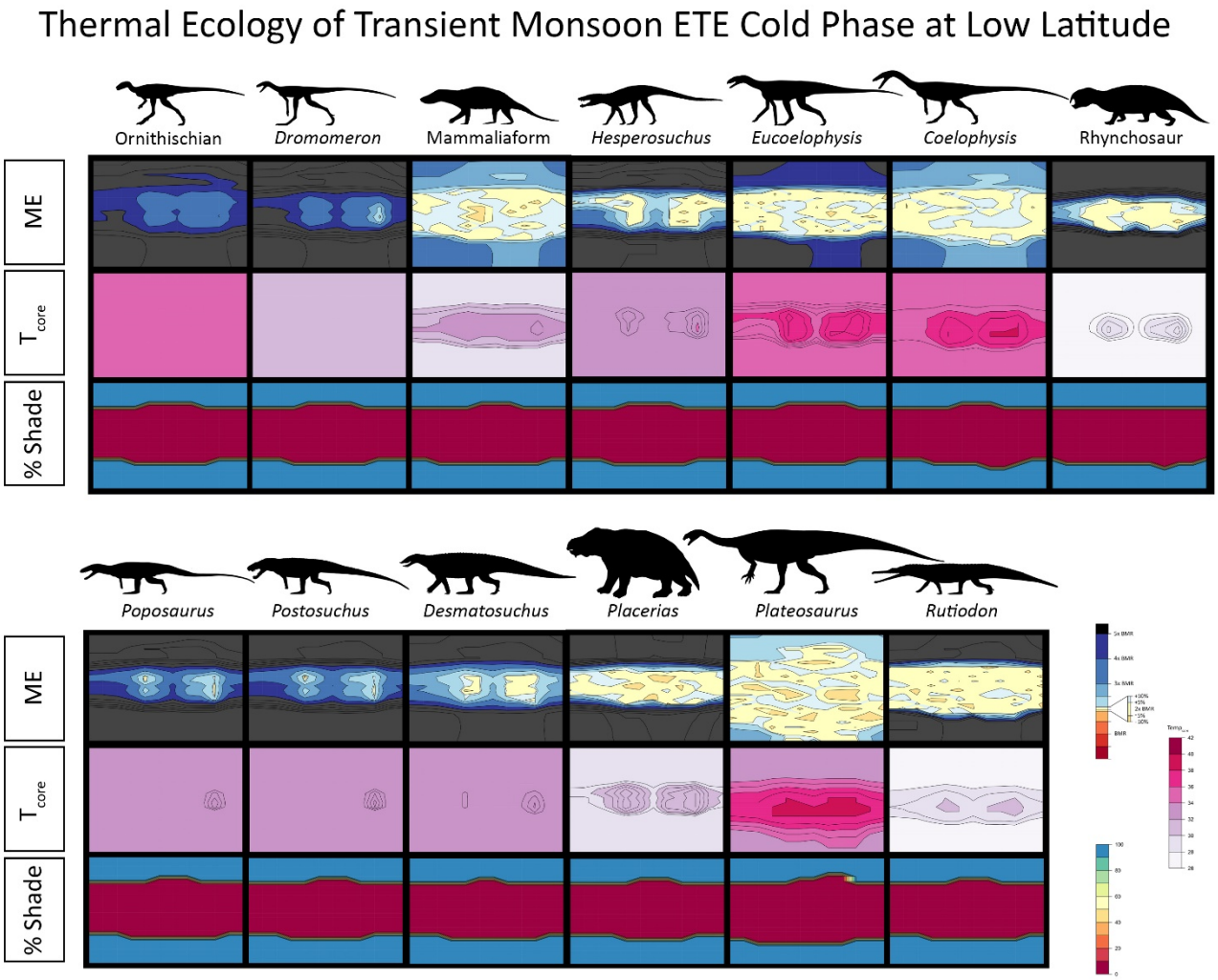

Fig. 1-15. Thermal performance in an ETE monsoon cold ecosystem at low latitude. *Species are arranged from smallest to largest left to right and top to bottom. Burrowing enabled plots can be seen in Fig. 1-9. Full size color keys can be found in Figs. 1-4 through 1-7. Abbreviations: ME, metabolic energy; T_{core}, core temperature; % Shade, amount of time per hour an animal must seek out shade to thermoregulate.*

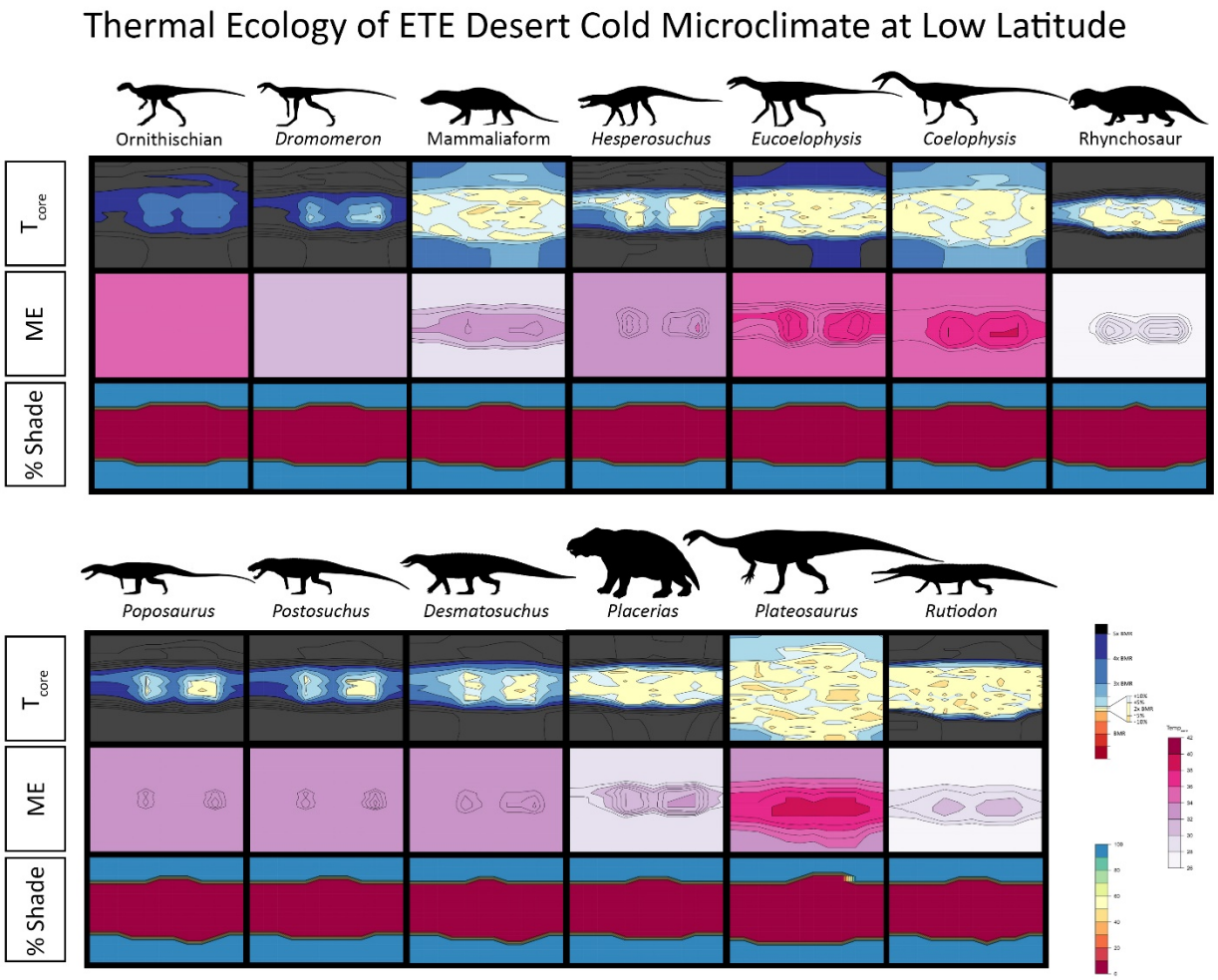

Fig. 1-16. Thermal performance in an ETE transient cold arid ecosystem at low latitude. *Species are arranged from smallest to largest left to right and top to bottom. Burrowing enabled plots can be seen in Fig. 1-9. Full size color keys can be found in Figs. 1-4 through 1-7. Abbreviations: ME, metabolic energy; T_{core}, core temperature; %Shade, amount of time per hour an animal must seek out shade to thermoregulate.*

pre-ETE low latitude climates would have placed significant stress on *Dromomeron.*

The mammaliaform fares even better with a burrow than without, although it shifts to a more diurnal foraging regime compared to the pre-ETE low latitude climate. With burrowing enabled *Hesperosuchus* can thermoregulate effectively through the ETE transient cold phase model year (Fig. 1-17), though with an increased need for cover when foraging. The rhynchosaur

appears non-viable even with burrowing allowed. It must burn high levels of ME even when burrowing, and regardless of physiological and behavioral attempts at thermoregulation its body temperature hovers between 26-28C almost year-round. Especially with such a short period of time in which to adapt to a changing climate, it appears unlikely the rhynchosaur population could have survived in either low latitude microclimate.

Turning to non-burrowing taxa, the silesaurid *Eucoelophysis* is also challenged to thermoregulate in the ETE transient cold environment, with implausibly high ME levels overnight for most of the year (Figs. 1-15 & 1-16). While not as dire as the thermal conditions in the rhynchosaur, for a taxa that had not previously needed to use hibernation or brumation this

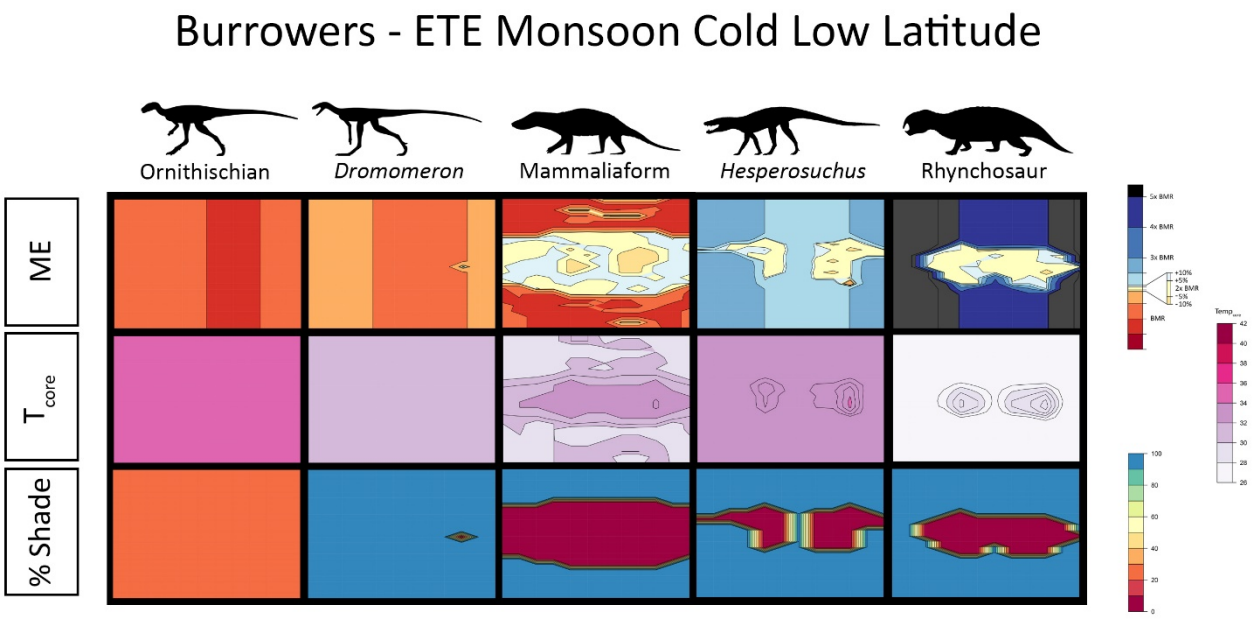

Fig. 1-17. Thermal ecology with burrowing enabled an ETE transient cold monsoon environment at 12 degrees latitude. *Species are arranged from smallest to largest left to right. Red areas in the metabolic energy plots are due to lowered thermoregulation costs while in a burrow, not from heat stress. Full size color keys can be found in Figs. 1-4 through 1-7. Abbreviations: ME, metabolic energy; T_{core}, core temperature; % Shade, amount of time per hour an animal must seek out shade to thermoregulate.*

would be a largely unavoidable cold stress for nine months of the year. The non-burrowing dinosaurs *Coelophysis* and *Plateosaurus* can thermoregulate within reasonable temperature and metabolic parameters all day throughout the model year. *Plateosaurus* appears to be better suited to the ETE transient cold phase than the low latitude pre-ETE environments, with a significant reduction in midday heat stress.

The larger non-dinosaurs fair much worse. All require excessive ME rates overnight year-round. *Poposaurus* and *Postosuchus* spend 6 months of the year never getting ME below 3x BMR during the day. *Desmatosuchus* is only moderately better. *Placerias* and *Rutiodon* maintain reasonable ME during the day but cannot do so for extended overnight periods throughout the year. Notably, the daytime T_{core} of *Placerias* no longer rises above its target core temperature as it had in pre-ETE microclimates, which would reduce the utility of social huddling for warmth. Given that *Rutiodon*, *Desmatosuchus*, and presumably socially-reinforced *Placerias* previously had no need of dormancy in pre-ETE environments this would have been significant cold stress, even if it did not cause immediate death due to lack of calories.

Turning to the high latitude transient cold ETE microclimate, colder temperatures and greater seasonality emphasize the disparity between taxa seen at low latitudes. There is again high stress on *Dromomeron,* a non-viable rhynchosaur, with the other burrowers fine if burrowing is enabled. With it off only the mammaliaform would be able to thermoregulate effectively. The non-burrowing dinosaurs effectively thermoregulate year-round, although signs of minor cold stress appear, as ME rates 3-4x BMR start to dominate night hours year-round.

The large non-dinosaurs are clearly non-viable at high latitudes during the transient ETE cold phase. *Poposaurus* and *Postosuchus* are never able to bring ME below excessive levels. *Desmatosuchus* and *Placerias* get into the still cold-stressed 4-5x BMR range ME for 6-8 hours

during summer months, but otherwise cannot reduce ME to plausible levels. *Rutiodon* is likewise stuck at non-viable levels of ME for most of the year. If any of these taxa were to survive the transient cold phase off the ETE, it did not happen at high latitudes. Given the similarity at low latitudes, an argument can be made that the rhynchosaur, *Poposaurus*, *Postosuchus*, *Desmatosuchus*, *Placerias*, and *Rutiodon*, and other similar members of their clades could not have been reasonably expected to survive the initial transient cold phase of the End Triassic Extinction.

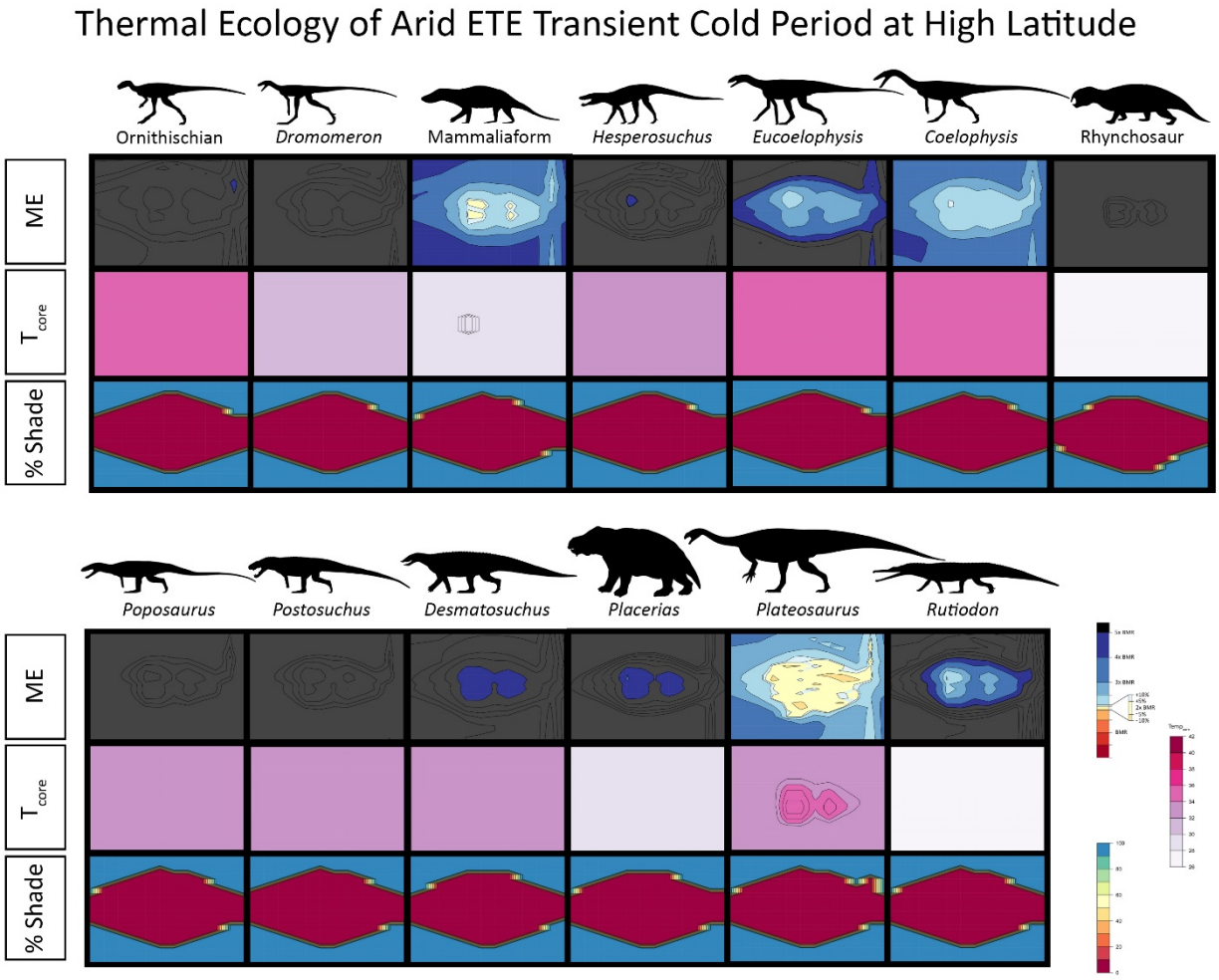

Fig. 1-18. Thermal performance in an arid ETE transient cold ecosystem at high latitude. *Species are arranged from smallest to largest left to right and top to bottom. Burrowing enabled plots can be seen in Fig. 1-9. Full size color keys can be found in Figs. 1-4 through 1-7. Abbreviations: ME, metabolic energy; T_{core}, core temperature; %Shade, amount of time per hour an animal must seek out shade to thermoregulate.*

Thermal Ecology of the ETE Global Warming Phase

It is not universally agreed that there was a transient cold phase component to the ETE (Heimdal, et al., 2020), and we have clearly not modeled every possible combination of climates and latitudes. To test the impact of a prolonged ETE global warming phase (~4-10+ kyr, cf. Heimdal, et al., 2020; Landwehrs, et al., 2020) on the Late Triassic taxa, all were run against a temperature increase of up to 4C above pre-ETE climates, at low latitudes in both monsoon and arid conditions. Landwehrs, et al. (2020) found the warming phase accompanied by an increase in monsoon-driven precipitation, so only a monsoon climate was modeled for the high latitude ETE global warming phase. The results of the arid microclimate run differed less than 1% in any values of the monsoon ETE global warming phase run (Fig 1-19, S.1-5) that only the monsoon ETE results are figured and reported here.

Among burrowing taxa, when burrowing is not allowed the mammaliaform and the rhynchosaur both show significant levels of midday heat stress in their ME rates. Looking at changes in T_{core}, the rhynchosaur is experience significantly more heat stress, as during midday hours its body temperature elevates from a targeted T_{core} of 30C all they way up to 37C. Without being able to retreat to a burrow it risk heat-stroke on a daily basis. The small ornithischian reaches a higher T_{core} of 40C, but with a target T_{core} of 38C this would be significantly less physiological stress, which is reflected its more favorable ME usage. This suggests that should prolonged dispersal without access to a burrow be required, the rhynchosaur and perhaps the mammaliaform would be in trouble. With burrowing enabled (Fig. 1-20), all five burrowing taxa thermoregulate withing reasonable bounds. The rhynchosaur T_{core} tops out at a more reasonable 34C.

Turning to non-burrowing taxa, *Placerias, Rutiodon*, and to a lesser degree *Plateosaurus* exhibit midday ME heat-stress through varying portions of the year. With ~2,000 years too little time to evolve nocturnal adaptations, the loss of daily foraging time could be a significant source

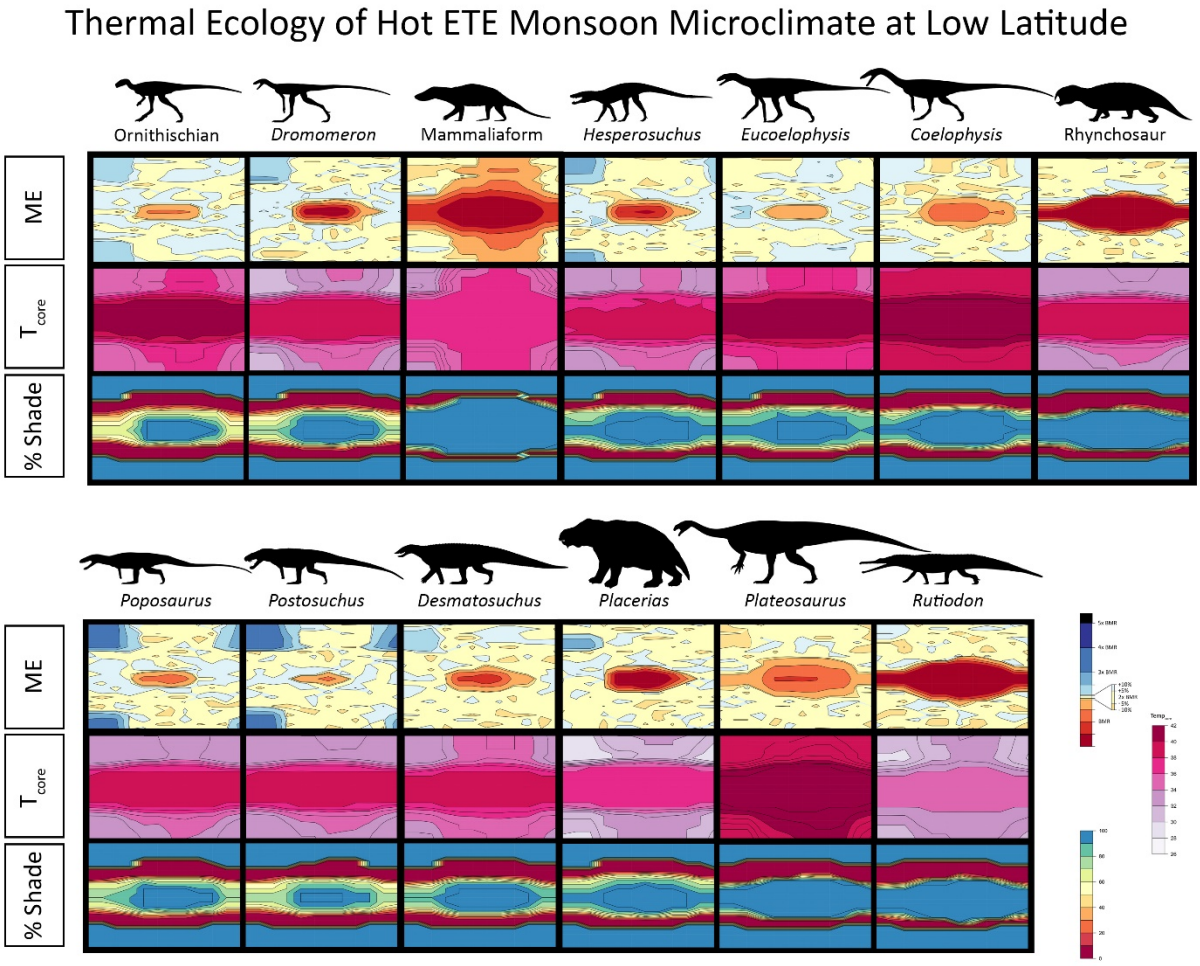

Fig. 1-19. Thermal performance in a monsoon ETE global warming phase at low latitude. *Species are arranged from smallest to largest left to right and top to bottom. Burrowing enabled plots can be seen in Fig. 1-9. Full size color keys can be found in Figs. 1-4 through 1-7. Abbreviations: ME, metabolic energy; T_{core}, core temperature; %Shade, amount of time per hour an animal must seek out shade to thermoregulate.*

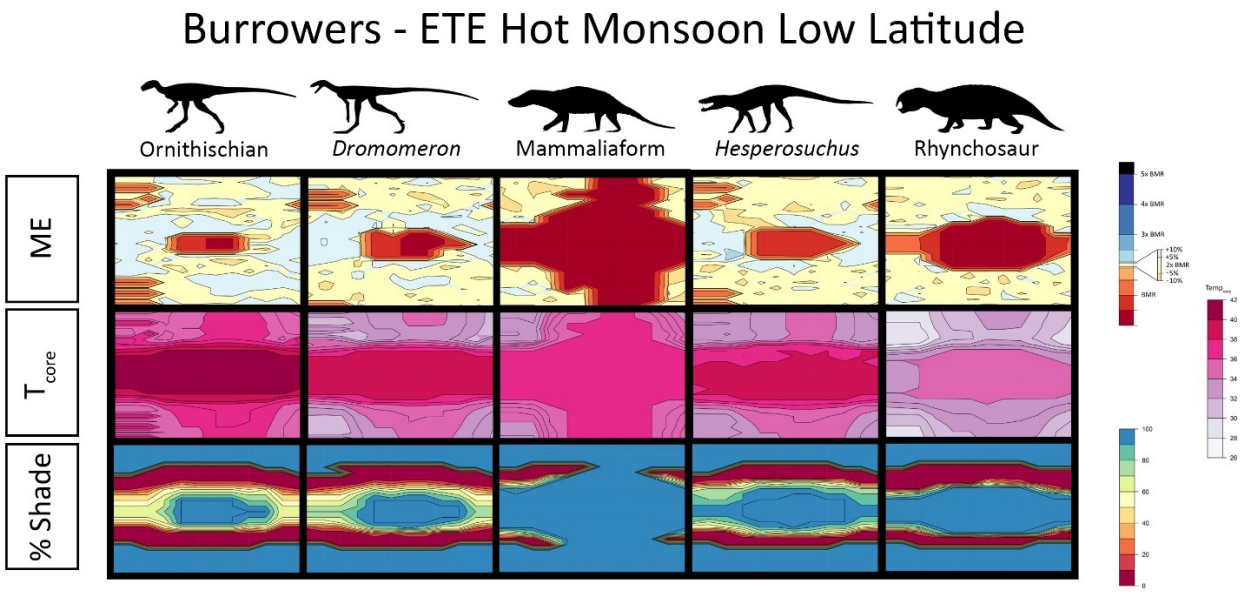

Fig. 1-20. Thermal ecology with burrowing enabled an ETE monsoon global warming environment at 12 degrees latitude. *Species are arranged from smallest to largest left to right. Red areas in the metabolic energy plots are due to lowered thermoregulation costs while in a burrow, not from heat stress. Full size color keys can be found in Figs. 1-4 through 1-7. Abbreviations: ME, metabolic energy; T_{core}, core temperature; % Shade, amount of time per hour an animal must seek out shade to thermoregulate.*

of stress, especially in the case of *Placerias*, which loses 4-6 hours of daylight foraging time from mid-April to mid-September. The herbivorous *Desmatosuchus*, *Placerias*, and *Plateosaurus* also must seek shade for most of their daylight hours, meaning they must either find forested areas to forage in during the day, or gather sufficient food during crepuscular activity hours.

If this were a stable climate scenario the three herbivores might be expected to disperse over time to more favorable geographic regions, but given the geologically short period of time these thermal constraints would have manifested as higher mortality rates, lowered growth rates, and reduced fecundity (Abell, 1999; Westphal, 2016). Moving to higher latitudes, even if temporally possible, would have been unlikely to be more favorable. While average temperatures at higher latitudes are a bit lower in the microclimate model, the prolonged day lengths at higher latitude offset this during summer months, resulting in similar heat stress to rhynchosaur and the

large herbivores, only with stronger seasonality reducing heat stress mildly in winters and increased mildly in summers (Fig. 1-21). The bipedal carnivorous pseudosuchians *Poposaurus* and *Postosuchus* thermoregulate effectively in the ETE global warming microclimates regardless of latitude or precipitation levels, although if they were previously diurnal shade seeking in the middle of the day would have required them to shift to more crepuscular or even nocturnal

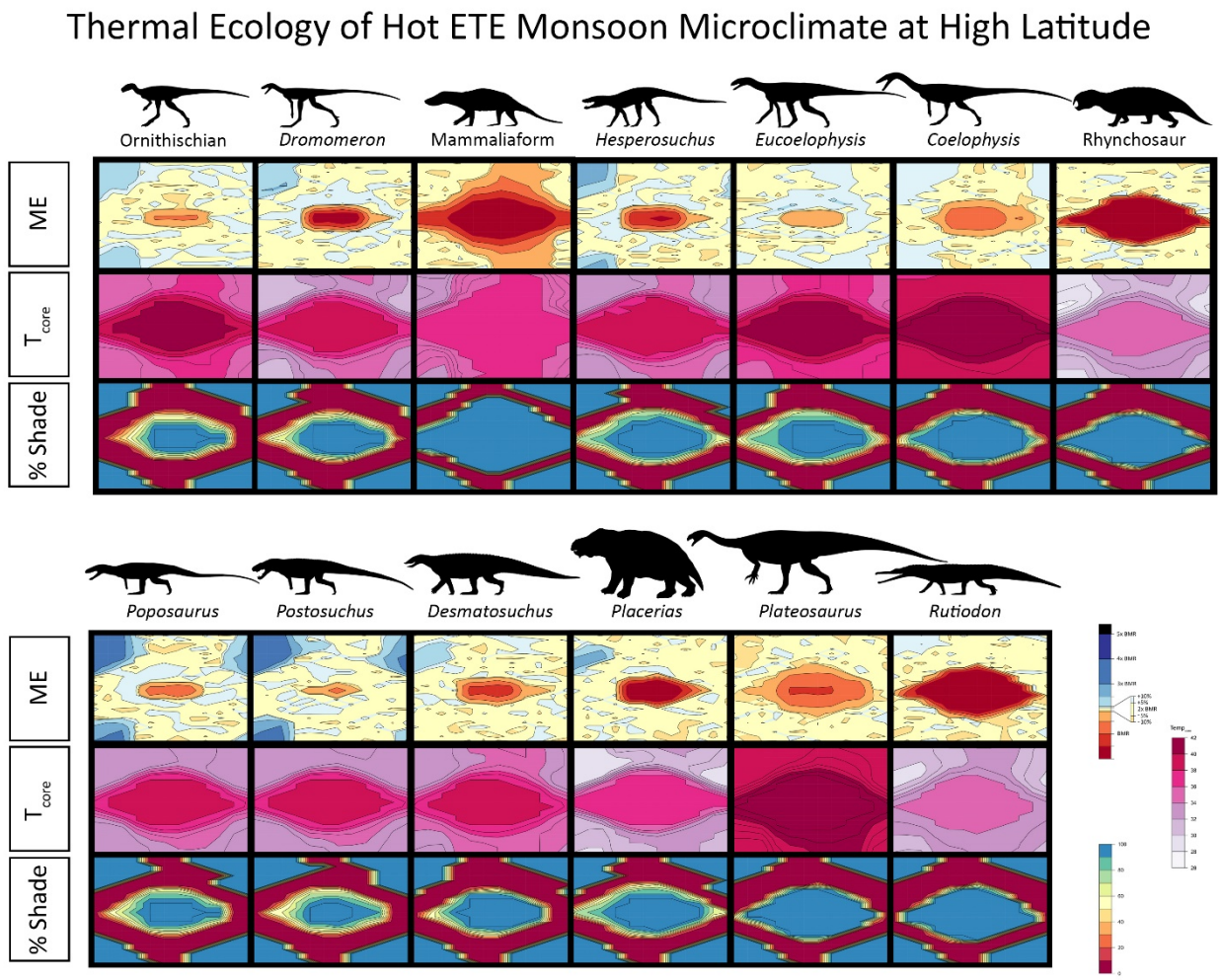

Fig. 1-21. Thermal performance in an ETE monsoon global warming phase at high latitude. *Species are arranged from smallest to largest left to right and top to bottom. Burrowing enabled plots can be seen in Fig. 1-9. Full size color keys can be found in Figs. 1-4 through 1-7. Abbreviations: ME, metabolic energy; T_{core}, core temperature; %Shade, amount of time per hour an animal must seek out shade to thermoregulate.*

behavioral patterns. The strong seasonal change in shade seeking behaviors in global warming ETE scenarios at high latitude apply to all non-burrowing species (Fig. 1-21), though how large, rapid changes in seasonal activity patterns effect non-cathemeral species is currently not well understood.

Thermal Ecology of Extreme ETE Global Warming Phase

The ETE environmental modeling of Landwehrs, et al. (2020) used for the prior ETE global warming temperatures were based on 5,300 Gt of carbon emission. Other authors (e.g. Ruhl et al. 2011; Heimdal, et al., 2020) have found emission pulses of 8,800-12,000+ Gt. To test scenarios with higher atmospheric CO_2 "extra hot" microclimate models were created with an extra +2C increase in average temperature (Table. 1-2; S1). These included monsoon and arid climates at low latitude, however as with the prior ETE model, the difference between arid and monsoon microclimates were insignificant, so the arid results are not figured or reported separately. An extra hot monsoon ETE global warming microclimate was also run at high latitude (55^{o}) as in previous runs.

In extra hot ETE global warming environments at low latitude all taxa start to show heat stress at midday, most for 6-12 months out of the year (Fig. 1-22). In addition to midday heat stress, shade seeking in all species greatly expands at midday, resulting in narrow bands of crepuscular foraging time available. The non-burrowing dinosaurs *Coelophysis* and *Plateosaurus* exhibit the least amount of heat stress, as seen in their less extreme reduction in ME when trying to maintain T_{core} at midday. This is followed by *Eucoelophysis and the small ornithischian (non-burrowing).* When not allowed to burrow, the rhynchosaur and especially the mammaliaform exhibit heat stress with ME and shade seeking. Enabling burrowing results in all burrowers spending midday sheltered, presumably engaging in crepuscular or nocturnal activity. For the

mammaliaform this worsens the heat problem, as it does not cool off and loses almost the entirety of its non-shade foraging time.

If carnivorous pseudosuchians *Poposaurus* and *Postosuchus* could successfully shift to crepuscular hunting times from obligate diurnal activity pre-ETE they could avoid significant

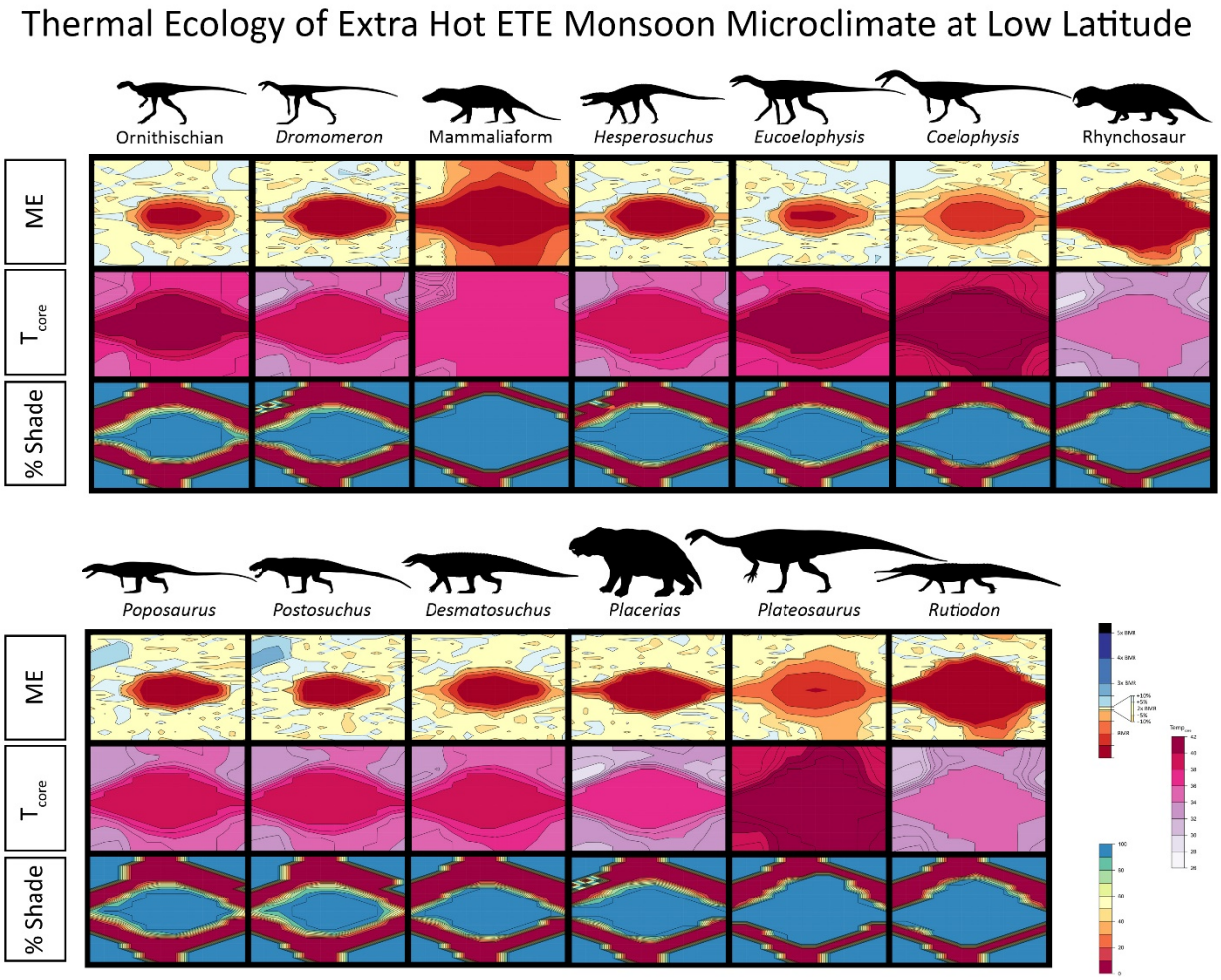

Fig. 1-22. Thermal performance in an extra hot ETE monsoon ecosystem at low latitude. *Species are arranged from smallest to largest left to right and top to bottom. Burrowing enabled plots can be seen in Fig. 1-9. Full size color keys can be found in Figs. 1-4 through 1-7. Abbreviations: ME, metabolic energy; T_{core}, core temperature; %Shade, amount of time per hour an animal must seek out shade to thermoregulate.*

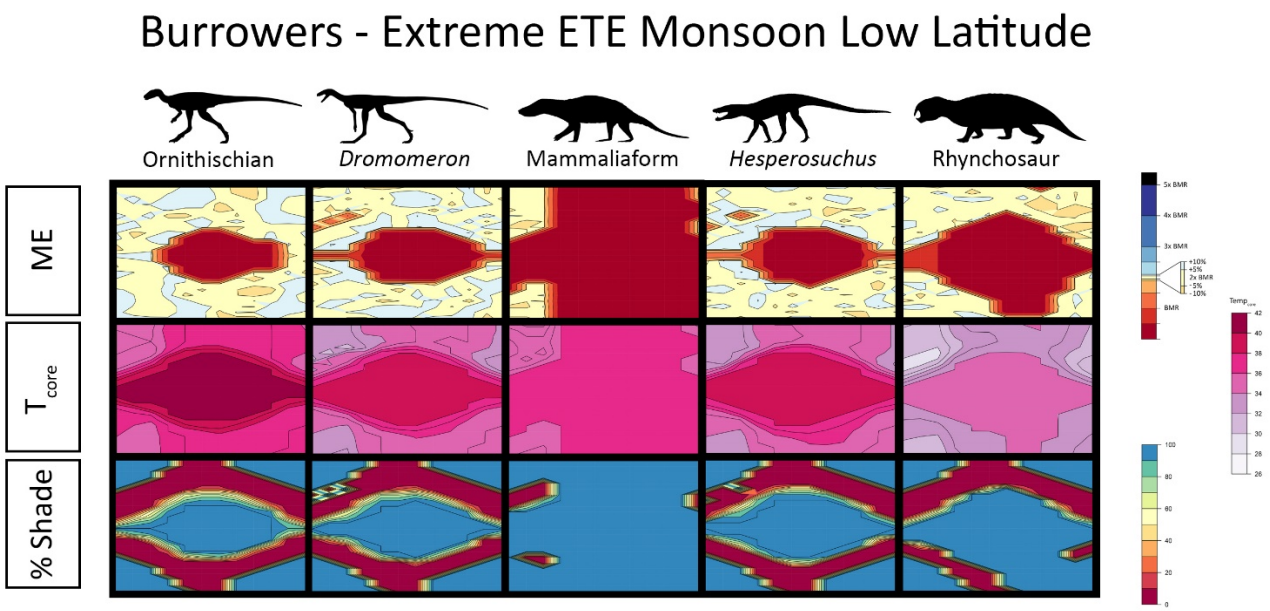

Fig. 1-23. Thermal ecology with burrowing enabled of an extreme ETE monsoon global warming environment at 12 degrees latitude. *Species are arranged from smallest to largest left to right. Red areas in the metabolic energy plots are due to lowered thermoregulation costs while in a burrow, not from heat stress. Full size color keys can be found in Figs. 1-4 through 1-7. Abbreviations: ME, metabolic energy; T_{core}, core temperature; % Shade, amount of time per hour an animal must seek out shade to thermoregulate.*

heat stress, although the potential impact of rapid changes to behavior and circadian regulation are not well understood. *Rutiodon* may have already been nocturnal in pre-ETE environments, so the greater amount of heat stress at midday would presumably have been tolerable. Large herbivores are less frequently nocturnal, so the increased amount of midday heat stress and shrinking time to forage without seeking shade may have been a larger problem for *Desmatosuchus* and *Placerias.*

In the high latitude extreme heat global warming phase microclimate model, midday heat stress reduces for about an hour a day for all non-burrowing taxa, but significant heat stress occurs during more months of the year (Fig. 1-24). Shade seeking behavior increases in all taxa,

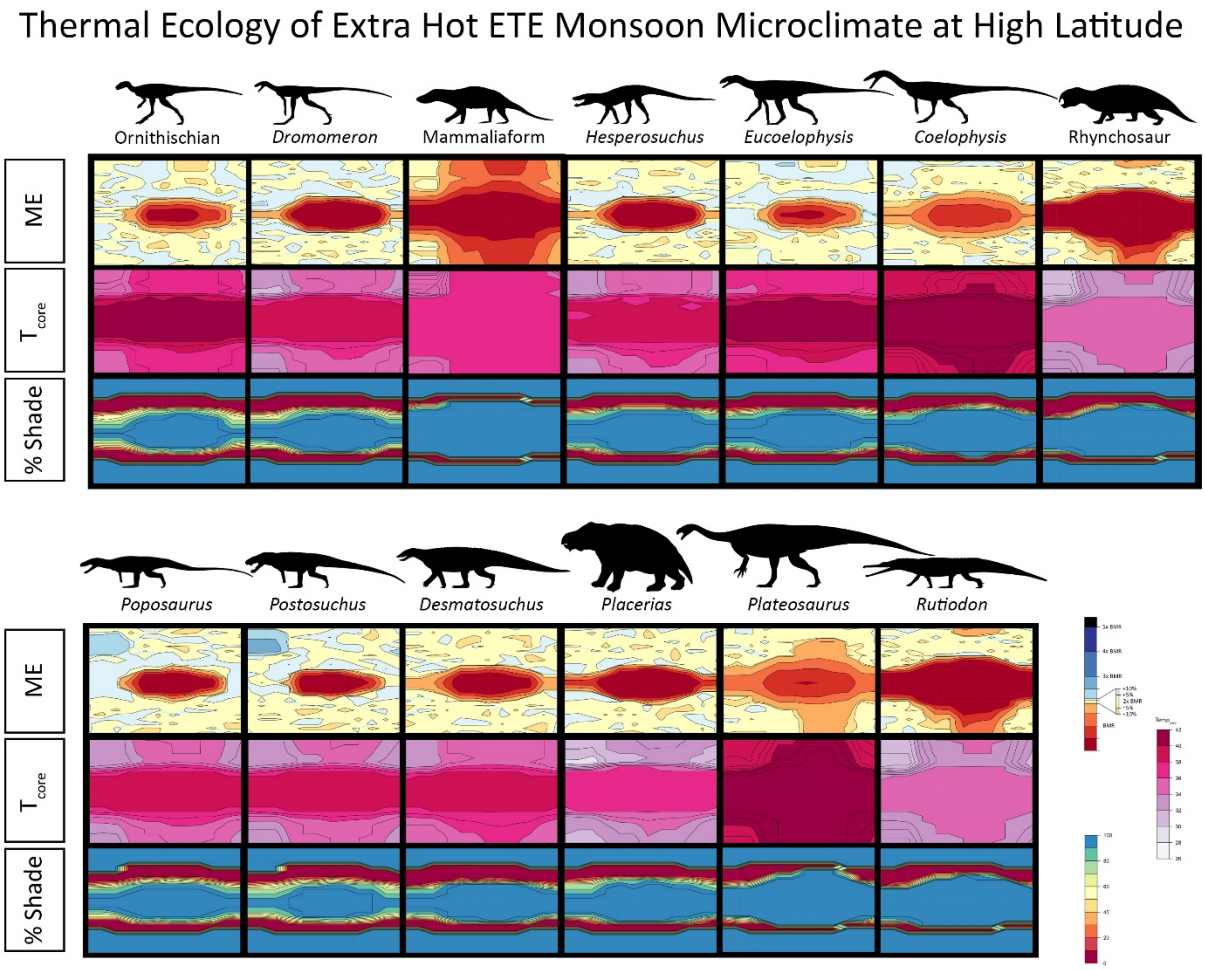

Fig. 1-24. Thermal performance in an extra hot ETE monsoon ecosystem at high latitude. *Species are arranged from smallest to largest left to right and top to bottom. Burrowing enabled plots can be seen in Fig. 1-9. Full size color keys can be found in Figs. 1-4 through 1-7. Abbreviations: ME, metabolic energy; T_{core}, core temperature; %Shade, amount of time per hour an animal must seek out shade to thermoregulate.*

resulting in even narrower bands of unshaded foraging time, particularly in the mammaliaform. Reduced foraging time would presumably apply even more stress to the large herbivores, as foraging for enough plant mass to sustain 280-850 kg animals in 4-9 hour days, or alternatively by braving significant heat stress would be challenging. The higher latitude microclimate does little to alter the thermal constraints of *Poposaurus, Postosuchus* or *Rutiodon*, implying that had they survived the transient cold phase they might have avoided extinction at the ETE.

Discussion

Mechanistic modeling of thermal ecology in Niche Mapper has seen widespread success among extant taxa (Kearney & Porter, 2009; Mathewson & Porter, 2013; Long, et al., 2014; Dudley, et al., 2016). Application of Niche Mapper to extinct taxa has recently been thoroughly vetted for Triassic dinosaurs (Lovelace, et al., 2020). These tools were leveraged to examine the thermal ecology of 13 taxa in Late Triassic ecosystems and investigate thermal stresses and potential causes of extinction selectivity during the End Triassic Extinction.

Late Triassic microclimate results are congruous with previously inferred activity patterns and fossil paleobiogeogrpahy

Pre-ETE microclimate model results provide insights into several features of late Triassic ecosystems. While organisms can be flagged as diurnal, nocturnal, etc. within Niche Mapper, all potential activity patterns were allowed during model runs so thermal constraints rather than preconceived assumptions would drive model taxa activity patterns. Thus, the mammaliaform was found to be nocturnal because its combination of size, burrowing, incipient mammalian endothermy, and mammalian epidermal insulation performed better by being active at night, not due to previous hypotheses. That Niche Mapper results match up with morphological evidence from olfactory and auditory anatomy (Luo, 2011; Angielczyk & Schmitz, 2014) and from ancestral genetic studies of vision genes (Wu, et al., 2017) supports the efficacy of mechanistic modeling. The results do provide a novel perspective on evolutionary mechanisms in this scenario, as it suggests that burrowing and nocturnality evolved in mammaliaformes due to the thermal constraints they encountered, not due to some nebulous concept of competition with diurnal dinosaurs as is commonly suggested (c.f. Schmitz & Motani, 2011; Wu, et al., 2017).

The results contradict the idea of a simple diurnal/nocturnal split between archosaurs and stem-mammals. While some archosaurs like *Poposaurus* and *Desmatosuchus* were restricted to diurnal activity, in low latitudes *Coelophysis* was found to be most likely nocturnal, crepuscular, or cathemeral, a result consistent with the activity pattern of a congeneric relative (Schmitz & Motani, 2011). The lack of thermal constraint on activity time suggests the potential for cathemeral activity in small burrowing ornithischian dinosaurs, while insectivorous silesaurids best functioned within crepuscular activity periods.

Pre-ETE thermal ecology also explains observed paleobiogeographical patterns. It has already been noted that low latitude heat stress on *Plateosaurus* is consistent with it and other large sauropodomorphs being found predominantly at higher latitudes (Lovelace, et al., 2020), but the restriction to low latitudes of modeled taxa like *Poposaurus* and *Postosuchus* (Gauthier, et al., 2011; Weinbaum, 2013), as well as the restriction over time of large phytosaurs like *Rutiodon* to lower latitudes (Fig. 1-14) are also consistent with the fossil record.

The Transient Cold Phase Explains Terrestrial Extinction Selectivity Across the ETE

While both the transient cold phase and both modeled global warming phases placed significant thermal stress on most of the modeled taxa, perhaps the most surprising finding is that the transient cold phase is much more consistent with extinction selectivity during the ETE (see Table 1-3). Rhynchosaurs, *Rutiodon*, *Desmatosuchus*, *Poposaurus*, *Postosuchus*, *Dromomeron* and *Eucoelophysis*, all taxa that went extinct during the ETE, were found to be either non-viable or highly stressed in the transient cold phase. Meanwhile, the dinosaurs, mammaliaform and small burrowing crocodilian *Hesperosuchus* all received little to no thermal stress from the transient cold phase.

Taxa	Status	Cold LL	Cold HL	Warm 1 LL	Warm 1 HL	Warm 2 LL	Warm 2 HL
Placerias	Extinct	High stress	Non-viable	High stress	High stress	High stress	High stress
Mammaliaform	Survive	No stress	No stress	Low stress	Low stress	High stress	High stress
Rhynchosaur	Extinct	Non-viable	Non-viable	Low stress	Low stress	Stress	High stress
Rutiodon	Extinct	High stress	Non-viable	Low stress	Low stress	Stress	Stress
Desmatosuchus	Extinct	High stress	Non-viable	Stress	Stress	High stress	High stress
Poposaurus	Extinct	Non-viable	Non-viable	Low stress	Low stress	Stress	Stress
Postosuchus	Extinct	Non-viable	Non-viable	Low stress	Low stress	Stress	Stress
Hesperosuchus	Survive	Low stress	Little stress	Low stress	Low stress	Stress	Stress
Dromomeron	Extinct	High stress	High stress	Low stress	Low stress	Stress	Stress
Eucoelophysis	Extinct	High stress	High stress	Low stress	Low stress	Stress	Stress
Ornithischian	Survive	No stress	No stress	Low stress	Low stress	Stress	High stress
Plateosaurus	Survive	No stress	Low stress	Stress	Stress	Stress	High stress
Coelophysis	Survive	No stress	Low stress	Low stress	Low stress	Stress	Stress

Table 2-3. Summary of survivorship and levels of thermal stress during the ETE. *Abbreviations: Cold, transient cold phase; HL, high latitude; LL, low latitude; Warm 1, global warming phase based on Landwehrs, et al. (2020); Warm 2, hotter global warming phase.*

During the global warming phase thermal stress was applied to all species, but was largely indiscriminate and does not match the pattern of ETE selectivity (Table 1-3). For example, large herbivores saw some of the highest stress levels, but fossils show that large herbivorous dinosaurs (cf. *Plateosaurus*) survived the ETE, while large herbivorous stem-mammals and pseudosuchians (cf. *Placerias* and *Desmatosuchus*) did not. Bipedal carnivorous pseudosuchians (cf. *Poposaurus* and *Postosuchus*) go extinct during the ETE, but they get only

minimal thermal pressure induced even during the most extreme global warming microclimate employed.

This is not to discount the problems global warming produces (e.g. Botkin, et al., 2007), nor to deny a key role for global warming in the ETE. Refugia of more amenable microclimates may have allowed pockets of stressed taxa to survive the ETE cold phase, non-linear biotic interactions may have occurred that could offset some foraging-related stress (Lindström, S., 2016; van de Schootbrugge & Wignall, 2016), or the brevity of the transient cold phase all could result in highly stressed taxa during the transient cold phase requiring prolonged thermal stress from the global warming phase and/or an associated increase in global warming-linked natural disasters such as wildfires (Belcher, et al., 2010) to fully drive them to extinction. It should also be noted that these results only apply to terrestrial amniotes. But given the perfectly congruous results between only taxa that went extinct and a high degree of stress experienced by those taxa during the transient cold phase, the cold phase provides the most robust explanation for the pattern of extinction and survival observed among terrestrial amniotes during the End Triassic Extinction.

The importance of burrowing and dormancy are often overlooked in vertebrate paleoecology

A reoccurring result was the importance of burrowing for small and medium-sized taxa. For small animals this was true regardless of metabolic rate or target T_{core}, while at larger sizes uninsulated or ectothermic taxa were more likely to need the thermal isolation of a burrow. Even larger taxa like *Poposaurus,* which at 75 kg and lacking any obvious adaptations to burrowing is not an ideal candidate, would probably have been able to more effectively thermoregulate if it had been modeled with burrowing enabled, especially at high latitudes (e.g. Figs. 1-10 to 1-12). This should not be a surprising finding, as using a burrow or other thermally isolated zone to

escape unfavorable thermal conditions is widespread in extant animals (Martin, 2017). Yet the physiological importance of utilizing burrows and the impact they have on size evolution and potential barriers to geographic dispersal in Paleozoic and Mesozoic tetrapods are under-discussed, and finding evidence of burrowing in archosaurs is often treated as an unexpected discovery (e.g. de Souza Varhalho, et al., 2005; Varricchio, et al., 2007).

A similar result is the importance of metabolic dormancy during thermally stressful seasonality. Utilizing some form of metabolic dormancy is widespread among small animals today (Guppy, et al., 1994; Withers & Cooper, 2010) and may have been important to the origin of mammalian sleeping patterns (Rial, et al., 2010). In the pre-ETE Triassic microclimates, taxa at higher latitude often would have endured lower thermal stress and reduced energy budgets if brumation, torpor, or hibernation were enabled.

Incorporating burrows and improved understanding of metabolic dormancy will likely be key to modeling the paleobiogeographic niches of small vertebrates in high latitudes in Paleozoic and Mesozoic ecosystems.

Conclusions

Applying the mechanistic niche modeling software Niche Mapper to representative taxa in Late Triassic microclimates reproduces activity times and latitudinal occupancy congruent with expectations from the fossil record. Simulating the same taxa within transient cold and prolonged global warming environments modeled for terrestrial End Triassic Extinction climates reproduces the same survivorship pattern seen in the fossil record. Surprisingly, most of the selectivity seems to occur in the transient cold period, with subsequent global warming phases playing a less-selective role in applying potential extinction pressure to all modeled taxa, perhaps

with the species hardest hit during the cold phase unable to survive the rapid reversal of climates. These results also show burrowing and metabolic dormancy are necessary and underrated components for understanding geographic distributions of small taxa in deep time.

Acknowledgements

I would like to thank Warren Porter for creating Niche Mapper (making this endeavor possible) and his constant encouragement as we developed ideas around testing extinct animals. Thanks to David Lovelace, who was instrumental in those discussions and who encouraged me to join the project. Thanks to Dave and Ben Linzmeier for working on R scripts that sped up multiple simulation runs; thanks are also due for their patience when my R skills were a bit rusty. Paul Matthewson must be thanked profusely for his work on the Niche Mapper code base, and for clarifying input values as we adapted it to modeling long dead animals. Aaron Kufner, Adam Fitch, and Calvin So worked on earlier versions of several of the taxa models and contributed to discussions on all things Triassic.

Supplemental Data

S.1-1. Microclimate input file:

https://figshare.com/articles/Microclimate_Biophysical_input_filee_-_Dissertation/12455825

S.1-2. Biophysical input file:

https://figshare.com/articles/Biophysical_model_inputs_-_Dissertation/12455828

S.1-3. All Niche Mapper plots (no burrowing):

https://figshare.com/articles/Raw_Niche_Mapper_output_plots_no_burrowing_/12480155

S.1-4. All burrowing Niche Mapper plots (burrowing enabled):

https://figshare.com/articles/Raw_Niche_Mapper_plots_with_burrowing_allowed/12480158

S.1-5. Raw output files from Niche Mapper simulation:

https://figshare.com/articles/Niche_Mapper_Output_Files/12485894

References

Abell, A.J., 1999. Variation in clutch size and offspring size relative to environmental conditions in the lizard *Sceloporus virgatus*. *Journal of Herpetology*, pp.173-180.

Angielczyk, K.D. and Schmitz, L., 2014. Nocturnality in synapsids predates the origin of mammals by over 100 million years. *Proceedings of the Royal Society B: Biological Sciences*, *281*(1793), p.20141642.

Angilletta, M.J., Cooper, B.S., Schuler, M.S. and Boyles, J.G., 2010. The evolution of thermal physiology in endotherms. *Front Biosci E*, *2*, pp.861-881.

Agnolín, F.L. and Rozadilla, S., 2018. Phylogenetic reassessment of Pisanosaurus mertii Casamiquela, 1967, a basal dinosauriform from the Late Triassic of Argentina. *Journal of Systematic Palaeontology*, *16*(10), pp.853-879.

Andrews, R.M. and Pough, F.H., 1985. Metabolism of squamate reptiles: allometric and ecological relationships. *Physiological Zoology*, *58*(2), pp.214-231.

Bajdek, P., Qvarnström, M., Owocki, K., Sulej, T., Sennikov, A.G., Golubev, V.K. and Niedźwiedzki, G., 2016. Microbiota and food residues including possible evidence of pre-mammalian hair in Upper Permian coprolites from Russia. *Lethaia*, *49*(4), pp.455-477.

Bajdek, P., Owocki, K. and Niedźwiedzki, G., 2014. Putative dicynodont coprolites from the Upper Triassic of Poland. *Palaeogeography, Palaeoclimatology, Palaeoecology*, *411*, pp.1-17.

Barlett, P.N. and Gates, D.M., 1967. The energy budget of a lizard on a tree trunk. *Ecology*, *48*(2), pp.315-322.

Belcher, C.M., Mander, L., Rein, G., Jervis, F.X., Haworth, M., Hesselbo, S.P., Glasspool, I.J. and McElwain, J.C., 2010. Increased fire activity at the Triassic/Jurassic boundary in Greenland due to climate-driven floral change. *Nature Geoscience*, *3*(6), pp.426-429.

Bennett, A.F., 1978. Activity metabolism of the lower vertebrates. *Annual Review of Physiology*, *40*(1), pp.447-469.

Berner, R.A., Beerling, D.J., Dudley, R., Robinson, J.M. and Wildman Jr, R.A., 2003. Phanerozoic atmospheric oxygen. *Annual Review of Earth and Planetary Sciences*, *31*(1), pp.105-134.

Berner, R.A. and Kothavala, Z., 2001. GEOCARB III: a revised model of atmospheric CO_2 over Phanerozoic time. *American Journal of Science*, *301*(2), pp.182-204.

Botha-Brink, J. and Smith, R.M.H. 2011. Osteohistology of the Triassic Archosauromorphs *Prolacerta*, *Proterosuchus*, *Euparkeria*, and *Erythrosuchus* from the Karoo Basin of South Africa. *Journal of Vertebrate Paleontology,* 31: 1238-1254. *Paleontology* 31: 1238–1254.

Botha-Brink, J., 2017. Burrowing in Lystrosaurus: preadaptation to a postextinction environment?. *Journal of Vertebrate Paleontology*, *37*(5), p.e1365080.

Botha-Brink, J. and Angielczyk, K.D., 2010. Do extraordinarily high growth rates in Permo-Triassic dicynodonts (Therapsida, Anomodontia) explain their success before and after the end-Permian extinction?. *Zoological Journal of the Linnean Society*, *160*(2), pp.341-365.

Botkin, D.B., Saxe, H., Araujo, M.B., Betts, R., Bradshaw, R.H., Cedhagen, T., Chesson, P., Dawson, T.P., Etterson, J.R., Faith, D.P. and Ferrier, S., 2007. Forecasting the effects of global warming on biodiversity. *Bioscience*, *57*(3), pp.227-236.

Brusatte, S.L., Niedźwiedzki, G. and Butler, R.J., 2011. Footprints pull origin and diversification of dinosaur stem lineage deep into Early Triassic. *Proceedings of the Royal Society B: Biological Sciences*, *278*(1708), pp.1107-1113.

Brusatte, S.L., Benton, M.J., Desojo, J.B. and Langer, M.C., 2010. The higher-level phylogeny of Archosauria (Tetrapoda: Diapsida). *Journal of Systematic Palaeontology*, *8*(1), pp.3-47.

Butler, R.J., Brusatte, S.L., Reich, M., Nesbitt, S.J. and Schoch, R.R., 2011. The Sail-Backed Reptile *Ctenosauriscus* from the Latest Early Triassic of Germany and.

Butler, R.J., 2010. The anatomy of the basal ornithischian dinosaur Eocursor parvus from the lower Elliot Formation (Late Triassic) of South Africa. *Zoological Journal of the Linnean Society*, *160*(4), pp.648-684.

Cabreira, S.F., Kellner, A.W.A., Dias-da-Silva, S., da Silva, L.R., Bronzati, M., de Almeida Marsola, J.C., Müller, R.T., de Souza Bittencourt, J., Batista, B.J.A., Raugust, T. and Carrilho, R., 2016. A unique Late Triassic dinosauromorph assemblage reveals dinosaur ancestral anatomy and diet. *Current Biology*, *26*(22), pp.3090-3095.

Campione, N.E., Barrett, P.M. and Evans, D.C., 2020. On the Ancestry of Feathers in Mesozoic Dinosaurs. In *The Evolution of Feathers* (pp. 213-243). Springer, Cham.

Capriolo, M., Marzoli, A., Aradi, L.E., Callegaro, S., Dal Corso, J., Newton, R.J., Mills, B.J., Wignall, P.B., Bartoli, O., Baker, D.R. and Youbi, N., 2020. Deep CO 2 in the end-Triassic Central Atlantic Magmatic Province. *Nature communications*, *11*(1), pp.1-11.

Chatterjee, S., 1985. Postosuchus, a new thecodontian reptile from the Triassic of Texas and the origin of tyrannosaurs. *Philosophical Transactions of the Royal Society of London. B, Biological Sciences*, *309*(1139), pp.395-460.

Clarke, A. and Pörtner, H.O., 2010. Temperature, metabolic power and the evolution of endothermy. *Biological Reviews*, *85*(4), pp.703-727.

Clark, J.M., Sues, H.D. and Berman, D.S., 2001. A new specimen of Hesperosuchus agilis from the Upper Triassic of New Mexico and the interrelationships of basal crocodylomorph archosaurs. *Journal of Vertebrate Paleontology*, *20*(4), pp.683-704.

Cleveland, D.M., Nordt, L.C. and Atchley, S.C., 2008. Paleosols, trace fossils, and precipitation estimates of the uppermost Triassic strata in northern New Mexico. *Palaeogeography, Palaeoclimatology, Palaeoecology*, *257*(4), pp.421-444.

Colbert, E. 1952. *A pseudosuchian reptile from Arizona*. Bulletin of the American Museum of Natural History. 99(10).

Crompton, A.W., Taylor, C.R. and Jagger, J.A., 1978. Evolution of homeothermy in mammals. *Nature*, *272*(5651), pp.333-336.

Datta, P.M., 2005. Earliest mammal with transversely expanded upper molar from the Late Triassic (Carnian) Tiki Formation, South Rewa Gondwana Basin, India. *Journal of Vertebrate Paleontology*, *25*(1), pp.200-207.

Davies, J., Marzoli, A., Bertrand, H., Youbi, N., Ernesto, M. and Schaltegger, U., 2017. End-Triassic mass extinction started by intrusive CAMP activity. *Nature communications*, *8*(1), pp.1-8.

de Souza Carvalho, I., Campos, A.D.C.A. and Nobre, P.H., 2005. Baurusuchus salgadoensis, a new crocodylomorpha from the Bauru Basin (Cretaceous), Brazil. *Gondwana Research*, *8*(1), pp.11-30.

Desojo, J.B., Ezcurra, M.D. and Kischlat, E.E., 2012. A new aetosaur genus (Archosauria: Pseudosuchia) from the early Late Triassic of southern Brazil. *Zootaxa*, *3166*(1–33).

Dubiel, R.F., Parrish, J.T., Parrish, J.M. and Good, S.C., 1991. The Pangaean megamonsoon: evidence from the Upper Triassic Chinle Formation, Colorado Plateau. *Palaios*, pp.347-370.

Dudley, P.N., Bonazza, R. and Porter, W.P., 2016. Climate change impacts on nesting and internesting leatherback sea turtles using 3D animated computational fluid dynamics and finite volume heat transfer. *Ecological Modelling*, *320*, pp.231-240.

Dudley, P.N., Bonazza, R. and Porter, W.P., 2013. Consider a Non-S pherical Elephant: Computational Fluid Dynamics Simulations of Heat Transfer Coefficients and Drag Verified Using Wind Tunnel Experiments. *Journal of Experimental Zoology Part A: Ecological Genetics and Physiology*, *319*(6), pp.319-327.

Dunham, A., Overall, K., Porter, W., & Forster, C. 1989. Implications of ecological energetics and biophysical and developmental constraints for life-history variation in dinosaurs. *Geological Society of America Special Papers*, *238*, 1-20.

Dróżdż, D., 2018. Osteology of a forelimb of an aetosaur Stagonolepis olenkae (Archosauria: Pseudosuchia: Aetosauria) from the Krasiejów locality in Poland and its probable adaptations for a scratch-digging behavior. *PeerJ*, *6*, p.e5595.

Eagle, R.A., Tütken, T., Martin, T.S., Tripati, A.K., Fricke, H.C., Connely, M., Cifelli, R.L. and Eiler, J.M., 2011. Dinosaur body temperatures determined from isotopic (13C-18O) ordering in fossil biominerals. *Science*, *333*(6041), pp.443-445.

Ezcurra, M.D., 2016. The phylogenetic relationships of basal archosauromorphs, with an emphasis on the systematics of proterosuchian archosauriforms. *PeerJ*, *4*, p.e1778.

Ezcurra, M.D., Montefeltro, F. and Butler, R.J., 2016. The early evolution of rhynchosaurs. *Frontiers in Ecology and Evolution*, *3*, p.142.

Ezcurra, M.D., 2006. A review of the systematic position of the dinosauriform archosaur *Eucoelophysis baldwini* Sullivan & Lucas, 1999 from the Upper Triassic of New Mexico, USA. *Geodiversitas*, *28*(4), pp.649-684.

Farlow, J.O., 1987. Speculations about the diet and digestive physiology of herbivorous dinosaurs. *Paleobiology*, *13*(1), pp.60-72.

Fiorillo, A.R., Padian, K. and Musikasinthorn, C., 2000. Taphonomy and depositional setting of the Placerias Quarry (Chinle Formation: Late Triassic, Arizona). *Palaios*, *15*(5), pp.373-386.

Fitzpatrick, M.J., Mathewson, P.D. and Porter, W.P., 2015. Validation of a mechanistic model for non-invasive study of ecological energetics in an endangered wading bird with counter-current heat exchange in its legs. *PloS one*, *10*(8), p.e0136677.

Franz, R., Hummel, J., Müller, D.W., Bauert, M., Hatt, J.M. and Clauss, M., 2011. Herbivorous reptiles and body mass: effects on food intake, digesta retention, digestibility and gut capacity, and a comparison with mammals. *Comparative Biochemistry and Physiology Part A: Molecular & Integrative Physiology*, *158*(1), pp.94-101.

Gates, D. M. 1969. Energy exchange in the biosphere.

Gates, D. M. 2012. *Biophysical ecology*. Courier Corporation.

Gauthier, J.A., Nesbitt, S.J., Schachner, E.R., Bever, G.S. and Joyce, W.G., 2011. The bipedal stem crocodilian Poposaurus gracilis: inferring function in fossils and innovation in archosaur locomotion. *Bulletin of the Peabody Museum of Natural History*, *52*(1), pp.107-126.

Gauthier, J. A. 1986. Saurischian monophyly and the origin of birds. Memoirs of the California Academy of Sciences, 8, 1-55.

Geiger, R., Aron, R.H. and Todhunter, P., 2009. *The climate near the ground*. Rowman & Littlefield.

Godefroit, P., Sinitsa, S.M., Dhouailly, D., Bolotsky, Y.L., Sizov, A.V., McNamara, M.E., Benton, M.J. and Spagna, P., 2014. A Jurassic ornithischian dinosaur from Siberia with both feathers and scales. *Science*, *345*(6195), pp.451-455.

Griffin, C.T., Bano, L.S., Turner, A.H., Smith, N.D., Irmis, R.B. and Nesbitt, S.J., 2019. Integrating gross morphology and bone histology to assess skeletal maturity in early dinosauromorphs: new insights from Dromomeron (Archosauria: Dinosauromorpha). *PeerJ*, *7*, p.e6331.

Grigg, G. and Beard, L., 2000. Hibernation by echidnas in mild climates: Hints about the evolution of endothermy?. In *Life in the cold* (pp. 5-19). Springer, Berlin, Heidelberg.

Guppy, M., Fuery, C.J. and Flanigan, J.E., 1994. Biochemical principles of metabolic depression. *Comparative Biochemistry and Physiology Part B: Comparative Biochemistry*, *109*(2-3), pp.175-189.

Hale, A., Merchant, M. and White, M., 2020. Detection and analysis of autophagy in the American alligator (Alligator mississippiensis). *Journal of Experimental Zoology Part B: Molecular and Developmental Evolution*, *334*(3), pp.192-207.

Hartman, S., Lovelace, D., Linzmeier, B., Mathewson, P., & Porter, W. 2016. Mechanistic physiological modelling predicts geographic distribution of Late Triassic tetrapods. In *Annual Meeting of the Society of Vertebrate Paleontology*, SVP 2016.

Hartman, S., Lovelace, D., Mathewson, Linzmeier, B. J., Porter, W. 2015. Using ecological modelling to quantify thermal constraints on two Late Triassic dinosaurs. Journal of Vertebrate Paleontology. Vol. 35, online supplement.

Heath, T.A., Hedtke, S.M. and Hillis, D.M., 2008. Taxon sampling and the accuracy of phylogenetic analyses. *Journal of Systematics and Evolution*, *46*(3), pp.239-257.

Heimdal, T.H., Jones, M.T. and Svensen, H.H., 2020. Thermogenic carbon release from the Central Atlantic magmatic province caused major end-Triassic carbon cycle perturbations. *Proceedings of the National Academy of Sciences*, *117*(22), pp.11968-11974.

Hendrickx, C., Hartman, S.A. and Mateus, O., 2015. An overview of non-avian theropod discoveries and classification. *PalArch's Journal of Vertebrate Palaeontology*, *12*(1).

Hudgins, Michael Naylor, Mark D. Uhen, and Linda A. Hinnov. "The evolution of respiratory systems in Theropoda and Paracrocodylomorpha, the end-Triassic extinction, and the role of Late Triassic atmospheric O_2 and CO_2." *Palaeogeography, Palaeoclimatology, Palaeoecology* 545 (2020): 109638.

Huene, F.R., 1913. A new phytosaur from the Palisades near New York. Bulletin of the AMNH; v. 32, article 15.

Hurlburt, G.R., Heckert, A.B. and Farlow, J.O., 2003. Body mass estimates of phytosaurs (Archosauria: Parasuchidae) from the Petrified Forest Formation (Chinle Group: Revueltian) based on skull and limb bone measurements. *New Mex Mus Nat Hist Sci Bull*, *24*, pp.105-13.

Huynh, T. T., & Poulsen, C. J. 2005. Rising atmospheric CO_2 as a possible trigger for the end-Triassic mass extinction. Palaeogeography, Palaeoclimatology, Palaeoecology, 217(3), 223-242.

Irmis, R.B., Nesbitt, S.J., Padian, K., Smith, N.D., Turner, A.H., Woody, D. and Downs, A., 2007a. A Late Triassic dinosauromorph assemblage from New Mexico and the rise of dinosaurs. *Science*, *317*(5836), pp.358-361.

Irmis, R.B., Parker, W.G., Nesbitt, S.J. and Liu, J., 2007b. Early ornithischian dinosaurs: the Triassic record. *Historical Biology*, *19*(1), pp.3-22.

Ji, Q., Luo, Z.X., Yuan, C.X. and Tabrum, A.R., 2006. A swimming mammaliaform from the Middle Jurassic and ecomorphological diversification of early mammals. *Science*, *311*(5764), pp.1123-1127.

Kearney, M.R., Shamakhy, A., Tingley, R., Karoly, D.J., Hoffmann, A.A., Briggs, P.R. and Porter, W.P., 2014. Microclimate modeling at macro scales: a test of a general microclimate model integrated with gridded continental-scale soil and weather data. *Methods in Ecology and Evolution*, *5*(3), pp.273-286.

Kearney, M., & Porter, W. 2009. Mechanistic niche modelling: combining physiological and spatial data to predict species' ranges. *Ecology letters*, *12*(4), 334-350.

Kearney, M., & Porter, W. P. 2004. Mapping the fundamental niche: physiology, climate, and the distribution of a nocturnal lizard. *Ecology*, *85*(11), 3119-3131.

Kielan-Jaworowska, Z., Cifelli, R.L. and Luo, Z.X., 2005. *Mammals from the age of dinosaurs: origins, evolution, and structure*. Columbia University Press.

Kammerer, C.F., Nesbitt, S.J. and Shubin, N.H., 2011. The first silesaurid dinosauriform from the Late Triassic of Morocco. *Acta Palaeontologica Polonica*, *57*(2), pp.277-284.

Klein, N., Foth, C. and Schoch, R.R., 2017. Preliminary observations on the bone histology of the Middle Triassic pseudosuchian archosaur Batrachotomus kupferzellensis reveal fast growth with laminar fibrolamellar bone tissue. *Journal of Vertebrate Paleontology*, *37*(4), p.e1333121.

Koteja, P., 1991. On the relation between basal and field metabolic rates in birds and mammals. *Functional Ecology*, pp.56-64.

Kreith, F. Black, W.Z. 1980. Basic Heat Transfer. 1st ed. New York:Harper & Row.

Knutsen, E.M. and Oerlemans, E., 2020. The last dicynodont? Re-assessing the taxonomic and temporal relationships of a contentious Australian fossil. *Gondwana Research*, *77*, pp.184-203.

Kundrát, M., 2004. When did theropods become feathered?—evidence for pre-archaeopteryx feathery appendages. *Journal of Experimental Zoology Part B: Molecular and Developmental Evolution*, *302*(4), pp.355-364.

Landwehrs, J.P., Feulner, G., Hofmann, M. and Petri, S., 2020. Climatic fluctuations modeled for carbon and sulfur emissions from end-Triassic volcanism. *Earth and Planetary Science Letters*, *537*, p.116174.

Lecuona, A. and Desojo, J.B., 2012. Hind limb osteology of Gracilisuchus stipanicicorum (Archosauria: Pseudosuchia). *Earth and Environmental Science Transactions of the Royal Society of Edinburgh*, *102*(2), pp.105-128.

Legendre, L.J., Segalen, L. and Cubo, J., 2013. Evidence for high bone growth rate in Euparkeria obtained using a new paleohistological inference model for the humerus. *Journal of Vertebrate Paleontology*, *33*(6), pp.1343-1350.

Legendre, L., 2014. Did crocodiles become secondarily ectothermic?: a paleohistological approach (Doctoral dissertation).

Leigh, S.R., 2001. Evolution of human growth. Evolutionary Anthropology: Issues, News, and Reviews: Issues, News, and Reviews, 10(6), pp.223-236.

Levy, O., Dayan, T., Kronfeld-Schor, N., & Porter, W. P. 2012. Biophysical modeling of the temporal niche: from first principles to the evolution of activity patterns. *The American Naturalist*, *179*(6), 794-804.

Li, C., Wu, X.C., Cheng, Y.N., Sato, T. and Wang, L., 2006. An unusual archosaurian from the marine Triassic of China. *Naturwissenschaften*, *93*(4), pp.200-206.

Lin, T.E., Chen, T.Y., Wei, H.L., Richard, R. and Huang, S.P., 2019. Low cold tolerance of the invasive lizard Eutropis multifasciata constrains its potential elevation distribution in Taiwan. *Journal of thermal biology*, *82*, pp.115-122.

Lindström, S., 2016. Palynofloral patterns of terrestrial ecosystem change during the end-Triassic event–a review. *Geological Magazine*, *153*(2), pp.223-251.

Liu, Y., Chi, H., Li, L., Rossiter, S.J. and Zhang, S., 2018. Molecular data support an early shift to an intermediate-light niche in the evolution of mammals. *Molecular biology and evolution*, *35*(5), pp.1130-1134.

Lovelace, D.M., Hartman, S.A., Mathewson, P.D., Linzmeier, B.J. and Porter, W.P., 2020. Modeling Dragons: Using linked mechanistic physiological and microclimate models to explore environmental, physiological, and morphological constraints on the early evolution of dinosaurs. *Plos one*, *15*(5), p.e0223872.

Lovelace, D. 2014. Triassic Macrostratigraphy of the Western United States. In *STRATI 2013* (pp. 1203-1206). Springer International Publishing.

Lucas, S.G. and Tanner, L.H., 2007. Tetrapod biostratigraphy and biochronology of the Triassic–Jurassic transition on the southern Colorado Plateau, USA. *Palaeogeography, Palaeoclimatology, Palaeoecology*, *244*(1-4), pp.242-256.

Lucas, S.G. and Heckert, A.B., 2002. Skull of the dicynodont Placerias from the Upper Triassic of Arizona. *New Mexico Mus Nat Hist Sci Bull*, *21*, pp.127-130.

Luo, Z.X., Meng, Q.J., Ji, Q., Liu, D., Zhang, Y.G. and Neander, A.I., 2015. Evolutionary development in basal mammaliaforms as revealed by a docodontan. *Science*, *347*(6223), pp.760-764.

Luo, Z.X., 2007. Transformation and diversification in early mammal evolution. *Nature, 450*(7172), pp.1011-1019.

Lutz, R.L. and Lutz, J.M., 1997. *Komodo, the living dragon*. Dimi Press.

Mallison, H. 2010. The digital Plateosaurus I: body mass, mass distribution, and posture assessed using CAD and CAE on a digitally mounted complete skeleton. *Palaeontologia Electronica*, *13*(2), 8A.

Maloney, S.K., 2008. Thermoregulation in ratites: a review. *Australian Journal of Experimental Agriculture*, *48*(10), pp.1293-1301.

Mathewson, P. D., & Porter, W. P. 2013. Simulating polar bear energetics during a seasonal fast using a mechanistic model.

Martin, A.J., 2017. *The evolution underground: burrows, bunkers, and the marvelous subterranean world beneath our feet*. Pegasus Books.

Martinez, R.N. and Alcober, O.A., 2009. A basal sauropodomorph (Dinosauria: Saurischia) from the Ischigualasto Formation (Triassic, Carnian) and the early evolution of Sauropodomorpha. *PLoS One*, *4*(2).

McCullough, E.C. and Porter, W.P., 1971. Computing clear day solar radiation spectra for the terrestrial ecological environment. *Ecology*, *52*(6), pp.1008-1015.

McKechnie, A.E. and Wolf, B.O., 2004. The allometry of avian basal metabolic rate: good predictions need good data. *Physiological and Biochemical Zoology*, *77*(3), pp.502-521.

McKellar, R.C., Chatterton, B.D., Wolfe, A.P. and Currie, P.J., 2011. A diverse assemblage of Late Cretaceous dinosaur and bird feathers from Canadian amber. *Science*, *333*(6049), pp.1619-1622.

McNab, B.K., 2008. An analysis of the factors that influence the level and scaling of mammalian BMR. *Comparative Biochemistry and Physiology Part A: Molecular & Integrative Physiology*, *151*(1), pp.5-28.

McPhee, B.W., Bordy, E.M., Sciscio, L. and Choiniere, J.N., 2017. The sauropodomorph biostratigraphy of the Elliot Formation of southern Africa: Tracking the evolution of Sauropodomorpha across the Triassic–Jurassic boundary. *Acta Palaeontologica Polonica*, *62*(3), pp.441-465.

Meng, Q.J., Ji, Q., Zhang, Y.G., Liu, D., Grossnickle, D.M. and Luo, Z.X., 2015. An arboreal docodont from the Jurassic and mammaliaform ecological diversification. *Science, 347*(6223), pp.764-768.

Mole, M.A., Rodrigues DÁraujo, S., Van Aarde, R.J., Mitchell, D. and Fuller, A., 2016. Coping with heat: behavioural and physiological responses of savanna elephants in their natural habitat. *Conservation physiology*, *4*(1).

Molnar, J.L., Pierce, S.E., Bhullar, B.A.S., Turner, A.H. and Hutchinson, J.R., 2015. Morphological and functional changes in the vertebral column with increasing aquatic adaptation in crocodylomorphs. *Royal Society Open Science*, *2*(11), p.150439.

Mukherjee, D. and Ray, S., 2014. A new H yperodapedon (A rchosauromorpha, R hynchosauria) from the U pper T riassic of I ndia: implications for rhynchosaur phylogeny. *Palaeontology*, *57*(6), pp.1241-1276.

Müller, R.T. and Dias-da-Silva, S., 2019. Taxon sample and character coding deeply impact unstable branches in phylogenetic trees of dinosaurs. *Historical Biology*, *31*(8), pp.1089-1092.

Myhrvold, N.P., 2016. Dinosaur metabolism and the allometry of maximum growth rate. *PloS one*, *11*(11).

Nesbitt, S.J., 2011. The early evolution of archosaurs: relationships and the origin of major clades. *Bulletin of the American Museum of Natural History*, *2011*(352), pp.1-292.

Nesbitt, S., 2007. The anatomy of Effigia okeeffeae (Archosauria, Suchia), theropod-like convergence, and the distribution of related taxa. *Bulletin of the american Museum of Natural history*, *2007*(302), pp.1-84.

Noy-Meir, I., 1974. Desert ecosystems: higher trophic levels. *Annual Review of Ecology and systematics*, *5*(1), pp.195-214.

Olsen, P.E., Shubin, N.H. and Anders, M.H., 1987. New Early Jurassic tetrapod assemblages constrain Triassic-Jurassic tetrapod extinction event. *Science*, *237*(4818), pp.1025-1029.

Otero, A., Cuff, A.R., Allen, V., Sumner-Rooney, L., Pol, D. and Hutchinson, J.R., 2019. Ontogenetic changes in the body plan of the sauropodomorph dinosaur Mussaurus patagonicus reveal shifts of locomotor stance during growth. *Scientific reports*, *9*(1), pp.1-10.

Owen-Smith, N., 1979. Assessing the foraging effeciency of a large herbivore, the kudu. *South African Journal of Wildlife Research-24-month delayed open access*, *9*(3-4), pp.102-110.

Padian, K., Li, C. and Pchelnikova, J., 2010. The trackmaker of Apatopus (Late Triassic, North America): implications for the evolution of archosaur stance and gait. *Palaeontology*, *53*(1), pp.175-189.

Parrish, J.T., 1993. Climate of the supercontinent Pangea. *The Journal of Geology*, *101*(2), pp.215-233.

Paul, G. S. 1997. Dinosaur models: the good, the bad, and using them to estimate the mass of dinosaurs. In DinoFest International: Proceedings of a Symposium Sponsored by Arizona State University. Academy of Natural Sciences, Philadelphia (pp. 129-154).

Peczkis, J., 1995. Implications of body-mass estimates for dinosaurs. *Journal of Vertebrate Paleontology*, *14*(4), pp.520-533.

Peterson, M.E., Daniel, R.M., Danson, M.J. and Eisenthal, R., 2007. The dependence of enzyme activity on temperature: determination and validation of parameters. *Biochemical Journal*, *402*(2), pp.331-337.

Plumb, G.E. and Dodd, J.L., 1993. Foraging ecology of bison and cattle on a mixed prairie: implications for natural area management. *Ecological Applications*, *3*(4), pp.631-643.

Pond, C.M., 1992. An evolutionary and functional view of mammalian adipose tissue. *Proceedings of the Nutrition Society*, *51*(3), pp.367-377.

Pontzer, H., Allen, V. and Hutchinson, J.R., 2009. Biomechanics of running indicates endothermy in bipedal dinosaurs. *PloS one*, *4*(11).

Porter, W.P. and Kearney, M., 2009. Size, shape, and the thermal niche of endotherms. *Proceedings of the National Academy of Sciences*, *106*(Supplement 2), pp.19666-19672.

Porter,W. & Mitchell J. 2006. Method and system for calculating the spatial-temporal effects of climate and other environmental conditions on animals. In: Office UP, editor. 11-0E Wisconsin Alumni Research Foundation; B http://www.patentstorm.us/patents/7155377-fulltext.html.

Porter, W.P., Vakharia, N., Klousie, W.D. and Duffy, D., 2006. Po'ouli landscape bioinformatics models predict energetics, behavior, diets, and distribution on Maui. *Integrative and Comparative Biology*, *46*(6), pp.1143-1158.

Porter, W.P., Mitchell, J.W., Beckman, W.A. and DeWitt, C.B., 1973. Behavioral implications of mechanistic ecology. *Oecologia*, *13*(1), pp.1-54.

Porter, W. P., & Gates, D. M. 1969. Thermodynamic equilibria of animals with environment. *Ecological monographs*, *39*(3), 227-244.

Preto, N., Kustatscher, E., & Wignall, P. B. 2010. Triassic climates—State of the art and perspectives. Palaeogeography, Palaeoclimatology, Palaeoecology, 290(1), 1-10.

Prochnow, S.J., Nordt, L.C., Atchley, S.C. and Hudec, M.R., 2006. Multi-proxy paleosol evidence for middle and late Triassic climate trends in eastern Utah. *Palaeogeography, Palaeoclimatology, Palaeoecology*, *232*(1), pp.53-72.

QGIS.org (2019). QGIS Geographic Information System. Open Source Geospatial Foundation Project. http://qgis.org

Qvarnström, M., Wernström, J.V., Piechowski, R., Tałanda, M., Ahlberg, P.E. and Niedźwiedzki, G., 2019. Beetle-bearing coprolites possibly reveal the diet of a Late Triassic dinosauriform. *Royal Society open science*, *6*(3), p.181042.

R Core Team. 2013. R: A language and environment for statistical computing. R Foundation for Statistical Computing, Vienna, Austria. URL http://www.R-project.org/.

Ramezani, J., Fastovsky, D.E. and Bowring, S.A., 2014. Revised chronostratigraphy of the lower Chinle Formation strata in Arizona and New Mexico (USA): high-precision U-Pb geochronological constraints on the Late Triassic evolution of dinosaurs. *American Journal of Science*, *314*(6), pp.981-1008.

Ray, S. and Chinsamy, A., 2003. Functional aspects of the postcranial anatomy of the Permian dicynodont Diictodon and their ecological implications. *Palaeontology*, *46*(1), pp.151-183.

Retallack, G.J., 2013. Permian and Triassic greenhouse crises. *Gondwana Research*, *24*(1), pp.90-103.

Rey, K., Amiot, R., Fourel, F., Abdala, F., Fluteau, F., Jalil, N.E., Liu, J., Rubidge, B.S., Smith, R.M., Steyer, J.S. and Viglietti, P.A., 2017. Oxygen isotopes suggest elevated thermometabolism within multiple Permo-Triassic therapsid clades. *Elife*, *6*, p.e28589.

Rial, R.V., Akaârir, M., Gamundí, A., Nicolau, C., Garau, C., Aparicio, S., Tejada, S., Gené, L., González, J., De Vera, L.M. and Coenen, A.M., 2010. Evolution of wakefulness, sleep and hibernation: from reptiles to mammals. *Neuroscience & Biobehavioral Reviews*, *34*(8), pp.1144-1160.

Ricklefs, R.E., Konarzewski, M. and Daan, S., 1996. The relationship between basal metabolic rate and daily energy expenditure in birds and mammals. *The American Naturalist*, *147*(6), pp.1047-1071.

Ricqlès, A. de, Padian, K., Knoll, F., and Horner. J.R. 2008. On the origin of high growth rates in archosaurs and their ancient relatives: complementary histological studies on Triassic archosauriforms and the problems of a "phylogenetic signal" in bone histology. *Annales de Paléontologie,* 94: 57–76.

Ricqlès, A.J., Padian, K. and Horner, J.R., 2003, April. On the bone histology of some Triassic pseudosuchian archosaurs and related taxa. In *Annales de Paléontologie* (Vol. 89, No. 2, pp. 67-101). Elsevier Masson.

Ruhl, M., Bonis, N. R., Reichart, G. J., Damsté, J. S. S., & Kürschner, W. M. 2011. Atmospheric carbon injection linked to end-Triassic mass extinction. Science, 333(6041), 430-434.

Sander, P.M. 2000.Seebacher, F., 2001. A new method to calculate allometric length-mass relationships of dinosaurs. *Journal of Vertebrate Paleontology*, *21*(1), pp.51-60.

Schachner, E.R., Irmis, R.B., Huttenlocker, A.K., Sanders, K., Cieri, R.L. and Nesbitt, S.J., 2020. Osteology of the Late Triassic Bipedal Archosaur Poposaurus gracilis (Archosauria: Pseudosuchia) from Western North America. *The Anatomical Record*, *303*(4), pp.874-917.

Scheyer, T.M., Desojo, J.B. and Cerda, I.A., 2014. Bone histology of phytosaur, aetosaur, and other archosauriform osteoderms (Eureptilia, Archosauromorpha). *The Anatomical Record*, *297*(2), pp.240-260.

Sellwood, B.W. and Valdes, P.J., 2006. Mesozoic climates: General circulation models and the rock record. *Sedimentary geology*, *190*(1-4), pp.269-287.

Sereno, P.C. and Arcucci, A.B., 1994. Dinosaurian precursors from the Middle Triassic of Argentina: Lagerpeton chanarensis. *Journal of Vertebrate Paleontology*, *13*(4), pp.385-399.

Seymour, R.S., 2013. Maximal aerobic and anaerobic power generation in large crocodiles versus mammals: implications for dinosaur gigantothermy. *PLoS One*, *8*(7).

Seymour, R.S., Bennett-Stamper, C.L., Johnston, S.D., Carrier, D.R. and Grigg, G.C., 2004. Evidence for endothermic ancestors of crocodiles at the stem of archosaur evolution. *Physiological and Biochemical Zoology*, *77*(6), pp.1051-1067.

Seymour, R.S. and Lillywhite, H.B., 2000. Hearts, neck posture and metabolic intensity of sauropod dinosaurs. *Proceedings of the Royal Society of London. Series B: Biological Sciences*, *267*(1455), pp.1883-1887.

Skoczylas, R., 1981. Thermoregulation in dinosaurs. In *Contributions to thermal physiology* (pp. 249-251). Pergamon.

Small, B.J., 1985. The Triassic thecodontian reptile Desmatosuchus: osteology and relationships (Doctoral dissertation, Texas Tech University).

Soberon, J., & Peterson, A. T. 2005. Interpretation of models of fundamental ecological niches and species' distributional areas.

Sookias, R. B., Benson, R. B., & Butler, R. J. 2012. Biology, not environment, drives major patterns in maximum tetrapod body size through time. *Biology letters*, *8*(4), 674-677.

Spielmann, J.A., Lucas, S.G. and Hunt, A.P., 2013. The first Norian (Revueltian) rhynchosaur: Bull Canyon Formation, New Mexico, USA. *New Mexico Museum of Natural History and Science Bulletin*, *61*, pp.562-566.

Spotila, J. R. 1980. Constraints of body size and environment on the temperature regulation of dinosaurs. In A cold look at warm-blooded dinosaurs (American Association for the Advancement of Science Selected Symposium 28). Westview, Boulder, Colo (pp. 233-252).

Spotila, J. R., Lommen, P. W., Bakken, G. S., & Gates, D. M. 1973. A mathematical model for body temperatures of large reptiles: implications for dinosaur ecology. *The American Naturalist*, *107*(955), 391-404.

Stevenson, R.D., 1985. The relative importance of behavioral and physiological adjustments controlling body temperature in terrestrial ectotherms. *The American Naturalist*, *126*(3), pp.362-386.

Stubbs, T.L., Pierce, S.E., Rayfield, E.J. and Anderson, P.S., 2013. Morphological and biomechanical disparity of crocodile-line archosaurs following the end-Triassic extinction. *Proceedings of the Royal Society B: Biological Sciences*, *280*(1770), p.20131940.

Sulej, T. and Niedźwiedzki, G., 2019. An elephant-sized Late Triassic synapsid with erect limbs. *Science*, *363*(6422), pp.78-80.

Thomas, C. D., Cameron, A., Green, R. E., Bakkenes, M., Beaumont, L. J., Collingham, Y. C., & Williams, S. E. 2004. Extinction risk from climate change. Nature, 427(6970), 145-148.

Træholt, C., 1995. Notes on the burrows of the water monitor lizard, Varanus salvator. *Malayan Nature Journal*, *49*, pp.103-112.

Ugalde, G.D., Müller, R.T., de Araújo-Júnior, H.I., Dias-da-Silva, S. and Pinheiro, F.L., 2018. A peculiar bonebed reinforces gregarious behaviour for the Triassic dicynodont Dinodontosaurus. *Historical Biology*, pp.1-9.

van de Schootbrugge, B. and Wignall, P.B., 2016. A tale of two extinctions: converging end-Permian and end-Triassic scenarios. *Geological Magazine*, *153*(2), pp.332-354.

Varricchio, D.J., Martin, A.J. and Katsura, Y., 2007. First trace and body fossil evidence of a burrowing, denning dinosaur. *Proceedings of the Royal Society B: biological sciences*, *274*(1616), pp.1361-1368.

Veiga, F.H., Soares, M.B. and Sayão, J.M., 2014. Osteohistology of hyperodapedontine rhynchosaurs from the Upper Triassic of Southern Brazil. *Acta Palaeontologica Polonica*, *60*(4), pp.829-836.

Walker, A.D., 1961. Triassic reptiles from the Elgin area: Stagonolepis, Dasygnathus and their allies. *Philosophical Transactions of the Royal Society of London. Series B, Biological Sciences*, *244*(709), pp.103-204.

Weather Spark Data 1: Average weather in Tamale, Ghana. https://weatherspark.com/y/42343/Average-Weather-in-Tamale-Ghana-Year-Round

Weather Spark Data 2: Average weather in Timbuktu, Mali. https://weatherspark.com/y/36520/Average-Weather-in-Timbuktu-Mali-Year-Round

Wedel, M.J., 2009. Evidence for bird-like air sacs in saurischian dinosaurs. *Journal of Experimental Zoology Part A: Ecological Genetics and Physiology*, *311*(8), pp.611-628.

Weinbaum, J.C., 2013. Postcranial skeleton of Postosuchus kirkpatricki (Archosauria: Paracrocodylomorpha), from the upper Triassic of the United States. *Geological Society, London, Special Publications*, *379*(1), pp.525-553.

Werner, J. and Griebeler, E.M., 2014. Allometries of maximum growth rate versus body mass at maximum growth indicate that non-avian dinosaurs had growth rates typical of fast growing ectothermic sauropsids. *PloS one*, *9*(2).

Westphal, M.F., Stewart, J.A., Tennant, E.N., Butterfield, H.S. and Sinervo, B., 2016. Contemporary drought and future effects of climate change on the endangered blunt-nosed leopard lizard, Gambelia sila. *PloS one*, *11*(5).

Whiteside, J. H., Grogan, D. S., Olsen, P. E., & Kent, D. V. 2011. Climatically driven biogeographic provinces of Late Triassic tropical Pangea. *Proceedings of the National Academy of Sciences*, *108*(22), 8972-8977.

Wickham, H. 2016. *ggplot2: Elegant Graphics for Data Analysis*. Springer-Verlag New York. ISBN 978-3-319-24277-4. https://ggplot2.tidyverse.org.

Withers, P.C. and Cooper, C.E., 2010. Metabolic depression: a historical perspective. In *Aestivation* (pp. 1-23). Springer, Berlin, Heidelberg.

Wolfe, J.L., Bradshaw, D.K. and Chabreck, R.H., 1987. Alligator feeding habits: new data and a review. *Gulf of Mexico Science*, *9*(1), p.1.

Wu Y, Wang H, Hadly EA. 2017. Invasion of ancestral mammals into dim-light environments inferred from adaptive evolution of the phototransduction genes. Scientific reports. 2017 Apr 20;7:46542.

Xing, L., McKellar, R.C., Xu, X., Li, G., Bai, M., Persons IV, W.S., Miyashita, T., Benton, M.J., Zhang, J., Wolfe, A.P. and Yi, Q., 2016. A feathered dinosaur tail with primitive plumage trapped in mid-Cretaceous amber. *Current Biology*, *26*(24), pp.3352-3360.

Xu, X., Zheng, X. and You, H., 2009. A new feather type in a nonavian theropod and the early evolution of feathers. *Proceedings of the National Academy of Sciences*, *106*(3), pp.832-834.

Yang, Z., Jiang, B., McNamara, M.E., Kearns, S.L., Pittman, M., Kaye, T.G., Orr, P.J., Xu, X. and Benton, M.J., 2019. Pterosaur integumentary structures with complex feather-like branching. *Nature ecology & evolution*, *3*(1), pp.24-30.

Zheng, X.T., You, H.L., Xu, X. and Dong, Z.M., 2009. An Early Cretaceous heterodontosaurid dinosaur with filamentous integumentary structures. *Nature*, *458*(7236), pp.333-336.

Chapter 2

Constraining torso dimensions in Mesozoic archosaurs

Abstract

To apply mechanistic niche modeling to extinct tetrapods it is necessary to constrain estimates of dimension and volume. Consensus methods exist for estimating head and tail proportions from complete fossil specimens, and organismal results are largely insensitive to errors in estimating limb volume. In contrast, errors in estimating torso dimensions have a disproportionate impact on overall organismal volumetric estimates. Here I demonstrate for the first time that missing singleton dorsal vertebra can be estimated to a high fidelity for Mesozoic archosaurs, though more complex models fail. I also show that typical 'mammal-style' vertical anterior ribs are limited almost entirely to mammals themselves. Improper rib angulation and anterior shifting of the pectoral girdle results in erroneously long torsos in archosaurs, increasing total organism volume estimates by 10% or more. Since rib angulation errors are widespread in literature reconstructions, museum mounts, and virtual specimens that are derived from them, this a largely unrecognized source of bias in volumetric mass estimates, and the paleobiological inferences that derive from them.

Introduction

Reconstructing the skeletal and life proportions of extinct vertebrates has been a goal since at least the late 18th century (Bru, 1796; Piñero, 1988; Rudwick, 1992), and it could be argued that earlier attempts ascribing legendary beasts to fossil remains were similarly, if less rigorously interested (Mayor, 2001 & 2007). As more complete skeletal remains were discovered, comparative anatomists produced surprisingly modern reconstructions of extinct mammals by the mid-19th century (Owen, 1860; Rudwick, 1993). Mesozoic archosaurs, and in particular Mesozoic dinosaurs traditionally lacked agreed-upon modern analogs to form the basis

of rigorous reconstructions, and attempts varied widely (e.g. Holland, 1906; Tornier, 1909; Hay, 1910; cf. Rudwick, 1992).

In the early 20th century as photographic equipment became more widespread a series of papers documenting mounts of Mesozoic vertebrates were published (e.g. Gilmore, 1912; Andrews, 1915; Gilmore, 1918 & 1932; Sternberg, 1942), but again there was a lack of consistency in assumptions about extant analogs, and therefore little consistency in the anatomical inferences of mounts, a trend that continued throughout the century (Carpenter et al., 1994; Vidal, et al., 2020). After the flurry of interest in newly mounted specimens, scientific interest in rigorously established proportions for Mesozoic archosaurs waned, and for the latter half of the 20th century was largely restricted to publications on volumetric mass estimates and center of gravity calculations (e.g. Colbert, 1962; Alexander, 1989, Paul, 1997). At the same time interest in establishing proportions in Mesozoic archosaurs became driven by the modernization of 'paleoart', as illustrators and artistically-inclined paleontologists attempted to bring more rigor to artistic reconstructions (Paul, 1987 and papers therein; Paul & Chase, 1989; Witton, et al., 2012).

As computing became faster and 3D digitizing became more accessible over the last two decades, the ability to produce 3D data sets from entire fossil skeletons, and to analyze the resulting 'virtual specimens' has become more common (e.g. Chapman, et al., 1999; Gunga, et al., 2007; Mallison, 2007; 2010a; 2010b; Hutchinson, et al., 2011). Advances in Light Detection and Range (LiDAR) scans and photogrammetry (Bates, et al., 2009; Stoinski, et al., 2011; Mallison & Wings, 2014; Das, et al., 2017) and the creation of searchable online repositories of digital datasets (e.g. DigiMorph.org; MorphoBank.org; MorphoSource.org) have accelerated the rate of 'virtual anatomy' publications analyzing proportions, volume, mass, muscle dynamics,

and center of gravity in Mesozoic archosaurs (Hutchinson, et al., 2011; Sellers, et al., 2012; Bates, et al., 2015; Clauss, et al., 2016).

The fundamental assumption underlying physiological modelling of extinct taxa is that basic proportions and volumes can be estimated reliably for extinct animals (Hartman, et al., 2015; Wang, et al., 2018; Lovelace, et al., 2020). For most body segments this appears reasonable. Skulls and mandibles closely approximate the overall dimensions of the head (Holliday, 2009; Nabavizadeh, 2020). Soft-tissue reconstructions of extinct tetrapod limbs are fairly conservative (Dilkes, 1999; Burch, 2015; Wang, et al., 2017), and volumetric modeling of extant tetrapods show that cranial and limb volume errors as a fraction of overall mass have a minor impact on the final mass of the model (Paul, 1997). Neck volumes in non-sauropod Mesozoic archosaurs are small enough that disagreements in modeling rarely have a large impact on final volume (Paul, 1997). Tails are straightforward to model when known from reasonably complete material (Persons & Currie, 2010; 2011; Mallison, et al., 2015; Snively, et al., 2019), and the problems with incomplete tails are being addressed elsewhere (Junchang & Hone, 2012; Hone, 2012; Hone, personal communication).

More problematic is constraining dimensions and volume of the torso in Mesozoic archosaurs. The torso makes up the majority of volume in the tetrapod bauplan, exceeding 50% of total volume in most tetrapod taxa (Talbot & McCulloch, 1965; Paul, 1997; Hutchinson, 2011), so relatively small errors in reconstructing torso dimensions can have large consequences in estimating an organism's mass and center of gravity (cf. Bates, et al., 2015). This is a challenge not just for mechanistic physiological modeling, but to many paleobiology research topics as mass is a fundamental arbiter of growth rates (Myhrvold, 2016), specific metabolic rate (McNab, 2009), carrying capacity (Kooijman, 2000), locomotion cost (Dececchi, 2020) and

dynamics (Gatesy, et al., 2009; Hutchinson, et al., 2011), the thermodynamics of epidermal insulation (Steudel, et al., 2014), inertial properties (Henderson, 1999), etc.

Methodological barriers to testing comparative torso interpretations

Explicit testing of competing anatomical inferences that impact torso dimensions would allow researchers to quantify those differences, and with time perhaps a broader consensus would emerge. A recurring methodological challenge to this process when estimating torso dimensions the last two decades is the emphasis on overly-simple meshes created via LiDAR scans (Bates, et al., 2009; Sellers et al., 2012;) or photogrammetry (Clauss et al., 2016; Brassey, et al., 2015) of mounted skeletons. To speed up processing and analysis, the resulting digitized point clouds are frequently processed into a single mesh consisting of the entire skeleton, or broken into a couple of large chunks (cf. Clauss, et al., 2016) positioned according to the unmanipulated spatial data from the mount. Crucially, this results in torso elements maintaining the same spatial configuration as the original mount (e.g. Bates, et al., 2009; Sellers, et al., 2012; Clauss et al., 2016) without the possibility of moving individual torso elements to test competing hypotheses or to account for improperly estimated missing data that may be part of the mounted specimen. This process has been lauded as fast and repeatable, but it also captures all errors and assumptions inherent in the mount, which are then passed on to the analysis when used as the basis for computational volumes (Sellers, et al., 2012).

It should hardly need stating, but museum mounts are not equivalent to CT scans of extant taxa (cf. Carpenter et al., 1994; Carpenter, 1997). This is especially true with Mesozoic archosaurs, not only because they have historically had wider-ranging debates about anatomical interpretation than Neogene mammals (e.g. compare Wood, 2006 vs Schwartz, et al., 2007), but because they are subject to additional errors due to their size and taphonomy. The incomplete

nature of many Mesozoic archosaur remains (Dodson, 1990; Hone, 2012; Taylor, 2015) make Mesozoic archosaur mounts more likely to be composites of multiple specimens and/or or to have extensive artistic reconstruction of missing bones (Carpenter et al., 1994; Hutchinson, et al., 2011; Vidal, et al., 2020). The delicate nature and sheer size of many Mesozoic archosaur specimens makes the physical act of supporting museum mounts challenging, and armatures are necessarily designed with safety and accessibility placed at a premium over anatomical concerns (Carpenter et al., 1994; Carpenter, 1997; Meiri, 2004; Mallison, 2010a; 2010b), and if delicate vertebral elements are replaced with more robust artistic sculptures major errors can be added to a mount (e.g. Paul, 1988).

The data presented by Clauss, et al. (2016) provide evidence of inconsistency within Mesozoic archosaur museum mounts. Their methodology consisted of projecting convex hull bounding volumes on photogrammetrically reproduced museum mounts. With scans of Neogene mammals they found predictable diet and allometry-based differences in torso scaling relative to size that were expected on physiological grounds (Claus, et al., 2016). In contrast, Clauss et al. (2016) found no pattern based on ecomorph or size for their Paleozoic and Mesozoic taxa. While it cannot be ruled out that non-mammal amniotes simply do not follow the same volumetric relationships (cf. Lavin, et al., 2008), it seems unlikely that they follow no pattern at all. The dataset, the most complete sample of virtual skeletons to date (n=126 specimens) cannot be tested with alternate anatomical configurations, nor with attempts to account for postmortem distortion as the torsos are single mesh objects.

This is not a problem inherent to virtual data sets but a reflection of choices made about digitizing and processing. Chapman, et al. (1999), Hartman & Shinkle (2006), Mallison (2010b; 2010c) and Brassey, et al. (2015) digitized and processed individual bone elements, so each

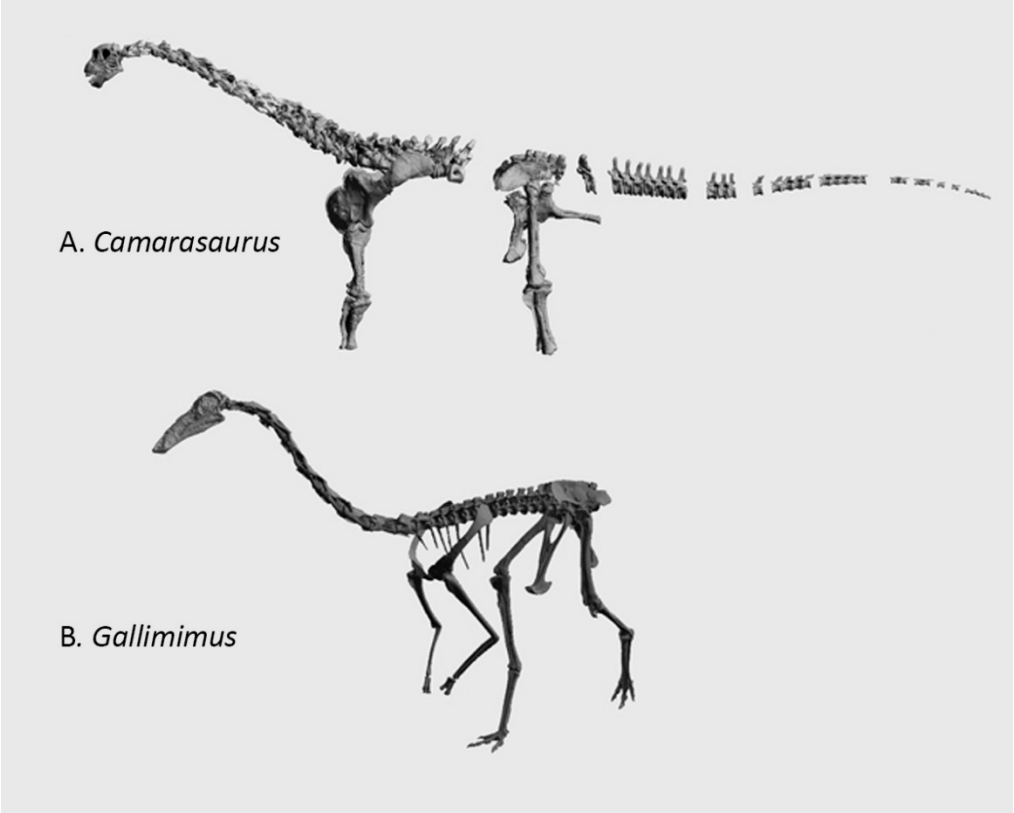

Fig. 2-1. Virtual skeletons produced by a small team at the Wyoming Dinosaur Center. *Specimens were scanned with a Steinbichler T-SCAN laser wand tracked by an Optotrak 3020 optical positioning unit. Point meshes of individual fossil elements were processed in Polyworks and placed into anatomical positions in (the now defunct) Softimage XSI.*

virtual element can be individually manipulated to test competing anatomical inferences (cf. Mallison, 2010a & 2012b). While this added complexity takes more time, digitizing, processing, and manipulating elements into skeletons can be achieved by individuals or small teams, even at small museums in a reasonable amount of time (cf. Shinkle & Hartman, 2006; Mallison, 2010a; Fig. 2-1).

Interpretive barriers to robust estimates of torso dimensions

I define "torso" for purposes of this paper as the body segment of an organism that extends from the anterior-most extent of the pectoral girdle to the posterior extent of the gut

cavity – in archosaurs this is generally the anterior surface of the pubes or (with some ornithischians) ischia (Macaluso & Tschopp, 2018). In crown group Aves the digestive tract continues to the posterior end of the ischia, extending the "torso" beyond the legs, but crown Aves are beyond the scope of this project and are generally not subject to the same uncertainties of estimation regarding torso anatomy. The relevant avian morphological changes occur very close to the avian crown, so the condition can be ignored for Mesozoic archosaurs (Hutchinson, 2001).

A key element of estimating torso dimensions is the length of the vertebral column. While it seems straightforward to measure a complete series of dorsal vertebrae, it is complicated by the absence of unpreserved soft tissue in the form of intervertebral cartilage, which in extant taxa can increase portions of vertebral column length from ~4% all the way up to 24% in some juveniles (Taylor & Wedel, 2013; Taylor, 2014). Recent CT examination of pathologically fused tail vertebrae in a hadrosaurian dinosaur suggests a quite small amount of intervertebral cartilage (Rothschild, et al., 2019), but since alligators and birds vary in the type of intervertebral articular tissue in different portions of their vertebral column (Taylor & Wedel, 2013), it is not clear how well this would generalize to other Mesozoic archosaurs. Intervertebral cartilage thickness appears to vary more in young animals, and especially in the cervical column (Taylor & Wedel, 2013; Taylor, 2014), so while an important aspect for estimating neck posture and length, it will not be addressed further here. A second challenge with measuring the length of vertebral columns stems from missing elements. Published reconstructions of missing vertebral elements can vary widely in the length of missing or cross-scaled vertebrae (e.g. Ibrahim, et al., 2014; Bates, et al., 2015), so a method for modeling missing elements is presented below.

Within Mesozoic archosaurs the pelvis is fused to the sacrum and generally immobile, so there is little debate over how pelvic girdle anatomy effects torso shape (Carrier & Farmer, 2000; Hutchinson, 2001; Claessens, 2004). While pectoral girdle orientation has been debated for some quadrupedal dinosaurs (e.g. Paul, 1987; Wood, 2006; Schwartz, et al., 2007), volumetric modeling demonstrates pectoral girdle orientation itself has a minor impact on torso dimensions in Mesozoic archosaurs (Paul, 1997; Hartman, 2012). This is because archosaurs retain the primitive tetrapod condition of a pectoral girdle tightly interlocked with sternal elements that are seated firmly against the rib cage (Burke, 1991; McGonnell, 2001; Remes, 2008; Claessens, 2015), so regardless of orientation the entire girdle still sits in roughly the same position relative to the anterior textent of the ribcage (Fig. 2-2). The fit of the pectoral girdle onto the rib cage,

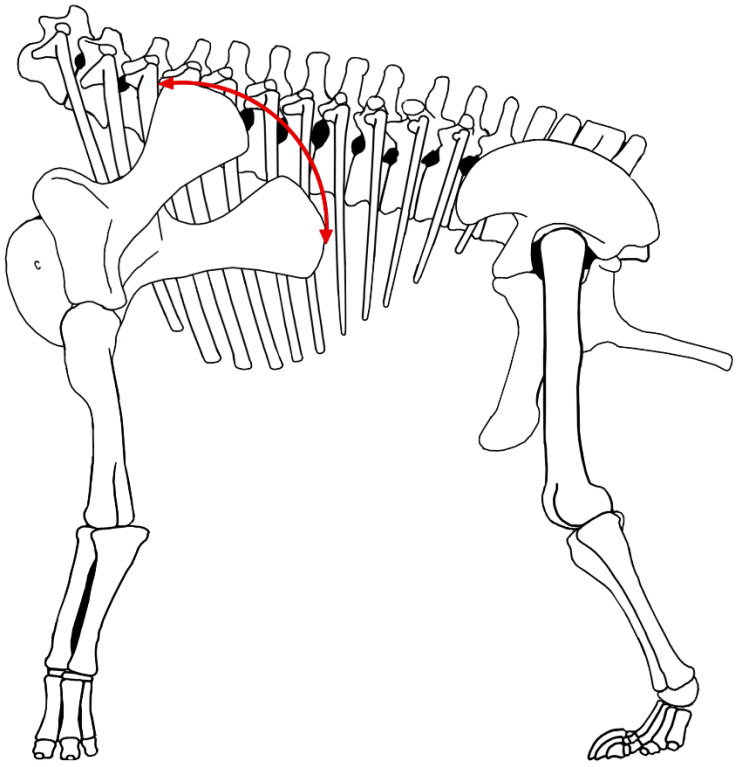

Fig. 2-2. Scapular orientation has minimal influence on torso dimensions. *While interpretations of sauropod scapular orientation have varied from nearly vertical (Schwartz, et al., 2007) to horizontal (Wood, 2006), they are still constrained to sit up against the rib cage, so have minimal impact on overall torso dimensions.*

however, is strongly influenced by the inferred angulation of anterior ribs (Paul, 1997; Remes, 2008; Hartman, 2012). The amount of difference in pectoral girdle displacement due to rib orientation, and therefore overall torso dimensions is non-trivial. Figure 2-3 shows a series of rigorous skeletal reconstructions of *Camarasaurus lentus* (methodology as described in Wang, et al., 2017; modified after Paul & Chase, 1989) utilizing a series of competing interpretations of anterior rib orientation, ranging from vertical to strongly angled posteriorly. Even if all else was held equal, the difference in rib angulation results in torso length increase of 87 cm from 265 to 352 cm. *Camarasaurus* is a fairly wide-bodied animal, so at a height of 220 cm if approximated as a cylinder for use in Niche Mapper (Chapter 1; Lovelace, et al., 2020) the increase in torso volume would be 13.4 m^3 vs 10.1 m^3. In most cases this is probably an underestimate of the difference; because archosaur ribs are double headed and the heads articulate at an oblique angle on the vertebrae (Paul, 1997; Brocklehurst, et al., 2017; Brocklehurst, et al., 2019), so angling ribs anteriorly also rotates them outwards, broadening the ribcage and further inflating torso volume.

Explicit consideration of rib angulation in Mesozoic archosaurs based on articulated remains has generally reached the conclusion that anterior ribs were swept posteriorly (Carpenter, 1984; Paul, 1987; 1997; Remes, 2008; Paul, 2019), but it has not reached widespread acceptance in mounted specimens nor in studies of virtual specimens (Bates, et al., 2009; Hutchinson, et al., 2011; Stoinski, et al., 2011; Sellers, et al., 2012; Bates, et al., 2015; Clauss, et al., 2016). In published analyses of multiple virtual specimens, variation in rib angulation may vary strongly between specimens (e.g. Hutchinson, et al., 2011; Clauss, et al., 2016), resulting in a clear source of error when comparing masses or center of gravities between species and/or individuals.

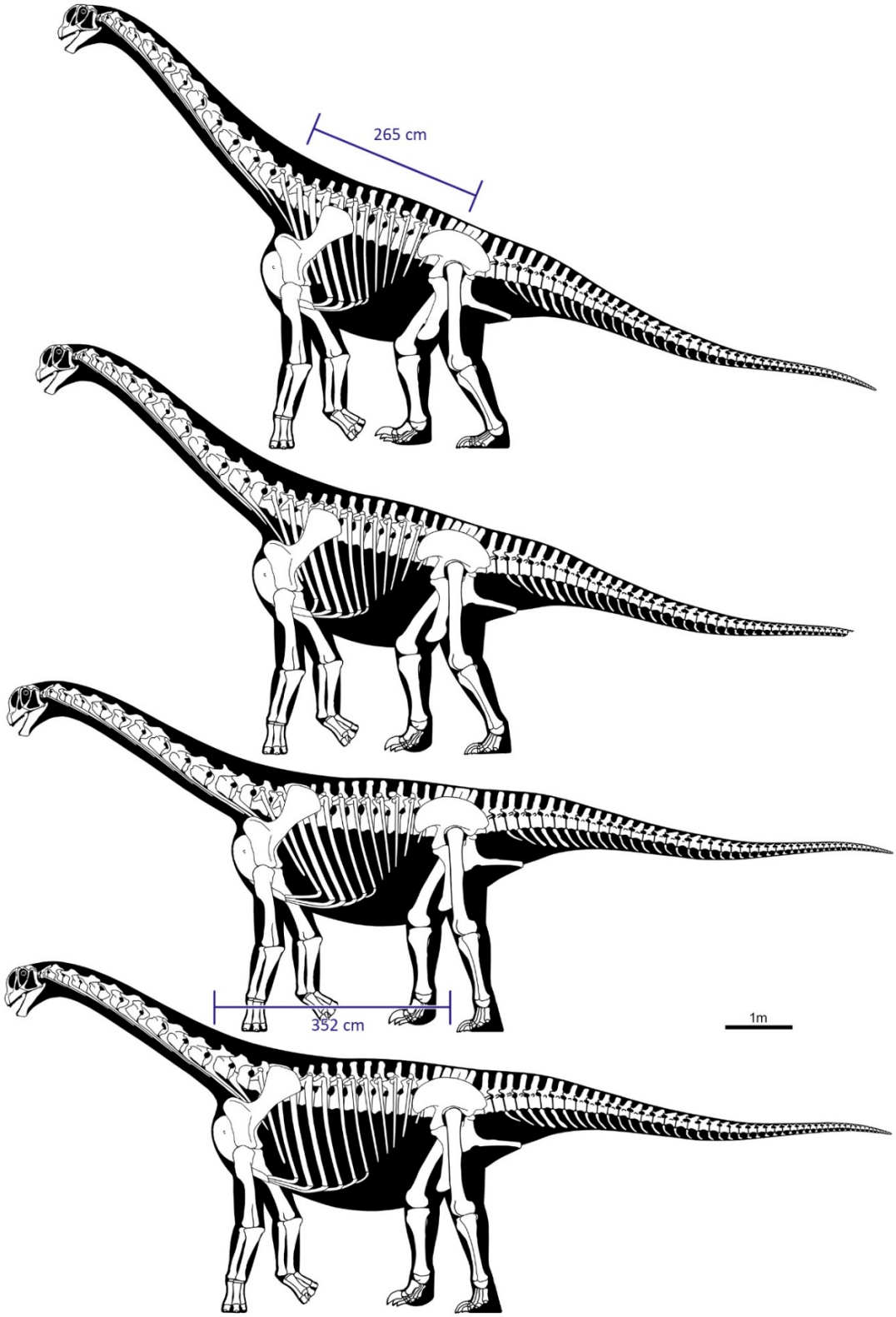

Fig. 2-3. Impact of rib angulation on torso proportions in Camarasaurus lentus. *As anterior ribs become more vertical (from top to bottom) the pectoral girdle must move anteriorly, increasing torso length by 87 cm.*

Even in living vertebrates quantifying rib angulation is difficult. Non-invasive 2D data collection like X-rays are imperfect representations of a curved 3D structure, and even with CT scan data finding repeatable landmarks is difficult, and is currently explored predominantly for modeling pathological medical conditions in humans (e.g. Klinder, et al., 2007; Wang, et al., 2016). While the rib cages of mammals are challenging to model (Streat, 2018), in archosaurs the rib cage moves extensively during respiration (Brocklehurst, et al., 2017; 2019) making it more difficult to establish base conditions. Yet it remains important to rule out unlikely rib angulations to reduce the amount of error in virtual specimens and provide solid phylogenetic context to rib angulation where possible.

I evaluated two methods for estimating missing vertebral data, a segmented regression model and a simple averaging of surrounding vertebrae. I find Mesozoic dinosaur dorsal vertebrae are not amenable to regression modeling approaches, but estimating singleton missing vertebral length data via simple averaging shows robust correlation with real measurements, providing a concrete method of restoring missing data in some scenarios. I also expand on existing descriptive work of rib angulation in tetrapods to provide a wider phylogenetic framework for understanding rib angulation in Mesozoic archosaurs, and demonstrate that incorrect rib angulation significantly increases mass their estimates.

Methods

Estimating missing vertebral data

I compiled a dataset (Suppl. S.2-1) of vertebral length measurements for 15 extant taxa (1 mammal, 1 tuatara, 2 lizards, 4 alligators and 7 birds) and 26 extinct taxa (1 basal saurischian, 9 theropods, 14 sauropodomorphs and 2 ornithischians). Measurements taken in person were

measured in an anteroposterior direction along the centrum using digital calipers and rounded to the nearest tenth of a millimeter. This was supplemented by literature values (listed in S.2-1), which are recorded to the same level of precision as presented in their original papers, though converted to millimeters as necessary for consistency.

Initial data exploration confirmed qualitative observations that vertebral lengths do not follow a simple linear trend of increasing or decreasing vertebral length along the dorsal column. Since at least some taxa (e.g. *Sinraptor*, Fig. 2-4) appeared to exhibit a clear breakpoint in vertebral length scaling, I employed segment regression (aka 'broken line regression') in R (R Core Team, 2013) to generate an initial general linear model regression of vertebral length against vertebral column position. This was used as an input in the R package *segmented* (Muggeo, 2017) to apply a Davies' test to see if there was a break point. The Davies' test method was used as it is the most appropriate for small sample sizes (Muggeo, 2017). The resulting data was plotted, along with break point position (if any), trend lines and r-squared values.

I also ran a simple estimation model appropriate for individual missing vertebral elements surrounded by elements of known length in adjacent positions. The estimated element length was calculated as the average of the two surrounding elements. To test the efficacy of this simple method of estimation against known values a replacement length was calculated for every vertebral measurement collected, except for the first and last vertebrae in each column, since cervical and sacral values were not always available and edge effects from using adjacent developmental segments could potentially skew results. This resulted in 318 estimated lengths paired with measured vertebral lengths. These were organized into a data frame by biological group (Suppl. S.2-2), including all-extant taxa, all-extinct taxa, and standard dinosaurian clades

(due to their shift from bipedal to quadrupedal locomotion sauropodomorphs were further subdivided into quadrupedal eusauropods and a separate grade of bipedal 'prosauropods').

Utilizing the general stats package in R, a regression was run against each group of real and estimated vertebral length values to ensure there was a linear relationship between real and estimated values. Each subgroup's real and estimated length data were subjected to a Shapiro-Wilks normality test and, since several of the data sets are large, were also plotted as Q-Q plots. Since all but one dataset failed normality testing, Spearman's correlation r was calculated for each group to test the strength of correlation between real and estimated vertebral lengths.

Rib angulation

To provide broader phylogenetic context for rib angulation I used non-invasive data sets for extant specimens, include CT scan data available from Morphosource.org and Digimorph.com, supplemented with photos supplied by commercial producers of diaphonized specimens. Diaphonization is a process of selective staining and chemical alteration that can provide an unobstructed view of bones or other internal elements in otherwise whole specimens (cf. Oommen, 2015). For extinct taxa this was supplemented by photos and literature reports of exceptionally well-preserved taxa.

To quantify the impact of competing interpretations of rib angulation I used double graphic integration (GDI; Jerison, 1973; Murray & Vickers-Rich, 2004) to estimate the mass of 3 dinosaur taxa, *Tyrannosaurus, Giganotosaurus,* and *Dreadnoughtus.* All three were selected because they have previously been part of mast estimate debates (Calvo, 2000; Hutchinson, et al., 2011; Bates, et al., 2015; Paul, 2019). GDI requires orthogonal outlines in dorsal and lateral view, which are broken into a series of evenly spaced slices and measured for width and height.

Each slice is treated as an ellipse, which allows for calculation of average cross-sectional area per body segment, which is then multiplied by the length of each body segment. Depending on the complexity of shape in the organism's outline, 30-50 slices were measured along the anteroposterior axis using the Photoshop measure tool, along with an additional 6-7 slices per limb (Suppl. S2-4). Applying literature-derived specific gravities to each volume provides mass estimates for each individual segment, as well as the entire organism.

Orthogonal views were prepared following a modified protocol detailed in Wang, et al., 2017 (which itself was adapted from Paul & Chase, 1989). Orthogonal views were produced using Photoshop CC versions 20 & 21. Individual bones were scaled based high-resolution photos exhibiting minimal parallax. Where possible virtual scaling was set according to scale bars photographed in the same plane as the specimens, using Photoshop's Custom Scaling tool (Image -> Analysis -> Set Measurement Scale), otherwise they were scaled according to published measurements. Bones were illustrated so that individual measurements end at the edge of the white portion of the bone, as opposed to the middle or outside of the black bounding line. Limb posture is informed by Hutchinson & Gatesy, (2000) and Gatesy (2002), while soft-tissue depths for silhouettes was drawn from literature and dissections.

Results

Vertebral length results

Results from segmented linear regression of vertebral length vs vertebral position are presented in Figures 2-4 and 2-5. Vertebral series were found to either be absent a breakpoint (n=2), or to have a single breakpoint (n=14), resulting in two fitted lines per series of dorsal vertebrae. For the dinosaurian taxa analyzed it is clear no generalizable segmented linear model

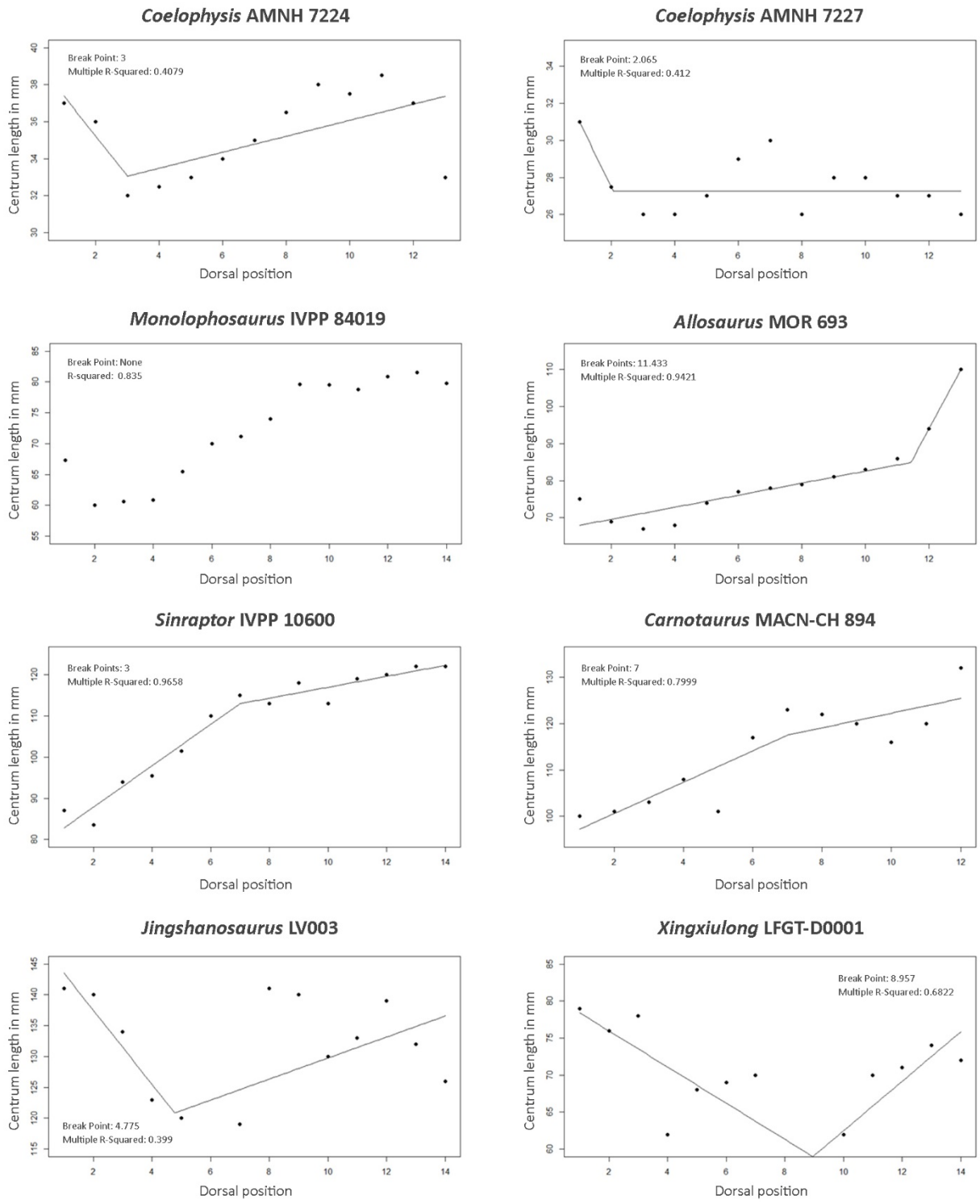

Fig. 2-4. Results of segmented linear regression of dorsal vertebral lengths vs vertebral position. *The first 6 taxa are theropods, the bottom two are 'prosauropods' (non-eusauropod sauropodomorphs).*

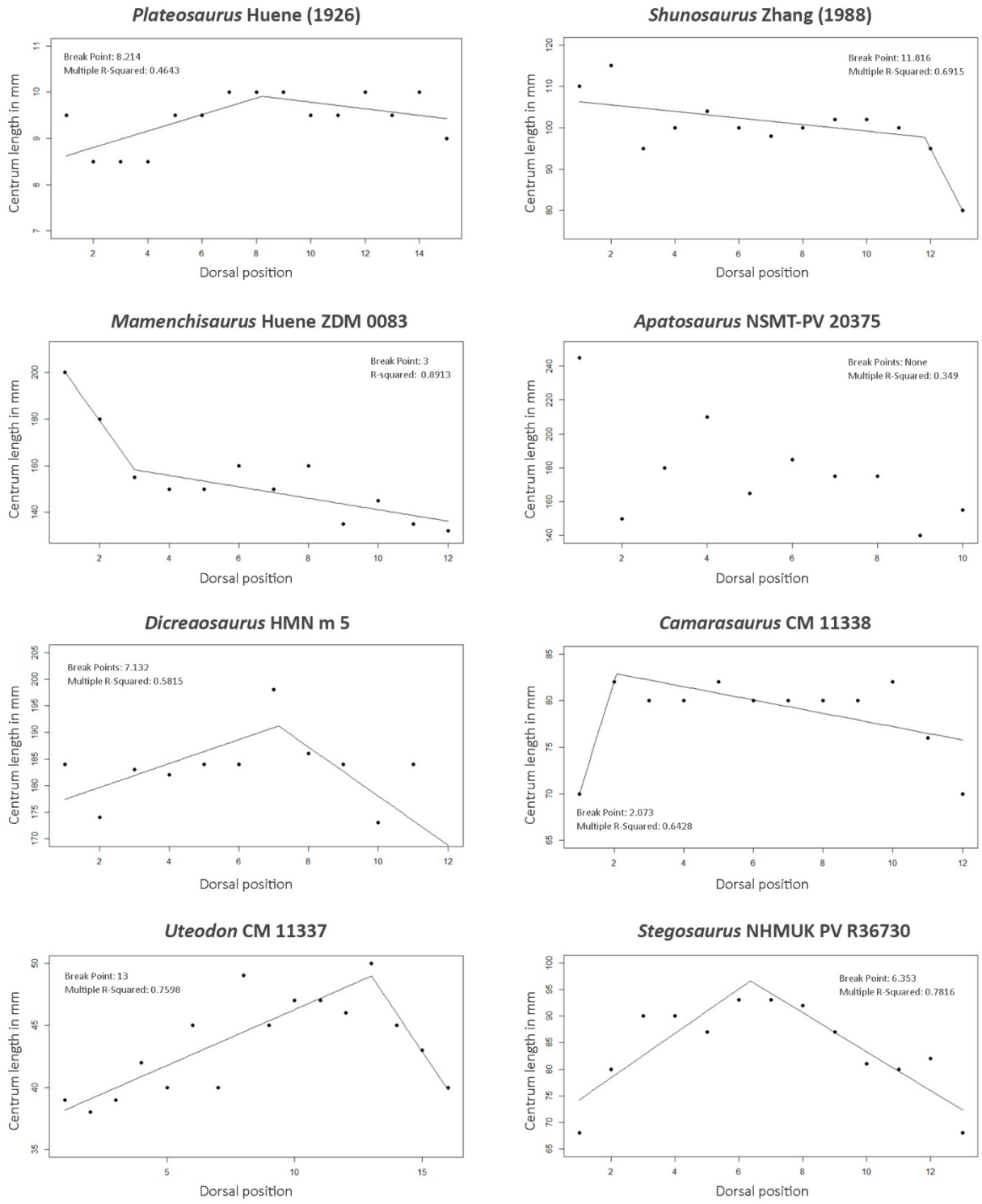

Fig. 2-5. Additional results of segmented linear regression of dorsal vertebral lengths vs vertebral position.
Plateosaurus is a 'prosauropod', Uteodon and Stegosaurus are ornithischians, remaining taxa are eusauropods.

Table 2-1. Summary statistics for correlation analysis of 'simple model' estimated vertebral lengths and actual vertebral lengths.

Clade	n pairs	p-value	Spearman's R
Extant combined	90	2.20E-16	0.9790
Extinct combined	228	2.20E-16	0.9931
Theropoda	74	2.20E-16	0.9950
'Prosauropods'	50	2.20E-16	0.9303
Eusauropoda	81	2.20E-16	0.9222
Ornithischians	23	8.43E-09	0.8948

can be fit to all taxa. There also is no apparent phylogenetic pattern, whether between close relatives (e.g. *Sinraptor* and *Allosaurus*, Fig. 2-4) or even among members of the same species (*Coelophysis*, Fig. 2-4) there was no consistency to either the position of the breakpoint nor the angle of the slopes of each segment.

Turning to the 'simple model' for estimating missing singleton vertebral lengths by averaging surrounding vertebrae, a summary table of Pearson's r for estimated vs real vertebral lengths can be found in Table 2.1. All groups were found to have highly significant results (p-values of 8.43E-09 or lower) and strongly correlate (0.8948 or higher). The correlation between real and estimated vertebral lengths of all dinosaurs combined (Pearson's r = 0.9931) was stronger than the correlation for all extant species (0.9790). 'Prosauropods' (non-eusauropod sauropodomorphs), eusauropods and ornithischians were somewhat less strongly correlated, although even at the lowest value of 0.8948 the estimated vertebral lengths were highly correlated with the real ones. Linear regressions of estimated vs real (i.e. measured) vertebral lengths are plotted in figures 2-6 and 2-7.

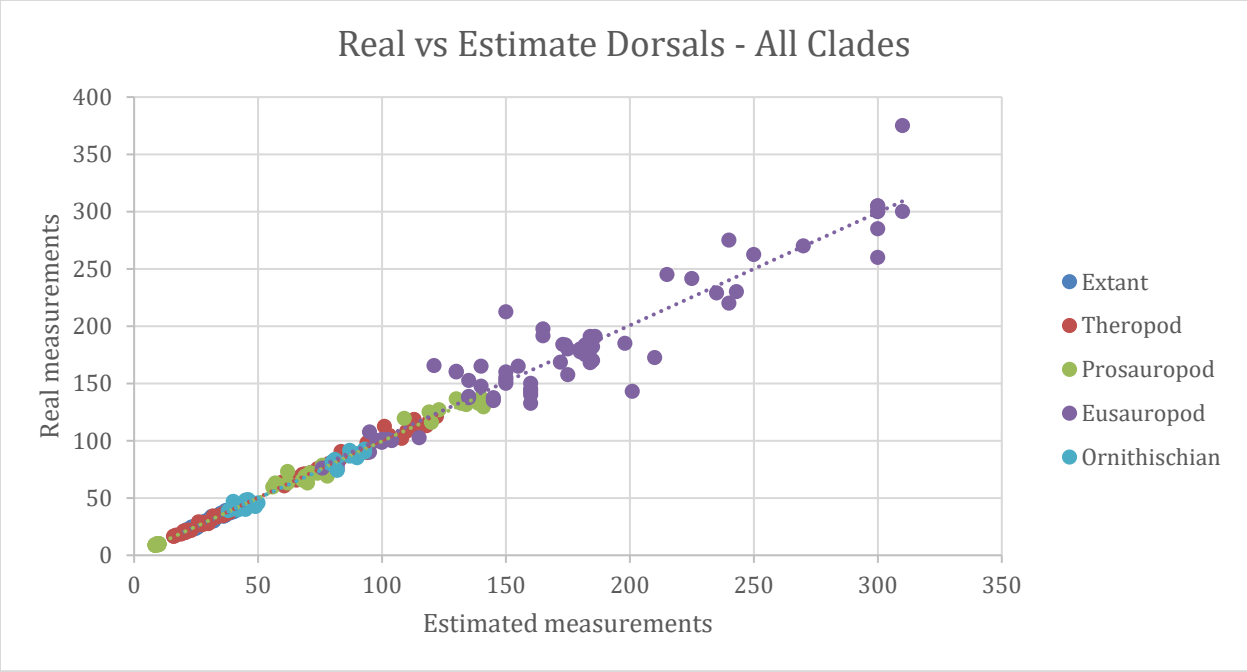

Fig. 2-6. Linear regression of 'simple model' estimated vertebral lengths vs their real counterparts. *All sub-groups plotted. Sauropod vertebrae are so large they compress other group results into the lower left of the diagrams.*

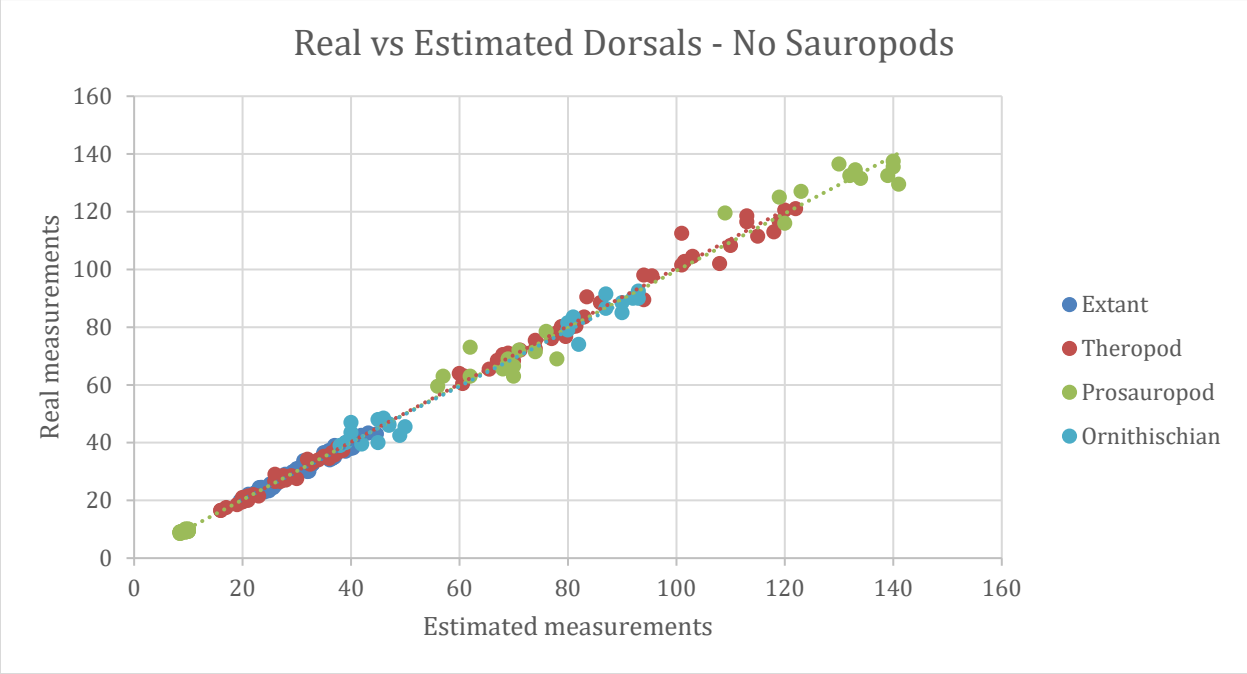

Fig. 2-7. Linear regression of 'simple model' estimated vertebral lengths vs their real counterparts*. Plotted without eusauropods to improve legibility of other results.*

Rib angulation results

Basal tetrapods and outgroups

Fish clades are highly variable, with the potential for no ribs in some taxa, and two sets (a dorsal and ventral set) of ribs in some actinopterygians (Romer, 1974). Angulation in the ventral ribs of actinopterygians is also variable, although many have anterior ribs with a posteriorly swept angulation, it is not universal (Fig. 2-8). Moving closer to tetrapods, actinistian and dipnoan ribs generally do not ossify, although the Triassic actinistian *Diplurus* had a surprisingly ossified skeleton for a coelocanth relative (Schaeffer, 1952), and rib angulation is strongly backswept (Fig. 2-9A). A survey of stem tetrapods shows all specimens sufficiently prepared or non-invasively scanned from elpistostegids to ichthyostegids to diadectimorphs all show strong, consistent posterior angulation of the ribs (Fig. 2-9, cf. Watson, 1918; Coates, 1996; Kennedy, 2010; Pierce, et al., 2012). Although stem tetrapods are often restored with vertically aligned anterior rib angulation, it is not supported by articulated remains.

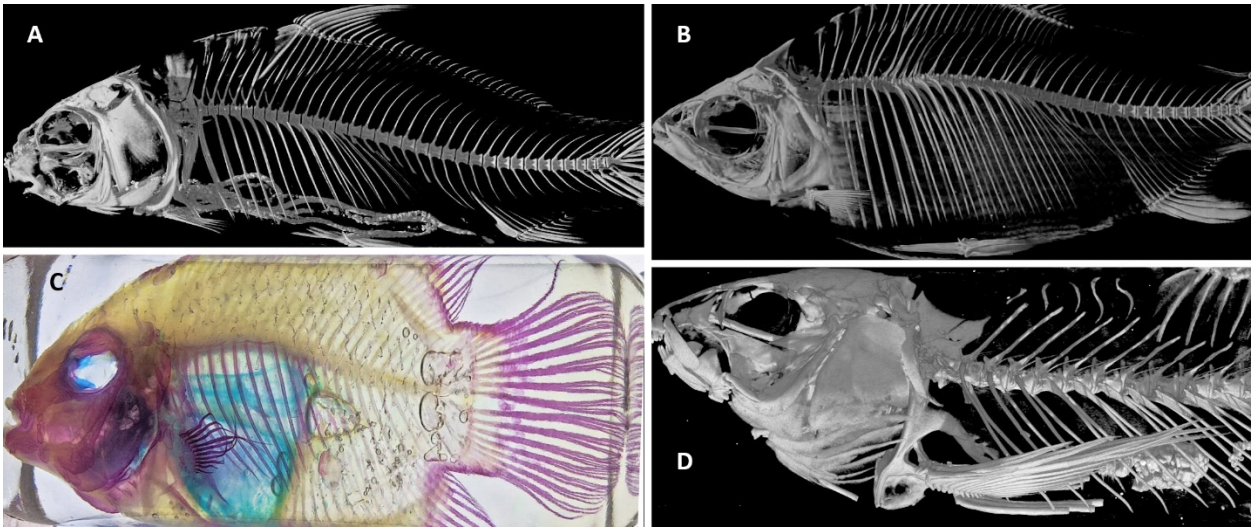

Fig. 2-8. Examples of actinopterygian fish rib angulation. *A. CT scan data of Carpiodes (DigiMorph Staff, 2016); B. CT scan data of Xenocharax (Humphries, 2006); C. Diaphonized parrot cichlid, courtesy Elliott Gustafson; D. CT scan data of Characidiumseen (DigiMorph Staff, 2010).*

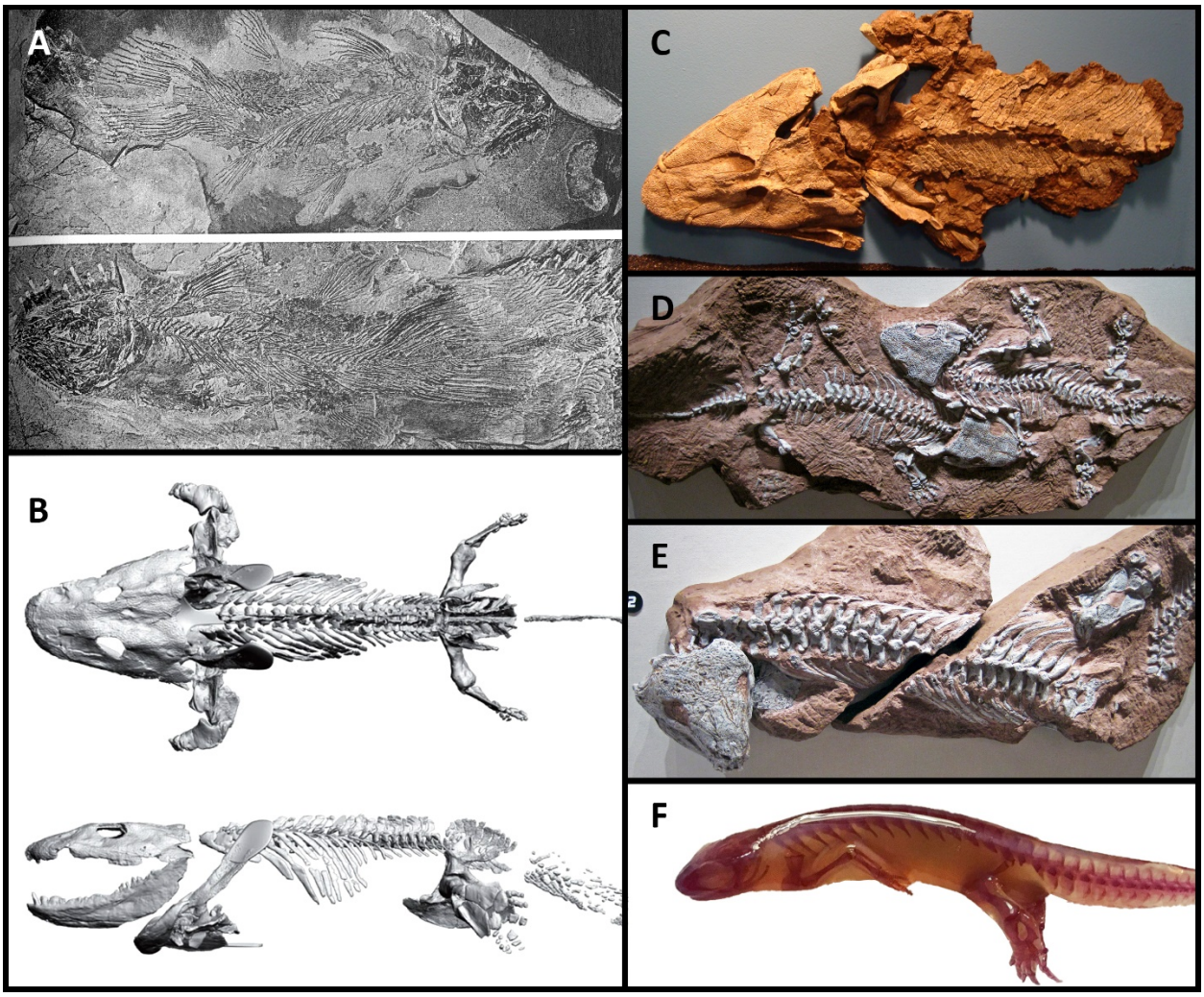

Fig. 2-9. Rib angulation in rhipidistians. *Anterior dorsal ribs are swept posteriorly in Diplurus (A) a Triassic coelacanth (Schaeffer, 1952), stem-tetrapods Ichthyostega (B, Pierce, et al., 2012) Tiktaalik (C, Solà, 2012), Seymouria (D, St. John, 2011), Diadectes (E, St. John, 2011) and extant salamanders (F, courtesy Darwin and Wallace Store).*

Non-archosaur diapsids

Moving closer to Archosauria, non-archosaur diapsids are known from extensive extant (squamates, testudines, and *Tuatara*) and fossil examples. Extant diapsids generally exhibit a uniform pattern of rib angulation with the anterior ribs angled posteriorly, and in most species all ribs angled posteriorly (Fig. 2-10). Turtle ribs, which fuse onto their carapace are highly modified from the general diapsid condition (Hirasawa, 2013; Wang, 2013), with anterior dorsal

ribs angled anteriorly, middorsal ribs angled laterally, and posterior ribs angled posteriorly. This condition is herein not considered a good model for archosaurs, and the Permian stem-turtle *Eunotosaurus* has anterior ribs which are also angled strongly posteriorly (Lyson & Bever, 2013). Extant snakes show a large degree of angular motion in their ribs during rectilinear motion (Lissmann, 1950), but it appears to be different degrees of posteriorly angulation, and the neutral position adopted when not in motion is also swept posteriorly (Fig. 2-10E). While fossils

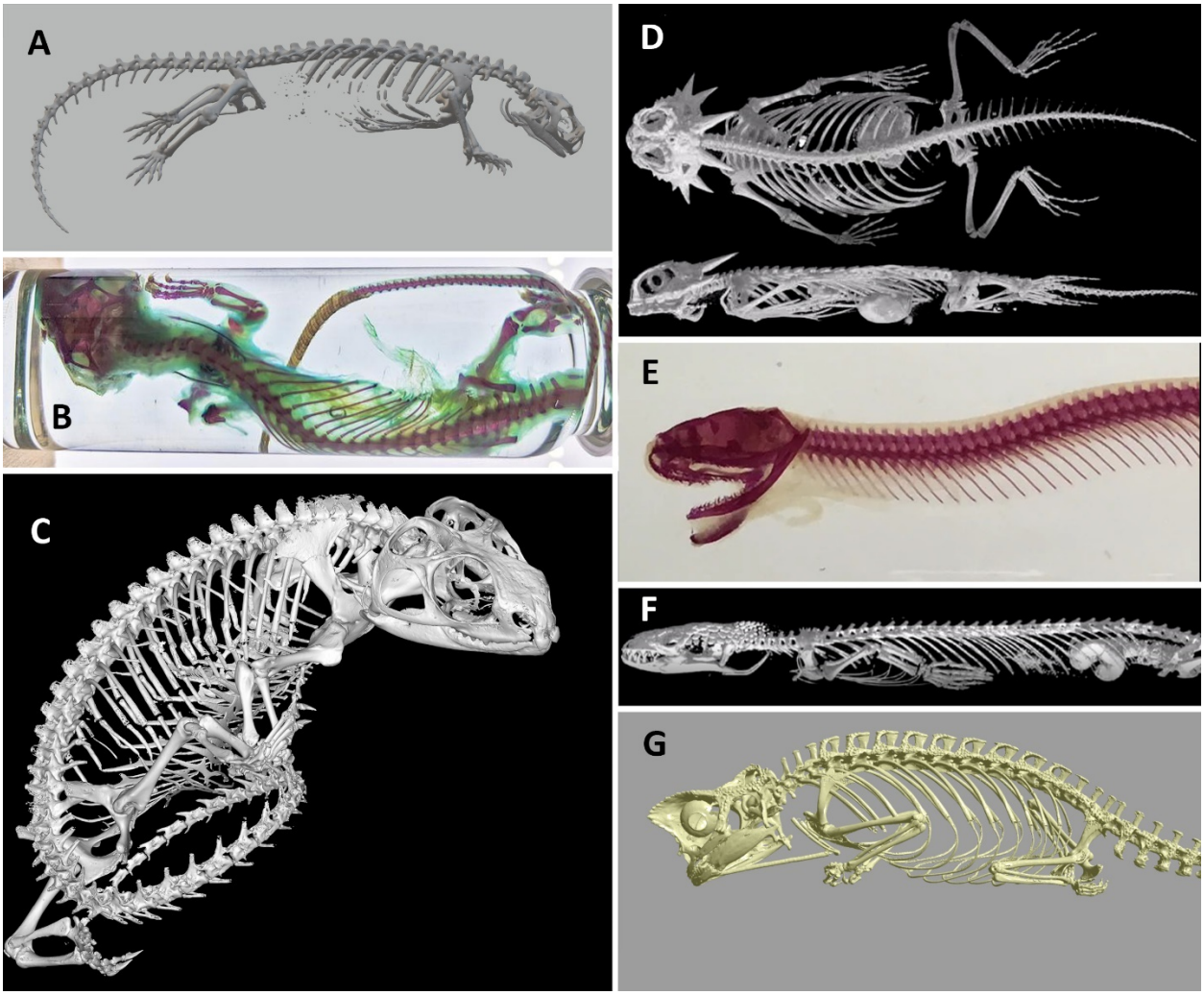

Fig. 2-10. Rib angulation in non-archosaur diapsids. *Outside of turtles (see text) posteriorly swept ribs appear to be universal among living non-archosaur squamates such as Moloch (A, Pianka, 2003), Varanus (B, courtesy Elliott Gustafson), Phrynosoma (D, Hodges, 2001), Neroidia (E, courtesy Darwin and Wallace Store), Heloderma (F, Bonine, 2005), and Brookesia (G, MorphoSource[1]). It is also the condition in Tuatara (C, courtesy John Hutchinson).*

run the risk of distortion relative to non-invasive examination of extant taxa, articulated specimens of fossil taxa show a similar pattern, including the neodiapsid *Younginia* (Ezcurra, 2016), the archosauriforms *Euparkeria* and *Proterosuchus* (see Fig. 15 of Ezcurra, 2016), and the rhynchosaur *Hyperodapedon* (Benton 1983). Strongly backswept anterior ribs are also found in well-preserved specimens of aquatic taxa such as the plesiosaur *Rhomaleosaurus* (Smith & Benson, 2014) and ichthyosaurs like *Ichthyosaurus* (Lomax & Massare) and *Stenopterygius* (e.g. Maxwel, 2012).

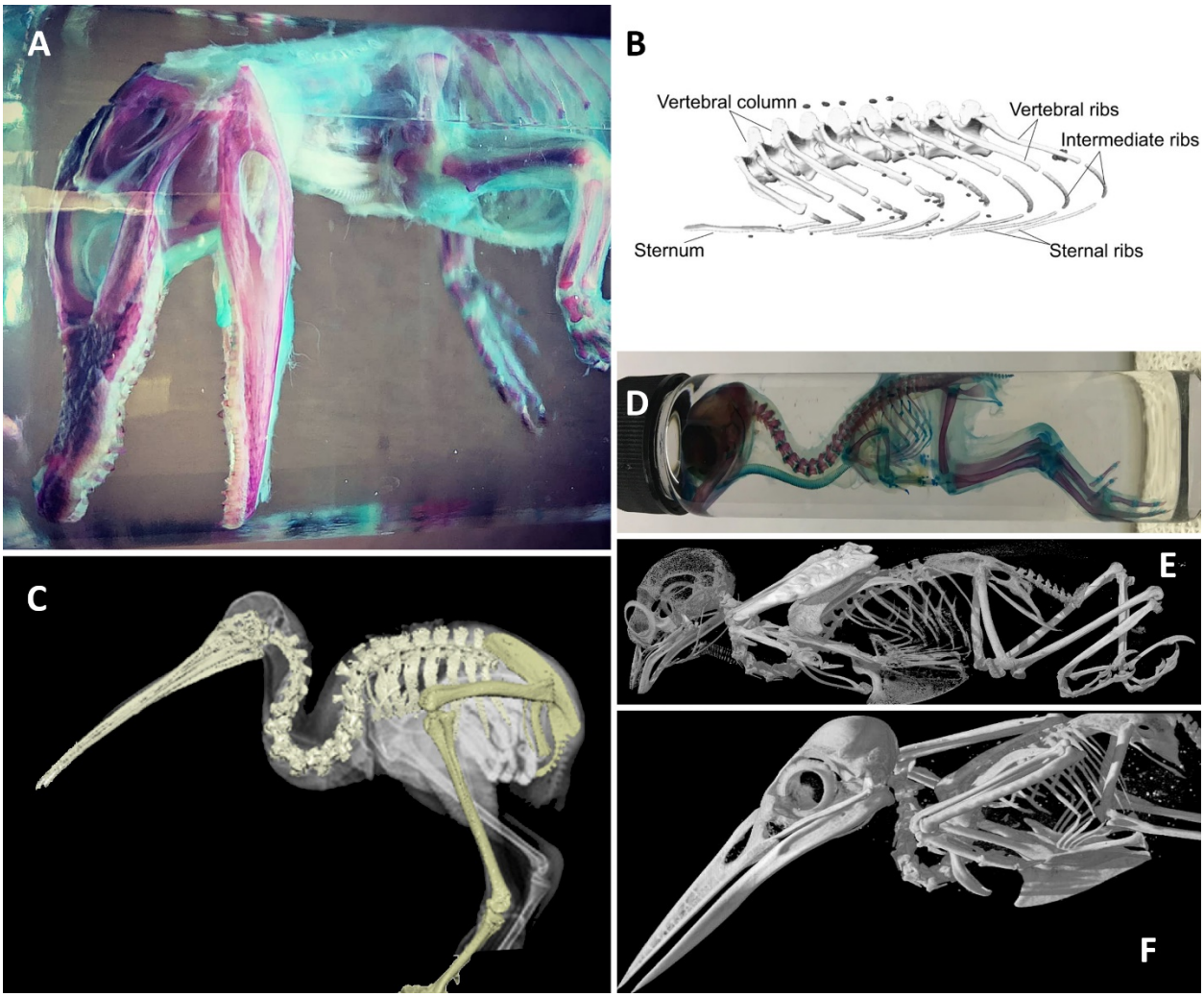

Fig. 2-11. Rib angulation in extant archosaurs. *Dorsal ribs are strongly angled back in juvenile (A) and adult (B, XROMM data, Brocklehurst, et al., 2017) Alligator. This is less true in flightless birds like Apteryx (C, Abourachid, et al., 2019) but anterior ribs are strongly swept back in flying birds as seen in juvenile Colinus (D) and adult Machaeropterus (E, Bostwick, et al., 2012) and Alcedo (F, DigiMorph, 2004). A & D courtesy Elliott Gustafson.*

Archosaurs

Turning to extant archosaurs, crocodilians ribs are strongly angled posteriorly, althoughtheir posterior ribs are often angled ever more than their anterior ribs, cause the ribcage to 'spread out' distally (Fig. 2-11A&B). Crocodilians also use extensive rib motion while breathing (Brocklehurst, et al., 2017). Volant avians generally have anterior ribs that are strongly sloping posteriorly, but their posterior ribs are frequently much less so, resulting in ribcages that are 'bunched together' distally (Fig.2-11D-F). Secondarily flightless avians like *Apteryx* (Fig 2-11C) and *Tinamotis* (cf. Digimorph Staff, 2005) have more vertical ribs, although these and larger ratites (cf. Patterson, 1983) seem to be the only exceptions among extant avians.

Shifting to Mesozoic archosaurs, well preserved croc-line and bird-line archosaur specimens all show evidence of anterior dorsal ribs that are angled posteriorly (Fig. 2-12). This includes Triassic pseudosuchians like the bipedal *Poposaurus* (cf. Schachner, et al., 2020 Fig. 2) to Cretaceous notosuchians like *Araripesuchus* (cf. Sereno & Larsson, 2009 Fig. 23), and neosuchians including extant taxa (Fig. 2-11).

Mesozoic dinosaur taxa also exhibit consistent posterior angulation of anterior ribs (Fig. 2-12). Posterior rib angulation varies more extensively among Mesozoic dinosaurs. Many sauropods have posterior ribs that are more vertical, creating a 'bunching up' of the distal ribcage reminiscent of extant dinosaurs (Fig. 2-12E, cf. Paul, 1997). Derived ornithischians exhibit a more extreme form of the bunched rib cage, with changes in angulation from anterior ribs angled strongly posteriorly grading into posterior ribs angled vertically or even anteriorly such that the distal ends of ribs in the middle of the thoracic region are nearly in contact with one another (e.g. Fig. 1-12A&B; Brown, 1916; Paul, 1987; Evans & Reisz, 2007). Theropods and small ornithischians appear more variable in the angulation of their posterior ribs, but this variability

Fig. 2-12. Rib angulation in Mesozoic archosaurs. *Anterior dorsal ribs are strongly angled back in well-preserved ornithischians like Brachylophosaurus (A) and Chasmosaurus (B, Currie, et al., 2016), theropod Anchiornis (C, Pei, et al., 2017), thalattosuchian Steneosaurus (D), and the sauropod Camarasaurus (E, St. John, 2012).*

does not directly impact torso dimensions since the posterior boundary of the torso is defined by the pelvic girdle.

Synapsids

Mammals and stem-mammals are beyond the scope of this work, but it is worth noting the overall configuration of the 'typical mammalian' ribcage, and that it is not actually universal to all extant mammals. Several placental mammal clades have greatly reduced connections

between the scapula and the sternum (Fig. 2-13A; cf. Cavendish, 2010). In these taxa anterior rib angulation ranges from vertical to sloping anteriorly, while the posterior ribs angle posteriorly, resulting in a 'spread out' distal end of the ribcage generally perceived to be typical of mammals (cf. Knight, 2013). In monotremes, which have robust pectoral girdles that firmly interact with the sternum, rib angulation is quite different, with the anterior ribs exhibiting the strongly swept posterior angulation seen in most other amniotes (Fig. 2-13B).

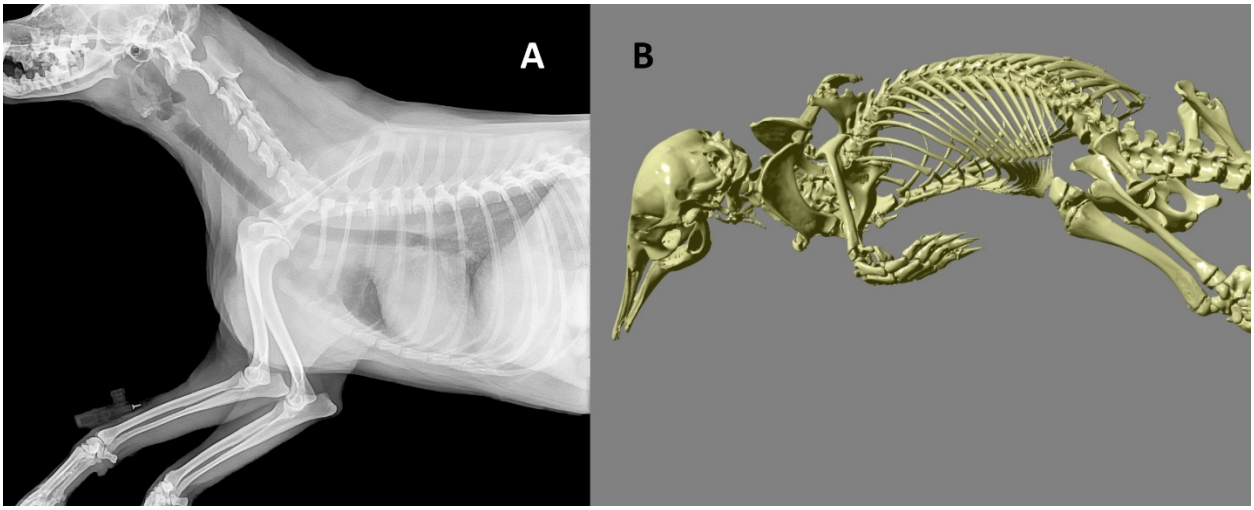

Fig. 2-13. Rib angulation in extant mammals. *X-ray of domesticated Canis (A) and CT scan data of Ornithorhyncus (B, MorphoSource[2]).*

Quantifying the impact of rib angulation inference on mass reconstructions

Artificially altering the anterior rib angulation to vertical in taxa that otherwise have posteriorly swept ribs alters their torso dimensions by anteriorly displacing the pectoral girdle, increasing torso length and girth. Below are conservative estimates of the impact of different rib angulations (vertical and 'articulated') presented for four Mesozoic dinosaur taxa (Figs. 2-14 to 2-17 and Table 2-2). These are considered conservative, as due to limitations of estimating oblique 3D movement in 2D orthogonal reconstructions torso and neck volumes were

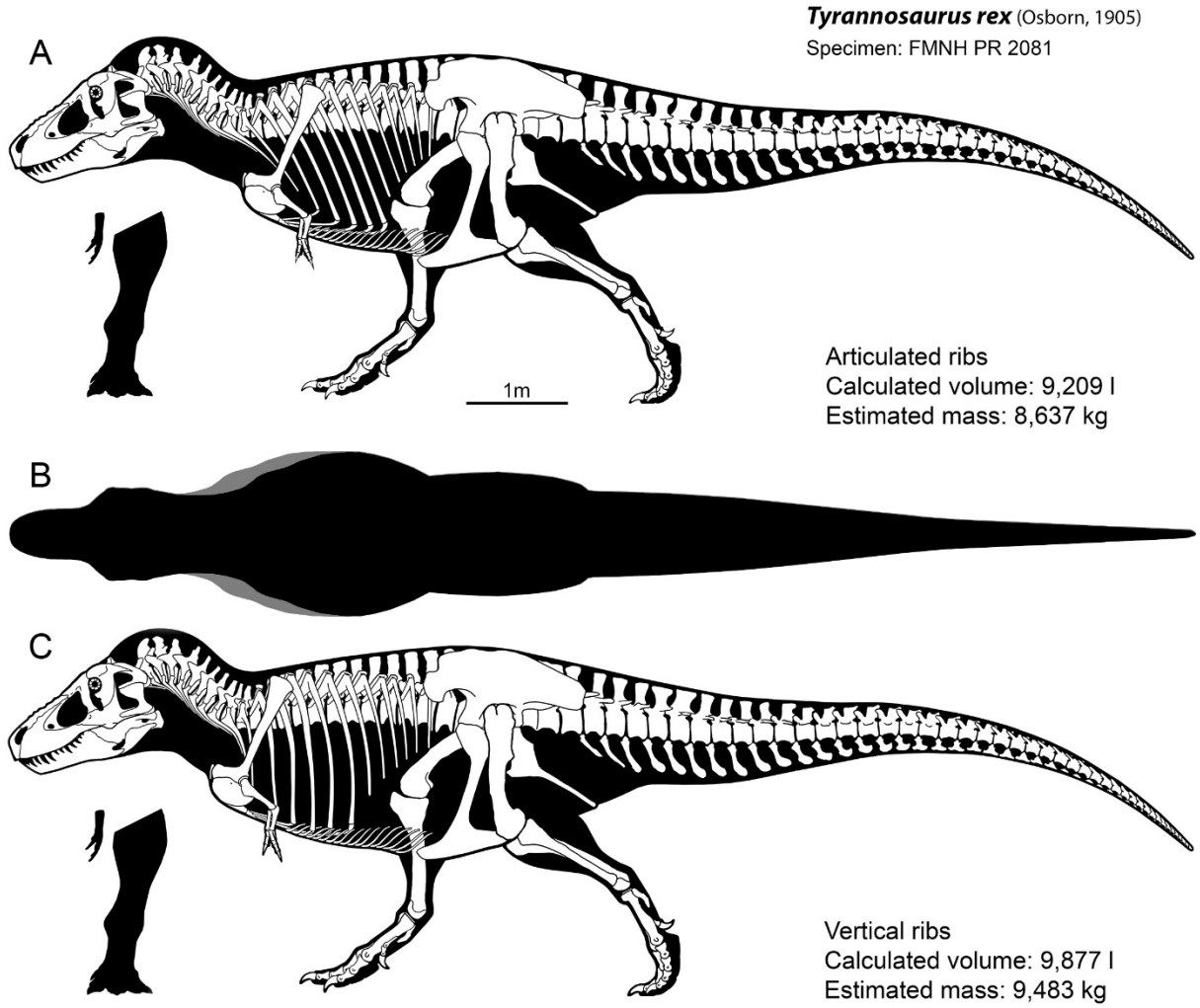

Figure 2-14. Volumetric impact of rib orientation in Tyrannosaurus. *Top skeletal with ribs restored after articulated specimens, bottom restored with vertically oriented rib shafts.*

Table 2-2. Comparative impact of rib orientation on volumetric estimates. *'Volume' refers to the most likely scenario of rib angulation like almost all non-mammals, 'Alt Volume' to calculations based on vertical anterior ribs and an anteriorly displaced pectoral girdle.*

Taxa	Volume	Alt Volume	% Increase
Tyrannosaurus	9433	10412	10.4
Giganotosaurus	7460	8208	10.0
Dreadnoughtus	36683	40151	9.5

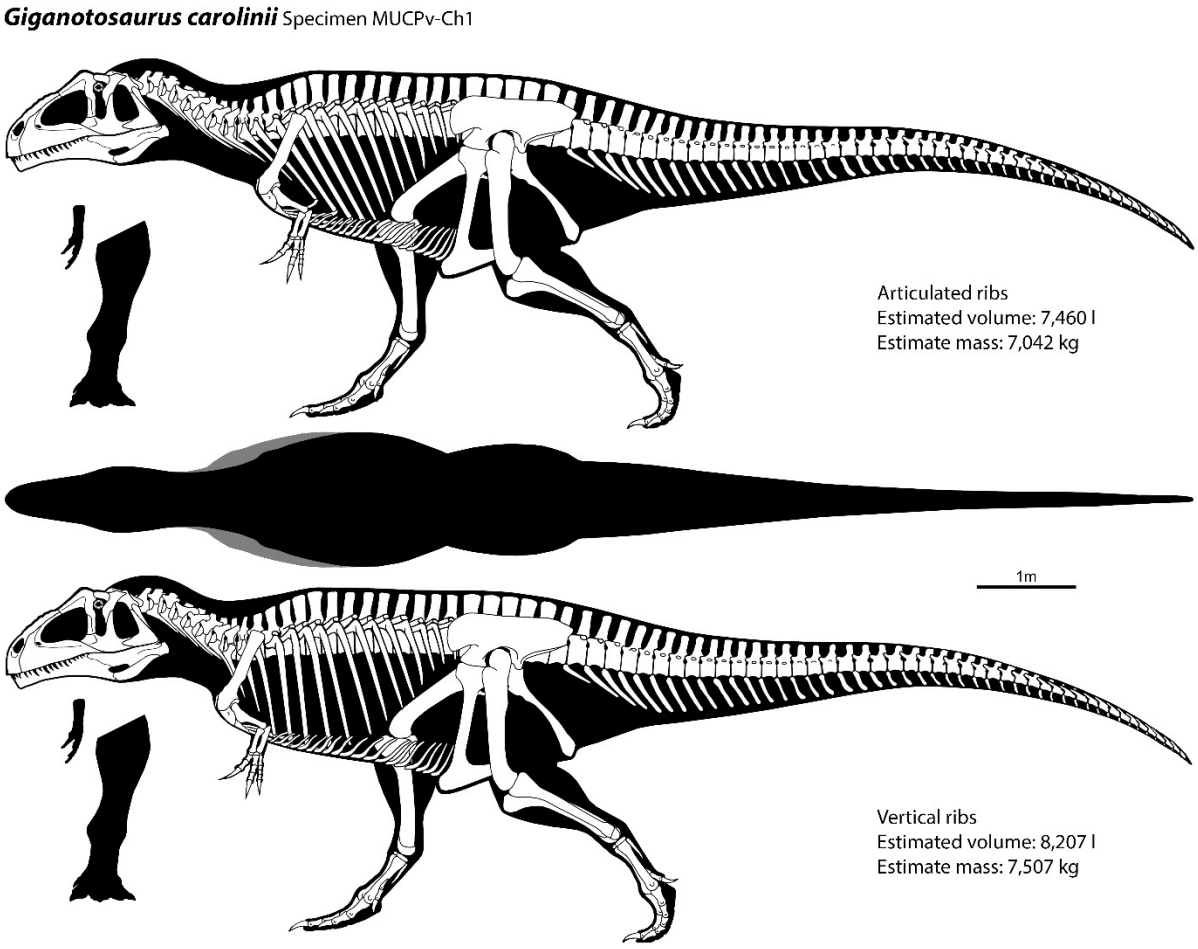

Fig. 2-15. Volumetric impact of rib orientation in Giganotosaurus. *Top skeletal with ribs restored after other articulated larger theropod specimens, bottom restored with vertically oriented rib shafts.*

'telescoped' to their alternate lengths, but rotating the ribs forward on their obliquely oriented rib heads would also widen the torso making real-life gains in volume (and hence mass) larger.

Discussion

Paleobiological inferences for extinct organisms, especially those known from incomplete remains will always carry an inherent and unavoidable degree of error (cf. Prothero,

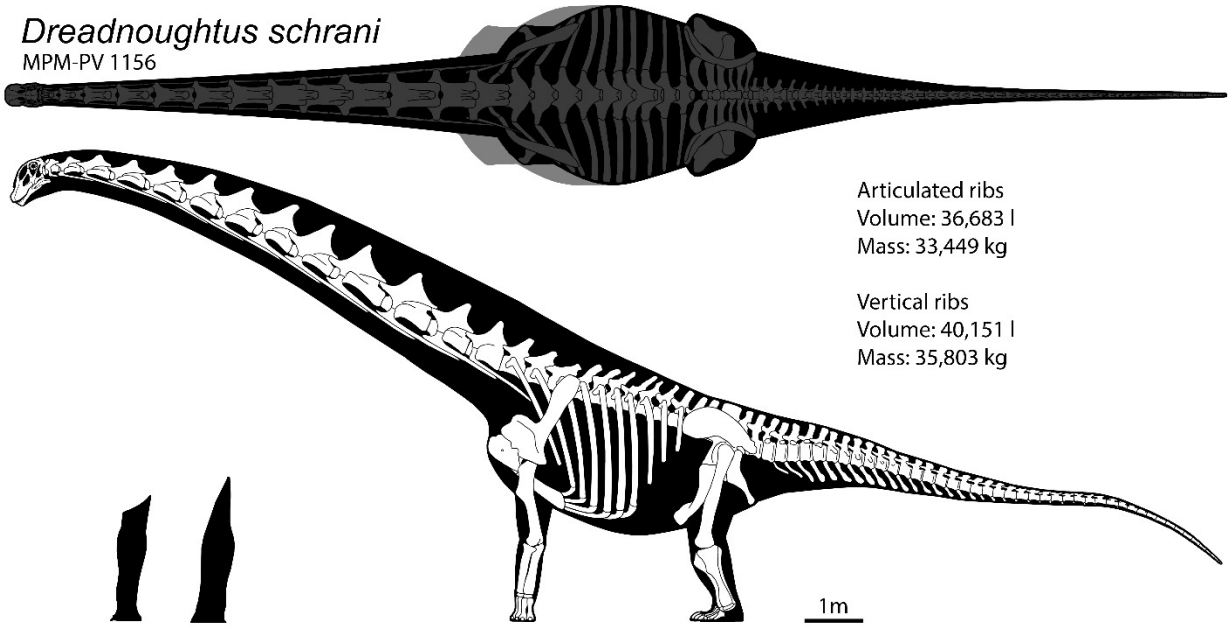

Fig. 2-16. Volumetric impact of rib orientation in Dreadnoughtus. *Light gray area in dorsal view indicates extension with vertical ribs.*

2007). But we must still strive to refine assumptions via careful observation and phylogenetic context, modeling of problems where possible, and quantification of the range of values competing inferences imply. I have presented several lines of data that can improve estimation of torso dimensions in Mesozoic archosaurs and quantify the result of choosing difference inferences in rib angulation.

When it comes to restoring missing vertebral length data for archosaurs, Mesozoic dinosaur taxa, at least, exhibit no consistency and frequently little explanatory power when applying regression models to the dorsal vertebral series (Fig. 2-4 & 2-5). Segmented regression in *Mamenchisaurus* (Fig. 2-5) and especially *Allosaurus* and *Sinraptor* (Fig. 2-4) did produce models with high explanatory power, and if you needed to estimate the length of a misplaced dorsal vertebrae from one of those specimens you could apply a regression model for the

purpose. Unfortunately, models are not consistent between closely related taxa, nor even between individuals of the same species (*Coelophysis*, Fig. 2-4). The limited number of taxa with multiple specimens (and even smaller number with documented measurements for multiple specimens) makes it impossible to advocate for GLM or segmented regression models for estimating missing vertebral length data in the dorsal column. There is some hope for caudal vertebral series, which follow a simpler pattern of linear changes (Grillo & Azevedo, 2011).

Griffin & Nesbitt (2016) found high variance in postnatal development rates was the plesiomorphic condition for archosaurs, and anomalously high variance in growth rates as the plesiomorphic and widespread condition among non-avian dinosaurs. The ability to grow rapidly when climate and food allowed, but to slow growth rates down during periods of low resource availability (cf. Griffin & Nesbitt, 2016; Lovelace, et al., 2020) may explain the lack of success in finding generalizable models of change in vertebral length in the dorsal series. The same explanation could potentially result in higher morphological variation in other portions of the skeleton, which for taxa named for morphological differences may be something that needs to be further explored.

Despite anomalous variance in growth rates, vertebral column development and differentiation are regulated via genetic signaling that results in smoothed transitions between individual elements (Minelli & Fusco, 2004), even if not in the overall trend of the vertebral column (cf. Fig. 2-4 & 2-5). While specific data is sparse for archosaurs, a combination of the initiating developmental genetics processes and the fact that cell signaling growth factors are themselves transmitted via diffusion (cf. Muhlhausler, et al., 2009) may account for the strong correlation between estimated and actual vertebral lengths using the simple model of averaging the lengths of adjacent vertebrae (Table 2-1, Figs. 2-6 & 2-7). The obvious limitation is this only

applies to a specific scenario of missing data, when there is no more than one adjoining vertebra missing at a time. But it is not an uncommon situation within vertebrate paleontology (e.g. Zhang, 1988; Tschopp & Mateus, 2017), and workers can adopt it when appropriate with confidence that they are using a highly correlated, data-driven methodology.

While the complexity and mobility of rib cages awaits larger 3D data sets before quantitative descriptions become widespread, placing qualitative observations into a phylogenetic context provides insight into the pattern of rib angulation in tetrapods. Despite the preponderance of vertical (or anteriorly) oriented ribs in museum mounts of non-mammalian taxa (cf. Paul, 1997) and LiDAR or photogrammetry studies based on them (e.g. Bates, et al., 2009; Sellers, et al., 2012; Clauss et al., 2016), non-invasive observations of extant tetrapods (Figs. 2-8 to 2-11) and close inspection of well-preserved and articulated extinct taxa (Figs. 2-9 & 2-12) show anterior ribs with vertical orientations are extremely rare outside of mammals. Instead, it appears the ancestors of tetrapods had anterior rib angulations that were posteriorly swept (Fig. 2-9), and this basic pattern of rib angulation was retained through the ancestors of amniotes (Fig. 2-9; Schaeffer, 1952; St. John, 2011; Pierce, et al., 2012; Solà, 2012). The same posteriorly swept rib angulation is seen across fossil and extant non-archosaur diapsids (Fig. 2-10; Watson, 1918; Coates, 1996; Kennedy, 2010; Pierce, et al., 2012). Since this same general pattern is found in extant crocodilians and volant avians (Fig. 2-11), posteriorly swept ribs should be the null hypothesis for non-mammalian tetrapods of all types.

For Mesozoic dinosaurs, the fact that secondarily flightless avians show a more vertical rib angulation in their anterior rib cage than other diapsids does raise the intriguing possibility that in reducing flight function and pectoral girdle size they could be expressing some prior developmental pathway. This can be dismissed by examination of well-preserved Mesozoic

dinosaur specimens, which consistently show strong, posteriorly swept rib angulation in the anterior rib cage (e.g. Fig. 2-12; Brown, 1916; Paul, 1987; Evans & Reisz, 2007; St. John, 2012; Currie, et al., 2016; Pei, et al., 2017). This turns out to be non-trivial, as the impact of shifting between a typical non-mammal ribcage restoration and a vertically oriented 'typical mammal' rib cage for organismal volume estimates is 10% or more (Table 2-2). It may be tempting to invoke such strategies when describing an organism that contends for the title of 'largest ever', but such comparisons should be made utilizing consistent and best-supported inferences (cf. Bates, et al., 2015), or at least by making explicit the difference in mass estimates forced by alternate anatomical inference and adjusting comparative data to match.

It is not clear how widespread the condition of vertical rib angulation is outside of placental mammals (Fig. 2-13). Extant monotremes follow the typical tetrapod pattern of anterior ribs with a strong posterior angulation (Fig. 2-13B), raising the question of when did the 'typical' mammal rib cage pattern evolve, and under what circumstances? Since monotremes share the plesiomorphic condition of having a pectoral girdle with well-developed sternal articulations, it may be speculated that only in mammals that reduced the connection between their pectoral girdles and sternal elements will we find the 'spread out' distal rib cage configuration with a vertical or anteriorly-oriented set of anterior ribs. If so, non-mammalian synapsids may also deserve a detailed analysis of rib angulation, despite a preponderance of 'typical' mammalian rib angulations in museum mounts (cf. Clauss, et al., 2016) and technical reconstructions (cf. Romer, 1974) for non-mammalian synapsids.

Conclusions

Mass is a fundamental aspect of biological and ecological processes, and a core input for mechanistic thermal niche modeling. In extinct vertebrates, estimating mass is particularly sensitive to errors in torso dimensions, which may occur when reconstructing missing data or incorrectly inferring rib angulation in the anterior portion of the ribcage. Estimating missing vertebral lengths by averaging the lengths of immediately surrounding vertebrae strongly correlates with known vertebral measurements in extinct and extant taxa. More complex models are not effective for reconstructing larger numbers of missing vertebral lengths in Mesozoic dinosaurs, potentially due to their anomalously high variance in postnatal growth. Finally, nearly all non-mammalian tetrapods living and extinct have anterior ribs that are angled strongly in a posterior direction, including examples of well-preserved, articulated Mesozoic archosaurs. If virtual specimen analyses account for proper rib angulation they can eliminate a source of consistent bias in bounding volume analyses that may be inflating mass estimates by 10% or more.

Acknowledgements

Thanks are due to the UW Zoological Museum for access to specimens. Many thanks are due to Darwin and Wallace: A Nature & Fossil Store, and Elliott Gustafson of Aphelion Necrology for photos of diaphonized specimens. And finally, thanks to John Hutchinson for the tuatara CT scan image in Fig. 2-10C.

Supplemental data

S.2-1. Anteroposterior centrum length measurements, in mm:

https://figshare.com/articles/Vertebral_length_database/12525872

S.2-2. Estimate and real vertebral lengths collated by biological group

https://figshare.com/articles/Estimated_and_real_vertebral_lengths_collated_by_testing_group/12526247

S.2-3. Vertebral length vs estimate correlation statistics – simple model:

https://figshare.com/articles/Simple_vertebral_length_estimate_correlation_statistics/12526205

S.2-4. Mass calculations spreadsheet:

https://figshare.com/articles/Mass_Estimate_Calculation_Spreadsheet/12552134

References

Abourachid, A., Castro, I. and Provini, P., 2019. How to walk carrying a huge egg? Trade-offs between locomotion and reproduction explain the special pelvis and leg anatomy in kiwi (Aves; Apteryx spp.). *Journal of anatomy*, *235*(6), pp.1045-1056.

Alexander, R.M., 1989. *Dynamics of dinosaurs and other extinct giants*. Columbia University Press.

Andrews, C.W., 1915. Note on a Mounted Skeleton of *Ophthalmosaurus icenicus*, Seeley. *Geological Magazine*, *2*(4), pp.145-146.

Bates, K. T., Falkingham, P. L., Macaulay, S., Brassey, C., & Maidment, S. C. 2015. Downsizing a giant: re-evaluating *Dreadnoughtus* body mass. *Biology letters*, *11*, 6, 20150215.

Bates, K.T., Manning, P.L., Hodgetts, D. and Sellers, W.I., 2009. Estimating mass properties of dinosaurs using laser imaging and 3D computer modelling. *PLoS One*, *4*(2), p.e4532.

Benson, R. B., Campione, N. E., Carrano, M. T., Mannion, P. D., Sullivan, C., Upchurch, P., & Evans, D. C. 2014. Rates of dinosaur body mass evolution indicate 170 million years of sustained ecological innovation on the avian stem lineage. PLoS Biol, 12(5), e1001853.

Benton, M.J., 1983. The Triassic reptile Hyperodapedon from Elgin: functional morphology and relationships. *Philosophical Transactions of the Royal Society of London. B, Biological Sciences*, *302*(1112), pp.605-718.

Bonine, K., 2005. *Heloderma suspectum* (On-line), Digital Morphology. Accessed June 22, 2020 at http://digimorph.org/specimens/Heloderma_suspectum/juvenile/whole/.

Bostwick, K., Riccio, M.L., Humphries, J.M. 2012, *Machaeropterus deliciosa* (On-line), Digital Morphology. Accessed June 22, 2020 at http://digimorph.org/specimens/Machaeropterus_deliciosa/.

Brassey, C.A., Maidment, S.C. and Barrett, P.M., 2015. Body mass estimates of an exceptionally complete *Stegosaurus* (Ornithischia: Thyreophora): comparing volumetric and linear bivariate mass estimation methods. *Biology letters*, *11*(3), p.20140984.

Brocklehurst, R.J., Moritz, S., Codd, J., Sellers, W.I. and Brainerd, E.L., 2019. XROMM kinematics of ventilation in wild turkeys (*Meleagris gallopavo*). *Journal of Experimental Biology*, *222*(23).

Brocklehurst, R.J., Moritz, S., Codd, J., Sellers, W.I. and Brainerd, E.L., 2017. Rib kinematics during lung ventilation in the American alligator (*Alligator mississippiensis*): an XROMM analysis. *Journal of Experimental Biology*, *220*(17), pp.3181-3190.

Brown, B., 1916. Corythosaurus casuarius: skeleton, musculature and epidermis. Bulletin of the AMNH; v. 35, article 38.

Bru, J.B., 1796. Descripción del esqueleto en particular, según las observaciones hechas al tiempo de armarle y colocarle en este Real Gabinete. *Garriga, Descripción*, pp.1-16.

Burch, S., 2015. *Osteological, myological, and phylogenetic trends of forelimb reduction in nonavian theropod dinosaurs* (Doctoral dissertation, The Graduate School, Stony Brook University: Stony Brook, NY.).

Burke, A.C., 1991. Proximal elements in the vertebrate limb: evolutionary and developmental origin of the pectoral girdle. In *Developmental patterning of the vertebrate limb* (pp. 385-394). Springer, Boston, MA.

Burness, G. P., Diamond, J., & Flannery, T. 2001. Dinosaurs, dragons, and dwarfs: the evolution of maximal body size. Proceedings of the National Academy of Sciences, 98(25), 14518-14523.

Calvo, J.O., 2000. New specimen of Giganotosaurus carolinii (Coria & Salgado, 1995), supports it as the largest theropod ever found. *Gaia*, *15*, pp.117-122.

Carpenter, K., 1997. Dinosaurs as Museum Exhibits. *The Complete Dinosaur*, pp.150-164.

Carpenter, K., Madsen, J. H., & Lewis, A. 1994. Mounting of fossil vertebrate skeletons. Vertebrate paleontological techniques, 1, 285-322.

Carrier, D.R. and Farmer, C.G., 2000. The evolution of pelvic aspiration in archosaurs. *Paleobiology*, *26*(2), pp.271-293.

Cavendish, M., Corporation, 2010. *Mammal Anatomy: An Illustrated Guide*. Marshall Cavendish.

Chapman, R.E., Andersen, A.F. and Jabo, S.J., 1999. Construction of the virtual Triceratops: procedures, results, and potentials. *Journal of Vertebrate Paleontology*, *19*(3), p.58.

Claessens, L.P., 2015. Anatomical transformations and respiratory innovations of the archosaur trunk. *Great transformations in vertebrate evolution*, pp.91-106.

Claessens, L.P., 2004. Archosaurian respiration and the pelvic girdle aspiration breathing of crocodyliforms. *Proceedings of the Royal Society of London. Series B: Biological Sciences*, *271*(1547), pp.1461-1465.

Clauss, M., Nurutdinova, I., Meloro, C., Gunga, H. C., Jiang, D., Koller, J., ... & Hellwich, O. 2016. Reconstruction of body cavity volume in terrestrial tetrapods. Journal of anatomy.

Coates, M.I., 1996. The Devonian tetrapod *Acanthostega gunnari* Jarvik: postcranial anatomy, basal tetrapod interrelationships and patterns of skeletal evolution. *Earth and Environmental Science Transactions of The Royal Society of Edinburgh*, *87*(3), pp.363-421.

Colbert, E.H., 1962. The weights of dinosaurs. *American Museum Novitates*, 2076, pp.1-16.

Currie, P.J., Holmes, R.B., Ryan, M.J. and Coy, C., 2016. A juvenile chasmosaurine ceratopsid (Dinosauria, Ornithischia) from the Dinosaur Park Formation, Alberta, Canada. *Journal of Vertebrate Paleontology*, *36*(2), p.e1048348.

Das, A.J., Murmann, D.C., Cohrn, K. and Raskar, R., 2017. A method for rapid 3D scanning and replication of large paleontological specimens. *PloS one*, *12*(7), p.e0179264.

Davies, R. B. 2002. Hypothesis testing when a nuisance parameter is present only under the alternative: linear model case. *Biometrika*, 89, 484–489

Dececchi, T.A., Mloszewska, A.M., Holtz Jr, T.R., Habib, M.B. and Larsson, H.C., 2020. The fast and the frugal: Divergent locomotory strategies drive limb lengthening in theropod dinosaurs. *PloS one*, *15*(5), p.e0223698.

DigiMorph Staff, 2016, *Carpiodes cyprinus* (On-line), Digital Morphology. Accessed June 22, 2020 at http://digimorph.org/specimens/Carpiodes_cyprinus/body/.

DigiMorph Staff, 2010, *Characidium* sp. (On-line), Digital Morphology. Accessed June 22, 2020 at http://digimorph.org/specimens/Characidium_sp/.

DigiMorph Staff, 2004, *Alcedo cristata* (On-line), Digital Morphology. Accessed June 21, 2020 at http://digimorph.org/specimens/Alcedo_cristata/whole/.

Dilkes, D.W., 1999. Appendicular myology of the hadrosaurian dinosaur *Maiasaura peeblesorum* from the Late Cretaceous (Campanian) of Montana. *Transactions-Royal Society of Edinburgh*, *90*(2), pp.87-125.

Dodson, P., 1990. Counting dinosaurs: how many kinds were there?. *Proceedings of the National Academy of Sciences*, *87*(19), pp.7608-7612.

Evans, D.C. and Reisz, R.R., 2007. Anatomy and relationships of *Lambeosaurus magnicristatus*, a crested hadrosaurid dinosaur (Ornithischia) from the Dinosaur Park Formation, Alberta. *Journal of Vertebrate Paleontology*, *27*(2), pp.373-393.

Ezcurra, M.D., 2016. The phylogenetic relationships of basal archosauromorphs, with an emphasis on the systematics of proterosuchian archosauriforms. *PeerJ*, *4*, p.e1778.

Fleming, A., Kishida, M. G., Kimmel, C. B., & Keynes, R. J. 2015. Building the backbone: the development and evolution of vertebral patterning. *Development*, *142*, 10, pp 1733-1744.

Gatesy, S.M., Bäker, M. and Hutchinson, J.R., 2009. Constraint-based exclusion of limb poses for reconstructing theropod dinosaur locomotion. *Journal of Vertebrate Paleontology*, *29*(2), pp.535-544.

Gatesy, S.M., 2002. Locomotor evolution on the line to modern birds. *Mesozoic birds: above the heads of dinosaurs*, *432*, p.447.

Gilmore, C.W., 1932. On a newly mounted skeleton of Diplodocus in the United States National Museum. *Proceedings of the United States National Museum*.

Gilmore, C.W., 1918. A newly mounted skeleton of the armored dinosaur, *Stegosaurus stenops*, in the United States National Museum. *Proceedings of the United States National Museum*.

Gilmore, C.W., 1912. The mounted skeletons of *Camptosaurus* in the United States National Museum. *Proceedings of the United States National Museum*.

Griffin, C.T. and Nesbitt, S.J., 2016. Anomalously high variation in postnatal development is ancestral for dinosaurs but lost in birds. *Proceedings of the National Academy of Sciences*, *113*(51), pp.14757-14762.

Grillo, O.N. and Azevedo, S.A., 2011. Recovering missing data: estimating position and size of caudal vertebrae in Staurikosaurus pricei Colbert, 1970. *Anais da Academia Brasileira de Ciências*, *83*(1), pp.61-72.

Gunga, H.C., Suthau, T., Bellmann, A., Friedrich, A., Schwanebeck, T., Stoinski, S., Trippel, T., Kirsch, K. and Hellwich, O., 2007. Body mass estimations for *Plateosaurus engelhardti* using laser scanning and 3D reconstruction methods. *Naturwissenschaften*, *94*(8), pp.623-630.

Hamm, C.A., Mallison, H., Hampe, O., Schwarz, D., Mews, J., Blobel, J., Issever, A.S. and Asbach, P., 2018. Efficiency, workflow and image quality of clinical computed tomography scanning compared to photo-grammetry on the example of a *Tyrannosaurus rex* skull from the maastrichtian of Montana, USA. *J Paleontol Tech*, *21*, pp.1-13.

Hartman, S., Lovelace, D., Mathewson, Linzmeier, B. J., Porter, W. 2015. Using ecological modelling to quantify thermal constraints on two Late Triassic dinosaurs. Journal of Vertebrate Paleontology. Vol. 35, online supplement.

Hartman, S. 2012. Investigating the impact of competing interpretations of pectoral girdle placement and appendicular function on sauropod head height. In *Journal of Vertebrate Paleontology.* Vol. 32, pp. 106-106.

Hartman, S. and Shinkle, L., 2006, September. Estimating osteological neutral position in saudopod axial skeletons: Comparing two-dimensional and three-dimensional methods of analysis. In *Journal of Vertebrate Paleontology* (Vol. 26, No. 3, pp. 73A-73A).

Hay, O.P., 1910, January. On the manner of locomotion of the dinosaurs especially Diplodocus, with remarks on the origin of the birds. In *Proceedings of the Washington Academy of Sciences* (Vol. 12, pp. 1-25). Washington Academy of Sciences.

Henderson, D.M., 1999. Estimating the masses and centers of mass of extinct animals by 3-D mathematical slicing. *Paleobiology*, pp.88-106.

Hirasawa, T., Nagashima, H. and Kuratani, S., 2013. The endoskeletal origin of the turtle carapace. *Nature Communications*, *4*, p.2107.

Hodges, W., 2001 *Phrynosoma taurus* (On-line), Digital Morphology. Accessed May 2, 2020 at http://digimorph.org/specimens/Phrynosoma_taurus/embryo/

Holland, W.J., 1906. *The Osteology of Diplodocus Marsh: With Special Reference to the Restoration of the Skeleton of Diplodocus Carnegiei Hatcher, Presented by Mr. Andrew Carnegie to the British Museum, May 12, 1905*. authority of the Board of Trustees of the Carnegie Institute.

Holliday, C.M., 2009. New insights into dinosaur jaw muscle anatomy. *The Anatomical Record: Advances in Integrative Anatomy and Evolutionary Biology: Advances in Integrative Anatomy and Evolutionary Biology*, *292*(9), pp.1246-1265.

Hone, D. W. 2012. Variation in the tail length of non-avian dinosaurs. *Journal of Vertebrate Paleontology*, *32*, 5, 1082-1089.

Humphries, J., 2006. *Xenocharax spilurus* (On-line), Digital Morphology. Accessed June 22, 2020 at http://digimorph.org/specimens/Xenocharax_spilurus/whole/.

Hutchinson, J. R., Bates, K. T., Molnar, J., Allen, V., & Makovicky, P. J. 2011. A computational analysis of limb and body dimensions in *Tyrannosaurus rex* with implications for locomotion, ontogeny, and growth. *PLoS One*, *6*(10), e26037.

Hutchinson, J.R., 2001. The evolution of pelvic osteology and soft tissues on the line to extant birds (Neornithes). *Zoological Journal of the Linnean Society*, *131*(2), pp.123-168.

Hutchinson, J.R. and Gatesy, S.M., 2000. Adductors, abductors, and the evolution of archosaur locomotion. *Paleobiology*, *26*(4), pp.734-751.

Ibrahim, N., Sereno, P. C., Dal Sasso, C., Maganuco, S., Fabbri, M., Martill, D. M., ... & Iurino, D. A. 2014. Semiaquatic adaptations in a giant predatory dinosaur. *Science*, *345*(6204), 1613-1616.

Jerison, H. J. 1973. Evolution of the brain and intelligence. Academic. *New York*, 482.

Junchang, L.Ü. and Hone, D.W., 2012. A new Chinese anurognathid pterosaur and the evolution of pterosaurian tail lengths. *Acta Geologica Sinica-English Edition*, *86*(6), pp.1317-1325.

Kennedy, N.K., 2010. Redescription of the postcranial skeleton of *Limnoscelis paludis* Williston (Diadectomorpha: Limnoscelidae) from the upper Pennsylvanian of El Cobre Canyon, northern New Mexico. *New Mexico Museum of Natural History and Science Bulletin*, *49*, pp.211-220.

Klinder, T., Lorenz, C., Von Berg, J., Dries, S.P., Bülow, T. and Ostermann, J., 2007, October. Automated model-based rib cage segmentation and labeling in CT images. In *International Conference on Medical Image Computing and Computer-Assisted Intervention* (pp. 195-202). Springer, Berlin, Heidelberg.

Knight, C., 2013. *Animal drawing: anatomy and action for artists*. Courier Corporation.

Kooijman, S.A.L.M., 2000. *Dynamic energy and mass budgets in biological systems*. Cambridge university press.

Lavin, S.R., Karasov, W.H., Ives, A.R., Middleton, K.M. and Garland Jr, T., 2008. Morphometrics of the avian small intestine compared with that of nonflying mammals: a phylogenetic approach. *Physiological and biochemical zoology*, *81*(5), pp.526-550.

Lomax, D.R. and Massare, J.A., 2017. Two new species of *Ichthyosaurus* from the lowermost Jurassic (Hettangian) of Somerset, England. *Papers in Palaeontology*, *3*(1), pp.1-20.

Lovelace, D.M., Hartman, S.A., Mathewson, P.D., Linzmeier, B.J. and Porter, W.P., 2020. Modeling Dragons: Using linked mechanistic physiological and microclimate models to explore environmental, physiological, and morphological constraints on the early evolution of dinosaurs. *PloS one*, *15*(5), p.e0223872.

Lyson, T.R., Bever, G.S., Scheyer, T.M., Hsiang, A.Y. and Gauthier, J.A., 2013. Evolutionary origin of the turtle shell. *Current Biology*, *23*(12), pp.1113-1119.

Macaluso, L. and Tschopp, E., 2018. Evolutionary changes in pubic orientation in dinosaurs are more strongly correlated with the ventilation system than with herbivory. *Palaeontology*, *61*(5), pp.703-719.

Mallison, H., Pittman, M. and Schwarz, D., 2015. *Using crocodilian tails as models for dinosaur tails* (No. e1653). PeerJ PrePrints.

Mallison, H. and Wings, O., 2014. Photogrammetry in paleontology—a practical guide. *Journal of Paleontological Techniques*, *12*(12), pp.1-31.

Mallison, H., 2010a. The digital *Plateosaurus* I: body mass, mass distribution, and posture assessed using CAD and CAE on a digitally mounted complete skeleton. *Palaeontologia Electronica*, *13*(2), p.8A.

Mallison, H., 2010b. The digital *Plateosaurus* II: an assessment of the range of motion of the limbs and vertebral column and of previous reconstructions using a digital skeletal mount. *Acta Palaeontologica Polonica*, *55*(3), pp.433-458.

Mallison, H., 2010c. CAD assessment of the posture and range of motion of *Kentrosaurus aethiopicus* Hennig 1915. *Swiss Journal of Geosciences*, *103*(2), pp.211-233.

Mallison, H., 2007. Virtual dinosaurs-Developing computer aided design and computer aided engineering modeling methods for vertebrate paleontology. Tübingen: Eberhard-Karls-Universität Tübingen.

Maxwell, E.E., 2012. New metrics to differentiate species of *Stenopterygius* (Reptilia: Ichthyosauria) from the Lower Jurassic of Southwestern. *Journal of Paleontology*, *86*(1), pp.105-115.

Mayor, A. 2007. Fossil legends of the first Americans. Princeton University Press.

Mayor, A. 2001. The first fossil hunters: paleontology in Greek and Roman times. Princeton University Press.

McGonnell, I.M., 2001. The evolution of the pectoral girdle. *Journal of Anatomy*, *199*(1-2), pp.189-194.

McNab, B.K., 2009. Ecological factors affect the level and scaling of avian BMR. *Comparative Biochemistry and Physiology Part A: Molecular & Integrative Physiology*, *152*(1), pp.22-45.

Meiri, S., 2004. *The museology of dinosaurs: in search of the authentic museum dinosaur*. University of Leicester (United Kingdom).

Minelli, A. and Fusco, G., 2004. Evo-devo perspectives on segmentation: model organisms, and beyond. *Trends in ecology & evolution*, *19*(8), pp.423-429.

MorphoSource[1] ARK: ark:/87602/m4/M11261. Shared via CC BY-NC license, retrieved from: http://www.morphosource.org/Detail/MediaDetail/Show/media_id/8808

MorphoSource[2] ARK: ark:/87602/m4/M65300. Shared via CC BY-NC license, retrieved from: http://www.morphosource.org/Detail/MediaDetail/Show/media_id/35370

Muhlhausler, B.S., Duffield, J.A., Ozanne, S.E., Pilgrim, C., Turner, N., Morrison, J.L. and McMillen, I.C., 2009. The transition from fetal growth restriction to accelerated postnatal growth: a potential role for insulin signaling in skeletal muscle. *The Journal of physiology*, *587*(17), pp.4199-4211.

Murray, P. F., & Vickers-Rich, P. (2004). Magnificent mihirungs: the colossal flightless birds of the Australian dreamtime. Indiana University Press.

Muggeo, V.M., 2017. Interval estimation for the breakpoint in segmented regression: a smoothed score-based approach. *Australian & New Zealand Journal of Statistics*, **59**, 311-322. .

Myhrvold, N.P., 2016. Dinosaur metabolism and the allometry of maximum growth rate. *PloS one*, *11*(11), p.e0163205.

Nabavizadeh, A., 2020. New reconstruction of cranial musculature in ornithischian dinosaurs: implications for feeding mechanisms and buccal anatomy. *The Anatomical Record*, *303*(2), pp.347-362.

Oommen, A., 2015. The artful science of diaphonization. *Science Connected Magazine*. https://magazine.scienceconnected.org/2015/07/the-artful-science-of-diaphonization/

Owen, R., 1860. Palaeontology, or a systematic summary of extinct animals and their geological relations. Adam and Charlos Black. 420 pages.

Patterson, C., 1983. *Osteology, Myology, Evolution and Paleobiogeography of the Emu, Dromaius Spp.(family Casuariidae: Dromaiinae)*. Monash University.

Paul, G., 2019. Determining the largest known land animal: a critical comparison of differing methods for restoring the volume and mass of extinct animals. *Annals of Carnegie Museum*, *85*(4), pp.335-358.

Paul, G. S. 1997. Dinosaur models: the good, the bad, and using them to estimate the mass of dinosaurs. In DinoFest International: Proceedings of a Symposium Sponsored by Arizona State University. Academy of Natural Sciences, Philadelphia. pp. 129-154.

Paul, G.S. and Chase, T.L., 1989. Reconstructing extinct vertebrates. *The guild handbook of scientific illustration*, pp.239-256.

Paul, G.S., 1988. The brachiosaur giants of the Morrison and Tendaguru with a description of a new subgenus, *Giraffatitan*, and a comparison of the world's largest dinosaurs Proceedings of the North American Paleontological Conference IV: The Golden Age of Dinosaurs. *Hunteria*, 2(3).

Paul, G.S. 1987. The science and art of reconstructing the life appearance of dinosaurs and their relatives: a rigorous how-to guide. In Dinosaurs Past and Present Volume II, Natural History Museum of Los Angeles County

Pei, R., Li, Q., Meng, Q., Norell, M.A. and Gao, K.Q., 2017. New specimens of *Anchiornis huxleyi* (Theropoda: Paraves) from the Late Jurassic of northeastern China. *Bulletin of the American Museum of Natural History*, *2017*(411), pp.1-67.

Persons IV, W.S. and Currie, P.J., 2011. Dinosaur speed demon: the caudal musculature of *Carnotaurus sastrei* and implications for the evolution of South American abelisaurids. *PloS one*, *6*(10), p.e25763.

Pierce, S.E., Clack, J.A. and Hutchinson, J.R., 2012. Three-dimensional limb joint mobility in the early tetrapod Ichthyostega. *Nature*, *486*(7404), pp.523-526.

Pianka, E., 2003. *Moloch horridus*"(On-line), Digital Morphology. Accessed May 1, 2020 at http://digimorph.org/specimens/Moloch_horridus/whole/

Piñero, J.M.L., 1988. Juan Bautista Bru (1740–1799) and the description of the genus *Megatherium*. Journal of the History of Biology, 21(1), pp.147-163.

Prothero, D.R., 2007. *Evolution: what the fossils say and why it matters*. Columbia University Press.

R Core Team. 2013. R: A language and environment for statistical computing. R Foundation for Statistical Computing, Vienna, Austria. URL http://www.R-project.org/.

Remes, K., 2008. Evolution of the pectoral girdle and forelimb in Sauropodomorpha (Dinosauria, Saurischia): osteology, myology and function. *Munich: Fakultät für Geowissenschaften, Ludwig-Maximilians-Universität*, *355*.

Romer, A.S., 1974. *Vertebrate paleontology* (No. 566 ROM).

Rudwick, M.J., 1992. *Scenes from deep time: early pictorial representations of the prehistoric world*. University of Chicago Press.

Schaeffer, B., 1952. The Triassic coelacanth fish *Diplurus*, with observations on the evolution of the Coelacanthini. *Bulletin of the American Museum of Natural History*, *99*(2), p.27.

Schwarz, D., Frey, E. and Meyer, C.A., 2007. Novel reconstruction of the orientation of the pectoral girdle in sauropods. *The Anatomical Record: Advances in Integrative Anatomy and Evolutionary Biology*, *290*(1), pp.32-47.

Sellers, W.I., Hepworth-Bell, J., Falkingham, P.L., Bates, K.T., Brassey, C.A., Egerton, V.M. and Manning, P.L., 2012. Minimum convex hull mass estimations of complete mounted skeletons. *Biology Letters*, *8*(5), pp.842-845.

Sereno, P. and Larsson, H., 2009. Cretaceous crocodyliforms from the Sahara. *ZooKeys*, *28*.

Shinkle, L. and Hartman, S., 2006, September. Utilizing 3D laser scans and commercially available software to create and analyze virtual morphological data sets. In *Journal of Vertebrate Paleontology* (Vol. 26, No. 3, pp. 125A-125A).

Smith, A.S. and Benson, R.B., 2014. Osteology of *Rhomaleosaurus thorntoni* (Sauropterygia: Rhomaleosauridae) from the Lower Jurassic (Toarcian) of Northamptonshire, England. *Monographs of the Palaeontographical Society*, *168*(642), pp.1-40.

Snively, E., O'Brien, H., Henderson, D.M., Mallison, H., Surring, L.A., Burns, M.E., Holtz Jr, T.R., Russell, A.P., Witmer, L.M., Currie, P.J. and Hartman, S.A., 2019. Lower rotational inertia and larger leg muscles indicate more rapid turns in tyrannosaurids than in other large theropods. *PeerJ*, *7*, p.e6432.

Solà, E. Distributed unmodified under a CC-BY-SA 3.0 license: https://creativecommons.org/licenses/by-sa/3.0/legalcode

St. John, j., 2012. Distributed unmodified under a CC-BY 2.0 license: https://creativecommons.org/licenses/by/2.0/legalcode

St. John, j., 2011. Distributed unmodified under a CC-BY 2.0 license: https://creativecommons.org/licenses/by/2.0/legalcode

Sternberg, C.M., 1942. New restoration of a hooded duck-billed dinosaur. *Journal of Paleontology*, pp.133-134.

Steudel, K., Porter, W.P. and Sher, D., 1994. The biophysics of Bergmann's rule: a comparison of the effects of pelage and body size variation on metabolic rate. *Canadian Journal of Zoology*, *72*(1), pp.70-77.

Stoinski, S., Suthau, T. and Gunga, H.C., 2011. Reconstructing body volume and surface area of dinosaurs using laser scanning and photogrammetry. *Biology of the Sauropod dinosaurs: understanding the life of giants. Indiana University Press, Bloomington*, pp.94-115.

Streat, J., 2018. Revising the Dead Art of Skeleton Preparation for Today's Museum Collections. *Biodiversity Information Science and Standards*.

Talbot, L.M. and McCulloch, J.S.G., 1965. Weight estimations for East African mammals from body measurements. *The Journal of Wildlife Management*, pp.84-89.

Taylor, M.P., 2015. *Almost all known sauropod necks are incomplete and distorted* (No. e1767). PeerJ PrePrints.

Taylor, M.P., 2014. Quantifying the effect of intervertebral cartilage on neutral posture in the necks of sauropod dinosaurs. *PeerJ*, *2*, p.e712.

Taylor, M. P., & Wedel, M. J. 2013. The effect of intervertebral cartilage on neutral posture and range of motion in the necks of sauropod dinosaurs. *PLoS One*, *8*(10), e78214.

Tornier, G., 1909. Wie war der Diplodocus carnegii wirklich gebaut. Sitzungsbericht der Gesellschaft naturforschender Freunde zu Berlin, 4, pp.193-209.

Tschopp, E. and Mateus, O., 2017. Osteology of Galeamopus pabsti sp. nov.(Sauropoda: Diplodocidae), with implications for neurocentral closure timing, and the cervico-dorsal transition in diplodocids. *PeerJ*, *5*, p.e3179.

Vidal, D., Ortega, F. and Sanz, J.L., 2020. Sauropodomorph skeletal mounts as scientific devices for testing hypotheses. *Journal of Iberian Geology*, pp.1-17.

Wang, X., Pittman, M., Zheng, X., Kaye, T.G., Falk, A.R., Hartman, S.A. and Xu, X., 2017. Basal paravian functional anatomy illuminated by high-detail body outline. *Nature Communications*, *8*(1), pp.1-6.

Wang, Y., Cao, L., Bai, Z., Reed, M.P., Rupp, J.D., Hoff, C.N. and Hu, J., 2016. A parametric ribcage geometry model accounting for variations among the adult population. *Journal of biomechanics*, *49*(13), pp.2791-2798.

Wang, Y., Porter, W., Mathewson, P.D., Miller, P.A., Graham, R.W. and Williams, J.W., 2018. Mechanistic modeling of environmental drivers of woolly mammoth carrying capacity declines on St. Paul Island. *Ecology*, *99*(12), pp.2721-2730.

Wang, Z., Pascual-Anaya, J., Zadissa, A., Li, W., Niimura, Y., Huang, Z., Li, C., White, S., Xiong, Z., Fang, D. and Wang, B., 2013. The draft genomes of soft-shell turtle and green sea turtle yield insights into the development and evolution of the turtle-specific body plan. *Nature genetics*, *45*(6), pp.701-706.

Watson, D.M.S., 1918, December. On Seymouria, the most primitive known reptile. In *Proceedings of the Zoological Society of London* (Vol. 88, No. 3-4, pp. 267-301). Oxford, UK: Blackwell Publishing Ltd.

Witton, M., Naish, D. and Conway, J., 2014. State of the Palaeoart. *Palaeontologia Electronica*, *17*(3), pp.17-3.

Wood, J.M., 2006. A Study of Carasaurus'(Dinosaura: Sauropodomorph) Torso and its Biomechanical Implications.

Zhang, G. 2009. An evo-devo view on the origin of the backbone: evolutionary development of the vertebrae. *Integrative and comparative biology*.

Zhang, Y., 1988. The Middle Jurassic dinosaur fauna from Dashanpu, Zigong, Sichuan. Vol. 1. Sauropod Dinosaurs (I) *Shunosaurus*. Sichuan Publishing House.

Chapter 3

A new paravian dinosaur from the Late Jurassic of North America supports a late acquisition of avian flight

Scott Hartman[1], Mickey Mortimer[2], William R. Wahl[3], Dean Lomax[4], Jessica Lippincott[3] & David M. Lovelace[5]

[1]Department of Geoscience, University of Wisconsin-Madison, Madison, WI, USA

[2]Maple Valley, WA, USA

[3]Wyoming Dinosaur Center, 110 Carter Ranch Road, Thermopolis, WY, USA

[4]The University of Manchester, School of Earth and Environmental Sciences, Manchester, UK

[5]University of Wisconsin Geology Museum, University of Wisconsin-Madison, Madison, Wisconsin, United States

Abstract

The last two decades have seen a remarkable increase in the known diversity of basal avialans and their paravian relatives. The lack of resolution in the relationships of these groups combined with attributing the behavior of specialized taxa to the base of Paraves has clouded interpretations of the origin of avialan flight. Here we describe *Hesperornithoides miessleri* gen. et sp. nov., a new paravian theropod from the Morrison Formation (Late Jurassic) of Wyoming, USA, represented by a single adult or subadult specimen comprising a partial, well-preserved skull and postcranial skeleton. Limb proportions firmly establish *Hesperornithoides* as occupying a terrestrial, non-volant lifestyle. Our phylogenetic analysis emphasizes extensive taxonomic sampling and robust character construction, recovering the new taxon most parsimoniously as a troodontid close to *Daliansaurus*, *Xixiasaurus* and *Sinusonasus.* Multiple alternative paravian topologies have similar degrees of support, but proposals of basal paravian archaeopterygids, avialan microraptorians, and *Rahonavis* being closer to Pygostylia than archaeopterygids or unenlagiines are strongly rejected. All parsimonious results support the hypothesis that each early paravian clade was plesiomorphically flightless, raising the possibility that avian flight originated as late as the Late Jurassic or Early Cretaceous.

Introduction

Paravians are an important radiation of winged coelurosaurs more closely related to birds than to *Oviraptor*, that include dromaeosaurids, troodontids, unenlagiines, halszkaraptorines and archaeopterygids in addition to derived avialans. Despite robust support for their monophyly, the interrelationships and composition of these groups remains contentious with recent studies alternatively favoring joining troodontids and dromaeosaurids as Deinonychosauria (Hu et al.,

2018; Lefèvre et al., 2017; Shen et al., 2017; Godefroit et al., 2013a; Senter et al., 2012; Turner et al., 2012), placing troodontids closer to Aves than dromaeosaurids (Gianechini et al., 2018; Cau et al., 2017; Foth and Rauhut, 2017; Lee et al., 2014a; Foth et al., 2014; Godefroit et al., 2013b), joining dromaeosaurids and avialans to form Eumaniraptora to the exclusion of troodontids (Agnolin and Novas, 2013) or merely recovering an unresolved trichotomy between the three (Cau et al., 2015; Brusatte et al., 2014).

This lack of phylogenetic resolution has been attributed to a combination of rapid rates of evolution at the base of Paraves (Brusatte, et al., 2014) and a lack of sampling of taxa from outside the hugely prolific Late Jurassic and Early Cretaceous fossil beds of eastern China. In particular, Middle and Late Jurassic taxa *Archaeopteryx*, *Anchiornis*, *Aurornis*, *Eosinopteryx*, and *Xiaotingia* have been recovered variously as basal dromaeosaurids, basal troodontids, archaeopterygids, or non-archaeopterygid avialans (e.g. Turner, et al., 2007; Xu, et al., 2011; Senter et al., 2012; Godefroit, et al., 2013a, b). Incomplete taxonomic sampling and unresolved relationships of basal avialans hinders tests of hypotheses for the origin of flight, and the order of acquisition of flight-associated characters in stem avians.

Here we report a new paravian theropod, *Hesperornithoides miessleri* gen. et sp. nov., collected from the Morrison Formation near Douglas, Wyoming, USA, based on a largely complete skull and associated postcranial elements (Lovelace, 2006; Wahl, 2006). We also present a significantly expanded and updated phylogenetic analysis of maniraptorans that clarifies paravian relationships, as well as the acquisition of flight-related characters in stem avians.

Materials & Methods

Specimen curation

WYDICE-DML-001 (formerly WDC DML-001) was collected on private property in 2001 (see Locality & Geologic Context below). In 2005 it was donated to the Big Horn Basin Foundation, a research and educational non-profit 501(c)3 formed in 1995 to be curated and made available for research. In 2016 the Wyoming Dinosaur Center and the Big Horn Basin Foundation merged to form a new non-profit organization, renamed The Wyoming Dinosaur Center, Inc. At that point WYDICE-DML-001 was transferred to the new non-profit, where it will be accessible to researchers in perpetuity. If the Wyoming Dinosaur Center, Inc. should ever cease to exist the donation agreement requires the specimen be transferred to the University of Wyoming's paleontological collections, ensuring it will always be available for research.

The electronic version of this article in Portable Document Format (PDF) will represent a published work according to the International Commission on Zoological Nomenclature (ICZN), and hence the new names contained in the electronic version are effectively published under that Code from the electronic edition alone. This published work and the nomenclatural acts it contains have been registered in ZooBank, the online registration system for the ICZN. The ZooBank LSIDs (Life Science Identifiers) can be resolved and the associated information viewed through any standard web browser by appending the LSID to the prefix http://zoobank.org/. The LSID for this publication is: urn:lsid:zoobank.org:pub:6325E8D2-0AAF-4ECD-9DF2-87D73022DC93. The online version of this work is archived and available from the following digital repositories: PeerJ, PubMed Central and CLOCKSS.

Preparation

Multiple cycles of mechanical micro-preparation have been performed on the specimen since discovery. The specimen was collected in several blocks and later reassembled in the lab to reproduce the original in-field association. In 2004 the skull and body block were scanned at the University of Texas High-Resolution X-ray Computed Tomography Facility in Austin, Texas. Segmentation of the scan data was completed in Object Research System's Dragonfly v1.1 software to help visualize preserved elements and internal morphology. Internal cavities, such as those seen in long bones and pleurocoels were filled with the mineral barite. The high electron density of barite precluded segmentation of many of the postcranial elements due to poor visualization. During physical preparation most of the specimen was left in the minimal amount of host matrix to preserve the original association but reveal as much morphology as possible.

Systematic Paleontology

Theropoda Marsh, 1881

Maniraptora Gauthier, 1986

Paraves Sereno, 1997

Deinonychosauria Gauthier, 1986

Troodontidae Gilmore, 1924

Hesperornithoides miessleri gen. et sp. nov.

Holotype

WYDICE-DML-001 (Wyoming Dinosaur Center, Thermopolis), a single, partially articulated skeleton consisting of most of an articulated skull and mandibles missing the anteriormost portions, hyoids, five cervical vertebrae, first dorsal vertebra, isolated anterior dorsal rib, portions of twelve caudal vertebrae, five chevrons, partial left scapula and coracoid, portions of the proximal left humerus and distal right humerus, left ulna and radius, radiale, semilunate carpal, left metacarpals I-III, manual phalanges III-2 and 3, manual unguals I, II, and III, ilial fragment, most of an incomplete femur, right and left tibiae and fibulae, left astragalus and calcaneum, portions of right and left metatarsal packets2, left pedal phalanges III-1, III-2, III-3, IV-1, IV-2, IV-3, IV-4, and pedal unguals II and III and the proximal portion of IV.

Etymology

'Hesper', (Greek) referring to the discovery in the American West, 'ornis', (Greek) for bird and 'oeides', (Greek) for similar, referring to the avian-like form of derived paravians. The trivial epithet honors the Miessler family, who have been avid supporters of the project.

Occurrence

Douglas, Converse County, Wyoming, USA; middle portion of Morrison Formation, which has been variously dated between Oxfordian and Tithonian in age (Trujillo, 2006; Trujillo et a., 2014), associated vertebrate fossils include the sauropod *Supersaurus*, a stegosaurid plate, and isolated large theropod teeth.

Diagnosis

A paravian with the following derived characters: pneumatic jugal (also in *Zanabazar* and some eudromaeosaurs among maniraptorans); short posterior lacrimal process (<15% of

ventral process length, measured from internal corner; also present in *Zanabazar*, *Archaeopteryx* and *Epidexipteryx*); quadrate forms part of lateral margin of paraquadrate foramen; small external mandibular fenestra (<12% of mandibular length; also in *Zhenyuanlong* and *Dromaeosaurus* among non-avian paravians); humeral entepicondyle >15% of distal humeral width (also in some avialans); manual ungual III subequal in size to ungual II (also in *Daliansaurus*, IGM 100/44 and *Mahakala*); mediodistal corner of tibia exposed anteriorly (also in *Archaeopteryx* and *Jeholornis*).

Locality & Geologic Context

In the summer of 2001, members of the Tate Geological Museum were excavating a large sauropod dinosaur (*Supersaurus vivianae*; see Lovelace et al., 2007) at the Jimbo Quarry in the Morrison Formation near Douglas, Wyoming (Fig. 3-1). WYDICE-DML-001 (aka the 'Lori' specimen; see Wahl, 2006) was discovered during the removal of overburden from the quarry. The accidental nature of the discovery directly impacted the recovery of the delicately preserved specimen, resulting in some portions being damaged or lost during collection.

The Morrison Formation in central Wyoming is considered undivided adding to the difficulty in long distance correlation (Trujillo, 2006; Trujillo et al., 2006; Trujillo et al., 2014). Very fine (100 μm) euhedral zircons have been observed in heavy mineral separates from a smectite rich mudstone within 0.5 m above and a mixed smectite-illite mudstone below the interval in which WYDICE-DML-001 was discovered.

The Jimbo Quarry (Unit 1 of Fig. 3-2) is an isolated discrete unit with an uneven upper and lower surface that is interpreted to be a hyperconcentrated flow resulting from post-fire soil destabilization (Lovelace, 2006). WYDICE-DML-001 was discovered in a fine grained muddy

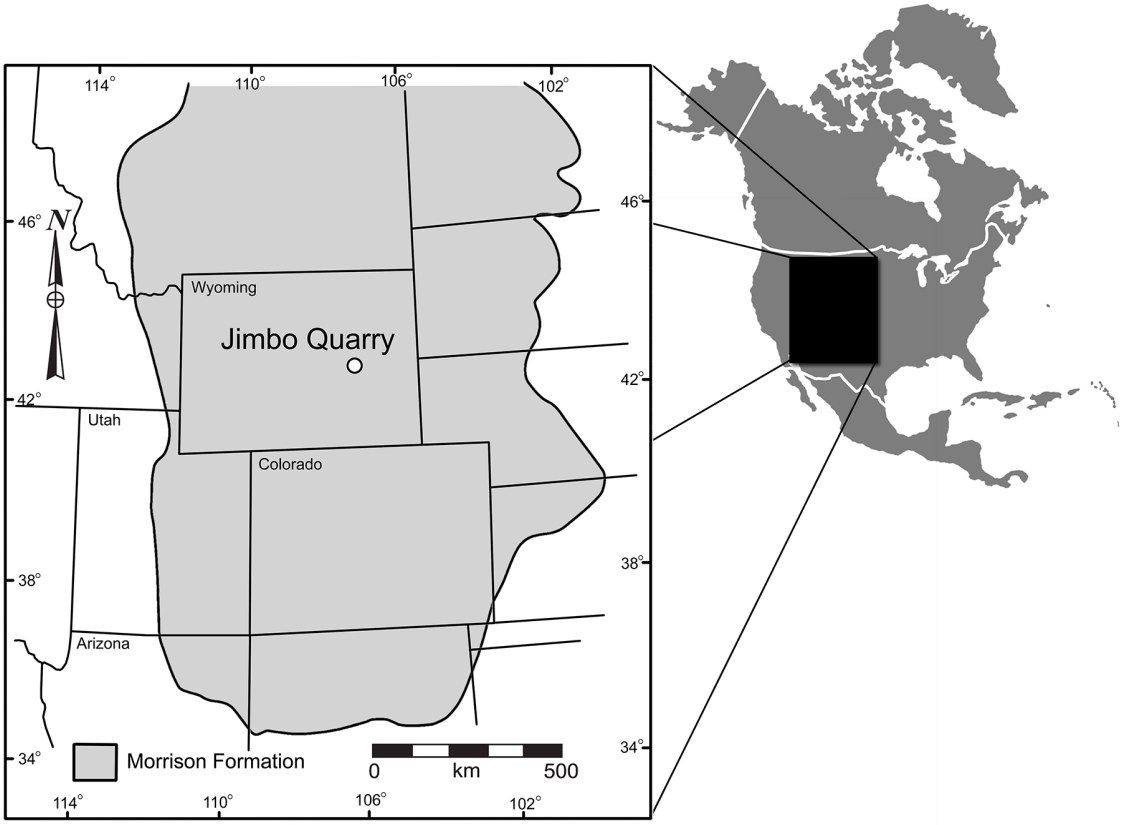

Figure 3-1. Geographic relationship of the Jimbo Quarry and the majority of the Morrison Formation, Late Jurassic, USA. *Formation outcrop and map data based on paleobiodb.org.*

sandstone that immediately overlies the Jimbo Quarry (Unit 2 of Fig. 3-2); this unit fines upwards over 10-20 cm into the first 1.5 m of mixed smectite-illite mudstone of Unit 3 (Fig. 3-2). Unit 3 exhibits 6 discrete micritic limestone layers that overly the first 1.5 m of mudstone and are each differentiated by 20-50 cm of mixed smectite-illite mudstones with abundant charophytes and conchostraca (Lovelace, 2006).

The first four meters of strata overlying the Jimbo Quarry have been interpreted as representing a cyclical rise and fall of the local water table in a marginal lacustrine or wetland environment (Lovelace, 2006) similar to those seen in the Big Horn Basin of Wyoming

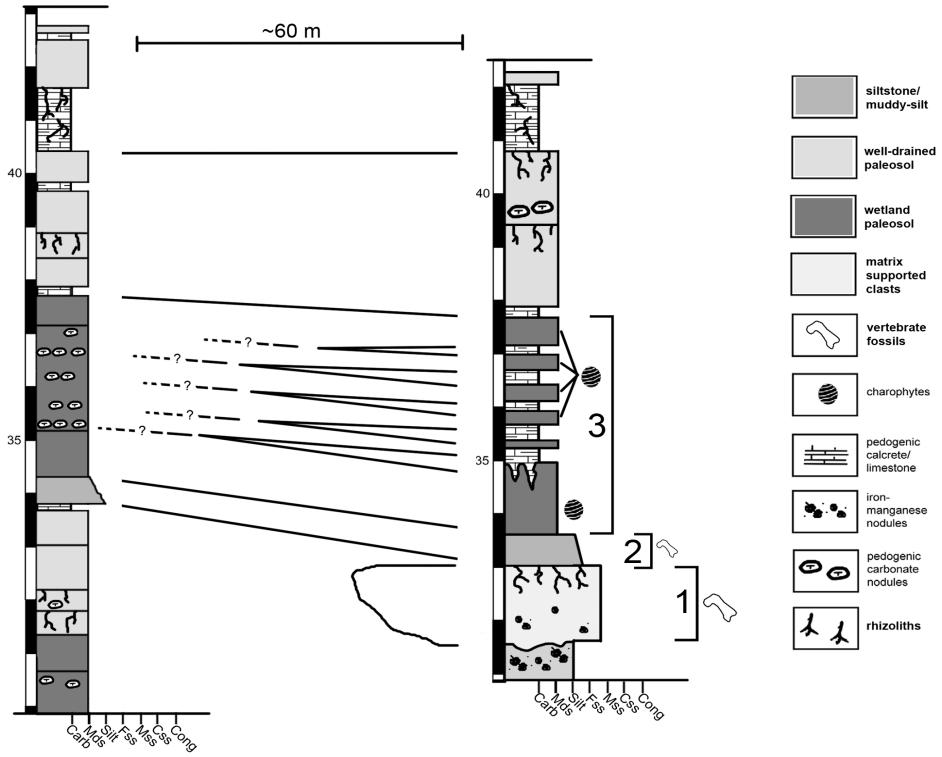

Figure 3-2. Condensed stratigraphic sections demonstrating the lateral variability near the Jimbo Quarry.

(Jennings et al., 2011). The concentrated presence of barite in long bones and pleurocoels is consistent with a saturated microenvironment where free sulfur is available due to organic decay; this has been observed elsewhere in marginal lacustrine and wetland environments within the Morrison of Wyoming (Jennings & Hasiotis, 2006; Jennings et al., 2011). The interpretation of a wetlands or marginal lacustrine environment is supported by XRD of clay minerals, presence of freshwater algae and arthropods, and the lack of sedimentary structures indicative of fluvial transport.

WYDICE-DML-001 is preserved in partial articulation with little evidence of dissociation. The presence of organic material at the distal end of several manual and pedal

unguals is consistent with the preservation of a keratinous sheath; no other soft-tissue preservation was observed. Much of the thoracic region is absent, although the relative positioning of the remaining elements (Fig. 3-3) suggests an animal in a resting position. Given the autochthonous nature of deposition it appears that *Hesperornithoides* was an inhabitant of wetland environments for at least a portion of its life history.

Description

WYDICE-DML-001 has an estimated length of 89 cm (Figs. 3-4 & 3-5, Table 3-1). The hind legs are folded in a crouching or resting position, the head is turned to the side underneath the left manus, and the preserved mid-caudal series wraps around the torso, reminiscent of the sleeping posture preserved in *Mei* and *Sinornithoides* (Xu and Norell, 2004; Gao et al. 2012; Russell and Dong, 1994). *Hesperornithoides* is compared below both to other paravians and to other small Morrison coelurosaurs.

Ontogenetic status

Visual inspection under 100x magnification showed neural arches are fused with fully obliterated synchondroses sutures on all preserved vertebrae, ruling out a hatchling or juvenile individual (sensu Hone, et al., 2016). Adult or subadult status is reinforced by general skeletal proportions (Fig. 3-5, Tables 3-1 & 3-2), as WYDICE-DML-001 lacks a relatively enlarged cranium or other allometric proportions associated with early ontogenetic stages. WYDICE-DML-001 does not exhibit signs of advanced ageing, as the skull and proximal tarsal sutures lack evidence of obliteration by co-ossification. Without histological analysis the ontogenetic stage cannot be resolved beyond “adult or subadult”, but either designation would result in minimal

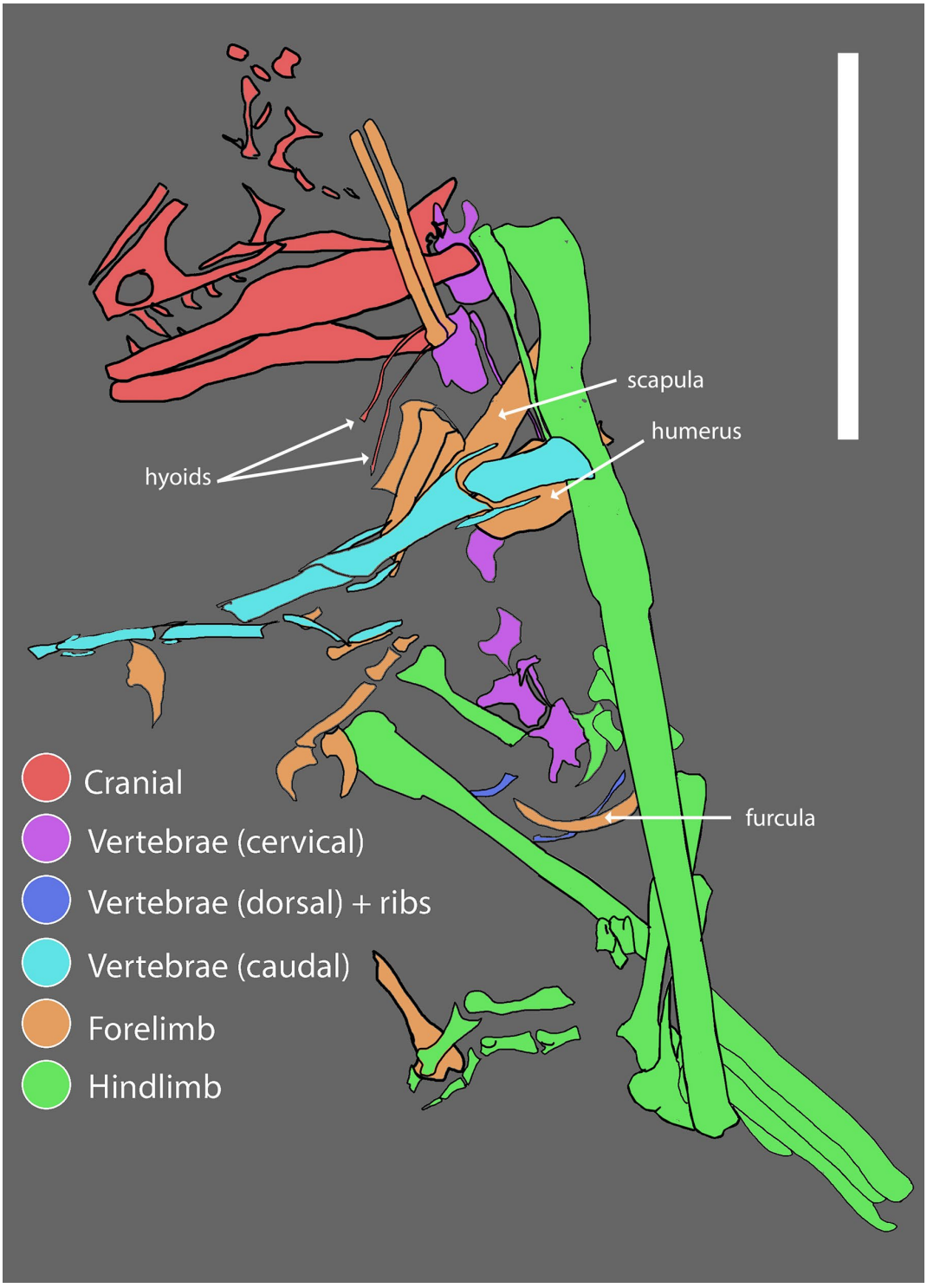

Figure 3-3. Reconstructed quarry map. *Association of skeletal elements assembled from 3D scans of specimen blocks prior to final mechanical preparation.*

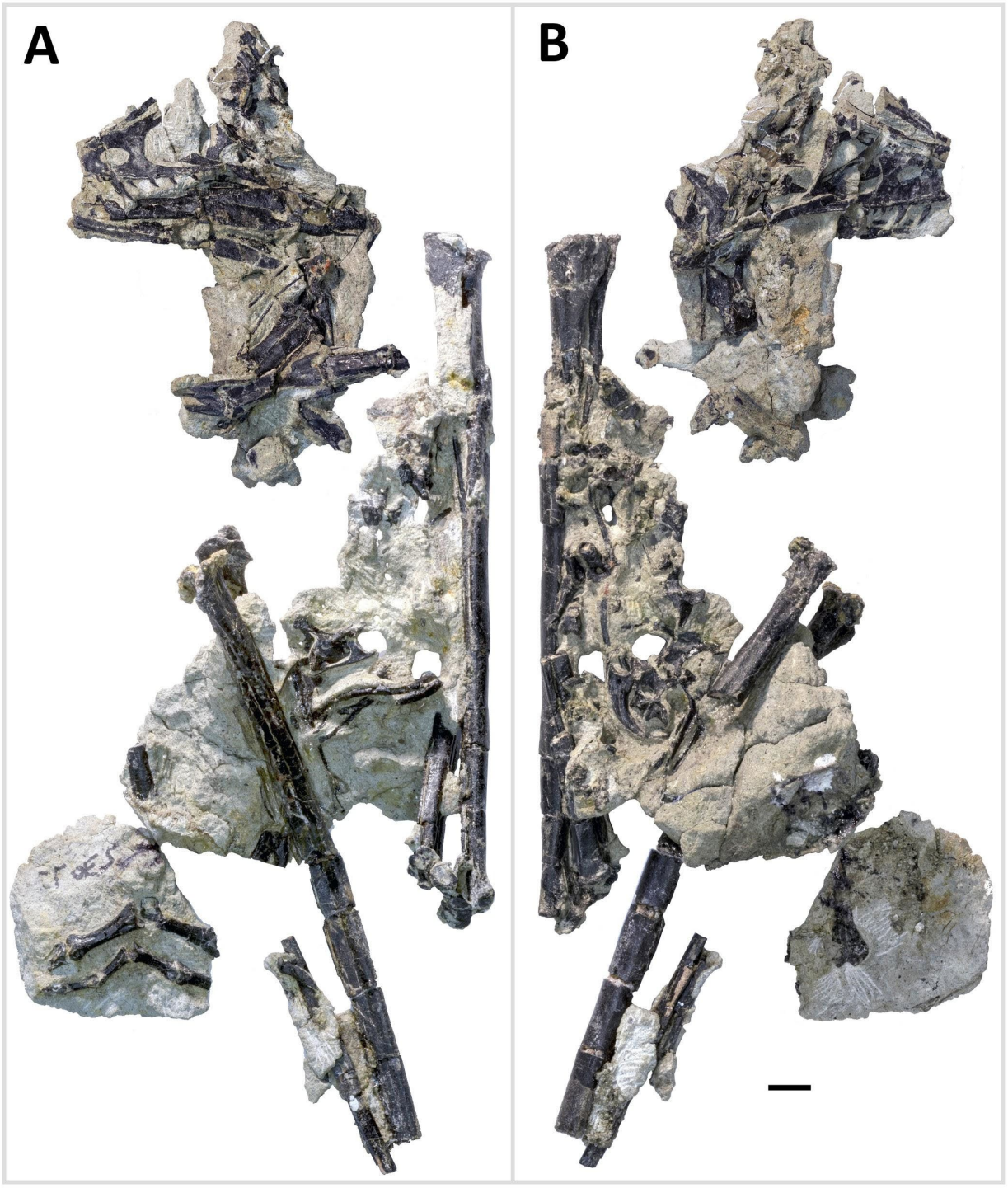

Figure 3-4. Primary blocks of WDC DM-001. *"Left" (A) and "right" (B) sides of the blocks after final preparation (B). Scale bar = 1 cm.*

additional linear skeletal growth, making the estimated 1 meter total length (Table 3-1) of *Hesperornithoides* is therefore substantially smaller than other relatively complete theropods from the Morrison Formation (Foster, 2003). The same can be said about individual elements, for example the humerus of WYDICE-DML-001 is 29% the length of the *Coelurus* holotype, 17% the length of the *Tanycolagreus* holotype and 28% the length of the *Ornitholestes* holotype.

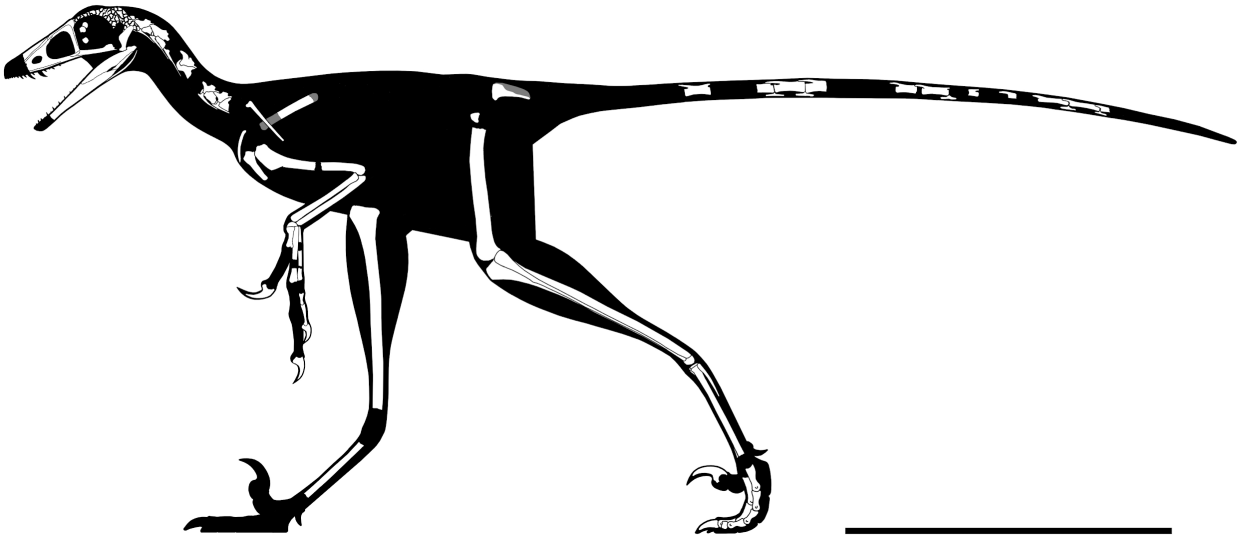

Figure 3-5. Rigorous skeletal reconstruction of WDC DML-001. *Scale bar = 25 cm.*

Skull

Cranial elements are preserved in a separate "skull block" (Figs. 3-3 & 3-4) prepared so both the right and left skull elements are largely visible in lateral view; some palatal elements are visible on the right side of the block. The right jugal, lacrimal, and posterior process of the maxilla are articulated and well preserved; the right quadrate is also exposed (Fig. 3-6). The skull and mandible exhibit some lateral compression with the left side being dorsally displaced (Fig. 3-6). The braincase suffers from both inadvertent damage during collection (some natural molds of

Element	Longest measurement (mm)	Other measurement (mm)
SKULL		
ventral length* (maxilla to quadrate)	39.5	
longest maxillary tooth crown	6.4	
shortest erupted tooth crown	2.1	
mandible* (missing anterior end)	42.5	
maxilla jugal ramus height	3.4	
AXIAL (centrum length)		
CV3	11.7	
CV4	est 14	
CV?6	14.5	
CV8	13.7	
CV9	11.7	
proximo/mid caudal	20.8	
CA B (mid caudal)	22.2	max height = 6
CA C (mid caudal)	22.3	
CA E (mid caudal)*	23.6	max height = 4.9
CA H (distal caudal)	18.2	3.2
CA I (distal caudal)	17.5	2.5
LENGTH ESTIMATES		
head	66	
neck	108	
dorsals	130	
sacrum	45	
caudal	540	
total	889	

Table 3-1. Measurements of the axial skeleton of WYDICE-DML-001.

broken elements exist) and pre-depositional disruption of elements. Posterior skull roof elements are progressively displaced dorsally; the left jugal is dorsoventrally rotated out of position underlying the posterior process of the maxilla. A portion of the lower half of the left lacrimal is exposed in lateral view; a medial impression of the mid-lacrimal is also visible. The premaxillae, as well as anteriormost portions of the maxillae, nasals, and dentaries were unfortunately destroyed during discovery of the specimen.

The skull is triangular in lateral aspect as seen in most basal paravians and enough of the snout is preserved to show the external naris was not enlarged. The maxilla exhibits an extensive, sharp-rimmed antorbital fossa containing a D-shaped antorbital fenestra, a large maxillary fenestra, and the posterior margin of a promaxillary fenestra (Fig. 3-6). This rim is also found in derived members of Sinovenatorinae (Xu et al., 2002: Fig. 1a; Xu et al., 2011: Fig. S1a; Xu et al., 2017: Fig. 2a), Microraptoria (Xu and Wu, 2001: Fig. 4B; Pei et al., 2014: Fig. 2) and some archaeopterygid specimens (Pei et al., 2017a: Fig. 5; Rauhut et al., 2018: Fig. 8A). Similar to most dromaeosaurids and *Halszkaraptor* (Godefroit et al., 2008: Fig. 4; Lu and Brusatte, 2015: Fig. 2; Zheng et al., 2009: Fig. 2a; Cau et al., 2017: Fig. 3b), the maxillary fenestra is dorsally displaced within the antorbital fossa (Fig. 3-7). The maxillary fenestra is positioned far from the unpreserved anterior edge of the antorbital fossa and is not set within a concavity unlike some dromaeosaurids. There is an accessory fossa posteroventral to the fenestra however, as in *Zhenyuanlong* (Lu and Brusatte, 2005: Fig. 2) but less developed than in microraptorians. A robust external ascending process separates the nasal and elongate antorbital fossa until the anterior margin of the antorbital fenestra. Segmented CT data shows medially there is an

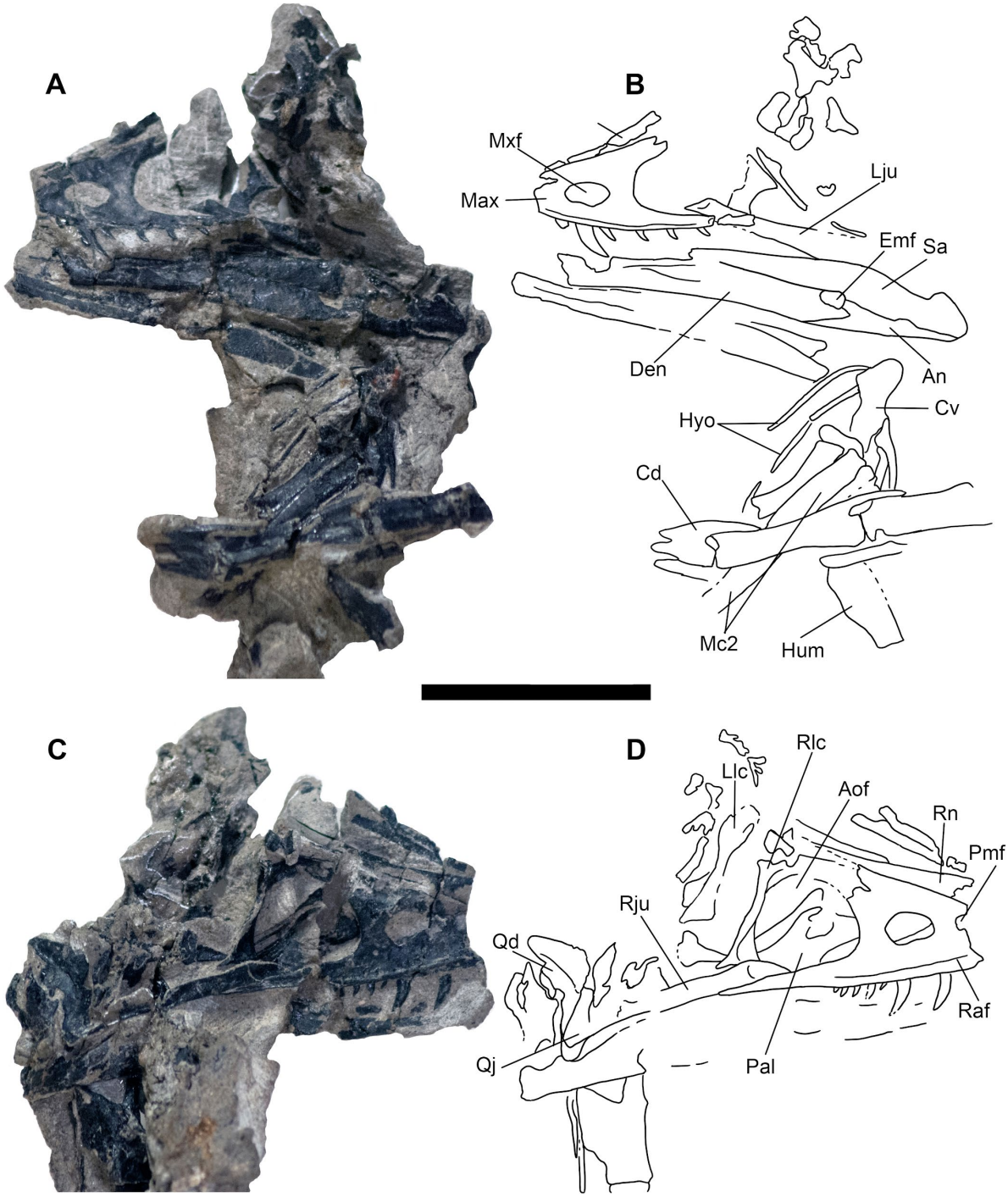

Figure 3-6. Skull block and interpretive drawing. *Skull block in left lateral (A, B) and right lateral (C, D) views. Abbreviations: An, angular; Aof, antorbital fenestra; Cd, mid caudal vertebrae; Cv, cervical vertebra; Den, dentary; Emf, external mandibular fenestra; Hyo, hyoids; Hum, humerus; Lju, left jugal; Llc, left lacrimal; Max, maxilla; Mc2, metacarpal II; Mxf, maxillary fenestra; Pal, palatine; Pmf, promaxillary fenestra; Qd, quadrate; Qj, quadratojugal; Raf, ridge under antorbital fossa; Rju, right jugal; Rlc, right lacrimal; Rn, right nasal; Sa, surangular. Scale bar = 5 cm.*

extensive palatal shelf placed more ventrally than in eudromaeosaurs (Fig. 3-7), and posteriorly the jugal process is shallow. Both promaxillary and epiantral recesses are developed, the postantral pila does not extend into the antorbital fenestra as it does in some dromaeosaurids, and the palatal shelf does not extend dorsally to be visible laterally as it does in *Saurornitholestes* and *Atrociraptor* (Fig. 3-7). Compared to *Ornitholestes*, the maxilla has a larger maxillary fenestra, a medial fenestra for the maxillary antrum (Witmer, 1997:42) and an external dorsal process that ends sooner so that the nasal contacts the antorbital fossa.

The incomplete nasals are unfused with smooth external surfaces which have no significant transverse convexity. The portion adjacent to the antorbital fossa on the left nasal lacks accessory pneumatic foramina. Both lacrimals are preserved, lacking horns but possessing the lateral expansion on the dorsal edge typical of pennaraptorans. A foramen is present in the posterodorsal corner of the antorbital fossa, here scored as pneumatic, but given similar structures have been considered to house the lacrimal duct (e.g. Fig. 5A in Yin et al., 2018 for *Sinovenator*), more objective criteria are needed. The posterior lacrimal process is short (Fig. 3-8), unlike most long-tailed paravians, but also present in *Zanabazar*, *Archaeopteryx* and *Epidexipteryx* (Barsbold, 1974: plate 1 Fig. 1b; Rauhut, 2013: Fig. 1A; Zhang et al., 2008: Fig. 1c). The lacrimal differs from *Tanycolagreus* in lacking a dorsally projecting horn (Carpenter et al., 2005a: Fig. 2.4G), and from *Ornitholestes* in having a laterally projecting antorbital process, both more similar to maniraptoriforms. The ventral process is strongly expanded distally and has a lateral lamina which never fully overlaps the medial lamina. The jugal is dorsoventrally low but lateromedially compressed beneath the orbit and laterotemporal fenestra. Segmented CT data indicates that unlike most maniraptorans (exceptions are *Zanabazar*, *Velociraptor* and *Deinonychus*; Norell et al., 2009:34; Barsbold and Osmolska, 1999:200; Witmer, 1997:45) and

Ornitholestes (Witmer, 1997:45), the jugal is pneumatic (Fig. 3-9) with a large opening in the antorbital fossa. The anterior end is only slightly expanded and there is no foramen medially at the level of the postorbital process. Along its ventral edge, there is a longitudinal ridge extending most of the way under the orbit. The jugal and postorbital contact completely separates the orbit from the infratemporal fenestra.

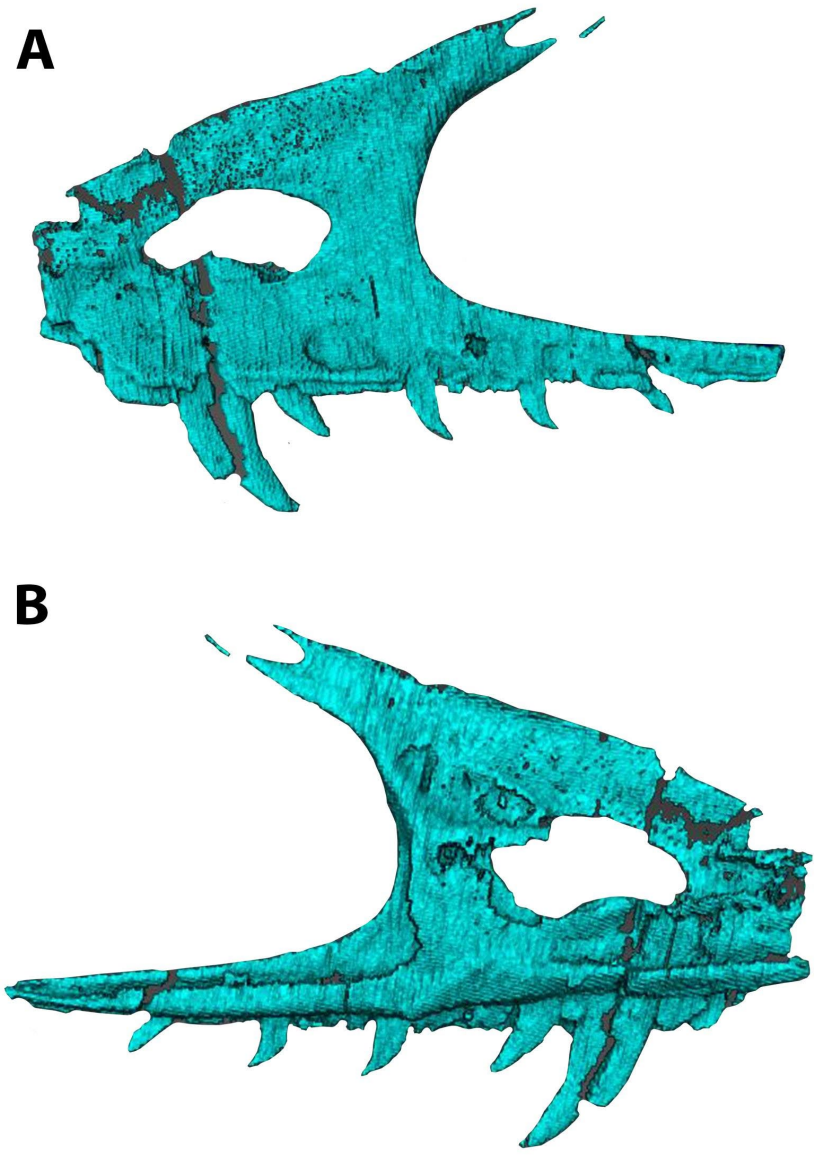

Figure 3-7. Segmented left maxilla of WDC DML-001. *Shown in lateral (A) and medial (B) views.*

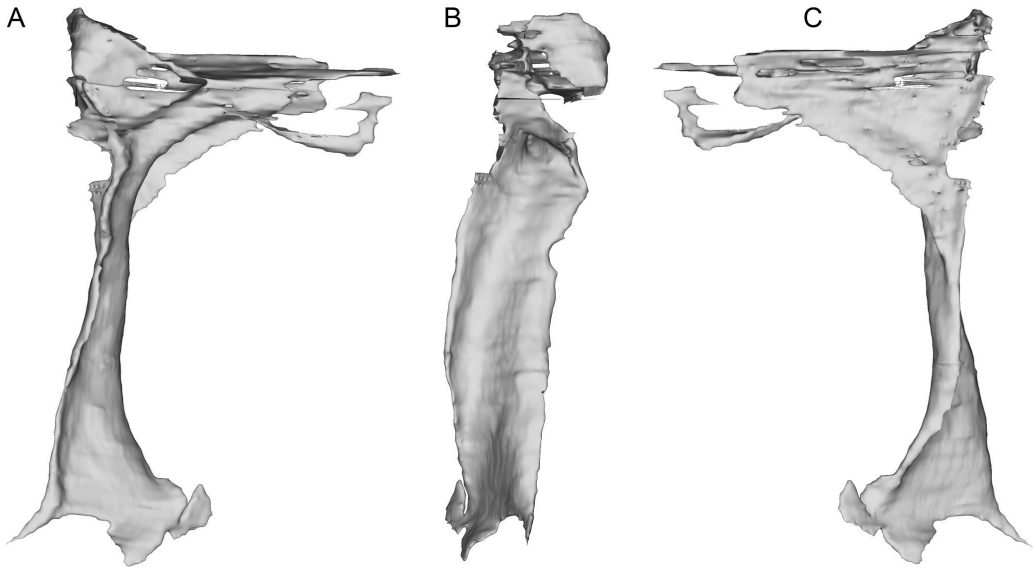

Figure 3-8. Segmented right lacrimal of WDC DML-001*. Shown in lateral (A), posterior (B) and medial (C) views.*

Figure 3-9. Segmented left jugal of WDC DML-001. *Shown in medial (A), lateral (B) and anterolateral oblique (C) views.*

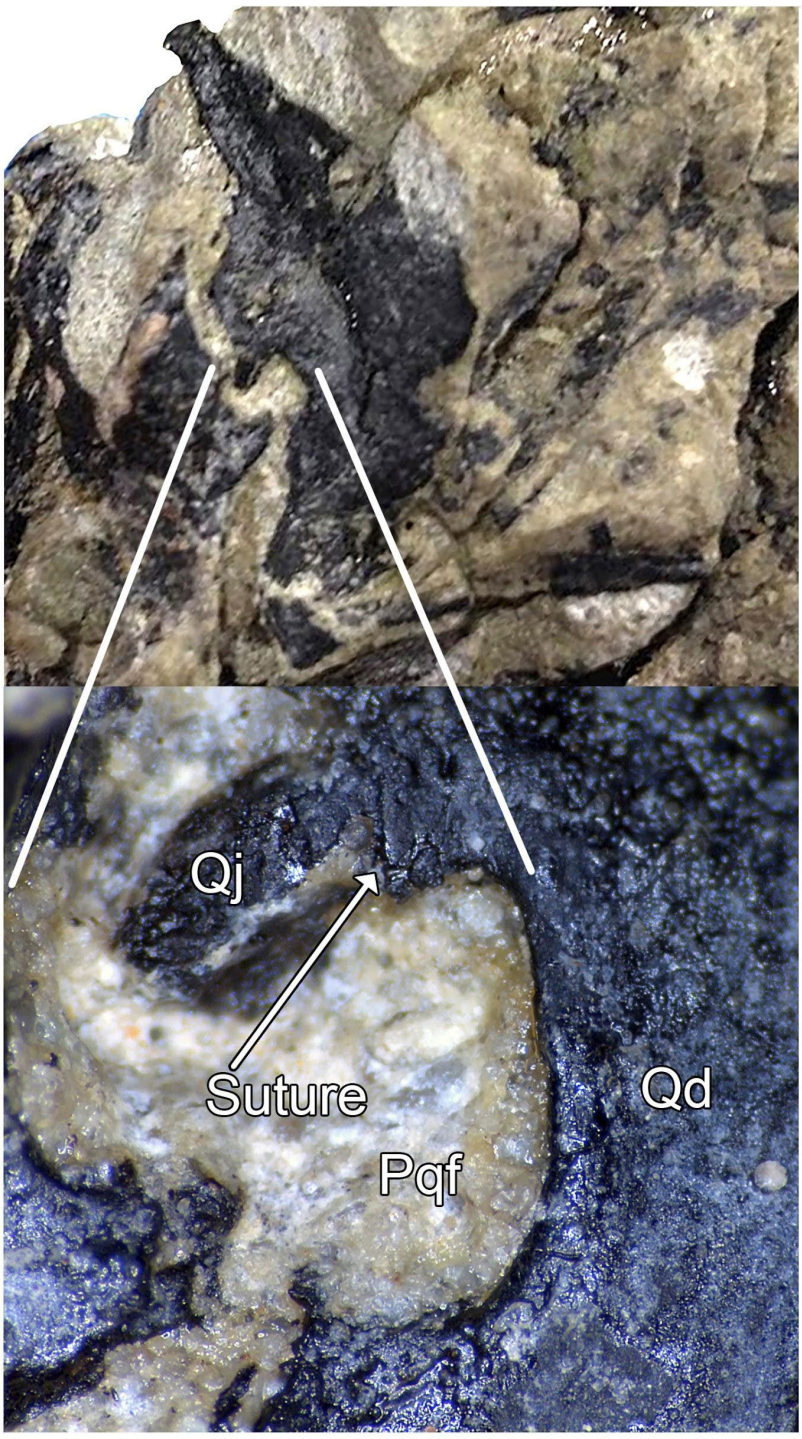

Figure 3-10. Paraquadrate foramen of WDC DML-001. *Paraquadrate foramen and inset detail showing the contribution of the quadrate to the paraquadrate foramen. Abbreviations: Pqf, paraquadrate foramen; Qd, quadrate; Qj, quadratojugal.*

The postorbital, squamosal, quadratojugal, palatine and perhaps pterygoid cannot be exposed via mechanical preparation in sufficient detail to score characters from. Interference from barite inclusions in the anterior cervical vertebrae have frustrated multiple CT scan attempts. Proportions of suborbital bones suggest a parietal shorter than the frontal. Both quadrates are preserved and partially exposed from surrounding matrix, showing a planar articulation with the quadratojugal and bicondylar distal articulations. CT scans show the quadrate is pneumatized as in troodontids but unlike *Ornitholestes*, with a fossa on the posterior surface. It partially encloses the small paraquadrate foramen laterally unlike *Tanycolagreus* (Carpenter et al., 2005a: Fig. 2.4O) and other maniraptorans (Fig. 3-10; compare to e.g. Barsbold et al., 1987: plate 49 Fig. 4; Xu and Wu, 2001: Fig. 4D; Burnham, 2004: Fig. 3.10B; Hu et al., 2009: Fig. S2d; Gao et al., 2012: Fig. 2A; Xing et al., 2013: Fig. S1; Cau et al., 2017: Fig. 3a; Gianechini et al., 2017: Fig. 5; Yin et al., 2018: Fig. 7A). Note in figure 3-10 there is a vertical suture at the top center of the closeup image and that bone to the left of that is a fragment of quadratojugal adhering to the quadrate.

Mandible & dentition

The left and right mandibles are complete save for the anterior portion of the dentaries that were destroyed during discovery. The lateral surface of the posterior left mandible is well exposed, however the dorsolateral dentary is largely obscured by the overlying maxillary teeth and associated matrix and must be described from segmented CT scan data. The posteriormost right mandible is laterally exposed and the medial surface of the dentary is visible on the left side of the skull block. The labial dentary groove widening posteriorly is clearly visible; initially described as a troodontid character (Hartman et al., 2005; Wahl, 2006) it is here resolved as a symplesiomorphy seen also in some microraptorians, unenlagiines, *Halszkaraptor* and most

archaeopterygids (Xu and Wu, 2001: Fig. 6; Paul, 2002: plate 7A; Gianechini and Apesteguia, 2011: Fig. 2Ag; Pei et al., 2014: Fig. 2; Cau et al., 2017:S23; Gianechini et al., 2017: Fig. 1-2; Lefèvre et al., 2017: Fig. 2; Pei et al., 2017a: Fig. 5). The groove is absent in *Ornitholestes* however, and the dentary differs from that referred to *Coelurus* in not being downturned (Carpenter, et al., 2005b: Fig. 3.3). Whether the new taxon's dentaries are entirely straight or slightly upturned anteriorly is uncertain due to the missing anterior tips. The slender dentaries lack a posterolateral shelf and have a deep Meckelian groove positioned at approximately midheight. *Hesperornithoides* has a small external mandibular fenestra (<11% of mandibular length; Fig. 3-5B) unlike most other maniraptorans except for *Zhenyuanlong* and *Dromaeosaurus* (Currie, 1995: Fig. 7A; Lu and Brusatte, 2015: Fig. 2). No coronoid is obvious despite a well preserved in situ mandible, but we conservatively score the taxon unknown given the reduced state of this element in some maniraptoriforms. Posteriorly, the surangular is shallower than the dentary at the anterior border of the external mandibular fenestra (Fig. 3-6A), has a very long suture with the dentary anterior to this fenestra, and lacks a pronounced coronoid eminence and or a process invading the fenestra.

The lack of anteriormost portions of the mandible and maxilla prevent determination of changes in size or spacing of alveoli, but in both elements the posterior teeth are smallest and the left maxilla preserves an anterior crown base smaller than the next tooth, the largest in the series. At least ten maxillary teeth and eleven dentary teeth were present, with the total count being perhaps ~14 and ~17. Teeth are relatively large and recurved and possess well developed mesial serrations as in most dromaeosaurids, *Troodon* and *Caihong* (Hu et al., 2018:4). The serrations

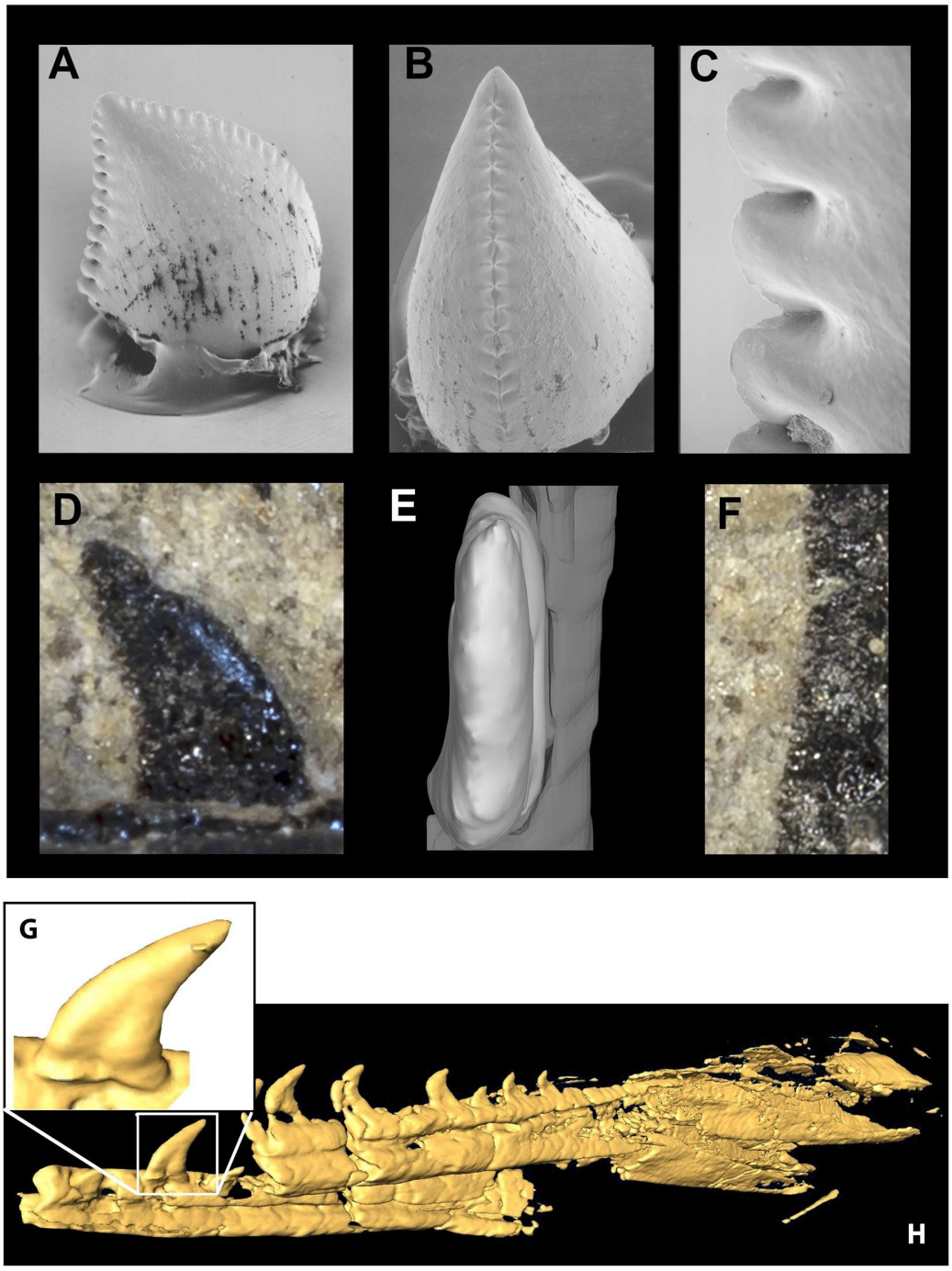

Figure 3-11. Mandible and comparative tooth morphology of Koparion and Hesperornithoides. *Tooth of Koparion in 'side' (A) and mesial (B) views, and a detail of the distal serrations (C). Hesperornithoides maxillary tooth in labial view (E), rendered from CT data in mesial view (F), inset details of segmented tooth and segmented oblique view of anterior mandibular elements of Hesperornithoides (G). Photo credit (A-C): Dan Chure.*

on the mesial carinae of maxillary teeth are smaller than the distal serrations as in basal dromaeosaurids. Mesial serrations are restricted to the apical third of the crown and appear absent in some teeth. Serrations are small (5.5 per mm distally) as in *Sinusonasus*, *Liaoningvenator* and some sinovenatorines, and not apically hooked. Similar to the condition described for *Serikornis*, the maxillary teeth are anisodont with crown height of the largest exposed teeth twice the size of others (Lefèvre, et al., 2017: Fig. 2). There is a slight mesiodistal constriction between tooth root and crown in fully erupted teeth (Fig. 3-11G) unlike *Ornitholestes* and most dromaeosaurids except some microraptorians (Xu et al., 2000: Fig. 2d; Xu and Li, 2016: Fig. 3), although no proximal expansion of the root is present. Both root and crown are labiolingually compressed, and the enamel shows no trace of longitudinal grooves. Chure (1994) previously described an isolated tooth from the Morrison Formation of Utah as the troodontid *Koparion douglassi*. This tooth differs from *Hesperornithoides* teeth in being more recurved, labiolingually wide (Basal Width / FABL ~.72 compared to ~.45), possessing large serrations as in derived troodontids, exhibiting mesial serrations that extend to within two serration lengths of the crown base, and possessing blood pits (Fig. 3-11). While it may belong to a derived troodontid, serration size and extent was extremely homoplasic in our phylogenetic results suggesting caution should be applied. Paired hyoids are preserved as thin parallel rod-like structures on the left side of the skull block; posteriorly the hyoids overlie the medioposterior surface of the right mandible.

Axial skeleton

The axial skeleton is distributed across three blocks (Fig. 3-4). Six presacral vertebrae are preserved on the “body block”, three anterior cervicals, two mid-cervicals and a cervicodorsal (Fig. 3-12). Three articulated mid-anterior caudals are found on the skull block, and the

remaining caudal vertebrae are preserved on the “hand block”, some as natural molds. Cervical centrum measurements indicate a cervicofemoral ratio (~0.95) similar to anchiornithines (0.81-1.01), troodontids (0.83-1.08) and dromaeosaurids (1.02-1.04) but shorter than *Halszkaraptor* (2.65) or *Archaeopteryx* (1.21-1.37). The axis is partially preserved, possessing epipophyses that extend past the postzygapophyseal tips. The third cervical centrum is over four times longer than tall posteriorly extending past the neural arch, with amphicoelous articular surfaces, a transversely convex ventral surface and a single pair of pleurocoels posterior to the parapophysis (Fig. 3-12B). CT cross sections and broken surfaces reveal additional cavities, including those extending into the zygapophyses (Fig. 3-12C). The neural spines are long and low, centered on the neural arch. Contra initial reports (Hartman et al., 2005; Wahl, 2006) some of the cervical ribs extend beyond the posterior margin of the centra. Cervical ribs begin broad in cross-section but thin rapidly in length to an almost hair-like diameter (Fig. 3-12E). Initial mechanical preparation missed this thinning, and it appears that other paravians described as having short cervical ribs may also be in need of additional preparation to ensure accurate scoring of this character (S.H., personal observation). Two cervical vertebrae are preserved with fused cervical ribs, consistent with a subadult or adult individual.

A single anterior dorsal vertebra is preserved (Fig. 3-12F). Its centrum is longer than wide or tall, posteriorly concave and has a pleurocoel behind the parapophysis with no lateral fossa. The anteroventral centrum is hidden by matrix, preventing determination of hypapophyseal height. Separated hyposphenes are present posteriorly. The transverse processes are short according to our newly quantified version of this classic TWiG character. It has a fan-shaped and moderately tall neural spine.

Appendicular Element	Longest measurement (mm)	Addl. measurement (mm)
coracoid*	height 21.4	width 14.6
Left humerus* (proximal portion)	26.9	shaft - 32.5
Left ulna/radius	46.4	
Left MCI	16.9	
MCII + carpals* (missing distal end)	61	
manus phalanx III-2	7	
manus phalanx III-3	18.2	
manual ungual I	17.1	
manual ungual II	15.5	
manual ungual III	14.4	
Left femur* (missing proximal end)	93.9	
Left tibia	168	
Right tibia* (missing distal end)	153	
Left MT packet* (proximal portion)	55.2	
Left pes phalanx III-1	26.3	
Left pes phalanx III-2	17.3	
Left pes phalanx IV-2	13.2	
Left pes phalanx IV-3*	est 8.5	
Left pes phalanx IV-4	6.9	
pedal ungual III	13.6	basal height 3.7
Left pedal ungual IV		

Table 3-2. Measurements of the appendicular skeleton of WYDICE-DML-001.

Portions of at least 3 caudals are preserved on the hand skull block, an additional 9 caudals are preserved on the hand block, several as natural molds. The 12 caudals provide good representation from mid and distal portions of the tail (Fig. 3-5, 3-8G and 3-8H). Caudal

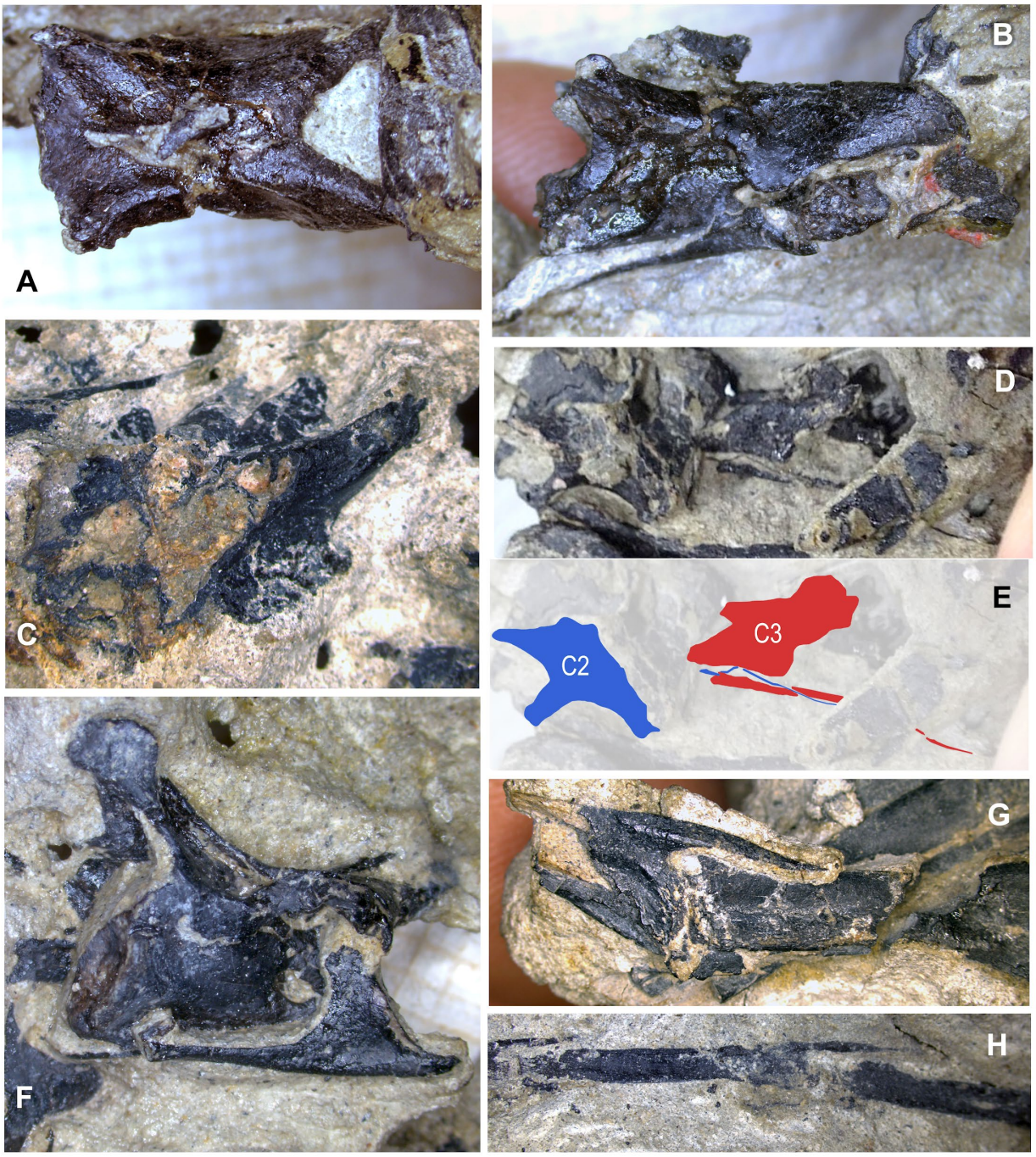

Figure 3-12. Select axial elements of WDC DML-001*. Cervical vertebra three in dorsal (A) and right lateral (B) views. (C) Mid-cervical vertebra in cross-section. Photo and schematic of association between axis and cervical three (D, E). Cervicodorsal in right lateral view (F). Articulated middle (G) and distal (H) caudal vertebrae in right lateral views.*

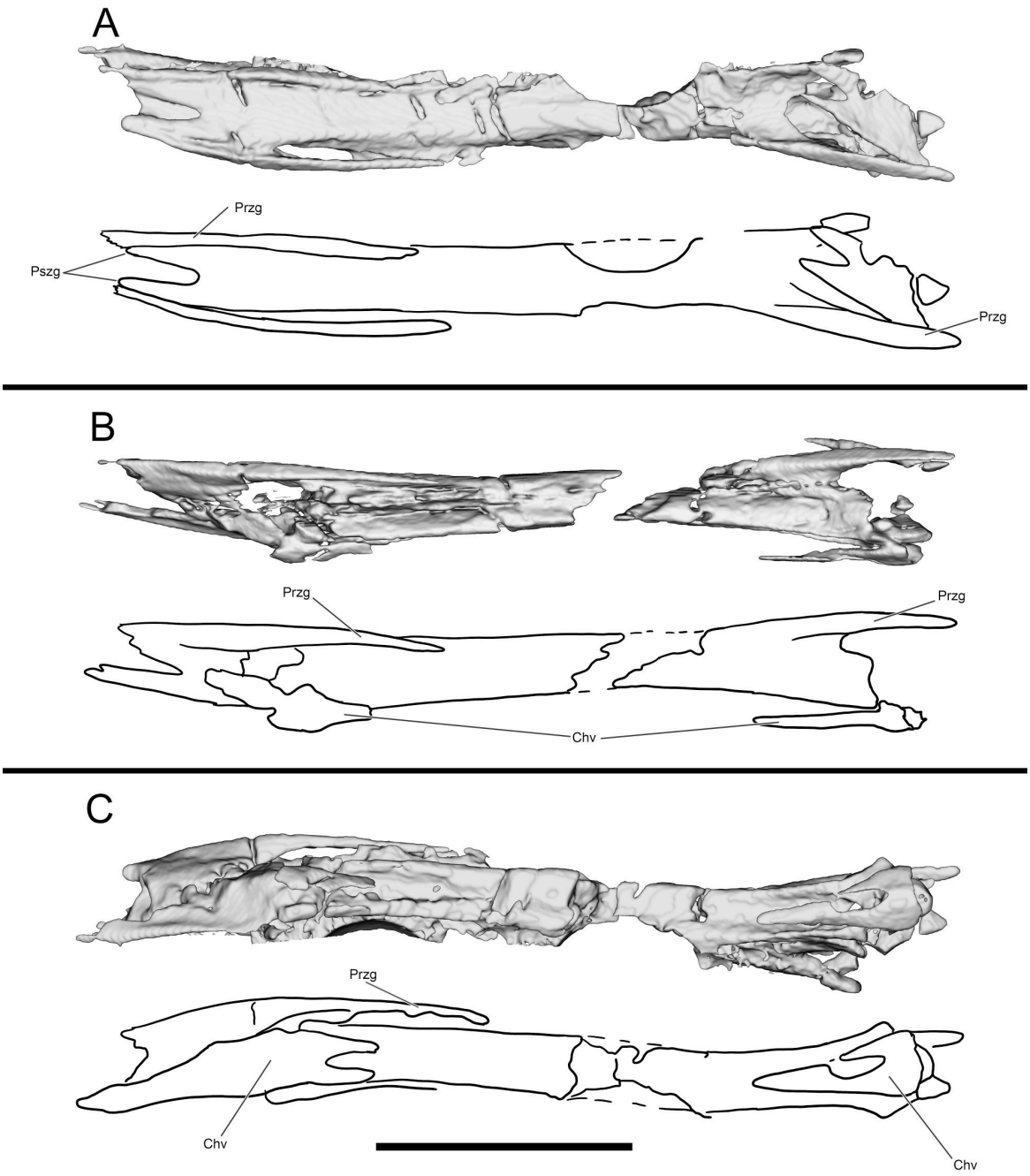

Figure 3-13. Segmented and interpretive drawing of middle caudal vertebrae of WDC DML-001. *In dorsal (A), right lateral (B) and ventral (C) view. Anterior is to the right in all views. Abbreviations: Chv, chevron; Przg, prezygapophysis; Pszg, postzygapophysis. Scale bar = 1cm.*

morphology suggests a distinct transition from shorter proximal caudals to elongate mid and distal caudal centra. The neural spines transition from well-developed on more proximal caudals to absent in mid-caudals, whereas *Coelurus* has low spines even on distal caudal vertebrae (Makovicky, 1995). The distal caudals have transversely flat dorsal surfaces between the zygapophyses, and while the distalmost elements develop a negligible concavity, it is never comparable to the sulcus found in other troodontids. Distal caudal prezygapophyses are between 33-100% of central length (Figs. 3-12H and 3-13), as in *Scansoriopteryx*, some troodontids, *Caihong* and jeholornithids (Currie and Dong, 2001: Fig. 5A; Czerkas and Yuan, 2002: Fig. 13; Zhou and Zhang, 2002: Fig. 1b-c; Xu and Wang, 2004: Fig. 1; Norell et al., 2009: Fig. 32A-B; Hu et al., 2018: Fig. 2e) but unlike the shorter prezygapophyses of *Coelurus* (Carpenter et al., 2005b: Fig. 3.6C). Unlike microraptorians and eudromaeosaurs, these processes lack bifurcation. The mid and distal caudals have a longitudinal sulcus on the lateral surface where centra meet neural arches, which is primitive for paravians, being present in unenlagiines, *Liaoningovenator*, archaeopterygids and *Jeholornis* (Motta et al., 2017:174; Shen et al., 2017: Fig. 4A). CT scans reveal pneumatopores within a fossa on the lateral surface of some caudal vertebrae. Ventrally, distal caudal centra exhibit a deep longitudinal groove. Mid-caudal chevrons are dorsoventrally flat but without highly elongate processes, and bifid anteriorly and posteriorly unlike those of *Ornitholestes* (Carpenter et al., 2005b: Fig. 3.6B") or other non-paravians.

Pectoral girdle & forelimb

The pectoral girdle is poorly preserved, but a large and robust furcula was preserved in association with the cervicodorsal vertebra on the body block. The boomerang-shaped furcula has an angle of approximately 80 degrees and curves posteriorly in lateral view. No hypocleidium or posterior groove are evident, and the furcula lacks strong anteroposterior

compression unlike most paravians besides *Velociraptor* (Norell and Makovicky, 1999:7). Remaining pectoral girdle elements include a portion of a strap-like scapula without a dorsal flange (preserved in part as natural mold on the body and skull blocks), and most of an enlarged coracoid, consistent with the pectoral girdle of other paravians. The coracoid possesses a posterior fossa and supracoracoid foramen but lacks signs of proximal pneumaticity.

The left forelimb is largely complete, missing the distal portion of the humeral shaft and the non-ungual phalanges of digits I and II; these elements are distributed across the skull, body, and hand blocks. The proximal half of the left humerus has been mechanically prepared to be fully free of matrix. The distal half of the right humerus is preserved on the body block, providing a nearly complete composite humerus. The ulna and radius are shorter than the humerus, and the resulting forearm is proportionately short (estimated forelimb to hindlimb ratio of .58, Table 3-1) as seen in *Mahakala*, *Mei*, *Tianyuraptor*, *Caihong*, *Zhenyuanlong*, *Austroraptor* and *Halszkaraptor* (Xu and Norell, 2004: supp. table 4; Novas et al., 2008: table 1; Zheng et al., 2009: table 1; Turner et al., 2011: table 1; Lu and Brusatte, 2015: supp. info. 1; Cau et al., 2017: supp. table 1; Hu et al., 2018: supp. table 1), and was clearly incapable of flapping flight.

The humerus is significantly shorter than the femur (0.63) and slender. The deltopectoral crest is proximally restricted, roughly triangular and projects closer to perpendicular to the head's long axis (Fig. 3-14E). *Hesperornithoides*' crest lacks the fenestra found in some microraptorians and the distinct lateral scar (Fig. 3-14F) seen in *Coelurus*, attributed to the m. pectoralis superficialis by Carpenter et al., (2005:60, Fig. 3.8B). The humeral head is anteriorly concave and proximally convex, and not separated from the bicipital crest by a capital groove. Well projected medially but unprojected anteriorly, this crest is proximodistally short but has a

straight inner edge. There is no trace of a pneumatricipital fossa or foramen in the proximal humerus. Distally the humerus is well expanded and exhibits an enlarged entepicondyle, over 15% of distal humeral width (Fig. 3-14D). Among maniraptorans, this is otherwise only seen in avialans such as *Zhongjianornis*, *Sapeornis*, *Jixiangornis*, *Confuciusornis* and various ornithothoracines (Chiappe et al., 1999: Fig. 38; Zhou and Zhang, 2003: Fig. 7a).

Unlike any of the three well preserved Morrison basal coelurosaurs, the distal ulna is highly compressed dorsoventrally to be over twice as wide as tall. It is also dissimilar from *Coelurus* and *Tanycolagreus* in being straight in side view (Carpenter et al., 2005a: Fig. 2.10B-C; Carpenter et al., 2005b: Fig. 3.8C-D). The distal end lacks significant proximoventral development of the articular surface, is roughly straight in dorsal perspective and has no well defined radial sulcus. The radius itself is over 70% of ulnar width at midshaft, exhibits no obvious groove or scaring posterodorsally on the shaft but does possess a distodorsal flange typical of pennaraptorans.

The semilunate carpal is preserved next to, but slightly displaced from the metacarpal packet on the skull block. It is not well exposed on the surface of the block, but CT scans reveal a well-developed semilunate morphology with a transverse trochlear groove (Fig. 3-14A). This is unlike the unfused distal carpal I of the much larger *Coelurus* specimen YPM 2010 which is more oblong than semilunate (Carpenter et al., 2005b: Fig. 3.9A). *Tanycolagreus* fuses the distal carpals but the resulting structure is very flat instead of semilunate (Carpenter et al.,

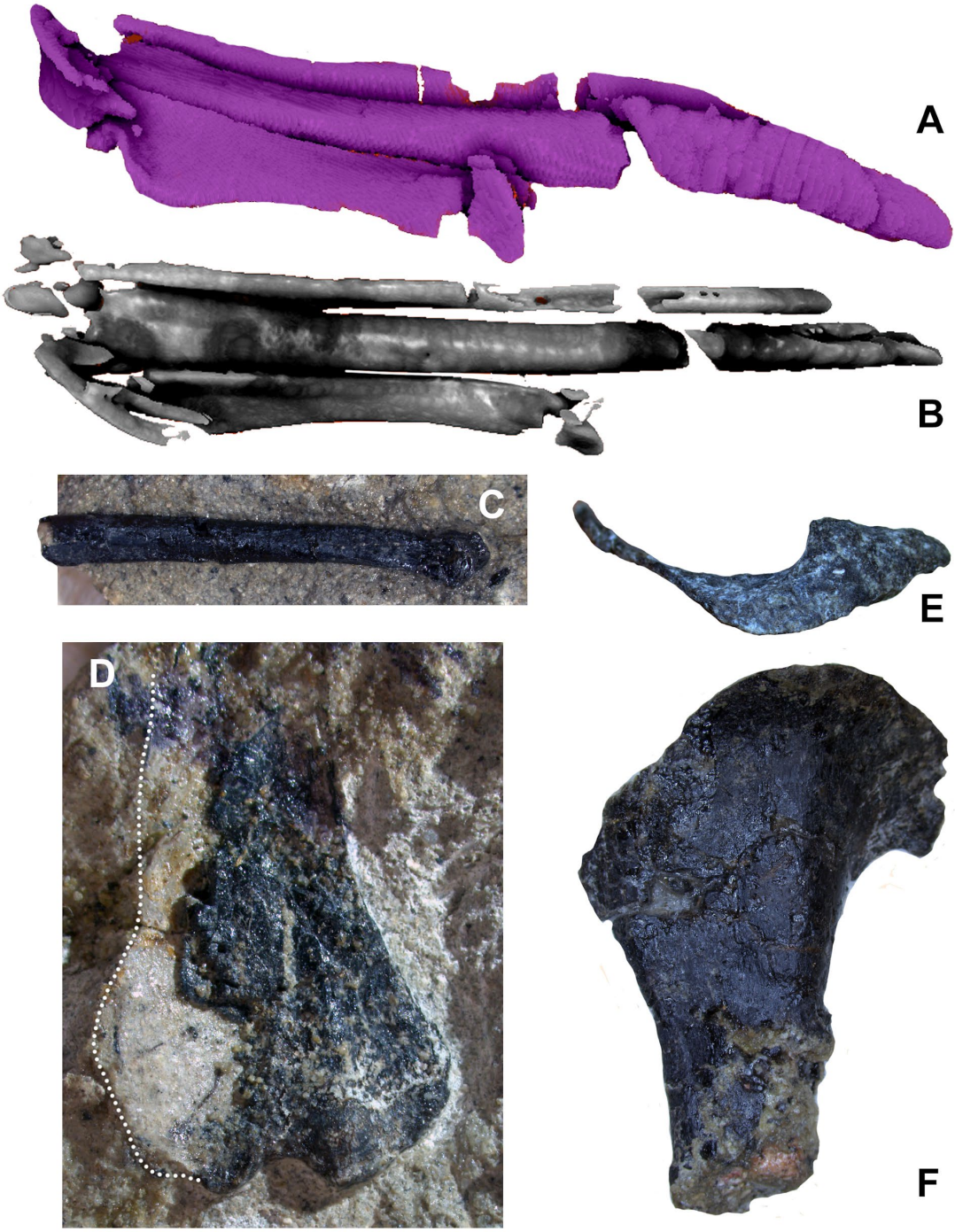

Figure 3-14. Forelimb elements of WDC DML-001. *Segmented left carpals and metacarpals in oblique (A) and extensor (B) views. (C) Distal portion of right MCIII in lateral view. (D) Distal end of right humerus in anterior view. Proximal end of left humerus in proximal (E) and lateral view (F).*

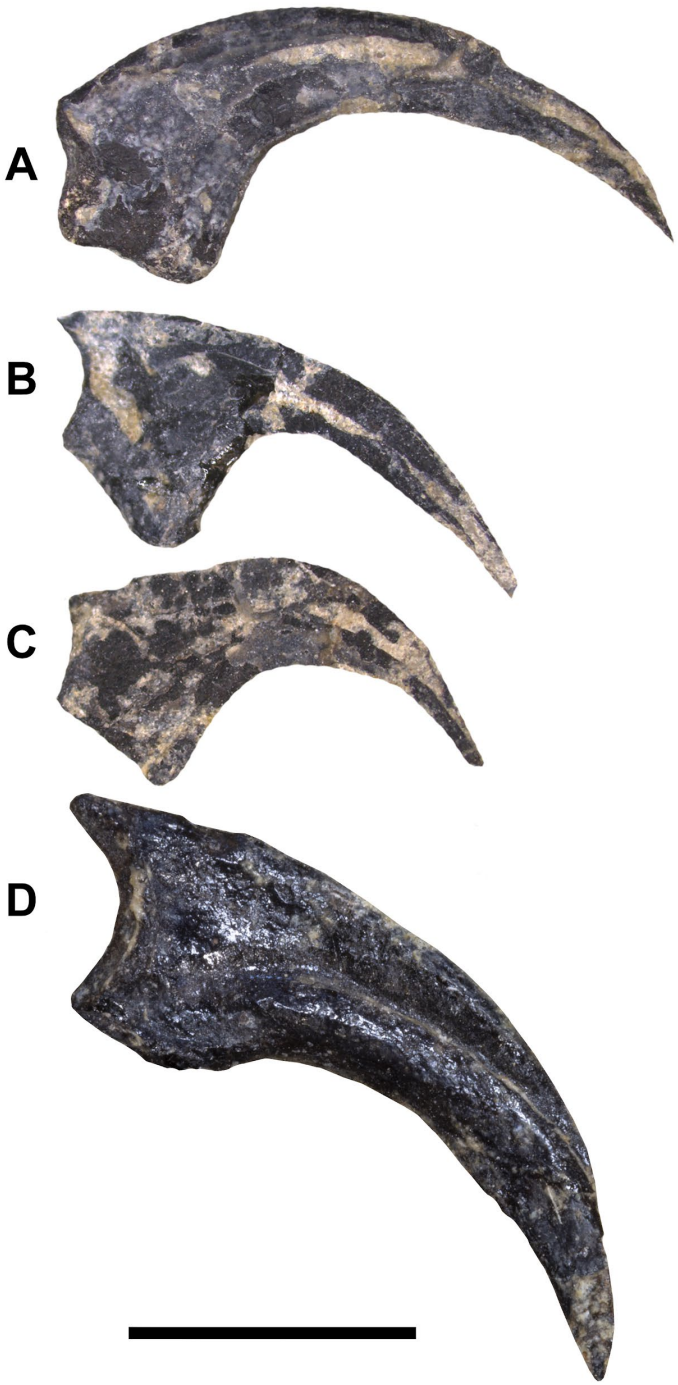

Figure 3-15. Select hindlimb elements of WDC DML-001*. Proximal end of left metatarsal packet in posterior (A) and anterior (B) views. (C) Right metatarsal I in medial view. (D) Cross-section through left metatarsals from distal perspective, anterior is to the bottom. (E) Enlarged pes ungual II: red shading is inferred to be preserved sheath material. (F) Cross-section through the left tibia at mid-shaft.*

2005a: Fig. 2.11E-F; note the radiale is mistakenly identified as the semilunate). The size of the semilunate shows it covered most or all of the proximal ends of metacarpals I and II. A well-developed mediodorsal process was present for articulation with the first metacarpal.

Metacarpal (MC) I is complete, while MC II-III are both missing the distal-most articular condyles; the left MC's can be seen on the right side of the skull block. An isolated distal MC III is also preserved from the other manus. Preserved phalanges are located on the hand block, with the exception of an isolated manual ungual. MC I is the shortest and most robust metacarpal (Fig. 3-14B), featuring an extensor flange as in paravians (Gishlick, 2002) but unlike *Ornitholestes* or *Tanycolagreus*. Its distal end is deeply ginglymoid, with the lateral condyle extending further ventrally. The metacarpals become progressively less robust laterally and there is no bowing of MC III. Metacarpal III is more robust than in *Tanycolagreus* however, where it is much narrower than half the width of metacarpal II (Carpenter et al., 2005a: Fig. 2.12B). Metacarpal II exhibits a dorsal scar for the m. extensor carpi ulnaris longus equivalent to the intermetacarpal process in some Aves, which Gishlick (2002) recovered as exclusive to Pennaraptora.

The articulated digit III is exposed on the hand block in medial view, along with phalanx II-1 and manual ungual II in lateral view. Phalanx III-3 is longer than the combined lengths of

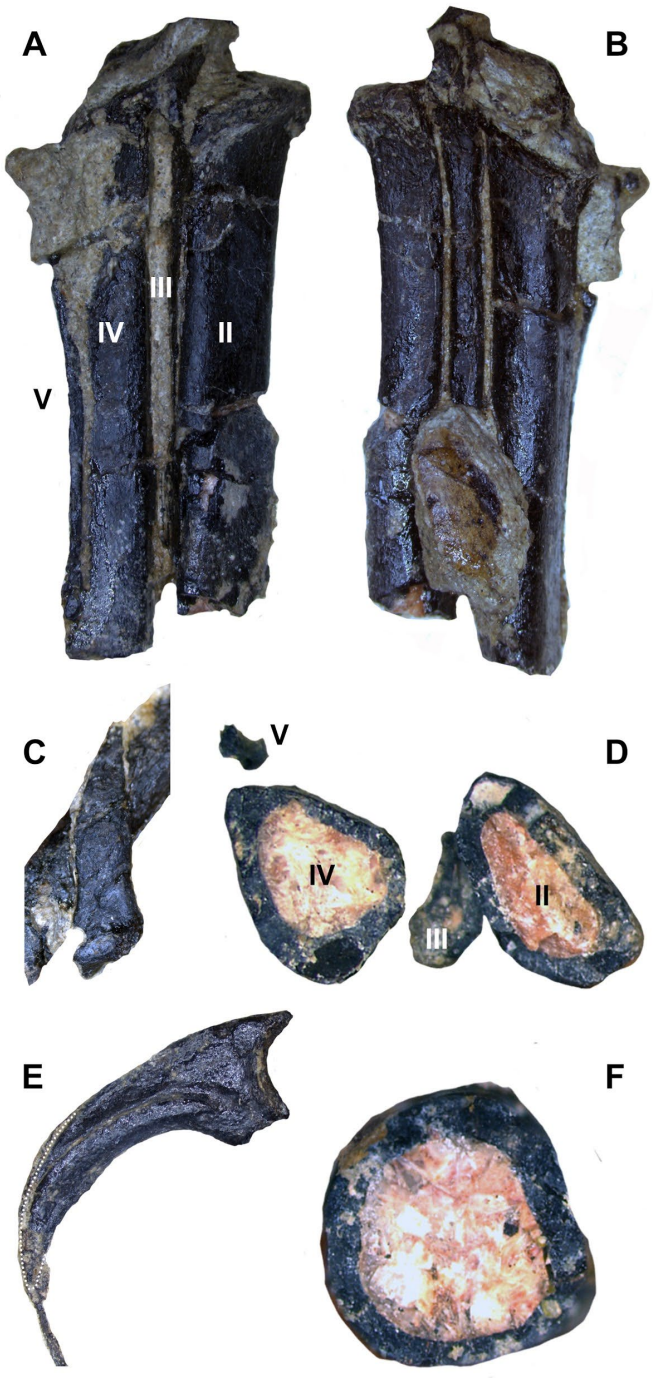

Figure 3-16. Unguals of WDC DML-001*. (A) Left manus ungual I in medial view. (B) Left manus ungual II in medial view. (C) Left manus ungual III in medial view. (D) Pes ungual II (mirrored for ease of comparison) with trenchant sickle morphology. Scale bar = 1 cm.*

III-1 and III-2. Manual unguals are large, raptorial, and trenchant. They have well-developed, proximally placed flexor tubercles and lack a proximodorsal lip (Fig. 3-15). An isolated ungual reported as an enlarged pes ungual II by Hartman et al. (2005) is reinterpreted as manual ungual I, as the dorsal margin arches significantly above the articular facet when the latter is held vertically, and the large flexor tubercle extends significantly beyond the palmar side of the articular facet (cf. Senter, 2007b). Manual ungual III is subequal in size to ungual II (Fig. 15B-C) unlike *Tanycolagreus* (Carpenter et al., 2005a: Fig. 2.12A) and most paravians except *Daliansaurus*, troodontid IGM 100/44 and *Mahakala* (Barsbold et al., 1987: plate 50 Fig. 2-4; Turner et al., 2011: Fig. 29; Shen et al., 2017: Table 1).

Pelvic girdle & hind limb

An isolated block contains much of the ilial postacetabular process, partly as an impression that can nonetheless be reconstructed precisely via CT scans. Unlike the condition in *Ornitholestes* (Carpenter et al., 2005b: fig. 3.10A; note the ilium is photographed at a slight ventral angle and that the postacetabular process is blunt if viewed perpendicular to the blade-M.M. pers. obs., AMNH 619), the postacetabular process is distally pointed in lateral view, has only a shallow brevis fossa and possesses a laterally projecting ventral lobe like some basal dromaeosaurids and troodontids. *Hesperornithoides* possesses a concavity along the dorsal edge of its postacetabular process. Originally considered an unenlagiine synapomorphy (Makovicky et al., 2005:S15), the condition has proven to be widespread among theropods.

Hind limb elements are all preserved on the body block. The hind limbs are elongate relative to individual vertebrae, as in most coelurosaurs including *Archaeopteryx* and *Jeholornis* (Dececchi & Larsson, 2013). The left femur has been entirely prepared off of the block prior to

reattachement, and is missing only the head and proximal-most portion; enough of the shaft is preserved to establish the absence of a fourth trochanter as in the vast majority of pennaraptorans but unlike *Coelurus* and *Tanycolagreus* (Carpenter et al., 2005b:66; Carpenter et al., 2005a: Fig. 2.14B). Notable among previously described Morrison paravian postcrania, proximal femur BYU 2023 (Jensen and Padian, 1989) only overlaps with WYDICE-DML-001 at midshaft where it also lacks a fourth trochanter. Our analysis recovered BYU 2023 as a deinonychosaur that could belong to a troodontid or dromaeosaurid *Hesperornithoides* without an increase in tree length (see Positions of taxa pruned a posteriori in the supplementary information), but further comparison is limited. Distally, our specimen lacks a significant extensor groove or medial epicondyle, and has a lateral condyle which is not projected distally and is separated from both the medial condyle and ectocondylar tuber.

The left tibia and fibula are exposed almost completely, with the anterior portion of the shafts buried in the body block. Proximally the tibia is longer than wide, with a deep incisura tibialis and anteriorly projected cnemial crest that diverges from the shaft at a high angle. No medial cnemial crest is developed. *Hesperornithoides* is similar to *Sinovenator*, the *Almas* holotype and *Achillobator* among paravians in having a lateral tibial condyle that extends anteriorly to overlap the incisura tibialis (Perle et al., 1999: plate XII Fig. 12C; Xu et al., 2002: Fig. 1h; Pei et al., 2017b: Fig. 9). This is unlike the condition in *Tanycolagreus* (Carpenter et al., 2005a: Fig. 2.14K). The proximally placed fibular crest is separated from the proximal condyles and has a longitudinal groove on its posterior edge. Distally, the lateral malleolus is covered by the proximal tarsals but the medial malleolus is distally exposed.

The fibula extends the full length of the tibia but is extremely reduced in diameter. Most of the shaft is less than 1 mm at maximum thickness. Broken portions reveal the fibula lacks

trabecular bone, being hollow and exceptionally thin walled. *Hesperornithoides* also differs from *Tanycolagreus* in that its fibula is subequal in transverse width anteriorly and posteriorly, whereas the latter genus exhibits a posterior tapering (Carpenter et al., 2005a: Fig. 2.14K).

The astragalus and calcaneum are tightly appressed to the distal ends of the tibia and fibula but are not co-ossified to them or each other. The ascending process of the astragalus is elongate unlike *Coelurus* (Carpenter et al., 2005b: Fig. 3.12A), though narrow unlike most paravians except for *Anchiornis* and *Scansoriopteryx* (Czerkas and Yuan, 2002: Fig. 20; Hu et al., 2009: Fig. S4d). It is separated from the astragalar body by a transverse groove and contacts the fibula at its lateral edge. Similar to avialans and most troodontids (Xu, 2002: Fig. 47D; Ji et al., 2011: Fig. 3F; Zanno et al., 2011: Fig. 9D; Xu et al., 2012: Fig. 1K; Brusatte et al., 2013:67) but in contrast to *Coelurus* and *Tanycolagreus* (Carpenter et al., 2005b: Fig. 3.12E; Carpenter et al., 2005a: Fig. 2.14L), the astragalocalcanear anterior intercondylar groove is deep (over 20% of tarsal depth).

The left metatarsus is preserved in articulation with the zeugopod and is almost completely exposed on the body block. Distal tarsals are not fused to the metatarsals, which are themselves also unfused. Although the left metatarsus is incomplete distally, it clearly displays a sub-arctometatarsalian condition (Fig. 3-16A, B, & D) unlike *Tanycolagreus* and *Ornitholestes* (Carpenter et al., 2005a: Fig. 2.15B; Carpenter et al., 2005: Fig. 3.13A), with metatarsal III being constricted along the shaft but not excluded in anterior view. The metatarsus is quite different from *Ornitholestes*, being slender and closely appressed with transversely compressed metatarsals (Fig. 16D; compare to Fig. 13C in Holtz, 1994). Metatarsal III further differs from all three well preserved Morrison basal coelurosaurs in being straight in proximal view instead of L-shaped (Carpenter et al., 2005a: Fig. 2.15C; Carpenter et al., 2005b: Fig. 3.13A, D- based on

medial margin of proximal metatarsal IV for *Coelurus*). Posteriorly, metatarsal III is exposed as a narrow sliver along its proximal length. MT II is not slender as in derived troodontids, and it and MT III lack tubercles for the m. cranialis tibialis. Only a posterior portion of the distal metatarsals is mechanically exposed, and they are not well resolved in the CT data. Metatarsal I is straight with no torsion, and has a slightly constricted neck just before the incompletely preserved distal condyles (Fig. 3-16C). A slender metatarsal V is preserved in articulation at the posterolateral edge of metatarsal IV (Fig. 3-16A, D). Due to distal breakage it is uncertain if the element is elongated as in dromaeosaurids.

Left pes digits III and IV are preserved in articulation with the plantar and lateral surface exposed at the base of the body block. As in *Archaeopteryx*, toes III and IV are subequal in length, proportions that appear less specialized for functional didactyly, with digit IV being substantially shorter and less robust than digit III (Mayr, et al., 2007: Fig. 13). Pedal phalanx IV-4 is shorter than IV-3, associated with cursoriality more than arboreality or grasping. Proximal portions of pedal unguals III and IV are preserved; they are compressed in section, do not appear to be strongly curved and lack enlarged flexor tubercles. An isolated ungual was found that is strongly recurved and trenchant, exhibiting an intermediately expanded flexor tubercle (Fig. 3-15D). The isolated ungual differs from manual unguals in having a dorsal margin that does not arch above the articular facet when the facet is vertical. Given the differences from the manual unguals and the articulated III & IV pedal unguals, we interpret this as an enlarged semi-raptorial pedal ungual II. It also preserves a filigree of organic material that is consistent with previously published remnants of keratin sheaths (Fig. 4-14E; Schweitzer, 2011).

Phylogenetic analysis

Phylogenetic methods

Almost every large-scale coelurosaur analysis from the past two decades is ultimately a derivative of Norell et al. (2001) and have come to be known as Theropod Working Group (TWiG) analyses. While TWiG can refer to the core group of AMNH affiliated researchers, we use it more inclusively to encompass the myriad analyses and derivatives based on their dataset (Supplemental figure S1). This widespread adoption has made the TWiG dataset arguably the most successful lineage of dinosaur phylogenetic analyses to date. Most subsequent iterations add one to several taxa and a few to several characters to a preexisting version of the matrix. While this practice has resulted in character and taxon list stability between coelurosaur analyses, it has also led to endemic issues in the compilation of data matrices. Jenner (2004) identified similar concerns for metazoan cladistics, finding that taxon selection and sampling, uncritical copying of scores, and poorly formed character states have been overlooked and can compromise the validity of topologies recovered by phylogenetics programs that use these as their primary data. In light of this, rather than adding *Hesperornithoides* to an existing TWiG matrix we have instead begun an overhaul of the TWiG dataset to comply with modern ideals of data matrix construction.

Subsequent TWiG analyses and derivatives have not added characters and taxa in a single "lineage" of analyses, but instead have formed "clades" of analyses that increasingly diverge in content (see Fig. S1). So for example modern analyses derived from Senter (2007a) such as Senter et al. (2012), and those derived from Turner (2008) such as Brusatte et al. (2014) have over a hundred characters not found in the other. A similar pattern occurs with taxonomic sampling; most new paravians are added individually or in small groups to a version of the

TWiG matrix but these additions are frequently not propagated to subsequent analyses. To date no analysis has added all, or even most, newly discovered taxa to a single matrix. We follow the advice of Jenner (2004) that authors should attempt to include all previously proposed characters and terminal taxa, while explicitly justifying omissions. To this end we have attempted to include every character from all TWiG papers published through 2012, with the goal to continually add characters from other analyses in future iterations. Each excluded character from these studies is justified under Excluded Characters in the Supplementary Information.

We have also scored almost every named Mesozoic maniraptoromorph known from more than single elements or teeth (the seven exceptions are noted under Excluded Taxa in the Supplementary Information), as well as twenty-eight unnamed specimens. Five recent examples of Aves were included, the palaeognath *Struthio* and the neognaths *Chauna*, *Anas*, *Meleagris* and *Columba*. The Tertiary *Lithornis* and *Qinornis* were also included as both have been suggested to be outside Aves by some authors, as were *Palaeotis*, *Anatalavis*, *Presbyornis*, *Sylviornis*, *Gallinuloides*, *Paraortygoides* and *Foro* as basal representatives of modern clades. Historically, TWiG analyses have focused on coelurosaurs while using *Sinraptor dongi* and *Allosaurus* as outgroups. As some taxa have been alternatively recovered as ceratosaurs or coelurosaurs (e.g. *Deltadromeus*, *Afromimus*), we tested the current character list against an exhaustive sample of Mesozoic averostrans with *Dilophosaurus* as the outgroup. This enabled us to test the content of Maniraptoromorpha and provided us with a more representative outgroup sample than merely *Sinraptor* and *Allosaurus*. However, while the coelurosaur characters utilized do recover many traditional clades outside Maniraptoromorpha, the topology of this section should not be viewed as well supported since characters specific to e.g. ceratosaurs, megalosauroids and carnosaurs are lacking.

One issue is that many TWiG analyses (a notable exception being Senter [2007a]) reuse scorings from prior analyses they were derived from, even when additional data has been published. This can perpetuate errant scores and fails to account for more recent discoveries, publications and interpretations. As an example, *Harpymimus* has been scored identically for only three cranial characters in every TWiG analysis not derived from Senter (2007a) since Norell et al.'s (2001) original up through Turner et al. (2012). Even analyses which focused on basal ornithomimosaurs (e.g. Makovicky et al., 2010) sometimes failed to utilize Kobayashi and Barsbold's (2005) redescription of *Harpymimus* for updated scorings. We address this by reexamining and rescoring each character for every taxon based on direct personal examination, high resolution photographs and/or literature published through 2018.

Perhaps more importantly, we have set out to improve character selection and construction. It is often unappreciated that accurate character scores are only useful if the characters and states themselves are objective, independent and formed so that phylogenetics programs will correctly interpret proposed homology. Existing TWiG state definitions are often unquantified, which hinders future authors from scoring taxa consistently or objectively determining accuracy of published scores. Composite characters, which score multiple variables in a single character, are also common. Correlated characters have increasingly become an issue in analysis lineages as authors add data from other analyses that are not independent of characters already in their matrix. Other issues we addressed included eliminating the use of "absent" as a state in a transformational character (Sereno, 2007:582-584), character traits constructed with discontinuous quantified states (so that certain ranges of values aren't covered by any state) and those that include a state merely scoring for any condition except those specified by the other states (Jenner, 2004:301-302). We have begun the process of resolving

these issues by quantifying 163 characters, isolating 240 composite states into single variables (often using the other variables to form new characters), and excluding 36 correlated characters (see Excluded Characters in the Supplementary Information). Our character list includes details of how each character has been changed from previously published versions. When possible, newly quantified character states have been formulated to best match the taxon distribution for each originally subjective character. All characters have been rewritten in the logical structure advocated by Sereno (2007) to reduce ambiguity and variability between analyses.

The resulting matrix includes 700 characters and 501 OTUs. Ten characters are parsimony-uninformative among our 389 maniraptoromorphs (excluding the possibly tyrannosauroid megaraptorans, coelurids and proceratosaurids in this and the following taxon totals, to ensure similar content). These are retained pending future expansions of the analysis, leaving 690 parsimony-informative characters among our taxon sample of maniraptoromorphs. This makes it the second largest character sample and the largest taxonomic sample in a TWiG analysis of maniraptoromorphs to date, compared to other recent iterations of each TWiG lineage- Gianechini et al. (2018) (700 parsimony-informative characters for their 135 maniraptoromorph OTUs), Foth and Rauhut (2017) (534 such characters and 120 such OTUs), Brusatte et al. (2014) (666 such characters and 127 such OTUs), Agnolin and Novas (2013) (405 such characters and 80 such OTUs) and Senter et al. (2012) (367 such characters and 98 such OTUs).

The data matrix was analyzed with TNT 1.5 (Goloboff and Catalano, 2016). After increasing the ‘Max. trees’ under ‘Memory’ in ‘Settings’ to 99999, an initial 'New Technology search' using 'Sect. Search', 'Ratchet', 'Drift' and 'Tree fusing' was run, as a 'Driven search' to 'Find min. length' 15 times. The level was checked every 3 hits, and Sect. Search settings were

changed to ‘For selections of size . . .’ ‘ …above’ 45 and RSS settings to ‘Factor for number of selections’ 84 and ‘Max. sector size’ 267. This search was stopped after 100 hours at a length of 12132 steps. A series of 'New Technology search'es using 'Sect. Search' (with ‘CSS’ unchecked), 'Ratchet', 'Drift' and 'Tree fusing' were run from ‘RAM’ which located trees 12128 steps in length. Constraint analyses were run using a file containing one shortest tree, unchecking ‘Settings’ ‘Lock trees’, checking ‘Trees’ ‘View’ and moving OTUs (left click, right click) to fulfill the constraint. An initial ‘Traditional search’ of ‘trees from RAM’ with 100 ‘Max. trees’ and ‘enforce constraints’ was then run, followed by a 'New Technology search' with 10000 ‘Max trees’ using 'Sect. Search' (with ‘CSS’ unchecked), 'Ratchet', 'Drift' and 'Tree fusing' from ‘RAM’ using ‘Enforce constraints.’ These traditional and new technology searches were alternated until the length was unchanged for three searches. Constraint analysis results which were shorter than 12128 steps were combined as the only trees in a new file which was itself analyzed as a 'New Technology search' with 99999 ‘Max trees’ using 'Sect. Search' (with ‘CSS’ unchecked), 'Ratchet', 'Drift' and 'Tree fusing' from ‘RAM’ until no shorter trees were recovered. A ‘Traditional search' of 'trees from RAM' with default parameters was then performed to more fully explore the final treespace.

Phylogenetic Results

The analysis resulted in >99999 most parsimonious trees with a length of 12123 steps. The recovered trees had a Consistency Index of 0.073, and a Retention Index of 0.589. Figure 3-17 presents a summary of the strict consensus tree after the a posteriori pruning of several taxa with multiple possible positions (see Supplementary Information for complete results). Megaraptorans and a clade of proceratosaurids and coelurids branch first after tyrannosauroids, yet both groups are often recovered as members of the latter clade in analyses sampling more

characters relevant rootward of Maniraptoromorpha. Indeed, megaraptorans or the coelurid-proceratosaurid group can be constrained to Tyrannosauroidea in only four steps, while it takes 10 steps to move the next closest taxon to birds, *Ornitholestes*. As *Ornitholestes* has never been recovered as a tyrannosauroid either, it is considered the most basal well supported member of Maniraptoromorpha here.

Compsognathids emerge closer to maniraptoriforms than *Ornitholestes*, and several taxa usually considered members of that family (e.g. *Huaxiagnathus*, *Juravenator*, *Mirischia*, *Sinocalliopteryx*) branch off more basally. As all previously suggested characters (e.g. Peyer, 2006:880; Brusatte, 2013:559) connecting these taxa to *Compsognathus* were utilized, our increased data sampling supports the more reduced Compsognathidae recovered here. This version of the family includes several controversial taxa. As described in the Supplementary Information, *Sciurumimus'* placement away from *Compsognathus* in the analyses used by Rauhut et al. (2012) was due almost entirely to misscorings in the original versions of those analyses and only one of its characters unexpected in a basal maniraptoromorph is not used in our analysis. As it requires seven steps to move to Megalosauroidea, the compsognathid dentification is better supported. *Aorun* was recently recovered as an alvarezsauroid by Xu et al. (2018) based on four characters, one of which we include (our 29) and another (proximodistal oblique ridge on tibia bracing astragalar ascending process) seemingly present in *Compsognathus* as well (Peyer, 2006: Fig. 10; scored unknown by Xu et al.). Constraining it to be an alvarezsauroid in our matrix adds 17 steps, so seems to be highly unlikely. Similarly, *Haplocheirus* falls out in Compsognathidae instead of its traditional position as a basal alvarezsauroid. Eight characters used by Choiniere et al. (2010) to place it in the latter clade were not included, but it also requires nine steps to constrain there in our analysis even with the

inclusion of the supposedly intermediate *Xiyunykus* and *Bannykus*. This suggests neither a compsognathid nor an alvarezsauroid identification is well supported and more study is needed.

Another area with less support than suggested by consensus is the base of Maniraptoriformes, where we recover alvarezsauroids and therizinosaurs as the first branching maniraptorans as in most recent studies. However, only four steps are required to get a result similar to Sereno's (1999) where alvarezsauroids are sister to ornithomimosaurs and therizinosaurs sister to that pair. Similarly, while we recover a pairing of alvarezsauroids and therizinosaurs to the exclusion of pennaraptorans, placing therizinosaurs closer to the latter clade merely needs three additional steps. Positioning alvarezsauroids sister to Pennaraptora or putting therizinosaurs just outside Maniraptoriformes are slightly less parsimonious at six steps each, but the once popular topology of a therizinosaur-oviraptorosauria clade is much less likely at 13 steps longer.

Among ornithomimosaurs, *Deinocheirus* and the odd *Hexing* form the first branching clade unlike Lee et al. (2014b) where the former is well nested sister to *Garudimimus*. As we use all valid characters from that analysis placing *Deinocheirus* close to *Garudimimus* and *Beishanlong*, and it takes 14 steps to constrain that result, it is here rejected. However, the

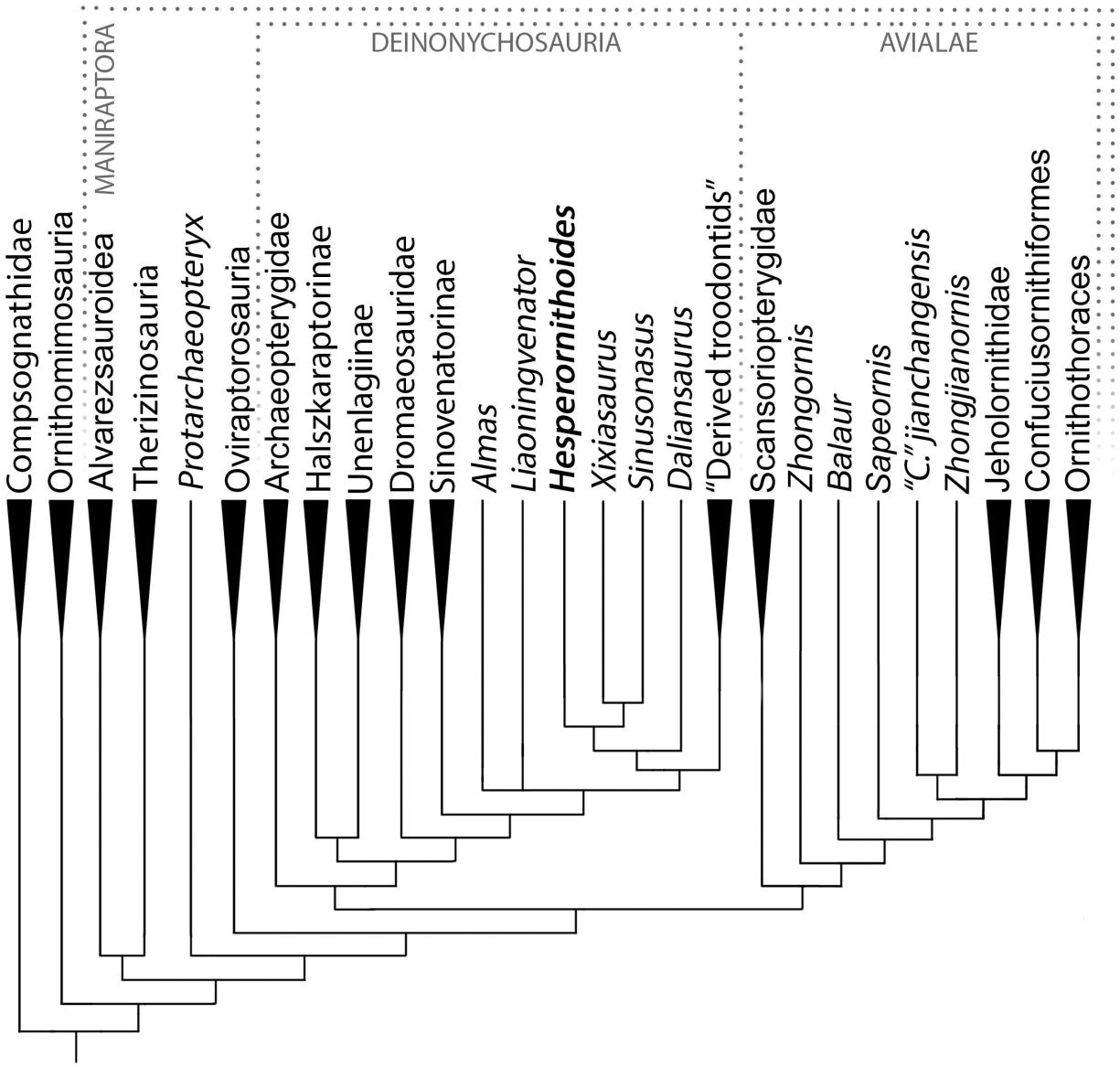

Figure 3-17. Summary phylogenetic diagram resulting from this phylogenetic analysis. *Strict consensus tree of maniraptoromorphs after a posteriori pruning with higher level taxa condensed (length = 12123). The uncondensed tree and positions of pruned taxa can be seen in the Supplemental Data.*

Mongolian giant can be placed within the toothless ornithomimosaur clade using merely four additional steps, so its basal position may change as the referred material is more fully described. Early Cretaceous American *Arkansaurus* and *Nedcolbertia* are both resolved as

ornithomimosaurs for the first time. Few characters have been proposed to organize taxa within Ornithomimosauria and many taxa lack detailed descriptions or justified alpha taxonomy. Thus our topology should be be regarded as tentative (e.g. the placement of *Harpymimus* within toothed ornithomimosaurs can be changed with only two steps), but the consensus pairing of *Anserimimus* with *Gallimimus* and *Struthiomimus* with *Dromiceiomimus* requires eight more steps, so deserves additional scrutiny.

Therizinosauroidea retains standard relationships among basal taxa, with *Falcarius*, *Jianchangosaurus*, *Beipiaosaurus* and *Alxasaurus* successively closer to therizinosaurids. *Martharaptor* has several equally parsimonious positions as a therizinosaur less closely related to *Therizinosaurus* than *Alxasaurus*, matching the position recovered by Senter et al. (2012). The topology is similar to the latest major study, Zanno's 2010 TWiG analysis whose data was fully utilized, in that *Suzhousaurus*, *Erliansaurus* and *Neimongosaurus* are outside a clade including *Nanshiungosaurus*, *Nothronychus* spp., *Erlikosaurus* and *Segnosaurus*.

Fukuivenator has a poorly specified position at the base of Maniraptora, emerging as the first branching alvarezsauroid, but moving to a basal therizinosauroid position with only two steps. A more stemward position seems more likely than a relationship with dromaeosaurids as suggested in its original description or Cau (2018), as it can be a coelurid with only four more steps, but takes seven steps to be sister to Pennaraptora and 11 steps to be paravian. The next branching alvarezsauroid is *Nqwebasaurus*, as also recovered by Dal Sasso and Maganuco (2007), which requires six steps to be an ornithomimosaur or seven steps to be closer to Pennaraptora. All but two characters recovered by Choiniere et al. (2012) as supporting an ornithomimosaurian placement were included, so the alvarezsauroid alternative is stronger. A compsognathid position as in Novas et al. (2012) is ten steps longer so even less likely.

Rounding out the controversial basal ornithomimosaurs is *Pelecanimimus,* recovered as the first branching alvarezsauroid based on characters such as an elongate anterior maxillary ramus (311:1), posterior tympanic recess in the otic recess (27:1), lateral teeth set in grooves (302:1), over 30 dentary teeth (90:3) and a proximally expanded metacarpal II (370:0). Constraining it as an ornithomimosaur only requires two additional steps however, where it emerges just above *Shenzhousaurus* as in MacDonald and Currie (2018). As only two of their characters supporting an ornithomimosaurian identification were not used by us, and only one from Brusatte et al. (2014), its true position is unclear pending a detailed osteology such as Perez-Moreno's (2004) unreleased description.

As in Xu et al.'s (2018) new analysis, *Patagonykus* and *Bonapartenykus* are outside Alvarezsauridae, but unlike that study *Xiyunykus* and *Bannykus* join them as patagonykines. Alvarezsaurid *Patagonykus* requires four steps, and Xu et al.'s new genera follow, while placing the new genera more stemward than *Patagonykus* only takes two steps. Thus neither of these arrangements should be viewed as heavily favored until Xu et al.'s taxa are described in detail. Within Parvicursorinae, not all characters from Longrich and Currie's (2009) alvarezsaurid analysis were included, but we recovered a clade including only *Mononykus*, *Shuvuuia*, *Parvicursor* and the Tugrik taxon as in derivatives of that study. *Heptasteornis* is recovered as an alvarezsaurid, supporting Naish and Dyke (2004). Note while the controversial *Kinnareemimus* fell out as a tyrannosauroid in the shortest trees, only three steps move it to Ornithomimosauria and four to Alvarezsauroidea. Similarly, while *Kol* resolves as a relative of *Avimimus* as suggested by Agnolin et al. (2012), a single step places it in Alvarezsauridae.

Protarchaeopteryx emerges as the sister group of Pennaraptora, but changes to the first branching oviraptorosaur with merely two steps and the first branching paravian with three steps,

suggesting no strong signal for this poorly preserved specimen. Placing it in Archaeopterygidae as originally proposed and supported by Paul (2002) requires 11 additional steps however, which strongly outnumber the few valid published characters for such an arrangement. Oviraptorosaurs include *Similicaudipteryx* as their first branching member and unusually places *Incisivosaurus* closer to caenagnathoids than *Caudipteryx* and within Oviraptoridae itself. It only requires a single step to make *Incisivosaurus* the sister taxon of Caenagnathoidea, and three steps to make the first branching oviraptorosaur, so any of these positions are plausible. Forcing *Incisivosaurus* and *Protarchaeopteryx* to be sister taxa as in Senter et al. (2004) requires six steps, and the duo resolves as the first branching oviraptorosaur clade. Within Caenagnathoidea, our results should be considered incomplete pending incorporation of characters from Maryanska et al. (2002) and its derivatives. Notable similarities to (Lee et al., 2019) include *Nomingia* as an oviraptorid and a clade of *Nemegtomaia* and *Heyuannia*. Major differences include non-caenagnathoid *Ganzhousaurus* (1 step needed to make oviraptorid; emerges sister to *Heyuannia*), caenagnathid *Avimimus* (3 steps to place outside Caenagnathoidea) and *Machairasaurus* (2 steps needed to make oviraptorid; emerges basalmost), and oviraptorid *Microvenator* (1 step needed to make caenagnathid, 3 steps to move it outside Caenagnathoidea), *Gigantoraptor* (4 steps needed to make caenagnathid; emerges basalmost) and *Beibeilong* (2 steps needed to make caenagnathid; second branching after *Microvenator*). Maryanska et al.'s heterodox hypothesis of avialan oviraptorosaurs requires 12 additional steps despite the inclusion of proposed intermediates such as *Epidexipteryx* and *Sapeornis*. As we use a far greater maniraptoromorph taxon and character sample (Maryanska et al., 2002 includes 16 such taxa and 162 parsimony-informative characters), and only lack two characters they use to support avialan oviraptorosaurs, the traditional content for Paraves is significantly more parsimonious.

A Deinonychosauria including troodontids and dromaeosaurids was recovered as in many recent analyses. Positioning troodontids closer to Aves than dromaeosaurids only requires a single additional step, but non-eumaniraptoran troodontids are less parsimonious at six more steps. Scansoriopterygids form the first branch of Avialae, matching their stratigraphic placement, and constraining them as basal paravians instead is only one step longer. Their other suggested position as oviraptorosaurs requires 12 more steps though, so is unlikely. While *Pedopenna* emerges as a scansoriopterygid in the MPTs, one step moves the fragmentary specimen to Archaeopterygidae instead. The juvenile *Zhongornis* branches next, with alternative positions in Scansoriopterygidae or Confuciusornithiformes being four and five steps longer respectively. *Balaur* follows and only moves to Dromaeosauridae with eight additional steps, supporting its placement in Avialae by Cau et al., 2015. The branching order of Jehol non-ornithothoracine birds has been contentious, with our matrix supporting *Sapeornis* branching first, followed by jeholornithids then confuciusornithiforms. Jeholornithids branching first is only three steps longer, but *Sapeornis* branching last as in some recent analyses requires twelve more steps. Note *Changchengornis* moves one node to Confuciusornithiformes in merely two steps and *Jinguofortis* joins *Chongmingia* in only three steps. Our analysis supports the latter's position close to Ornithothoraces as in p2 of Wang et al.'s (2016) figure 7, whereas moving it to their p1 more stemward of *Jeholornis* and *Sapeornis* requires 11 more steps.

Characters supporting enantiornithine monophyly and phylogeny are not strongly sampled, making this portion of the tree provisional. Despite this, several proposed clades were recovered including Pengornithidae, *Liaoningornis* plus *Eoalulavis*, *Sinornis* plus *Cathayornis*, and Longipterygidae with *Longipteryx* outside a clade containing *Longirostravis*, *Shanweiniao* and *Rapaxavis*. One proposed clade which is strongly rejected is Bohaiornithidae, requiring 16

additional steps to make monophyletic using Wang et al.'s (2014) content. Among controversial taxa, *Evgenavis* and *Qiliania* can move to Confuciusornithiformes using only three steps and one step respectively, *Liaoningornis* and *Hollanda* can move to Ornithuromorpha in four steps each, and *Vorona* requires six steps to move to that clade. The proposed pairings of *Aberratiodontus* and *Yanornis* (Zhou et al., 2008) and *Ambiortus* and *Otogornis* (Kurochkin, 1999) are unparsimonious at eight and 17 additional steps. Among taxa closer to crown Aves, the grade of taxa stemward of *Bellulornis* are usually resolved as enantiornithines and can move there in one to five steps depending on the OTU. Thus, their position may be revised given the inclusion of more enantiornithine characters, whereas e.g. *Bellulornis* and *Archaeorhynchus* would take 14 and 17 steps to move to Enantiornithes respectively so are solidly closer to Aves.

Our analysis includes all of Clarke's lineage of ornithuromorph characters (originating from Clarke, 2002) as incorporated into Turner et al.'s (2012) TWiG analysis, so should be a good test for this portion of the tree. *Bellulornis* is the sister taxon to Ornithuromorpha, followed by a pairing of *Archaeorhynchus* and *Patagopteryx* as in Zheng et al. (2018). Placing the latter genus closer to carinates than *Gansus* as in some recent analyses requires nine more steps. Songlingornithidae is recovered, but Hongshanornithidae forms a grade and requires 10 more steps to constrain with Wang et al.'s (2015) content. With Field et al.'s (2018) new *Ichthyornis* data included, it falls out sister to hesperornithines, but the alternatives with either toothed taxon being closer to Aves only need four additional steps each. *Eogranivora* and the poorly described *Xinghaiornis* form the first branching carinates, followed by *Iaceornis* and *Apsaravis*. *Lithornis* is just outside Aves, but can be a palaeognath in five additional steps. While the character list was not designed to resolve Aves, consensus clades are largely recovered, including the recently recognized Vegaviidae and an anseriform *Teviornis*.

Incorporating the new data from Rauhut et al. (2018) on *Archaeopteryx* and Pei et al. (2017a) on *Anchiornis* nests the former genus in the clade usually called Anchiornithinae, making this entire group Archaeopterygidae. As in Xu et al. (2011) we recover archaeopterygids as deinonychosaurs, but both the traditional *Archaeopteryx* position closer to Aves and the common *Anchiornis* position sister to troodontids require a single additional step each. Even making archaeopterygids sister to dromaeosaurids requires merely four more steps, but placing them on the paravian stem as Lefevre et al. (2017) recovered for anchiornithines is 15 steps longer. As only two of their characters supporting this stemward placement were unused by us, that position is rejected here. Among complete archaeopterygids *Caihong* is notably labile and can be a dromaeosaurid with only two more steps, given its mesially serrated teeth and unreduced distal caudal prezygapophyses.

As in Senter et al. (2012) and Cau (2018) our trees pair unenlagiines and halszkaraptorines, but uniquely places this Unenlagiidae sister to the dromaeosaurid plus troodontid clade. Unenlagiids can take their traditional position sister to other dromaeosaurids in trees one step longer where archaeopterygids pair with troodontids, or can be placed closer to Aves as in Agnolin and Novas (2013) in trees one step longer where archaeopterygids are in this position as well. *Mahakala* is only weakly connected to *Halszkaraptor*, becoming a basal paravian in one step, but eight new characters proposed as halszkaraptorine synapomorphies by Cau et al. (2017) were not used so this may be an artifact. *Hulsanpes* emerges as a dromaeosaurine in the shortest trees, but only takes two steps to move to Halszkaraptorinae. The briefly described taxon *Ningyuansaurus* resolves as the sister taxon to *Mahakala* but becomes a basal paravian in one more step and an oviraptorosaur as originally proposed in four steps. It should be reexamined, but characters such as the low iliofemoral ratio (261:1), low ischiopubic

ratio (187:3) and enlarged pedal ungual II (224:1) are more like paravians than oviraptorosaurs. For the first time the European *Pyroraptor* and *Ornithodesmus* are recovered as unenlagiines, which would match biostratigraphically with the presence of traditionally Gondwanan clades such as spinosaurids, carcharodontosaurids and abelisaurs in the Cretaceous of Europe. Giant *Dakotaraptor* also falls out in this group instead of sister to *Dromaeosaurus* as in DePalma et al. (2015), but the latter study did not provide their scorings for the genus although we used all their characters. Moving it to Dromaeosauridae only takes three steps, but it resolves as a basal taxon instead of a eudromaeosaur. The unenlagiine *Rahonavis* had previously been recovered by Agnolin and Novas (2013) and trees based on Cau's analysis as closer to Aves in a similar position to *Jeholornis*. We recover it nested in Unenlagiinae, and it takes ten additional steps to move closer to Aves than archaeopterygids and other unenlagiines. We analyzed every character supporting this in Agnolin and Novas' matrix, so the unenlagiine consensus seems strong, especially as four of their characters connecting *Rahonavis* with more derived birds are correlated with having long wings.

Tianyuraptor is recovered as the most basal dromaeosaurid but can be placed in Microraptoria with one step and closer to eudromaeosaurs in two steps. Similarly, *Zhenyuanlong* is a microraptorian in the shortest trees, but can be nearer to eudromaeosaurs in two steps as well. Constraining the two to be sister taxa to simulate the synonymy suggested by Makovicky et al. (2018) is only four steps longer, and the pair emerge on the eudromaeosaur branch. We recover *Bambiraptor* as an early branching microraptorian as in Senter et al. (2004), with *Variraptor* as its sister taxon. However, *Bambiraptor* moves closer to eudromaeosaurs as in Senter et al. (2012) and Cau et al. (2017) with the addition of a single step, and *Variraptor* can join Unenlagiinae with the other European taxa in only three steps. Fragmentary *Yurgovuchia* is

sister to Eudromaeosauria and requires four steps to place close to *Utahraptor* and *Achillobator* as in Senter et al. (2012) despite using all of their characters supporting this. *Deinonychus* joins *Utahraptor* and *Achillobator* to form a large dromaeosaurid clade not previously hypothesized, which is most parsimoniously outside Dromaeosaurinae plus Velociraptorinae, but can be moved to either subfamily in two steps. This group also includes the controversial *Yixianosaurus*, which takes seven steps to move to a more stemward position in Maniraptora as in Dececchi et al. (2012), 10 steps to be a basal paravian as in Foth et al. (2014) and 13 steps to place by scansoriopterygids as originally proposed by its describers. Another new coalition is a Dromaeosaurinae including *Saurornitholestes*, *Atrociraptor*, *Tsaagan*, *Linheraptor* and *Itemirus*, though the first two were recovered as close relatives by Longrich and Currie (2009) and *Tsaagan* and *Linheraptor* have been proposed to be synonymous by several authors and were resolved as sister taxa by Cau et al. (2017). Our results agree with most recent studies in placing *Adasaurus* in Velociraptorinae, along with the newly analyzed *Luanchuanraptor* and unnamed Djadochta specimen IGM 100/980. Although *Acheroraptor* and *Velociraptor? osmolskae* resolve as microraptorians, a single step nests the former in Eudromaeosauria, and two steps joins the latter to *V. mongoliensis*, so these jaw-based taxa are not strong evidence of Late Cretaceous microraptorians. Conversely, the Campanian *Hesperonychus* holotype emerges as an avialan at least as close to Aves as *Balaur* despite all of its microraptorian-like characters being used. Three steps are needed to constrain it to Microraptoria. Agnolin and Novas (2013) uniquely proposed microraptorians to be in Avialae (under their junior synonym Averaptora), but as we included all their characters supporting this arrangement and still find it takes 14 additional steps to constrain, we strongly reject the hypothesis.

The recently named Sinovenatorinae are the first branching troodontids, including not only *Mei* and the eponymous *Sinovenator*, but also *Xiaotingia*, *Jianianhualong* and unnamed IGM 100/140 described by Tsuijhiji et al. (2015). Troodontid characters present in *Xiaotingia* but not anchiornithines include distally positioned obturator process (183:2), and characters shared with sinovenatorines include large posterior surangular foramen (80:2), capital groove in humerus (458:1), metacarpal III extending distally past metacarpal II (640:1), laterally ridged ischium (182:2) and enlarged pedal ungual II (224:1). Forcing *Xiaotingia* into Archaeopterygidae requires nine more steps, which strongly suggests it is not a member considering we included all of the TWiG data originally used to place it there. Alternative placements as a non-anchiornithine avialan (Lee et al., 2014a), a dromaeosaurid (Senter et al., 2012) and a scansoriopterygid relative (Lefevre et al., 2017) are eight, five and 26 more steps respectively. *Jianianhualong* and IGM 100/140 were originally recovered as closer to troodontines by their describers, and both can move there with a single step. One node closer to troodontines are *Almas*, possibly referrable perinates IGM 100/972 and 100/974, and a clade of *Liaoningvenator* and unnamed Ukhaa Tolgod specimen IGM 100/1128. *Almas* and IGM 100/1128 were recovered as jinfengopterygines by Turner et al. (2012) but the eponymous *Jinfengopteryx* has a highly unstable position in our analysis, equally capable of joining with these taxa or falling out in Sinovenatorinae. Even a position in Archaeopterygidae as in Ji et al. (2005) is only three steps longer, and a basal paravian position as in Foth et al. (2014) is just four steps longer. In comparison, moving *Liaoningvenator* to group with anchiornithines as in Shen et al. (2017a) requires 10 steps. *Zanabazar*, *Linhevenator*, *Talos* and *Troodon* sensu lato form a derived group of troodontines, with *Saurornithoides*, *Urbacodon*, *Gobivenator* and *Byronosaurus* successively more distant sister taxa. The classic Early Cretaceous specimen IGM 100/44 branches first in the

final troodontid clade, with *Daliansaurus* and a pairing of *Xixiasaurus* and *Sinusonasus* successively closer to our new taxon *Hesperornithoides*. *Daliansaurus* and *Sinusonasus* were recovered as sinovenatorines by Shen et al. (2017b) and can be constrained there in four and six steps respectively.

Finally, constraint analyses were used to test alternative placements for *Hesperornithoides*. In order to quantify the likelihood of it being a juvenile *Ornitholestes*, *Coelurus* or *Tanycolagreus*, we constrained trees pairing *Hesperornithoides* with each Morrison OTU. These were 11, 15 and 16 steps longer respectively than the most parsimonious trees, corroborating the abundant character evidence described above that *Hesperornithoides* is not referable to a Morrison non-maniraptoriform. While not unique, troodontid synapomorphies such as the pneumatic quadrate (60:1), anterior cervical centra which extend posterior to their neural arches (104:1), and the deep tibiotarsal intercondylar groove (206:1) place *Hesperornithoides* within that clade. Characters like the small dental serrations (92:1), elongate but not hypertrophied distal caudal prezygapophyses (127:1), straight ulna (367:0), dorsally projected curve on manual ungual I (378:1) and enlarged manual ungual III (391:1) are homoplasic but combine to position the new taxon with *Daliansaurus*, *Xixiasaurus* and *Sinusonasus*. Yet like its contemporary *Archaeopteryx*, *Hesperornithoides* can easily move to different positions in the paravian tree. A placement as the first branching dromaeosaurid is just two steps longer, supported by the dorsally placed maxillary fenestra (321:1), mesial dental serrations (89:0) and large lateral teeth (91:0). This may be more compatible stratigraphically, but moving *Hesperornithoides'* clade to a more stemward position in Troodontidae outside Sinovenatorinae, the *Liaoningvenator*-like taxa and derived troodontids is also only two steps longer. Similarly, in trees two steps longer than the MPTs where troodontids are avialans, *Hesperornithoides* can be

the first branching taxon closer to Aves than troodontids based on homoplasic characters such as the short posterodorsal lacrimal process (44:0/1). Two additional steps also place the taxon in contemporaneous Archaeopterygidae, sister to *Caihong* which shares character states 89:0, 91:0 and 127:1. Despite the uncertainty of its position within Paraves however, *Hesperornithoides* is strongly supported as a member of the Deinonychosauria plus Avialae clade, as even constraining it to the paravian stem requires 15 additional steps.

Discussion

Hesperornithoides miessleri adds another small-bodied theropod to the list of dinosaur taxa from the well-studied Morrison Formation (e.g. Foster, 2003), reinforcing the importance of continued exploration and excavation of well-sampled formations. Regardless of its position within Paraves, *Hesperornithoides* is significant given the previous lack of Jurassic troodontids or dromaeosaurids known from non-dental remains, or of Jurassic avialans and/or archaeopterygids from the Americas. If it is a troodontid as the most parsimonious trees suggest, it would establish the presence of multiple species in the Jurassic of North America in conjunction with *Koparion douglassi* (though see Holtz, Brinkman & Chandler, 1998).

Our phylogenetic analysis and constraint tests suggest that the appearance of consensus in TwiG derivatives may often be one of multiple equally plausible alternatives, from the topology of early maniraptoriform clades to the structure of Paraves. Indeed, a single step separates several different paravian phylogenies including such heterodox concepts as an archaeopterygid-troodontid sister group and a pairing of troodontids and dromaeosaurids exclusive of unenlagiids. Yet this does not mean anything goes, as multiple proposed topologies were rejected by our data. These include alvarezsauroid *Aorun*, paravian *Fukuivenator*,

deinocheirid *Garudimimus*, the therizinosaur-oviraptorosaur clade, avialan oviraptorosaurs, oviraptorosaurian scansoriopterygids, *Yixianosaurus* or *Xiaotingia* sister to scansoriopterygids, basal paravian archaeopterygids, avialan microraptorians, *Rahonavis* closer to Pygostylia than archaeopterygids or unenlagiines, pygostylian *Sapeornis* and Bohaiornithidae with its original content. This realm of plausibility has not always been made obvious in prior TWiG analyses, as few explicitly test alternative topologies. When alternatives are tested, the likelihood of their reality may be understated such as when Turner et al. (2012) reported as we do that only one step is necessary to recover troodontids in Avialae instead of Deinonychosauria. Yet they still stated "Deinonychosaurian monophyly is well supported in the present cladistic analysis and has been consistently recovered in all TWiG analyses after the original Norell et al. (2001) analysis". This illustrates the importance of viewing cladograms as a network of more or less likely relationships instead of a new "correct" topology. Given the propensity of authors to reuse previous scorings and character constructions, repeated phylogenetic results may result in a false impression of confidence not justified by constraint analysis. We urge authors going forward to be vigilant in checking old character scorings, to formulate uncorrelated and quantifiable new characters scoring for single variables when expanding past analyses, and to check alternative topologies' strength.

Even considering the range of parsimonious maniraptoran topologies, our phylogenetic results provide important observations on the origin of avian flight. Basal maniraptoran clades such as alvarezsauroids and therizinosaurs are unambiguously non-volant. Short-armed *Protarchaeopteryx* lies near the divergence of oviraptorosaurs and paravians, while basal oviraptorosaurs exhibit a grade of short-armed basal taxa including *Similicaudipteryx, Caudipteryx* and *Avimimus* (Table 3-3). Within Paraves we find unambiguously non-flying taxa

at the base of all clades regardless of topology. *Archaeopteryx* (humerofemoral ratio 112-124%) is nested within shorter-armed Tiaojishan taxa (78-104%) that lack feathers adapted for advanced aerodynamic locomotion (Saitta, Gelernter & Vinther, 2017; Pan, et al., 2019) whether *Caihong* is an archaeopterygid or a dromaeosaurid. Halszkaraptorines are short-armed, and if *Mahakala* and/or *Ningyuansaurus* are basal paravians instead these support the hypothesis even further. Long-armed *Rahonavis* is deeply nested in Unenlagiinae, as is *Microraptor* within Dromaeosauridae even if *Tianyuraptor*, *Zhenyuanlong* and *Bambiraptor* are allowed several steps to be closer to eudromaeosaurs. All troodontids have humeri 70% or less of femoral length with the exception of *Xiaotingia* (Table 3-3), including the early *Hesperornithoides* if it is a member. Moving the latter to Dromaeosauridae or Avialae would only cement the pattern further.

This pattern of short-armed basal members of paravian outgroups and subclades (Fig. 3-18) is important for understanding the timing of avian flight acquisition, as individuals with humerofemoral ratios of 70% or less lack the wing-loading to generate significant horizontal or vertical thrust (Dececchi et al. 2016). This contradicts hypotheses of neoflightlessness in oviraptorosaurs (Maryanska, Osmolska, & Wolsan, 2002; Feduccia & Czerkas, 2015) or paravians in general (Paul, 2002), and also contradicts plesiomorphically volant dromaeosaurids (Xu, et al., 2003). The recently discovered *Yi* suggests that at least some scansoriopterygids developed a divergent, parallel form of aerial locomotion (Xu, et al., 2015), but given the

Taxa	H/F Ratio	Taxa	H/F Ratio
Ningyuansaurus	0.56	*Deinonychus*	0.76-0.80
Protarchaeopteryx	0.70	*Austroraptor*	0.47
Similicaudipteryx	0.59	*Buitreraptor*	0.91
Caudipteryx	0.47	*Unenlagia*	0.72
Mahakala	0.50	*Dakotaraptor*	0.57
Mei	0.52-0.55	*Archaeopteryx*	1.12-1.24
Sinovenator	0.68	*Serikornis*	0.90
Xiaotingia	0.85	*Anchiornis*	0.96-1.04
Jianianhualong	0.70	*Eosinopteryx*	0.78
Jinfengopteryx	0.70	*Aurornis*	0.88
Liaoningvenator	0.59	*Halszkaraptor*	0.60
Sinornithoides	0.59	*Scansoriopteryx*	1.06-1.12
Hesperornithoides	0.56	*Yandangornis*	0.75
Tianyuraptor	0.65	*Epidexipteryx*	0.98
Caihong	0.59	*Zhongornis*	1.04
Zhenyuanlong	0.63	*Zhongjianornis*	1.48
NGMC 91	0.92	*Sapeornis*	1.57-1.88
Changyuraptor	0.97	*Jeholornis*	1.40-1.47
Sinornithosaurus	0.92	*Jixiangornis*	1.34-1.56
Microraptor	0.79-0.92	*Eoconfuciusornis*	1.11-1.30
Zhongjianosaurus	0.73	*Chongmingia*	1.18
Bambiraptor	0.85	*Confuciusornis*	1.14-1.27

Table 3-3. Humeral/femoral ratios of paravian theropods.

significant epidermal and morphological differences between *Yi*'s forelimb anatomy and avian wings it seems most likely to have occurred independently of avian flight. This holds true whether scansoriopterygids are early branching avialans or basal paravians. The most parsimonious interpretation of our results is a series of parallel appearances of non-avian aerodynamic locomotion within microraptorians, unenlagiids, archaeopterygids and scansoriopterygids.

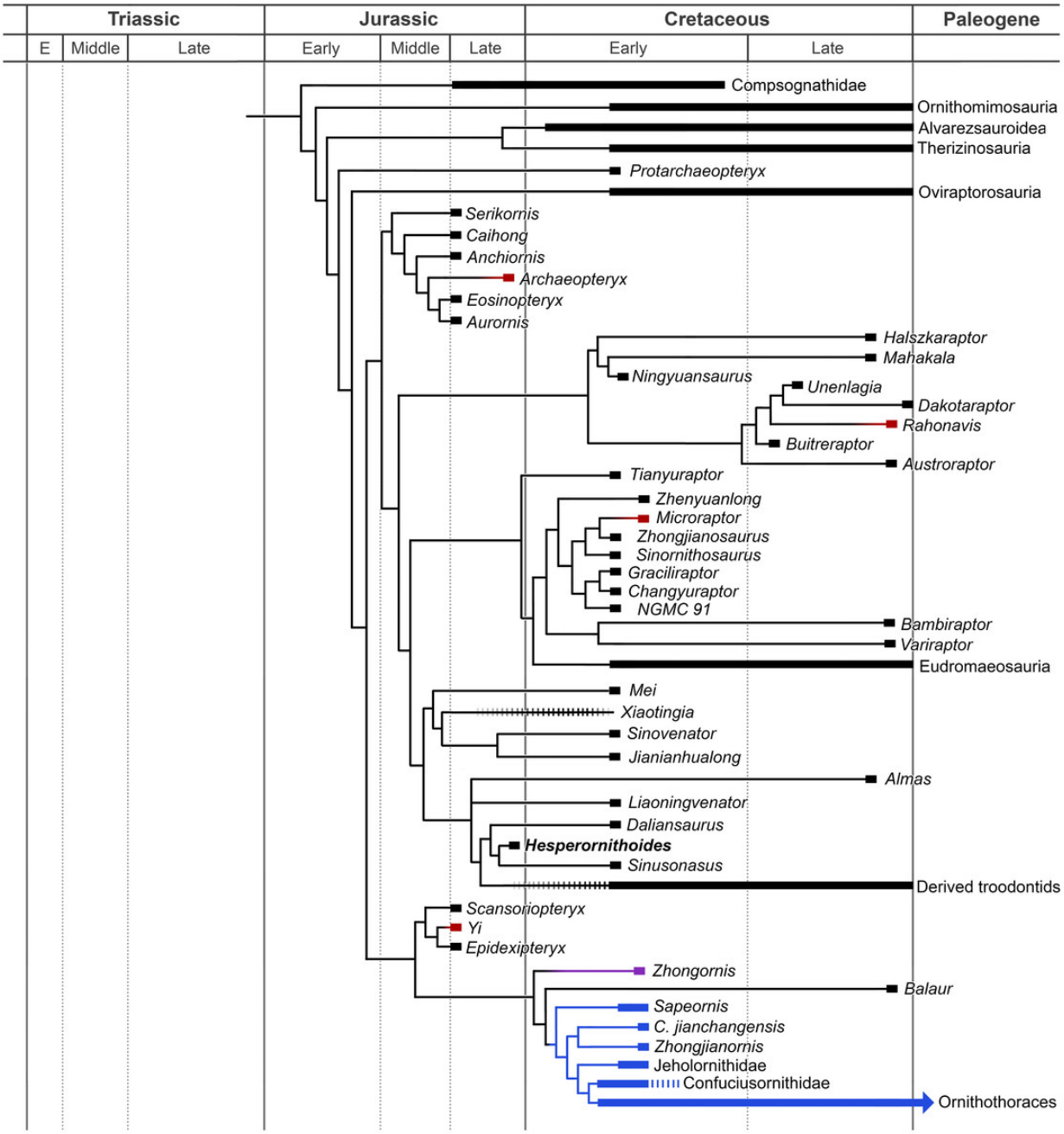

Figure 3-18. Partially expanded, time calibrated phylogenetic results. *Clades containing potentially volant taxa (red) are expanded to show their position nested within flightless taxa (black). Taxa exhibiting aerial locomotion directly connected to crown clade Aves are colored blue. Zhongornis is colored purple to reflect the uncertainty revolving around this juvenile specimen.*

Traditional attempts to understand the origin of avian flight have centered on the use of well-known, supposedly intermediary taxa such as *Archaeopteryx* and *Microraptor* to serve as key evolutionary stages (e.g. Ostrom, 1979; Xu, Zhou, & Wang, 2003). Our results (Fig. 3-18) suggest that whatever aerial locomotion these taxa may have engaged in, they did not give rise to avialan flight. Models of avian flight origins based on these taxa may be misinterpreting the sequence of character acquisition that resulted in crown avian flight. The embedding of putatively flighted *Rahonavis, Archaeopteryx* (though see Federico, et al., 2019)*,* and *Microraptor* within clades that lack evidence of aerial locomotion is consistent with prior students that found the morphology of most non-avialan paravians as functionally more similar to terrestrial than arboreal birds and mammals (e.g. Dececchi & Larsson, 2011; Angolin, et al., 2019; Federico, et al., 2019). This supports a non-volant terrestrial ecomorph as the basal condition for the major paravian clades, supporting numerous previous studies demonstrating that key flight preadaptations up to and including vaned feathers and well-developed wings evolved in terrestrial contexts millions of years prior to the origin of crown avian flight (e.g. Makovicky & Zanno, 2011; Brusatte, et al., 2014; Dececchi, et al., 2016; Cau, 2018).

With the morphologically divergent and potentially volant *Yi* (Xu, et al., 2015) nested within a non-flying clade of basal avialans, one counter-intuitive result is that even avialans may have been plesiomorphically flightless. Though not a novel hypothesis (e.g. Ostrom, 1979; Speakman & Thompson, 1994; Dececchi & Larsson, 2011), it suggests the possibility for a surprisingly late acquisition of avian flight. Though new Jurassic fossils have the potential to push the origin of avian flight deeper in time, at the moment our first branching preserved examples are the Early Cretaceous *Zhongjianornis*, *Sapeornis* and possibly *Zhongornis* (Fig. 3-18). Investigating the differences in flight capabilities and mode of life between them,

confuciusornithids and more crownward avialans may be the most fruitful line of inquiry for understanding the transition to true avian flight.

The pattern of character acquisition, adult body reduction size (Bensen, et al., 2014), and parallel emergences of aerodynamic locomotion within Paraves suggests one possible solution to the traditional dichotomy of arboreal vs. terrestrial habitats in the origin of avian flight. While short-armed, non-arboreal alvarezsauroids, oviraptorosaurs, troodontids, and dromaeosaurs demonstrate that wings and other key characters associated with avian flight evolved in a terrestrial context, it is notable that clearly volant avialans like *Zhongjianornis,* and clades with putatively aerial behavior such as microraptorians, some archaeopterygids and scansoriopterygids exhibit the strongest evidence among paravians for arboreal or semi-arboreal behavior. This suggests a model wherein small size and increasing approximations of the flight stroke allowed some clades of terrestrial paravians to utilize wing assisted incline running to access trees or other subvertical substrates previously not accessible (Tobalske & Dial, 2007; Dececchi et al., 2016). From there the utility of gliding or flap-descent (Norberg, 1985; Rayner, 1988) provides a logical selective pressure that could generate several parallel experiments with aerial behavior, only one of which led directly to avian flight.

Conclusions

We have described *Hesperornithoides miessleri*, a new paravian theropod from the Late Jurassic of North America. We ran a phylogenetic analysis based on previous TWiG datasets with expanded taxonomic sampling and recovered it as a troodontid, the oldest diagnostic specimen from North America known from more than teeth. *Hesperornithoides* was clearly a non-volant, terrestrial theropod that spent at least a portion of its life in a marginal lacustrine or

wetland environment. The terrestrial and flightless lifestyle is consistent with the base of Paraves, and with the base of paravian subclades, suggesting that avian flight evolved within Avialae, most likely in the Late Jurassic or Early Cretaceous.

Acknowledgements

We would like to thank Howard and Helen Miessler for their support and generosity. We also thank volunteers from both the Tate Geological Museum and the Wyoming Dinosaur Center who aided the excavation. Thanks are due to Levi Shinkle for additional photography of WYDICE-DML-001 NS to Dan Chure for supplying photographs of *Koparion*. High resolution CT scans were carried out at UT-Austin, with additional CT work provided by the UW-Madison WIMR and Hot Springs County Memorial Hospital. We would like to thank Alexander Averianov, Hebert Bruno Campos, Andrea Cau, Gareth Dyke, Federico Gianechini, Michael Habib, Jaime Headden, Rutger Jansma, Zhiheng Li, Heinrich Mallison, Phil Senter, Lindsay Zanno and others who provided unpublished data on specimens, and the AMNH staff for allowing access to their collections. A final thanks is due to Oliver Rauhut and an anonymous reviewer, whose feedback greatly improved the manuscript.

References

Agnolin, Federico, & Novas, Fernando E. 2013. Avian ancestors: A review of the phylogenetic relationships of the theropods Unenlagiidae, Microraptoria, *Anchiornis* and Scansoriopterygidae. Springer Netherlands. 96 pp. DOI: 10.1007/978-94-007-5637-3_1

Agnolin, Powell, Novas and Kundrat, 2012. New alvarezsaurid (Dinosauria, Theropoda) from uppermost Cretaceous of north-western Patagonia with associated eggs. Cretaceous Research. 35, 33-56. DOI: 10.1016/j.cretres.2011.11.014

Agnolin, F., Motta, M.J., Brisson, F., Lo Coco, G. and Novas, F.E., 2018. Paravian phylogeny and the dinosaur-bird transition: An Overview. Frontiers in Earth Science, 6, p.252. DOI: 10.3389/feart.2018.00252

Barsbold, 1974. Saurornithoididae, a new family of small theropod dinosaurs from Central Asia and North America. Palaeontologia Polonica. 30, 5-22.

Barsbold and Osmólska, 1999. The skull of *Velociraptor* (Theropoda) from the Late Cretaceous of Mongolia. Acta Palaeontologica Polonica. 44(2), 189-219.

Barsbold, Osmolska and Kurzanov, 1987. On a new troodontid (Dinosauria, Theropoda) from the Early Cretaceous of Mongolia. Acta Palaeontologica Polonica. 32(1-2), 121-132.

Benson, R.B., Campione, N.E., Carrano, M.T., Mannion, P.D., Sullivan, C., Upchurch, P. and Evans, D.C., 2014. Rates of dinosaur body mass evolution indicate 170 million years of sustained ecological innovation on the avian stem lineage. PLoS Biology, 12, 5, DOI: 10.1371/journal.pbio.1001853

Brusatte, 2013. The phylogeny of basal coelurosaurian theropods (Archosauria: Dinosauria) and patterns of morphological evolution during the dinosaur-bird transition. PhD thesis, Columbia University. 944 pp.

Brusatte, S. L., Lloyd, G. T., Wang, S. C., & Norell, M. A. 2014. Gradual assembly of avian body plan culminated in rapid rates of evolution across the dinosaur-bird transition. Current Biology, 24, 2386-2392. DOI: 10.1016/j.cub.2014.08.034

Burnham, 2004. New information on *Bambiraptor feinbergi* (Theropoda: Dromaeosauridae) from the Late Cretaceous of Montana. In Currie, Koppelhus, Shugar and Wright (eds.). Feathered Dragons. Studies on the transition from dinosaurs to birds. Indiana University Press. 67-111.

Carpenter, Miles and Cloward, 2005a. New small theropod from the Upper Jurassic Morrison Formation of Wyoming. In Carpenter (ed.). The Carnivorous Dinosaurs. Indiana University Press. 23-48.

Carpenter, K., Miles, C., Ostrom, J.H. and Cloward, K., 2005b. Redescription of the small maniraptoran theropods *Ornitholestes* and *Coelurus* from the Upper Jurassic Morrison Formation of Wyoming. In Carpenter (ed.). Carnivorous Dinosaurs. Indiana University Press. 49-71.

Cau, 2018. The assembly of the avian body plan: A 160-million-year long process. Bollettino della Società Paleontologica Italiana. 57(1), 1-25. DOI: 10.4435/BSPI.2018.01

Cau, A., Brougham, T., & Naish, D. 2015. The phylogenetic affinities of the bizarre Late Cretaceous Romanian theropod *Balaur bondoc* (Dinosauria, Maniraptora): dromaeosaurid or flightless bird? PeerJ 3, e1032. DOI: 10.7717/peerj.1032

Cau A., Beyrand, V., Voeten, D. F. A. E., Fernandez, V., Tafforeau, P., Stein, K., Barsbold, R., Tsogtbaatar, K., Currie, P. J. & Godefroit, P. 2017. Synchrotron scanning reveals

amphibious ecomorphology in a new clade of bird-like dinosaurs. Nature, 552, 395-399. DOI: 10.1038/nature24679

Chiappe, Ji, Ji and Norell, 1999. Anatomy and systematics of the Confuciusornithidae (Theropoda: Aves) from the Late Mesozoic of northeastern China. Bulletin of American Museum of Natural History. 242, 1-89. DOI: 10.1642/0004-8038(2000)117[0836:AASOTC]2.0.CO;2

Choiniere, Forster and de Klerk, 2012. New information on *Nqwebasaurus thwazi*, a coelurosaurian theropod from the Early Cretaceous (Hauteriverian?) Kirkwood Formation in South Africa. Journal of African Earth Sciences. 71-72, 1-17. DOI: 10.1016/j.jafrearsci.2012.05.005

Choiniere, Xu, Clark, Forster, Guo and Han, 2010. A basal alvarezsauroid theropod from the Early Late Jurassic of Xinjiang, China. Science. 327, 571-574. DOI: 10.1126/science.1182143

Chure, D. J. 1994. *Koparion douglassi*, a new dinosaur from the Morrison Formation (Upper Jurassic) of Dinosaur National Monument; the oldest troodontid (Theropoda: Maniraptora). Brigham Young University Geology Studies, 40(1), 11-15.

Clarke, 2002. The morphology and systematic position of *Ichthyornis* Marsh and the phylogenetic relationships of basal Ornithurae. Ph.D. dissertation, Yale University. 532 pp.

Currie, 1995. New information on the anatomy and relationships of *Dromaeosaurus albertensis* (Dinosauria: Theropoda). Journal of Vertebrate Paleontology. 15(3), 576-591. DOI: 10.1080/02724634.1995.10011250

Currie and Dong, 2001. New information on Cretaceous troodontids (Dinosauria, Theropoda) from the People's Republic of China. Canadian Journal of Earth Sciences. 38(12), 1753-1766. DOI: 10.1139/e01-065

Czerkas and Yuan, 2002. An arboreal maniraptoran from Northeast China. Feathered Dinosaurs and the Origin of Flight. The Dinosaur Museum Journal. 1, 63-95.

Dal Sasso and Maganuco, 2011. *Scipionyx samniticus* (Theropoda: Compsognathidae) from the Lower Cretaceous of Italy: Osteology, ontogenetic assessment, phylogeny, soft tissue anatomy, taphonomy, and palaeobiology. Memorie della Società Italiana di Scienze Naturali e del Museo Civico di Storia Naturale di Milano. 281 pp.

Dececchi, T. A. & Larsson, H. C. 2013. Body and limb size dissociation at the origin of birds: uncoupling allometric constraints across a macroevolutionary transition. Evolution, 67, 2741-2752. DOI: 10.1111/evo.12150

Dececchi, T. A., Larsson, H. C., & Habib, M. B. 2016. The wings before the bird: an evaluation of flapping-based locomotory hypotheses in bird antecedents. PeerJ, 4, e2159. DOI: 10.7717/peerj.2159

Dececchi, Larsson and Hone, 2012. *Yixianosaurus longimanus* (Theropoda: Dinosauria) and its bearing on the evolution of Maniraptora and ecology of the Jehol fauna. Vertebrata PalAsiatica. 59(2), 111-139.

DePalma, Burnham, Martin, Larson and Bakker, 2015. The first giant raptor (Theropoda: Dromaeosauridae) from the Hell Creek Formation. Paleontological Contributions. 14, 16 pp. DOI: 10.17161/paleo.1808.18764

Feduccia, A. and Czerkas, S.A., 2015. Testing the neoflightless hypothesis: propatagium reveals flying ancestry of oviraptorosaurs. Journal of ornithology, 156(4), pp.1067-1074.

Field, Hanson, Burnham, Wilson, Super, Ehret, Ebersole and Bhullar, 2018. Complete *Ichthyornis* skull illuminates mosaic assembly of the avian head. Nature. 557, 96-100. DOI: 10.1038/s41586-018-0053-y

Foster, J.R., 2003. Paleoecological Analysis of the Vertebrate Fauna of the Morrison Formation (Upper Jurassic), Rocky Mountain Region, USA: Bulletin 23 (Vol. 23). New Mexico Museum of Natural History and Science.

Foth, C., & Rauhut, O.W.M. 2017. Re-evaluation of the Haarlem *Archaeopteryx* and the radiation of maniraptoran theropod dinosaurs. BMC Evolutionary Biology. 17:236. DOI: 10.1186/s12862-017-1076-y

Foth, C., Tischlinger, H., & Rauhut, O.W.M. 2014. New specimen of *Archaeopteryx* provides insights into the evolution of pennaceous feathers. Nature. 511, 79-82. DOI: 10.1038/nature13467

Gao, C., Morschhauser, E.M. , Varricchio, D.J., Liu, J., & Zhao, B. 2012. A second soundly sleeping dragon: New anatomical details of the Chinese troodontid *Mei long* with implications for phylogeny and taphonomy. PLoS ONE, 7, e45203. DOI: 10.1371/journal.pone.0045203

Gauthier, J. A. 1986. Saurischian monophyly and the origin of birds. Memoirs of the California Academy of Sciences, 8, 1-55.

Gianechini and Apesteguiia, 2011. Unenlagiinae revisited: Dromaeosaurid theropods from South America. Anais da Academia Brasileira de Ciências. 83(1), 163-195.

Gianechini, Makovicky and ApesteguÍa, 2017. The cranial osteology of *Buitreraptor gonzalezorum* Makovicky, ApesteguÍa, and AgnolÍn, 2005 (Theropoda, Dromaeosauridae), from the Late Cretaceous of Patagonia, Argentina. Journal of Vertebrate Paleontology. e1255639. DOI: 10.1080/02724634.2017.1255639

Gianechini, Makovicky, Apesteguía and Cerda, 2018. Postcranial skeletal anatomy of the holotype and referred specimens of *Buitreraptor gonzalezorum* Makovicky, Apesteguía and Agnolín 2005 (Theropoda, Dromaeosauridae), from the Late Cretaceous of Patagonia. PeerJ. 6:e4558. DOI: 10.7717/peerj.4558

Gilmore, 1924. On *Troodon validus*, an orthopodous dinosaur from the Belly River Cretaceous of Alberta, Canada. Department of Geology, University of Alberta Bulletin. 1, 1-43.

Gishlick, 2002. The functional morphology of the forelimb of *Deinonychus antirrhopus* and its importance for the origin of avian flight. PhD thesis, Yale University. 142 pp.

Goloboff, P. A. & Catalano, S. A. 2016. TNT version 1.5, including a full implementation of phylogenetic morphometrics. Cladistics, 32, 221-238. DOI: 10.1111/cla.12160

Godefroit, Currie, Li, Shang and Dong, 2008. A new species of *Velociraptor* (Dinosauria: Dromaeosauridae) from the Upper Cretaceous of northern China. Journal of Vertebrate Paleontology. 28(2), 432-438. DOI: 10.1671/0272-4634(2008)28[432:ANSOVD]2.0.CO;2

Godefroit, P., Cau, A., Dong-Yu, H., Escuillié, F., Wenhao, W. & Dyke, G. 2013b. A Jurassic avialan dinosaur from China resolves the early phylogenetic history of birds. Nature, 498, 359-362. DOI: 10.1038/nature12168

Godefroit, P., Demuynck, H., Dyke, G., Hu, D., Escuillie, F. & Claeys, P. 2013a. Reduced plumage and flight ability of a new Jurassic paravian theropod from China. Nature Communications, 4, 1394. DOI: 10.1038/ncomms2389

Hartman, S., Lovelace, D. & Wahl, W. 2005. Phylogenetic assessment of a maniraptoran from the Morrison Formation. In: Journal of Vertebrate Paleontology, 25, 3, pp. 67A-68A. DOI: 10.1080/02724634.2005.10009942

Holtz, 1994. The arctometatarsalian pes, an unusual structure of the metatarsus of Cretaceous Theropoda (Dinosauria: Saurischia). Journal of Vertebrate Paleontology. 14(4), 480-519. DOI: 10.1080/02724634.1995.10011574

Holtz Jr, T.R., Brinkman, D.L. and Chandler, C.L., 1998. Denticle morphometrics and a possibly omnivorous feeding habit for the theropod dinosaur *Troodon*. Gaia, 15, pp.159-166.

Hone, D.W., Farke, A.A. and Wedel, M.J., 2016. Ontogeny and the fossil record: what, if anything, is an adult dinosaur?. Biology letters, 12(2), p.20150947. DOI: 10.1098/rsbl.2015.0947

Hu, Hou, Zhang and Xu, 2009. A pre-*Archaeopteryx* troodontid theropod from China with long feathers on the metatarsus. Nature. 461, 640-643. DOI: 10.1038/nature08322

Hu, D., Clarke, J. A., Eliason, C. M., Qiu, R., Li, Q., Shawkey, M. D., Zhao, C., D'Alba, L., Jiang, J., & Xu, X. 2018. A bony-crested Jurassic dinosaur with evidence of iridescent plumage highlights complexity in early paravian evolution. Nature Communications. 9, 217. DOI: 10.1038/s41467-017-02515-y

Jenner, 2004. The scientific status of metazoan cladistics: Why current research practice must change. Zoologica Scripta. 33, 293-310. DOI: 10.1111/j.0300-3256.2004.00153.x

Jennings, D. & Hasiotis, S. 2006. Taphonomic analysis of a dinosaur feeding site using Geographic Information Systems (GIS), Morrison Formation, southern Bighorn Basin, Wyoming, USA. Palaios, 21, 480-492. DOI: 10.2110/palo.2005.P05-062R

Jennings, D. S., Lovelace, D. M. & Driese, S. G. 2011. Differentiating paleowetland subenvironments using a multi-disciplinary approach: An example from the Morrison formation, South Central Wyoming, USA. Sedimentary Geology, 238, 23-47. DOI: 10.1016/j.sedgeo.2011.03.005

Jensen and Padian, 1989. Small pterosaurs and dinosaurs from the Uncomphagre fauna (Brushy Basin Member, Morrison Formation: ?Tithonian), Late Jurassic, western Colorado. Journal of Paleontology. 63(3), 364-373. DOI: 10.1017/S0022336000019533

Ji, Ji, Lu, You, Chen, Liu and Liu, 2005. First avialan bird from China (*Jinfengopteryx elegans* gen. et sp. nov.). Geological Bulletin of China. 24(3), 197-205.

Ji, Atterholt, O'Connor, Lammana, Harris, Li, You and Dodson, 2011. A new, three-dimensionally preserved enantiornithine bird (Aves: Ornithothoraces) from Gansu Province, north-western China. Zoological Journal of the Linnean Society. 162, 201-219. DOI: 10.1111/j.1096-3642.2010.00671.x

Kirkland, J. I., Zanno, L. E., Sampson, S. D., Clark, J. M., & DeBlieux, D. D. 2005. A primitive therizinosauroid dinosaur from the Early Cretaceous of Utah. Nature. 435, 84-87. DOI: 10.1038/nature03468

Kobayashi and Barsbold, 2005. Anatomy of *Harpymimus okladnikovi* Barsbold and Perle 1984 (Dinosauria; Theropoda) of Mongolia. In Carpenter (ed.). The Carnivorous Dinosaurs. 97-126.

Kurochkin, 1999. The relationships of the Early Cretaceous *Ambiortus* and *Otogornis* (Aves: Ambiortiformes). Smithsonian Contributions to Paleobiology. 89, 275-284.

Lee, M, S, Cau, A., Naish, D., & Dyke, G. J. 2014a. Sustained miniaturization and anatomical innovation in the dinosaurian ancestors of birds. Science. 345(6196), 562-566. DOI: 10.1126/science.1252243

Lee, Lee, Chinsamy, Lu, Barsbold and Tsogtbaatar, 2019. A new baby oviraptorid dinosaur (Dinosauria: Theropoda) from the Upper Cretaceous Nemegt Formation of Mongolia. PLoS ONE. 14(2), e0210867. DOI: 10.1371/journal.pone.0210867

Lee, Barsbold, Currie, Kobayashi, Lee, Godefroit, Escuillie and Tsogtbaatar, 2014b. Resolving the long-standing enigmas of a giant ornithomimosaur *Deinocheirus mirificus*. Nature. 515, 257-260. DOI: 10.1038/nature13874

Lefèvre, U., Cau, A., Cincotta, A., Hu, D., Chinsamy, A., Escuillié, F. & Godefroit, P. 2017. A new Jurassic theropod from China documents a transitional step in the macrostructure of feathers. The Science of Nature, 104, 74. DOI: 10.1007/s00114-017-1496-y

Longrich and Currie, 2009. *Albertonykus borealis*, a new alvarezsaur (Dinosauria: Theropoda) from the Early Maastrichtian of Alberta, Canada: Implications for the systematics and ecology of the Alvarezsauridae. Cretaceous Research. 30(1), 239-252. DOI: 10.1016/j.cretres.2008.07.005

Lovelace, D. M. 2006. An Upper Jurassic Morrison Formation fire-induced debris flow: Taphonomy and paleoenvironment of a sauropod (Sauropoda: *Supersaurus vivianae*) locality, east-central Wyoming. Paleontology and Geology of the Upper Jurassic Morrison Formation, 36, 47-56.

Lovelace, D. M., Hartman, S. A., & Wahl, W. R. 2007. Morphology of a specimen of *Supersaurus* (Dinosauria, Sauropoda) from the Morrison Formation of Wyoming, and a re-evaluation of diplodocid phylogeny. Arquivos do Museu Nacional, Rio de Janeiro, 65, 527-544.

Lu and Brusatte, 2015. A large, short-armed, winged dromaeosaurid (Dinosauria: Theropoda) from the Early Cretaceous of China and its implications for feather evolution. Scientific Reports. 5, 11775. DOI: 10.1038/srep11775

Macdonald and Currie, 2018. Description of a partial *Dromiceiomimus* (Dinosauria: Theropoda) skeleton with comments on the validity of the genus. Canadian Journal of Earth Sciences. 56(2), 129-157. DOI: 10.1139/cjes-2018-0162

Makovicky, 1995. Phylogenetic aspects of the vertebral morphology of Coelurosauria (Dinosauria: Theropoda). M.S. thesis, University of Copenhagen. 311 pp.

Makovicky, P.J. and Zanno, L.E., 2011. Theropod diversity and the refinement of avian characteristics. In Living Dinosaurs (pp. 9-29). Wiley, Hoboken.

Makovicky, Gorscak and Zhou, 2018. A new specimen of the large-bodied dromaeosaurid *Tiuanyuraptor* provides new insights on microraptorine anatomy, taxonomy, and plumage evolution. Journal of Vertebrate Paleontology. Program and Abstracts, 2018. 174.

Makovicky, Li, Gao, Lewin, Erickson and Norell, 2010. A giant ornithomimosaur from the Early Cretaceous of China. Proceedings of the Royal Society B. 277, 191-198. DOI: 10.1098/rspb.2009.0236

Marsh, O. C., 1881. Principal characters of American Jurassic dinosaurs. Part V. American Journal of Science, 21, 417-423.

Maryanska, T., Osmolska, H., & Wolsan, M. 2002. Avialan status for Oviraptorosauria. Acta Palaeontologica Polonica. 47 (1), 97-116.

Matthew, W. D., & Brown, B. 1922. The family Deinodontidae, with notice of a new genus from the Cretaceous of Alberta. Bulletin of the American Museum of Natural History. 46(6), 367-385.

Mayr, G., Pohl, B., Hartman, S. & Peters, D. S. 2007. The tenth skeletal specimen of Archaeopteryx. Zoological Journal of the Linnean Society, 149, 97-116. 10.1111/j.1096-3642.2006.00245.x

Motta, Egli and Novas, 2017. Tail anatomy of *Buitreraptor gonzalezorum* (Theropoda, Unenlagiidae) and comparisons with other basal paravians. Cretaceous Research. 83, 168-181. DOI: 10.1016/j.cretres.2017.09.004

Naish, D., & Dyke, G. J. 2004. *Heptasteornis* was no ornithomimid, troodontid, dromaeosaurid or owl: The first alvarezsaurid (Dinosauria: Theropoda) from Europe. Neus Jahrbuch für Geologie und Paläontologie. 7 , 385-401.

Norberg, U.M., 1985. Evolution of vertebrate flight: an aerodynamic model for the transition from gliding to active flight. The American Naturalist, 126(3), pp.303-327. DOI: 10.1086/284419

Norell and Makovicky, 1999. Important features of the dromaeosaurid skeleton II: Information from newly collected specimens of *Velociraptor mongoliensis*. American Museum Novitates. 3282, 45 pp.

Norell, M. A., Clark, J. M. & Makovicky, P. J. 2001. Phylogenetic relationships among coelurosaurian theropods. In: Gauthier, J. & Gall, L. F. (eds.). New Perspectives on the Origin and Early Evolution of Birds. Proceedings of the International Symposium in Honor of John H. Ostrom, 49-67.

Norell, Makovicky, Bever, Balanoff, Clark, Barsbold and Rowe, 2009. A review of the Mongolian Cretaceous dinosaur *Saurornithoides* (Troodontidae: Theropoda). American Museum Novitates. 3654, 63 pp. DOI: 10.1206/648.1

Novas, Ezcurra, Agnolin, Pol and Ortiz, 2012. New Patagonian Cretaceous theropod sheds light about the early radiation of Coelurosauria. Revista del Museo Argentino de Ciencias Naturales. 14(1), 57-81.

Novas, Pol, Canale, Porfiri and Calvo, 2008. A bizarre Cretaceous theropod dinosaur from Patagonia and the evolution of Gondwanan dromaeosaurids. Proceedings of the Royal Society B. 276(1659), 1101-1107. DOI: 10.1098/rspb.2008.1554

Ostrom, J.H., 1979. Bird Flight: How Did It Begin? Did birds begin to fly “from the trees down” or “from the ground up”? Reexamination of Archaeopteryx adds plausibility to an" up from the ground" origin of avian flight. American Scientist, 67(1), pp.46-56.

Padian, K., Hutchinson, J. R. & Holtz Jr, T. R. 1997. Phylogenetic definitions and nomenclature of the major taxonomic categories of the theropod dinosaurs. Journal of Vertebrate Paleontology. 17(3), 68A. DOI: 10.1080/02724634.1997.10011028

Pan, Y., Zheng, W., Sawyer, R.H., Pennington, M.W., Zheng, X., Wang, X., Wang, M., Hu, L., O’Connor, J., Zhao, T. and Li, Z., 2019. The molecular evolution of feathers with direct evidence from fossils. Proceedings of the National Academy of Sciences, p.3018-3023. DOI: 10.1073/pnas.1815703116

Paul, 2002. Dinosaurs of the Air. The Johns Hopkins University Press, Baltimore. 460 pp.

Pei, Li, Meng, Gao and Norell, 2014. A new specimen of *Microraptor* (Theropoda: Dromaeosauridae) from the Lower Cretaceous of western Liaoning, China. American Museum Novitates. 3821, 28 pp. DOI: 10.1206/3821.1

Pei, Li, Meng, Norell and Gao, 2017a. New specimens of *Anchiornis huxleyi* (Theropoda: Paraves) from the Late Jurassic of northeastern China. Bulletin of the American Museum of Natural History. 411, 66 pp. DOI: 10.1206/0003-0090-411.1.1

Pei, Norell, Barta, Bever, Pittman and Xu, 2017b. Osteology of a new Late Cretaceous troodontid specimen from Ukhaa Tolgod, Ömnögovi Aimag, Mongolia. American Museum Novitates. 3889, 47 pp. DOI: 10.1206/3889.1

Perez-Moreno, 2004. *Pelecanimimus polyodon*: Anatomía, sistemática y paleobiología de un Ornithomimosauria (Dinosauria: Theropoda) de Las Hoyas (Cretácico Inferior; Cuenca, España). PhD thesis. Universidad Autónoma de Madrid. 149 pp.

Perle, Norell and Clark, 1999. A new maniraptoran theropod - *Achillobator giganticus* (Dromaeosauridae) - from the Upper Cretaceous of Burkhant, Mongolia. Contribution no. 101 of the Mongolian-American Paleontological Project. 1-105.

Peyer, 2006. A reconsideration of *Compsognathus* from the Upper Tithonian of Canjuers, southeastern France. Journal of Vertebrate Paleontology. 26(4), 879-896. DOI: 10.1671/0272-4634(2006)26[879:AROCFT]2.0.CO;2

Rauhut, 2013. New observations on the skull of *Archaeopteryx*. Paläontologische Zeitschrift. 88(2), 211-221. DOI: 10.1007/s12542-013-0186-0

Rauhut, Foth and Tischlinger, 2018. The oldest *Archaeopteryx* (Theropoda: Avialiae): A new specimen from the Kimmeridgian/Tithonian boundary of Schamhaupten, Bavaria. PeerJ. 6:e4191. DOI: 10.7717/peerj.4191

Rauhut, Foth, Tischlinger and Norell, 2012. Exceptionally preserved juvenile megalosauroid theropod dinosaur with filamentous integument from the Late Jurassic of Germany. Proceedings of the National Academy of Sciences. 109(29), 11746-11751. DOI: 10.1073/pnas.1203238109\

Rayner, J.M., 1988. The evolution of vertebrate flight. Biological Journal of the Linnean Society, 34(3), pp.269-287. DOI:10.1111/j.1095-8312.1988.tb01963.x

Russell, D. A., & Dong, Z-M. 1994. A nearly complete skeleton of a new troodontid dinosaur from the Early Cretaceous of the Ordos Basin, Inner Mongolia, People's Republic of China. Canadian Journal of Earth Sciences. 30(10), 2163-2173. DOI: 10.1139/e93-187

Saitta, E.T., Gelernter, R. and Vinther, J., 2018. Additional information on the primitive contour and wing feathering of paravian dinosaurs. Palaeontology, 61, 273-288. DOI: 10.1111/pala.12342

Schweitzer, M. H. 2011. Soft tissue preservation in terrestrial Mesozoic vertebrates. Annual Review of Earth and Planetary Sciences, 39, 187-216. DOI: 10.1146/annurev-earth-040610-133502

Sears, K. E., Behringer, R. R., Rasweiler, J. J. & Niswander, L. A. 2006. Development of bat flight: morphologic and molecular evolution of bat wing digits. Proceedings of the National Academy of Sciences, 103, 6581-6586. DOI: 10.1073/pnas.0509716103

Senter, P. 2007a. A new look at the phylogeny of Coelurosauria. Journal of Systematic Palaeontology, 5, 429-463. DOI: 10.1017/S1477201907002143

Senter, P. 2007b. A method for distinguishing dromaeosaurid manual unguals from pedal “sickle claws”. Bulletin of the Gunma Museum of Natural History, 11, 1-6.

Senter, P. 2011. Using creation science to demonstrate evolution 2: Morphological continuity within Dinosauria. Journal of Evolutionary Biology, 24, 2197-2216. DOI: 10.1111/j.1420-9101.2011.02349.x

Senter, Barsbold, Britt and Burnham, 2004. Systematics and evolution of Dromaeosauridae. Bulletin of Gunma Museum of Natural History. 8, 1-20.

Senter, P., Kirkland, J. I., DeBlieux, D. D., Madsen, S & Toth, N. 2012. New dromaeosaurids (Dinosauria: Theropoda) from the Lower Cretaceous of Utah, and the evolution of the dromaeosaurid tail. PLoS ONE, 7, e36790. DOI: 10.1371/journal.pone.0036790

Sereno, P.C. 1997. The origin and evolution of dinosaurs. Annual Review of Earth and Planetary Sciences, 25, 435-489. DOI: 10.1146/annurev.earth.25.1.435

Sereno, 1999. The evolution of dinosaurs. Science. 284, 2137-2147. DOI: 10.1126/science.284.5423.2137

Sereno, 2007. Logical basis for morphological characters in phylogenetics. Cladistics. 23, 565-587. DOI: 10.1111/j.1096-0031.2007.00161.x

Shen, Zhao, Gao, Lű and Kundrát, 2017a. A new troodontid dinosaur (*Liaoningvenator curriei* gen. et sp. nov.) from the Early Cretaceous Yixian Formation in western Liaoning province. Acta Geoscientica Sinica. 38(3), 359-371. DOI: 10.3975/cagsb.2017.03.06

Shen, C., Lű, J., Kundrát, M., Brusatte, S. L. & Gao, H. 2017b. A new troodontid dinosaur from the Lower Cretaceous Yixian Formation of Liaoning Province, China. Acta Geologica Sinica, 91, 763-780. DOI: 10.1111/1755-6724.13307

Speakman, J.R. and Thomson, S.C., 1994. Flight capabilities of *Archaeopteryx*. Nature, 370(6490), 514. DOI: 10.1038/370514a0

Tobalske, B. W., & Dial, K. P. 2007. Aerodynamics of wing-assisted incline running in birds. Journal of Experimental Biology, 210, 1742-1751. DOI: 10.1242/jeb.001701

Trujillo, K. 2006. Clay mineralogy of the Morrison Formation and its use in long distance correlation and paleoenvironmental analysis. In: Foster, J. R. & Lucas, S. G. (Eds.), Paleontology and Geology of the Upper Jurassic Morrison Formation. New Mexico Museum of Natural History and Science Bulletin, 17–24.

Trujillo, K., Chamberlain, K. & Strickland, A. 2006. Oxfordian Park: U/Pb ages from SHRIMP analysis for the Upper Jurassic Morrison Formation of southeastern Wyoming with implications for biostratigraphic correlations. Journal of Vertebrate Paleontology, Suppl. 26:3, 132. DOI: 10.1080/02724634.2006.10010069

Trujillo, K., Foster, J., Hunt-Foster, R. & Chamberlain, K. A. 2014. U/Pb age for the Mygatt-Moore Quarry, Upper Jurassic Morrison Formation, Mesa County, Colorado. Volumina Jurassica, 12, 107-114. DOI: 10.5604/17313708 .1130132

Tsuihiji, Barsbold, Watabe, Tsogtbaatar, Suzuki and Hattori, 2015. New material of a troodontid theropod (Dinosauria: Saurischia) from the Lower Cretaceous of Mongolia. Historical Biology. 28(1-2), 128-138. DOI: 10.1080/08912963.2015.1005086

Turner, 2008. Phylogenetic relationships of paravian theropods. PhD Thesis. Columbia University. 666 pp.

Turner, A. H., Makovicky, P. J. & Norell, M. 2012. A review of dromaeosaurid systematics and paravian phylogeny. Bulletin of the American Museum of Natural History, 371, 1-206.

Turner, Pol and Norell, 2011. Anatomy of *Mahakala omnogovae* (Theropoda: Dromaeosauridae), Tögrögiin Shiree, Mongolia. American Museum Novitates. 3722, 66 pp. DOI: 10.1206/3722.2

Turner, A. H., Pol, D., Clarke, J. A., Erickson, G. M. & Norell, M. A. 2007. A basal dromaeosaurid and size evolution preceding avian flight. Science, 317, 1378-1381. DOI: 10.1126/science.1144066

Wahl, W. R. 2006. Osteology and phylogenetic relationships of a new small maniraptoran from the Upper Jurassic of Wyoming. Master's thesis, Fort Hays State University. 97 pp.

Wang, Zhou, O'Connor and Zelenkov, 2014. A new diverse enantiornithine family (Bohaiornithidae fam. nov.) from the Lower Cretaceous of China with information from two new species. Vertebrata PalAsiatica. 52(1), 31-76.

Wang, Wang, Wang and Zhou, 2016. A new basal bird from China with implications for morphological diversity in early birds. Scientific Reports. 6, 19700. DOI: 10.1038/srep19700

Wang, Zheng, O'Connor, Lloyd, Wang, Wang, Zhang and Zhou, 2015. The oldest record of Ornithuromorpha from the Early Cretaceous of China. Nature Communications. 6:6987. DOI: 10.1038/ncomms7987

Witmer, 1997. The evolution of the antorbital cavity of archosaurs: A study in soft-tissue reconstruction in the fossil record with an analysis of the function of pneumaticity. Journal of Vertebrate Paleontology. Memoir 3. 17(1), 1-73. DOI: 10.1080/02724634.1997.10011027

Xing, Persons, Bell, Xu, Zhang, Miyashita, Wang and Currie, 2013. Piscivory in the feathered dinosaur *Microraptor*. Evolution. 67(8), 2441-2445. DOI: 10.1111/evo.12119

Xu, 2002. Deinonychosaurian fossils from the Jehol Group of Western Liaoning and the coelurosaurian evolution. PhD Thesis. Chinese Academy of Sciences. 325 pp.

Xu and Li, 2016. A new microraptorine specimen (Theropoda: Dromaeosauridae) with a brief comment on the evolution of compound bones in theropods. Vertebrata PalAsiatica. 54(4), 153-169.

Xu, X., & Norell, M.A. 2004. A new troodontid dinosaur from China with avian-like sleeping posture. Nature. 431, 838-841. DOI: 10.1038/nature02898

Xu and Wang, 2004. A new troodontid (Theropoda: Troodontidae) from the Lower Cretaceous Yixian Formation of Western Liaoning, China. Acta Geologica Sinica. 78(1), 22-26. DOI: 10.1111/j.1755-6724.2004.tb00671.x

Xu and Wu, 2001. Cranial morphology of *Sinornithosaurus millenii* Xu et al. 1999 (Dinosauria: Theropoda: Dromaeosauridae) from the Yixian Formation of Liaoning, China. Canadian Journal of Earth Sciences. 38, 1739–1752. DOI: 10.1139/e01-082

Xu, Zhou and Wang, 2000. The smallest known non-avian theropod dinosaur. Nature, 408, 705-708. DOI: 10.1038/35047056

Xu, X., You, H., Du, K. & Han, F. 2011. An *Archaeopteryx*-like theropod from China and the origin of Avialae. Nature, 475, 465-470. DOI: 10.1038/nature10288

Xu, Norell, Wang, Makovicky and Wu, 2002. A basal troodontid from the Early Cretaceous of China. Nature. 415, 780-784. DOI: 10.1038/415780a

Xu, Zhao, Sullivan, Tan, Sander and Ma, 2012. The taxonomy of the troodontid IVPP V 10597 reconsidered. Vertebrata PalAsiatica. 50(2), 140-150.

Xu, Currie, Pittman, Xing, Meng, Lu, Hu and Yu, 2017. Mosaic evolution in an asymmetrically feathered troodontid dinosaur with transitional features. Nature Communications. 8:14972. DOI: 10.1038/ncomms14972

Xu, Kobayashi, Lu, Lee, Liu, Tanaka, Zhang, Jia and Zhang, 2011. A new ornithomimid dinosaur with North American affinities from the Late Cretaceous Qiupa Formation in Henan Province of China. Cretaceous Research. 32(2), 213-222. DOI: 10.1016/j.cretres.2010.12.004

Xu, X., Zheng, X., Sullivan, C., Wang, X., Xing, L., Wang, Y., Zhang, X., O'Connor, J.K., Zhang, F. and Pan, Y., 2015. A bizarre Jurassic maniraptoran theropod with preserved evidence of membranous wings. Nature, 521(7550), p.70.

Xu, Choiniere, Tan, Benson, Clark, Sullivan, Zhao, Han, Ma, He, Wang, Xing and Tan, 2018. Two Early Cretaceous fossils document transitional stages in alvarezsaurian dinosaur evolution. Current Biology. 28, 1-8. DOI: 10.1016/j.cub.2018.07.057

Yin, Pei and Zhou, 2018. Cranial morphology of *Sinovenator changii* (Theropoda: Troodontidae) on the new material from the Yixian Formation of western Liaoning, China. PeerJ 6:e4977. DOI: 10.7717/peerj.4977

Zanno, 2010. A taxonomic and phylogenetic re-evaluation of Therizinosauria (Dinosauria: Maniraptora). Journal of Systematic Palaeontology. 8(4), 503-543. DOI: 10.1080/14772019.2010.488045

Zanno, Varricchio, O'Connor, Titus and Knell, 2011. A new troodontid theropod, *Talos sampsoni* gen. et sp. nov., from the Upper Cretaceous western interior basin of North America. PLoS ONE. 6(9), e24487. DOI: 10.1371/journal.pone.0024487

Zhang, Zhou, Xu, Wang and Sullivan, 2008. A bizarre Jurassic maniraptoran from China with elongate ribbon-like feathers. Nature. 455, 1105-1108. DOI: 10.1038/nature07447

Zheng, O'Connor, Wang, Wang and Zhou, 2018. Reinterpretation of a previously described Jehol bird clarifies early trophic evolution in the Ornithuromorpha. Proceedings of the Royal Society B. 285, 20172494. DOI: 10.1098/rspb.2017.2494

Zheng, Xu, You, Zhao and Dong, 2009. A short-armed dromaeosaurid from the Jehol Group of China with implications for early dromaeosaurid evolution. Proceedings of the Royal Society B. 277, 211-217. DOI: 10.1098/rspb.2009.1178

Zhou and Zhang, 2002. A long-tailed, seed-eating bird from the Early Cretaceous of China. Nature. 418, 405-409. DOI: 10.1038/nature00930

Zhou and Zhang, 2003. Anatomy of the primitive bird *Sapeornis chaoyangensis* from the Early Cretaceous of Liaoning, China. Canadian Journal of Earth Sciences. 40, 731-747. DOI: 10.1139/e03-011

Zhou, Clarke and Zhang, 2008. Insight into diversity, body size and morphological evolution from the largest Early Cretaceous enantiornithine bird. Journal of Anatomy. 212, 565-577. DOI: 10.1111/j.1469-7580.2008.00880.x

Supplemental Appendices

Supplement A - Coauthored paper underlying Chapter 1:

Modeling Dragons: Using linked mechanistic physiological and microclimate models to explore environmental, physiological, and morphological constraints on the early evolution of dinosaurs

David M. Lovelace[1*], Scott A. Hartman[2], Paul D. Mathewson[3], Benjamin J. Linzmeier[2] & Warren P. Porter[3*]

[1] University of Wisconsin Geology Museum, Department of Geosciences, University of Wisconsin-Madison, Madison, Wisconsin, United States of America

[2] Department of Geoscience, University of Wisconsin-Madison, Madison, Wisconsin, United States of America

[3] Department of Integrative Biology, University of Wisconsin-Madison, Madison, Wisconsin, United States of America

Abstract

We employed the widely-tested biophysiological modeling software, Niche Mapper™ to investigate the metabolic function of the Late Triassic dinosaurs *Plateosaurus* and *Coelophysis* during global greenhouse conditions. We tested a variety of assumptions about resting metabolic rate, each evaluated within six microclimate models that bound paleoenvironmental conditions at 12° N paleolatitude, as determined by sedimentological and isotopic proxies for climate within the Chinle Formation of the southwestern United States. Sensitivity testing of metabolic variables and simulated "metabolic chamber" analyses support elevated "ratite-like" metabolic rates and intermediate "monotreme-like" core temperature ranges in these species of early saurischian dinosaur. Our results suggest small theropods may have needed partial to full epidermal insulation in temperate environments, while fully grown prosauropods would have likely been heat stressed in open, hot environments and should have been restricted to cooler microclimates such as dense forests or higher latitudes and elevations. This is in agreement with the Late Triassic fossil record and may have contributed to the latitudinal gap in the Triassic prosauropod record.

Introduction

Paleontologists have long inferred the biology of extinct organisms from morphological correlates and paleoenvironmental context. Hypotheses derived from morphology rely on extant phylogenetic bracketing and modern analogs for support [1,2]; lack of inferential specificity may come from trimmed phylogenetic trees or increased distance from extant relatives [3]. Spatiotemporally derived hypotheses suffer from confounding factors related to bias in the stratigraphic record [4-6]. These biases can be tempered by using physics-based constraints to model a broad range of paleobiological phenomena.

All animals, living and extinct are constrained by physics. Gravity exerts control on the maximum size attained by terrestrial clades, from spiders to sauropods [7], and biological thermodynamics constrains the rate heat is produced as well as its transfer to and from the environment [8]. Robust biophysiological models, such as Niche Mapper™ are built on the fundamental principles of heat and mass flux into and out of individuals [9]. Morphology (e.g. posture, insulation, color, and body part dimensions), behavior (e.g. seeking shade, sunning, fur or feather erection, varying activity level and location), and physiology (e.g. metabolic rate, peripheral blood flow, respiratory and cutaneous water loss) can accelerate or retard heat exchange with the surrounding environment, setting temporal and spatial constraints (boundary conditions) for animal function.

For decades ecologists have modeled the physics of heat transfer to understand ecological and biogeographic constraints of modern organisms [10-25]. Biophysiological models have only been sparsely applied to deep time investigations [e.g. 26,27]. For paleoecologists, the paleobiogeographic distribution of an extinct organism is harder to test with respect to organismal physiology. For instance, it has been noted that there is an absence of large (>~1000 kg) prosauropod dinosaurs in the well-studied tropical to subtropical latitudes during the Late Triassic (e.g., the Chinle Formation of southwestern U.S.), while smaller (<~100 kg) theropod dinosaurs and their closest relatives are quite common [28]. In contrast, both large and small (~10-100 kg) prosauropods as well as small theropods are well represented in temperate latitudes. A number of hypotheses have been proposed to explain this pattern, including exclusion via high temperatures and environmental fluctuations, increased severity and frequency of wildfires, aridity, and precipitation patterns [28]. These hypotheses are difficult to test explicitly without the use of biophysical modeling.

The paleobiogeographic distribution of *Plateosaurus* and *Coelophysis* along with associated paleoclimate proxies from fossil localities provide boundary conditions to test hypotheses of environmental exclusion due to physiological limitations. We applied Niche Mapper to test a range of physiological possibilities for two adult-sized Late Triassic dinosaurs, the ~20 kg theropod *Coelophysis bauri* (Cope 1887) and the ~1000 kg prosauropod *Plateosaurus engelhardti* (von Meyer 1837) to quantitatively test the thermal constraint hypothesis. We performed sensitivity analyses to determine the relative contributions of climate, body mass, shape, diet, insulation, and the efficiencies of respiratory, digestive, and muscle systems, as well as feasible daily core temperature range and resting metabolic rate on total energy requirements. The integration of biophysiological and microclimate models offers a potentially powerful means of testing feasible physiologies and behaviors of extinct organisms against known fossil distribution and their associated paleoenvironments.

Materials and methods

We employed the mechanistic modeling program Niche Mapper, developed at UW-Madison [29]. Niche Mapper is compartmentalized into generic microclimate and animal submodels that each contain momentum, heat, and mass transfer equations. The microclimate model has 51 variables relating to seasonality, insolation, shade, wind, air temperature, humidity, cloud, and soil properties. The biophysical model is composed of 270 morphological, physiological, and behavioral parameters previously described in detail and tested over a wide range of animal taxa including reptiles, amphibians, birds, mammals, and insects [e.g., 12,13,15,16,23,30-39]. The user is able to control how many days (1 to 365) and how those days are distributed throughout the year, and how many of the variables (such as air temperature, feather density, or body mass) vary for each modeled day (see S1 Appendix).

Fundamentally, Niche Mapper calculates hourly energy and mass expenditures that can predict survivorship based on reasonable bounds of thermal stress and resource availability. Paleoenvironmental bounds for the microclimate model are derived from environmental proxies preserved within the rock record and data from analogous modern environments, when applicable. Measurements of skeletal dimensions parameterize a simple geometric volume that approximates the shape of the animal. The range of metabolic rates known from modern tetrapods bounds modeled rates. These boundaries allowed us to explore a reasonable parameter space although the model could easily be extended to explore unique circumstances and test novel hypotheses.

As an additional test of our Triassic microclimate models and as a point of comparison we modelled *Varanus komodoensis* (Komodo dragon), using the same methodology implemented for our dinosaur models. We compared our modeled results against observational data for *V. komodoensis* [40-42] activity patterns, food requirements, body size and body temperature (S2 Appendix).

The microclimate model

The microclimate model calculates hourly air temperatures, wind speeds, and relative humidity profiles, solar and thermal long wavelength infrared radiation, ground surface and subsurface temperatures available to an animal [11,29,43,44]. Local environments at mean animal height are used for heat balance calculations (Fig S1-1).

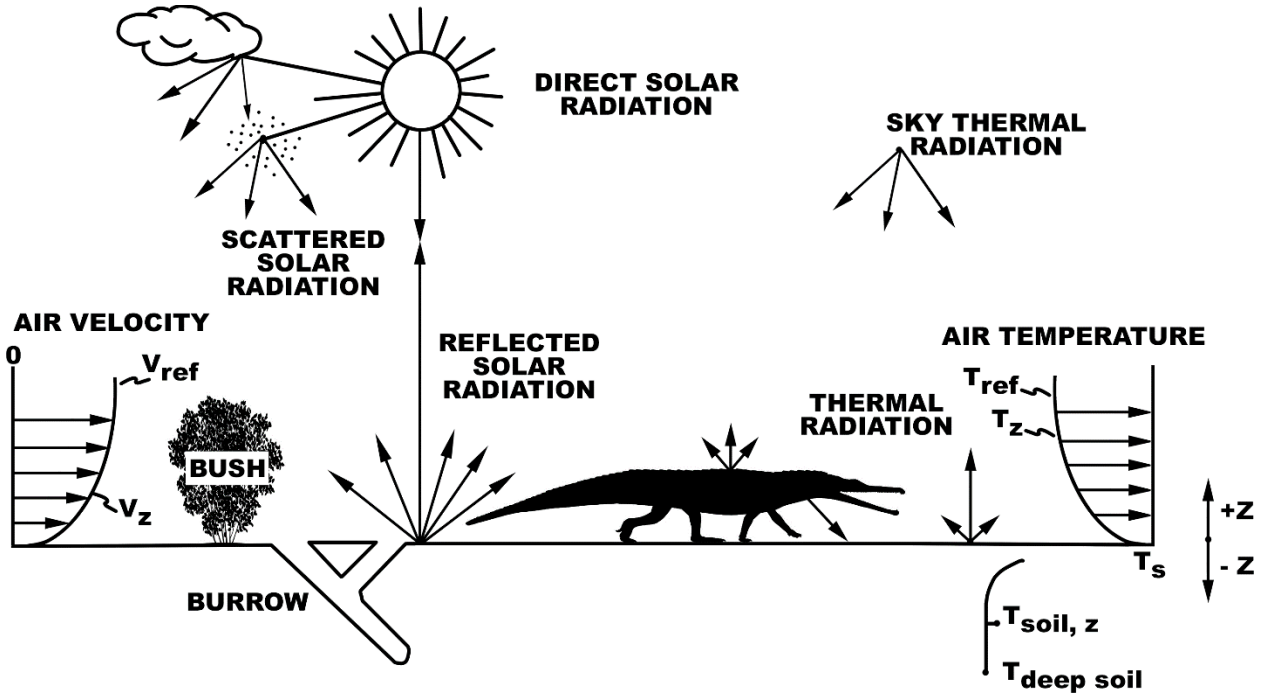

Fig S1-1. Organism-environment heat balance interactions. *The reptile's heat and mass balances that influence body temperature are determined by where it chooses to be each hour to remain within its preferred body temperature range. Niche Mapper allows it to find a location each hour where it can remain active, or not, if necessary, to optimize its body temperature and/or water balance.*

The microclimate model fits a sinusoidal curve to user-specified maximum and minimum daily air temperatures, wind speeds, cloud cover, and relative humidity to estimate hourly values. We set minimum air temperature, minimum wind speed, maximum relative humidity and cloud cover to occur at sunrise. Maximum air temperature, maximum wind speed, and minimum relative humidity and cloud cover are set to occur one hour after solar noon [45]. Clear sky solar radiation is calculated based on date, hour of day, and geographic location adjusted for cloud cover and overhead vegetation [43,46]. Paleosolar calculations for insolation were computed from Laskar et al. [47] using the *palinsol* program in R [48]. Because of uncertainties in deep time insolation we used modern values as a first step. However, we recognize there is variability in insolation not only in deep time, but also on shorter timescales due to precession, obliquity,

and eccentricity. Cloud cover also reduces solar radiation intensity at ground level and provides thermal cover by trapping longwave radiation that would otherwise escape to the sky, increasing the sky's radiant temperature [29,44,45,49].

Long wavelength thermal radiation from clear sky and clouds were computed using empirical air temperature correlations from the literature [50,51]. Substrate thermal radiation was computed hourly from the numerical solution of a one dimensional finite difference transient heat balance equation for the ground. Hourly outputs from the microclimate model specify above and belowground local microclimates in the sunniest and shadiest sites specified by the user.

Microclimate Model Parameterization in Deep Time

In order to test the hypothesis that large dinosaurs such as *Plateosaurus* were restricted from tropical latitudes primarily due to thermal constraints we chose to use the well sampled Late Triassic strata of the Chinle Formation of western North America as a model for our Late Triassic paleoenvironment. Although these strata are currently located at 35 degrees north, the Chinle was originally deposited between 5 and 10 degrees north paleolatitude [52]. We used published local and regional paleoclimate data derived from the Chinle Formation; these data include sedimentary proxies for paleotemperature and precipitation [52-54], global climate models [55], and global geochemical compilations [56,57]. We used these data to constrain our microclimate model to best represent a tropical Late Triassic environment and considered this the 'hot' microclimate model. This is not the most extreme temperatures proposed for the Late Triassic Chinle Formation [58], making our modeled environment a conservative estimate for testing whether high temperatures excluded large dinosaurs from the region. Our cold microclimate is an conservative approximation of paleoclimates in upper Triassic strata in central

and northern Europe (~35-45 ºN; [55,59,60]) where *Plateosaurus* is a relatively common constituent in fossil assemblages. In order to aid comparison and avoid interactions of variables, annual distribution of microclimate data was maintained across the hot and cold microclimates and only the temperature values were adjusted to model a cooler temperate microclimate as a first-order approximation of higher latitudes. A moderate microclimate was also modeled to represent areas intermediate between hot and cold microclimates. Air temperature are modeled at the average height of the organisms being examined for each hour (Fig. S1-2). Paleolatitude is modeled as 12 ºN, with an elevation of 150 m [54].

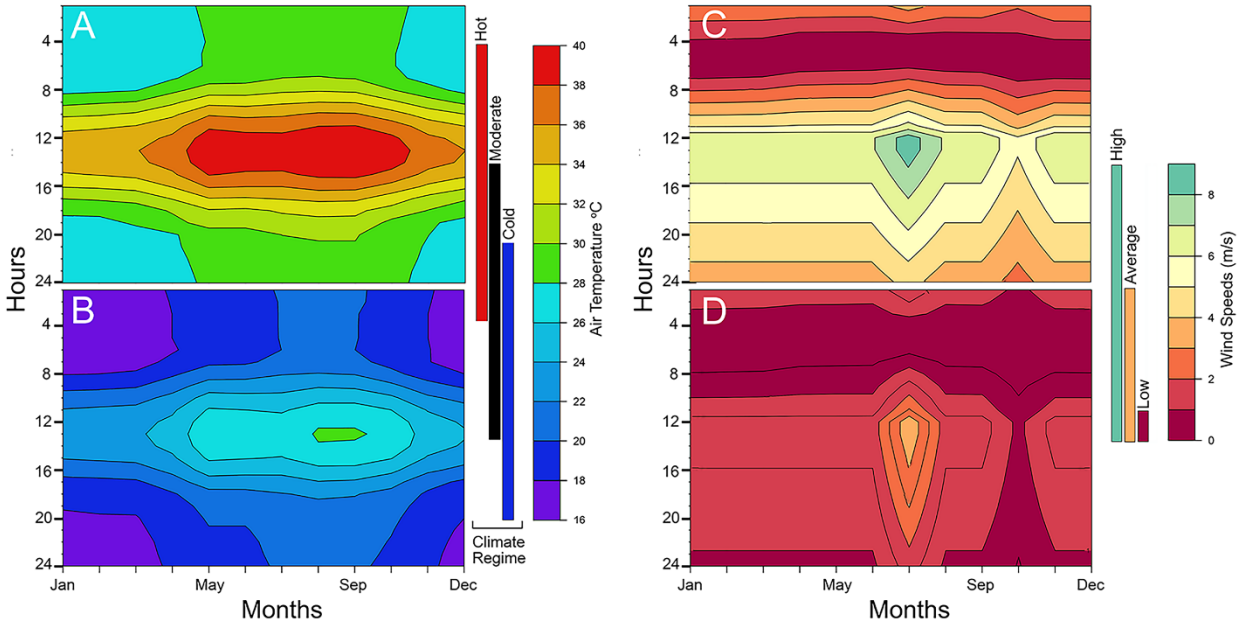

Fig S1-2. Heatmaps of microclimate air temperature and wind speed at average animal height for each modeled hour. *We use a turbulent velocity and temperature profile where the most significant changes occur within the first 15 cm from the ground. The microclimates are the same for both Coelophysis (shown) and Plateosaurus. (A) hot and B) cold climate regimes, C) high and D) low wind speeds.*

Because the resolution of paleoclimate proxies are time-averaged it is difficult to determine an annual pattern for the microclimate model. As such, historic climate data from modern analogues provide a means to establish realistic annual patterns otherwise indiscernible in the rock record. We selected regions similar to paleogeographic reconstructions of the Chinle

formation with respect to elevation, temperature and precipitation regimes, latitude, and general position on the continent; two locations in western Africa (Tamale, Ghana and Timbuktu, Mali) act as modern analogues for this study. Numeric values for the microclimate model were determined by multi-proxy data in the geological record whenever possible (see Table S1-1).

Table S1-1. Microclimate parameters inferred from geologic proxies, GCM's, and modern analogues.

Parameter	**Model**	**Source**	**Modeled Range**
Air Temperature	microclimate	[52]	Cold: 16–30 °C; warm: 20–34 °C; hot: 26–40 °C; **see Fig 2**
Relative Humidity	microclimate	[55,61]	'Dry' 13-65%; 'Wet' 48-96%
Cloud Cover	microclimate	[61]	50-90%
Wind Speeds	microclimate	[62,63]	1-4 m/s; **see Fig 2**
Atmospheric $\%O_2$	biophysical	[56]	$\%O_2 = 18$
Atmospheric $\%CO_2$	biophysical	[54,57]	$\%CO_2 = 0.13$

The biophysical model

Gross organismal morphology (head, neck, torso, legs, tail) are modeled as simple geometric shapes (e.g., cylinders, spheres, truncated cones, or ellipsoids; S3 Appendix). These geometries have known or measurable heat transfer properties and temperature profile equations that simplify solving the heat balance equation when there is distributed internal heat generation [e.g., 36,64,66]. Each body part can be modeled with up to three concentric layers: 1) a solid central geometry of tissue uniformly generating heat; 2) if present, a surrounding layer of

insulating subcutaneous fat is modeled as a hollow heat conducting geometry; 3) a surrounding layer of insulating fur or feathers, modeled as a hollow porous medium (see below). Net metabolic heat produced by the central flesh layer must be transferred through the fat layer to the skin surface, where is it either dissipated via cutaneous evaporation, convection and infrared thermal radiation (naked), or transferred through the fur/feather layer if present, then lost by convection and infrared thermal radiation to the environment. Heat is transferred through the

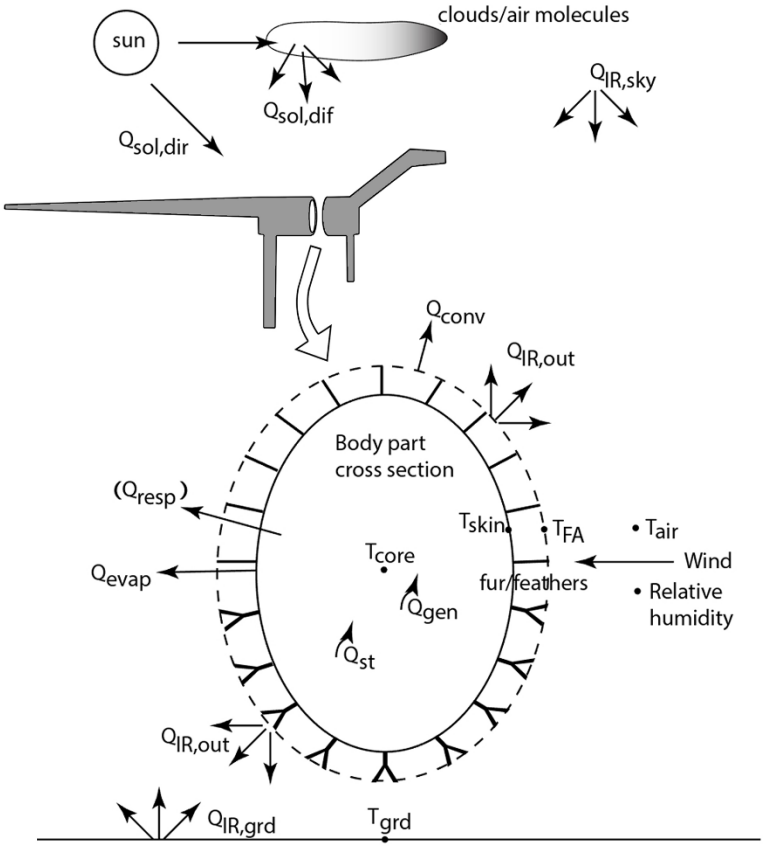

Fig S1-3. Heat transfer pathways between modeled organism and environment. *Cross-section of a body segment (e.g., elliptical cylindrical torso of distributed heat generating flesh surrounded by an optional layer of fat (not shown), then skin surrounded by porous insulation whose properties may be the same or different dorsally vs. ventrally). The flesh is generating metabolic heat throughout the body (Qmet) and exchanging (Qresp, Qevap, QIRnet, Qconv, Qsol) heat with its environment as modeled by Niche Mapper (adapted from Porter et al. [23]). The transient model also includes a heat storage term, Qst, for the flesh. A full list of symbols and abbreviations can be found in the text.*

fur/feathers by parallel thermal radiation and conduction through the air between the insulation elements and through the fur or feathers [36,66] and is lost to the environment via thermal radiation and convection. If the animal is lying down and has ventral insulation, it is compressed by an amount defined by the user and heat is conducted to or from the substrate at the insulation surface. Heat from solar radiation can also be absorbed through the skin (naked) or fur/feather layer (insulated), contributing to the heat load that must be dissipated (Fig S1-3).

Provided with the local environmental conditions from the microclimate model and biophysical properties of the organism, the animal model calculates radiative (Q_{rad}), convective (Q_{conv}), solar (Q_{sol}), and evaporative (respiratory: Q_{resp} and cutaneous: Q_{evap}) heat fluxes between the animal and its microenvironment to solve a heat balance equation (1) for a metabolic rate, Q_{met}, that satisfies (1) and is consistent with the status of its core and skin temperatures and environmental conditions:

$$Qmet - Qresp - Qst - Qevap = Qrad + Qconv - Qsol \quad (1)$$

If the animal has a fur or feather layer, an additional parameter (*Qfur*) must be added to account for heat flow through the insulating fur or feather layer:

$$Qmet - Qresp - Qs - Qevap = Qfur = Qrad + Qconv - Qsol \quad (2)$$

where Q_{fur} represents the heat flux through the fur or feather layer via parallel conductive and radiative processes. For more detailed explanations of heat flux through porous media such as fur or feathers and solving for steady state conditions see Porter et al. [36], Porter and Kearney [67] and Mathewson and Porter [17].

For each hour of every model day the heat balance equation is solved for individual body parts and summed to provide the total metabolic rate (W) for the entire animal that will allow it to maintain a target core temperature in that hour's range of environmental conditions. Users can specify a basal metabolic rate multiplier to simulate activity in the heat balance calculations, as well as muscle efficiency, which is the proportion of that additional activity expenditure contributes to the animal's heat balance (i.e., 0% means that the mechanical work (activity) is 100% efficient with no excess heat produced; 99% means that 99% of the metabolic effort is lost as heat and needs to be considered in the heat balance). We assumed a mammal-like 20% muscle efficiency for activity with 80% of the chemical energy for activity going to heat. Although a ~35% muscle efficiency may be more reasonable for archosaurs, it is less well documented [68]; we performed a sensitivity analysis to test the effect of differing muscle efficiencies (see below).

If the total animal metabolic rate deviates from user-specified variation in the target metabolic rate (i.e., expected basal metabolic rate x activity multiplier) for the hour being modeled, physiological options, followed by behavioral options, are engaged to prevent the animal from being too hot or too cold by decreasing or increasing metabolic expenditure on heat production respectively.

User selected physiological options are engaged in the following order when individually enabled: 1) incrementally erect fur or feathers to increase insulation; 2) incrementally increase or

decrease flesh thermal conductivity, simulating vasodilation or vasoconstriction of peripheral blood vessels; 3) incrementally increase or decrease core temperature, simulating temporary, bounded positive or negative heat storage; 4) incrementally increase the amount of surface area that is wet to increase evaporative heat loss, simulating sweating (if allowed); and 5) incrementally decrease oxygen extraction efficiency to increase respiratory heat loss, simulating panting.

If physiological changes are not sufficient to thermoregulate, behavioral thermoregulation options are engaged and the animal can seek shade, swim, wade, climb, or enter a burrow to achieve cooler environmental conditions. The user defines which behaviors are possible for the modeled organism; for instance, it is unlikely that an 850 kilogram prosauropod is burrowing or climbing trees to behaviorally thermoregulate, so these options would not be utilized. If the animal is too cold (i.e. the requisite metabolism is greater than the resting metabolic rate x the activity multiplier), the user can allow the animal to enter a burrow or seek vegetative shelter or get out of the wind. These options also reduce radiant heat loss to the sky by providing overhead structures (e.g. forest canopy or burrow ceiling) with warmer radiant temperatures than the open sky. Users can also allow model animals to make postural changes such as curling up to minimize surface area for heat exchange with the environment if the animal is too cold.

The heat balance is re-solved after each incremental thermoregulatory change until either 1) the metabolic rate that balances the heat budget equation is within the percent error of the target metabolic rate or 2) thermoregulatory options are exhausted. In the case of the latter, the metabolic rate that balances the heat budget equation that is closest to the target rate is used for that hour. Hourly metabolic rates and water losses are integrated over the day to calculate daily metabolic rate and water loss, which can then be used to calculate food and water requirements.

The day's water and energy requirements are then used to compute the respiratory and digestive system inputs and outputs using molar balances as described below.

The heat and mass balance of an organism are connected by metabolic rate, a 'biological fire' that requires fuel and oxygen. The daily metabolic rate that releases heat (*Qmet*) sets the daily mass balance requirements for the respiratory and digestive systems (Fig 4). Diet composition (proteins, carbohydrates, lipids, percent water) specify how much mass must be absorbed ($\mathbf{m_{abs}}$) from the gut to meet metabolic demands. Digestive efficiency divided into the mass absorbed determines the mass of food that must be ingested per day ($\boldsymbol{m_{in}}$) to meet energy requirements. Mass excreted ($\boldsymbol{m_{out}}$) is the difference between mass in and mass absorbed.

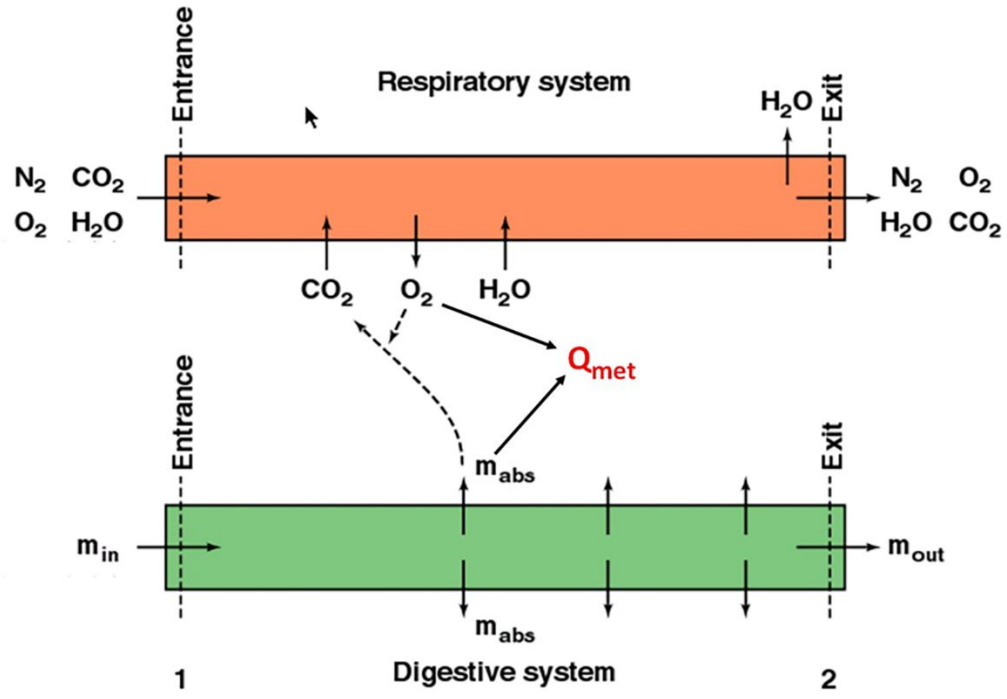

Fig S1-4. Internal mass balance models coupled to heat transfer. *System diagram for the respiratory and digestive system driven by the metabolic rate, Qmet.*

The respiratory system functions in an analogous manner. Diet utilization and activity rates determine the amount of oxygen needed and carbon dioxide produced. Oxygen required divided by the respiratory extraction coefficient specifies the mass of air that must enter the respiratory system, given the atmospheric composition of oxygen per unit volume. Humidity of the incoming air is increased to saturated air at lung (body) temperature, so respiratory water loss can also be computed. Recovery of water vapor during exhalation through cooler nostrils is also calculated.

Biophysical Model Parameterization in Deep Time

Key *morphological* and *behavioral* model inputs are summarized in Tables S1-2 & S1-3. For *behavioral* thermoregulation, we allowed animals to hide from wind (if too cool), seek shade during the day (if too hot), seek shade at night (e.g., simulating vegetative cover slowing the rate of radiative heat loss seen in open sky conditions), be active in the shade (day and night), postural changes to minimize surface area if cold and inactive, or maximize surface area if hot. For *physiological* thermoregulation we allowed for panting (too hot), increased and decreased flesh conductivity (to simulate vasoconstriction/vasodilation when cold/hot), if dermal insulation (fur/feathers) is present they can piloerect/ptiloerect, or changes in regulated body temperature within the user specified maximum and minimum body temperature range. Sweating was not enabled due to phylogenetic constraints. Sensitivity analyses were performed to test which behavior, or interaction of multiple behaviors, had the strongest effect. Since legs and tail consist of mostly muscle, bone and tendon, we allowed the temperature in limb and tail segments to reach 50% of the difference between the torso-segment junction and ambient air or ground temperatures [c.f.,12,69].

Table S1-2. Morphological parameters of porous insulation modeled and skin or insulation surface solar reflectivity.

Variable			No Insulation	Top-only Insulation	Full Insulation	Reference and comment
Insulation	Length (mm)	Dorsal*	0	30	30	[Based on 69–72]
		Ventral*	0	0	30	
	Depth (mm)	Dorsal*	0	10	10	
		Ventral*	0	0	10	
	Density (elements/cm^2)		0	2000	2000	[37 Fig 25,73]
	Insulation/skin reflectivity (%)		15	15	15	Porter, marine iguana, unpub. data
	Pilo/ptiloerection		No	Yes**	Yes**	

Insulation element density estimated assuming that 1) feathers evolved by selection for a follicle that would grow an emergent tubular appendage [73] early 'feathers' were similar to stage 1 or 2 in the developmental pattern of modern feathers, i.e. cylindrical in shape. 3) that the minimum hair density that substantially reduces heat loss (reduces metabolic heat generation that sets body temperature) is approximately 800–1000 'hairs' /cm^2 [37 Fig 25].

* head, neck, torso, and tail

**only when behaviors are enabled

https://doi.org/10.1371/journal.pone.0223872.t002

Determining rates of metabolism

To determine a range of metabolic rates for extinct taxa within our modeled microclimate, we simulated a spectrum of different metabolic rates. We evaluated 5 different resting metabolic rates (RMRs) ranging from a typical ectothermic squamate to endothermic eutherian metabolisms. An RMR from the lower avian range (ratite) and two lower mammal (monotreme and eutherian) RMRs were calculated from empirical regressions utilizing phylogenetic and ecological constraints [e.g.,75,76], while the squamate, and an additional eutherian RMR were calculated using empirical models derived from oxygen consumption or CO_2 production measurements with an assumed respiratory quotient [7,83]. These regressions implicitly include the presence or absence of epidermal insulation of extant species as well as their size and shape, but the data provide a range of values for estimating the span of modern mass-specific metabolic rates(S1 Table).

Using the calculated masses (S3 Appendix) and the empirical equations above we generated five different mass-specific resting metabolic rates for *Coelophysis* and *Plateosaurus*,

labeled: squamate, monotreme, marsupial, ratite, and eutherian. We analysed the thermoneutral range for each RMR in a virtual metabolic chamber simulation within Niche Mapper. We chose to conduct the remainder of the model simulations with low (squamate), moderate (monotreme), and high (ratite) RMRs representing a

Table S1-3. Parameters for metabolic rates, diet, and behavior.

Variable			Value		Reference and comment
			Plateo	*Coelo*	
Squamate	Metabolic rate		70.1 W	3.4 W	[7]
	Core temp (˚C)	Maximum	40		
		Target	38		
		Minimum	25		
Ratite	Metabolic rate		301 W	24 W	[74,75]
	Core temp (˚C)	Maximum	40		[76]
		Target	38		[76]
		Minimum	36		
Fat mass as % of body mass			5		[74,75]
Sweat ok?			No		
Activity Multiplier**			2		[77]
Food	High Browser	% protein*	10		[78]
		% fat*	0		
		% carbohydrate*	88		
		% dry matter	25		
		Digestive efficiency (%)	60		
		Fecal water (%)	60		[79]
		Uric acid (%)	60		[79]
	Low Browser	% protein*	10		[78]
		% fat*	0		
		% carbohydrate*	88		
		% dry matter	44		
		Digestive efficiency (%)	60		
		Fecal water (%)	60		[79]
		Uric acid (%)	60		[79]
	Carnivore	% protein*	60		[80]
		% fat*	38		
		% carbohydrate*	0		
		% dry matter	66.7		
		Digestive efficiency (%)	85		
		Fecal water (%)	46		[81]
		Uric acid (%)	27		[81]
Behavior	Ground seeking shade		Y	Y	
	Night shade		Y	Y	
	Seek shelter from wind		Y	Y	
	Posture	Sleeping	Posture 3		Legs lumped into torso, head & neck on ground
		Resting in shade	Posture 3		Legs lumped into torso, head & neck on ground
		Inactive posture	Posture 3		Legs lumped into torso, head & neck on ground

'*Plateo*' = *Plateosaurus* and '*Coelo*' = *Coelophysis*.

* based on % dry mass

** Activity multiplier = field metabolic rate (FMR) / basal metabolic rate (BMR). FMR is calculated as FMR = 4.82*weight^(0.734)

https://doi.org/10.1371/journal.pone.0223872.t003

possible range of metabolic rates based on phylogenetic position. It is unlikely that basal dinosaurs had metabolic rates elevated above extant ratites, or below extant squamates.

Diets

In the Niche Mapper model, the primary outputs influenced by diet are daily values for discretionary water (kg/day) and food requirement (kg/day). The diet (required caloric intake) is calculated based on daily energy expenditure, user-supplied values for percent protein, fat, carbohydrates, and dry mass of the food, and the animal's assimilation efficiency (Table 3). The amount of water initially available to the organism is calculated from the diet-assigned dry mass and the amount of food consumed (e.g., total food mass - dry mass = total available free water from food). Metabolic water production is computed from diet composition and metabolic rate [84 p. 489, 695]. Daily water loss is the total of cutaneous water evaporation (if sweating were allowed; we did not allow sweating) and water lost through respiration and excretion (in mammal-based models this includes water loss through feces and urine, in non-mammal models water loss through urine is ignored). If the daily water budget is negative, the organism must drink water to make up the volume; thus,discretionary water reflects the debt or credit of the total water budget after all modeled physiological needs are met. A user defined digestive efficiency controls the amount of incoming calories (food mass) that is required by the model organism to meet its metabolic needs (Table S1-3).

Coelophysis has long been considered a predatory theropod [85,86] and *Plateosaurus* is usually described as a herbivorous prosauropod, but omnivery is not excluded [6]. To assess the impact of varying inferences of diet on food and water requirements *Coelophysis* and

Plateosaurus were both modeled as carnivores and as high and low browsing herbivores. The diet in the high browsing scenario is comprised of primarily high % dry matter (e.g., 40-50% dry mass) such as conifers (8.3 MJ/kg dry mass), ginkgos (8.6 MJ/kg dry mass), and cycads (6.1 MJ/kg dry mass) [79,87]. Low browsing diets were primarily composed of ferns (7.7 MJ/kg dry mass) and *Equisetum* (11.6 MJ/kg dry mass) which contain much higher water content (e.g., 25-30% dry mass) [79,87]. A positive discretionary water budget would indicate the animal is getting most of its water from its food source as well as metabolic water and may not require regular access to drinking water extending its potential geographic range.

Energy requirements

We developed an R script to interface Niche Mapper with a modifiable database containing climate (Table 1) and physiological variables (Tables S1-2 & S1-3) for each of the experimental simulations, which were assessed for 6 unique climates [hot, moderate, cold] x [arid, humid]. For each simulation Niche Mapper calculated hourly interactions between the organisms and their environment over a 24 hour period at mid-month for a calendar year (12 total model days).

In all of our modeled simulations, each species is given the potential ability to be active every hour of the day (24 hours). The amount of metabolic heat production (W) needed to maintain the target core temperature throughout the day is determined by multiplying the resting metabolic rate (Table 4) by an activity multiplier (2.0 in our study; [78]). The resultant is the daily target metabolic rate (MJ/day):

$$RMR(W) \times 2.0 \times 86{,}400(s/day) / 1.0 \times 10^{6}\ J / MJ \quad (3)$$

Thus any decrease in activity hours represents periods of the modeled day when the animal is heat stressed and must decrease activity to lower its metabolic heat production. If the animal is cold stressed or within its active thermoneutral zone it will maintain 24 hour activity. However, if it is cold stressed the animals metabolic heat production and by extension, food consumption, must increase accordingly.

We define the *active* thermoneutral zone as the zone where an activity multiplier > 1 is expanding the temperature range in which the animals internal heat production balances the heat loss to the external environment (steady state condition). In contrast, a *resting* thermoneutral zone is the temperature range when the activity multiplier is 1.

Table S1-4. Annual predicted energy budget (MJ/year) for both dinosaur species.

		Resting Metabolic Rate (W)			Daily Metabolic Rate (MJ)			Annual Metabolic Rate (MJ)		
	Mass (kg)	Ecto RMR*	Mono RMR**	Ratite RMR**	Ecto DMR	Mono DMR	RatiteDMR	Ecto YMR	Mono YMR	Ratite YMR
Coelo	15	2.6	9.7	17.5	0.45	1.67	3.02	163.08	610.29	1102.58
	21	3.4	12.3	22.2	0.59	2.13	3.83	214.36	778.64	1397.75
	30	4.5	16.0	28.5	0.79	2.76	4.92	286.62	1008.05	1797.36
	40	5.7	19.7	34.9	0.99	3.40	6.03	362.43	1241.48	2201.49
	50	6.9	23.1	40.9	1.19	4.00	7.06	434.87	1459.16	2576.55
	60	8.0	26.4	46.5	1.38	4.56	8.03	504.72	1665.06	2929.96
Plateo	600	52.7	139.8	235.5	9.11	24.16	40.70	3325.34	8819.21	14854.63
	850	70.1	179.9	301.1	12.12	31.09	52.03	4422.46	11348.73	18989.15
	1150	89.9	224.0	372.6	15.53	38.70	64.38	5668.06	14125.16	23499.42
	1600	117.8	284.4	470.3	20.36	49.15	81.26	7430.36	17940.35	29659.90
	2000	141.5	334.3	550.4	24.44	57.77	95.10	8921.95	21085.98	34712.93
	3000	197.2	448.4	732.5	34.08	77.48	126.57	12440.32	28280.29	46199.32

See text for explanation of under and over estimates of mass (kg). Green highlighted mass and data are our chosen optimal masses for each species.

* [7]

*[74,75]

https://doi.org/10.1371/journal.pone.0223872.t004

Four physiological conditions were used to test the viability of each modeled organism under six microclimate conditions mentioned above (see Table 1). Low (squamate) and high (ratite) resting metabolic rates were calculated based on equations from McNab [75,76] and McMahon [7], each of which were analyzed with a broad squamate-like core temperature range (CTR), which ranged from 26-40°C, moderate monotreme-like CTR (32-40°C), and a narrow ratite-like CTR (36-40°C). All CTRs were assigned a target core temperature of 38°C.

Metabolic Chamber

Metabolic chamber simulations in Niche Mapper were used to evaluate the specific impact of different physiological inferences and their impact on the temperatures in which model animals were predicted to be cold or heat stressed. In the metabolic chamber simulations, all temperatures (ground, sky, and air) are set equal to one another, no solar input is allowed, a constant, negligible wind speed of 0.1 m/s is used, along with a constant 5% relative humidity. Animals are modeled "at rest" in a standing posture with no activity multiplier. In order to identify lower and upper critical temperature boundaries for each animal, heat balance calculations were performed along a range of temperatures (0-51°C) that exceeded the minimum and maximum air temperatures within which organisms could maintain thermoneutrality [65]. This process was repeated for each proposed metabolic rate.

Sensitivity Analyses

Niche Mapper is an effective tool for modeling extant organisms where direct measurements can be applied. Modeling organisms in deep-time is faced with a number of challenges where direct measurements are not possible. Variables such as air temperature, core temperature range, resting metabolic rate, and insulatory structures have a significant effect on

the modeled organisms annual metabolic energy and are tested for and visualized in each modeled experiment. Additional parameters, such as muscle efficiency, digestion, and respiration, as well as mass estimates, skin reflectivity, and insolation factors related to latitude are independently tested for model sensitivity. In order to determine how sensitive the model was to these additional parameters, a bounded range that includes our hypothesized values were modeled for each parameter.

For instance, there is uncertainty as to the color of skin or insulatory structures in most extinct animals. For our purposes, it is known that a lighter color absorbs less solar radiation, a darker color absorbs more and this variable could be easily selected for in a given environment [88-90]. To test the effect of color on total metabolic energy requirements we modeled the skin of *Plateosaurus* and the uninsulated *Coelophysis* as well as the proto-feathers for the top-only and fully insulated *Coelophysis* with 5 states ranging from high to low reflectivity (light to dark color, respectively) in both our cold and hot microclimate.

Similarly we tested main and interactive effects of parameters related to climate (i.e.,temperature, wind, relative humidity, cloud cover). To assess the relative effect of these parameters we used the metric of total annual energy for each species and determined how annual metabolic expenditure would change relative to the target value for all variables individually and combined. This approach allowed us to evaluate the main effects of each of these variables as well as possible interactions between them. To determine main effects and interactions of the variables on annual metabolic expenditures for *Plateosaurus* and *Coelophysis* we used a 2^4 (climate) full factorial design and Yates' algorithm for analysis of effects [91]; minimum and maximum data are outlined in Table 1.

Results

Sensitivity analyses

The strength of our modeled results, in part, relies on understanding how the model responds to ranges of values for variables that are not directly measurable in deep-time. We conducted the following analyses to quantify the advantage or disadvantage our chosen values would impact on the model results: skin/insulation reflectivity, muscle efficiency, respiratory efficiency, digestive efficiency, the effect of latitude, and mass estimates; a summary of these results follows - further details and figures are provided in supplemental data (S4 Appendix).

Skin and insulation color (reflectivity) was analyzed from 10 – 60% (15% was our chosen model value). It was observed that the disparity in ME between high and low reflectivity values increased with increasing cold stress. For example, the more cold-stressed the model was (i.e., >4-5 x RMR), the greater advantage low reflectivity values (darker color) had. However, there was a negligible effect of reflectivity for models whose annual ME was near target (e.g., between 2x and 3x RMR). Similarly, muscle efficiency ranged from 20 – 50% efficient (20% was our chosen model value) and the disparity between the lowest and highest values for a given model increased as cold-stress increased (see S4 Appendix); there was a negligible effect for models whose RMR was between 2 and 3x resting. An analysis of respiratory efficiency ranged from 10 – 30% (we chose a min-max value of 15-20%) and there was virtually no change in annual ME regardless of which parameter was used.

Digestive efficiency was analyzed with a range of 70 – 85% efficiency (we chose 85%) for the carnivorous diet, and 30-70% (we chose 60%) for the herbivorous diets (see S4 Appendix for discussion). All diet parameters are independent of metabolic calculations and thus did not

affect annual ME. Varying the efficiency of digestion provides us with a range of annual wet food requirements. These values can be used to compare with reasonable rates of browsing (or prey acquisition/consumption) relative to modern analogs. For instance, even at the lower extreme, a 30% digestive efficiency for *Plateosaurus* would require ~8000 kg wet-food per year; this is ~22 kg of wet-food per day, which is on par with similarly sized extant browsing mammals such as the black rhinoceros [92,93].

Because we are using our cold microclimate as a proxy for higher latitudes we also tested our models at 45°N [e.g., 55,59,60]. The primary effect of increasing latitude was a result of increased daylight hours midyear and decreased daylight hours during the winter months. This is most apparent in the increased hours/day that core temperature was maintained, midyear, and decreased during the winter months relative to those observed at 12°N. The model is more sensitive to microclimate temperatures than variance in insolation due to increased latitude between12 and 45°N.

The parameters outlined above had relatively small effects on metabolic needs of the modeled organisms that were able to maintain an annual ME between 2 and 3x RMR. However, we realize these effects can be cumulative and are more significant at the boundaries of a modeled organisms' temperature tolerance where small changes can be the difference between survival or death. There is also the potential effect of interaction between parameters. To test the main and interactive effects of four primary climate parameters (temperature, humidity, wind speed, and cloud cover) a 2^4 factorial design and Yates' algorithm [91] was analyzed (S4 Fig 6). Temperature had 2-10 times the effect of wind, and both humidity and cloud cover were insignificant. Variables that have the greatest impact, such as temperature, CTR, RMR, and insulation are presented below with a range of inputs for each experiment.

Mass estimates

Mass estimates can vary widely for a given taxon depending on methodology [94-99]. Niche Mapper uses a user-supplied mass and distributes that mass, with assigned densities, among each body segment (head, neck, torso, front legs, hind legs, and tail). We tested our modeled organisms with 6 mass estimates from a low to an extreme high mass in both the hot and cold microclimate. In addition to increasing the estimated mass we also accounted for the necessary increase in RMR with mass (see Table S1-4).

Linear measurements of a *Coelophysis* specimen (AMNH 7224) yield a skeletal length of 2.61 m. With an estimated average density of 0.97 kg/l our *Coelophysis* model has a mass of 21 kg. This is consistent with previously assigned masses [94, pg. 260] of 15-20 kg for a 'gracile' and 'robust' skeleton, respectively. It is unlikely that the mass exceeds 30 kg for the skeletal dimensions used for this analysis of mass estimates. We tested the effect of increased mass via increasing the diameter of the model's body segments (i.e., making it thicker) with mass assignments of 15, 21, 30, 40, 50, and 60 kg (see S4 Figure 7). The 40, 50, and 60 kg masses are extreme (nonviable) overestimates to test the model. Results for monthly metabolic energy with a high (ratite-like) RMR and CTR (relative to target) for the uninsulated, top-only insulated, and fully insulated *Coelophysis* model demonstrate the effect of mass and insulation in hot and cold microclimates (Fig S1-5). Results for varied RMR and CTR for the 21 kg *Coelophysis* follow.

The uninsulated model resulted in extreme cold-stress for the lower three sizes in the hot microclimate, and all 6 mass estimates in the cold microclimate. When increased to top-only insulation the severity of cold-stress decreased, but the model was still excessively cold-stressed

in the cold microclimate. The hot microclimate resulted in more months where the model was able to maintain its target metabolic energy, including summer months of the lower three size estimates and all months for the largest three mass estimates. The fully insulated model shows heat-stress during the summer

		Coelophysis Uninsulated Mass (kg)					
	Month	15	21	30	40	50	60
Hot microclimate	J	173	157	141	131	124	118
	F	172	156	141	130	123	118
	M	170	154	140	129	123	118
	A	156	143	131	122	115	111
	M	143	131	121	114	108	105
	J	142	131	120	113	109	104
	J	137	126	116	109	105	102
	A	132	123	114	107	103	101
	S	133	123	114	108	104	101
	O	140	129	118	111	106	104
	N	158	145	131	122	116	112
	D	173	156	141	130	123	118
Cold microclimate	J	335	290	249	221	203	190
	F	332	286	246	218	200	188
	M	326	281	241	214	197	185
	A	303	262	225	201	186	175
	M	267	234	205	186	172	162
	J	274	237	207	186	173	164
	J	285	246	212	189	175	165
	A	258	225	198	179	167	157
	S	260	226	199	180	168	158
	O	258	227	200	182	169	160
	N	311	269	232	206	191	179
	D	332	287	246	219	201	189

	Coelophysis Top-only Insulated Mass (kg)					
Month	15	21	30	40	50	60
J	125	114	105	102	100	99
F	124	114	106	101	101	100
M	124	114	106	100	101	100
A	117	108	102	101	101	100
M	108	102	101	102	101	99
J	108	102	101	100	101	99
J	105	102	100	100	101	100
A	103	101	100	99	99	97
S	103	101	99	99	99	98
O	106	101	101	101	101	100
N	116	107	101	100	100	101
D	124	114	105	102	99	99
J	228	197	170	151	139	131
F	227	196	168	150	138	130
M	223	193	166	148	137	129
A	209	180	155	141	131	125
M	185	163	144	132	124	118
J	189	165	144	132	125	119
J	195	168	146	132	123	117
A	178	156	139	128	120	114
S	179	157	140	128	121	114
O	178	158	141	129	121	116
N	212	184	158	143	132	126
D	225	195	168	149	138	131

	Coelophysis Fully Insulated Mass (kg)					
Month	15	21	30	40	50	60
J	102	101	100	98	97	95
F	101	101	101	98	97	95
M	102	101	100	98	97	95
A	101	100	98	96	93	91
M	95	93	89	86	86	86
J	95	92	89	86	85	85
J	94	90	87	86	84	82
A	91	88	84	84	82	80
S	90	88	84	84	82	80
O	96	93	91	87	87	87
N	100	98	96	94	92	90
D	102	100	98	96	96	93
J	108	103	101	101	101	102
F	108	103	101	102	101	101
M	108	103	101	101	101	101
A	106	100	101	100	101	101
M	102	100	101	100	99	100
J	102	100	102	101	100	100
J	102	101	100	101	101	100
A	102	101	100	100	101	100
S	102	101	100	100	100	99
O	102	101	101	101	100	100
N	105	100	101	101	101	100
D	108	102	101	101	100	102

Fig S1-5. Effect of mass estimate (Coelophysis) on annual energy. *The matrix reflects the effect of size and insulation for Coelophysis in a hot and cold microclimate. Dark blue = >10% above target ME; light blue = 5-10% above target ME; green = +/- 5% of target ME; light orange = 5-10% below target ME; and dark orange = >10% below target ME.*

months in the hot microclimate, gradually increasing in severity and temporal extent with increased mass. Under the cold microclimate, the model met target metabolic energy for all but the 15 kg *Coelophysis*, which exhibited minor cold-stress within the winter months (between 5 and 10% above target).

Our linear dimensions for *Plateosaurus* were taken from GPIT/RE/7288, a six meter long skeleton with a femoral length of 635 mm. With an estimated density of 0.97 kg/l the model has a mass of 850 kg. This is in line with mass estimates for moderate sized *Plateosaurus* specimens

(i.e., 5.67 m skeleton [595 mm femoral length] with a mass between 660-782 kg using a 0.89-1.05 kg/l density respectively; [98]). Other *Plateosaurus* mass estimates include a 6.5 m long skeleton (1073 kg using polynomial method [99]) and a 920 kg mass determined by stylopodial circumference using a 685 mm femoral length [100].

To test the effect of different mass estimates, we chose to take the same skeletal dimensions and increase or decrease the diameter of body segments (assigned densities remained constant). We ran experiments assuming a total mass of 600, 850, 1150, 1600, 2000, and 3000 kg (Fig S1-6; see also S4 Figure 8). The first three states (600-1150 kg) more likely capture a realistic mass estimate range for the skeleton and are representative of mass estimates in the literature for this specimen [97-100]. The last three states (1600-3000 kg) were used to observe how an extreme (nonviable) overestimate of mass would affect the model results. Results for monthly metabolic energy with a high (ratite-like) RMR and CTR (relative to target) for the *Plateosaurus* model demonstrate the effect mass has for hot and cold microclimates (Fig S1-6). Results for varied RMR and CTR for the 850 kg *Plateosaurus* follow.

The 600 kg model was mildly heat stressed in the hot microclimate during peak summer temperatures, however it was excessively cold (ME ~15-20% above target) in the cold microclimate. Under the hot microclimate, the 850 kg model we identified as most likely for our 6 m skeleton met its target ME during the cooler winter and spring/fall seasons, but experienced significant heat stress (ME ~10% below target) during peak summer temperatures. As mass increased, this trend was amplified in the hot microclimate producing excessive heat stressed models. The 850 kg model experienced modest cold stress in the winter months, while the four largest mass estimates met expected target values within the cold microclimate.

Diet of Plateosaurus

It has been suggested [87] that *Equisetum* would have been a favored food source (from a nutritional point of view) due to its higher degradability (e.g., 11.6 MJ/kg dry matter) relative to various conifers or *Ginko* (8.3, 8.6 MJ/kg dry mass, respectively). However, given the high water content of *Equisetum* (~70% [79]) relative to conifers (~44% [79]) the degradable energy per kilogram of wet mass (what the animal actually consumes) is nearly identical: 3.5 MJ/kg wet mass (*Equisetum*) vs 3.6 MJ/kg wet mass (various conifers) [79,87]. The various ferns reported by Hummel and others [87] have nearly 75% water content and yield 7.7 MJ/kg dry mass (or 2.1 MJ/kg wet mass). Thus, an animal eating dominantly ferns will need to consume 60% more vegetative mass than an organism whose diet is primarily composed of conifers or horsetails.

The diet component of the model, although extremely useful for certain questions, is calculated based on the resulting metabolic energy outputs. Factors such as digestive efficiency, food nutrient composition, waste products (urea/feces), and gut retention time affect the food and water requirements, but do not directly affect metabolic energy calculations. In the two modeled herbivorous diet scenarios the high-browsing animals display substantial differences in the volume of food required per day relative to low browsing animals. This is due to differences in the %dry mass, where the higher the %dry mass, the greater non-water component is available for digestion (see above, and S1-Fig 8). *Plateosaurus*, as a high browser with ratite RMR and CTR in the cold microclimate meets the calculated target food intake (blue filled pentagon, Fig S1-8). The

	Plateosaurus Mass (kg)					
Month	600	850	1150	1600	2000	3000
J	99	99	98	94	94	84
F	99	99	98	94	94	84
M	100	99	98	94	94	84
A	99	98	97	88	89	78
M	96	92	89	77	79	68
J	95	92	89	77	79	68
J	95	92	88	75	77	65
A	92	89	85	71	73	62
S	93	89	85	71	73	62
O	95	93	89	76	78	68
N	99	97	95	86	88	77
D	100	98	97	92	93	82
J	119	107	100	100	100	98
F	118	106	99	100	99	98
M	118	106	100	99	98	98
A	114	104	99	98	98	98
M	110	101	99	99	99	98
J	110	100	99	99	98	98
J	108	100	101	98	98	98
A	106	99	100	98	98	97
S	107	100	100	98	98	97
O	108	100	101	99	98	98
N	115	104	98	98	98	98
D	119	107	100	101	99	98

Fig S1-6. Effect of mass estimate (Plateosaurus) on annual energy. *The matrix reflects the effect of size and insulation for Plateosaurus in a hot and cold microclimate. Dark blue = >10% above target ME; light blue = 5-10% above target ME; green = +/- 5% of target ME; light orange = 5-10% below target ME; and dark orange = >10% below target ME.*

lower than target values for high browsing in the hot microclimate demonstrate a decrease in activity below 2 times RMR, likely due to heat stress.

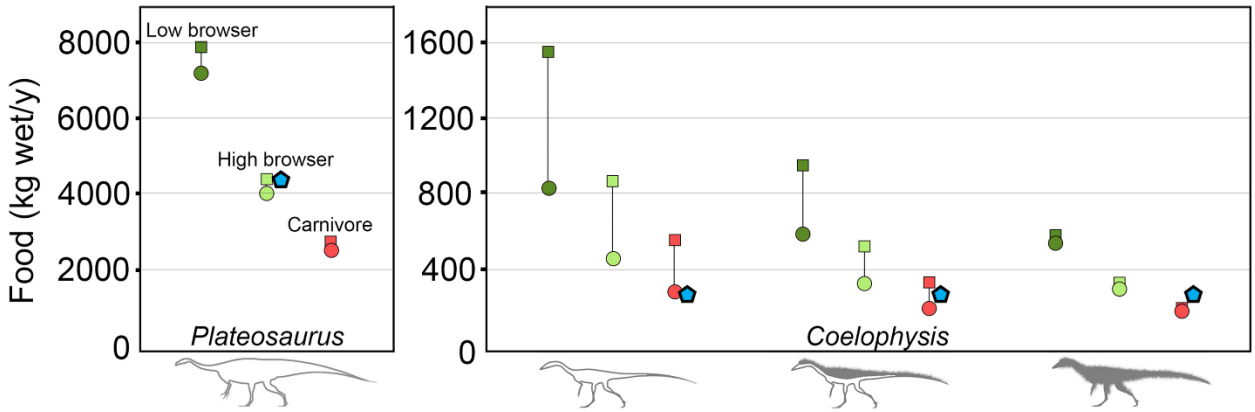

Fig S1-7. Dietary variability with diet type and insulation. *The amount of food needed to maintain the specified (target) core body temperature throughout the year varies with diet type. Diet types: low browser herbivore (dark green); high browser herbivore (light green); and carnivore (red). Climate conditions also affect the quantity of food required to maintain core temperatures in hot (closed circles) and cold (closed squares) climates; annual target food intake in kilograms for each species is denoted by a closed blue pentagon when Plateosaurus = high browser and Coelophysis = carnivore. Data represent each species with a ratite RMR and CTR.*

Diet of Coelophysis

The incremental addition of insulation to *Coelophysis* produced a corresponding decrease in overall food requirement. The uninsulated *Coelophysis* (ratite RMR/CTR) with a carnivorous diet in the hot climate requires ~300 kg/y, which is near the calculated target food intake requirement of 310 kg/y (blue filled pentagons of Fig S1-7). However, with full insulation the annual intake is only 200 kg/y, suggesting heat stress has an impact on activity through a reduction in metabolic heat production during some parts of the year, thus requiring less food intake. Under cold climate conditions the uninsulated *Coelophysis* with a carnivorous diet requires more than twice the target food intake to maintain an elevated, ratite like core temperatures, while a fully insulated individual is slightly heat stressed requiring less than the

target food intake. This heat stress is overcome with a slight reduction in insulation or a broadening of CTR (see below).

It is notable that the absolute difference between the cold and hot climate annual food requirements decreases non-linearly as insulation increases similar to that reported by Porter [101]. There is a 6% difference in the annual food budget between hot and cold climates for the fully insulated *Coelophysis* and an 8.8% difference for *Plateosaurus* for all diets (carnivorous/herbivorous). In contrast, the difference in annual food budget under cold and hot climates for the top-only insulated and uninsulated *Coelophysis* increases to 36% and 46% respectively for the cold climates relative to warm climates. These differences in food requirements for small dinosaurs with little to no insulation are directly related to the decrease of thermal heat flux from the body due to increased insulation for fully insulated *Coelophysis* or having a large adult body size like *Plateosaurus*.

Metabolic chamber simulation results

Within the metabolic chamber simulation that spanned 0-50°C, *Plateosaurus* displayed a greater range of temperatures where it could remain in its active-thermoneutral zone relative to the small bodied uninsulated and top-only insulated *Coelophysis*. The fully insulated *Coelophysis* exhibited a similar breadth of thermoneutrality range as the *Plateosaurus* (Fig S1-8). For each stepwise increase in resting metabolic rate (RMR; from squamate to eutherian) two general trends were observed: 1) thermoneutral zone breadth increased and 2) the maximum and minimum thermoneutral temperature values each shifted to lower values. This trend is more apparent in the larger bodied *Plateosaurus*. For example, *Plateosaurus* with a ratite-like core temperature range (CTR) of 38±2°C can maintain thermoneutrality with a squamate grade RMR

in air temperatures between 32-45°C and between 15-36°C with a ratite grade RMR. There is an 8°C increase in the absolute thermoneutral range from squamate to ratite RMR, while the maximum air temperature shifts negatively by 9°C.

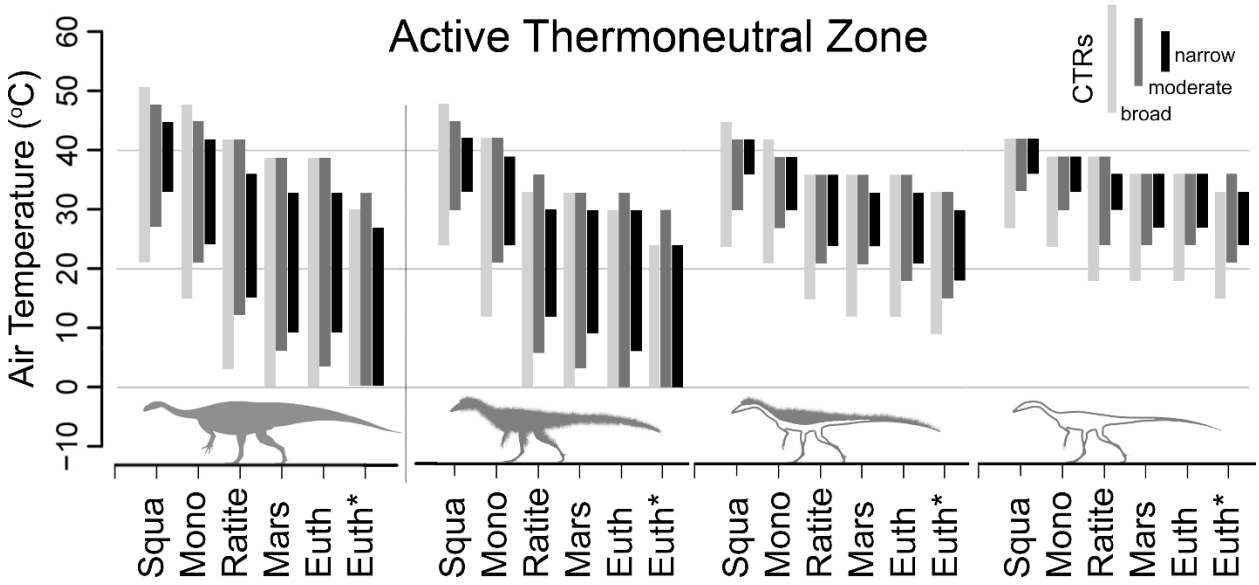

Fig S1-8. Active thermoneutral zones of Plateosaurus and variably insulated Coelophysis. *Shaded areas represent the active thermoneutral zone determined from 18 metabolic chamber experiments for Plateosaurus and Coelophysis (fully insulated, top-only, and uninsulated) with RMR ranging from squamates to eutherians based on published regression equations [7,75,76]. Light gray = broad CTR (26-40°C); dark gray = moderate CTR (32-40°C); black = high CTR (36-40°C). Target T_{core} = 38°C. The active thermoneutral zones for the top-only and fully insulated Coelophysis were calculated with the ptiloerection behavioral function enabled.*

Varying the amount of external insulation in the form of filamentous 'proto'-feathers made a substantial difference in thermoneutral temperature ranges. An uninsulated *Coelophysis* could maintain thermoneutrality over an 6-10°C temperature range (Fig S1-8). With a ratite RMR and CTR (38±2°C) the thermoneutral range of an uninsulated *Coelophysis* was 30-36°C. As dermal insulation was added the overall pattern observed was similar to that seen with increased BMR; i.e., there was a stepwise decrease in maximum and minimum thermoneutral

temperature, but an overall increase in total range. The thermoneutral range relative to the uninsulated model was extended moderately 0-3°C (depending on metabolic rate) in the top-only insulated *Coelophysis*. A fully insulated *Coelophysis* had a substantial decrease in the lower end of its thermoneutral range while minimally decreasing its upper bound (12-30°C); the fully insulated *Coelophysis* more than doubled its active thermoneutral air temperature range. The net effect of insulation allows a fully insulated *Coelophysis* to maintain thermoneutrality across a much broader temperature range in colder environments compared to the non-insulated *Coelophysis*, although this is at the cost of lowering the maximum tolerable air temperature.

To test the effect of variable CTRs as well as RMRs we simulated a broad (26-40°C), moderate (32-40°C), and narrow (36-40°C) core temperature range for each of the 6 RMRs (Fig 8). The same trends were observed with the broad and moderate CTR as seen in the narrow CTR simulations, however the absolute range was greatest in the broad CTR and intermediate in the moderate CTR, and lowest in the narrow CTR discussed above. We also tested the model with four different *target* core body temperatures, 38, 35, 32 and 29°C with a narrow (±2°C) and broad(+2/-13°C) CTR for both species to compare their active thermoneutral zones under these conditions. As the target core temperature was stepped down, the overall thermoneutral range remained effectively the same, but the absolute minimum and maximum air temperature values shifted negatively ~ 2-3°C for each 3°C step down in target core temperature. The results for the four target core temperatures under ratite-like and squamate-like CTR are shown in S4 Figures 9 & 10, respectively.

Effects of resting metabolic rate and core temperature range

Each model simulation paired different physiological combinations of resting metabolic rate (RMR; squamate, monotreme, and ratite grade metabolic rates) with a broad, moderate, or narrow core temperature range (CTR), each with a 38°C target core temperature (26-40°C, 32-40°C, and 36-40°C, respectively), under cold, moderate, and hot climates for the two dinosaur species. The results of these experiments yielded hourly outputs that were plotted as annual heatmaps for core body temperature, metabolic energy (contoured in multiples of RMR), and hours in open versus shaded conditions (see Fig S1-9 for explanation of heatmaps).

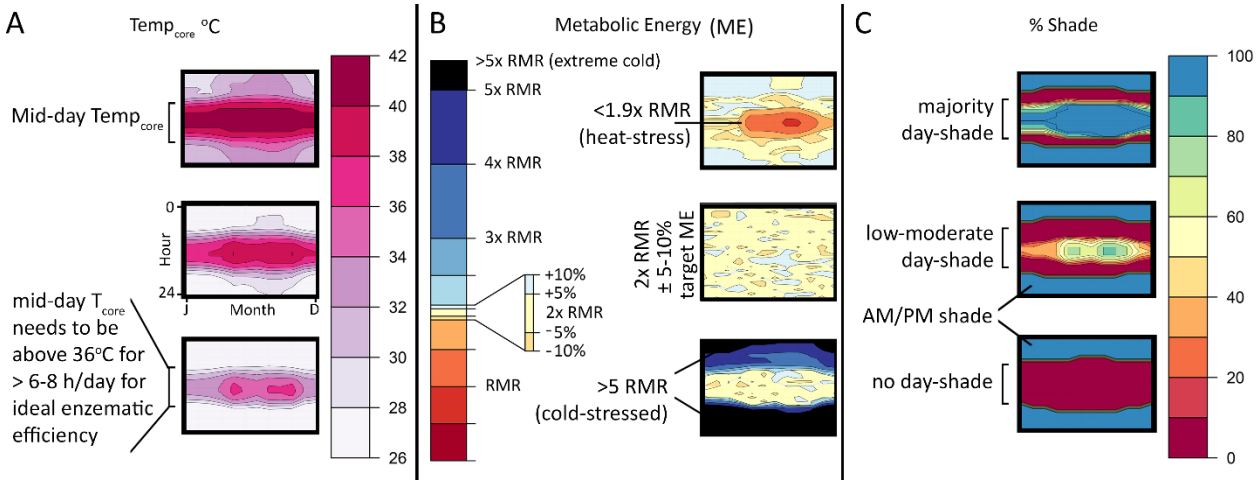

Fig S1-9. Heatmaps of T_{core}, metabolic energy (ME), and % shade. *Heatmaps provide a quick quantitative tool for visualizing results on an hourly basis across the year. A) Top; example of narrow CTR heatmap where $36<T_{core}<40$ ~6-8 hrs per day. Bottom; $36<T_{core}<38$ ~0-3 hrs per day (e.g., cold stressed). B) Top; Metabolic energy (ME) heatmap displaying heat stress during mid-day hours, mid-year. Middle; ME heatmap displaying a reasonable range around 2x RMR. Bottom; results of a cold-stressed model with ME exceeding 5x RMR. C) Heatmaps demonstrating a high (top), moderate (middle), and low (bottom) daylight hours shade requirement.*

Coelophysis (uninsulated).

The uninsulated *Coelophysis* model results show a high degree of cold stress for all but 3 of the 27 possible RMR/CTR/microclimate combinations (Fig S1-10).The two best fits are the moderate and upper RMR with broad CTR in the hot microclimate. However, under all RMR/CTR combinations *Coelophysis* is cold stressed in the cold microclimate. Even if paleotemperatures of high latitude localities were only slightly cooler (moderate) than equatorial (hot) conditions modeled herein, the uninsulated *Coelophysis* still shows signs of cold stress (i.e., T_{core} does not reach 35°C for more than 4 hours a day, for over half of the year; 3 months of the year never reach 35°C at all). This lends support to a requirement of some form of insulation or thermoregulatory behavior under all model conditions, leaving room for the possibility that uninsulated adult *Coelophysis* could exceed modeled temperatures in the hot microclimate.

Because many ectothermic animals have the potential to decrease their internal temperatures below the 26°C lower bound we used in the broad, squamate-grade CTR, we also modeled the uninsulated *Coelophysis* with a 10°C lower temperature bound to ensure we capture the lowest extremes of core temperature. *Coelophysis* was modeled in the hot and cold microclimate for the month of May (northern hemisphere early summer). These data were plotted along with the November (southern hemisphere early summer) temperature profile for the largest known extant predatory ectothermic terrestrial vertebrate, *Varanus komodoensis*, as a frame of reference (Fig S1-11). In the hot microclimate T_{core} for *Coelophysis* responded similarly to *V. komodoensis* during the modeled month. However, during the winter months the squamate-grade *Coelophysis* was slightly cold stressed without the ability to burrow like *V. komodoensis* (we assume *Coelophysis* does not burrow). In the cold microclimate T_{core} does not exceed 30°C

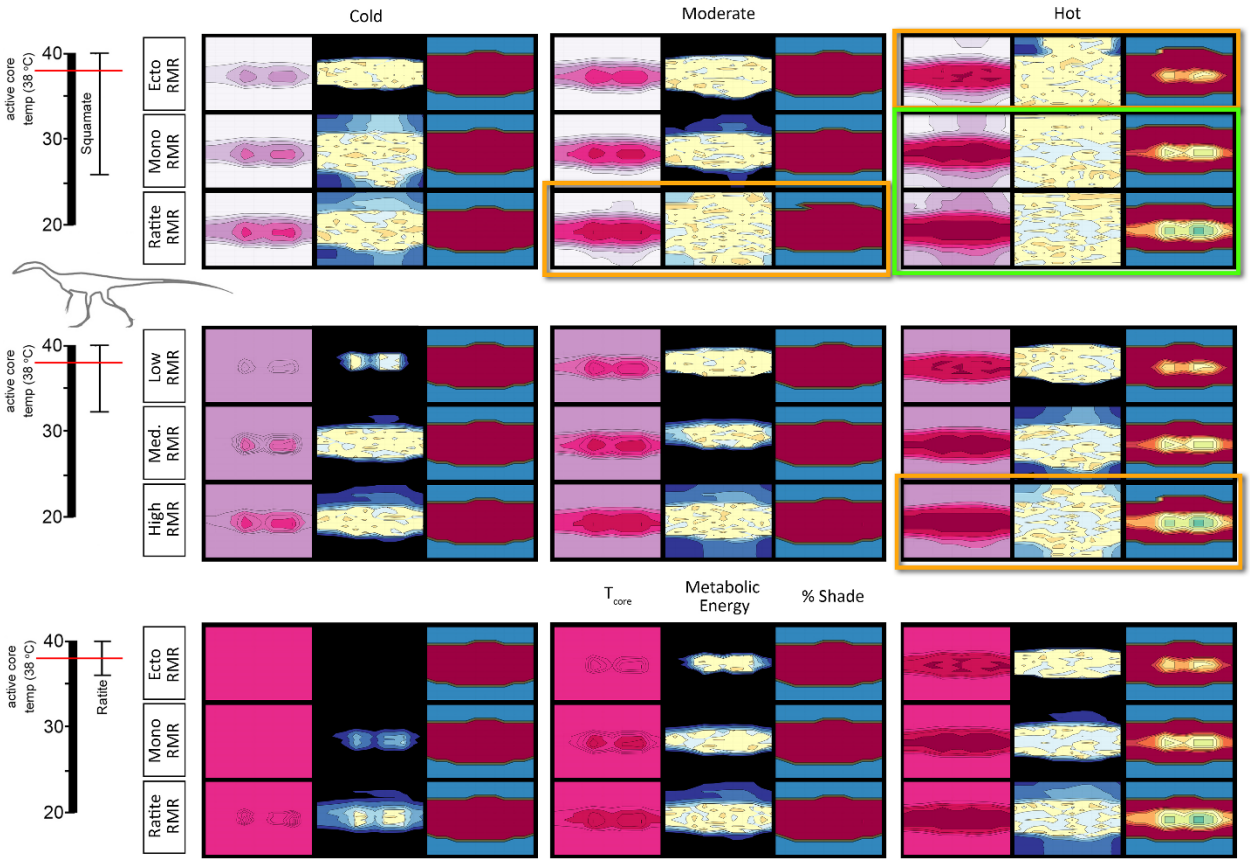

Fig S1-10. T_{core}, ME, and %shade heatmaps for Coelophysis (uninsulated). *Heatmaps representing the hourly results across the modeled year the three dominant variables: microclimate (hot, moderate, and cold), RMR (low, moderate, and high), CTR (broad, moderate, and narrow) for an uninsulated Coelophysis. See figure 9 for key. Two most likely scenarios for survivability are outlined in bright green, the three edge conditions are outlined in orange; all other conditions are considered to be non-viable.*

for more than 5 months of the year demonstrating severe cold stress for the uninsulated *Coelophysis* (non-viable).

With a 10-40°C CTR the lowest ambient air temperature in the cold microclimate was above the lower (10°C) CTR threshold, thus, it was possible for the organism to thermoregulate and maintain its target ME by dropping its core temperature rather than increase its metabolic rate (see S4 Figure 11). This did not affect the daily core temperature results between 26 and 40°C which are identical as the

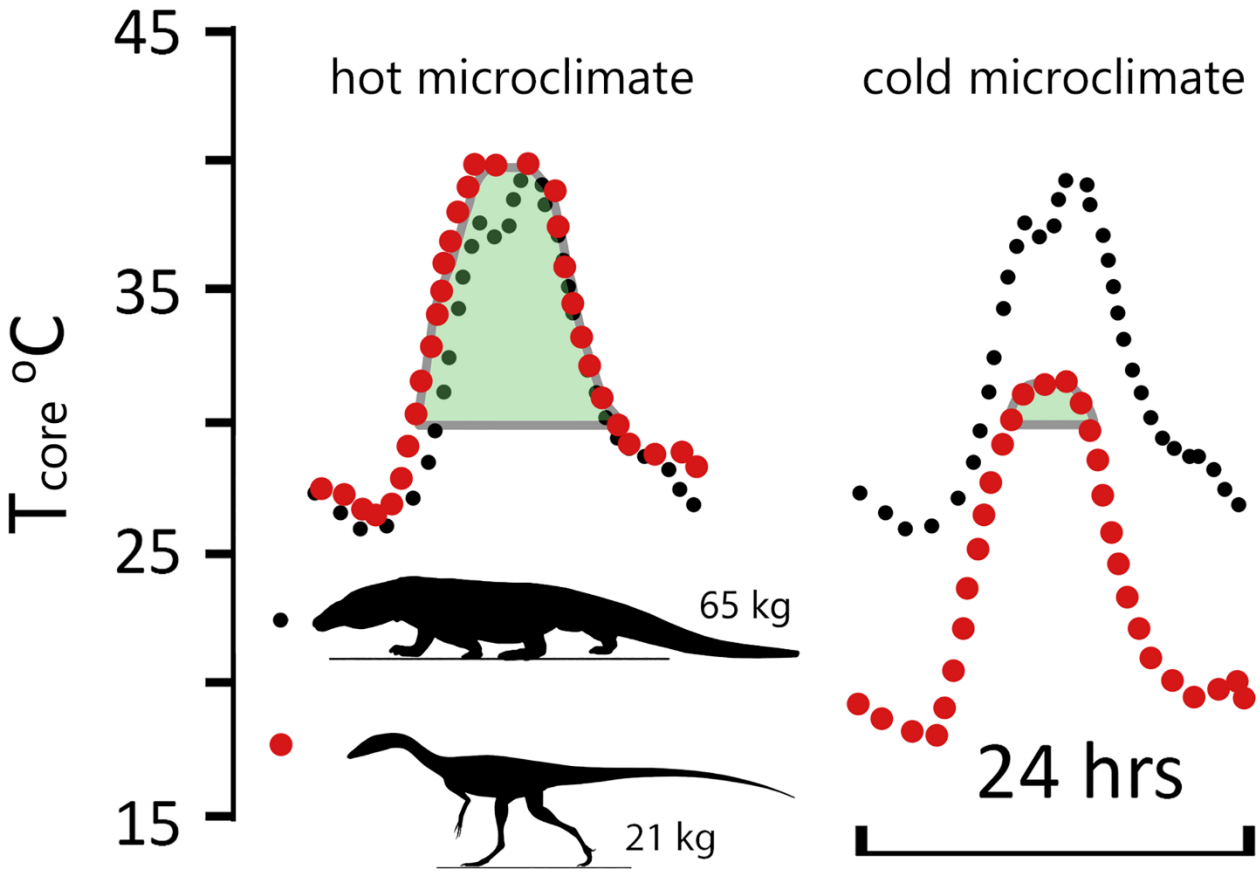

Fig S1-11. Comparison of daily temperature curves for Varanus and Coelophysis (uninsulated). *Daily temperature curves for hot and cold microclimates for the 15th of May (uninsulated Coelophysis) and November (Varanus komodoensis) [40]. There is strong agreement between the low RMR and broad CTR Coelophysis and V. komodoensis in the hot microclimate. Coelophysis modeled in the cold microclimate was significantly cold stressed. Green shaded area represents duration of day with* $T_{core} > 30°C$.

prior broad CTR experiment above; the animal is still significantly cold-stressed.

Coelophysis (top-only insulation)

With the addition of insulation to the top-half of *Coelophysis* the severity of cold-stress decreased and the number of viable RMR/CTR/microclimate combinations increased to 6 of 27 (Fig S1-12). Under the hot microclimate with a broad CTR, all RMR conditions met ME targets and were able to maintain a core temperature above 35°C. As the microclimate shifted to the

moderate condition, the lower RMR was excluded; all RMR were excluded under the cold microclimate. As the CTR reached the moderate range, only the moderate and upper RMR were

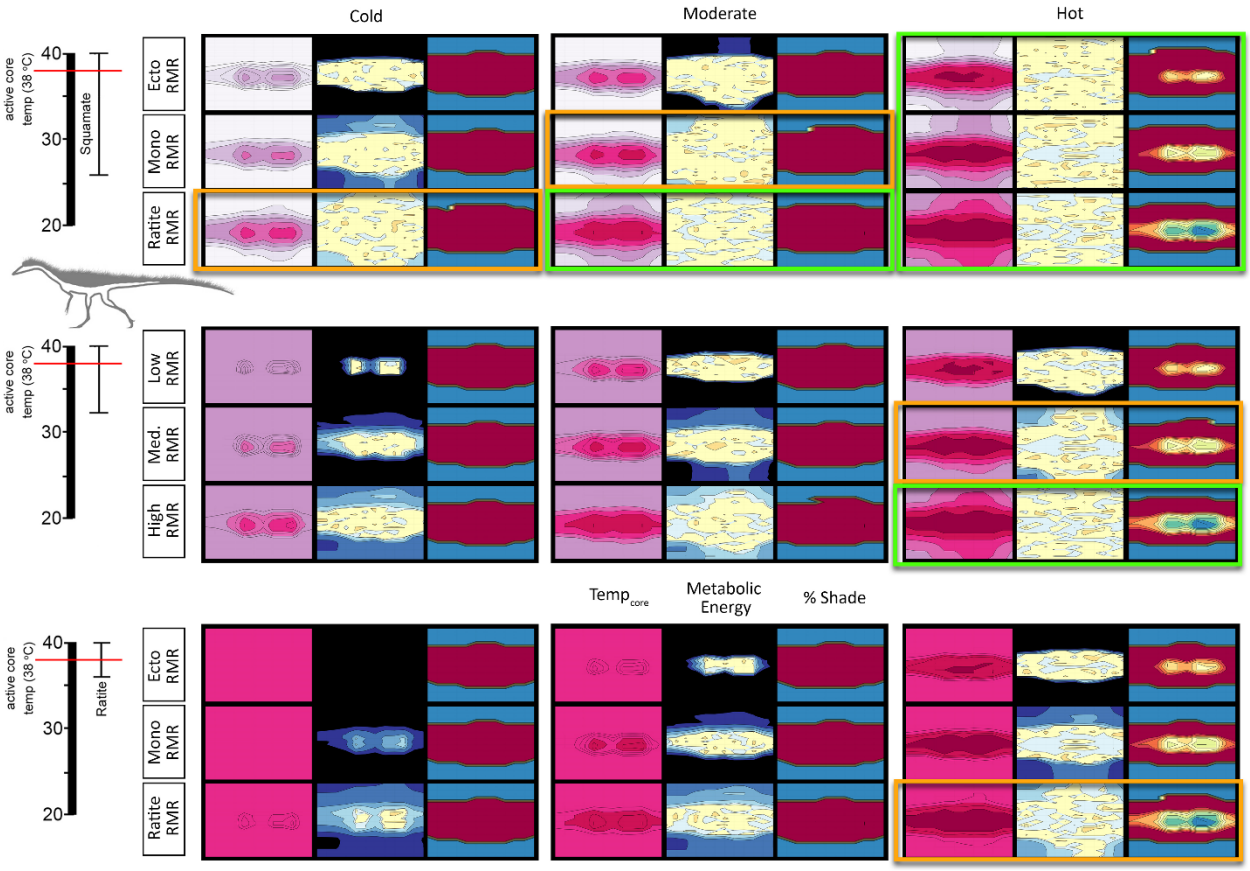

Fig S1-12. T_{core}, ME, and %shade heatmaps for Coelophysis (top-only insulated). *Heatmaps representing the hourly results across the modeled year the three dominant variables: microclimate (hot, moderate, and cold), RMR (low, moderate, and high), CTR (broad, moderate, and narrow) for a top-only insulated Coelophysis. See figure 9for key. Five most likely scenarios for survivability are outlined in bright green, the four edge conditions are outlined in orange; all other conditions are considered to be non-viable.*

considered feasible under the hot microclimate. The narrow CTR excluded all RMR in all microclimates.

Coelophysis (full insulation)

With a fully insulated *Coelophysis* the severity of cold-stress further decreased and the number of viable RMR/CTR/microclimate combinations increased to 10 of 27; heat stress was

evident in all 3 CTRs with an upper RMR under the hot microclimate (Fig S1-13). The fully insulated *Coelophysis* was cold stressed in the cold and moderate microclimates with a broad CTR. However, it was able to maintain its ME target and sustain a core temperature greater than 34-36°C for at least half of dial hours with a broad CTR and: lower RMR in the hot microclimate; moderate RMR in moderate and hot microclimates; upper RMR in cold and moderate microclimates. Raising the CTR to the moderate condition excluded all lower RMRs as well as the moderate RMR condition in the moderate microclimate. A narrow CTR resulted in the loss of the remaining moderate RMR in the hot microclimate; only the upper RMR in moderate and cold microclimates were able to meet their ME target.

Plateosaurus

Plateosaurus exhibits a similar response to that seen in the fully insulated *Coelophysis*; the number of viable RMR/CTR/microclimate combinations was 10 of 27; heat stress was evident in all 3 CTRs with a ratite RMR under the hot microclimate (Fig S1-14). With a lower RMR and broad CTR, *Plateosaurus* was cold stressed in the early morning hours under cold conditions and didn't exceed 30°C body temperature for more than half of the calendar year. The moderate microclimate fared only slightly better, but the ME still exceeded target by ~10%. This same physiology modeled in the hot microclimate demonstrated a core temperature of 28-30°C during morning hours and reached target core temperatures by midday.

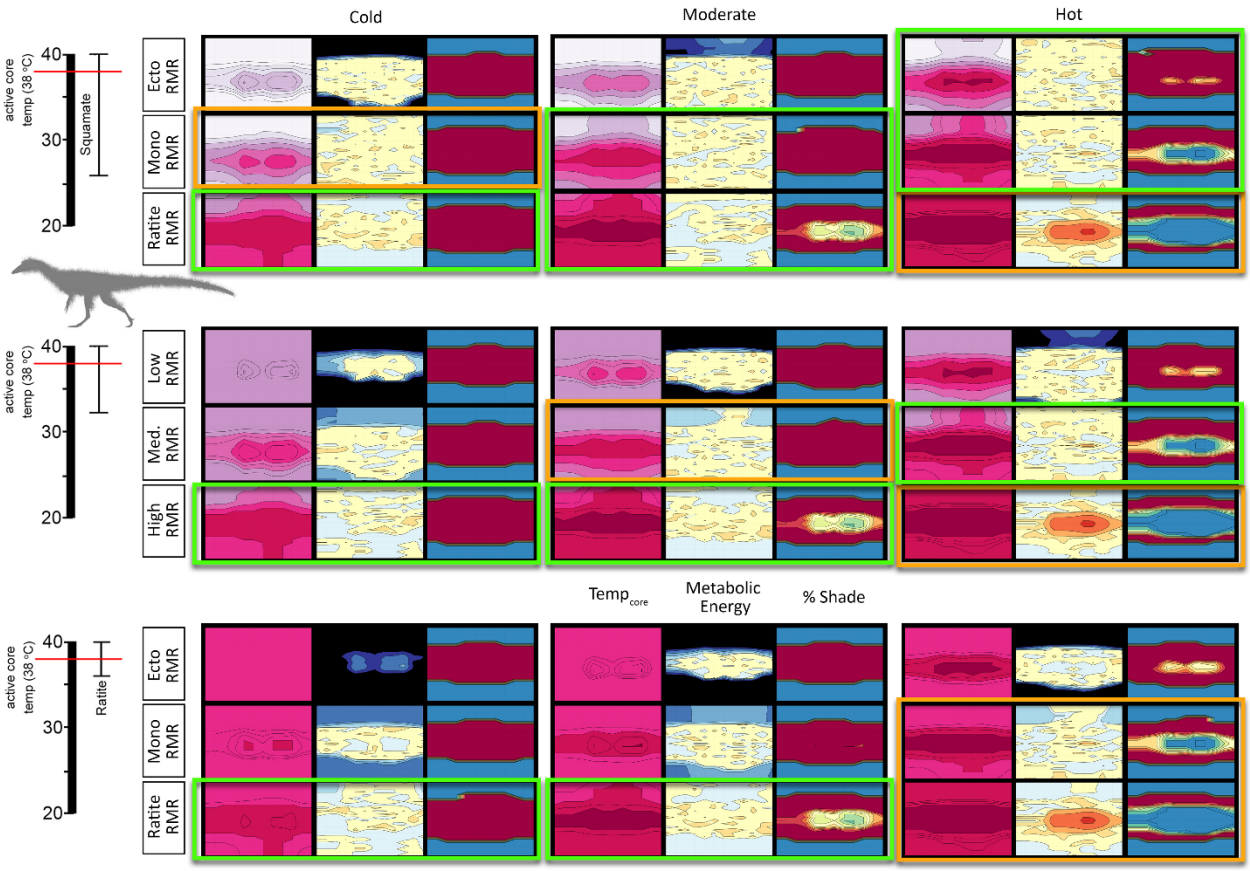

Fig S1-13. T_{core}, ME, and %shade heatmaps for Coelophysis (fully insulated). *Heatmaps representing the hourly results across the modeled year the three dominant variables: microclimate (hot, moderate, and cold), RMR (low, moderate, and high), CTR (broad, moderate, and narrow) for a fully insulated Coelophysis. See figure 9for key. Tenmost likely scenarios for survivability are outlined in bright green, the six edge conditions are outlined in orange; all other conditions are considered to be non-viable.*

When the CTR reached the moderate level, all lower RMR were excluded due to significant cold stress, as was the moderate RMR in the cold microclimate. The moderate RMR met its ME target in the hot microclimate, but its ME slightly exceeded its target goal in the moderate microclimate and exceeded its ME target under the cold microclimate. The final step to a narrow CTR increased the cold stress previously observed in the moderate and cold microclimate with a moderate RMR, the model slightly exceeded its ME target under the cold

microclimate with an upper RMR. The model met its ME target under the moderate microclimate with an upper RMR.

Microclimate wind effects

Because the wind was the second strongest main effect in our yates analysis (see S4) we further explored this effect using *Coelophysis* and *Plateosaurus* with an upper RMR and narrow CTR. For *Coelophysis*, the magnitude of wind effects varies substantially depending on the degree of insulation, ptiloerection, and climate (Fig S1-15). Daily variation in wind speeds from 0.1 to 2.0 m/s affects total annual energy requirements from approximately 2000 (hot microclimate) to 3400 MJ/y (cold microclimate) without insulation down to approximately 1400 (hot microclimate) to 1800 MJ/y (cold microclimate) when fully insulated *without* ptiloerection (30 mm insulation depth); the fully insulated (with ptiloerection enabled) was ~1500 MJ/y. Ptiloerection was not activated until the model required >2x RMR to maintain *target* core temperatures.

We tested 5 insulatory conditions for each climate: 1) no insulation, 2) 15 mm depth top half only (only the top half of the animal had insulation), 3) 30 mm depth top half only with, 4) 15 mm depth fully insulated, and 5) 30 mm depth fully insulated. Fully insulated animals only engaged ptiloerection in the coldest microclimate. When the feather depth of the fully insulated animal decreased from 30 to 15 mm its energetic response was similar to that of the 30 mm top-only insulation; thus decreased insulation depth is equivalent to greater depth with only top surfaces insulated.

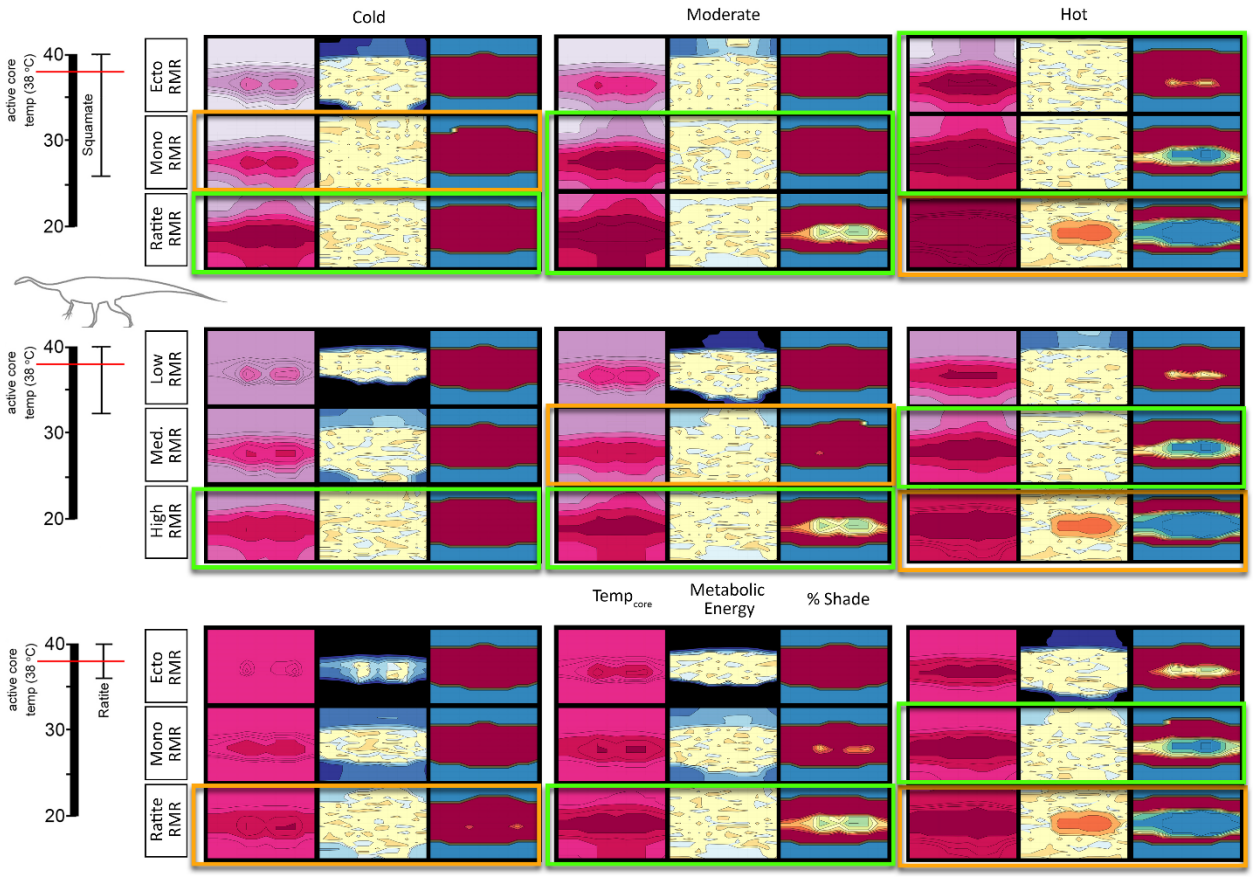

Fig S1-14. T_{core}, ME, and %shade heatmaps for Plateosaurus. *Heatmaps representing the hourly results across the modeled year the three dominant variables: microclimate (hot, moderate, and cold), RMR (low, moderate, and high), CTR (broad, moderate, and narrow) for a Plateosaurus. See figure 9for key. Ten most likely scenarios for survivability are outlined in bright green, the six edge conditions are outlined in orange; all other conditions are considered to be non-viable.*

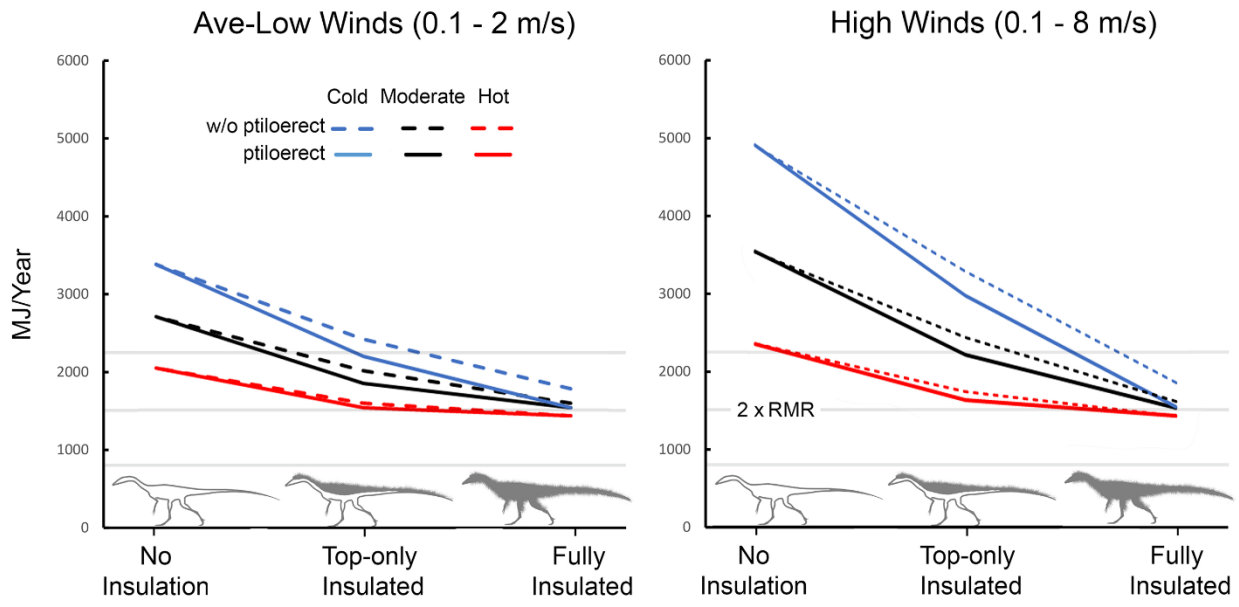

Fig S1-15. Energetic cost of wind exposure for Coelophysis. *As temperature increases (blue, black, and red lines, respectively) ptiloerection was less beneficial with increased insulation volume. (e.g., fully insulated Coelophysis does not significantly benefit by implementing ptiloerection at hot temperatures but the presence of feathers broadens its active thermoneutral zone). The three light gray horizontal lines represent, from bottom to top, resting, twice resting (e.g., ME target), and three times resting metabolic rate to indicate the likely range of activity levels for the size, shape, and degree of insulation for Coelophysis.*

Wind did not have as large of an impact on the modeled *Plateosaurus*, although wind was the second strongest effect observed in the Yates analyses. *Plateosaurus* was able to maintain its target core temperature under the moderate and hot microclimates for average and high speed winds. In low speed winds moderate and cold microclimates were at the lower *target* boundary (-5% of 2x RMR), while the hot microclimate caused notable heat stress (-10% of 2x RMR; Fig 16). This stresses the importance of behavior for the model to seek shelter from or take advantage of higher wind conditions for thermoregulation.

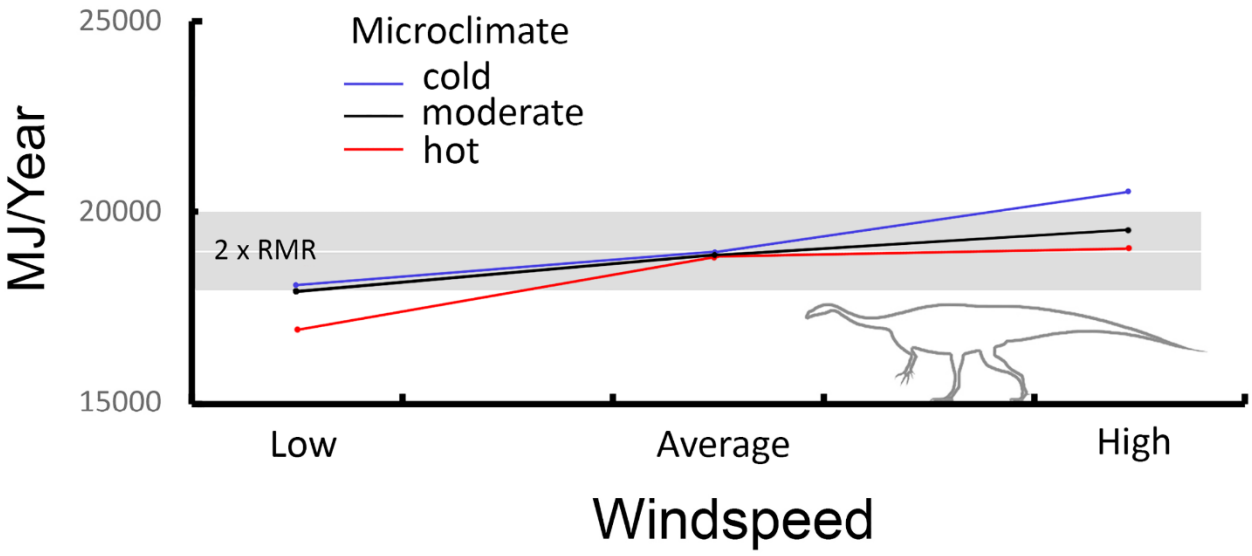

Fig S1-16. Energetic costs of wind exposure for Plateosaurus. *Under low wind speeds Plateosaurus is moderately to notably heat stressed (cold/moderate and hot, respectively). Target ME is maintained in all microclimates for average winds, and in the hot microclimate with high winds. Plateosaurus becomes cold stressed with high winds in the cold microclimate. Red line = hot microclimate, blue line = cold microclimate, black line = moderate microclimate.*

Discussion

Mechanistic physiological modeling of extant organisms accurately predicts environmental range with high fidelity [19,20,31,32,69]. This has been leveraged to generate hypotheses of how organisms respond to habitat expansion, contraction, and altered geographic ranges associated with changing climate on local and global scales [12,18,40,102]. Niche Mapper in particular has demonstrated the ability to predict metabolic expenditure as a function of environmental conditions for a broad sample of vertebrates in microclimates ranging from arctic to tropical [13,17,20,32,34]. Our efforts have focused on extending Niche Mapper to generate and test biophysical hypotheses against known paleobiogeographic distributions, phylogenetic position, and life histories for two extinct animals in deep time. While we lack detailed empirical profiles for the physiology of extinct animals, we can explore different

combinations of morphological and physiological characteristics to determine their effect on energetics, behavior, and animal distributions.

We utilized a variety of stable isotope and geochemical systems to infer mean annual temperature, mean annual precipitation, atmospheric O_2 and CO_2, and relative humidity in the Late Triassic of Western North America [55,103-105]. These and other sedimentary paleoenvironmental proxies [e.g., 52] were employed to refine global climate model data used to construct our microclimate models. We also decoupled our organismal models from specific microclimate models using Niche Mapper's virtual metabolic chamber function to determine an active thermoneutral temperature range for modeled taxa. Determining the overlap in thermoneutral zones of organisms and mapping them against their paleobiogeographic distributions [e.g., 15,23] provides an independent test of plausible paleophysiologies.

Deep-time model uncertainty

In our deep-time implementation of Niche Mapper, we have been forced to make a series of assumptions. We assume the distribution of fossils are evidence of the presence of a viable population of organisms in that time and place. We further assume that the range of extant tetrapod physiology (e.g. newts to birds) bound possible physiologies for these Triassic organisms. At this time we find no convincing evidence that a physiology outside of observed modern bounds existed for these organisms. We also assume paleoclimate proxies provide reasonably accurate reconstructions of local environments and that parameters which do not have reliable proxies (i.e. wind speed, cloud cover) can be bound by modern environments with similar temperature-precipitation regimes. We further assume that conditions not currently possible were likewise not possible in the Triassic (e.g. 100 km/hr constant winds, annually).

Some uncertainty in model interpretation may be created by these assumptions, and additional uncertainty may derive from the absence of fossil evidence required to constrain behavioral thermoregulation such as the use of burrows, shelters, or torpor as a means of altering heat transfer to and from the environment.

Suites of inferences are testable. If a modeled combination of physiology, shape, behavior, insulation, and climate do not produce a viable organism in a location where there are fossils, then clearly the hypothesized input parameters are flawed. For instance, if we were to find skin impressions of multiple *Coelophysis* without insulating integument at high latitudes, but model results suggest uninsulated individuals were not viable it might be necessary to add adipose, enable torpor, allow burrowing for behavioral thermoregulation, or reassess the inferred microclimate to allow for the maintenance of a viable population. If remains of *Plateosaurus* (or similar sized prosauropods) are found in areas we have predicted thermal exclusion, then our current hypothesis would need to be rejected and the model would need to incorporate these new constraints to generate new testable hypotheses. It is also possible for the model to generate several equally parsimonious solutions. In some situations sheltering (i.e., burrows) or elevating metabolic rate may provide equally viable solutions. Moreover, our modeled organisms are adult forms of specific clades and are not representative of the ecosystem as a whole. Nor do we assume that juveniles from hatchling to subadult will be modeled with similar parameters as each other, or their adult counterpart - each ontogenetic stage may have different combinations of physiology, shape, behavior, insulation and niche availability. It is beyond the scope of this study to model each stage of ontogeny. To further explore and test the viability of our models future work will need to generate ontogenetic series for each species, and contemporaneous taxa at high latitudes such as small archosaurs, amphibians, and lepidosaurs known to co-occur with

Plateosaurus and *Coelophysis*. This ability to incorporate new data allows for future refinement of the model and for new testable hypotheses to be generated, akin to the process of generating and testing phylogenetic hypotheses.

Plateosaurus

Our results demonstrate that an adult *Plateosaurus* could have maintained its target metabolic energy (ME) in hot environments with either a squamate-like core temperature range (CTR) and resting metabolic range (RMR), or with a monotreme-like RMR at moderate to narrow CTR. A shift from hot to moderate or colder environments, however, required at minimum a ratite-like RMR with a moderate CTR. Modeling *Plateosaurus* with a ratite-like narrow CTR and upper RMR resulted in heat stress in hot environments, full viability in moderate environmental temperatures, and slight cold stress in our coldest environments (Fig 17).

Modeling *Plateosaurus* with a squamate RMR was non-viable for all moderate and cold microclimates regardless of CTR. The greater viability of *Plateosaurus* with elevated RMRs in Late Triassic environments is consistent with isotopic estimates derived from dinosaur teeth and eggs which suggests an elevated core temperature between 36-38°C for the sauropod lineage [106-110]. Additionally, a squamate-like broad core temperature would be near the lower limits of enzymatic efficiency (regardless of ontogeny) seen in large extant herbivores. This would translate to an inhibition of rapid growth, counter to rates of growth reported from *Plateosaurus* bone histology [111,112].

The temperate paleobiogeography of *Plateosaurus* and other Triassic sauropodomorphs precludes squamate-level RMRs and CTRs. If *Plateosaurus* was maintaining a narrow internal

core temperature range then a ratite-like RMR and narrower CTR would be required. Physiological acclimatization including seasonally variable metabolic rates, variable fat stores, or changes in thermal conductivity to the ground could potentially facilitate this, as these mechanisms do in extant endothermic animals [e.g., 113,114]. We conclude that *Plateosaurus* most likely had a moderate core temperature range coupled with an elevated ratite-like resting metabolic range.

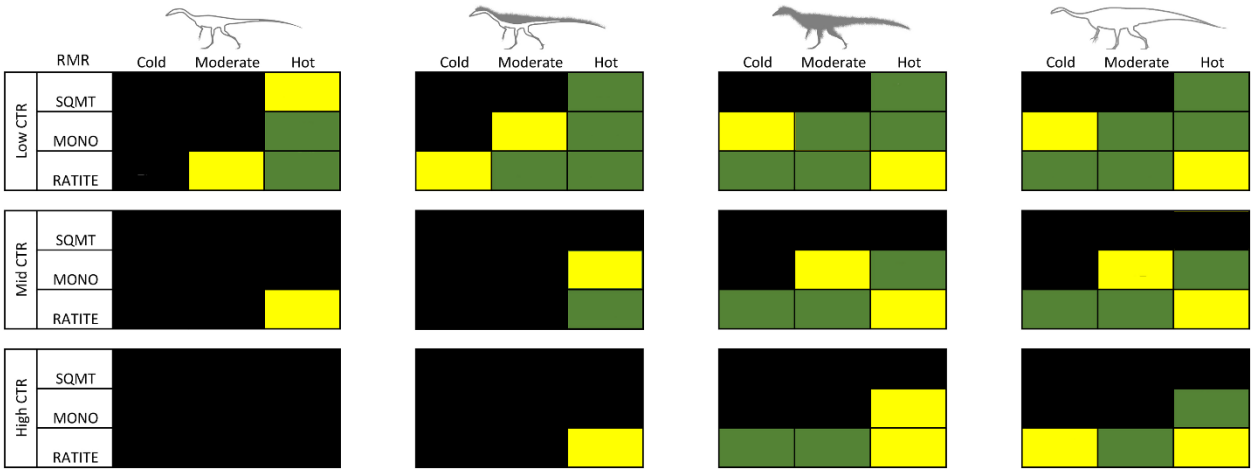

Fig S1-17. Summary of viable, conditional tolerance, and non-viable results. *The matrix provides a summary of viable combinations of resting metabolic rate (RMR) and core temperature range (CTR) within cold, moderate, and hot microclimates. Green = viable; black = non-viable; yellow = conditional tolerance (e.g., a possible but extreme endmember of viability).*

As previously mentioned we only modeled an adult *Plateosaurus*. A viable population would require survival of all ontogenetic stages through reproductive age. Preliminary simulations of isometrically scaled 'juvenile' (10-100kg) *Plateosaurus* suggest they would require either an RMR elevated above ratite grade (between marsupial and eutherian grade for a 10 kg individual, decreasing with mass) and a moderate CTR (i.e., no defence of stable core temperature), insulation (feathers or subdermal adipose), shelter (burrow or nest) or some combination of these to survive in the cold microclimate during the coldest 4 months of the year.

The 10 and 20 kg ‘juveniles’ were viable with only the addition of sheltering behavior in the moderate microclimate. Modeling allometrically smaller individuals coupled to growth rates [111,112] is a necessary next step. It is known that juvenile (nestling) sauropodomorphs such as *Mussaurus* were not only allometrically different than adults (e.g., proportionally taller skulls with short snout and larger eyes, and shorter tails and necks), they were functionally different as obligate quadrupeds that only later in ontogeny gained a bipedal stance [115, 116]. It is likely that there are significant differences that will need to be accounted for when modeling juvenile vs. adult forms.Although modelling an entire ontogenetic series is beyond the scope of the current study, it’s a logical step for future studies to investigate.

Coelophysis

When *Coelophysis* is modeled without insulation while possessing either a narrow or moderate CTR it experiences excessive cold stress in all environments regardless of RMR. Non-insulated *Coelophysis* modeled with a broad CTR is able to meet its target thermoregulation in hot environments with either a monotreme or ratite-like RMR, but remains non-viable due to cold stress under all other conditions. When *Coelophysis* is modeled with a squamate-like RMR and CTR its daily T_{core} profile is similar to an adult komodo dragon, each under early summer conditions (see results above). However, the uninsulated *Coelophysis* exhibits cold stress in winter months. Cold stress can be alleviated by decreasing the lower CTR bound by 2°C, but this does not alter peak temperatures, which remain below target core temperatures with a squamate RMR. Uninsulated *Coelophysis* remains cold stressed in the moderate and cold environments as a squamate. In short, a non-insulated *Coelophysis* would be viable only in hot environments with a broad CTR, and a moderate to high RMR.

Dorsal epidermal insulation increases the capacity of *Coelophysis* to maintain its daily target ME in moderate environments with a broad CTR and ratite-like RMR. All RMRs were viable in the hot microclimate with a broad CTR. The addition of dorsal insulation made a moderate CTR viable, but only with a ratite-like RMR within hot environments. Half-insulated *Coelophysis* was non-viable with a ratite-like CTR in all environments and in all cold environments regardless of CTR.

The fully insulated *Coelophysis* was viable in a broader range of temperatures. A squamate-like RMR is required in the hot environment with a broad CTR for a fully insulated *Coelophysis.* A monotreme-like RMR is non-viable due to cold stress in colder environments regardless of CTR. *Coelophysis* with a monotreme-like RMR is viable in hot (moderate to broad CTR) and moderate (broad CTR only) microclimates. Cold and moderate environments are accessible to fully insulated *Coephysis* with moderate to narrow CTRs with a ratite-like RMR, although heat stress occurs during peak summer temperatures in the hot microclimate.

Isotope paleothermometry of theropod teeth and eggshell indicates elevated RMRs and core temperature ranges above the levels of extant squamates [107,109,117]. Eagle and others [107] performed a clumped-isotope analysis on oviraptorosaur eggs and concluded the egg-layer had an average core temperature of 31.9 ±2.9°C . The studied oviraptorosaurs had a mass broadly similar to *Coelophysis*, though they were more deeply nested within Coelurosauria; the analyzed specimens were found in deposits at a high paleolatitude (> 45°N) during time of deposition [118]. An average core temperature much lower than 32°C would likely inhibit metabolic efficiencies necessary for elevated growth rates reported for *Coelophysis* [119,120].

Lowering the target core temperature from 38°C to 32°C changes viable combinations of RMR, CTR, and insulation for *Coelophysis*. Squamate-like RMR and CTR are viable within hot environment models only; under both moderate and cold microclimates squamate-like uninsulated *Coelophysis* experiences extreme cold stress (with T_{core} rarely exceeding 30°C for more than a few hours a day, S4 Appendix Figure 12 & Table 1). The half-insulated *Coelophysis* with a ratite-like RMR and CTR was viable in moderate to hot environments. Fully insulated *Coelophysis* with a ratite-like RMR was viable in cold and moderate environments but is still heat stressed in the hot microclimate. Fully- to half-insulated *Coelophysis* with ratite-like RMR are viable in all environments with both elevated (38°C) and lowered (32°C) *target* core temperatures (S4 Appendix Table 1). These results support an elevated RMR for *Coelophysis* with a moderate to narrow CTR.

Integrating model results with the fossil record

Body fossils of coelophysoids are known from equatorial through temperate paleolatitudes, while larger bodied plateosaurid body fossils are found in subtropical and temperate climates, but are absent from equatorial paleolatitudes (Fig S1-18). Given that the paleogeographic range of the two modeled species extends to temperate latitudes we substitute our cold microclimate model as a conservative surrogate for temperatures at subtropical to temperate latitudes [see 55,59,60]. Even if temperatures at higher latitudes were not as extreme as our modeled cold microclimate, they are certainly bound by our moderate microclimate. *Plateosaurus* modeled at 45°N paleolatitude demonstrate that air temperature has a much greater effect than change in insolation (i.e. solar energy input), supporting the use of our low latitude cold (or moderate) microclimate as an analog for temperate latitudes.

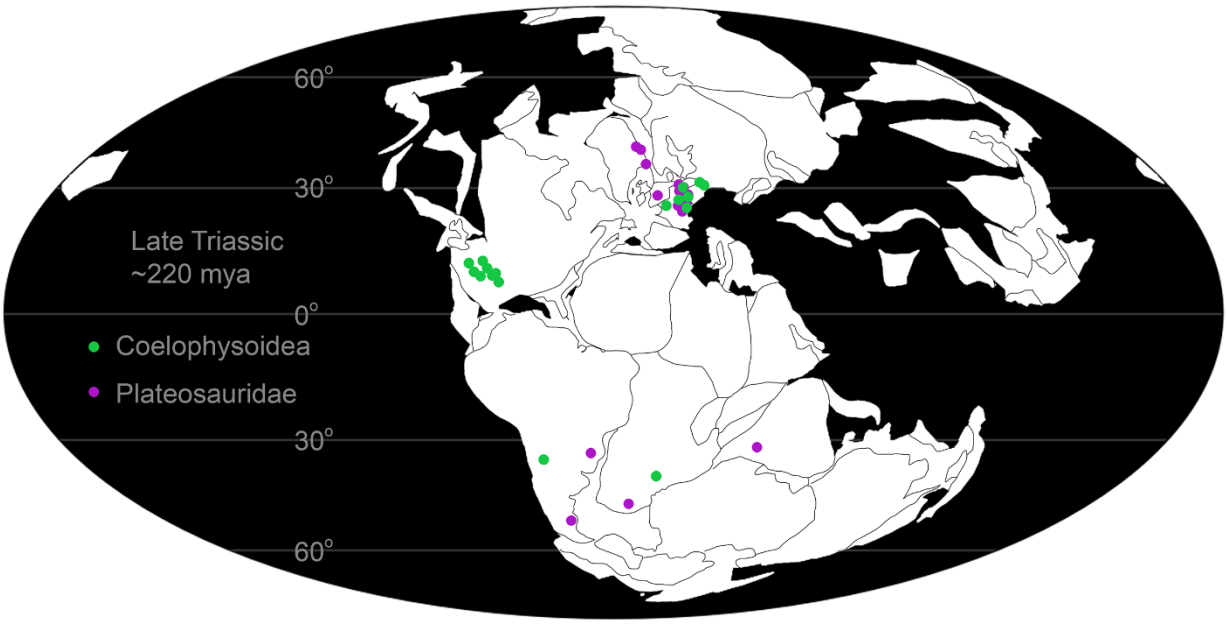

Fig S1-18. Paleogeographic distribution of body fossils for members of Coelophysoidea and Plateosauridae. *Note the absence of Plateosauridae at tropical latitudes. Data from paleobiodb.org.*

Skeletons of large bodied *Plateosaurus* and other large Late Triassic prosauropods (e.g., *Antetonitrus* (Yates and Kitching 2003), *Unaysaurus* (Leal and others 2004), and *Efraasia* (von Huene 1908)) have not been found in a paleogeographic gap extending through tropical latitudes. Conversely, large bodied dinosaurs are well known from cooler subtropical to temperate latitudes, consistent with our results for *Plateosaurus* in moderate to cooler environments.

Although no prosauropod body fossils have been found, the Late Triassic vertebrate track record of North America contains traces that have been attributed to medium-sized prosauropods (i.e., *Evazoum* (Nicosia and Loi 2003) formerly *Pseudotetrasauropus* (Ellenberger 1965), see [121]). The trackmakers would have been similar in size to Early Jurassic skeletons of the ~100 kg *Seitaad* (Sertich and Loewen 2010) and *Sarahsaurus* (Rowe and others 2011). There remains some doubt that the trackmakers are actually dinosaurian [121]. However, tracksites from latest

Triassic-Early Jurassic sites in northeastern New Mexico have been more confidently attributed to a larger sauropod dinosaur [121]. Notably, the locations of all described prosauropod/sauropod trackways are near the edges of local highlands on the Late Triassic-Early Jurassic landscape, where they would have had access to more appropriate microclimates (Fig S1-19).

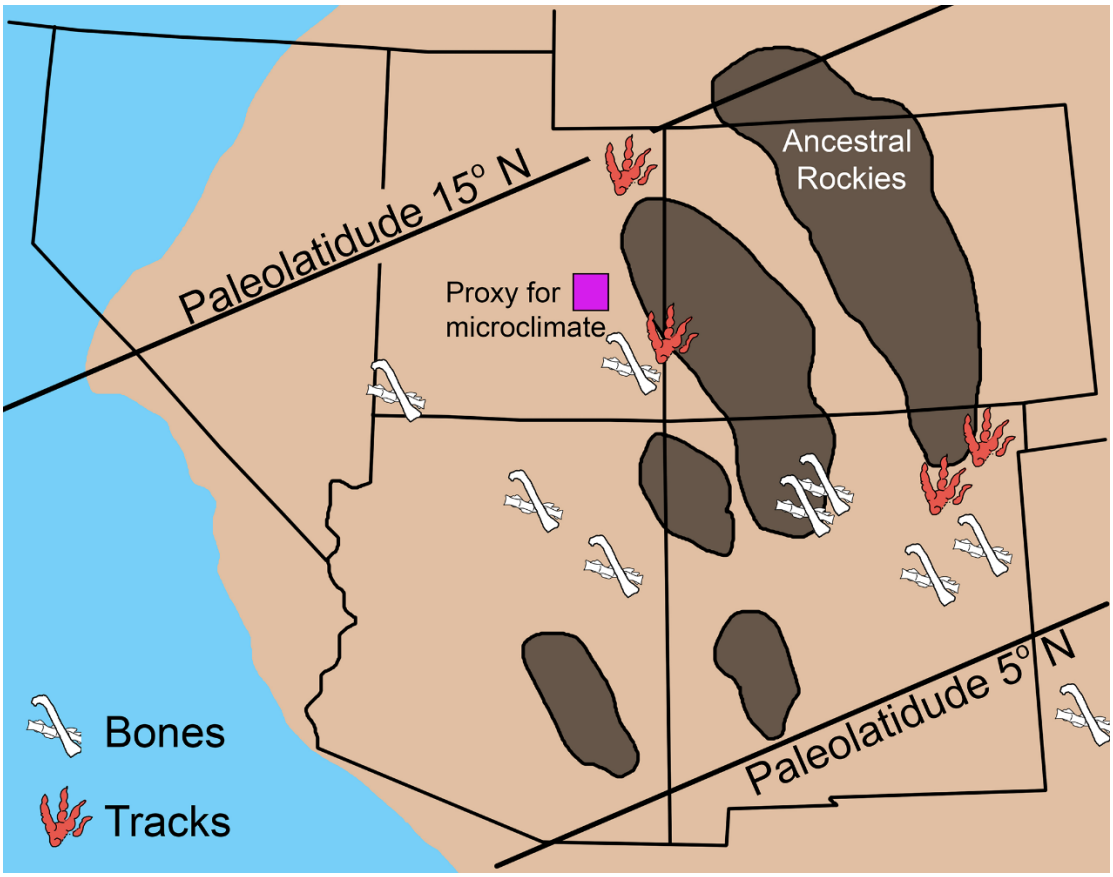

Fig S1-19. Track locations attributed to prosauropods and bones of Coelophysis in the late Triassic of the western USA. *Purple square = field localities from which proxy microclimate data used in this study were previously published [52]. Bones = localities with known coelophysoid body fossils.*

Whiteside and others [28] argued for climate driven environmental and vegetative instability as a dominant factor for the exclusion of large dinosaurs from the Late Triassic tropics. While we cannot rule that out, our results suggest heat stress alone would have been a

significant barrier for *Plateosaurus*-sized dinosaurs. We suggest environmental temperatures limited large bodied prosauropods from greater appearance in tropical latitudes during the Late Triassic. Prosauropods may have been present in cooler environments such as forested areas and higher elevations, but these depositional environments are less conducive to fossil preservation compared to the hotter environments encountered in lowland floodplains of the Chinle Formation [122,123]. Utilizing dense vegetative cover or higher elevations could explain the absence of body fossils in Chinle floodplain deposits but allow for the rare occurrence of trackways attributed to prosauropod-like track makers surrounding elevated cores of the ancestral rockies (Fig 19).

It should also be noted that there are no small bodied prosauropod species known from the tropics, in contrast to several taxa known from temperate latitudes (i.e., *Thecodontosaurus* (Morris 1843) and *Pantydraco* (Galton and others 2007). Our preliminary results from isometrically scaled 'juvenile' *Plateosaurus* demonstrate 10 to 100 kg individuals are viable in the hot microclimate under the same physiological parameters (among others) as the viable adult form modeled in the cold microclimate. This is consistent with the presence of Late Triassic prosauropod-like tracks and ~100 kg Early Jurassic body fossils. Although we maintain that heat stress is a limiting factor to large bodied prosauropods in the tropics it is possible other factors such as insurmountable paleogeographic or environmental barriers, or preservational biases account for the paucity of smaller morphs within the Chinle depocenter.

Large size alone is not a limiting factor for the Late Triassic Chinle paleoecosystem. Several large bodied vertebrates inhabited this region, including the ~1000 kg dicynodont *Placerias* (Lucas 1904) and the ~2000 kg phytosaur *Rutiodon* (Emmons 1856). Both of these taxa are capable of terrestrial locomotion but are thought to exhibit hippo-like and crocodile-like

aquatic behavior and niche occupation respectively [124-126]. Spending time in water enhances heat dissipation and allows for viable large size existence in hot equatorial climates [e.g., 40]. There is no anatomical evidence to suggest prosauropods like *Plateosaurus* exhibit similar behaviors, but it cannot be excluded as a potential thermoregulatory behavior.

Other behaviors such as burrowing or hibernation were excluded in our study as they are unlikely means of temperature regulation for adult *Coelophysis* and *Plateosaurus*. However, several smaller dinosaurs from temperate latitudes later in the Mesozoic are known or suspected burrowers [127,128]. It is not outside the realm of possibility that juvenile *Plateosaurus* (or other small prosauropods such as the 15 kg *Thecodontosaurus*) would have leveraged the benefits of burrowing. Fossorial behavior would allow for exploitation of more stable microhabitats in environments with higher variance in daily or annual air temperature. It is well known that small squamates, as well as the large *Varanus* and crocodylian *Alligator* use burrowing behaviors to thermoregulate, surviving extreme weather events and even wildfires [40,129,130].

A potential discrepancy with our results is the presence of small-medium bodied taxa contemporaneous with *Plateosaurus* such as *Thecodontosaurus*, early turtles (i.e, Proganochelys), and gracile crocodylomorphs (i.e., *Terrestrisuchus*) which would likely model as cold stressed during the winter nights if provided similar behavior parameters without the benefit of dermal insulation or greater size. These high latitude species almost certainly employed alternate thermoregulatory strategies such as burrowing, aestivation, or hibernation, much like their modern descendants. It may be that denning (burrowing) behavior was an ancestral state for crocodyliformes [131]. It should be noted too, that while *Terrestrisuchus* and its relatives may not have had epidermal insulation (currently phylogenetically constrained to Ornithodira), either croc-line archosaurs or archosaurs in general may have had elevated resting

metabolic rates based on respiratory anatomy [132], upright locomotion [133] and inferred growth rates [134]. Investigating the impact of those metabolic and behavioral inferences on non-dinosaurian archosaurs is an exciting avenue of potential research, for ourselves and others who adopt mechanistic modeling techniques.

Insulation in Triassic theropods

Late Triassic theropod body and trace fossils are well known from tropical latitudes in contrast to the skeletal and ichnological fossil record of prosauropods. The 21 kg *Coelophysis* is best represented in the body fossil record of the Chinle Formation (Fig S1-19), and other coelophysoids are known globally at higher latitudes (Fig S1-18). The basal saurischian *Chindesaurus* (Long and Murray 1995) - which at the least filled a theropod-like ecological role - along with basal theropods *Daemonosaurus* (Sues and others 2011) and *Tawa* (Nesbit and others 2011) as well as the neotheropod *Camposaurus* (Hunt and others 1998) are all known from body fossils within the Chinle Formation. There are also abundant trackways attributable to theropod dinosaurs throughout the region.

According to several independent methods of mass estimation [e.g. 94,100] adult theropod taxa from this formation were near 20 kilograms. Body fossils of coelophysoids such as *Zupaysaurus* (Arcucci and Coria 2003), *Liliensternus* (Welles 1984), *Procompsognathus* (Fraas 1913), and *Coelophysis rhodesiensis* (Raath 1969) are known from subtropical to temperate paleolatitudes. *C. rhodesiensis* was discovered in temperate southern paleolatitudes and is similar in size to Chinle coelophysoids. *Zupaysaurus* and *Liliensternus* would have been around 100 kg heavier than *Coelophysis*.

Coelophysis and other primitive theropods had a bipedal upright stance and a narrow, laterally compressed body that reduces solar cross-section when the sun is overhead while maximizing surface to volume ratio, enhancing radiative cooling relative to more round-bodied taxa [11]. When the sun was low in the sky laterally compressed animals have greater behavioral flexibility in adjusting their solar radiation cross-section, either by facing towards the sun to minimize their cross-section or by orienting themselves perpendicular to the sun, making their solar absorption equivalent to more rotund organisms. In both cases the change produces a reduction in solar absorption during peak thermal stress, allowing for higher metabolic rates during the day [101]. Our model results show this bauplan is appropriate in warm environments, but without insulation individuals would have been at a distinct disadvantage in cooler climates.

A major difference between our *Plateosaurus* and *Coelophysis* models is the inclusion of the aforementioned states of dermal insulation in the form of primitive filamentous structures for *Coelophysis*. Filamentous and/or quill-like structures are known in a wide range of coelurosaurian theropods, basal ornithischians such as *Tianyulong* (Zheng and others 2009) and *Kulindadromeus* (Godefroit and others 2014), as well as the more derived ornithischian *Psittacosaurus* (Osborn 1923). Comparisons of pterosaurian pycnofibers and dinosaurian quill structures has led to the suggestion that the epidermal insulatory structures may be the primitive conditions for Ornithodira (i.e the most recent common ancestor of pterosaurs, dinosaurs and all their descendants; [135]). This hypothesis has been questioned by character optimization analyses [136], though they acknowledge that Early Jurassic theropod resting imprints with epidermal structures [137] makes proto-feathered Triassic theropods plausible.

In the absence of definitive skin impressions, our model can add to the discussion on the need for insulatory structures in *Coelophysis* [126-128]. We have not added such structures to

Plateosaurus, as there are no prosauropod or sauropod body (or trace) fossils that demonstrate insulatory epidermal structures. If insulatory coverings were primitive to Dinosauria, it is likely they were lost as sauropodomorphs increased in size - increased mass alone can expand tolerance of cooler temperatures and stabilize internal temperature variation, but not without its own energetic costs. There is also the possibility that insulation is present in the hatchlings of some larger species and is lost during ontogeny, though scales are known in some embryonic titanosaur sauropods [141].

Skeletal remains of *C. bauri* (our model) are well known from Chinle deposits best represented by our hot microclimates while similarly sized *C. rhodesiensis* is well known from the Elliot Formation (Zimbabwe) which was deposited in a temperate southern hemisphere paleolatitude with a seasonally cold winter [55,60]. Thus, the paleogeographic range of small-bodied coelophysoids extends from northern low tropical latitudes through temperate latitudes of both hemispheres. This is a broad latitudinal and environmental range for coelophysoids in the 20 kilogram size range. Given the lack of evidence of significantly different metabolic adaptations in these closely-related basal theropods, any biophysical scenario must satisfy both the hot and cold microclimates. While no single biophysical condition (i.e., combination of CTR/RMR) satisfies the disparity in climate regimes that *Coelophysis* inhabited, varying the amount and location of insulation covering its body solves this apparent paradox.

The addition of complete insulation coverage of filamentous structures to our modeled *Coelophysis* produced similar results to those of the much larger non-insulated *Plateosaurus*. Our results demonstrate that both *Plateosaurus* and a fully insulated *Coelophysis* would have been heat stressed in the hot Chinle microclimate, limiting their distribution to temperate and

boreal latitudes or high elevations (or dense forested areas) at more equatorial latitudes as mentioned above.

In extant taxa the density of insulatory structures vary with ontogeny and by season [138,142,143]. Temperature acclimatization to both hot and cold climates is a well-documented phenomenon in birds and mammals. It has been shown that cold-acclimated birds can have greater feather density, higher resting metabolic rates, and reduced evaporative cooling compared to heat-acclimated birds of the same species [see 114].

Recent studies of growth and postnatal development in early dinosaurs (e.g., *C. bauri* and *C. rhodesiensis*) and dinosauromorphs (e.g., the silesaurid *Asilisaurus* (Nesbitt and others 2010)) suggest high variation in developmental sequence and body size at skeletal maturity was likely the ancestral condition [139,144]. This differs from the moderate to low intraspecific variation in growth seen in extant archosaurs [144]. Griffin and Nesbitt [144] suggest anomalously high variability in *Coelophysis* body size at skeletal maturity may be epigenetically controlled. Higher variability in metabolic rate and core temperature range (and thus physiological efficiencies such as digestion) is consistent with increased variability in size at skeletal maturity. This size variance combined with evidence of increased respiratory efficiency [145-147] and locomotion energetics [148-150] suggests increased RMR within basal dinosaurs (or their immediate ancestors) was linked to increasing aerobic scope, as opposed to enzymatic efficiency, parental care, or increased eurythermy [e.g., 151-153].

Future research

With the need to document how to adapt Niche Mapper for modeling extinct organisms, we have restricted our present work to the adult states of *Coelophysis* and *Plateosaurus,* in

environments in which they are known to occur. Ontogenetic shifts in physiology (e.g., declining metabolic rates with age/size), thermoregulatory behavior, or insulation (e.g., dermal or subdermal) should all be taken into account in future work. Clearly, hatchlings through sub adult members of a population must have survived to adulthood in our modeled climates, whether through physiological, environmental, or behavioral means. Likewise, phylogenetically disparate but spatiotemporally contemporaneous species should be incorporated in future studies to further test ecological hypotheses.

Mechanistic modeling of physiological and environmental conditions to test for viable physiological combinations in multiple environments is a relatively new tool for deep time applications. The simulations described above outline the primary components necessary for exploring paleophysiology in deep time with Niche Mapper. The relative effect of temperature, resting metabolic rate, core temperature range, size, and epidermal insulation are much greater than those of skin/fur/feather color, or muscle, respiration, and digestive efficiencies. We do not suggest these other parameters are trivial, rather they are more suited to 'fine tuning' the model, as seen in extant examples previously mentioned, or where circumstances are favorable for a specific extinct taxa [i.e., 102]. Niche Mapper is a powerful tool that can be leveraged to address a diverse array of evolutionary questions in deep time pertaining to paleoecological carrying capacity, paleobiogeographic distribution, and survivorship across major extinction boundaries.

Conclusions

Mechanistic models in Niche Mapper use phylogenetically-constrained physiological parameters to determine habitable microclimates for a given taxon. Based on our results, prosauropods like *Plateosaurus* would have had a resting metabolic rate close to that of modern

ratites, although we cannot rule out variance in this clade's core temperature range being intermediate to that predicted for extant ratites and squamates of their size. This is not unexpected given their phylogenetic position relative to known ectothermic and endothermic crown members and is suggestive of an acquisition of elevated metabolic rates prior to the narrowing of core temperature ranges in defense of a stable core temperature. Similarly, we suggest *Coelophysis* was more likely to maintain a ratite-like resting metabolic rate than a monotreme or squamate-like RMR. A core temperature range intermediate to extant ratites and squamates is also suggested, similar to *Plateosaurus*. The presence of variable depth, density, and distribution of epidermal insulation would not only allow for a broader range of environmental tolerances, it appears to be a physiological necessity for *Coelophysis* and likely for most small ornithodirans as they increased their resting metabolic rates above ancestral levels.

Our results illustrate the interconnected nature of morphology, physiology, environmental variables and how they constrain organismal energetics, behavior, and geographic distribution. Niche Mapper is a flexible tool that can be applied to extinct organisms in deep time whose body shapes have no direct modern analog.

Acknowledgements

The authors would like to thank Aaron Kufner and Adam Fitch for discussion and productive feedback on earlier versions of the manuscript and Andrew Zaffos for help troubleshooting R code. Thanks also goes to the numerous colleagues who have acted as sounding boards and provided critical evaluations of this work as it progressed over the last few years; their efforts are greatly appreciated. A special thanks to two anonymous reviewers whose

suggestions vastly improved an earlier draft of this manuscript, and the reviews of Dr.'s DJ Button and R. Kosma for their constructive comments.

Supporting Information

S1 Appendix. Niche Mapper Variables

S2 Appendix. Model test using Varanus komodoensis on Komodo Island

S3 Appendix. Parameterizing biophysical model dimensions for fossil vertebrates.

S4 Appendix. Sensitivity analyses and additional figures

S1 Table. Target resting metabolic rates for classes of animals.

References

1 Bryant HN, Russell AP. The role of phylogenetic analysis in the inference of unpreserved attributes of extinct taxa. Phil Trans Royal Soc B. 1992; 337(1282): 405-418.

2 Witmer LM. The extant phylogenetic bracket and the importance of reconstructing soft tissues in fossils. In: Thomason J, editor. Functional Morphology in Vertebrate Paleontology; 1995.19-33.

3 Hunt, G. Measuring rates of phenotypic evolution and the inseparability of tempo and mode. Paleobiology. 2012; 38(3): 351-373.

4 Peters SE. Genus extinction, origination, and the durations of sedimentary hiatuses. Paleobiology. 2006; 32(3): 387-407.

5 Barrett PM, McGowan AJ, Page V. Dinosaur diversity and the rock record. Proc. R. Soc. B Biol. Sci. 2009; 276: 2667-2674.

6 Dunhill AM, Hannisdal B, Benton, MJ. Disentangling rock record bias and common-cause from redundancy in the British fossil record. Nat Comm. 5:4818.

7 McMahon TA. Using body size to understand the structural design of animals: quadrupedal locomotion. J Applied Physiol. 1975; 39(4): 619-627.

8 Haynie DT. Biological Thermodynamics. Cambridge: Cambridge UP, 2001.

9 Porter WP. Heat Balances in Ecological Contexts. In: Johnson EA, Martin YE, editors. A Biogeoscience Approach to Ecosystems.2016; 49-87.

10 Barlett PN, Gates DM. The energy budget of a lizard on a tree trunk. Ecology. 1967; 48: 315-322.

11 Dudley PN, Bonazza R, Porter WP. Consider a Non-Spherical Elephant: Computational Fluid Dynamics Simulations of Heat Transfer Coefficients and Drag Verified Using Wind Tunnel Experiments. J Exp Biol. 2013; 319(6): 319-327.

12 Dudley PN, Bonazza R, Porter WP. Climate change impacts on nesting and internesting leatherback sea turtles using 3D animated computational fluid dynamics and finite volume heat transfer. Ecol Model. 2016; 320: 231-240.

13 Fitzpatrick MJ, Mathewson PD, Porter WP. Validation of a mechanistic model for non-Invasive study of ecological energetics in an endangered wading bird with counter-current heat exchange in its legs. PLoS One. 2015; 10(8): e0136677.

14 Levy O, Dayan T, Kronfeld-Schor N, Porter WP. Biophysical modeling of the temporal niche: from first principles to the evolution of activity patterns. Am Nat. 2012; 179(6): 794-804.

15 Long RA, Bowyer RT, Porter WP, Mathewson PD, Monteith KL, Findholt SL, et al. Linking habitat selection to fitness-related traits in herbivores: the role of the energy landscape. Oecologia. 2016; 181(3): 709-720.

16 Mathewson PD, Moyer-Horner L, Beever EA, Briscoe NJ, Kearney M,
Yahn JM, et al. Mechanistic variables can enhance predictive models of endotherm distributions: the American pika under current, past, and future climates. Glob Change Biol. 2016; 23(3): 1048-1064.

17 Mathewson PD, Porter WP. Simulating polar bear energetics during a seasonal fast using a mechanistic model. PLoS One. 2013; 8: e72863.

18 Mitchell NJ, Hipsey MR, Arnall S, McGrath G, Bin Tareque H, Kuchling G, et al. Linking eco-energetics and eco-hydrology to select sites for the assisted colonization of Australia's rarest reptile. Biology. 2013; 2(1): 1-25.

19 Kearney M, Phillips BL, Tracy CR, Christian KA, Betts G, Porter WP. Modelling species distributions without using species distributions: the cane toad in Australia under current and future climates. Ecography. 2008; 31: 423-434.

20 Kearney M, Porter WP, Williams C, Ritchie S, Hoffmann AA. Integrating biophysical models and evolutionary theory to predict climatic impacts on species' ranges: the dengue mosquito Aedes aegypti in Australia. Funct Ecol. 2009; 23(3): 528-538.

21 Kearney MR, Wintle BA, Porter WP. Correlative and mechanistic models of species distribution provide congruent forecasts under climate change. Conserv Lett. 2010; 3(3): 203-213.

22 Norris KS. Color adaptation in desert reptiles and its thermal relationships. In: Milstead WM, editor. Lizard Ecology a Symposium, University of Missouri Press; 1967. 162-229.

23 Porter WP, Mitchell JW, Beckman WA, DeWitt CB. Behavioral implications of mechanistic ecology: Thermal and behavioral modeling of desert ectotherms and their microenvironment. Oecologia. 1973; 13: 1-54.

24 Porter WP, Budaraju S, Stewart WE, Ramankutty N. Calculating climate effects on birds and mammals: impacts on biodiversity, conservation, population parameters, and global structure. Am Zool. 2000; 40: 597-630.

25 Porter WP, Sabo JL, Tracy CR, Reichman O, Ramankutty N. Physiology on a landscape scale: plant-animal interactions. Integr Comp Biol. 2002; 42(3): 431-453.

26 Spotila JR, Lommen PW, Bakken GS, Gates DM. A mathematical model for body temperatures of large reptiles: implications for dinosaur ecology. Am Nat. 1973; 107(955): 391-404.

27 Dunham AE, Overall, KL, Porter WP, Forster CA. Implications of ecological energetics and biophysical and developmental constraints for life-history variation in dinosaurs. Geol S Am S. 1989; 238: 1-20.

28 Whiteside JH, Lindström S, Irmis RB, Glasspool IJ, Schaller MF, Dunlavey M, Nesbitt SJ, Smith ND, Turner AH, Extreme ecosystem instability suppressed tropical dinosaur dominance for 30 million years. PNAS. 2015; 112(26): 7909-7913.

29 Porter WP, Mitchell JW. Method and system for calculating the spatial-temporal effects of climate and other environmental conditions on animals. In: Office UP, editor. 11-0E Wisconsin Alumni Research Foundation; B [Internet], 2006: http://www. patentstorm.us/patents/7155377-fulltext.html.

30 Briscoe NJ, Handasyde KA, Griffiths SR, Porter WP, Krockenberger A, Kearney MR. Tree-hugging koalas demonstrate a novel thermoregulatory mechanism for arboreal mammals. Biol Lett. 2014; 10(6): 20140235.

31 Bartelt PE, Klaver RW, Porter, WP. Modeling amphibian energetics, habitat suitability, and movements of western toads, Anaxyrus (= Bufo) boreas, across present and future landscapes. Ecol Model. 2010; 221(22): 2675-2686.

32 Deville A-S, Labaude S, Robin J-P, Béchet A, Gauthier-Clerc M, Porter WP, et al. Impacts of extreme climatic events on the energetics of
long-lived vertebrates: the case of the greater flamingo facing cold spells in the Camargue. J Exp Biol. 2014; 217: 3700-3707.

33 Huang S-P, Chiou C-R, Lin T-E, Tu M-C, Lin C-C, Porter WP. Future advantages in energetics, activity time, and habitats predicted in a high-altitude pit viper with climate warming. Funct Ecol. 2013; 27: 446-458.

34 Long RA, Bowyer RT, Porter WP, Mathewson PD, Monteith KL, Kie JG. Behavior and nutritional condition buffer a large-bodied endotherm against direct and indirect effects of climate. Ecol Monogr. 2014; 84(3): 513-532.

35 Kingsolver JG. Thermal and hydric aspects of environmental heterogeneity in the pitcher plant mosquito. Ecol Monogr. 1979; 49(4): 357-376.

36 Porter W, Vakharia N, Klousie W, Duffy D. Po'ouli landscape bioinformatics models predict energetics, behavior, diets, and distribution on Maui. Integr Comp Biol. 2006; 46(6): 1143-1158.

37 Porter WP, Munger JC, Stewart WE, Budaraju S, Jaeger J. Endotherm energetics: from a scalable individual-based model to ecological applications. Aust J Zool. 1994; 42: 125-162.

38 Tracy CR. A model of the dynamic exchanges of water and energy between a terrestrial amphibian and its environment. Ecol Monogr. 1976; 46(3): 293-326.

39 Zhang Y, Mathewson PD, Zhang Q, Porter WP, Ran J. An ecophysiological perspective on likely giant panda habitat responses to climate change. Glob Change Biol. 2018; 1-13.

40 Auffenberg W. The behavioral ecology of the Komodo monitor. 1st ed. Gainesville:University Presses of Florida;1981.

41 Harlow HJ, Purwandana D, Jessop TS, Phillips JA. Body temperature and thermoregulation of Komodo dragons in the field. J Therm Biol. 2010; 35(7): 338-347.

42 McNab BK, Auffenberg W. The effect of large body size on the temperature regulation of the Komodo dragon, Varanus komodoensis. Comp Biochem Phys A. 1976; 55(4A): 345-350.

43 Kearney MR, Shamakhy A, Tingley R, Karoly DJ, Hoffmann AA, Briggs PR, et al. Microclimate modelling at macro scales: a test of a general microclimate model integrated with gridded continental-scale soil and weather data. Methods Ecol Evol. 2014; 5(3): 273-286.

44 Fuentes M, Porter W. Using a microclimate model to evaluate impacts of climate change on sea turtles. Ecol Model. 2013; 251: 150-157.

45 Geiger R. The climate near the ground. 1st ed. Cambridge; Harvard University Press: 1965.

46 McCullough EC, Porter WP. Solar Radiation Spectra for the Terrestrial Ecological Environment. Ecology. 1971; 52(6): 1008-1015.

47 Laskar J, Robutel P, Joutel F, Gastineau M, Correia ACM, Levard B. A long-term numerical solution for the insolation quantities of the Earth. Astron Astrophys. 2004; 428: 261-285.

48 Crucifix, M. Palinsol: Insolation for Palaeoclimate Studies. V.0.93 [Internet]; Available From: https://cran.r-project.org/web/packages/palinsol/index.html.

49 Gates DM. Energy exchange in the biosphere. 1st ed. New YorK; Harper and Row: 1962.

50 Swinbank WC. Long-wave radiation from clear skies. Quart J Roy Met Soc. 1963; 89: 339-348.

51 Idso SB, Jackson RD. Thermal radiation from the atmosphere. J. Geophys. Res. 1969; 74: 5397-5403.

52 Prochnow S, Nordt L, Atchley S, Hudec M. Multi-proxy paleosol evidence for middle and late Triassic

climate trends in eastern Utah. Palaeogeogr Palaeocl. 2006; 232(1): 53-72.

53 Sellwood B, Price G, and Shackleton N, Francis J. Sedimentary Facies as Indicators of Mesozoic Palaeoclimate. Phil Trans Royal Soc B. 1993; 341(1297: 225-233.

54 Cleveland DM, Nordt LC, Atchley SC. Paleosols, trace fossils, and precipitation estimates of the uppermost Triassic strata in northern New Mexico. Palaeogeogr Palaeocl. 2008; 257(4): 421-444.

55 Sellwood B, Valdes P. Mesozoic climates: General circulation models and the rock record. Sediment Geol. 2006; 190: 269-287.

56 Berner RA, Beerling DJ, Dudley R, Robinson JM, Widlman RA. Phanerozoic atmospheric oxygen. Annu Rev Earth Planet Sci. 2003; 31: 105-134.

57 Berner RA, Kothavala Z. Geocarb III: A Revised Model of Atmospheric CO_2 over Phanerozoic Time. Am J Sci. 2001; 301(2): 182-204.

58 Cleveland DM, Nordt LC, Dworkin SI, Atchley SC. Pedogenic carbonate isotopes as evidence for extreme climatic events preceding the Triassic-Jurassic boundary: Implications for the biotic crisis? GSA Bul. 2008; 120(11-12): 1408-1415.

59 Kutzbach JE. Idealized Pangean climates: Sensitivity toorbital change. Geol. Soc. Am. Spec. Pap. 1994; 289: 41–55.

60 Crowley TJ. Pangean climates.Geol. Soc. Am. Spec. Pap. 1994; 289: 25-39

61 Parrish J. Climate of the supercontinent Pangea. J Geol. 1993; 101(2): 215-233.

62 Weatherspark. Average weather in Accra, Ghana [Internet]. Available from: https://weatherspark.com/y/42343/Average-Weather-in-Tamale-Ghana- Year-Round.

63 Weatherspark. Average weather in Accra, Ghana [Internet]. Available from: https://weatherspark.com/y/36520/Average-Weather-in-Timbuktu-Mali- Year-Round.

64 Kreith F, Black WZ. Basic Heat Transfer. 1st ed. New York:Harper & Row;1980.

65 Bird RB, Stewart WE, Lightfoot WN. Transport Phenomena. 2nd ed. New York:John Wiley & Sons, Inc;2002.

66 Kowalski GJ, Mitchell JW. Heat transfer from spheres in the naturally turbulent, outdoor environment. J Heat Transf. 1976; 98(4): 649-653.

67 Porter WP, KearneyMR. Size, shape and the thermal niche of endotherms. P Natl Acad Sci USA. 2009; 106(Suppl.2): 19666-19672.

68 Smith NP, Barclay CJ, Loiselle DS. The efficiency of muscle contraction. Prog Biophys Mol Bio. 2005; 88(1): 1-58.

69 Natori Y, Porter WP. Habitat Evaluation for the Japanese Serow (Capricornis crispus) by Energetics Landscape Modeling. Ecol Applications. 2007; 17(5): 1441-1459.

70 Xu X, Zhao Q, Norell M, Sullivan C, Hone D, Erickson G, et al. A new feathered maniraptoran dinosaur fossil that fills a morphological gap in avian origin. Chinese Sci Bul. 2009; 54(3): 430-435.

71 Xu X, Zheng X, You H. Exceptional dinosaur fossils show ontogenetic development of early feathers. Nature. 2010; 464: 1338-1341.

72 Xu X, Zhou Z. Prum RO. Branched integumental structures in Sinornithosaurus and the origin of feathers. Nature. 2001; 410: 200-204.

73 Norell MA, Xu X. Feathered dinosaurs. Annu Rev Earth Planet Sci. 2005; 33: 277-299.

74 Prum and Brush 2002. The evolutionary origin and diversification of feathers. Quart Rev Biol. 2002; 77(3): 261-295.

75 McNab BK. An analysis of the factors that influence the level and scaling of mammalian BMR. Comp Biochem Phys A. 2008; 151(1): 5-28.

76 McNab BK. Ecological factors affect the level and scaling of avian BMR. Comp Biochem Phys A. 2009; 152(1): 22-45.

77 Schmidt-Nielsen K. Animal physiology: Adaptation and environment. 2nd ed. Cambridge: Cambridge University Press; 1979.

78 Nagy KA. Field metabolic rate and body size. J Exp Biol. 2005; 208(9): 1621-1625.

79 Weaver JC. The improbable endotherm: the energetics of the sauropod dinosaur Brachiosaurus. Paleobiology. 1983; 9(2): 173-182.

80 Nagy KA. Water and electrolyte budgets of a free-living desert lizard,Sauromalus obesus. J Comp Physiol. 1972; 79(1): 39-62.

81 Saadoun, A, Cabrera, MC. A review of the nutritional content and technological parameters of indigenous sources of meat in South America. Meat Sci. 2008; 80(3): 570-581.

82 Minnich JE, Shoemaker VH. Water and Electrolyte Turnover in a Field Population of the Lizard, Uma scoparia. Copeia. 1972; 1972(4): 650-659.

83 Roberts MF, Lightfoot EN, Porter WP. A new model for the body size–metabolism relationship. Physiol Biochem Zool. 2010; 83(3): 395-405.

84 Eckert R, Randall D. Animal Physiology Mechanisms and Adaptations. 2nd ed. New York:W. H. Freeman and Company;1983.

85 Farlow J, Hotz, T. The fossil record of predation in dinosaurs. Paleontological Society Papers. 2002; 8: 251-266.

86 Carpenter K. Forelimb biomechanics of nonavian theropod dinosaurs in predation. Senk Leth. 2002; 82(1): 59-75.

87 Hummel J, Gee CT, Südekum K-H, Sander PM, Nogge G, Clauss M. In vitro digestibility of fern and gymnosperm foliage: implications for sauropod feeding ecology and diet selection. Proc R Soc B. 2008; 275: 1015-1021.

88 Walsberg GE. Coat color and solar heat gain in animals. Bioscience. 1983; 33(2): 88-91

89 Norris KS. Color adaptation in desert reptiles and its thermal relationships. in Lizard ecology: a symposium. 1967; University of Missouri Press Columbus, Missouri.

90 Smith, K.R., et al., Color Change for Thermoregulation versus Camouflage in Free-Ranging Lizards. The American Naturalist. 0(0): p. 000-000.

91 Box GEP, Hunter WG, Hunter JS. Statistics for Experimenters. 1st ed. New York:John Wiley & Sons, Inc;1978.

92 Shipley LA. Grazers and Browsers: How Digestive Morphology Affects Diet Selection. Idaho Forest, Wildlife & Range Exp. Sta. Bull. 1999; 70: 20-27.

93 Schrader AM, Owen-Smith N, Ogutu JO. Blackwell Publishing Ltd How a mega-grazer copes with the dry season: food and nutrient intake rates by white rhinoceros in the wild. Func Ecol. 2006; 20: 376-384.

94 Paul GS. Dinosaur models: The good, the bad, and using them to estimate the mass of dinosaurs. In: Wolberg DL, Stumpand E, Rosenberg, GD, editors. Dinofest International. Proceedings of a symposium held at Arizona State University.1997;129-142.

95 Colbert EH. The weights of dinosaurs. American Museum Novitates. 1962; 2076: 1-16.

96 Alexander RM. Dynamics of dinosaurs and other extinct giants. Columbia University Press. 1989.

97 Gunga HC, Suthau T, Bellmann A, Friedrich A, Schwanebeck T, Stoinski T, Trippe T, Kirsch K, Hellwich O. Body mass estimations for Plateosaurus engelhardti using laser scanning and 3D reconstruction methods. Naturwissenschaften. 2007; 94(8): 623-630.

98 Mallison H. The Digital Plateosaurus I: Body mass, mass distribution and posture assessed using CAD and CAE on a digitally mounted complete skeleton. Palaeon Electron. 2010; 13(2): 8A 26p.

99 Seebacher F. A new method to calculate allometric length-mass relationships of dinosaurs. J Vertebr Paleontol. 2001; 21(1): 51-60.

100 Benson RBJ, Campione NE, Carrano MT, Mannion PD, Sullivan C, Upchurch P, et al. Rates of Dinosaur Body Mass Evolution Indicate 170 Million Years of Sustained Ecological Innovation on the Avian Stem Lineage. Plos One. 2014; 12(6): e1001896.

101 Porter WP. Nature's experiments on body shape and size have metabolic optima. Nature Lett. In review.

102 Wang Y, Porter W, Mathewson P, Miller P, Graham R, Williams J. Mechanistic modeling of environmental drivers of woolly mammoth carrying capacity and extinction on St. Paul Island, AK. Ecology. (in review). 2018.

103 Cerling TE, Quade J. Stable carbon and oxygen isotopes in soil carbonates. Geoph Monog. 1993; 78: 217-231.

104 Chan M. Triassic loessite of north-central Utah; stratigraphy, petrophysical character, and paleoclimate implications. J Sediment R. 1999; 69(2): 477-485.

105 Gázquez F, Morellón M, Bauska T, Herwartz D, Surma J, Moreno A, et al. Triple oxygen and hydrogen isotopes of gypsum hydration water for quantitative paleo-humidity reconstruction. Earth Panet Sc Lett. 2018; 481: 177-188.

106 Eagle RA, Tütken T, Martin TS, Tripati AK, Fricke HC, Connely M, et al. Dinosaur body temperatures determined from isotopic (13C-18O) ordering in fossil biominerals. Science. 2011; 333(6041): 443-445.

107 Eagle RA, Enriques M, Grellet-Tinner G, Pérez-Huerta A, Hu D, Tütken T, et al. Isotopic ordering in eggshells reflects body temperatures and suggests differing thermophysiology in two Cretaceous dinosaurs. Nat Comm. 2015; 6: 8296.

108 Barrick RE, Showers WJ, Fischer AG. Comparison of thermoregulation of four ornithischian dinosaurs and

a varanid lizard from the Cretaceous Two Medicine Formation: evidence from oxygen isotopes. Palaios. 1996; 11(4): 295-305.

109 Fricke HC, Rogers RR. Multiple taxon–multiple locality approach to providing oxygen isotope evidence for warm-blooded theropod dinosaurs. Geology. 2000; 28(9): 799-802.

110 Grady JM, Enquist BJ, Dettweiler-Robinson E, Wright NA, Smith FA. Evidence for mesothermy in dinosaurs. Science. 2014; 344(6189): 1268-1272.

111 Sander PM, Klein N, Buffetaut E, Cuny G, Suteethorn V, Loeuff JL. Adaptive radiation in sauropod dinosaurs: bone histology indicates rapid evolution of giant body size through acceleration. Org Divers Evol. 2004; 4(3): 165-173.

112 Klein N, Sander PM. Bone histology and growth of the prosauropod dinosaur Plateosaurus engelhardti von Meyer, 1837 from the Norian bonebeds of Trossingen (Germany) and Frick (Switzerland). Spec Pap Paleontol. 2007; 77: 169-206.

113 Chaffee RR, Roberts JC. Temperature acclimation in birds and mammals. Annu Rev Physiol. 1971; 33: 155-202.

114 Marsh RL, Dawson, WR. Avian adjustments to cold. In: Wang LCH, editor, Animal adaptations to cold. New York; Springer-Verlag: 205-253.

115 Amiot R, Lécuyer C, Buffetaut E, Escarguel G, Fluteau F, Martineau F. Oxygen isotopes from biogenic apatites suggest widespread endothermy in Cretaceous dinosaurs. Earth and Planet Sci. 2006; 246: 41-54.

116 Golovneva LB. The Maastrichtian (Late Cretaceous) climate in the Northern Hemisphere. Geological Society, London, Special Publications. 2000; 181: 43-54.

117 Erickson GM, Rogers KC, Yerby SA. Dinosaurian growth patterns and rapid avian growth rates. Nature. 2001; 412: 429-433.

118 Werner J, Griebeler EM. Allometries of Maximum Growth Rate versus Body Mass at Maximum Growth Indicate That Non-Avian Dinosaurs Had Growth Rates Typical of Fast Growing Ectothermic Sauropsids. PLoS One. 2014; 9: e88834.

119 Lockley MG, Lucas SG, Hunt AP. Eosauropus, a new name for a Late Triassic track: Further observations on the Late Triassic ichnogenus Tetrasauropus and related forms, with notes on the limits of interpretation. In: Harris et al., editors. The Triassic-Jurassic Terrestrial Transition. New Mexico Museum of Natural History and Science Bulletin 37; 2006. 192-198.

120 Brett CE, Baird, GC. Comparative taphonomy: a key to paleoenvironmental interpretation based on fossil preservation. Palaios. 1986; 1(3): 207-227.

121 Schopf, JM. Modes of fossil preservation. Rev Palaeobot Palyno. 1975; 20: 27-53.

122 Renesto S, Lombardo C. Structure of the tail of a phytosaur (Reptilia, Archosauria) from the Norian (Late Triassic) of Lombardy (Northern Italy). Riv Ital Paleontol S. 1999; 105(1): 135-144.

123 Marsicano CA, Mancuso AC, Palma RM, Krapovickas V. Tetrapod tracks in a marginal lacustrine setting (Middle Triassic, Argentina): Taphonomy and significance. Palaeogeogr Palaeocl. 2010; 291(3-4): 388-399.

124 Thomson TJ, Lovelace DM. Swim track morphotypes and new track localities from the Moenkopi and Red Peak Formations (Lower-Middle Triassic) with preliminary interpretations of aquatic behaviors. In: Lockley MG, Lucas SG, editors. Fossil footprints of North America. New Mexico Museum of Natural History and Science Bulletin 62; 2014. 103-128.

125 Yang Z, Jiang B, McNamara ME, Kearns SL, Pitman M, Kaye TG, Orr PJ, Xu X, Benton MJ. Pterosaur integumentary structures with complex feather-like branching. Nat Ecol Evol. 2019; 3(1): 24-30

126 Lennerstedt I. Seasonal variation in foot papillae of wood pigeon, pheasant and house sparrow. Comp Biochem Phys A. 1975; 51(3): 511-520.

127 Griffin CT, Nesbitt, SJ. Anomalously high variation in postnatal development is ancestral for dinosaurs but lost in birds. P Natl Acad Sci USA. 2016a; 113: 14757-14762.

128 Baron MG, Norman DB, Barrett PM. A new hypothesis of dinosaur relationships and early dinosaur evolution. Nature. 2017; 543: 501-506.

129 Varricchio DJ, Martin AJ, Katsura Y. First trace and body fossil evidence ofa burrowing, denning dinosaur. Proc Royal Soc Lond. 2007; B274: 1361–1368.

130 Martin AJ. Dinosaur burrows in the Otway Group (Albian) of Victoria, Australia, and theirrelation to Cretaceous polar environments. Cretaceous Research. 2009; 30: 1223–1237

131 Barnett LB. Seasonal changes in temperature acclimatization of the house sparrow Passer domesticus. Comp Biochem Phys A. 1970; 33: 559-578.

132 Møller, AP. The allometry of number of feathers in birds changes seasonally. Avian Res. 2015; 6: 2.

133 Griffin CT, Nesbitt, SJ. The histology and femoral ontogeny of the Middle Triassic (?late Anisian) dinosauriform Asilisaurus kongwe and implications for the growth of early dinosaurs. J Vertebr Paleontol. 2016b; 36(3): e1111224.

134 O'connor PM, Claessens LP. Basic avian pulmonary design and flow-through ventilation in non-avian theropod dinosaurs. Nature. 2005 Jul;436(7048):253.

135 Sereno PC, Martinez RN, Wilson JA, Varricchio DJ, Alcober OA, Larsson HC. Evidence for avian intrathoracic air sacs in a new predatory dinosaur from Argentina. PLoS one. 2008 Sep 30;3(9):e3303.

136 Wedel MJ. Evidence for bird-like air sacs in saurischian dinosaurs. J Exp Zool A Ecol Genet Physiol. 2009 Oct 1;311(8):611-28.

137 Carrier DR. The evolution of locomotor stamina in tetrapods: circumventing a mechanical constraint. Paleobiology. 1987 Jul;13(3):326-41.

138 Hutchinson JR, Gatesy SM. Dinosaur locomotion: beyond the bones. Nature. 2006 Mar 15;440(7082):292.

139 Pontzer H, Allen V, Hutchinson JR. Biomechanics of running indicates endothermy in bipedal dinosaurs. PLoS One. 2009 Nov 11;4(11):e7783.

140 Hopson JA. Endothermy, small size, and the origin mammalian reproduction. The American Naturalist. 1973; 107(955): 446-452.

141 Kemp TS. The origin of mammalian endothermy: a paradigm for the evolution of complex biological structure. Zool J Linn Soc. 2006; 147(4): 473-488.

142 Nespolo RF, Solano-Iguaran JJ, Bozinovic F. Phylogenetic analysis supports the aerobic-capacity model for the evolution of endothermy. Am Nat. 2017; 189(1): 13-27.

Supplement B – Non-chapter coauthored paper relevant to Chapter 3:

An Overview of Non- Avian Theropod Discoveries and Classification

Christophe Hendrickx*, Scott A. Hartman# & Octávio Mateus*

* Universidade Nova de Lisboa, CICEGe, Departamento de Ciências da Terra, Faculdade de Ciências e Tecnologia, Quinta da Torre, 2829-516, Caparica, Portugal & Museu da Lourinhã, 9 Rua João Luis de Moura, 2530-158, Lourinhã, Portugal

University of Wisconsin-Madison, Department of Geoscience, Madison, WI, 53715 USA

Abstract

Theropods form a taxonomically and morphologically diverse group of dinosaurs that include extant birds. Inferred relationships between theropod clades are complex and have changed dramatically over the past thirty years with the emergence of cladistic techniques. Here, we present a brief historical perspective of theropod discoveries and classification, as well as an overview on the current systematics of non-avian thero- pods. The first scientifically recorded theropod remains dating back to the 17th and 18th centuries come from the Middle Jurassic of Oxfordshire and most likely belong to the megalosaurid *Megalosaurus*. The latter was the first theropod genus to be named in 1824, and subsequent theropod material found before 1850 can all be referred to megalosauroids. In the fifty years from 1856 to 1906, theropod remains were reported from all continents but Antarctica. The clade Theropoda was erected by Othniel Charles Marsh in 1881, and in its current usage corresponds to an intricate ladder-like organi- zation of 'family' to 'superfamily' level clades. The earliest definitive theropods come from the Carnian of Argentina, and coelophysoids form the first significant theropod radiation from the Late Triassic to their extinction in the Early Jurassic. Most subsequent theropod clades such as ceratosaurs, allosauroids, tyrannosauroids, ornithomimosaurs, therizinosaurs, oviraptorosaurs, dromaeosaurids, and troodontids persisted until the end of the Cretaceous, though the megalosauroid clade did not extend into the Maas- trichtian. Current debates are focused on the monophyly of deinonychosaurs, the posi- tion of dilophosaurids within coelophysoids, and megaraptorans among neovenatorids. Some recent analyses have suggested a placement of dilophosaurids outside Coelo- physoidea, Megaraptora within Tyrannosauroidea, and a paraphyletic Deinonychosauria with troodontids placed more closely to avialans than dromaeosaurids.

Introduction

Theropods form a clade of bipedal tetrapods that include all carnivorous dinosaurs and birds. Along with other dinosaur clades, they appeared in the Late Triassic (Fig. S2-1) and rapidly acquired a worldwide distribution, as they are known on every continent, including Antarctica, by the Lower Jurassic (Tykoski and Rowe 2004). In the Middle Jurassic, small theropods gave rise to birds, which were the only dinosaurs to survive the Cretaceous-Paleocene

mass extinction event 66 million years ago (Fig. S2-1). By surviving to the catastrophe at the K–Pg boundary, birds subsequently diversified during the Cenozoic, occupying ecological niches left by non-avian dinosaurs (Padian and Chiappe 1998; Chiappe and Witmer 2002; Naish 2012). Consequently, theropods are one of the most successful groups of vertebrates and the most morphologically and taxonomically diverse clade of dinosaurs (Rauhut 2003*a*; Brusatte 2012; Holtz 2012).

Non-avian theropods (i.e., Theropoda excluding Avialae) were the dominant terrestrial predators in Mesozoic ecosystems worldwide (Rauhut 2003*a*; Holtz 2012). As for other clades of dinosaurs, they became extinct at the end of the Cretaceous, although their diversity and disparity remained high in the latest stage of the Cretaceous (Rauhut 2003*a*; Holtz et al. 2004; Upchurch et al. 2011; Brusatte et al. 2014). Non-avian theropods includes the large majority (if not all) of meat-eating dinosaurs, yet many theropod clades became secondarily adapted to herbivory (Xu et al. 2009*a*; Zanno et al. 2009; Holtz 2012), and several taxa have also been suggested to be omnivores (Holtz et al. 1998) and filter feeders (Norell et al. 2001). The theropod body plan remains relatively poorly modified during the evolution of the clade as non-avian theropods were exclusively bipedal and always showed an elongated neck and a long, often horizontally projected tail. Variation in the postcranium mostly occurs in the forelimb and manual morphology as well as the elongation of the neural spine. Some theropods like abelisaurids had short stubby arms bearing four short fingers (e.g., Ruiz et al. 2011; Burch and Carrano 2012) whereas others like therizinosaurids and dromaeosaurids possesses elongated forelimbs with three slender fingers bearing large claws (). On the other hand, there is a large range of skull shape in non-avian theropods, from the elongated skull of spinosaurids showing a terminal spatulate rosetta (Dal Sasso et al. 2005) to the short parrot-like skull with edentulous jaws of

oviraptorids (Xu and Han 2010). Recent discoveries of non-avian theropods such as the rodent-like faced *Incisivosaurus* (Xu et al. 2002*a*), the beaked *Limusaurus* (Xu et al. 2009*a*), the great crested *Guanlong* (Xu et al. 2006) and the long snouted *Buitreraptor* (Makovicky et al. 2005) indicate a particularly high variety of skull morphologies among this group of dinosaurs.

This work aims to give a brief history of the first discoveries of theropod remains and review our current knownledge on theropod classification, with an illustration of the skeletal reconstruction in a representative of all main theropod clade.

Historical background

First Discoveries

The discovery of the first theropod and dinosaur remains goes hand in hand with that of the first dinosaur material, as the totality of dinosaur bones and teeth that were uncovered and reported in the literature for the first time belong to theropods (Lebrun 2004). Interestingly, the discovery of theropod material reported in the 17th, 18th, and the first half of the 19th century all occurred in England and France, and have all been referred to megalosauroid theropod, with the large majority belonging to Megalosauridae. This can be explained by two main factors: 1) the emergence of vertebrate paleontology in Early modern Europe and early 19th century in Western Europe, and mostly England and France, with scientists like Georges Cuvier, Gideon Mantell, and Richard Owen; and 2) the excavation, at that time, of the first dinosaur remains in Middle Jurassic limestone quarries of Stonesfield (Oxfordshire) and Caen (Normandy), a period of time when megalosaurids were the dominant theropods in Europe.

Theropod fossils were unquestionably found all over the world by prescientific societies well before the 17th century, and the discovery of these unusual remains by locals typically

leaded to myths and legends (Buffetaut 1994; Lebrun 2004; Spalding and Sarjeant 2012). Theropod tracks from the Lower Cretaceous sandstones of Paraíba in Brazil were, for instance, considered by Amerindians to pertain to giant birds similar to living rheas (Leonardi 1984; Lebrun 2004). In the same way, theropod footprints from the Rhine Valley, in Germany, may have inspired the story of the dragon of Drachenfels slayed by the hero Siegfried (Kirchner 1941; Spalding and Sarjeant 2012).

The very first published record of a theropod bone is this of an incomplete femur described and figured by Robert Plot in his 1677 *Natural History of Oxfordshire*. The fossil was dug out from a quarry in the Parish of Cornwell, Oxfordshire, and probably pertains to the megalosaurid *Megalosaurus* (Delair and Sarjeant 1975, 2002). Plot (1677) correctly identified the bone as a distal femoral condyle (*capita femoris inferiora*), and wondered whether this partial femur belonged to an elephant brought in Britain by the Romans. Plot (1677), however, noted many differences with the femur of elephants and instead referred the bone to a human giant also brought by the Romans (Evans 2010). This portion of femur was reillustrated by English naturalist Richard Brookes (1763) who labeled the figure 'Scrotum humanum' given the shared morphology between the distal condyle and the men sexual organ. Although this binomial term was obviously used as a descriptive appellation by Brookes (Spalding and Sarjeant 2012), it has been proposed by some people as a valid scientific name, the first one given to a dinosaur, and a senior synonym of *Megalosaurus bucklandii* (Halstead 1970; Delair and Sarjeant 1975), a proposition which was, however, rejected by the International Zoological Commission (Halstead and Sarjeant 1993; Delair and Sarjeant 2002).

Isolated theropod teeth were first described and figured in 1699 by Welsh naturalist Edward Lhuyd in his catalogue of fossils and minerals *Lithophylacii Britannici Ichnographica*

(Lhuyd 1699). The specimen number 1328 (Lhuyd 1699, plate 16), originally ascribed to a fish by Lhuyd (1699), corresponds to an isolated tooth from the Middle Jurassic Great Oolite of Stonesfield. This shed tooth greatly resembles *Megalosaurus* teeth and most likely belongs to that taxon (Delair and Sarjeant 2002). Additional theropod findings reported in the 18th century literature include a limb bone from Stonesfield labelled specimen a.1 by John Woodward (1729) in his catalogue of British fossils from his personal collection. This section of limb bone is currently preserved in the Sedgwick Museum of Cambridge (specimen D.30.1) and, once again, likely pertains to *Megalosaurus* (Delair and Sarjeant 1975, 2002). It may, therefore, be the earliest-discovered bone that can still be identified as belonging to a theropod with confidence (Delair and Sarjeant 1975, 2002). Later, an incomplete femur described and illustrated by Platt (1758) was identified by him as belonging to a hippopotamus, a rhinoceros, or an unknown animal of large size; yet, this large femur, which is also from a slate pit at Stonesfield, was recently referred to *Megalosaurus bucklandii* by Evans (2010).

The first theropod taxon to be recognized as reptilian and formally described in the literature is, in fact, *Megalosaurus*, coined by William Buckland in 1824 (although the generic name was already announced by James Parkinson in 1822). Material originally ascribed to *Megalosaurus* included a right dentary with a well-preserved erupted tooth (OUMNH J13505), and post-cranial material consisting of ribs, hind-limbs, pelvic bones, and sacral and caudal vertebrae. As Buckland (1824) did not provide a species name to *Megalosaurus*, a type species, *Megalosaurus conybeari*, was first given by Ferdinand von Ritgen in 1826 (von Ritgen 1826). The latter, however, failed to provide a description and a diagnosis to the species, and Mantell (1827) was the first scientist to name and diagnose a theropod species, i.e., *Megalosaurus bucklandii*, which is currently accepted by the scientific community.

Streptospondylus altdorfensis (Meyer 1832) and *Poekilopleuron bucklandii* (Eudes-Deslongchamps 1837) are, in France, the first non-avian theropods to be described and figured in the literature, and the second and third Mesozoic theropods to be formally named after *Megalosaurus*. These two megalosaurids, which are now considered as valid species (Carrano et al. 2012), are only known from postcranial remains. The material of *Streptospondylus*, discovered in the Callovian Vaches Noires cliffs around 1770, was mixed with crocodilian remains, and interpreted as a crocodile by Cuvier (1808, 1812, 1824). On the other hand, remains of *Poekilopleuron* were correctly identified as belonging to a large reptile closely related to *Megalosaurus*. Unfortunately, the material was lost during World War II and only casts of the bones remain (Allain and Chure 2002).

The first valid non-avian coelurosaur to be formally described is *Nuthetes destructor* from the Purbeck Formation (Berriasian, Early Cretaceous) of Durlston Bay, Dorset. This tentative dromaeosaurid was erected by Owen (1854) based on an incomplete dentary and some isolated teeth originally assigned to a lizard or a varanid (Milner 2002). In North America, theropod remains discovered and reported in the literature for the first time are isolated teeth from the Upper Cretaceous of Montana (Breithaupt 1999). These teeth were briefly described by Leidy in 1856 and this American paleontologist erected two new species, *Troodon formosus* based on a single shed tooth, and *Deinodon horridus* based on several fragment of teeth. *Troodon* and *Deinodon* were originally classified as a lacertilian (lizard) and a relative of *Megalosaurus*, respectively (Leidy 1856). *Troodon* is now considered to be a valid species of troodontid (Currie 1987), whereas *Deinodon* has been synonymized with the better know tyrannosaurid *Albertosaurus* (Breithaupt 1999; Breithaupt and Elizabeth 2008). *Compsognathus longipes* (Wagner 1861) is the first non-avian theropod preserving a nearly complete and slightly

disarticulated skull (maxilla and quadrate included) to be discovered and reported in the literature. This theropod was briefly described by Wagner (1861) and remained one of the best known theropods for more than a century (Ostrom 1978).

History of Classification

The clade Dinosauria was erected as a tribe (or a sub-order) by Richard Owen in 1842 to contain three taxa of large reptiles, namely *Megalosaurus*, *Iguanodon* et *Hylaeosaurus*. Owen (1842) did not, however, include the already named *Poekilopleuron*, *Streptospondylus*, and *Suchosaurus*, all considered to be crocodilian taxa at that time. 'Goniopoda' was the first clade of dinosaurs to gather two valid theropod dinosaurs. This order was erected by Charles Drinker Cope in 1866 to encompass *Laelaps* (now known as *Dryptosaurus*; Brusatte et al. 2011) and 'probably' *Megalosaurus*. 'Goniopoda' was, by then, opposed to the 'Orthopoda' consisting of *Scelidosaurus*, *Hylaeosaurus*, *Iguanodon*, and *Hadrosaurus*.

Although the taxa 'Goniopoda' and 'Orthopoda' were used in Matthew and Brown's (1922) classification of theropods in the 20th century, these two groups were abandoned in favor of clades coined by Othniel Charles Marsh by the end of the 19th century. Marsh (1881) first erected the taxon Theropoda to contain the family Allosauridae, initially represented by the genera *Allosaurus*, *Creosaurus*, and *Labrosaurus*. The term 'Theropoda' derived from the old Greek words θηρίον, *thérion* meaning "wild beast, animal", and ποδος, *pous*, *podos* meaning "foot". Theropods, with "beast feet" were, at that time, separated from ornithopods, meaning "bird feet", and sauropods, meaning "reptiles feet", which were both coined by Marsh in 1871 and 1878, respectively. A year after naming the taxon Theropoda, Marsh (1882) already included six 'families' in this clade, nammely Megalosauridae, Zanclodontidae, Amphisauridae,

Labrosauridae, Coeluridae, and Compsognathidae. A few years later, Seeley (1887) used the orientation and morphology of the pubis to divide the clade of Dinosauria into two major groups, the Saurischia and the Ornithischia. Theropods and sauropodomorphs were grouped among saurischian dinosaurs with reptile-like pelvis, whereas ornithischians, with bird-like pelvis, included Stegosauria and Ornithopoda. Ironically, saurischian theropods with beast-like feet and a reptile-like pelvis were those to give rise to birds, instead of the ornithischians with a bird-like pelvis, and the ornithopods with bird-like feet. By the end of the 19th century, four valid theropod clades (Ceratosauridae, Megalosauridae, Compsognathidae, Omithomimidae) as well as two sauropodomorph (Plateosauridae, Anchisauridae) and four unrecognized archosaur clades (i.e., Labrosauridae, Dryptosauridae, Coeluridae, and Hallopidae) were gathered into the clade of Theropoda by Marsh (1895, 1896).

The classification of theropods was markedly affected by the work of Friedrich von Huene (1909, 1914*a*, *b*, 1923, 1926*a*, *b*, 1929, 1932) in the first half of the 20th century. Until 1932, this German paleontologist abandoned the taxon Theropoda and erected two new clades to encompass all saurischian dinosaurs, namely the Coelurosauria and the 'Pachypodosauria'. In most of Huene's classifications, coelurosaurs comprised theropods such as *Coelophysis*, *Ceratosaurus*, *Compsognathus*, *Proceratosaurus*, *Tyrannosaurus*, and *Ornithomimus*, whereas pachypodosaurs included the Carnosauria, consisting of *Megalosaurus*, *Spinosaurus*, and *Allosaurus* (formerly known as *Antrodemus*), as well as the Prosauropoda and the Sauropoda, two clade currently classified among sauropodomorphs. In the 1930s, Huene (1932) slightly changed his view on theropod systematics and abandoned the taxon 'Pachypodosauria'. At that time, saurischian dinosaurs included Coelurosauria, Carnosauria, Prosauropoda, and Sauropoda, and the separation between coelurosaurs and carnosaurs was mostly based on size criteria

(Rauhut 2003*a*). Among carnivorous saurischians, coelurosaurs, indeed, gathered relatively small, slenderly built, predaceous bipeds such as Coelophysidae (formerly known as 'Podokesauridae'), Compsognathidae, and Ornithomimidae, whereas carnosaurs encompassed large, heavily built predators with massive skulls such as Megalosauridae, Spinosauridae, Tyrannosauridae (formerly known as 'Dinodontidae'), and Allosauridae (Huene 1932).

In the beginning of the second half of the 20th century, Alfred Sherwood Romer (1956), in his authoritative book *Osteology of the Reptiles*, proposed a slightly modified version of the saurischian classification. This leading paleontologist separated saurischian dinosaurs into Theropoda and Sauropoda, and included all bipedal saurischians within theropods, namely the Prosauropoda, Coelurosauria, and Carnosauria. Romer (1956), however, followed the size criteria adopted by Huene (1932) and restricted carnosaurs to Teratosauridae (now considered to be a clade of rauisuchian archosaurs; e.g., Benton 1986), Megalosauridae (represented at that time by variate theropods such as *Ceratosaurus*, *Megalosaurus*, *Spinosaurus*, *Allosaurus*, *Carcharodontosaurus*, and *Proceratosaurus*), and Tyrannosauridae. From the 1960s to the beginning of the 1980s, authors working on theropods such as Walker (1964), Colbert (1964), Colbert and Russell (1969), Ostrom (1976*a*), and Russell (1984) did not deviate much from the classification scheme proposed by Romer (1956). Most of them, however, acknowledge that coelurosaurs and carnosaurs were likely to be grades rather than clades (Thulborn 1984). Nevertheless, a few authors like Barsbold (1977), Welles (1984) and Carroll (1988) did abandon the dichotomy between coelurosaurs and carnosaurs, and Barsbold (1977), for instance, included among theropods newly erected clades such as Oviraptorosauria (with Oviraptoridae), Deinonychosauria (with Dromaeosauridae and Troodontidae, formerly known as 'Saurornithoididae'), and Therizinosauria (formerly known as 'Deinocheirosauria').

The development of modern phylogenetic analyses in the early 1980s was a major step in the history of theropod systematic, and results of cladistic analyses radically changed the views on theropod phylogeny. If Thulborn (1984) was the first to investigate theropod interrelationships through a cladistic approach by addressing the systematics of *Archaeopteryx* and other stem-group birds, Gauthier's (1986) leading work on saurischian interrelationships was the first to define the bases of the current phylogenetic classification of non-avian theropods. Based on a cladistic analysis performed on a data matrix of 84 characters, Gauthier (1986) could confirm the monophyly of dinosaurs and corroborated Seeley's idea that Sauropodomorpha and Theropoda were sister-groups among Saurischia. The American paleontologist also recovered Theropoda as a well-supported clade divided into Ceratosauria and Tetanurae, and provided the first phylogenetic definition of theropods: birds and all saurischians that are closer to birds than to sauropodomorphs (Gauthier 1986). He finally recognized a dichotomy between Carnosauria and Coelurosauria among tetanuran theropods, and erected the clade Maniraptora to encompass coelurosaurs more derived than Ornithomimidae. At that time, Ceratosauria contained *Megapnosaurus*, *Coelophysis*, *Dilophosaurus*, and *Ceratosaurus*, carnosaurs included *Allosaurus*, *Acrocanthosaurus* and tyrannosaurids, and non-avian coelurosaurs comprised *Compsognathus*, *Ornitholestes*, and the Ornithomimidae, Caenagnathidae, and Deinonychosauria.

Since the pioneering phylogenetic work of Gauthier (1986), and with the availability of parsimony-based phylogenetic softwares, a large number of authors have investigated theropod interrelationships based on cladistic analyses, resulting in major changes in the theropod systematics. Novas (1992) was the first to include abelisaurids and tyrannosaurids among ceratosaurs and coelurosaurs, respectively (Rauhut 2003*a*), and Holtz (1994) first major

phylogenetic analysis recovered the clade Avetheropoda (erected by Paul 1988) to include Allosauridae and Coelurosauria (Fig. S2-3). The same year, Sereno et al. (1994) found that Megalosauroidea (formerly known as 'Torvosauroidea' and 'Spinosauroidea') formed the sister group of Avetheropoda (also known as 'Neotetanurae') and was divided into Megalosauridae (formerly known as 'Torvosauridae') and Spinosauridae (Fig. S2-3). Two years later, Sereno et al. (1996) found the new clade Allosauroidea, which gathered *Allosaurus*, Sinraptoridae, and Carcharodontosauridae, to be the sister-group of Coelurosauria. Following these preliminary analyses, Sereno's (1997, 1998, 1999) major phylogenetic analyses of dinosaurs allowed to define all main theropod clades such as Neotheropoda, Coelophysoidea, Megalosauroidea, Allosauroidea, Tyrannosauroidea, Ornithomimosauria ('Ornithomimoidea' *sensu* Sereno 1999), Therizinosauroidea, Paraves, and Deinonychosauria (Fig. S2-4).

Subsequent studies on theropod systematics, whose results are summarized by (Holtz 1998), Rauhut (2003*a*), Senter (2007), Carrano and Sampson (2008) and Carrano et al. (2012), allowed to better resolve the relationships of non-avian theropods and to define additional clades such as Noasauridae (Coria and Salgado 1998), Piatnitzkysauridae (Carrano et al. 2012), Megaraptora (Benson et al. 2010), and Proceratosauridae (Rauhut et al. 2010; Figs. S2-3–4). In 2014, the current consensus on non-avian theropod classification is based on the results of the most recent large scaled phylogenetic analyses obtained by Sues et al. (2011) for non-neotheropod Theropoda, Smith et al. (2007) and Ezcurra and Brusatte (2011) for non-averostran Neotheropoda, Pol and Rauhut (2012) and Tortosa et al. (2014) for Ceratosauria, Carrano et al. (2012) for non-coelurosaur Tetanurae, Loewen et al. (2013), Lü et al. (2014) and Porfiri et al. (2014) for Tyrannosauroidea, and Turner et al. (2012), Godefroit et al. (2013*a*) and Choiniere et al. (2014) for non-tyrannosauroid Coelurosauria (Figs. S2-3–4).

As noted by Turner et al. (2012), the theropod clade is now comprised of numerous well-supported 'family' or 'super-family'-level subclades that forms a pectinate, ladder-like organization, each rungs corresponding to a node-based clade that has not always received a name. Although the relationships between most theropod clades are currently well-understood, many aspects of theropod systematics remain controversial. Currently, debate mostly occurs in the phylogenetic placement of *Eoraptor* and/or herrerasaurids within non-theropod saurischians (e.g., Langer and Benton 2006; Alcober and Martinez 2010; Ezcurra 2010; Martinez et al. 2011; Sereno et al. 2013) or at the base of the theropod clade (Nesbitt et al. 2009; Ezcurra and Brusatte 2011; Nesbitt 2011; Sues et al. 2011; Langer and Ferigolo 2013; Fig. S2-3), and in the monophyly/paraphyly of Coelophysoidea (i.e., Coelophysidae + Dilophosauridae; e.g., Tykoski 2005; Yates 2005; Ezcurra and Cuny 2007; Ezcurra and Novas 2007; Smith et al. 2007; Nesbitt et al. 2009; Ezcurra and Brusatte 2011; Xing 2012) and Deinonychosauria (e.g., Senter 2011; Turner et al. 2012; Godefroit et al. 2013*a*, *b*; Choiniere et al. 2014; Foth et al. 2014; Tsuihiji et al. 2014). Recent debate also occurred in the position of megaraptorans within neovenatorid allosauroids (Benson et al. 2010; Carrano et al. 2012) or among tyrannosauroid coelurosaurs (Novas et al. 2013; Porfiri et al. 2014; Fig. S2-3).

Origin, evolution, and current classification

First Theropods

Theropoda can be defined as a stem-based taxon containing *Passer domesticus* and all taxa sharing a more recent common ancestor with it than with *Cetiosaurus oxoniensis* (Holtz and Osmólska 2004; Holtz 2012). Regardless of the inclusion of *Eoraptor* and herrerasaurids within

Theropoda, the oldest theropod remains come from the mid-Carnian (Early Late Triassic; ~235 Ma) of Argentina (Fig. S2-1). Similar to *Eoraptor lunensis* (Sereno et al. 2013; Fig. S2-5A) and the herrerasaurids *Herrerasaurus ischigualastensis* (Sereno and Novas 1994; Fig. S2-5B) and *Sanjuansaurus gordilloi* (Alcober and Martinez 2010), the oldest unquestionably theropod taxon, *Eodromaeus murphi* (Martinez et al. 2011), is from the Ischigualasto Formation of San Juan Province. *Eodromaeus*, *Eoraptor* and herrerasaurids were small to medium sized (1-4m long; (Brusatte et al. 2010*c*) bipedal saurischians with relatively elongated skulls and ventrodorsally high cranium. These primitive saurischians retained the ancestral dinosauromorph habit of obligate bipedality as well as the ziphodont dentition present in more primitive archosauriforms (Holtz 2012), so that they have been considered as carnivorous dinosaurs. However, *Eoraptor*, recently interpreted to be a basal sauropodomorph (Martinez et al. 2011; Sereno et al. 2013), bears some constricted crowns with pointed denticles leading to think that this primitive saurischian might have been omnivore (Sereno et al. 2013).

Tawa hallae (Nesbitt et al. 2009; Fig. S2-5C) and *Daemonosaurus chauliodus* (Sues et al. 2011) from the Norian and Rhaetian of New Mexico, respectively, are currently recovered between *Eodromaeus* and neotheropods (Fig. S2-3). Unlike *Eoraptor*, these two recently reported taxa possess the short subnarial gap present in basal neotheropods and an antorbital fossa restricted to the vicinity of the antorbital fenestra, as seen in *Herrerasaurus* (Nesbitt et al. 2009; Sues et al. 2011; Langer 2014). This condition, however, contrasts with the expanded antorbital fossa of *Eoraptor* and *Eodromaeus*. *Daemonosaurus* is particular in having a short and tall skull bearing procumbent premaxillary and dentary teeth (Sues et al. 2011). *Tawa* is closer to coelophysoids than *Daemonosaurus* and other primitive theropods in having a much more elongated snout and a more gracile body. Yet, *Tawa* shares with *Daemonosaurus* the greatly

enlarged maxillary teeth as well as a pneumatic fossae (pleurocoels) in the cervical vertebrae (Nesbitt et al. 2009; Sues et al. 2011).

Coelophysoidea and Dilophosauridae

Neotheropoda, the least inclusive clade containing *Coelophysis bauri* and *Passer domesticus* (Martinez et al. 2011; Allain et al. 2012), currently comprises theropods more derived than *Tawa* (Nesbitt et al. 2009; Nesbitt 2011; Sues et al. 2011). Among many derived features, neotheropods are characterized by an intramandibular joint, a hinge between the dentary and the postdentary bones (Holtz 2012). Current consensus on basal theropod phylogeny suggests that neotheropods encompass a first primitive branch referred as Coelophysoidea and a second more derived clade named Dilophosauridae (Fig. S2-3). The latter is thought to belong to Coelophysoidea by some authors (e.g., Carrano et al. 2005; Tykoski 2005; Ezcurra and Cuny 2007; Ezcurra and Novas 2007; Xing 2012), yet results of the most recent cladistic analyses recovered Dilophosauridae as a more derived clade of neotheropods, and the sister-group of Averostra (e.g., Smith et al. 2007; Nesbitt et al. 2009; Ezcurra and Brusatte 2011; Sues et al. 2011).

Coelophysoidea (*sensu* Ezcurra and Brusatte 2011) encompasses small to medium sized theropods (2-6m long) with slender skulls, and lightly built, gracile, and elongated bodies characterized by elongated cervical centra (Tykoski and Rowe 2004; Brusatte et al. 2010*c*; Holtz 2012). The first coelophysoids are already present in the Norian of Europe (*Procompsognathus*, *Camposaurus*; Sereno and Wild 1992; Rauhut and Hungerbühler 1998; Ezcurra and Brusatte 2011) and North America (*Coelophysis*; Fig. S2-6A). Although coelophysoids form the first radiation of theropod, they were the non-dominant terrestrial predators in the Late Triassic as

larger carnivores such as ornithosuchids, rauisuchians and phytosaurs were more abundant at that time (Brusatte et al. 2010*c*; Holtz 2012). Unlike these basal archosaurs, coelophysoids survived the Triassic/Jurassic boundary, and Jurassic coelophysoids are known from the Hettangian–Pliensbachian of South Africa (*Megapnosaurus rhodesiensis*) and North America (*Megapnosaurus kayentakatae*). *Megapnosaurus rhodesiensis* is sometimes known as '*Syntarsus*' *rhodesiensis* by some authors. However, as the genus name *Syntarsus* was already given to a beetle, the entomologists Ivie et al. (2001) replaced it by *Megapnosaurus*. *Zupaysaurus rougieri* (Arcucci and Coria 2003; Ezcurra 2007) and *Liliensternus liliensterni* (Huene 1934) from the Norian of Argentina and Germany, respectively, have been formerly classified as coelophysoids, but are currently seen as more derived neotheropod positioned between Coelophysoidea and Dilophosauridae (Nesbitt et al. 2009; Ezcurra and Brusatte 2011; Sues et al. 2011).

Dilophosauridae forms a poorly supported clade containing medium to large sized (4-7m long) theropods such as *Dilophosaurus wetherilli* (Welles 19841; Fig. S2-6B) and *Dracovenator regenti* (Yates 2005) from the Early Jurassic of North America and South Africa, respectively. Similar to coelophysoids, they possess a subnarial gap and anteriormost maxillary teeth facing anteroventrally, yet they share with averostrans a promaxillary fenestra and a reduced number of maxillary teeth (Holtz 2012). *Sinosaurus triassicus* (Hu 1993; Xing 2012) and *Cryolophosaurus ellioti* (Smith et al. 2007) from the Early Jurassic of China and Antarctica, respectively, were formerly interpreted as dilophosaurids and are now classified among basal tetanurans (Benson 2010*a*; Carrano et al. 2012; Xing 2012). The cranial crest of *Dilophosaurus*, *Cryolophosaurus*, and *Sinosaurus* seems, therefore, to be convergently acquired in these taxa and has evolved independently in dilophosaurids and basal tetanurans (Xing 2012). Although relatively common

and showing a high diversity in the Jurassic, coelophysoids and dilophosaurids became extinct at or near the end of Early Jurassic (Carrano and Sampson 2004; Ezcurra and Novas 2007).

Ceratosauria

Averostra, the least inclusive clade containing *Ceratosaurus nasicornis* and *Passer domesticus* (Allain et al. 2012), radiated into two main clades, namely the Ceratosauria and Tetanurae (Fig. S2-3). Basal averostrans are characterized by the oreinirostral condition of their head which is defined as a transversally narrow, and dorsoventrally high skull (Holtz 2012). The first averostrans are known from the Early Jurassic and are distributed widely across the globe as their remains have been found in China (*Sinosaurus*; Xing 2012), Antarctica (*Cryolophosaurus*; Smith et al. 2007), Africa (*Berberosaurus*; Allain et al. 2007), and possibly Europe ('*Saltriosaurus*'; Dal Sasso 2003; Benson 2010*b*). Ceratosaurs currently include a basal clade informally referred as 'elaphrosaurs', a more derived family named Ceratosauridae, and a major clade known as the Abelisauroidea (Carrano and Sampson 2008; Pol and Rauhut 2012; Tortosa et al. 2014). 'Elaphrosaurs' is a poorly known group of primitive ceratosaurs gathering theropods such as *Elaphrosaurus bambergi* from the Kimmeridgian–Tithonian of Tendaguru (Carrano and Sampson 2008), *Limusaurus inextricabilis* from the Oxfordian of China (Xu et al. 2009*a*; Fig. S2-6C), and *Spinotropheus gauthieri* from the Neocomian of Niger (Carrano and Sampson 2008). *Limusaurus*, the only elaphrosaur known from cranial material, possesses an edentulous skull and a body convergent with this of ornithomimids (Fig. S2-6C). Although recovered as an elaphrosaurid in all recent cladistic analyses (Pol and Rauhut 2012; Tortosa et al. 2014), *Limusaurus* may however be a noasaurid abelisauroid (Stiegler et al. 2014).

Ceratosauridae only contains two taxa, namely *Ceratosaurus* from the Kimmeridgian–Tithonian of North America (*C. nasicornis*; Gilmore 1920; Madsen and Welles 2000; Carrano and Sampson 2008; Fig. S2-7A) and Europe (*Ceratosaurus* sp.; (Mateus and Antunes 2000; Malafaia et al. 2014), and *Genyodectes serus* from the Aptian–Albian of Argentina (Rauhut 2004*a*). Ceratosaurids were large theropods (6-8 m long) characterized by strongly elongated maxillary teeth longer than the dentary height, and at least *Ceratosaurus* showed a fused nasal horn, two lacrimal horns, and osteoderms on the back (Marsh 1884; Gilmore 1920; Madsen and Welles 2000). Along with megalosaurids and allosaurids, ceratosaurids were apex predators in the Late Jurassic (Kimmeridgian–Tithonian) ecosystems of Europe and North America.

Abelisauroidea falls into two divergent subclades, the Noasauridae and Abelisauridae (Carrano and Sampson 2008; Pol and Rauhut 2012; Tortosa et al. 2014; Fig. S2-3). Noasaurids form a relatively poorly known group of small, slender abelisauroids with long forelimbs bearing well-developed claws (Agnolin and Chiarelli 2010). They are only known from the Cretaceous and may have already been present in the Barremian–early Aptian of Argentina (*Ligabueino*; Tortosa et al. 2014). Noasaurids are, however, well-known in the latest part of the Cretaceous in Gondwana as they have been unearthed in Maastrichtian deposits in Argentina (*Noasaurus*; Bonaparte and Powell 1980), Madagascar (*Masiakasaurus*; Carrano et al. 2002, 2011) and India (*Laevisuchus*; Huene and Matley 1933). *Masiakasaurus knopfleri* (Fig. S2-7B), the best known noasaurid taxon, shows the peculiarity of having procumbent dentary teeth with a constriction at the crown base and flutes on the lingual surface.

Abelisauridae is a well-supported clade of medium to large (5-9 m long) stubby-armed theropods with short rounded snout, and deep, heavily sculptured skulls bearing bony protuberances and poorly recurved teeth (Carrano and Sampson 2008; Brusatte 2012; Holtz

2012; Pol and Rauhut 2012). The inclusion of *Eoabelisaurus mefi* (Pol and Rauhut 2012) from the Aalenian-Bajocian of Patagonia within abelisaurids is subject of debate (Pol and Rauhut 2012; Tortosa et al. 2014) and the first definitive Abelisauridae, *Kryptops palaios*, comes from the Aptian–Albian of North Africa (Sereno and Brusatte 2008). Abelisaurids were the non-dominant predators in Gondwanian ecosystems in the Early Cretaceous and early Late Cretaceous of South America and North Africa, as they were supplanted by the larger spinosaurids and carcharodontosaurids during that time (Holtz 2012). Following the extinction and/or decline of Spinosauridae and Carcharodontosauridae after the Cenomanian-Turonian transition, abelisaurids became, however, apex predators in Africa, Europe, and South America in the latest part of the Cretaceous. The best-known taxa are from the Campanian-Maastrichtian of Europe and Gondwana and include *Majungasaurus crenatissimus* (Sampson et al. 1998; Sampson and Witmer 2007; Fig. S2-7C) from Madagascar, *Aucasaurus garridoi* (Coria et al. 2002) and *Carnotaurus sastrei* (Bonaparte et al. 1990; Carabajal 2011) from Argentina, *Rajasaurus narmadensis* (Wilson et al. 2003) from India, and *Arcovenator escotae* (Tortosa et al. 2014) from France.

Megalosauroidea

Tetanurae, the most inclusive clade containing *Passer domesticus* but not *Ceratosaurus nasicornis* (Allain et al. 2012), are characterized by an antorbital tooth row, the presence of a maxillary fenestra piercing the lateral wall of the maxilla, and interlocking tail vertebrae (Gauthier 1986; Benson 2010*a*; Carrano et al. 2012). Several relatively complete basal tetanurans are known from the Early and Middle Jurassic of China and Antarctica (i.e., *Sinosaurus*, *Cryolophosaurus*, and *Monolophosaurus*). These primitive tetanurans are recovered between basal averostrans and the recent clade Orionides which comprises two major radiations, the

Megalosauroidea and Avetheropoda (Carrano et al. 2012). The first one, Megalosauroidea, currently gathers three subclades, namely the Piatnitzkysauridae, Megalosauridae, and Spinosauridae (Fig. S2-3). Piatnitzkysauridae is the sister group of Megalosauria, divided into Megalosauridae and Spinosauridae. Piatnitzkysaurids currently comprise medium sized (5-6m long) American forms such as *Marshosaurus bicentesimus* (Madsen 1976*a*; Fig. S2-8A) from the Kimmeridgian-Tithonian of North-America, and *Piatnitzkysaurus floresi* (Bonaparte 1986; Rauhut 2004*b*) and *Condorraptor currumili* (Rauhut 2005) from the Bajocian–Callovian of Argentina. These basal megalosauroids are characterized by a maxilla with a short anterior ramus and vertically ridged interdental plates (Carrano et al. 2012).

Megalosauridae is a diversified clade of theropods restricted to the Middle to Late Jurassic, which suggests that they went extinct at the Jurassic-Cretaceous boundary (Carrano et al. 2012). Megalosaurids are medium to very large (4-10m long) theropods showing a relatively elongated skull lacking of cranial protuberances, and powerful arms bearing a large claw at digit one (Carrano et al. 2012). They are already known in the Bajocian of England (*Magnosaurus*, *Duriavenator*; Benson 2008*a*, 2010*b*) and include forms from the Bajocian-Callovian of England and France (*Megalosaurus*, Fig. S2-8B; *Eustreptospondylus*, *Dubreuillosaurus*; Allain 2002; Sadleir et al. 2008; Benson 2010*a*), the Kimmeridgian-Tithonian of North-America and Portugal (*Torvosaurus*; Britt 1991; Hendrickx and Mateus 2014*a*), the Late Jurassic of China (*Leshansaurus*; Li et al. 2009), and the Middle/Late? Jurassic of Africa (*Afrovenator*; Sereno et al. 1996). *Sciurumimus albersdoerferi*, a possible megalosaurid from the Kimmeridgian of Germany, is the most complete megalosauroid discovered so far (Rauhut et al. 2012). It is also the most primitive theropod that preserved direct evidence of filamentous integument, indicating

that protofeathers were already covering some tetanurans early in their evolution (Rauhut et al. 2012).

Spinosauridae, the sister group of Megalosauridae, is a very-well supported clade of overspecialized theropods united by an elongated crocodile-like skull, spatulated snout with sigmoid alveolar margins, fluted conical teeth with minute or no denticles, and an hypertrophied manual ungual (Charig and Milner 1997; Sereno et al. 1998; Sues et al. 2002). Such derived anatomical features, associated with direct evidence of gut contents, suggest that spinosaurids were, at least partially, piscivorous theropods, feeding also on dinosaurs and pterosaurs (Charig and Milner 1997; Buffetaut et al. 2004). Spinosaurids were large to very large theropods (8-17 m long) and include the largest terrestrial predators discovered hitherto. They were also characterized by elongated neural spines which evolved into a bony sail in some members (e.g., *Spinosaurus*, *Ichthyovenator*; Stromer 1915; Smith et al. 2006; Allain et al. 2012). Spinosaurid teeth seem to be already present in the Kimmeridgian – Tithonian of Tanzania (Buffetaut 2011; for a different opinion see Rauhut 2011), yet the first definitive spinosaurid is currently *Baryonyx walkeri* (Fig. S2-8C) from the Barremian of England and Portugal (Charig and Milner 1986; Mateus et al. 2011). Spinosauridae are also known from the Aptian-Albian of Niger (*Suchomimus*; Sereno et al. 1998) and Brazil (*Angaturama*, *Irritator*; Kellner and Campos 1996; Sues et al. 2002) and the most recent spinosaurid, *Spinosaurus aegyptiacus*, comes from the Cenomanian of North Africa (Stromer 1915; Dal Sasso et al. 2005).

Allosauroidea

Avetheropoda (also known as 'Neotheropoda'; e.g., Sereno et al. 1994; Sereno 1999; Allain et al. 2012), the least inclusive clade containing *Allosaurus fragilis* and *Passer domesticus*

(Allain et al. 2012), comprises two major subclades: the Allosauroidea, and the Coelurosauria (Fig. S2-3). Allosauroids were one of the dominant terrestrial predators in the Late Jurassic, Early Cretaceous, and early Late Cretaceous worldwide. Allosauroids are currently divided into four subclades: the Metriacanthosauridae, Allosauridae, Neovenatoridae, and Carcharodontosauridae (Fig. S2-3). Metriacanthosauridae (formerly known as the 'Sinraptoridae') is the most primitive one and mostly gathers forms from the Early and Late Jurassic of China such as *Sinraptor dongi* (Currie and Zhao 1993*a*), '*Yangchuanosaurus*' *hepigensis*, and *Yangchuanosaurus shangyouensis* (Dong et al. 1983). These taxa, which are known from very well-preserved and nearly complete skeletons, share a maxilla with a promaxillary fenestra larger than the maxillary fenestra, a pneumatic recess on the lateral surface of the ascending ramus, and the absence of an anterior ramus. *Metriacanthosaurus parkeri* (Huene 1923) from the Oxfordian of England is the only definitive non-Asian metriacanthosaurids reported hitherto (although *Lourinhanosaurus antunesi* from the Kimmeridgian-Tithonian of Portugal may also pertain to this clade; see Benson 2010*a*), and *Siamotyrannus isanensis* (Buffetaut et al. 1996) from the Barremian–Aptian of Thailand is, so far, the only metriacanthosaurid that lived in the Cretaceous (Carrano et al. 2012).

Allosauridae, a more derived clade of allosauroids and the sister-clade of Carcharodontosauria, is a small group of Kimmeridgian-Tithonian tetanurans comprising only four North American and Portuguese species, namely *Allosaurus fragilis* (Gilmore 1920; Madsen 1976*b*; Chure 2000; Loewen 2010; Fig. S2-9A), *Allosaurus europaeus* (Mateus et al. 2006), *Allosaurus* '*jimmadseni*' (Chure 2000; Loewen 2010), and *Saurophaganax maximus* (Chure 1995). Allosaurids were medium to large (8-10m long) theropods and one of the dominant predators in the Late Jurassic ecosystems of North America and Europe.

Carcharodontosauria falls into two subclades, the Neovenatoridae and the Carcharodontosauridae (Carrano et al. 2012). It is argued whether Neovenatoridae is a monospecific clade including the taxon *Neovenator salerii* (Brusatte et al. 2008; Fig. S2-9B) from the Hauterivian–Barremian of England, or a more inclusive clade gathering *Neovenator* and megaraptorans (Benson et al. 2010; Carrano et al. 2012; Novas et al. 2013; Zanno and Makovicky 2013; Porfiri et al. 2014). According to Benson et al. (2010), neovenatorids are united by postcranial synapomorphies such as a short and broad scapula and a pneumatic ilium. The recent discovery of a relatively well-preserved megaraptoran with cranial material seems, however, to provide better support for a placement of megaraptorans within Tyrannosauroidea, and megaraptorans are, therefore, described in the next paragraph.

Carcharodontosauridae, on the other hand, form a well-supported clade comprising medium to very large theropods (6-14m long) characterized by a massive and deep skull with sculptured facial bones, and cranial protuberances on the lacrimals and postorbitals. The first carcharodontosaurid is currently *Veterupristisaurus milneri* (Rauhut 2011) known from caudal vertebrae from the Kimmeridgian-Tithonian of Tanzania. In the Cretaceous, carcharodontosaurids became a diversified clade of allosauroids distributed worldwide. Due to their very large sized, carcharodontosaurids were at the apex of the food chain in most 'mid' Cretaceous ecosystems. The best preserved carcharodontosaurids are *Concavenator corcovatus* (Ortega et al. 2010) from the Barremian of Spain, *Acrocanthosaurus atokensis* (Harris 1998; Currie and Carpenter 2000; Eddy and Clarke 2011) and *Tyrannotitan chubutensis* (Canale et al. 2014) from the Aptian-Albian of North America and Argentina, respectively, *Carcharodontosaurus saharicus* (Rauhut 1995; Brusatte and Sereno 2007) from the Cenomanian of North Africa, *Giganotosaurus carolinii* (Coria and Salgado 1995; Calvo and Coria 1998; Fig.

S2-9C) and *Mapusaurus roseae* (Coria and Currie 2006) from the Cenomanian-?Santonian of Argentina, and *Shaochilong maortuensis* (Brusatte et al. 2010*b*) from the Turonian of China (Carrano et al. 2012). The carcharodontosaurid lineage may have extended to the latest part of the Cretaceous in South America as material assigned to Carcharodontosauridae have been reported from the Campanian-Maastrichtian of Brazil (e.g., Azevedo et al. 2013).

Basal Coelurosauria and Tyrannosauroidea

Coelurosauria, the most inclusive clade containing *Passer domesticus* Linnaeus 1758 but not *Allosaurus fragilis*, *Sinraptor dongi*, and *Carcharodontosaurus saharicus* (Godefroit et al. 2013*a*; Novas et al. 2013), is a also well-supported clade that contains a large diversity of herbivorous and carnivorous non-avian theropods as well as living birds. Coelurosaurs are, thereby, the most morphologically diverse theropod clade, and the only one to survive the K–Pg boundary. Members of this group differ from other more basal theropods by possessing an enlarged brains, a well-developed medial shelf on the maxilla, long and slender forearms and hands, and amphiplatyan cervical and anterior dorsal vertebrae (Holtz 2012; Turner et al. 2012). Coelurosaur interrelationships is complex and the clade include several well-separated coelurosaur groups nested in different subclades (Figs. S2-3–4). The oldest definite coelurosaurs are known from the Bathonian of Eurasia, and older coelurosaur remains may already come from the Early Jurassic of China (Zhao and Xu 1998; Barrett 2009). A current consensus on theropod systematics agrees that the basalmost clade of coelurosaurs is the Tyrannosauroidea (Fig. S2-3). There are, however, several coelurosaur taxa that fall outside Tyrannosauroidea, at the very base of Coelurosauria. These include *Aorun zhaoi* (Choiniere et al. 2014) and *Zuolong sallei* (Choiniere et al. 2010*a*) from the Oxfordian-Callovian of China, *Tanycolagreus topwilsoni* from the Kimmeridgian-Tithonian of Wyoming, *Tugulusaurus faciles* from the ?Valanginian–Albian

of China (Rauhut and Xu 2005), and *Bicentenaria argentina* from the Cenomanian of Argentina (Novas et al. 2012).

Due to the iconic status gained by *Tyrannosaurus rex* and the numerous tyrannosauroid specimens, tyrannosauroids are certainly the most studied and best known non-avian theropods (Brusatte et al. 2010*a*). The recent discovery of a large number of basal and derived tyrannosauroids increased dramatically the diversity of this group whose evolution is currently relatively well-understood. Tyrannosauroids encompass small to very large-bodied theropods (3-13 m long) characterized by premaxillary teeth significantly smaller than anterior maxillary teeth and with U-shaped cross-section, small premaxillae with elongated nasal and maxillary (subnarial) processes, and fused nasals (Holtz 2004, 2012; Brusatte et al. 2010*a*). The discovery of several well-preserved tyrannosauroids from China has revealed that the body of small to large primitive forms such as *Dilong paradoxus* (Xu et al. 2004) and *Yutyrannus huali* (Loewen et al. 2013; Lü et al. 2014; Porfiri et al. 2014) were covered with filamentous integument. Recent phylogenetic analyses of Tyrannosauroidea suggest that three main subclades independently radiated, namely the Proceratosauridae, Megaraptora, and Tyrannosauridae (Fig. S2-3).

The first and most primitive one, the Proceratosauridae, comprises small-bodied tyrannosauroids characterized by elaborated cranial crests (Brusatte et al. 2010*a*; Fig. S2-10A). Proceratosaurids originated in the Middle Jurassic of Eurasia as the oldest taxa are *Proceratosaurus bradleyi* (Rauhut et al. 2010) and *Kileskus aristotocus* (Averianov et al. 2010) from the Bathonian of England and Siberia, respectively. Proceratosaurids are also known from the Oxfordian of China (*Guanlong wucaii*; Xu et al. 2006; Fig. S2-10A), and the more recent member is currently *Sinotyrannus kazuoensis* (Ji et al. 2009) from the Albian of China (Brusatte et al. 2010*a*).

Primitive non-proceratosaurid tyrannosauroids encompass several small to medium sized forms from the Late Jurassic of Europe (*Aviatyrannis jurassica, Juratyrant langhami*; Rauhut 2003*b*; Benson 2008*b*; Brusatte and Benson 2013) and North America (*Stokesosaurus clevelandi*; Benson 2008*b*; Brusatte and Benson 2013), and the Early Cretaceous of China (*Dilong paradoxus*, *Yutyrannus huali*, *Xiongguanlong baimoensis*; Xu et al. 2004, 2012; Li et al. 2010). Based on the recent description of a relatively complete juvenile specimen of *Megaraptor namunhuaiquii*, megaraptorans seem to evolve from primitive tyrannosauroids more derived than proceratosaurids (Novas et al. 2013; Porfiri et al. 2014). Megaraptorans are gracile theropods characterized by an elongated skull, and elongated and robust forelimbs with enlarged thumb claws on digits I and II (Benson et al. 2010; Porfiri et al. 2014). They were distributed widely across the globe as they encompass *Fukuiraptor kitadaniensis* (Azuma and Currie 2000; Currie and Azuma 2006) from the Barremian of Japan, *Australovenator wintonensis* (Hocknull et al. 2009) from the Albian of Australia, *Aerosteon riocoloradensis* (Sereno et al. 2008) from the Campanian of North Argentina, and possibly *Eotyrannus lengi* (Hutt et al. 2001; Fig. S2-10B) from the Barremian of England. Megaraptorans seem also to extend to the end of the Cretaceous, with *Orkoraptor burkei* (Novas et al. 2008) from the Maastrichtian of Patagonia as the most recent member of this clade.

Tyrannosaurids are the most derived and the largest tyrannosauroids. Within Tyrannosauroidea, they show the derived features of having a large body size (6-12m long), robust and broad skulls with powerful jaws bearing incrassate teeth with long roots, and reduced forelimbs ended by two fingers (the third digit is vestigial and does not appear as a finger; Currie 2003; Holtz 2004, 2012; Brusatte et al. 2010*a*). Tyrannosaurids were apex predators in all Late Cretaceous ecosystems of North America and Asia. They were hypercarnivores and were able to

produce extremely powerful bite forces capable of crushing bones (Erickson et al. 1996; Bates and Falkingham 2012). Tyrannosaurids also possessed a higher degree of stereoscopic vision than other non-avian theropods, and their olfactory ratios is particularly high, suggesting a keener sense of smell (Stevens 2006; Witmer and Ridgely 2009; Zelenitsky et al. 2009). Studies have shown that they had accelerated grow rates and underwent important changes during ontogeny (Carr 1999; Erickson et al. 2004; Horner and Padian 2004). The best known tyrannosaurids are from the Campanian–Maastrichtian of Asia and North-America and include *Albertosaurus sarcophagus*, *Gorgosaurus libratus*, *Daspletosaurus torosus*, and *Tyrannosaurus rex* (Fig. S2-10C) from USA and Canada (e.g., Russell 1970; Molnar 1991; Brochu 2003; Currie 2003), and *Alioramus altai* and *Tarbosaurus baatar* from Mongolia (e.g., Hurum and Sabath 2003; Tsuihiji et al. 2011; Brusatte et al. 2012).

Compsognathidae and Ornithomimosauria

All recent large scaled cladistic analyses recovered Compsognathidae and Ornithomimosauria as the second and third basalmost clades of coelurosaurs, respectively (Csiki et al. 2010; Senter 2011; Turner et al. 2012; Godefroit et al. 2013*a*; Choiniere et al. 2014; Fig. S2-4). Compsognathids are characterized by a small body size (1-2.5m long), gracile and slender body, and elongated skull with slender jaws bearing ziphodont teeth (Fig. S2-11A). Given the fact that they mostly include immature individuals retaining a primitive and unspecialized anatomy, Compsognathidae have sometimes been considered as a paraphyletic clade, and some compsognathid taxa are recovered outside this clade in the phylogenetic analyses of some authors (e.g., Butler and Upchurch 2007; Godefroit et al. 2013*a*; Choiniere et al. 2014). Compsognathids typically include *Juravenator starki* (Chiappe and Göhlich 2010) and *Compsognathus longipes* (Bidar et al. 1972; Ostrom 1978; Peyer 2006; Fig. S2-11A) from the

Kimmeridgian-Tithonian of Germany and France, *Scipionyx samniticus* (Dal Sasso and Maganuco 2011) from the Albian of Italy, and *Huxiagnathus orientalis* (Hwang et al. 2004), *Sinocalliopteryx gigas* (Ji et al. 2007*a*), and *Sinosauropteryx prima* (Currie and Chen 2001; Ji et al. 2007*b*) from the Neocomian of China. Compsognathid feeding behavior is the best known among non-avian theropods, as stomach contents are preserved in both specimens of *Compsognathus* (Bidar et al. 1972; Ostrom 1976*a*; Evans 1994; Peyer 2006), *Huxiagnathus* (Hwang et al. 2004), *Scipionyx* (Dal Sasso and Maganuco 2011), and two specimens of *Sinosauropteryx* (Currie and Chen 2001; Ji et al. 2007*b*) and *Sinocalliopteryx* (Xing et al. 2012). These direct evidences reveal the fact that compsognathids ingested gastroliths and had an extremely diverse diet composed of fish, lizards, non-avian theropods (dromaeosaurids), primitive birds, and mammals. Similar to more basal tetanurans, evidences of filamentous integument in some exceptionally well-preserved compsognathids such as *Sinosauropteryx* (Currie and Chen 2001) and *Juravenator* (Chiappe and Göhlich 2010) suggest that protofeathers partially or extensively covered the body of these basal coelurosaurs. A recent study on the fossilized melanosomes in *Sinosauropteryx* has also revealed that the tail of this animal had stripes which exhibited chestnut to rufous (reddish-brown) tones (Zhang et al. 2010).

Maniraptoriformes, a node-based clade containing *Passer domesticus*, *Ornithomimus edmontonicus* and all their descendants (or the least inclusive clade containing *Passer domesticus* and *Ornithomimus edmontonicus*; Turner et al. 2012), mostly include herbivorous theropods that are partially or fully edentulous and/or possess reduced lanceolate crowns, and only some derived maniraptoriforms (i.e., dromaeosaurids) were reversely carnivorous (Holtz 2012). The first radiation of fully herbivorous theropods are ornithomimosaurs. The latter are small to very large (2-10m long) lightly built ostrich-like theropods characterized by a low and delicate skull,

slender neck, elongated forehands bearing three non-raptorial clawed fingers, and long powerful legs adapted for fast runs (Russell 1972; Makovicky et al. 2004; Kobayashi and Barsbold 2005*a*; Fig. S2-11B). The jaws of basal ornithomimosaurs bear a large number of small conical teeth, yet intermediate taxa possess small teeth restricted to the anterior extremity of the dentary and derived forms are fully edentulous and possess a rhamphotheca (some with columnar structures used as a filter-feeding system; Norell et al. 2001; for an alternative hypothesis, see Barrett 2005). Some derived ornithomimosaurs (ornithomimids) were the first theropods to possess both filamentous protofeathers and long shafted feathers (pennibrachium) on the forearms, forming wings (Zelenitsky et al. 2012). Ornithomimosaurs originated in the earliest part of the Cretaceous and the earliest member of this clade is currently *Nqwebasaurus thwazi* from the Berriasian–Valanginian of South Africa (Choiniere et al. 2012). *Pelecanimimus polyodon* (Pérez-Moreno et al. 1994) from the Hauterivian of Spain is, however, often seen as the basalmost taxon of Ornithomimosauria. Non-ornithomimid ornithomimosaurs with toothed lower jaws are mostly known from the Valanginian-Albian of China like *Hexing qingyi* (Liyong et al. 2012), *Beishanlong grandis* (Makovicky et al. 2010), *Shenzhousaurus orientalis* (Ji et al. 2003), and *Harpymimus okladnikovi* (Kobayashi and Barsbold 2005*b*). Edentulous ornithomimosaurs, including ornithomimids, are only known from the Upper Cretaceous of Asia and North America, and the best known taxa are *Garudimimus brevipes* (Kobayashi and Barsbold 2005*a*) and *Sinornithomimus dongi* (Kobayashi and Lü 2003) from the early Late Cretaceous of China, *Ornithomimus edmontonicus* and *Struthiomimus altus* (Russell 1972) from the Campanian-Maastrichtian of Canada, and *Gallimimus bullatus* (Osmólska et al. 1972; Fig. S2-11B) from the Maastrichtian of Mongolia.

Therizinosauria, Alvarezsauroidea and Oviraptorosauria

Maniraptora forms a stem-based clade containing *Passer domesticus* and all coelurosaurs closer to it than to *Ornithomimus edmontonicus* (or the most-inclusive clade containing *Passer domesticus* but not *Ornithomimus edmontonicus*; Turner et al. 2012). Maniraptorans are characterized by a well-developed lateral process of the quadrate, a large bony sternum with ossified sternal plates, and a semilunate carpal (Holtz 2012; Turner et al. 2012). Similar to ornithischians, many maniraptorans convergently acquired a pubis pointing backwards (Holtz 2012). *Ornitholestes hermanni* (Osborn 1903; Carpenter et al. 2005; Fig. S2-11C) from the Upper Jurassic of North America is typically considered to be the basalmost maniraptoran in the latest cladistic analyses, and the basalmost clade of Maniraptora is the Alvarezsauroidea (Fig. S2-4). Alvarezsauroids were small (1-2.5 m long) coelurosaurs characterized by a gracile and low skull with large cranial openings, elongated rostrum, and slender jaws bearing a large number of teeth that are at least, for some of them, lanceolate (Fig. S2-12A). The forelimbs of alvarezsauroids bear three fingers in which digit II and III are reduced in size and were even lost in some derived taxa (Longrich and Currie 2009*a*; Choiniere et al. 2010*b*; Xu et al. 2011*a*; Holtz 2012). The basalmost member is *Haplocheirus sollers* from the Oxfordian of China, and all alvarezsauroids more derived than *Haplocheirus* belong to Alvarezsauridae (Choiniere et al. 2010*a*). Alvarezsaurids are restricted to the Late Cretaceous of North-America, South-America, Asia, and Europe. They comprise taxa with a large number of minute and lanceolate crowns, short forelimbs bearing a single or much larger thumb with a massive claw, a pubis oriented backward, and elongated hind limbs adapted for cursioriality. The best known members are *Patagonykus puertai* (Novas 1997) from the Turonian-Coniacian of Argentina, *Albertonykus borealis* (Longrich and Currie 2009*a*) from the Maastrichtian of Canada, and the parvicursorines *Mononykus olecranus* (Perle et al. 1993, 1994), *Shuvuuia deserti* (Chiappe et al. 1998; Suzuki et

al. 2002; Fig. S2-12A) and *Ceratonykus oculatus* (Alifanov and Barsbold 2009) from the Campanian-Maastrichtian of Mongolia. Similar to more primitive tetanurans, alvarezsauroids such as *Shuvuuia* possessed filamentous integuments (Schweitzer et al. 1999).

Therizinosaurs are small to very large (2-10m long) 'prosauropod'-like theropods characterized by a small head bearing reduced and basally constricted crowns, an elongated neck, long and robust arms terminated by large claws, broad abdomen and pelvis, and a relatively vertical position of the body (Clark et al. 2004; Zanno 2010*a*; Fig. S2-12B). Therizinosaurs strictly inhabited North America and Asia in the Cretaceous. The most primitive member is currently *Falcarius utahensis* (Zanno 2006, 2010*b*) from the Barremian of Utah. *Jianchangosaurus yixianensis* (Pu et al. 2013) and *Beipiaosaurus inexpectus* (Xu et al. 1999*a*) are two basal therizinosaurs from the Early Cretaceous (Barremian?) of China slightly more derived than *Falcarius*. The body of these two primitive therizinosaurs was covered with filamentous integuments (Xu et al. 2009*b*; Pu et al. 2013), which suggests that most, if not all, therizinosaurs had protofeathers. Therizinosaur taxa more derived than *Jianchangosaurus* form the clade of Therizinosauroidea (Pu et al. 2013). *Jianchangosaurus* and therizinosauroids share a downturned anterior extremity of the dentary, large apically inclined denticles of the crowns, and an edentulous premaxilla bearing a rhamphotheca (which is possibly present in *Falcarius*). On the other hand, derived therizinosauroids (therizinosaurids) possess long scythe-like manual unguals, a backward pointing pubis, short and squat hind limbs, and feet formed by four toes touching the ground for body support (Clark et al. 2004; Zanno 2010*a*; Brusatte et al. 2012; Holtz 2012). The best known therizinosauroids are *Alxasaurus elesitaiensis* (Russell and Dong 1993) from the Albian of China, *Nothronychus graffami* (Zanno et al. 2009; Fig. S2-12B) from the Turonian of Utah, *Erlikosaurus andrewsi* and *Segnosaurus galbinensis* (Barsbold and Perle

1980; Barsbold 1983; Clark et al. 1994) from the Cenomanian-Turonian of Mongolia, and *Neimongosaurus yangi* (Zhang et al. 2001) from the Campanian-Maastrichtian of China (Zanno 2010*a*).

The clade gathering theropods more derived than therizinosaurs, and including Oviraptorosauria and Paraves, has been recently coined Pennaraptora based on definitive evidence of pennaceous feathers in pennaraptorans (Foth et al. 2014). Oviraptorosauria is a well-supported clade of small to large (1-8 m long) theropods easily recognizable by their short parrot-like beaked skull, forelimbs with elongated manual fingers, and short tails (Osmólska et al. 2004; Balanoff and Norell 2012; Holtz 2012; Lamanna et al. 2014; Fig. S2-12C). Oviraptorosaurs are restricted to the Cretaceous of Asia and North America, and most taxa come from the Campanian-Maastrichtian in those continents. Members of this clade were partially to strictly herbivorous coelurosaurs with an avian like brooding position over their nest (Clark et al. 1999; Varricchio et al. 2008; Zanno and Makovicky 2011). Similar to ornithomimosaurs, primitive oviraptorosaurs retained teeth that were lost through their evolution, and the large majority of oviraptorosaur taxa, gathered among the clade of Caenagnathoidea, were edentulous. The basalmost oviraptorosaur is currently *Incisivosaurus gauthieri* from the Aptian of China (Balanoff et al. 2009). *Incisivosaurus* shows the primitive condition of having dentulous maxillae and dentaries, and the peculiarity of bearing premaxillary teeth that are much larger than the lateral teeth (Xu et al. 2002*a*; Balanoff et al. 2009). Contemporaneous, yet more derived, non-caenagnathoid oviraptorosaurs such as *Caudipteryx zoui* and *Similicaudipteryx yixianensis* from China, only retained premaxillary teeth, and several well-preserved specimens preserved elaborated feathers such as remiges on the forelimbs, and rectrices on the caudal vertebrae (Ji et al. 1998; Zhou et al. 2000; He et al. 2008; Xu et al. 2010). This suggests that some, if not all,

oviraptorosaurs had feathered bodies and wings, yet they were too heavy to fly. Caenagnathoidea is divided into two main subclades, namely Oviraptoridae and Caenagnathidae (Osmólska et al. 2004; Longrich et al. 2013; Lamanna et al. 2014). Caenagnathids are characterized by fused dentaries, and long, shallow pneumatized mandibles, whereas oviraptorids had deeper lower jaws and an external naris extending over the antorbital fenestra (Longrich et al. 2013). Oviraptorids such as *Khaan mckennai* (Clark et al. 1999; Balanoff and Norell 2012; Fig. S2-12C) mostly inhabited xeric environments (i.e., deserts) whereas caenagnathids occurred in fluvial-dominated and costal floodplain environments (Longrich et al. 2013). Taxa belonging to both clades of Caegnathoidea convergently acquired cranial crests, as shown in *Citipati osmolskae* (Clark et al. 2002), *Nemegtomaia barsboldi* (Lü et al. 2004), and *Anzu wyliei* (Lamanna et al. 2014).

Paraves

The remaining maniraptorans, which comprise birds and two non-avian theropod clades typically gathered among deinonychosaurs, are grouped within Paraves (Fig. S2-4). The latter is defined as the least inclusive clade including *Passer domesticus* but not *Oviraptor philoceratops* (Godefroit et al. 2013*a*). Deinonychosauria, on the other hand, is either defined as a node-based clade containing the last common ancestor of *Troodon formosus* and *Velociraptor mongoliensis* and all of its descendants (Turner et al. 2012), or the most-inclusive clade containing *Dromaeosaurus albertensis* but not *Passer domesticus* (Godefroit et al. 2013*a*). Deinonychosaurs are typically divided into Dromaeosauridae and Troodontidae and encompass theropods that share a raptorial sickle-shaped claw on the retractable pedal digit II (Holtz 2012; Turner et al. 2012). Deinonychosauria was considered to be a very well-supported clade until recently (e.g., Turner et al. 2012), yet newly discovered basal paravians associated with the description of additional well-preserved specimens of *Archaeopteryx* (Mayr et al. 2005; Foth et al. 2014)

suggest that troodontids are more closely related to avialans than to dromaeosaurids, rendering the taxon Deinonychosauria paraphyletic or equivalent to Dromaeosauridae, pending on the phylogenetic definition given to this clade (e.g., Godefroit et al. 2013*a*; Choiniere et al. 2014; Foth et al. 2014; Fig. S2-4).

Dromaeosaurids are the only definitive carnivorous maniraptoriforms. They share ziphodont teeth, reduced pneumaticity of the braincase, and a hinge joint (ginglymus) on the distal end of metatarsal II that permits motion of the second toe and its associated hypertrophied claw (Norell and Makovicky 2004; Turner et al. 2012). Dromaeosaurids is a widespread group of very small to large bodied (0.6-7m long) paravians that were present on all continents by the Late Cretaceous. Although isolated teeth from the Late Jurassic of Europe have been assigned to the members of this clade (Zinke 1998; Lubbe et al. 2009; Hendrickx and Mateus 2014*b*), definitive dromaeosaurids currently range from the Barremian (China) to the Maastrichtian (North America). A large array of evidence indicates that some, and most likely all Dromaeosauridae were covered with filamentous integuments, and at least two dromaeosaurid taxa (i.e., *Microraptor* and *Changyuraptor*) possessed four wings (i.e., pennaceous fore- and hind limbs) with elaborated modern-like feathers (Xu et al. 1999*b*, 2001, 2003; Ji et al. 2001; Turner et al. 2007; Han et al. 2014). Unenlagiinae is the first radiation and the most basal lineage of Dromaeosauridae. These primitive dromaeosaurids are characterized by an elongated rostrum, unserrated teeth, and a vertically oriented pubis (Gianechini and Apesteguía 2011; Gianechini et al. 2011; Turner et al. 2012; Fig. S2-13A). They are exclusively found in the Upper Cretaceous of Gondwana, and are mostly known from Argentina, with the best preserved forms being *Buitreraptor gonzalezorum* from the Cenomanian (Makovicky et al. 2005; Fig. S2-13A),

Unenlagia comahuensis from the Turonian–Coniacian (Novas and Puerta 1997), and *Austroraptor cabazai* from the Maastrichtian (Novas et al. 2009).

The remaining dromaeosaurids, all characterized by a promaxillary fenestra, are classified among three subclades, namely Microraptorinae (also known as 'Microraptoria' *sensu* Senter et al. 2004, 2012*b*), Velociraptorinae and Dromaeosaurinae (Turner et al. 2012; Fig. S2-4). As suggested by the etymology of the clade name, microraptorines were small to very small (0.6–2m long) dromaeosaurids with aerial abilities (i.e., gliding, powered flight, or other semi-aerial locomotion) from the Early to Late Cretaceous of China and North America (Xu et al. 2003; Longrich and Currie 2009*b*; Han et al. 2014). The best preserved members of this clade, all from the Early Cretaceous of Liaoning in China, are *Microraptor* sp. (Hwang et al. 2002; Xu et al. 2003; O'Connor et al. 2011; Xing et al. 2013), *Sinornithosaurus millenii* (Xu et al. 1999*b*; Xu and Wu 2001; Gong et al. 2010), *Tianyuraptor ostromi* (Zheng et al. 2010), and *Changyuraptor yangi* (Han et al. 2014). *Hesperonychus elizabethae*, from the Campanian of Alberta, is the most recent microraptorines, and the only one found outside China (Longrich and Currie 2009*b*). Velociraptorinae gathers North American, Asian and possibly European dromaeosaurids characterized by pleurocoels in all dorsal vertebrae (Turner et al. 2012). Velociraptorines encompass the famous theropods *Velociraptor mongoliensis* from the Campanian of Mongolia (Sues 1977; Norell and Makovicky 1997, 1999; Barsbold and Osmólska 1999), *Deinonychus antirrhopus* from the Aptian–Albian of Montana (Ostrom 1969, 1976*b*), and *Bambiraptor feinbergi* from the Campanian of Montana (Burnham et al. 2000; Burnham 2004). *Balaur bondoc*, from the Maastrichtian of Romanian, may represent the only definitive velociraptorine from Europe (Csiki et al. 2010; Brusatte et al. 2013) although the most recent large scale phylogenetic analyses on coelurosaurs recovered it as a basal avialans (Godefroit et

al. 2013*a*; Foth et al. 2014). Dromaeosaurinae, the remaining subclade of dromaeosaurids, includes small to large-sized theropods with a lateral dentition bearing mesial denticles, a ventrodorsally tall jugal process of the maxilla, and a vertically oriented pubis (Turner et al. 2012). This clade mostly comprises North American dromaeosaurid taxa such as *Utahraptor ostrommaysorum* from the Barremian of Utah (Kirkland et al. 1993), and *Dromaeosaurus albertensis* (Colbert and Russell 1969; Currie 1995; Fig. S2-13B) and *Atrociraptor marshalli* (Currie and Varricchio 2004) from the Campanian of Alberta.

Troodontidae is a clade of lightly built maniraptorans known to include non-avian theropods with one of the smallest body sizes and one of the highest encephalization quotients (Makovicky and Norell 2004; Lü et al. 2010; Zanno et al. 2011; Tsuihiji et al. 2014). Troodontids share an anteroventrally inclined quadrate and jaws with a large number of small constricted teeth set in an open groove in the dentary (Makovicky and Norell 2004; Turner et al. 2012). The crowns are unserrated in basalmost forms and bear very large hooked denticles in derived taxa, which suggests an herbivorous or omnivorous diet in these theropods (Currie 1987; Holtz et al. 1998; Lü et al. 2010; Zanno and Makovicky 2011). Troodontids are known from the Cretaceous of Asia, North America, Europe, and India, and possibly from the Late Jurassic of China, depending on the troodontid affinities of newly discovered forms such as *Anchiornis*, *Xiaotingia*, and *Eosinopteryx* (Makovicky and Norell 2004; Hu et al. 2009; Vullo and Néraudeau 2010; Xu et al. 2011*b*; Turner et al. 2012; Godefroit et al. 2013*b*; Goswami et al. 2013). If *Troodon formosus* from the Campanian of Canada is the most famous troodontid and the first to be discovered (Russell 1948; Currie 1985, 1987; Currie and Zhao 1993*b*; Fig. S2-13C), the best preserved troodontid taxa all come from the Cretaceous of Asia. They include *Sinusonasus magnodens* (Xu and Wang 2004), *Mei long* (Xu and Norell 2004; Gao et al. 2012), and

Sinovenator changii (Xu et al. 2002*b*) from the Early Cretaceous of China, and *Byronosaurus jaffei* (Norell et al. 2000; Makovicky et al. 2003), *Gobivenator mongoliensis* (Tsuihiji et al. 2014), *Saurornithoides mongoliensis* and *Zanabazar junior* (Barsbold 1974; Norell et al. 2009) from the Campanian of Mongolia.

The recent discovery of a large number of paravian taxa closely related to birds such as *Anchiornis huxleyi* (Hu et al. 2009; Fig. S2-14A), *Xiaotingia zhengi* (Xu et al. 2011*b*), *Aurornis xui* (Godefroit et al. 2013*a*), and *Eosinopteryx brevipenna* (Godefroit et al. 2013*b*) allowed to redefine the relationships of the earliest avian theropods. The latter are typically gathered within Avialae, the most-inclusive clade containing *Passer domesticus* but not *Dromaeosaurus albertensis* or *Troodon formosus* (Godefroit et al. 2013*a*). The most basal and earliest avialan form was typically considered to be *Archaeopteryx* sp. (Fig. S2-14B) until the inclusion of these recently reported paravians into cladistic analyses. *Archaeopteryx* is either recovered as a deinonychosaur closely related to troodontids and dromaeosaurids (e.g., Xu et al. 2011*b*; Godefroit et al. 2013*b*; Xu and Pol 2014), or an avian theropod more derived than the basalmost avialans *Aurornis* and *Anchiornis* (e.g., Godefroit et al. 2013*a*; Foth et al. 2014). The anatomical distinctions between non-avian and avian theropods are, therefore, particularly subtle and varies between authors. According to Foth et al. (2014), who provided one of the largest and most recent cladistic analyses on coelurosaurs, Avialae are characterized by roots of dentary teeth subcircular in cross-section, extensive contact between pubes, humerus and femur subequal in thickness, and dorsal margin of antorbital fossa formed by lacrimal and nasal.

References

Agnolin, F. L. and Chiarelli, P. 2010. The position of the claws in Noasauridae (Dinosauria: Abelisauroidea) and its implications for abelisauroid manus evolution. *Paläontologische Zeitschrift* 84 (2): 293–300.

Alcober, O. A. and Martinez, R. N. 2010. A new herrerasaurid (Dinosauria, Saurischia) from the Upper Triassic Ischigualasto Formation of northwestern Argentina. *ZooKeys* (63): 55–81.

Alifanov, V. R. and Barsbold, R. 2009. *Ceratonykus oculatus* gen. et sp. nov., a new dinosaur (?Theropoda, Alvarezsauria) from the Late Cretaceous of Mongolia. *Paleontological Journal* 43 (1): 94–106.

Allain, R. 2002. Discovery of megalosaur (Dinosauria, Theropoda) in the middle Bathonian of Normandy (France) and its implications for the phylogeny of basal Tetanurae. *Journal of Vertebrate Paleontology* 22 (3): 548–563.

Allain, R. and Chure, D. J. 2002. *Poekilopleuron bucklandii*, the theropod dinosaur from the Middle Jurassic (Bathonian) of Normandy. *Palaeontology* 45 (6): 1107–1121.

Allain, R., Xaisanavong, T., Richir, P. and Khentavong, B. 2012. The first definitive Asian spinosaurid (Dinosauria: Theropoda) from the early cretaceous of Laos. *Naturwissenschaften* 99 (5): 369–377.

Allain, R., Tykoski, R., Aquesbi, N., Jalil, N.-E., Monbaron, M., Russell, D. and Taquet, P. 2007. An abelisauroid (Dinosauria: Theropoda) from the Early Jurassic of the High Atlas Mountains, Morocco, and the radiation of ceratosaurs. *Journal of Vertebrate Paleontology* 27 (3): 610–624.

Arcucci, A. B. and Coria, R. A. 2003. A new Triassic carnivorous dinosaur from Argentina. *Ameghiniana* 40 (2): 217–228.

Averianov, A. O., Krasnolutskii, S. A. and Ivantsov, S. V. 2010. A new basal coelurosaur (Dinosauria: Theropoda) from the Middle Jurassic of Siberia. *Proceedings of the Zoological Institute RAS* 314 (1): 42–57.

Azevedo, R. P. F. de, Simbras, F. M., Furtado, M. R., Candeiro, C. R. A. and Bergqvist, L. P. 2013. First Brazilian carcharodontosaurid and other new theropod dinosaur fossils from the Campanian–Maastrichtian Presidente Prudente Formation, São Paulo State, southeastern Brazil. *Cretaceous Research* 40: 131–142.

Azuma, Y. and Currie, P. J. 2000. A new carnosaur (Dinosauria: Theropoda) from the Lower Cretaceous of Japan. *Canadian Journal of Earth Sciences* 37 (12): 1735–1753.

Balanoff, A. M. and Norell, M. A. 2012. Osteology of *Khaan mckennai* (Oviraptorosauria: Theropoda). *Bulletin of the American Museum of Natural History*: 1–77.

Balanoff, A. M., Xu, X., Kobayashi, Y., Matsufune, Y. and Norell, M. A. 2009. Cranial osteology of the theropod dinosaur *Incisivosaurus gauthieri* (Theropoda: Oviraptorosauria). *American Museum Novitates* 3651: 1–35.

Barrett, P. M. 2005. The diet of ostrich dinosaurs (theropoda: Ornithomimosauria). *Palaeontology* 48 (2): 347–358.

Barrett, P. M. 2009. The affinities of the enigmatic dinosaur *Eshanosaurus deguchiianus* from the Early Jurassic of Yunnan Province, People's Republic of China. *Palaeontology* 52 (4): 681–688.

Barsbold, R. 1974. Saurornithoididae, a new family of small theropod dinosaurs from central Asia and North America. *Palaeontologia Polonica* 30: 5–22.

Barsbold, R. 1977. On the evolution of carnivorous dinosaurs (in rushian). *Transactions of the Joint Soviet Mongolian Paleontological Expedition* 4: 48–56.

Barsbold, R. 1983. Carnivorous dinosaurs from the Cretaceous of Mongolia. *Transactions of the Joint Soviet-Mongolian Paleontological Expedition* 19: 1–120.

Barsbold, R. and Perle, A. 1980. Segnosauria, a new infraorder of carnivorous dinosaurs. *Acta Palaeontologica Polonica* 25 (2): 187–195.

Barsbold, R. and Osmólska, H. 1999. The skull of *Velociraptor* (Theropoda) from the Late Cretaceous of Mongolia. *Acta Palaeontologica Polonica* 44 (2): 189–219.

Bates, K. T. and Falkingham, P. L. 2012. Estimating maximum bite performance in *Tyrannosaurus rex* using multi-body dynamics. *Biology Letters* 8 (4): 660–664.

Benson, R. B. J. 2008a. A redescription of '*Megalosaurus*' *hesperis* (Dinosauria, Theropoda) from the Inferior Oolite (Bajocian, Middle Jurassic) of Dorset, United Kingdom. *Zootaxa* 1931: 57–67.

Benson, R. B. J. 2008b. New information on *Stokesosaurus*, a tyrannosauroid (Dinosauria: Theropoda) from North America and the United Kingdom. *Journal of Vertebrate Paleontology* 28 (3): 732–750.

Benson, R. B. J. 2010a. A description of *Megalosaurus bucklandii* (Dinosauria: Theropoda) from the Bathonian of the UK and the relationships of Middle Jurassic theropods. *Zoological Journal of the Linnean Society* 158 (4): 882–935.

Benson, R. B. J. 2010b. The osteology of *Magnosaurus nethercombensis* (Dinosauria, Theropoda) from the Bajocian (Middle Jurassic) of the United Kingdom and a re-examination of the oldest records of tetanurans. *Journal of Systematic Palaeontology* 8 (1): 131–146.

Benson, R., Carrano, M. and Brusatte, S. 2010. A new clade of archaic large-bodied predatory dinosaurs (Theropoda: Allosauroidea) that survived to the latest Mesozoic. *Naturwissenschaften* 97 (1): 71–78.

Benton, M. J. 1986. The late Triassic reptile *Teratosaurus*—a rauisuchian, not a dinosaur. *Palaeontology* 29 (2): 293–301.

Bidar, A., Demay, L. and Thomel, G. 1972. *Compsognathus corallestris*: nouvelle espèce de dinosaurien théropode du Portlandien de Canjuers (sud-est de la France). *Annales du Muséum d'Histoire Naturelle de Nice* 1: 9–40.

Bonaparte, J. F. 1986. Les dinosaures (Carnosaures, Allosauridés, Sauropodes, Cétiosauridés) du Jurassique Moyen de Cerro Cóndor (Chubut, Argentina). *Annales de Paléontologie (Vert.-Invert.)* 72 (3): 247–289.

Bonaparte, J. F. and Powell, J. E. 1980. A continental assemblage of tetrapods from the Upper Cretaceous beds of El Brete, northwestern Argentina (Sauropoda-Coelurosauria-Carnosauria-Aves). *Mémoires de la Société Géologique de France, Nouvelle Série* 139: 19–28.

Bonaparte, J. F., Novas, F. E. and Coria, R. A. 1990. *Carnotaurus sastrei* Bonaparte, the horned, lightly built carnosaur from the Middle Cretaceous of Patagonia. *Natural History Museum of Los Angeles County Contributions in Science* 416 (416): 1–42.

Breithaupt, B. H. 1999. The first discoveries of dinosaurs in the American West. *Vertebrate Paleontology in Utah*: 59–65.

Breithaupt, B. H. and Elizabeth, H. 2008. Wyoming's *Dynamosaurus imperiosus* and other early discoveries of *Tyrannosaurus rex* in the rocky mountain West. *In*: Larson, P. L. and Carpenter, K. (eds.), *Tyrannosaurus Rex, the Tyrant King*, 57–61. Indiana University Press, Bloomington, Indiana.

Britt, B. B. 1991. Theropods of Dry Mesa Quarry (Morrison Formation, Late Jurassic), Colorado, with emphasis on the osteology of *Torvosaurus tanneri*. *Brigham Young University Geology Studies* 37: 1–72.

Brochu, C. A. 2003. Osteology of *Tyrannosaurus rex*: Insights from a nearly complete skeleton and high-resolution computed tomographic analysis of the skull. *Journal of Vertebrate Paleontology* 22 (sup4): 1–138.

Brookes, R. 1763. The Natural History of Waters, Earths, Stones, Fossils, and Minerals, with their Virtues, Properties, and Medicinal Uses: To Which is added, The Method in which LINNAEUS has treated these Subjects. Vol. 5. J. Newbery, London, pp.

Brusatte, S. L. 2012. *Dinosaur Paleobiology*. Wiley-Blackwell, 336pp.

Brusatte, S. L., Norell, M. A., Carr, T. D., Erickson, G. M., Hutchinson, J. R., Balanoff, A. M., Bever, G. S., Choiniere, J. N., Makovicky, P. J. and Xu, X. 2010a. Tyrannosaur paleobiology: new research on ancient exemplar organisms. *Science* 329 (5998): 1481–1485.

Brusatte, S. L. and Sereno, P. C. 2007. A new species of *Carcharodontosaurus* (Dinosauria: Theropoda) from the Cenomanian of Niger and a revision of the genus. *Journal of Vertebrate Paleontology* 27 (4): 902–916.

Brusatte, S. L., Benson, R. B. J. and Hutt, S. 2008. The osteology of *Neovenator salerii* (dinosauria: theropoda) from the wealden group (barreman) of the Isle of Wight. *Palaeontographical Society*: 1–75.

Brusatte, S. L., Benson, R. B. J. and Norell, M. A. 2011. The anatomy of *Dryptosaurus aquilunguis* (Dinosauria: Theropoda) and a review of its tyrannosauroid affinities. *American Museum Novitates* 3717: 1–53.

Brusatte, S. L., Carr, T. D. and Norell, M. A. 2012. The osteology of *Alioramus*, a gracile and long-snouted tyrannosaurid (Dinosauria: Theropoda) from the Late Cretaceous of Mongolia. *Bulletin of the American Museum of Natural History* 366: 1–197.

Brusatte, S. L., Chure, D. J., Benson, R. B. J. and Xu, X. 2010b. The osteology of *Shaochilong maortuensis*, a carcharodontosaurid (Dinosauria: Theropoda) from the Late Cretaceous of Asia. *Zootaxa* 2334: 1–46.

Brusatte, S. L., Nesbitt, S. J., Irmis, R. B., Butler, R. J., Benton, M. J. and Norell, M. A. 2010c. The origin and early radiation of dinosaurs. *Earth-Science Reviews* 101 (1–2): 68–100.

Brusatte, S. L., Vremir, M., Csiki-Sava, Z., Turner, A. H., Watanabe, A., Erickson, G. M. and Norell, M. A. 2013. The Osteology of *Balaur bondoc*, an Island-Dwelling Dromaeosaurid (Dinosauria: Theropoda) from the Late Cretaceous of Romania. *Bulletin of the American Museum of Natural History*: 1–100.

Brusatte, S. and Benson, R. B. J. 2013. The systematics of Late Jurassic tyrannosauroids (Dinosauria: Theropoda) from Europe and North America. *Acta Palaeontologica Polonica* 58 (1): 47–54.

Buckland, W. 1824. Notice on the *Megalosaurus* or great fossil lizard of Stonesfield. *Transactions of the Geological Society* 21: 390–397.

Buffetaut, E. 1994. *Les Dinosaures*. Presses Universitaires de France - PUF, Paris, 127pp.

Buffetaut, E. 2011. An early spinosaurid dinosaur from the Late Jurassic of Tendaguru (Tanzania) and the evolution of the spinosaurid dentition. *Oryctos* 10: 1–8.

Buffetaut, E., Suteethorn, V. and Tong, H. 1996. The earliest known tyrannosaur from the Lower Cretaceous of Thailand. *Nature* 381 (6584): 689–691.

Buffetaut, E., Martill, D. and Escuillié, F. 2004. Pterosaurs as part of a spinosaur diet. *Nature* 430 (6995): 33–33.

Burch, S. H. and Carrano, M. T. 2012. An articulated pectoral girdle and forelimb of the abelisaurid theropod *Majungasaurus crenatissimus* from the Late Cretaceous of Madagascar. *Journal of Vertebrate Paleontology* 32 (1): 1–16.

Burnham, D. A. 2004. New Information on *Bambiraptor feinbergi* (Theropoda: Dromaeosauridae) from the Late Cretaceous of Montana. *In*: Currie, P. J., Koppelhus, E. B., Shugar, M. A. and Wright, J. L. (eds.), *Feathered Dragons: Studies on the Transition from Dinosaurs to Birds*, 67–111. Indiana University Press, Bloomington, Indiana.

Burnham, D. A., Derstler, K. L., Currie, P. J., Bakker, R. T., Zhou, Z. and Ostrom, J. H. 2000. Remarkable new birdlike dinosaur (Theropoda: Maniraptora) from the Upper Cretaceous of Montana. *The Paleontological Institute, The University of Kansas* 13: 1–14.

Butler, R. J. and Upchurch, P. 2007. Highly incomplete taxa and the phylogenetic relationships of the theropod dinosaur *Juravenator starki*. *Journal of Vertebrate Paleontology* 27 (1): 253–256.

Calvo, J. O. and Coria, R. 1998. New specimen of *Giganotosaurus carolinii* (Coria & Salgado, 1995), supports it as the largest theropod ever found. *Gaia* 15: 117–122.

Canale, J. I., Novas, F. E. and Pol, D. 2014. Osteology and phylogenetic relationships of *Tyrannotitan chubutensis* Novas, de Valais, Vickers-Rich and Rich, 2005 (Theropoda: Carcharodontosauridae) from the Lower Cretaceous of Patagonia, Argentina. *Historical Biology* 0 (0): 1–32.

Carabajal, A. P. 2011. The braincase anatomy of *Carnotaurus sastrei* (Theropoda: Abelisauridae) from the Upper Cretaceous of Patagonia. *Journal of Vertebrate Paleontology* 31 (2): 378–386.

Carpenter, K., Miles, C., Ostrom, J. H. and Cloward, K. 2005. Redescription of the small maniraptoran theropods *Ornitholestes* and *Coelurus* from the Upper Jurassic Morrison Formation of Wyoming. *In*: Carpenter, K. (ed.), *The Carnivorous Dinosaurs*, 49–71. Indiana University Press, Bloomington, Indiana.

Carr, T. D. 1999. Craniofacial ontogeny in Tyrannosauridae (Dinosauria, Coelurosauria). *Journal of Vertebrate Paleontology* 19 (3): 497–520.

Carrano, M. T. and Sampson, S. D. 2004. A review of coelophysoids (Dinosauria: Theropoda) from the Lower Jurassic of Europe, with Comments on the Late History of the Coelophysoidea. *Neues Jahrbuch für Geologie und Paläontologie Monatshefte* 2004 (9): 537–558.

Carrano, M. T. and Sampson, S. D. 2008. The phylogeny of Ceratosauria (Dinosauria: Theropoda). *Journal of Systematic Palaeontology* 6 (2): 183–236.

Carrano, M. T., Sampson, S. D. and Forster, C. A. 2002. The osteology of *Masiakasaurus knopfleri*, a small abelisauroid (Dinosauria: Theropoda) from the Late Cretaceous of Madagascar. *Journal of Vertebrate Paleontology* 22 (3): 510–534.

Carrano, M. T., Hutchinson, J. R. and Sampson, S. D. 2005. New information on *Segisaurus halli*, a small theropod dinosaur from the Early Jurassic of Arizona. *Journal of Vertebrate Paleontology* 25 (4): 835–849.

Carrano, M. T., Loewen, M. A. and Sertich, J. J. W. 2011. New materials of *Masiakasaurus knopfleri* Sampson, Carrano, and Forster, 2001, and implications for the morphology of the Noasauridae (Theropoda: Ceratosauria). *Smithsonian Contributions to Paleobiology* 95: 1–53.

Carrano, M. T., Benson, R. B. J. and Sampson, S. D. 2012. The phylogeny of Tetanurae (Dinosauria: Theropoda). *Journal of Systematic Palaeontology* 10 (2): 211–300.

Carroll, R. L. 1988. *Vertebrate Paleontology and Evolution*. W. H. Freeman and Company, 698pp.

Charig, A. J. and Milner, A. C. 1986. *Baryonyx*, a remarkable new theropod dinosaur. *Nature* 324 (6095): 359–361.

Charig, A. J. and Milner, A. C. 1997. *Baryonyx walkeri*, a fish-eating dinosaur from the Wealden of Surrey. *Bulletin of the Natural History Museum* 53 (1): 11–70.

Chiappe, L. M. and Witmer, L. M. 2002. *Mesozoic Birds: Above the Heads of Dinosaurs*. University of California Press, 548pp.

Chiappe, L. M. and Göhlich, U. B. 2010. Anatomy of *Juravenator starki* (Theropoda: Coelurosauria) from the Late Jurassic of Germany. *Neues Jahrbuch für Geologie und Paläontologie Abhandlungen* 258 (3): 257–296.

Chiappe, L. M., Norell, M. A. and Clark, J. M. 1998. The skull of a relative of the stem-group bird *Mononykus*. *Nature* 392 (6673): 275–278.

Choiniere, J. N., Forster, C. A. and de Klerk, W. J. 2012. New information on *Nqwebasaurus thwazi*, a coelurosaurian theropod from the Early Cretaceous Kirkwood Formation in South Africa. *Journal of African Earth Sciences* 71–72: 1–17.

Choiniere, J. N., Clark, J. M., Forster, C. A. and Xu, X. 2010a. A basal coelurosaur (Dinosauria: Theropoda) from the Late Jurassic (Oxfordian) of the Shishugou Formation in Wucaiwan, People's Republic of China. *Journal of Vertebrate Paleontology* 30 (6): 1773–1796.

Choiniere, J. N., Xu, X., Clark, J. M., Forster, C. A., Guo, Y. and Han, F. 2010b. A basal alvarezsauroid theropod from the Early Late Jurassic of Xinjiang, China. *Science* 327 (5965): 571–574.

Choiniere, J. N., Clark, J. M., Forster, C. A., Norell, M. A., Eberth, D. A., Erickson, G. M., Chu, H. and Xu, X. 2014. A juvenile specimen of a new coelurosaur (Dinosauria: Theropoda) from the Middle–Late Jurassic Shishugou Formation of Xinjiang, People's Republic of China. *Journal of Systematic Palaeontology* 12 (2): 177–215.

Chure, D. J. 1995. A reassessment of the gigantic theropod *Saurophagus maximus* from the Morrison Formation (Upper Jurassic) of Oklahoma, USA. *Sixth Symposium on Mesozoic Terrestrial Ecosystems and Biota, Short Papers*: 103–106.

Chure, D. J. 2000. A new species of *Allosaurus* from the Morrison Formation of Dinosaur National Monument (Utah-Colorado) and a revision of the theropod family Allosauridae. Ph.D. Dissertation, Columbia University, New York, New York., 909pp.

Clark, J. M., Perle, A. and Norell, M. 1994. The skull of *Erlicosaurus andrewsi*, a late Cretaceous 'Segnosaur' (Theropoda, Therizinosauridae) from Mongolia. *American Museum Novitates* 3115: 1–39.

Clark, J. M., Norell, M. and Chiappe, L. M. 1999. An oviraptorid skeleton from the late Cretaceous of Ukhaa Tolgod, Mongolia, preserved in an avianlike brooding position over an oviraptorid nest. *American Museum Novitates* 3265: 1–36.

Clark, J. M., Norell, M. A. and Rowe, T. 2002. Cranial anatomy of *Citipati osmolskae* (Theropoda, Oviraptorosauria), and a reinterpretation of the holotype of *Oviraptor philoceratops*. *American Museum Novitates* 3364: 1–24.

Clark, J. M., Maryanska, T. and Barsbold, R. 2004. Therizinosauroidea. *In*: Weishampel, D. B., Dodson, P. and Osmólska, H. (eds.), *The Dinosauria, Second Edition*, 151–164. University of California Press, Berkeley, California.

Colbert, E. H. 1964. Relationships of the saurischian dinosaurs. *American Museum Novitates* 2181.

Colbert, E. H. and Russell, D. A. 1969. The small Cretaceous dinosaur *Dromaeosaurus*. *American Museum Novitates* 2380: 1–49.

Coria, R. A. and Salgado, L. 1995. A new giant carnivorous dinosaur from the Cretaceous of Patagonia. *Nature* 377 (6546): 224–226.

Coria, R. A. and Salgado, L. 1998. A basal Abelisauria Novas, 1992 (Theropoda-Ceratosauria) from the Cretaceous of Patagonia, Argentina. *Gaia* 15: 89–102.

Coria, R. A. and Currie, P. J. 2006. A new carcharodontosaurid (Dinosauria, Theropoda) from the Upper Cretaceous of Argentina. *Geodiversitas* 28 (1): 71–118.

Coria, R. A., Chiappe, L. M. and Dingus, L. 2002. A new close relative of *Carnotaurus sastrei* Bonaparte 1985 (Theropoda: Abelisauridae) from the Late Cretaceous of Patagonia. *Journal of Vertebrate Paleontology* 22 (2): 460–465.

Csiki, Z., Vremir, M., Brusatte, S. L. and Norell, M. A. 2010. An aberrant island-dwelling theropod dinosaur from the Late Cretaceous of Romania. *Proceedings of the National Academy of Sciences* 107 (35): 15357–15361.

Currie, P. J. 1985. Cranial anatomy of *Stenonychosaurus inequalis* (Saurischia, Theropoda) and its bearing on the origin of birds. *Canadian Journal of Earth Sciences* 22 (11): 1643–1658.

Currie, P. J. 1987. Bird-like characteristics of the jaws and teeth of troodontid theropods (Dinosauria, Saurischia). *Journal of Vertebrate Paleontology* 7 (1): 72–81.

Currie, P. J. 1995. New information on the anatomy and relationships of *Dromaeosaurus albertensis* (Dinosauria: Theropoda). *Journal of Vertebrate Paleontology* 15 (3): 576–591.

Currie, P. J. 2003. Cranial anatomy of tyrannosaurid dinosaurs from the Late Cretaceous of Alberta, Canada. *Acta Palaeontologica Polonica* 48 (2): 191–226.

Currie, P. J. and Zhao, X.-J. 1993a. A new carnosaur (Dinosauria, Theropoda) from the Jurassic of Xinjiang, People's Republic of China. *Canadian Journal of Earth Sciences* 30 (10): 2037–2081.

Currie, P. J. and Zhao, X.-J. 1993b. A new troodontid (Dinosauria, Theropoda) braincase from the Dinosaur Park Formation (Campanian) of Alberta. *Canadian Journal of Earth Sciences* 30 (10): 2231–2247.

Currie, P. J. and Carpenter, K. 2000. A new specimen of *Acrocanthosaurus atokensis* (Theropoda, Dinosauria) from the Lower Cretaceous Antlers Formation (Lower Cretaceous, Aptian) of Oklahoma, USA. *Geodiversitas* 22 (2): 207–246.

Currie, P. J. and Chen, P. 2001. Anatomy of *Sinosauropteryx prima* from Liaoning, northeastern China. *Canadian Journal of Earth Sciences* 38 (12): 1705–1727.

Currie, P. J. and Varricchio, D. J. 2004. A new dromaeosaurid from the Horseshoe Canyon Formation (upper Cretaceous) of Alberta, Canada. *In*: Currie, P. J., Koppelhus, E. B., Shugar, M. A. and

Wright, J. L. (eds.), *Feathered Dragons: Studies on the Transition from Dinosaurs to Birds.*, 112–132. Bloomington, Indiana.

Currie, P. J. and Azuma, Y. 2006. New specimens, including a growth series, of *Fukuiraptor* (Dinosauria, Theropoda) from the Lower Cretaceous Kitadani Quarry of Japan. *Journal of the Paleontological Society of Korea* 22 (1): 173–193.

Cuvier, G. 1808. Sur les ossements fossiles de crocodiles: et particulièrement sur ceux des environs du Havre et de Honfleur, avec des remarques sur les squelettes des Sauriens de la Thuringe. *Annales du Muséum d'Histoire naturelle de Paris* XII: 73–110.

Cuvier, G. 1812. Recherches sur les ossemens fossiles de quadrupèdes, où l'on rétablit les caractères de plusieurs espèces d'animaux que les révolutions du globe paroissent avoir détruites. Chez Deterville, 486pp.

Cuvier, G. 1824. Recherches sur les ossemens fossiles, où l'on rétablit les caractères de plusieurs animaux dont les révolutions du globe ont détruit les espèces. chez G. Dufour et E. D'Ocagne, libraires, quai Voltaire, 630pp.

Delair, J. B. and Sarjeant, W. A. 1975. The earliest discoveries of dinosaurs. *Isis*: 5–25.

Delair, J. B. and Sarjeant, W. A. S. 2002. The earliest discoveries of dinosaurs: the records re-examined. *Proceedings of the Geologists' Association* 113 (3): 185–197.

Dong, Z., Zhou, S. W. and Zhang, Y. 1983. Dinosaurs from the Jurassic of Sichuan. *Palaeontologica Sinica, New Series C* 162 (23): 1–136.

Eddy, D. R. and Clarke, J. A. 2011. New information on the cranial anatomy of *Acrocanthosaurus atokensis* and its implications for the phylogeny of Allosauroidea (Dinosauria: Theropoda). *PLoS ONE* 6 (3): e17932.

Erickson, G. M., Kirk, S. D. V., Su, J., Levenston, M. E., Caler, W. E. and Carter, D. R. 1996. Bite-force estimation for *Tyrannosaurus rex* from tooth-marked bones. *Nature* 382 (6593): 706–708.

Erickson, G. M., Makovicky, P. J., Currie, P. J., Norell, M. A., Yerby, S. A. and Brochu, C. A. 2004. Gigantism and comparative life-history parameters of tyrannosaurid dinosaurs. *Nature* 430 (7001): 772–775.

Eudes-Deslongchamps, J. A. 1837. Mémoire sur le Poekilopleuron bucklandii, grand saurien fossile, intermédiaire entre les crocodiles et les lézards, découvert dans les carrières de la Maladrerie, près Caen, au mois de juillet 1835. impr. A. Hardel, 144pp.

Evans, M. 2010. The roles played by museums, collections and collectors in the early history of reptile palaeontology. *Geological Society, London, Special Publications* 343 (1): 5–29.

Evans, S. E. 1994. The Solnhofen (Jurassic: Tithonian) genus *Bavarisaurus*: new material and a new interpretation. *Neues Jahrbuch fur Geologie und Palaontologie Abhandlungen* 192: 37–52.

Ezcurra, M. D. 2007. The cranial anatomy of the coelophysoid theropod *Zupaysaurus rougieri* from the Upper Triassic of Argentina. *Historical Biology* 19 (2): 185–202.

Ezcurra, M. D. 2010. A new early dinosaur (Saurischia: Sauropodomorpha) from the Late Triassic of Argentina: a reassessment of dinosaur origin and phylogeny. *Journal of Systematic Palaeontology* 8 (3): 371–425.

Ezcurra, M. D. and Cuny, G. 2007. The coelophysoid *Lophostropheus airelensis*, gen. nov.: a review of the systematics of '*Liliensternus*' *airelensis* from the Triassic–Jurassic outcrops of Normandy (France). *Journal of Vertebrate Paleontology* 27 (1): 73–86.

Ezcurra, M. D. and Novas, F. E. 2007. Phylogenetic relationships of the Triassic theropod *Zupaysaurus rougieri* from NW Argentina. *Historical Biology* 19 (1): 35–72.

Ezcurra, M. D. and Brusatte, S. L. 2011. Taxonomic and phylogenetic reassessment of the early neotheropod dinosaur *Camposaurus arizonensis* from the Late Triassic of North America. *Palaeontology* 54 (4): 763–772.

Foth, C., Tischlinger, H. and Rauhut, O. W. M. 2014. New specimen of *Archaeopteryx* provides insights into the evolution of pennaceous feathers. *Nature* 511 (7507): 79–82.

Gao, C., Morschhauser, E. M., Varricchio, D. J., Liu, J. and Zhao, B. 2012. A second soundly sleeping dragon: new anatomical details of the Chinese troodontid *Mei long* with implications for phylogeny and taphonomy. *PLoS ONE* 7 (9): e45203.

Gauthier, J. 1986. Saurischian monophyly and the origin of birds. *In*: Padian, K. (ed.), *The Origin of Birds and the Evolution of Flight*, Vol. 8, 1–55. Memoirs of the California Academy of Sciences, San Francisco, California.

Gianechini, F. A. and Apesteguía, S. 2011. Unenlagiinae revisited: dromaeosaurid theropods from South América. *Anais da Academia Brasileira de Ciências* 83 (1): 163–195.

Gianechini, F. A., Makovicky, P. J. and Apesteguía, S. 2011. The teeth of the unenlagiine theropod *Buitreraptor* from the Cretaceous of Patagonia, Argentina, and the unusual dentition of the Gondwanan dromaeosaurids. *Acta Palaeontologica Polonica* 56 (2): 279–290.

Gilmore, C. W. 1920. Osteology of the carnivorous Dinosauria in the United State National museum: with special reference to the genera *Antrodemus* (*Allosaurus*) and *Ceratosaurus*. *Bulletin of the United States National Museum* 110: 1–159.

Godefroit, P., Cau, A., Dong-Yu, H., Escuillié, F., Wenhao, W. and Dyke, G. 2013a. A Jurassic avialan dinosaur from China resolves the early phylogenetic history of birds. *Nature* 498: 359–362.

Godefroit, P., Demuynck, H., Dyke, G., Hu, D., Escuillié, F. and Claeys, P. 2013b. Reduced plumage and flight ability of a new Jurassic paravian theropod from China. *Nature Communications* 4: 1394.

Gong, E., Martin, L. D., Burnham, D. A. and Falk, A. R. 2010. The birdlike raptor *Sinornithosaurus* was venomous. *Proceedings of the National Academy of Sciences* 107 (2): 766–768.

Goswami, A., Prasad, G. V. R., Verma, O., Flynn, J. J. and Benson, R. B. J. 2013. A troodontid dinosaur from the latest Cretaceous of India. *Nature Communications* 4: 1703.

Halstead, L. B. 1970. *Scrotum humanum* Brookes 1763—the first named dinosaur. *Journal of Insignificant Research* 5: 14–15.

Halstead, L. B. and Sarjeant, W. A. S. 1993. Scrotum humanum Brookes—the earliest name for a dinosaur? *Modern Geology* 18: 221–224.

Han, G., Chiappe, L. M., Ji, S.-A., Habib, M., Turner, A. H., Chinsamy, A., Liu, X. and Han, L. 2014. A new raptorial dinosaur with exceptionally long feathering provides insights into dromaeosaurid flight performance. *Nature Communications* 5.

Harris, J. D. 1998. A reanalysis of *Acrocanthosaurus atokensis*, its phylogenetic status, and paleobiogeographic implications, based on a new specimen from Texas. *New Mexico Museum of Natural History and Science Bulletin* 13: 1–75.

He, T., Wang, X.-L. and Zhou, Z.-H. 2008. A new genus and species of caudipterid dinosaur from the Lower Cretaceous Jiufotang Formation of western Liaoning, China. *Vertebrata PalAsiatica* 46 (3): 178–189.

Hendrickx, C. and Mateus, O. 2014a. *Torvosaurus gurneyi* n. sp., the largest terrestrial predator from Europe, and a proposed terminology of the maxilla anatomy in nonavian theropods. *PLoS ONE* 9 (3): e88905.

Hendrickx, C. and Mateus, O. 2014b. Abelisauridae (Dinosauria: Theropoda) from the Late Jurassic of Portugal and dentition-based phylogeny as a contribution for the identification of isolated theropod teeth. *Zootaxa* 3759 (1): 1–74.

Hocknull, S. A., White, M. A., Tischler, T. R., Cook, A. G., Calleja, N. D., Sloan, T. and Elliott, D. A. 2009. New mid-Cretaceous (Latest Albian) dinosaurs from Winton, Queensland, Australia. *PLoS ONE* 4 (7): e6190.

Holtz, T. R. J. 1998. A new phylogeny of the carnivorous dinosaurs. *Gaia* 15: 5–61.

Holtz, T. R. J. 2004. Tyrannosauroidea. *In*: Weishampel, D. B., Dodson, P. and Osmólska, H. (eds.), *The Dinosauria. Second Edition*, 111–136. University of California Press, Berkeley, California.

Holtz, T. R. J. 2012. Theropods. *In*: Brett-Surman, M. K., Holtz, T. R. J. and Farlow, J. O. (eds.), *The Complete Dinosaur, Second Edition*, 347–378. Indiana University Press, Bloomington, Indiana.

Holtz, T. R. J. and Osmólska, H. 2004. Basal Saurischia. *In*: Weishampel, D. B., Dodson, P. and Osmólska, H. (eds.), *The Dinosauria. Second Edition*, 21–24. University of California Press, Berkeley, California.

Holtz, T. R. J., Brinkman, D. L. and Chandler, C. L. 1998. Denticle morphometrics and a possibly omnivorous feeding habit for the theropod dinosaur *Troodon*. *Gaia* 15: 159–166.

Holtz, T. R. J., Molnar, R. E. and Currie, P. J. 2004. Basal Tetanurae. *In*: Weishampel, D. B., Dodson, P. and Osmólska, H. (eds.), *The Dinosauria. Second Edition*, 71–110. University of California Press, Berkeley, California.

Holtz, T. R. 1994. The phylogenetic position of the Tyrannosauridae: implications for theropod systematics. *Journal of Paleontology* 68 (5): 1100–1117.

Horner, J. R. and Padian, K. 2004. Age and growth dynamics of Tyrannosaurus rex. Proceedings of the Royal Society of London. Series B: Biological Sciences 271 (1551): 1875–1880.

Hu, D., Hou, L., Zhang, L. and Xu, X. 2009. A pre-*Archaeopteryx* troodontid theropod from China with long feathers on the metatarsus. *Nature* 461 (7264): 640–643.

Hu, S. 1993. A new theropoda (*Dilophosaurus sinensis* sp. nov.) from Yunnan, China. *Vertebrata PalAsiatica* 31 (1): 65–69.

Huene, F. R. von. 1909. Skizze zu einer systematik und stammesgeschichte der dinosaurier. *Centralblatt für Mineralogie, Geologie und Paläontologie* 1909: 12–22.

Huene, F. R. von. 1914a. Das natürliche system der Saurischia. *Zentralblatt für Mineralogie, Geologiie, und Paläontologie B*: 154–158.

Huene, F. R. von. 1914b. Saurischia and Ornithischia. *Geological Magazine* 1 (10): 444–445.

Huene, F. R. von. 1923. Carnivorous Saurischia in Europe since the Triassic. *Bulletin of the Geological Society of America* 34: 449–458.

Huene, F. R. von. 1926a. On several known and unknown reptiles of the order Saurischia from England and France. *Journal of Natural History Series 9* 17 (101): 473–489.

Huene, F. R. von. 1926b. The carnivorous Saurischia in the Jura and Cretaceous formations, principally in Europe. *Revista del Museo de La Plata* 29: 35–167.

Huene, F. R. von. 1929. Kurze Übersicht über die Saurischia und ihre natürlichen Zusammenhänge. *Palaeontologische Zeitschrift* 11 (3): 269–273.

Huene, F. R. von. 1932. Die fossile Reptil-Ordnung Saurischia, ihre Entwicklung und Geschichte. *Monographien zur Geologie und Palaontologie, Series 1,* 4: 1–361.

Huene, F. R. von. 1934. Ein neuer Coelurosaurier in der thüringischen Trias. *Paläontologische Zeitschrift* 16 (3): 145–170.

Huene, F. R. von and Matley, C. A. 1933. The Cretaceous Saurischia and Ornithischia of the Central Provinces. *Memoirs of the Geological Survey of India, New Series* 21: 1–74.

Hurum, J. H. and Sabath, K. 2003. Giant theropod dinosaurs from Asia and North America: Skulls of *Tarbosaurus bataar* and *Tyrannosaurus rex* compared. *Acta Palaeontologica Polonica* 48 (2): 161–190.

Hutt, S., Naish, D., Martill, D. M., Barker, M. J. and Newbery, P. 2001. A preliminary account of a new tyrannosauroid theropod from the Wessex Formation (Early Cretaceous) of southern England. *Cretaceous Research* 22 (2): 227–242.

Hwang, S. H., Norell, M. A., Ji, Q. and Keqin, G. 2002. New specimens of *Microraptor zhaoianus* (Theropoda: Dromaeosauridae) from Northeastern China. *American Museum Novitates* 3381: 1–44.

Hwang, S. H., Norell, M. A., Qiang, J. and Keqin, G. 2004. A large compsognathid from the Early Cretaceous Yixian Formation of China. *Journal of Systematic Palaeontology* 2 (1): 13–30.

Ivie, M. A., Slipinski, S. A. and Wegrzynowicz, P. 2001. Generic Homonyms in the Colydiinae (Coleoptera: Zopheridae). *Insecta Mundi* 15 (1): 63–64.

Ji, Q., Ji, S. A. and Zhang, L. J. 2009. First large tyrannosauroid theropod from the Early Cretaceous Jehol Biota in northeastern China. *Geological Bulletin of China* 28 (10): 1369–1374.

Ji, Q., Currie, P. J., Norell, M. A. and Shu-An, J. 1998. Two feathered dinosaurs from northeastern China. *Nature* 393 (6687): 753–761.

Ji, Q., Ji, S., Lü, J. and Yuan, C. 2007a. A new giant compsognathid dinosaur with long filamentous integuments from lower Cretaceous of Northeastern China. *Acta Geologica Sinica* 81: 8–15.

Ji, Q., Norell, M. A., Gao, K.-Q., Ji, S.-A. and Ren, D. 2001. The distribution of integumentary structures in a feathered dinosaur. *Nature* 410 (6832): 1084–1088.

Ji, Q., Norell, M. A., Makovicky, P. J., Gao, K.-Q., Ji, S. and Yuan, C. 2003. An early ostrich dinosaur and implications for ornithomimosaur phylogeny. *American Museum Novitates* 3420: 1–19.

Ji, S., Gao, C., Liu, J., Meng, Q. and Qiang, J. 2007b. New Material of *Sinosauropteryx* (Theropoda: Compsognathidae) from Western Liaoning, China. *Acta Geologica Sinica - English Edition* 81 (2): 177–182.

Kellner, A. W. A. and Campos, D. A. 1996. First Early Cretaceous theropod dinosaur from Brazil with comments on Spinosauridae. *Neues Jahrbuch für Geologie und Paläontologie - Abhandlungen* 199 (2): 151–166.

Kirchner, H. 1941. Versteinerte Reptil-Fährten als Grundlage für den Drachenkampf in einem Heldenlied. *Zeitschrift der Deutschen Geologischen Gesellschaft*: 309–314.

Kirkland, J. I., Gaston, R. and Burge, D. 1993. A large dromaeosaur (Theropoda) from the Lower Cretaceous of eastern Utah. *Hunteria* 2 (10): 1–16.

Kobayashi, Y. and Lü, J.-C. 2003. A new ornithomimid dinosaur with gregarious habits from the Late Cretaceous of China. *Acta Palaeontologica Polonica* 48 (2): 235–259.

Kobayashi, Y. and Barsbold, R. 2005a. Reexamination of a primitive ornithomimosaur, *Garudimimus brevipes* Barsbold, 1981 (Dinosauria: Theropoda), from the Late Cretaceous of Mongolia. *Canadian Journal of Earth Sciences* 42 (9): 1501–1521.

Kobayashi, Y. and Barsbold, R. 2005b. Anatomy of *Harpymimus okladnikovi* Barsbold and Perle 1984 (Dinosauria; Theropoda) of Mongolia. *In*: Carpenter, K. (ed.), *The Carnivorous Dinosaurs*, 97–126. Indiana University Press, Bloomington, Indiana.

Lamanna, M. C., Sues, H.-D., Schachner, E. R. and Lyson, T. R. 2014. A new large-bodied oviraptorosaurian theropod dinosaur from the Latest Cretaceous of Western North America. *PLoS ONE* 9 (3): e92022.

Langer, M. C. 2014. The origins of Dinosauria: much ado about nothing. *Palaeontology* 57 (3): 469–478.

Langer, M. C. and Benton, M. J. 2006. Early dinosaurs: a phylogenetic study. *Journal of Systematic Palaeontology* 4 (04): 309–358.

Langer, M. C. and Ferigolo, J. 2013. The Late Triassic dinosauromorph *Sacisaurus agudoensis* (Caturrita Formation; Rio Grande do Sul, Brazil): anatomy and affinities. *Geological Society, London, Special Publications* 379: 353–392.

Lebrun, P. 2004. Dinosaures carnivores: une histoire naturelle des théropodes non aviaires. Tome 1: histoire des découvertes, anatomie et physiologie, phylogenèse, théropodes basaux et carnosauriens. Minéraux & Fossiles Hors-série n°18. CEDIM, 128pp.

Leidy, J. 1856. Notice of remains of extinct reptiles and fishes, discovered by Dr. F.V. Hayden in the Bad Lands of the Judith River, Nebraska Territory. *Proceedings of the Academy of Natural Sciences of Philadelphia* 8: 72–73.

Leonardi, G. 1984. Le impronte fossili di dinosauri. *In*: Ligabue, G. (ed.), *Sulle Orme Dei Dinosauri*, Vol. 9, 165–186. Erizzo for Le Societá del Gruppo ENI.

Lhuyd, E. 1699. *Lithophylacii Britannici ichnographia*. E Typographeo Clarendoniano, 284pp.

Li, D., Norell, M. A., Gao, K. Q., Smith, N. D. and Makovicky, P. J. 2010. A longirostrine tyrannosauroid from the Early Cretaceous of China. *Proceedings of the Royal Society B: Biological Sciences* 277 (1679): 183–190.

Li, F., Peng, G., Ye, Y., Jiang, S. and Huang, D. 2009. A new carnosaur from the Late Jurassic of Qianwei, Sichuan, China. *Acta Geologica Sinica* 83: 1203–1213.

Liyong, J., Jun, C. and Godefroit, P. 2012. A new basal ornithomimosaur (Dinosauria: Theropoda) from the Early Cretaceous Yixian Formation, Northeast China. *In*: Godefroit, P. (ed.), *Bernissart*

Dinosaurs and Early Cretaceous Terrestrial Ecosystems, 466–487. Indiana University Press, Bloomington, Indiana.

Loewen, M. A. 2010. Variation in the Late Jurassic theropod dinosaur *Allosaurus*: Ontogenetic, functional, and taxonomic implications. Ph.D. Dissertation, The University of Utah, Texas, Utah, USA, 326pp.

Loewen, M. A., Irmis, R. B., Sertich, J. J. W., Currie, P. J. and Sampson, S. D. 2013. Tyrant dinosaur evolution tracks the rise and fall of Late Cretaceous oceans. *PLoS ONE* 8 (11): e79420.

Longrich, N. R. and Currie, P. J. 2009a. *Albertonykus borealis*, a new alvarezsaur (Dinosauria: Theropoda) from the Early Maastrichtian of Alberta, Canada: implications for the systematics and ecology of the Alvarezsauridae. *Cretaceous Research* 30 (1): 239–252.

Longrich, N. R. and Currie, P. J. 2009b. A microraptorine (Dinosauria–Dromaeosauridae) from the Late Cretaceous of North America. *Proceedings of the National Academy of Sciences* 106 (13): 5002–5007.

Longrich, N. R., Barnes, K., Clark, S. and Millar, L. 2013. Caenagnathidae from the Upper Campanian Aguja Formation of West Texas, and a Revision of the Caenagnathinae. *Bulletin of the Peabody Museum of Natural History* 54 (1): 23–49.

Lü, J., Tomida, Y., Azunia, Y., Dong, Z. and Lee, Y. N. 2004. New oviraptorid dinosaur (Dinosauria: Oviraptorosauria) from the Nemegt Formation of Southwestern Mongolia. *Bulletin of the National Science Museum: Geology & paleontology* 30: 95–130.

Lü, J., Xu, L., Liu, Y., Zhang, X., Jia, S. and Ji, Q. 2010. A new troodontid theropod from the Late Cretaceous of central China, and the radiation of Asian troodontids. *Acta Palaeontologica Polonica* 55 (3): 381–388.

Lü, J., Yi, L., Brusatte, S. L., Yang, L., Li, H. and Chen, L. 2014. A new clade of Asian Late Cretaceous long-snouted tyrannosaurids. *Nature Communications* 5.

Lubbe, T. van der, Richter, U. and Knötschke, N. 2009. Velociraptorine dromaeosaurid teeth from the Kimmeridgian (Late Jurassic) of Germany. *Acta Palaeontologica Polonica* 54 (3): 401–408.

Madsen, J. H. 1976a. A second new theropod dinosaur from the Late Jurassic of east central Utah. *Utah geology* 3 (1): 51–60.

Madsen, J. H. 1976b. *Allosaurus fragilis*: A Revised Osteology. *Utah Geological Survey Bulletin* 109: 1–177.

Madsen, J. H. and Welles, S. P. 2000. *Ceratosaurus* (Dinosauria, Theropoda): a revised osteology. *Utah Geological Survey, Miscellaneous Publication* 00-2: 1–89.

Makovicky, P. J. and Norell, M. A. 2004. Troodontidae. *In*: Weishampel, D. B., Dodson, P. and Osmólska, H. (eds.), *The Dinosauria. Second Edition*, 184–195. University of California Press, Berkeley, California.

Makovicky, P. J., Kobayashi, Y. and Currie, P. J. 2004. Ornithomimosauria. *In*: Weishampel, D. B., Dodson, P. and Osmólska, H. (eds.), *The Dinosauria. Second Edition*, 137–150. University of California Press, Berkeley, California.

Makovicky, P. J., Apesteguía, S. and Agnolín, F. L. 2005. The earliest dromaeosaurid theropod from South America. *Nature* 437 (7061): 1007–1011.

Makovicky, P. J., Norell, M. A., Clark, J. M. and Rowe, T. 2003. Osteology and relationships of *Byronosaurus jaffei* (Theropoda: Troodontidae). *American Museum Novitates* 3402: 1–32.

Makovicky, P. J., Li, D., Gao, K.-Q., Lewin, M., Erickson, G. M. and Norell, M. A. 2010. A giant ornithomimosaur from the Early Cretaceous of China. *Proceedings of the Royal Society B: Biological Sciences* 277 (1679): 191–198.

Malafaia, E., Ortega, F., Escaso, F. and Silva, B. 2014. New evidence of *Ceratosaurus* (Dinosauria: Theropoda) from the Late Jurassic of the Lusitanian Basin, Portugal. *Historical Biology* 0 (0): 1–9.

Mantell, G. A. 1827. Illustrations of the Geology of Sussex: A General Viewof the Geological Relations of the South-Eastern Part of England, with Figures and Descriptions of the Fossils of Tilgate Forest. Lupton Relfe, London, 92pp.

Marsh, O. C. 1881. Principal characters of American Jurassic dinosaurs. Part V. *American Journal of Science (Series 3)* 21: 417–423.
Marsh, O. C. 1882. Classification of the Dinosauria. *American Journal of Science (Series 3)* 23: 81–86.
Marsh, O. C. 1884. Principal characters of the American Jurassic dinosaurs. Part VIII. The order Theropoda. *American Journal of Science, Series 3* 27: 329–340.
Marsh, O. C. 1895. On the affinities and classification of the dinosaurian reptiles. *American Journal of Science* (300): 483–498.
Marsh, O. C. 1896. *The dinosaurs of North America*. Washington, 462pp.
Martinez, R. N., Sereno, P. C., Alcober, O. A., Colombi, C. E., Renne, P. R., Montañez, I. P. and Currie, B. S. 2011. A basal dinosaur from the dawn of the dinosaur era in southwestern Pangaea. *Science* 331 (6014): 206–210.
Mateus, O. and Antunes, M. T. 2000. *Ceratosaurus* sp. (Dinosauria: Theropoda) in the Late Jurassic of Portugal. *Abstracts, 31st International Geological Congress*.
Mateus, O., Walen, A. and Antunes, M. T. 2006. The large theropod fauna of the Lourinhã Formation (Portugal) and its similarity to the Morrison Formation, with a description of a new species of *Allosaurus*. *New Mexico Museum of Natural History and Science Bulletin* 36: 123–129.
Mateus, O., Araújo, R., Natário, C. and Castanhinha, R. 2011. A new specimen of the theropod dinosaur *Baryonyx* from the early Cretaceous of Portugal and taxonomic validity of *Suchosaurus*. *Zootaxa* 2827: 54–68.
Matthew, W. D. and Brown, B. 1922. The family Deinodontidae, with notice of a new genus from the Cretaceous of Alberta. *Bulletin of the American Museum of Natural History* 46 (6): 367–385.
Mayr, G., Pohl, B. and Peters, D. S. 2005. A well-preserved *Archaeopteryx* specimen with theropod features. *Science* 310 (5753): 1483–1486.
Meyer, H. von. 1832. *Paleologica zur Geschichte der Erde*. Frankfurt am Main, 560pp.
Milner, A. C. 2002. Theropod dinosaurs of the Purbeck limestone group, Southern England. *Special Papers in Palaeontology* 68: 191–202.
Molnar, R. E. 1991. The cranial morphology of *Tyrannosaurus rex*. *Palaeontographica Abteilung A* 217 (4-6): 137–176.
Naish, D. 2012. Birds. *In*: Brett-Surman, M. K., Holtz, T. R. J. and Farlow, J. O. (eds.), *The Complete Dinosaur, Second Edition*, 379–423. Indiana University Press, Bloomington, Indiana.
Nesbitt, S. J. 2011. The early evolution of archosaurs: relationships and the origin of major clades. *Bulletin of the American Museum of Natural History*: 1–292.
Nesbitt, S. J., Smith, N. D., Irmis, R. B., Turner, A. H., Downs, A. and Norell, M. A. 2009. A complete skeleton of a Late Triassic saurischian and the early evolution of dinosaurs. *Science* 326 (5959): 1530–1533.
Norell, M. A. and Makovicky, P. J. 2004. Dromaeosauridae. *In*: Weishampel, D., Dodson, P. and Osmólska, H. (eds.), *The Dinosauria. Second Edition*, 196–209. University of California Press, Berkeley, California.
Norell, M. A., Makovicky, P. J. and Clark, J. M. 2000. A new troodontid theropod from Ukhaa Tolgod, Mongolia. *Journal of Vertebrate Paleontology* 20 (1): 7–11.
Norell, M. A., Makovicky, P. J. and Currie, P. J. 2001. Palaeontology: the beaks of ostrich dinosaurs. *Nature* 412 (6850): 873–874.
Norell, M. A., Makovicky, P. J., Bever, G. S., Balanoff, A. M., Clark, J. M., Barsbold, R. and Rowe, T. 2009. A review of the Mongolian Cretaceous dinosaur *Saurornithoides* (Troodontidae: Theropoda). *American Museum Novitates* 3654: 1–63.
Norell, M. and Makovicky, P. J. 1997. Important features of the dromaeosaur skeleton : information from a new specimen. *American Museum Novitates* 3215: 1–28.
Norell, M. and Makovicky, P. J. 1999. Important features of the dromaeosaurid skeleton. 2, Information from newly collected specimens of *Velociraptor mongoliensis*. *American Museum Novitates* 3282: 1–45.

Novas, F. E. 1992. La evolución de los dinosaurios carnivoros. *In*: Sanz, J. L. and Buscalioni, A. D. (eds.), *Los Dinosaurios Y Su Entorno Biotico: Actas Del Segundo Curso de Paleontología En Cuenca*, 126–163. Instituto 'Juan Valdez,' Cuenca, Spain.

Novas, F. E. 1997. Anatomy of *Patagonykus puertai* (Theropoda, Avialae, Alvarezsauridae), from the Late Cretaceous of Patagonia. *Journal of Vertebrate Paleontology* 17 (1): 137–166.

Novas, F. E. and Puerta, P. F. 1997. New evidence concerning avian origins from the Late Cretaceous of Patagonia. *Nature* 387 (6631): 390–392.

Novas, F. E., Ezcurra, M. D. and Lecuona, A. 2008. *Orkoraptor burkei* nov. gen. et sp., a large theropod from the Maastrichtian Pari Aike Formation, Southern Patagonia, Argentina. *Cretaceous Research* 29 (3): 468–480.

Novas, F. E., Pol, D., Canale, J. I., Porfiri, J. D. and Calvo, J. O. 2009. A bizarre Cretaceous theropod dinosaur from Patagonia and the evolution of Gondwanan dromaeosaurids. *Proceedings of the Royal Society B: Biological Sciences* 276 (1659): 1101–1107.

Novas, F. E., Ezcurra, M. D., Agnolin, F. L., Pol, D. and Ortíz, R. 2012. New Patagonian Cretaceous theropod sheds light about the early radiation of Coelurosauria. *Revista del Museo Argentino de Ciencias Naturales* 14 (1): 57–81.

Novas, F. E., Agnolín, F. L., Ezcurra, M. D., Porfiri, J. and Canale, J. I. 2013. Evolution of the carnivorous dinosaurs during the Cretaceous: The evidence from Patagonia. *Cretaceous Research* 45: 174–215.

O'Connor, J., Zhou, Z. and Xu, X. 2011. Additional specimen of *Microraptor* provides unique evidence of dinosaurs preying on birds. *Proceedings of the National Academy of Sciences* 108 (49): 19662–19665.

Ortega, F., Escaso, F. and Sanz, J. L. 2010. A bizarre, humped Carcharodontosauria (Theropoda) from the Lower Cretaceous of Spain. *Nature* 467 (7312): 203–206.

Osborn, H. F. 1903. *Ornitholestes hermanni*, a new compsognathoid dinosaur from the Upper Jurassic. *Bulletin of the American Museum of Natural History* 19: 459–464.

Osmólska, H., Roniewicz, E. and Barsbold, R. 1972. A new dinosaur, *Gallimimus bullatus* n. gen., n. sp.(Ornithomimidae) from the Upper Cretaceous of Mongolia. *Palaeontologia Polonica* 27: 103–143.

Osmólska, H., Currie, P. J. and Barsbold, R. 2004. Oviraptorosauria. *In*: Weishampel, D. B., Dodson, P. and Osmólska, H. (eds.), *The Dinosauria. Second Edition*, 165–183. University of California Press, Berkeley, California.

Ostrom, J. H. 1969. Osteology of *Deinonychus antirrhopus*, an unusual theropod from the Lower Cretaceous of Montana. *Bulletin Peabody Museum of Natural History* 30: 1–165.

Ostrom, J. H. 1976a. *Archaeopteryx* and the origin of birds. *Biological Journal of the Linnean Society* 8 (2): 91–182.

Ostrom, J. H. 1976b. On a new specimen of the Lower Cretaceous theropod dinosaur *Deinonychus antirrhopus*. *Breviora* 439: 1–21.

Ostrom, J. H. 1978. The osteology of *Compsognathus longipes* Wagner. *Zitteliana* 4: 73–118.

Owen, R. 1840. Odontography; or, A treatise on the comparative anatomy of the teeth; their physiological relations, mode of development, and microscopic structure, in the vertebrate animals. London, H. Baillière, 766pp.

Owen, R. 1842. Report on British fossil reptiles. *Report of the British Association for the Advancement of Science* 11 (1841): 60–294.

Owen, R. 1849. *A History of British Fossil Reptiles*. Cassell & company limited, 690pp.

Owen, S. R. 1854. On some fossil reptilian and mammalian remains from the Purbecks. *Quarterly Journal of the Geological Society of London* 10: 420–433.

Padian, K. and Chiappe, L. M. 1998. The origin and early evolution of birds. *Biological Reviews* 73 (1): 1–42.

Paul, G. S. 1988. Predatory Dinosaurs of the World: A Complete Illustrated Guide. Simon & Schuster, 464pp.

Pérez-Moreno, B. P., Sanz, J. L., Buscalioni, A. D., Moratalla, J. J., Ortega, F. and Rasskin-Gutman, D. 1994. A unique multitoothed ornithomimosaur dinosaur from the Lower Cretaceous of Spain. *Nature* 370 (6488): 363–367.

Perle, A., Chiappe, L. M. and Barsbold, R. 1994. Skeletal morphology of *Mononykus olecranus* (Theropoda: Avialae) from the Late Cretaceous of Mongolia. *American Museum Novitates* 3105: 1–29.

Perle, A., Norell, M. A., Chiappe, L. M. and Clark, J. M. 1993. Flightless bird from the Cretaceous of Mongolia. *Nature* 362 (6421): 623–626.

Peyer, K. 2006. A reconsideration of *Compsognathus* from the upper Tithonian of Canjuers, southeastern France. *Journal of Vertebrate Paleontology* 26 (4): 879–896.

Platt, J. 1758. An account of the fossile thigh-bone of a large animal, dug up at Stonesfield, near Woodstock. *Philosophical Transactions of the Royal Society of London* 50: 524–527.

Plot, R. 1677. The Natural History of Oxfordshire, Being an Essay Toward the Natural History of England. Printed at the Theater, Oxford, 378pp.

Pol, D. and Rauhut, O. W. M. 2012. A Middle Jurassic abelisaurid from Patagonia and the early diversification of theropod dinosaurs. *Proceedings of the Royal Society B: Biological Sciences* 279 (1741): 3170–3175.

Porfiri, J. D., Novas, F. E., Calvo, J. O., Agnolín, F. L., Ezcurra, M. D. and Cerda, I. A. 2014. Juvenile specimen of *Megaraptor* (Dinosauria, Theropoda) sheds light about tyrannosauroid radiation. *Cretaceous Research* 51: 35–55.

Pu, H., Kobayashi, Y., Lü, J., Xu, L., Wu, Y., Chang, H., Zhang, J. and Jia, S. 2013. An unusual basal therizinosaur dinosaur with an ornithischian dental arrangement from Northeastern China. *PLoS ONE* 8 (5): e63423.

Rauhut, O. W. M. 1995. Zur systematischen Stellung der afrikanischen Theropoden *Carcharodontosaurus* Stromer 1931 und *Bahariasaurus*Stromer 1934. *Berliner Geowissenschaften Abhlandlungen E* 16: 357–375.

Rauhut, O. W. M. 2003a. The interrelationships and evolution of basal theropod dinosaurs. *Special Papers in Palaeontology* 69: 1–213.

Rauhut, O. W. M. 2003b. A tyrannosauroid dinosaur from the Upper Jurassic of Portugal. *Palaeontology* 46 (5): 903–910.

Rauhut, O. W. M. 2004a. Provenance and anatomy of *Genyodectes serus*, a large-toothed ceratosaur (Dinosauria: Theropoda) from Patagonia. *Journal of Vertebrate Paleontology* 24 (4): 894–902.

Rauhut, O. W. M. 2005. Osteology and relationships of a new theropod dinosaur from the Middle Jurassic of Patagonia. *Palaeontology* 48 (1): 87–110.

Rauhut, O. W. M. and Xu, X. 2005. The small theropod dinosaurs *Tugulusaurus* and *Phaedrolosaurus* from the early Cretaceous of Xinjiang, China. *Journal of Vertebrate Paleontology* 25 (1): 107–118.

Rauhut, O. W. M., Milner, A. C. and Moore-Fay, S. 2010. Cranial osteology and phylogenetic position of the theropod dinosaur *Proceratosaurus bradleyi* (Woodward, 1910) from the Middle Jurassic of England. *Zoological Journal of the Linnean Society* 158 (1): 155–195.

Rauhut, O. W. M., Foth, C., Tischlinger, H. and Norell, M. A. 2012. Exceptionally preserved juvenile megalosauroid theropod dinosaur with filamentous integument from the Late Jurassic of Germany. *Proceedings of the National Academy of Sciences* 109 (29): 11746–11751.

Rauhut, O. W. 2004b. Braincase structure of the Middle Jurassic theropod dinosaur *Piatnitzkysaurus*. *Canadian Journal of Earth Sciences* 41 (9): 1109–1122.

Rauhut, O. W. 2011. Theropod dinosaurs from the Late Jurassic of Tendaguru (Tanzania). *Special Papers in Palaeontology* 86: 195–239.

Rauhut, O. W. and Hungerbühler, A. 1998. A review of European Triassic theropods. *Gaia* 15: 75–88.

Von Ritgen, F. A. 1826. Versuchte Herstellung einiger Becken urweltlichter Thiere. *Nova Acta Academiae Caesarea LeopoldinoCarolinae Germanicae Naturae Curiosorum* 13: 331–358.

Romer, A. 1956. *Osteology of the Reptiles*. University of Chicago Press, Chicago, 772pp.

Ruiz, J., Torices, A., Serrano, H. and López, V. 2011. The hand structure of *Carnotaurus sastrei* (Theropoda, Abelisauridae): implications for hand diversity and evolution in abelisaurids. *Palaeontology* 54 (6): 1271–1277.

Russell, D. A. 1970. Tyrannosaurs from the Late Cretaceous of western Canada. *National Museum of Natural Sciences Publications in Paleontology* 1: 1–34.

Russell, D. A. 1972. Ostrich dinosaurs from the Late Cretaceous of Western Canada. *Canadian Journal of Earth Sciences* 9 (4): 375–402.

Russell, D. A. 1984. A check list of the families and genera of North American dinosaurs. *Syllogeus* 53: 1–35.

Russell, D. A. and Dong, Z. 1993. The affinities of a new theropod from the Alxa Desert, Inner Mongolia, People's Republic of China. *Canadian Journal of Earth Sciences* 30 (10): 2107–2127.

Russell, L. S. 1948. The dentary of *Troödon*, a genus of theropod dinosaurs. *Journal of Paleontology* 22 (5): 625–629.

Sadleir, R., Barrett, P. M. and Powell, H. P. 2008. The anatomy and systematics of *Eustreptospondylus oxoniensis*, a theropod dinosaur from the Middle Jurassic of Oxfordshire, England. *Monograph of the Palaeontographical Society, London* 160: 1–82.

Sampson, S. D. and Witmer, L. M. 2007. Craniofacial anatomy of *Majungasaurus crenatissimus* (Theropoda: Abelisauridae) from the Late Cretaceous of Madagascar. *Journal of Vertebrate Paleontology* 27 (sup2): 32–104.

Sampson, S. D., Witmer, L. M., Forster, C. A., Krause, D. W., O'Connor, P. M., Dodson, P. and Ravoavy, F. 1998. Predatory dinosaur remains from Madagascar: implications for the Cretaceous biogeography of Gondwana. *Science* 280 (5366): 1048–1051.

Dal Sasso, C. 2003. Dinosaurs of Italy. *Comptes Rendus Palevol* 2 (1): 46–66.

Dal Sasso, C. and Maganuco, S. 2011. *Scipionyx samniticus* (Theropoda: Compsognathidae) from the Lower Cretaceous of Italy: osteology, ontogenetic assessment, phylogeny, soft tissue anatomy, taphonomy and palaeobiology. *Memorie della Società Italiana di Scienze Naturali e del Museo Civico di Storia Naturale di Milano* 37 (1): 1–281.

Dal Sasso, C., Maganuco, S., Buffetaut, E. and Mendez, M. A. 2005. New information on the skull of the enigmatic theropod *Spinosaurus*, with remarks on its size and affinities. *Journal of Vertebrate Paleontology* 25 (4): 888–896.

Schweitzer, M. h., Watt, J. a., Avci, R., Knapp, L., Chiappe, L., Norell, M. and Marshall, M. 1999. Beta-keratin specific immunological reactivity in feather-like structures of the Cretaceous Alvarezsaurid, Shuvuuia deserti. *Journal of Experimental Zoology* 285 (2): 146–157.

Seeley, H. G. 1887. On the classification of the fossil animals commonly named Dinosauria. *Proceedings of the Royal Society of London* 43 (258-265): 165–171.

Senter, P. 2007. A new look at the phylogeny of Coelurosauria (Dinosauria: Theropoda). *Journal of Systematic Palaeontology* 5 (4): 429–463.

Senter, P. 2011. Using creation science to demonstrate evolution 2: morphological continuity within Dinosauria. *Journal of Evolutionary Biology* 24 (10): 2197–2216.

Senter, P., Kirkland, J. I. and DeBlieux, D. D. 2012a. *Martharaptor greenriverensis*, a New Theropod Dinosaur from the Lower Cretaceous of Utah. *PLoS ONE* 7 (8): e43911.

Senter, P., Barsbold, R., Britt, B. B. and Burnham, D. A. 2004. Systematics and evolution of Dromaeosauridae (Dinosauria, Theropoda). *Bulletin of Gunma Museum of Natural History* 8: 1–20.

Senter, P., Kirkland, J. I., DeBlieux, D. D., Madsen, S. and Toth, N. 2012b. New dromaeosaurids (Dinosauria: Theropoda) from the Lower Cretaceous of Utah, and the evolution of the dromaeosaurid tail. *PLoS ONE* 7 (5): e36790.

Sereno, P. C. 1997. The origin and evolution of dinosaurs. *Annual Review of Earth and Planetary Sciences* 25 (1): 435–489.

Sereno, P. C. 1998. A rationale for phylogenetic definitions, with application to the higher-level taxonomy of Dinosauria. *Neues Jahrbuch fur Geologie und Palaontologie Abhandlungen* 210: 41–83.

Sereno, P. C. 1999. The Evolution of Dinosaurs. *Science* 284 (5423): 2137–2147.

Sereno, P. C., Beck, A. L., Dutheil, D. B., Gado, B., Larsson, H. C. E., Lyon, G. H., Marcot, J. D., Rauhut, O. W. M., Sadleir, R. W., Sidor, C. A., Varricchio, D. D., Wilson, G. P. and Wilson, J. A. 1998. A long-snouted predatory dinosaur from Africa and the evolution of spinosaurids. *Science* 282 (5392): 1298–1302.

Sereno, P. C. and Wild, R. 1992. *Procompsognathus*: theropod, 'thecodont' or both? *Journal of Vertebrate Paleontology* 12 (4): 435–458.

Sereno, P. C. and Novas, F. E. 1994. The skull and neck of the basal theropod *Herrerasaurus ischigualastensis*. *Journal of Vertebrate Paleontology* 13 (4): 451–476.

Sereno, P. C. and Brusatte, S. L. 2008. Basal abelisaurid and carcharodontosaurid theropods from the Lower Cretaceous Elrhaz Formation of Niger. *Acta Palaeontologica Polonica* 53 (1): 15–46.

Sereno, P. C., Martínez, R. N. and Alcober, O. A. 2013. Osteology of *Eoraptor lunensis* (Dinosauria, Sauropodomorpha). *Journal of Vertebrate Paleontology* 32 (sup1): 83–179.

Sereno, P. C., Wilson, J. A., Larsson, H. C. E., Dutheil, D. B. and Sues, H.-D. 1994. Early Cretaceous dinosaurs from the Sahara. *Science* 266 (5183): 267–271.

Sereno, P. C., Martinez, R. N., Wilson, J. A., Varricchio, D. J., Alcober, O. A. and Larsson, H. C. E. 2008. Evidence for avian intrathoracic air sacs in a new predatory dinosaur from Argentina. *PLoS ONE* 3 (9): e3303.

Sereno, P. C., Dutheil, D. B., Larochene, M., Larsson, H. C. E., Lyon, G. H., Magwene, P. M., Sidor, C. A., Varricchio, D. J. and Wilson, J. A. 1996. Predatory dinosaurs from the Sahara and Late Cretaceous faunal differentiation. *Science* 272 (5264): 986–991.

Smith, J. B., Lamanna, M. C., Mayr, H. and Lacovara, K. J. 2006. New information regarding the holotype of *Spinosaurus aegyptiacus* Stromer, 1915. *Journal of Paleontology* 80 (2): 400–406.

Smith, N. D., Makovicky, P. J., Hammer, W. R. and Currie, P. J. 2007. Osteology of *Cryolophosaurus ellioti* (Dinosauria: Theropoda) from the Early Jurassic of Antarctica and implications for early theropod evolution. *Zoological Journal of the Linnean Society* 151 (2): 377–421.

Spalding, D. E. A. and Sarjeant, W. A. S. 2012. Dinosaurs: The Earliest Discoveries. *In*: Brett-Surman, M. K., Holtz, T. R. J. and Farlow, J. O. (eds.), *The Complete Dinosaur, Second Edition*, 3–24. Indiana University Press, Bloomington, Indiana.

Stevens, K. A. 2006. Binocular vision in theropod dinosaurs. *Journal of Vertebrate Paleontology* 26 (2): 321–330.

Stiegler, J., Wang, S., Xu, X. and Clark, J. M. 2014. New anatomical details on the basal ceratosaur *Limusaurus* and implications for the Jurassic radiation of Theropoda. *74th Annual Meeting Society of Vertebrate Paleontology, Berlin, Germany. (November 5-8, 2014), Program and Abstracts*: 235.

Stromer, E. 1915. Ergebnisse der Forschungsreisen Prof. E. Stromers in den Wüsten Ägyptens. II. Wirbeltier-Reste der Baharîje-Stufe (unterstes Cenoman). 3. Das Original des Theropoden *Spinosaurus aegyptiacus* nov. gen., nov. spec. *Abhandlungen der Königlichen Bayerischen Akademie der Wissenschaften, Mathematisch- Physikalische Klasse* 28: 1–32.

Sues, H.-D. 1977. The skull of *Velociraptor mongoliensis*, a small Cretaceous theropod dinosaur from Mongolia. *Paläontologische Zeitschrift* 51 (3-4): 173–184.

Sues, H.-D., Frey, E., Martill, D. M. and Scott, D. M. 2002. *Irritator challengeri*, a spinosaurid (Dinosauria: Theropoda) from the Lower Cretaceous of Brazil. *Journal of Vertebrate Paleontology* 22 (3): 535–547.

Sues, H.-D., Nesbitt, S. J., Berman, D. S. and Henrici, A. C. 2011. A late-surviving basal theropod dinosaur from the latest Triassic of North America. *Proceedings of the Royal Society B: Biological Sciences* 278 (1723): 3459–3464.

Suzuki, S., Chiappe, L. M. and Dyke, G. J. 2002. A new specimen of *Shuvuuia deserti* Chiappe *et al.,* 1998, from the Mongolian late Cretaceous with a discussion of the relationships of alvarezsaurids to other theropod dinosaurs. *Contributions in Science* 194: 1–18.

Thulborn, R. A. 1984. The avian relationships of *Archaeopteryx*, and the origin of birds. *Zoological Journal of the Linnean Society* 82 (1-2): 119–158.

Tortosa, T., Buffetaut, E., Vialle, N., Dutour, Y., Turini, E. and Cheylan, G. 2014. A new abelisaurid dinosaur from the Late Cretaceous of southern France: Palaeobiogeographical implications. *Annales de Paléontologie* 100 (1): 63–86.

Tsuihiji, T., Watabe, M., Tsogtbaatar, K., Tsubamoto, T., Barsbold, R., Suzuki, S., Lee, A. H., Ridgely, R. C., Kawahara, Y. and Witmer, L. M. 2011. Cranial osteology of a juvenile specimen of *Tarbosaurus bataar* (Theropoda, Tyrannosauridae) from the Nemegt Formation (Upper Cretaceous) of Bugin Tsav, Mongolia. *Journal of Vertebrate Paleontology* 31 (3): 497–517.

Tsuihiji, T., Barsbold, R., Watabe, M., Tsogtbaatar, K., Chinzorig, T., Fujiyama, Y. and Suzuki, S. 2014. An exquisitely preserved troodontid theropod with new information on the palatal structure from the Upper Cretaceous of Mongolia. *Naturwissenschaften* 101 (2): 131–142.

Turner, A. H., Makovicky, P. J. and Norell, M. A. 2007. Feather quill knobs in the dinosaur *Velociraptor*. *Science* 317 (5845): 1721–1721.

Turner, A. H., Makovicky, P. J. and Norell, M. 2012. A review of dromaeosaurid systematics and paravian phylogeny. *Bulletin of the American Museum of Natural History* 371: 1–206.

Tykoski, R. S. 2005. Anatomy, ontogeny, and phylogeny of coelophysoid theropods. Ph.D. Dissertation, The University of Texas, Austin, Texas, 553pp.

Tykoski, R. S. and Rowe, T. 2004. Ceratosauria. *In*: Weishampel, D., Dodson, P. and Osmólska, H. (eds.), *The Dinosauria. Second Edition*, 47–70. University of California Press, Berkeley, California.

Varricchio, D. J., Moore, J. R., Erickson, G. M., Norell, M. A., Jackson, F. D. and Borkowski, J. J. 2008. Avian paternal care had dinosaur origin. *Science* 322 (5909): 1826–1828.

Vullo, R. and Néraudeau, D. 2010. Additional dinosaur teeth from the Cenomanian (Late Cretaceous) of Charentes, southwestern France. *Comptes Rendus Palevol* 9 (3): 121–126.

Wagner, A. 1861. Neue Beiträge zur Kenntnis der urweltlichen Fauna des lithographischen Schiefers; V. *Compsognathus longipes* Wagner. *Abhandlungen der Bayerischen Akademie der Wissenschaften* 9: 30–38.

Walker, A. D. 1964. Triassic reptiles from the Elgin Area: *Ornithosuchus* and the origin of carnosaurs. *Philosophical Transactions of the Royal Society of London. Series B, Biological Sciences* 248 (744): 53–134.

Welles, S. P. 1984. *Dilophosaurus wetherilli* (Dinosauria, Theropoda). Osteology and comparisons. *Palaeontographica Abteilung A* 185 (4-6): 85–180.

Wilson, J. A., Sereno, P. C., Srivastava, S., Bhatt, D. K., Khosla, A. and Sahni, A. 2003. A new abelisaurid (Dinosauria, Theropoda) from the Lameta Formation (Cretaceous, Maastrichtian) of India. *Contributions from the Museum of Paleontology, University of Michigan* 31 (1): 1–42.

Witmer, L. M. and Ridgely, R. C. 2009. New insights into the brain, braincase, and ear region of tyrannosaurs (Dinosauria, Theropoda), with implications for sensory organization and behavior. *The Anatomical Record: Advances in Integrative Anatomy and Evolutionary Biology* 292 (9): 1266–1296.

Woodward, J. M. D. 1729. An attempt towards a natural history of the fossils of England in a catalogue of the English fossils in the collection of J. Woodward, M.D. Printed for F. Fayram, J. Senex, and J. Osborn and T. Longman, 656pp.

Xing, L. 2012. *Sinosaurus* from southwestern China. MSc. Dissertation, University of Alberta, Edmonton, Alberta, Canada, 267pp.

Xing, L., Bell, P. R., Persons, W. S., Ji, S., Miyashita, T., Burns, M. E., Ji, Q. and Currie, P. J. 2012. Abdominal Contents from Two Large Early Cretaceous Compsognathids (Dinosauria:

Theropoda) Demonstrate Feeding on Confuciusornithids and Dromaeosaurids. *PLoS ONE* 7 (8): e44012.

Xing, L., Persons, W. S., Bell, P. R., Xu, X., Zhang, J., Miyashita, T., Wang, F. and Currie, P. J. 2013. Piscivory in the feathered dinosaur *Microraptor*. *Evolution* 67 (8): 2441–2445.

Xu, X., Sullivan, C., Pittman, M., Choiniere, J. N., Hone, D., Upchurch, P., Tan, Q., Xiao, D., Tan, L. and Han, F. 2011a. A monodactyl nonavian dinosaur and the complex evolution of the alvarezsauroid hand. *Proceedings of the National Academy of Sciences* 108 (6): 2338–2342.

Xu, X., Clark, J. M., Mo, J., Choiniere, J., Forster, C. A., Erickson, G. M., Hone, D. W. E., Sullivan, C., Eberth, D. A., Nesbitt, S., Zhao, Q., Hernandez, R., Jia, C., Han, F. and Guo, Y. 2009a. A Jurassic ceratosaur from China helps clarify avian digital homologies. *Nature* 459 (7249): 940–944.

Xu, X. and Wu, X.-C. 2001. Cranial morphology of *Sinornithosaurus millenii* Xu et al. 1999 (Dinosauria: Theropoda: Dromaeosauridae) from the Yixian Formation of Liaoning, China. *Canadian Journal of Earth Sciences* 38 (12): 1739–1752.

Xu, X. and Wang, X.-L. 2004. A new troodontid (Theropoda: Troodontidae) from the lower Cretaceous Yixian Formation of western Liaoning, China. *Acta Geologica Sinica* 78 (1): 22–26.

Xu, X. and Norell, M. A. 2004. A new troodontid dinosaur from China with avian-like sleeping posture. *Nature* 431 (7010): 838–841.

Xu, X. and Han, F. L. 2010. A new oviraptorid dinosaur (Theropoda: Oviraptorosauria) from the Upper Cretaceous of China. *Vertebrata PalAsiatica* 48: 11–18.

Xu, X. and Pol, D. 2014. *Archaeopteryx*, paravian phylogenetic analyses, and the use of probability-based methods for palaeontological datasets. *Journal of Systematic Palaeontology* 12 (3): 323–334.

Xu, X., Tang, Z. and Wang, X. 1999a. A therizinosauroid dinosaur with integumentary structures from China. *Nature* 399 (6734): 350–354.

Xu, X., Wang, X.-L. and Wu, X.-C. 1999b. A dromaeosaurid dinosaur with a filamentous integument from the Yixian Formation of China. *Nature* 401 (6750): 262–266.

Xu, X., Zhou, Z. and Prum, R. O. 2001. Branched integumental structures in *Sinornithosaurus* and the origin of feathers. *Nature* 410 (6825): 200–204.

Xu, X., Zheng, X. and You, H. 2009b. A new feather type in a nonavian theropod and the early evolution of feathers. *Proceedings of the National Academy of Sciences* 106 (3): 832–834.

Xu, X., Zheng, X. and You, H. 2010. Exceptional dinosaur fossils show ontogenetic development of early feathers. *Nature* 464 (7293): 1338–1341.

Xu, X., Cheng, Y.-N., Wang, X.-L. and Chang, C.-H. 2002a. An unusual oviraptorosaurian dinosaur from China. *Nature* 419 (6904): 291–293.

Xu, X., You, H., Du, K. and Han, F. 2011b. An *Archaeopteryx*-like theropod from China and the origin of Avialae. *Nature* 475 (7357): 465–470.

Xu, X., Norell, M. A., Wang, X., Makovicky, P. J. and Wu, X. 2002b. A basal troodontid from the Early Cretaceous of China. *Nature* 415 (6873): 780–784.

Xu, X., Zhou, Z., Wang, X., Kuang, X., Zhang, F. and Du, X. 2003. Four-winged dinosaurs from China. *Nature* 421 (6921): 335–340.

Xu, X., Norell, M. A., Kuang, X., Wang, X., Zhao, Q. and Jia, C. 2004. Basal tyrannosauroids from China and evidence for protofeathers in tyrannosauroids. *Nature* 431 (7009): 680–684.

Xu, X., Clark, J. M., Forster, C. A., Norell, M. A., Erickson, G. M., Eberth, D. A., Jia, C. and Zhao, Q. 2006. A basal tyrannosauroid dinosaur from the Late Jurassic of China. *Nature* 439 (7077): 715–718.

Xu, X., Wang, K., Zhang, K., Ma, Q., Xing, L., Sullivan, C., Hu, D., Cheng, S. and Wang, S. 2012. A gigantic feathered dinosaur from the Lower Cretaceous of China. *Nature* 484 (7392): 92–95.

Yates, A. M. 2005. A new theropod dinosaur from the Early Jurassic of South Africa and its implications for the early evolution of theropods. *Palaeontologia Africana* 41: 105–122.

Zanno, L. E. 2006. The pectoral girdle and forelimb of the primitive therizinosauroid *Falcarius utahensis* (Theropoda, Maniraptora): analyzing evolutionary trends within Therizinosauroidea. *Journal of Vertebrate Paleontology* 26 (3): 636–650.

Zanno, L. E. 2010a. A taxonomic and phylogenetic re-evaluation of Therizinosauria (Dinosauria: Maniraptora). *Journal of Systematic Palaeontology* 8 (4): 503–543.

Zanno, L. E. 2010b. Osteology of *Falcarius utahensis* (Dinosauria: Theropoda): characterizing the anatomy of basal therizinosaurs. *Zoological Journal of the Linnean Society* 158 (1): 196–230.

Zanno, L. E. and Makovicky, P. J. 2011. Herbivorous ecomorphology and specialization patterns in theropod dinosaur evolution. *Proceedings of the National Academy of Sciences* 108 (1): 232–237.

Zanno, L. E. and Makovicky, P. J. 2013. Neovenatorid theropods are apex predators in the Late Cretaceous of North America. *Nature Communications* 4.

Zanno, L. E., Gillette, D. D., Albright, L. B. and Titus, A. L. 2009. A new North American therizinosaurid and the role of herbivory in 'predatory' dinosaur evolution. *Proceedings of the Royal Society B: Biological Sciences* 276 (1672): 3505–3511.

Zanno, L. E., Varricchio, D. J., O'Connor, P. M., Titus, A. L. and Knell, M. J. 2011. A New Troodontid Theropod, *Talos sampsoni* gen. et sp. nov., from the Upper Cretaceous Western Interior Basin of North America. *PLoS ONE* 6 (9): e24487.

Zelenitsky, D. K., Therrien, F. and Kobayashi, Y. 2009. Olfactory acuity in theropods: palaeobiological and evolutionary implications. *Proceedings of the Royal Society B: Biological Sciences* 276 (1657): 667–673.

Zelenitsky, D. K., Therrien, F., Erickson, G. M., DeBuhr, C. L., Kobayashi, Y., Eberth, D. A. and Hadfield, F. 2012. Feathered non-avian dinosaurs from North America provide insight into wing origins. *Science* 338 (6106): 510–514.

Zhang, F., Kearns, S. L., Orr, P. J., Benton, M. J., Zhou, Z., Johnson, D., Xu, X. and Wang, X. 2010. Fossilized melanosomes and the colour of Cretaceous dinosaurs and birds. *Nature* 463 (7284): 1075–1078.

Zhang, X.-H., Xu, X., Zhao, X.-J., Sereno, P., Kuang, X.-W. and Tan, L. 2001. A long-necked therizinosauroid dinosaur from the Upper Cretaceous Iren Dabasu Formation of nei Mongol, People's Republic of China. *Vertebrata PalAsiatica* 39 (4): 283–294.

Zhao, X. and Xu, X. 1998. The oldest coelurosaurian. *Nature* 394 (6690): 234–235.

Zheng, X., Xu, X., You, H., Zhao, Q. and Dong, Z. 2010. A short-armed dromaeosaurid from the Jehol Group of China with implications for early dromaeosaurid evolution. *Proceedings of the Royal Society B: Biological Sciences* 277 (1679): 211–217.

Zhou, Z.-H., Wang, X.-L., Zhang, F.-C. and Xu, X. 2000. Important features of *Caudipteryx*-evidence from two nearly complete new specimens. *Vertebrata PalAsiatica* 38 (4): 243–265.

Zinke, J. 1998. Small theropod teeth from the Upper Jurassic coal mine of Guimarota (Portugal). *Paläontologische Zeitschrift* 72 (1): 179–189.

Figures

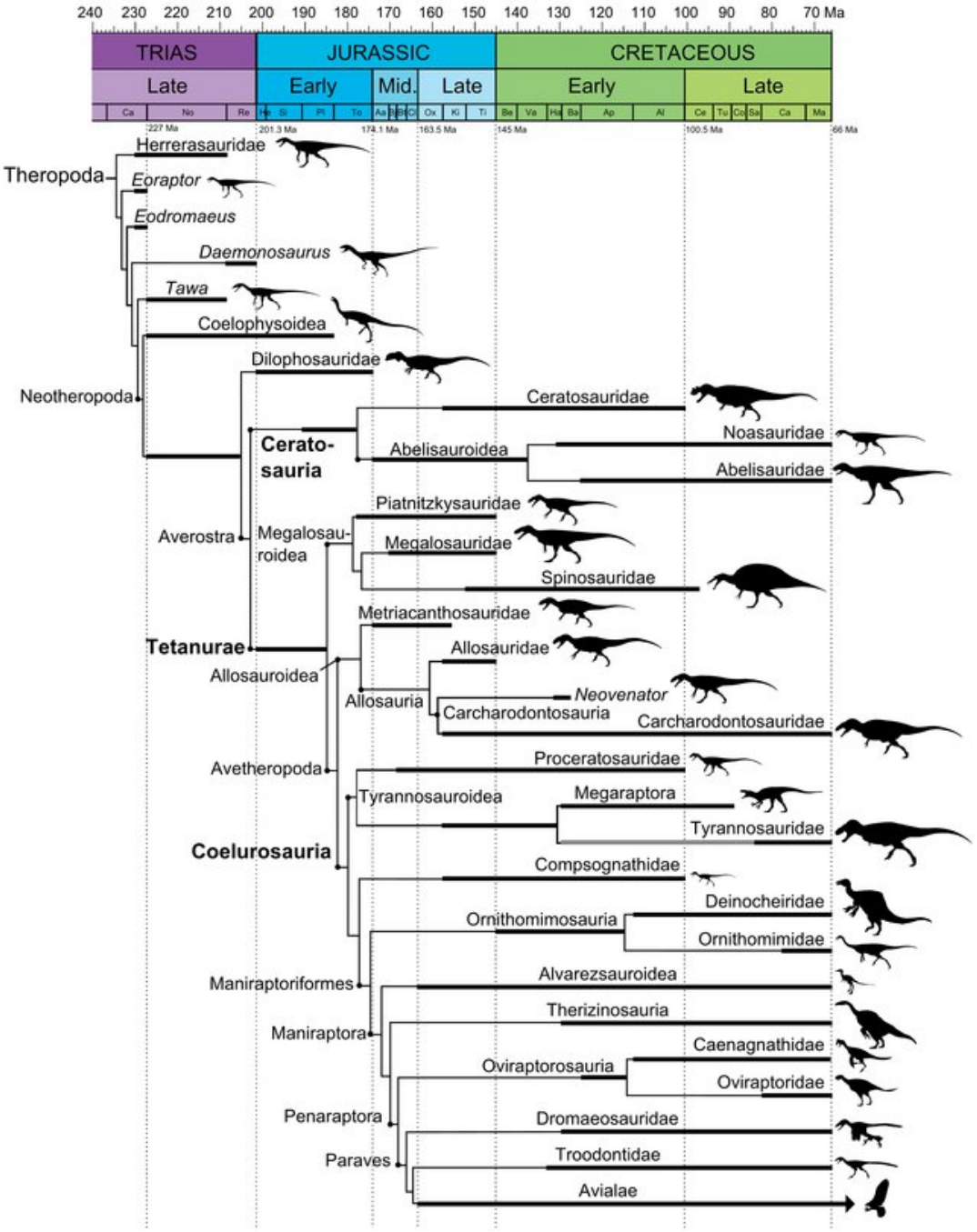

FIGURE S2-1. Phylogeny and stratigraphic distribution of theropod clades. *The phylogenetic classification of theropods follows the results of the cladistic analyses obtained by Sues et al. (2011) for non-neotheropod Theropoda, Smith et al. (2007) and Ezcurra and Brusatte (2011) for non-averostran Neotheropoda, Pol and Rauhut (2012) and Tortosa et al. (2014) for Ceratosauria, Carrano et al. (2012) for non-coelurosaur Tetanurae, Loewen et al. (2013), Lü et al. (2014) and Porfiri et al. (2014) for Tyrannosauroidea, and Turner et al. (2012), Godefroit et al. (2013a) and Choiniere et al. (2014) for non-tyrannosauroid Coelurosauria.*

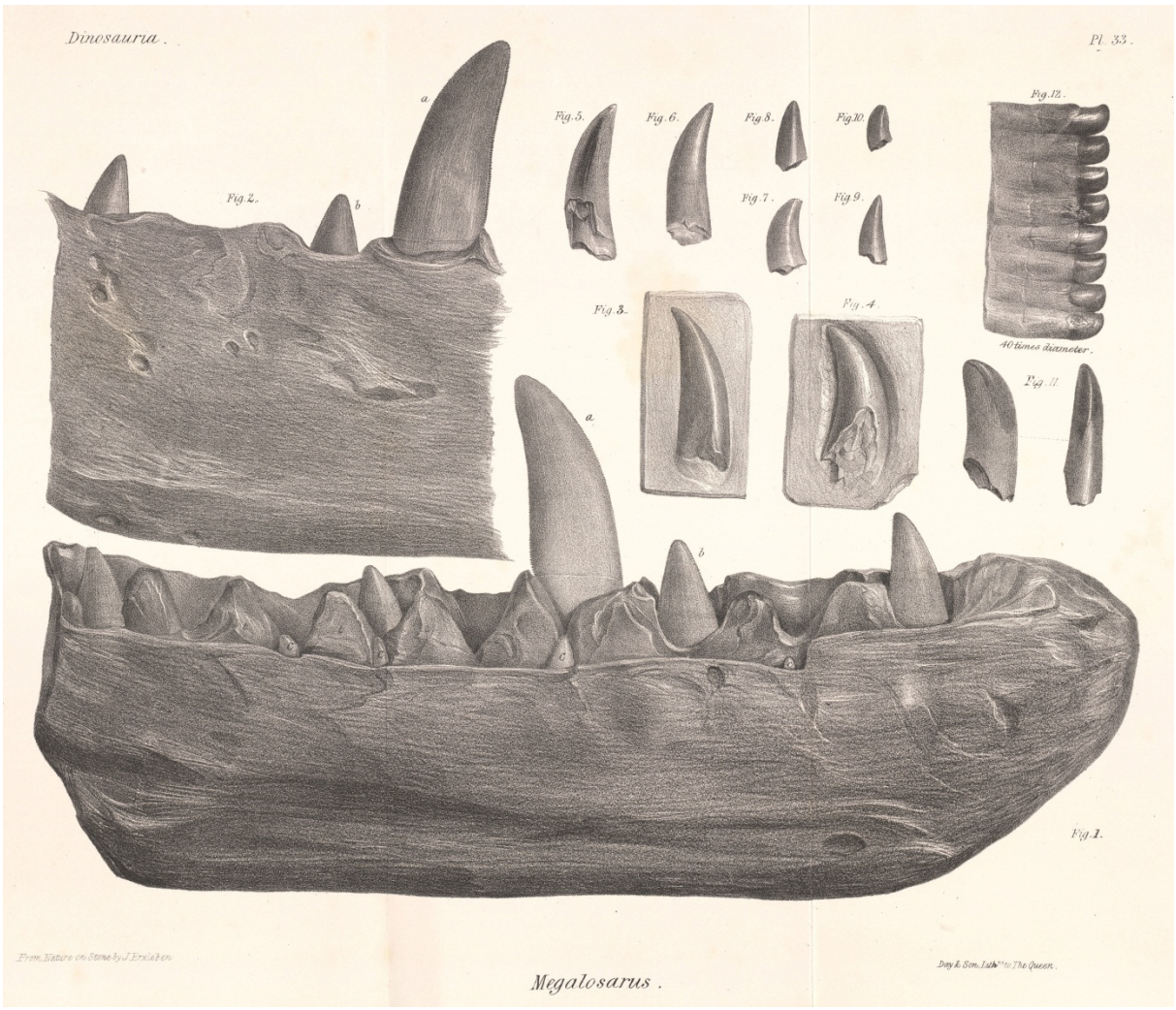

FIGURE S2-2. Dentary and isolated teeth of Megalosaurus bucklandii illustrated by Owen (1849-1884) in his book A History of British Fossil Reptile. *Megalosaurus is the first (non-avian) dinosaur to be illustrated and reported in the literature by Plot (1677), but also the first dinosaur to be formally named by Buckland (1824; for the genus) and Mantell (1827; for the species) based on the here illustrated dentary and other postcranial bones. Teeth belonging to this taxon were the first to be illustrated for a theropod by Lhuyd (1699), and the Megalosaurus dentition was the first one to be thoroughly described the literature by Owen (1840-1845) in his Odontography. Finally, both disarticulated dentary and maxilla of Megalosaurus bucklandii were the first theropod maxilla and dentary to receive a detailed description.*

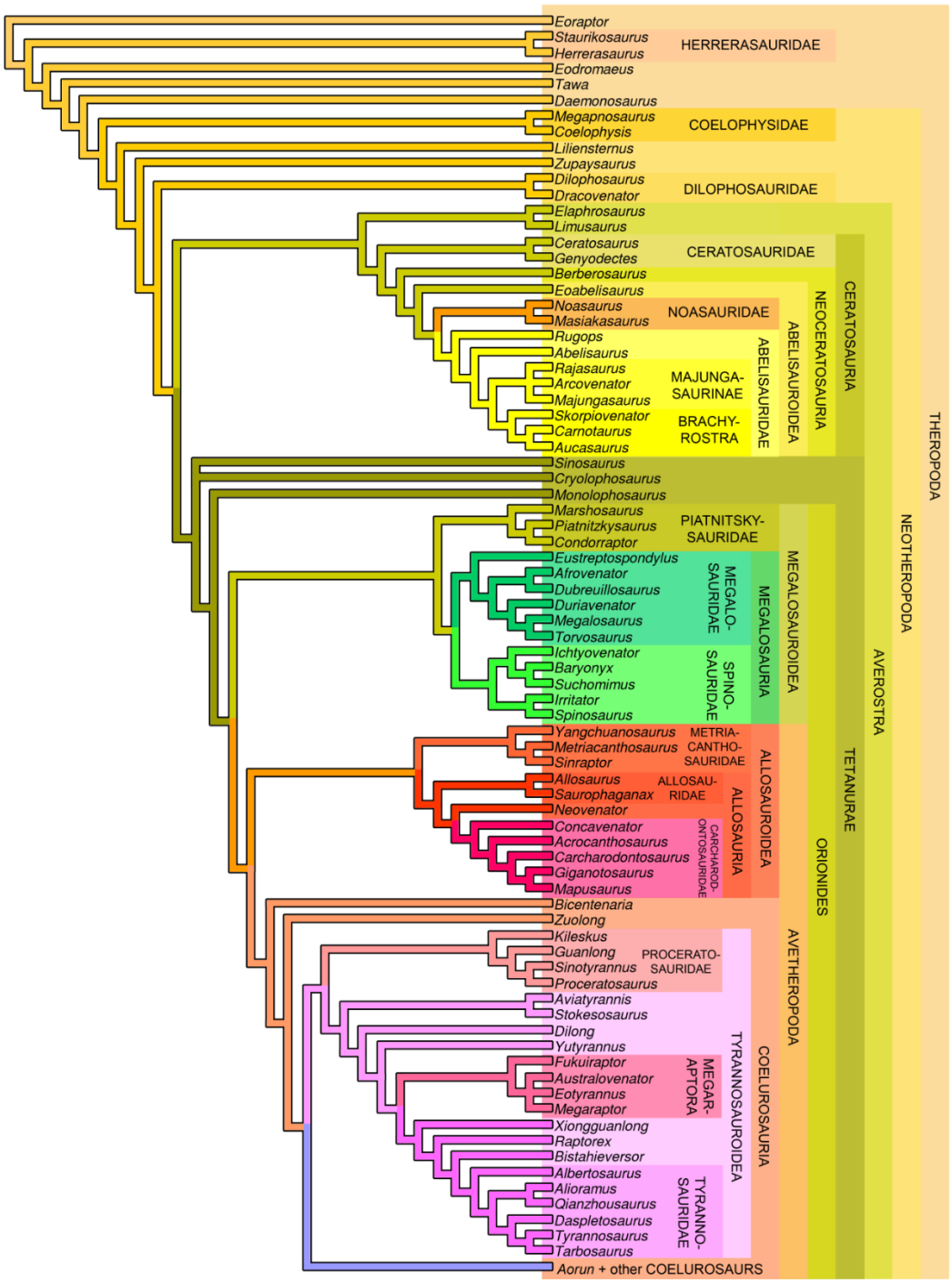

FIGURE S2-3. Cladogram of basal Theropoda showing the relationships of 'non-neocoelurosaur' theropod taxa. *The phylogenetic classification follows the results of the cladistic analyses obtained by Sues et al. (2011) for non-neotheropod Theropoda, Smith et al. (2007) and Ezcurra and Brusatte (2011) for non-averostran Neotheropoda, Pol and Rauhut (2012) and Tortosa et al. (2014) for Ceratosauria, Carrano et al. (2012) for non-coelurosaur Tetanurae, Loewen et al. (2013), Lü et al. (2014) and Porfiri et al. (2014) for Tyrannosauroidea, and Choiniere et al. (2014) for basalmost Coelurosauria.*

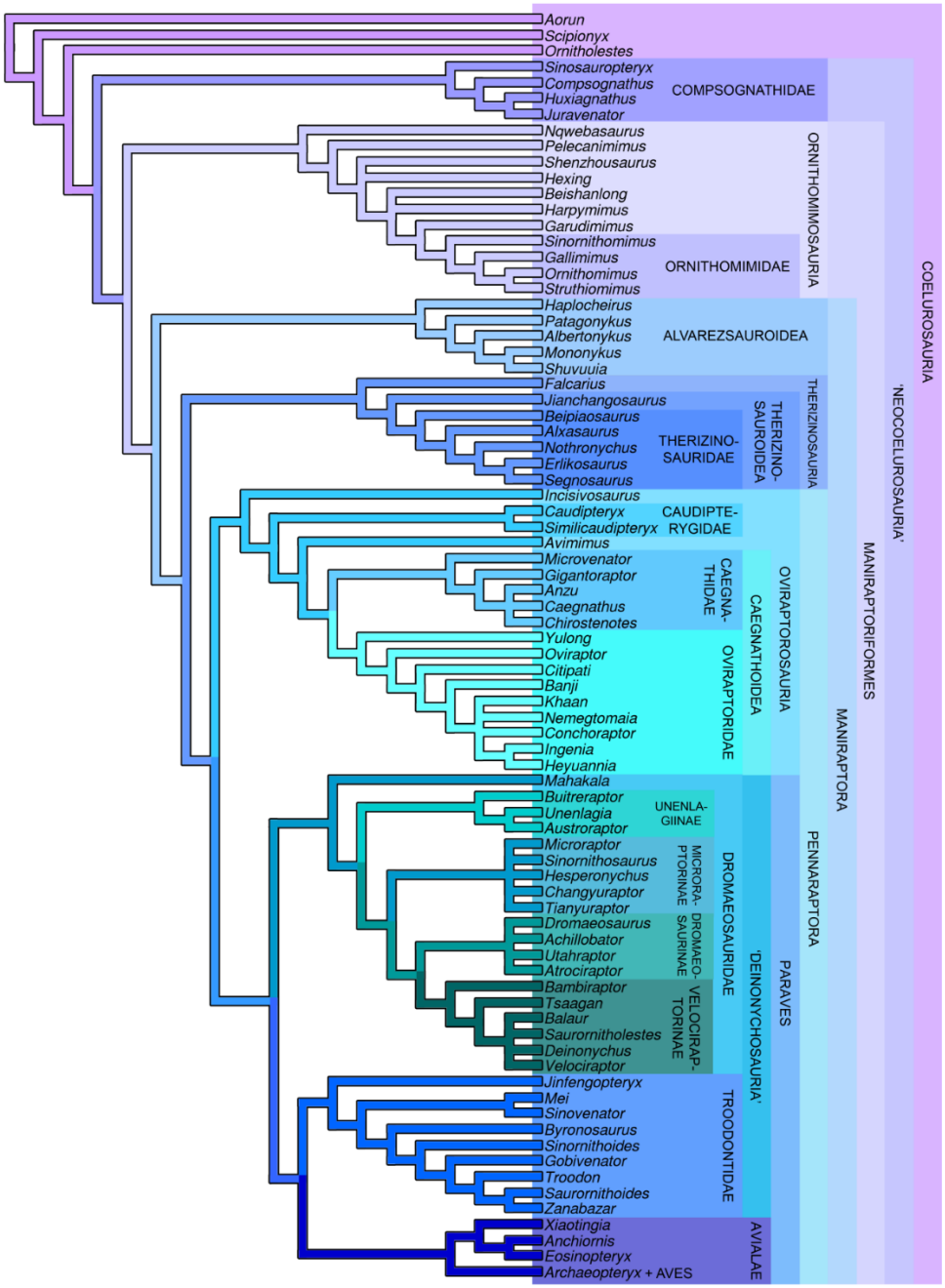

FIGURE S2-4. Cladogram of 'neocoelurosaur' Theropoda showing the relationships of non-tyrannosauroid coelurosaurs. *The phylogenetic classification follows the results of the cladistic analyses obtained by Choiniere et al. (2014) for basalmost Coelurosauria and Compsognathidae, Longrich and Currie (2009a) and Choiniere et al. (2010b) for Alvarezsauroidea, Choiniere et al. (2012) and Liyong et al. (2012) for Ornithomimosauria, Senter et al. (2012a) and Pu et al. (2013) for Therizinosauria, Lamanna et al. (2014) for Oviraptorosauria, Turner et al. (2012) for Paraves, and Foth et al. (2014) for Avialae.*

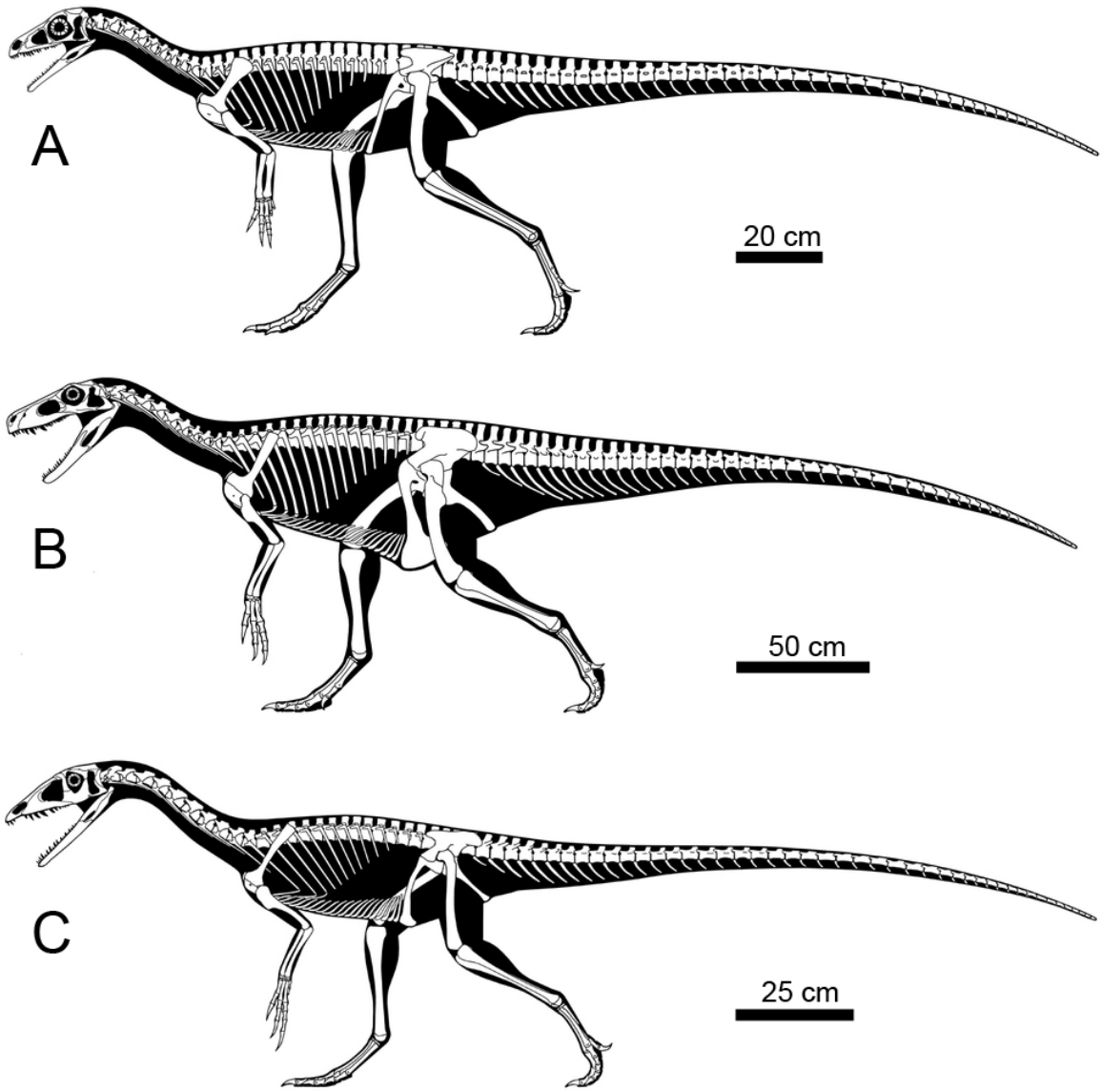

FIGURE S2-5. Skeletal reconstructions of three non-neotheropod saurischians (and possibly three basalmost theropods). *A, the possible primitive sauropodomorph Eoraptor lunensis; B, the herrerasaurid Herrerasaurus ischigualastensis; and C, the very basal theropod Tawa hallae. Reconstructions by © Scott Hartman.*

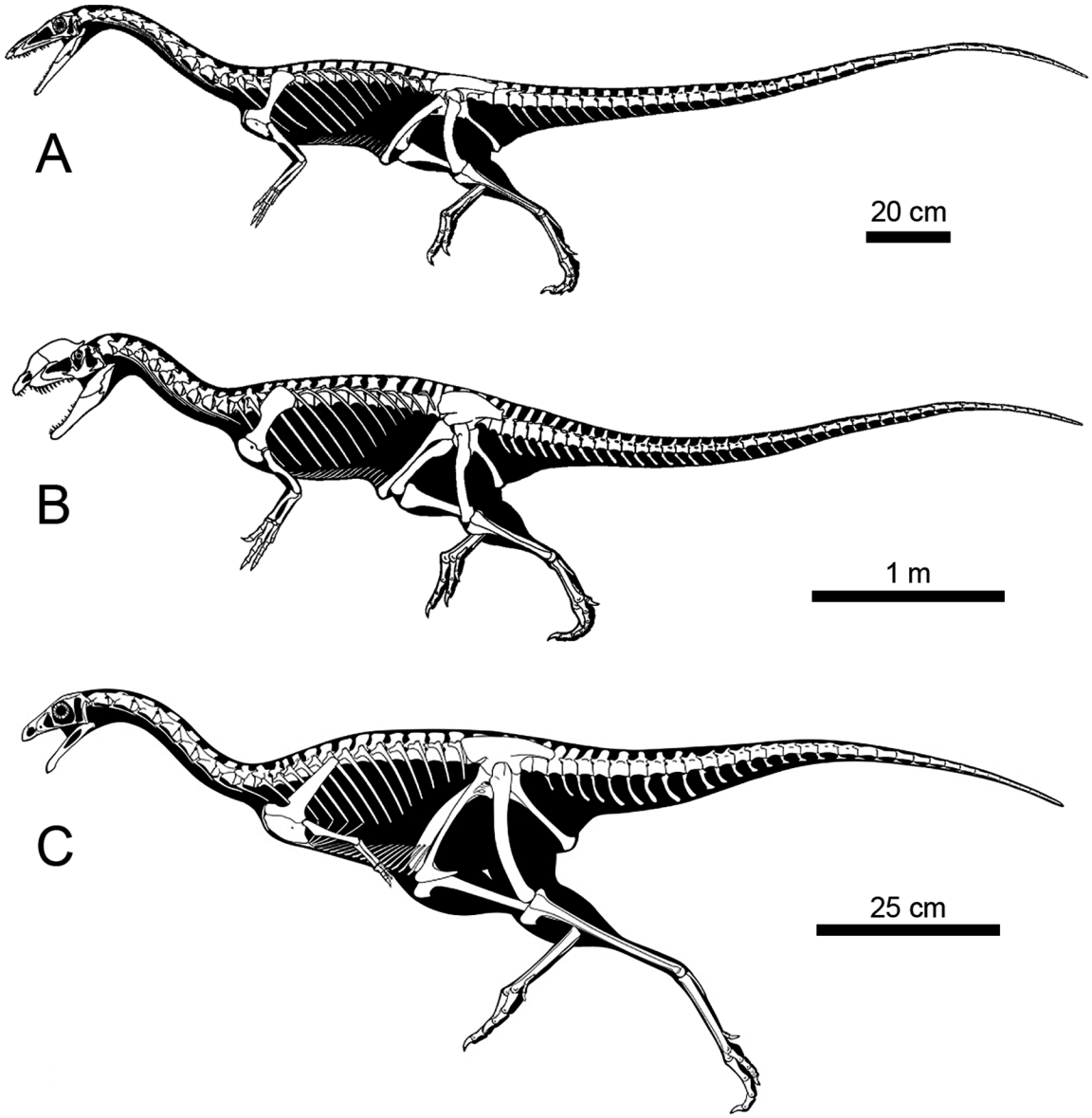

FIGURE S2-6. Skeletal reconstructions of two non-averostran neotheropods and one basal ceratosaur*. A) The coelophysoid Coelophysis bauri; B) The dilophosaurid Dilophosaurus wetherilli; C) The 'elaphrosaur' Limusaurus inextricabilis. Reconstructions by Gregory Paul for Coelophysis and Dilophosaurus (modified), and Ville Sinkkonen for Limusaurus (modified).*

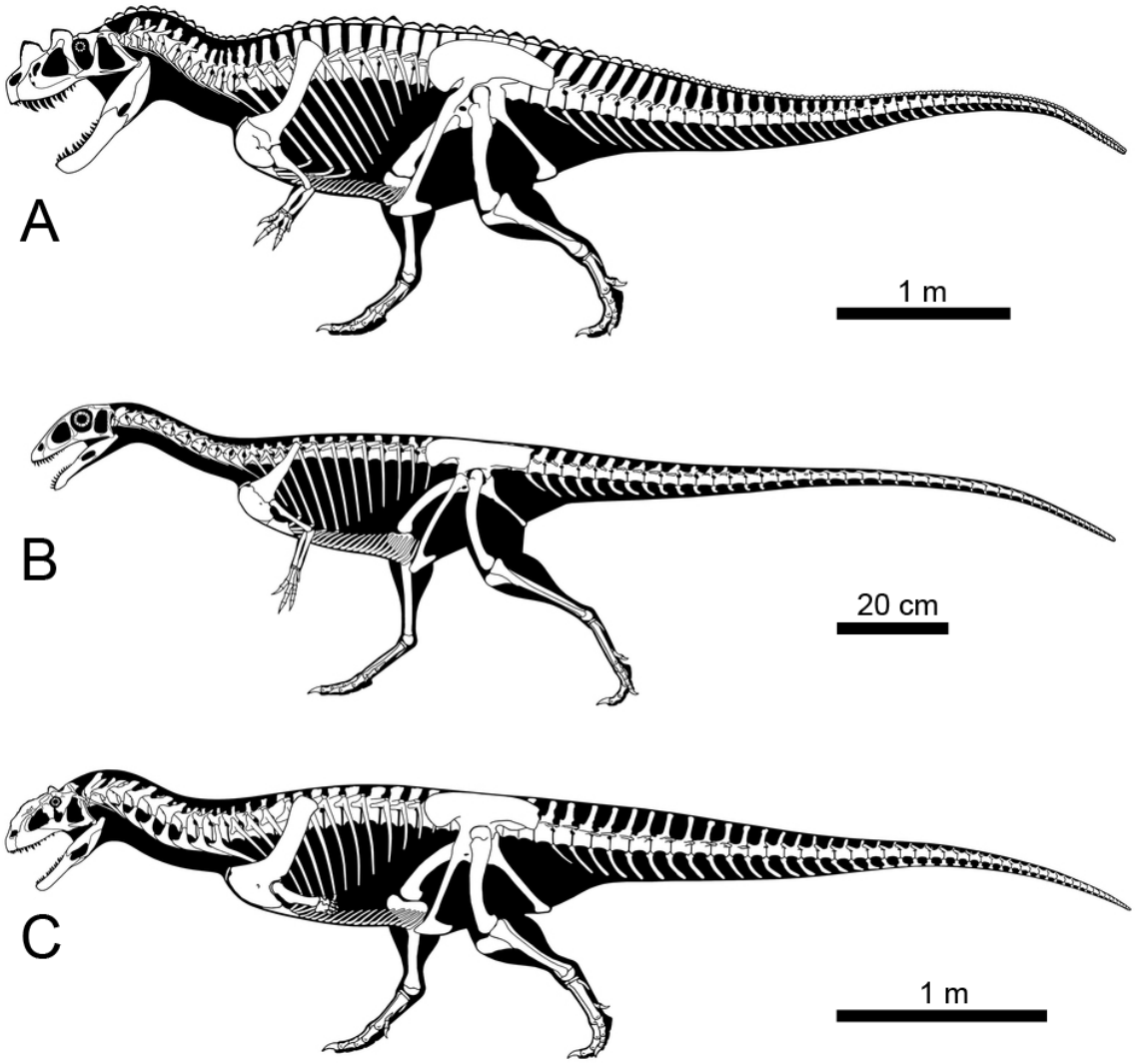

FIGURE S2-7. Skeletal reconstructions of three ceratosaurs*. A, the ceratosaurid Ceratosaurus nasicornis; B, the noasaurid Masiakasaurus knopfleri; C, the abelisaurid Majungasaurus crenatissimus. Reconstructions by © Scott Hartman.*

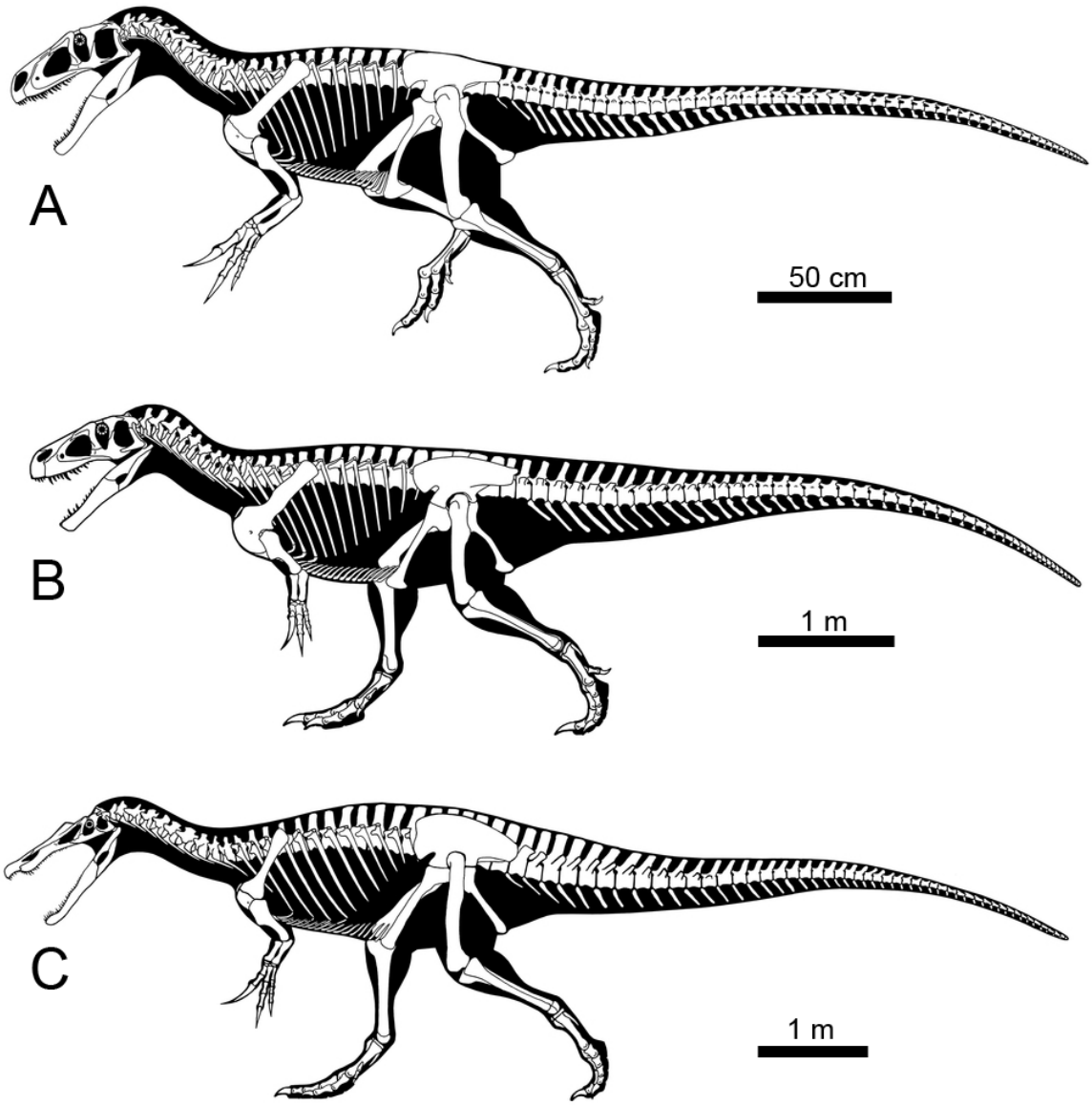

Fig. S2-8. Skeletal reconstructions of three megalosauroids*. A, the piatnitzkysaurid Marshosaurus bicentissimus; B, the megalosaurid Megalosaurus bucklandii; and C, the spinosaurid Baryonyx walkeri. Reconstructions by © Scott Hartman.*

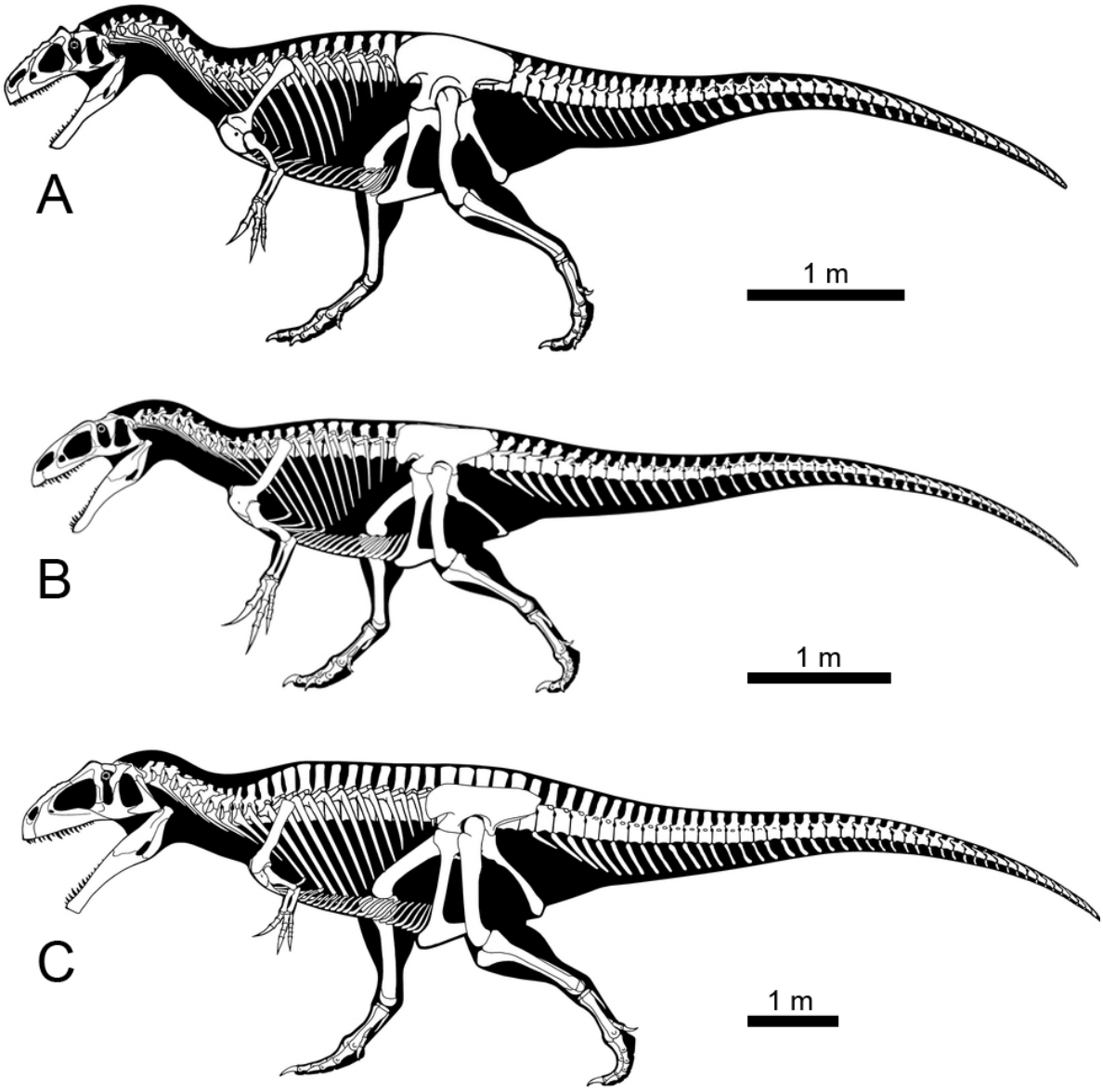

FIGURE S2-9. Skeletal reconstructions of three allosauroids. *A, the allosaurid Allosaurus 'jimmadseni'; B, the neovenatorid Neovenator salerii; and C, the carcharodontosaurid Giganotosaurus carolinii. Reconstructions by © Scott Hartman.*

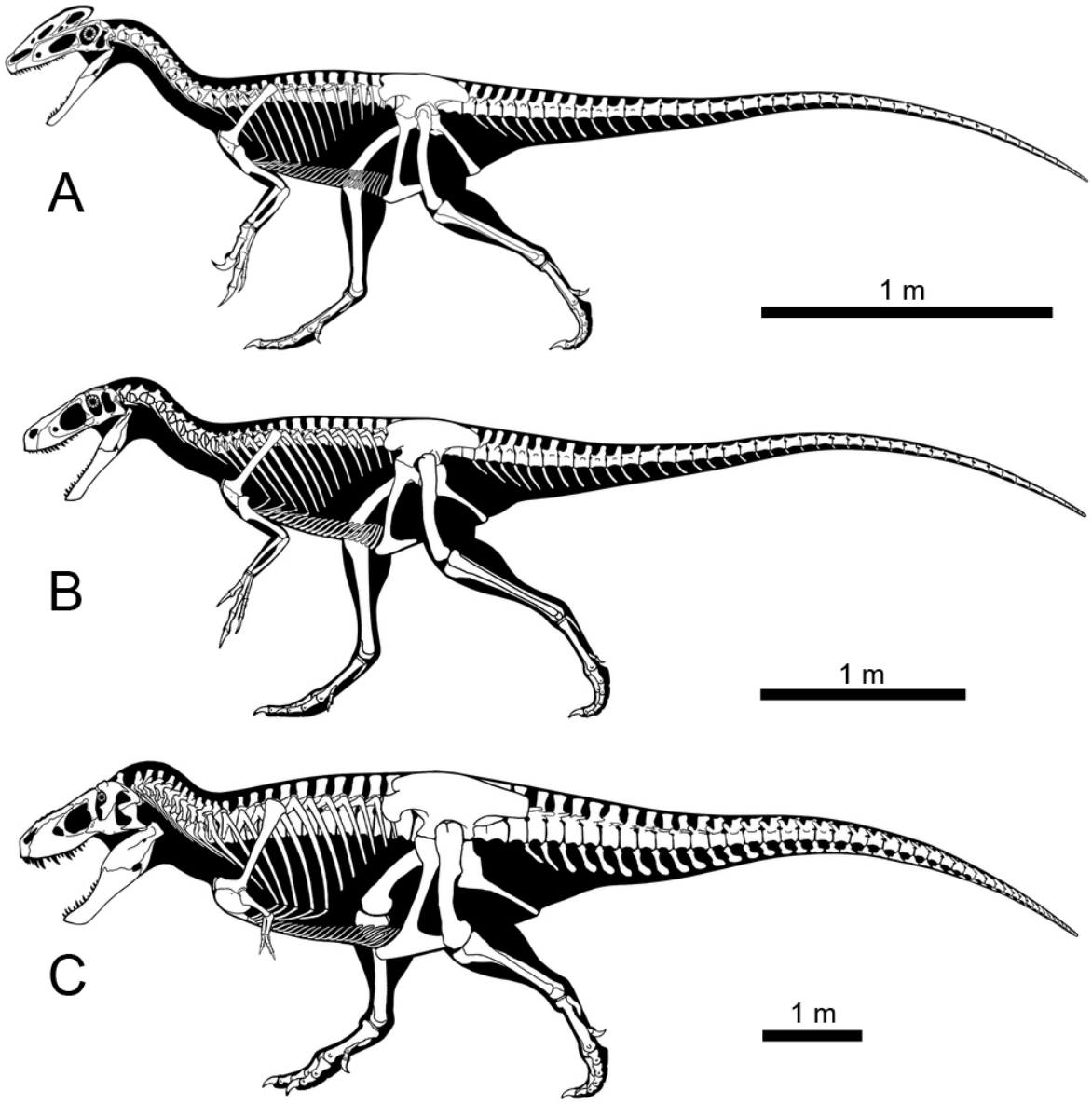

***FIGURE S2-10. Skeletal reconstructions of three tyrannosauroids**. A, the proceratosaurid Guanlong wucaii; B, the possible megaraptorid Eotyrannus lengi; and C, the tyrannosaurid Tyrannosaurus rex. Reconstructions by © Scott Hartman.*

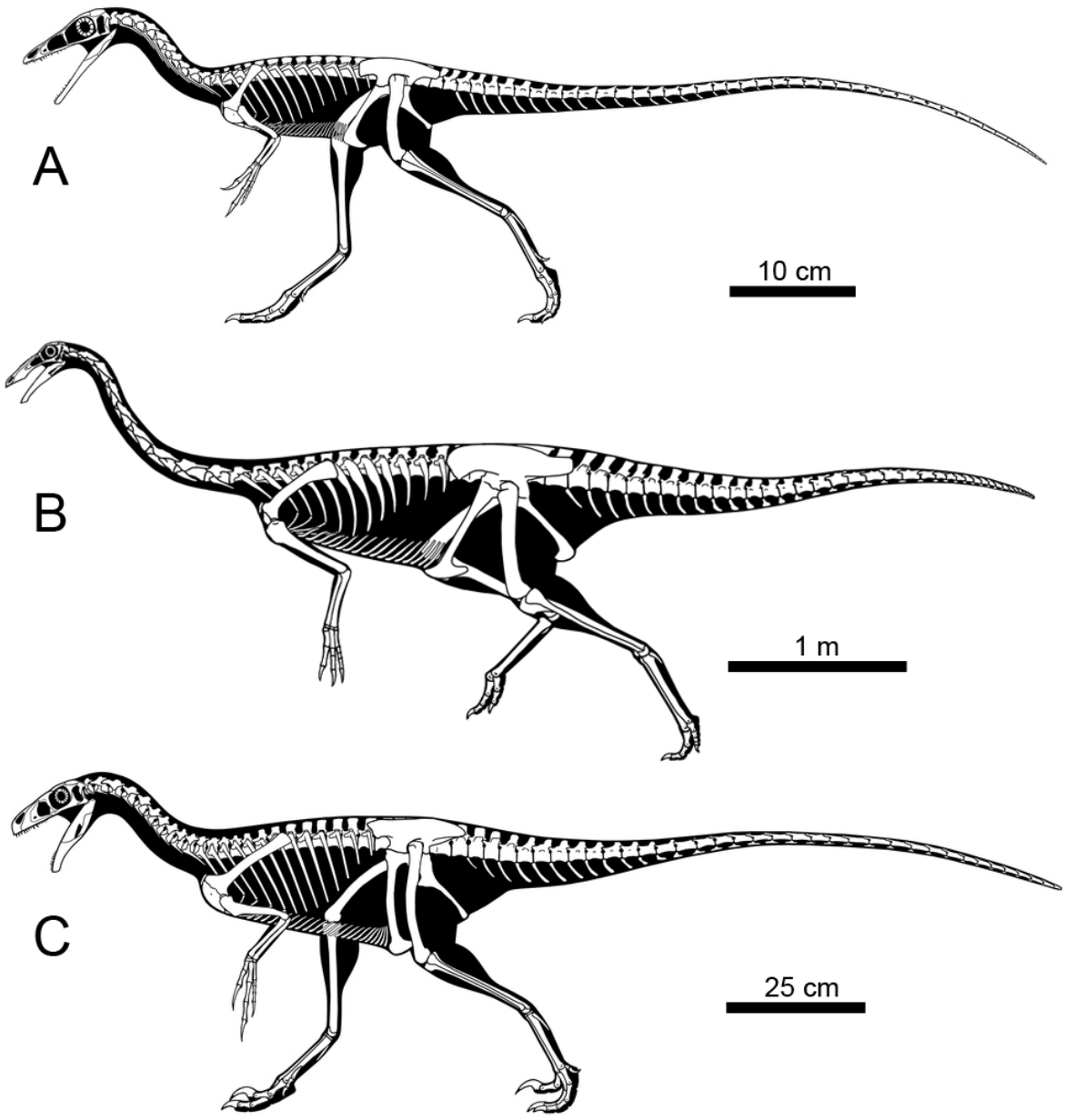

FIGURE S2-11. Skeletal reconstructions of three basal maniraptoriforms. *A, the compsognathid Compsognathus longipes; B, the ornithomimid Gallimimus bullatus; and C, the basal maniraptoran Ornitholestes hermanni. Reconstructions by © Scott Hartman.*

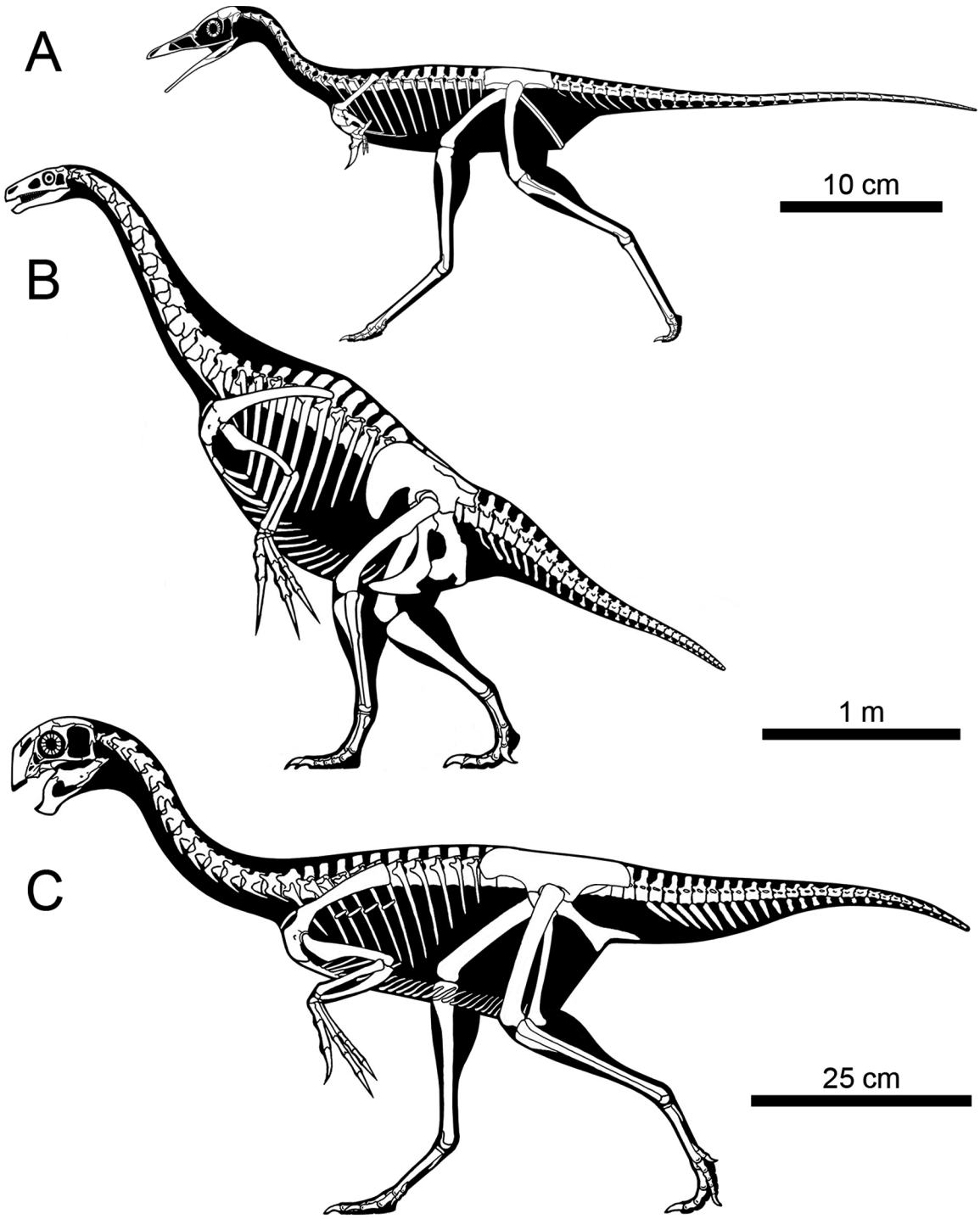

FIGURE S2-12. Skeletal reconstructions of three basal maniraptorans. *A) The alvarezsauroid Shuvuuia deserti; B) The therizinosauroid Nothronychus graffami; C) The oviraptorosaur Khaan mangas. Reconstructions by Scott Hartman.*

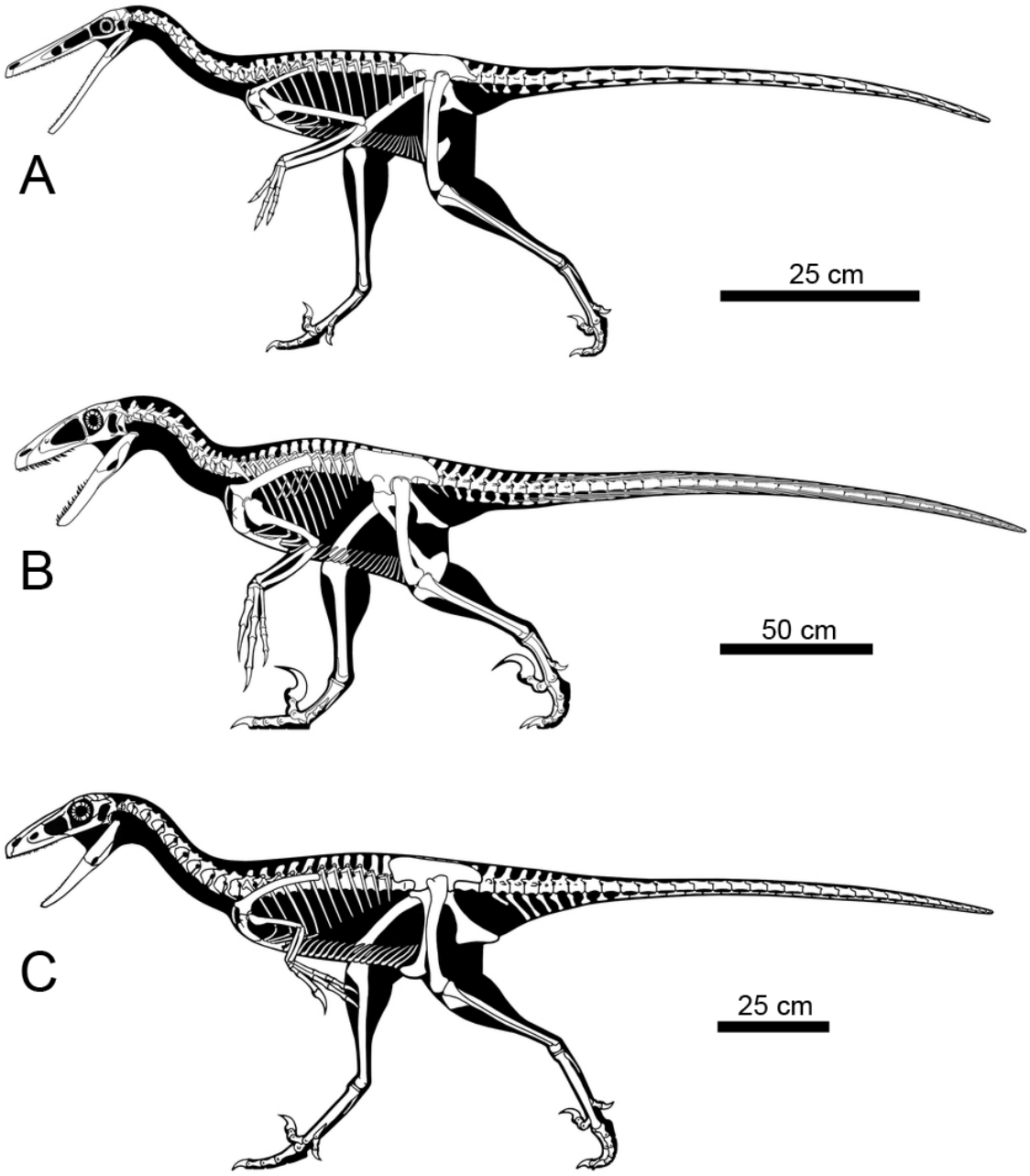

FIGURE S2-13. Skeletal reconstructions of three basal paravians. *A, the unenlagiine dromaeosaurid Buitreraptor gonzalezorum; B, the velociraptorine dromaeosaurid Deinonychus antirrhopus; and C, the troodontid Troodon formosus. Reconstructions by © Scott Hartman.*

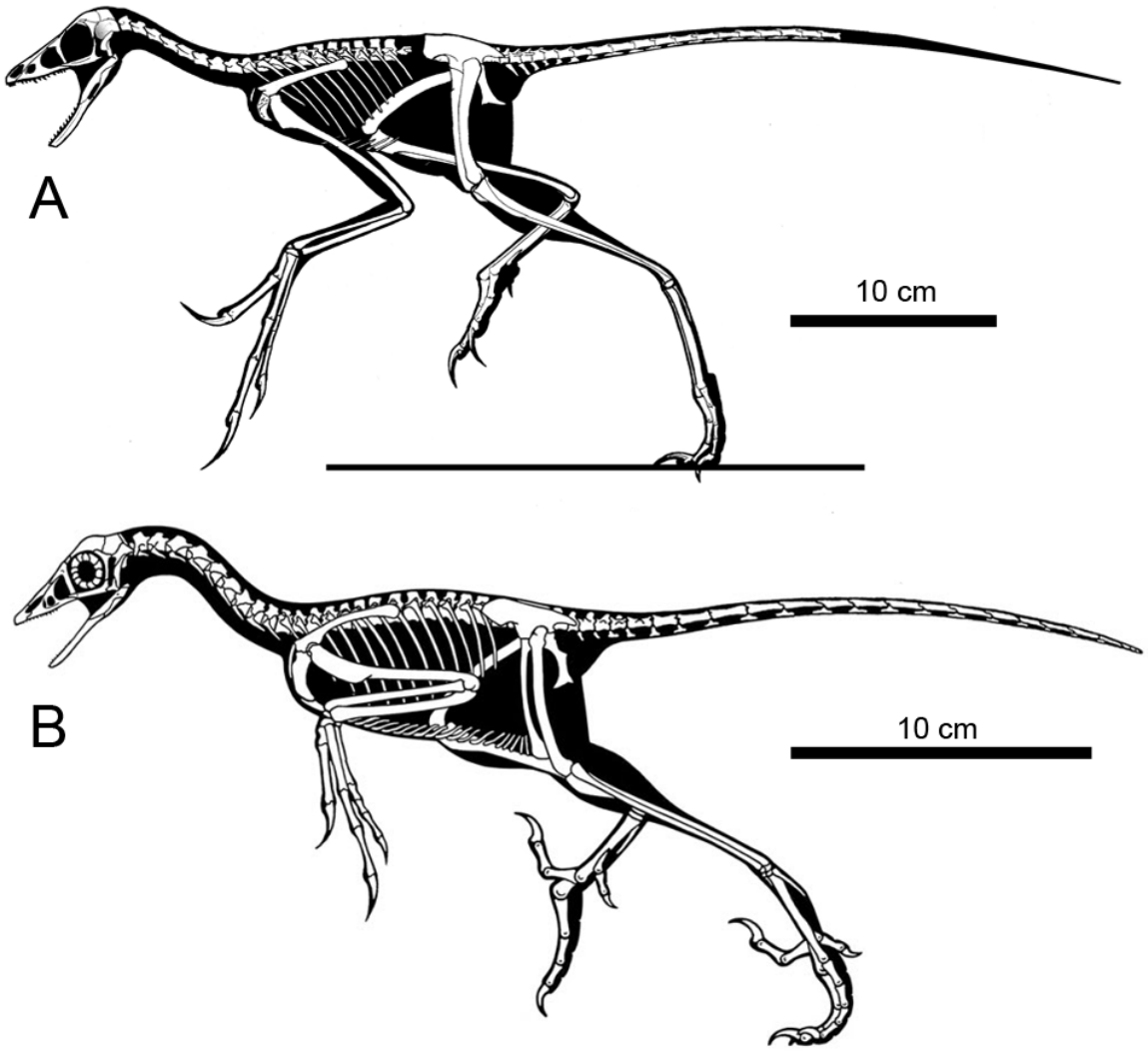

FIGURE S2-14. Skeletal reconstructions of two avialan theropods. *A, the basal avialan Anchiornis huxley; and B, the archaeopterygid Archaeopteryx sp. Reconstructions by © Jaime A. Headden for Anchiornis and © Scott Hartman for Archaeopteryx.*

Supplement C – Coauthored paper relevant to Chapter 3:

Basal paravian functional anatomy illuminated by the first high-detail body outline

Xiaoli Wang[1†], Michael Pittman[2†], Xiaoting Zheng[1,3], Thomas G. Kaye[4], Amanda R. Falk[5], Scott A. Hartman[6], Xing Xu[1,7]

[1]Institute of Geology and Paleontology, Linyi University, Linyi City, Shandong, 276005, China.
[2]Vertebrate Palaeontology Laboratory, Department of Earth Sciences, University of Hong Kong, Pokfulam, Hong Kong, China.
[3]Shandong Tianyu Museum of Nature, Pingyi, Shandong, 273300, China.
[4]Foundation for Scientific Advancement, 7023 Alhambra Drive, Sierra Vista, Arizona, 85650, United States of America.
[5]Department of Biology, Centre College, 600 West Walnut Street, Danville, Kentucky, 40422, United States of America.
[6]Department of Geoscience, University of Wisconsin-Madison, Lewis G. Weeks Hall for Geological Sciences, 1215 West Dayton Street, Madison, Wisconsin, 53706-1692, United States of America.
[7]Key Laboratory of Vertebrate Evolution and Human Origins of Chinese Academy of Sciences, Institute of Vertebrate Paleontology and Paleoanthropology, Chinese Academy of Sciences, Beijing, 100044, China.

Abstract

Body shape is a fundamental expression of organismal biology, but its quantitative reconstruction in fossil vertebrates is rare because it requires unusual specimens with pristine preservation. The body shape of basal paravians are inferred from their skeletons, feathers and knowledge of modern avian and crocodilian musculoskeletal anatomy. Due to the absence of fossilised soft tissue evidence, the functional consequences of basal paravian body shape and its implications on avian and flight origins are not yet fully understood. To address this, the first quantitative body outline of a fossil paravian *Anchiornis* is reconstructed based on high-definition images of soft tissues revealed by laser-stimulated fluorescence. This body outline confirms patagia-bearing arms, drumstick-shaped legs and a slender tail, features that were probably widespread among paravians, with forelimb patagia even known in non-paravian pennaraptorans. Finely preserved details also reveal similarities in propatagial and footpad form between basal paravians and modern birds extending their record to at least the Late Jurassic, with similar basal tetanuran footpads being even older. This new body outline and soft tissue details suggest significant functional decoupling between the legs and tail in at least some basal paravians and the number of seemingly modern propatagial traits they possess hint that feather patterning was a significant factor in how this decoupling was utilized for aerodynamic benefit.

Laser-stimulated fluorescence (LSF) imaging can broaden the scope of data available from fossils by revealing morphological details that are otherwise invisible under white or UV light conditions[1]. In this study, LSF imaging is performed on the four-winged dinosaur *Anchiornis*[2,3], one of a few key basal paravian theropods - including *Microraptor* and *Archaeopteryx* - whose osteology, feathering and aerodynamics have made profound contributions to understanding of avian origins and early flight evolution[3-8]. *Anchiornis* is

especially suited for this study because these aspects have not been fully realized even though it is the earliest four-winged paravian with long tibial and metatarsal feathers, which is a key feature of gliding-capable *Microraptor*[3,5,9]. *Anchiornis* is also represented by 229+ specimens[10], which greatly improves the chance of discovering rare soft tissue preservation with minimal taphonomic damage. The LSF data collected was used to produce and describe the first quantitative outlines of portions of the fossil paravian body. In providing much needed fossilised soft tissue evidence, the scope of indirect skeletal and feather evidence in determining basal paravian body shape will be better understood. Additionally, the utility of body shape inferences based on an extant phylogenetic bracket (EPB) approach can be gauged. The functional consequences of the new data and its implications on understanding of avian and flight origins is discussed.

LSF imaging recovered high fidelity outlines of the arms, legs and tail for *Anchiornis*, but head, neck and thorax outlines could not be reliably imaged (Fig. S3-1). The slender arm outline is widest across the propatagia (Figs. S3-1, 2). The latter are preserved at 69°-94° of elbow extension and are less widely extended than the smaller postpatagia (Supplementary Fig. S1; Table S1). There is no obvious alular patagium, unlike enantiornithine MCCMLH31444[11]. The propatagial surface is covered in almost evenly spaced - but not scattered[11] - spots that occasionally contain brown filamentous structures. The third manual digit is covered in small rounded reticulate scales (Suppl. Fig. S2). The outline interpreted as the margin of the soft tissue is approximately twice as thick as the phalanges of the third digit and has a smooth ventral surface without thick fleshy pads, as in the fingers of oviraptorosaur *Caudipteryx* (fig. 1, plate II of [12]).

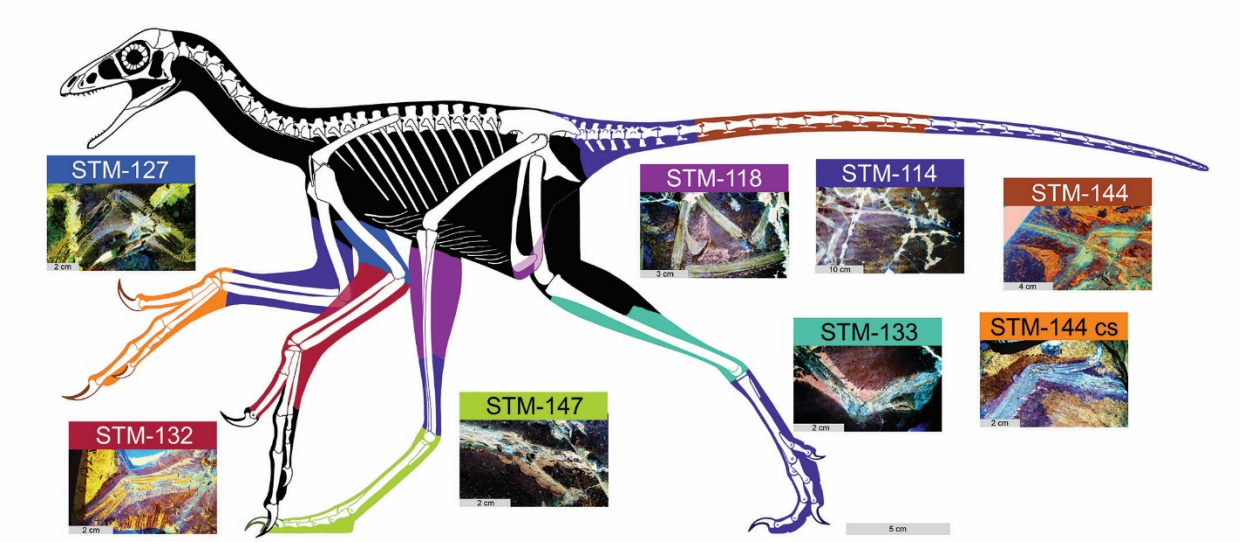

Fig. S3-1. Reconstructed body outline of basal paravian Anchiornis using scaled LSF images selected amongst 229 specimens. *Coloured areas represent different specimens and black ones are approximated from equivocal data. Skeleton predominantly reconstructed from STM-118 and its scale is 5cm. See Methods.*

The leg outlines are known up to the proximal end of the tibia and fibula and are widest at the proximal two-thirds of the latter (Fig. S3-1), the same shape in birds[13,14]. The feet have bird-like plantar footpads with interpad grooves exhibiting the typical arthal condition of theropods[15,16] (Figs. S3-1, 3). The footpads are covered in pebble-shaped reticulate scales (Fig. S3-3), but the dorsal foot scales are minimally discernible. There are pebble-shaped tibia scales and equivocal ankle scales (Suppl. Fig. S3).

The slender tail outline hugs the caudal vertebrae, but at its base it forms a gently concave margin from the third caudal to the tip of the posterior ramus of the ischium (Figs. S3-1, 4 [the ischium is not preserved in STM-0-114, but its position is inferred from STM-0-118 and other specimens]). The body outline follows the shape of the pubic boot and then ascends at a steep angle towards the distal end of the ischium.

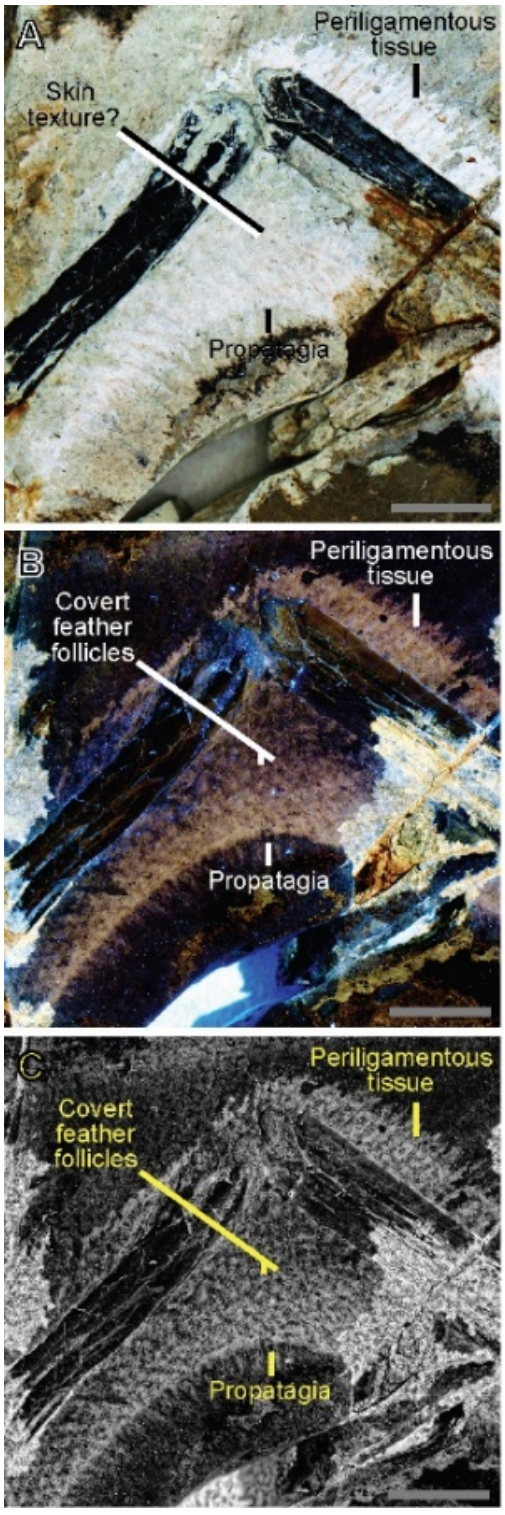

Fig. S3-2. Shallow propatagium of Anchiornis STM-0-127 at 95˚ of elbow extension. Almost regularly spotted skin texture are covert feather follicles. Scale is 1cm. (A) white light image, (B), LSF image, (C), LSF image with rank filter applied.

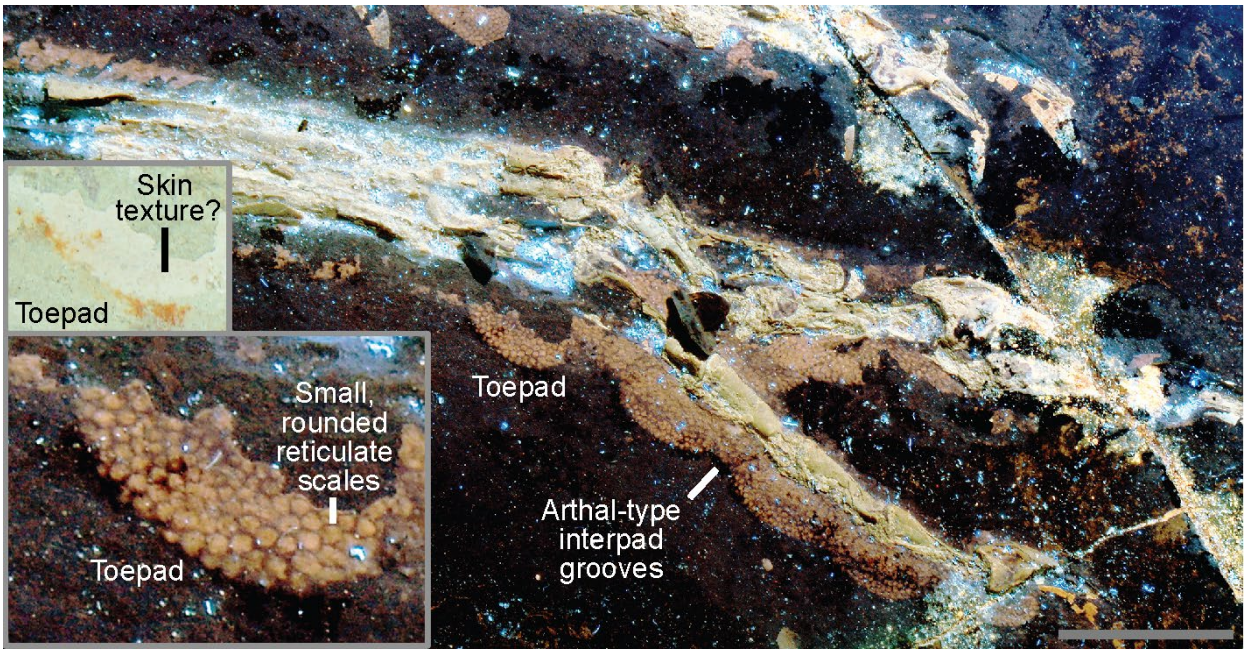

Fig. S3-3. Plantar footpads of Anchiornis STM-0-147. *These preserve reticulate scales and arthal-type interpad grooves. Scale is 1cm. Inset images of a footpad under white and laser light.*

The bird-like body outline reconstruction in Figure S3-1 confirms existing skeleton- and feather-based inferences and supports EPB-based studies of leg and tail shape[17,18]. The drumstick-shaped legs of *Anchiornis* (Fig. S3-1), and probably of most theropods, are concordant with the relatively slender foot and distal portion of the tibia and fibula as well as the broader proximal portion of the latter bones and the robust femur. The slender tail (Fig. S3-1) also fits the shallow and narrow caudal centra and their shallow chevron depths. The observed leg and tail outline are also in agreement with reconstructed theropod musculature using fossil bones studied through an EPB-based approach, validating this method. However, future studies will benefit

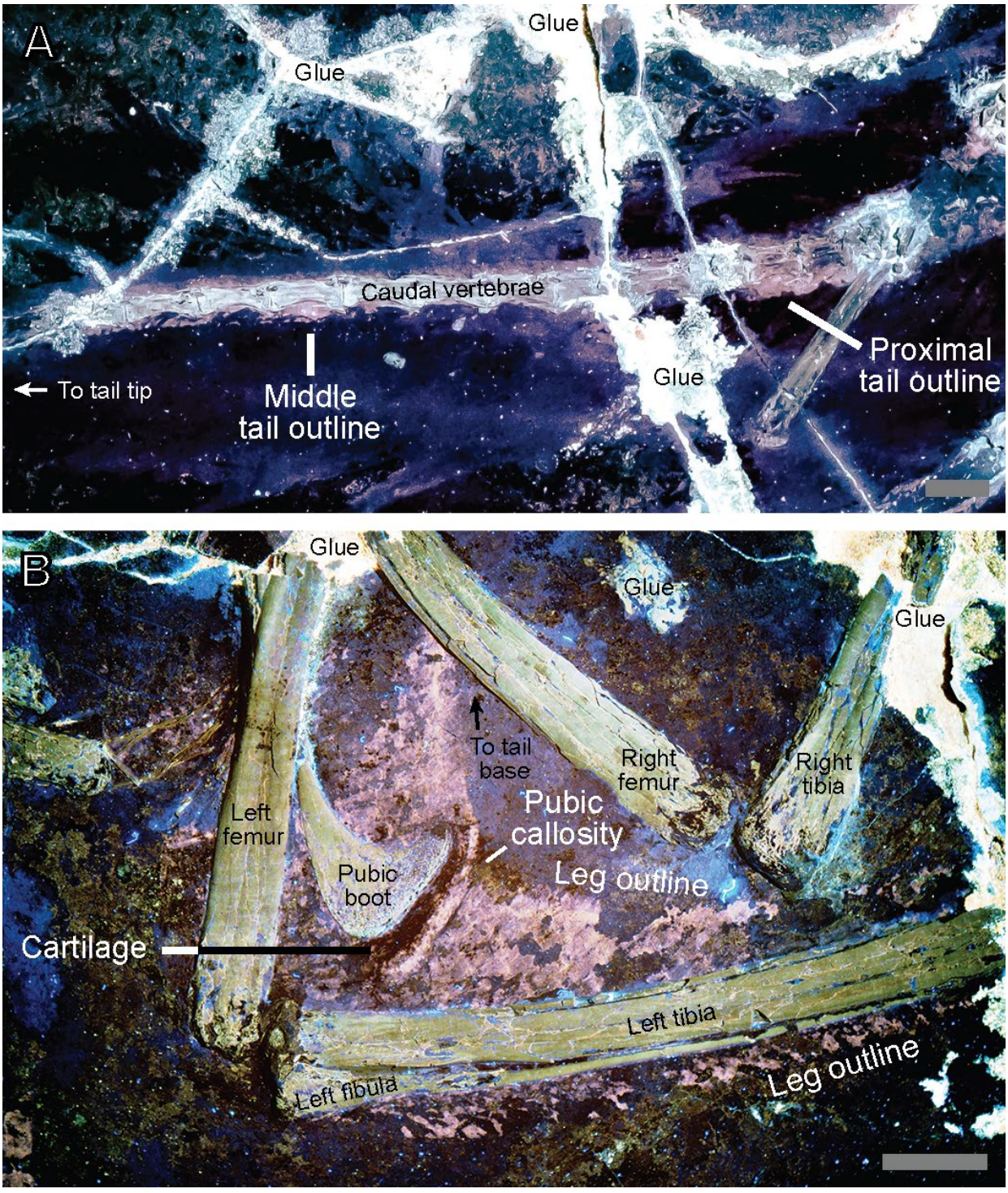

Fig. S3-4. Tail, leg and pubic boot outlines. *(A) Tail outline of STM-0-114. (B) Left leg and pubic boot outline of STM-0-118. The latter forms a potential cartilage-supported (black band) callosity. Scales are 1cm.*

from the new data in helping to better constrain leg muscles like the M. fibularis longus and M. gastrocnemius lateralis and tail muscles like the M. transversospinalis, M. ilio-ischio caudalis and M. ischio-ilio caudalis[13,17-21] (Figs. S3-1, 4). Scales from the tibia to the feet suggest that *Anchiornis* had podotheca like modern birds[15] and other tetanurans[13,16] (Suppl. Fig. S3). The toepads in particular are of modern avian aspect (Figs. S3-1, 3). Between the tail and legs, there is a potential cartilage-supported pubic callosity that may have been suited for partially supporting the animal as it rested on the ground (Fig. S3-4B). However, it could simply indicate that the individual (STM-0-118) had yet to reach maturity, although there are no clear indications of ontogenetic stage elsewhere in the specimen.

The *Anchiornis* propatagia observed in this study are the first direct examples among four-winged dinosaurs (see *Existing pennaraptoran propatagia* in Supplementary Information for purported example in *Archaeopteryx*[22]) and were associated with symmetrical feathering in life[3]. They show shape discrepancies with the halos preserved in the matrix around the bones, suggesting that the latter should not be taken at face value as fossilised soft tissues without complimentary evidence such as preserved feathering (*Microraptor*: Suppl. Figs. S2, S4; Fig. 2 of [23]). Modern avian propatagia form the leading edge of the aerofoil and help give it a cambered profile[24]. It makes major contributions to lift generation proximal to the wrist without which they cannot fly[25]. This function may have been possible in *Anchiornis* given that we already know that the movement of some four-winged dinosaurs through the air was limited by wing area[6], a wing property that propatagia help to increase. However, some living flightless carinate birds have similar propatagial muscle complexes to their volant relatives[26]. Propatagia also have a deep non-flight-related non-avian theropod origin e.g. those in *Caudipteryx* (fig. 4 of [23]; see

Supplementary Information: *Existing pennaraptoran propatagia*). Specimens STM-0-114, 127 and 132 have the best propatagia and their shallow depth (1.2-1.5mm) even at obtuse elbow angles indicates that the arm was not nearly fully extended when these individuals died. This implies that the propatagium was kept taut either by a form of ligamentum propatagiale[27] or by other portions of the propatagial muscle complex. They also suggest that *Anchiornis* could produce a relatively straight arm, a posture broadly found in many living gliding birds (e.g. comorants, albatrosses and pelicans). This indicates a previously unknown aspect of arm morphology differentiation at the earliest stages of paravian evolution (at least by the Oxfordian stage of the Late Jurassic[3]) that may even have been widespread. The aforementioned differentiation in arm morphology among basal paravians implies functional diversity that is in keeping with the diversity of arm feathers seen in four-winged paravians: symmetrically vaned in *Anchiornis*[3] and asymmetrically vaned in *Microraptor* and *Archaeopteryx*[5,9]. It also complements differences in the muscular control of basal paravian arms as implied by the presumably weaker muscle attachments to the non-ossified sterna of *Anchiornis* and *Archaeopteryx*, and presumably stronger muscle attachments to the ossified sterna of *Microraptor*[10]. The uncrossed and skin-bound second and third manual digits of *Anchiornis* (Figs. S3-1, Suppl. S5) formed a functionally didactyl hand, as in Enantiornithes[11]. The latter trait presumably helped to stiffen the postpatagium, but it is unclear whether it was present in other four-winged dinosaurs too (e.g. *Microraptor*: Fig. Suppl. S4). A stiffer feathered postpatagium in *Anchiornis* may have compensated for its aerodynamically inferior arm feathers to some degree, providing another example that basal paravians may have evolved multiple solutions to similar locomotor needs and challenges. Improved understanding of the interactions between functional parameters is therefore a crucial step towards a more holistic understanding of basal paravian function.

However, it is clear that there was a range of functional capabilities among basal paravian arms, including those used for aerodynamic purposes.

The well-preserved propatagial surface of *Anchiornis* (Fig. S3-2) shows the earliest known details of paravian covert feather attachment and arrangement[11,28]. In *Anchiornis*, regularly-spaced spots on the surface of the propatagium are interpreted as covert feather follicles (Fig. S3-2). These are not arranged in tracts - unlike modern birds - indicating little feather differentiation as seen in its plumage[3]. These are not closely packed near the leading edge of the wing which was covered incovert feathers that were comparatively longer than those of most living birds (Fig. Suppl. S5;[13]; fig. 1 of [24]). However, the diagonal orientation of these coverts (Figs. S3-1, Suppl. S5) is shared with living birds[24], indicating some degree of leading edge camber in the wings of *Anchiornis*. This is supported by the denser colouration of the propatagial leading edge, a 2D representation of the original 3D morphology[29] (Fig. Suppl. S3-2). Brown-coloured filamentous structures associated with some of the feather follicles appear to be fossilised *in situ* periligamentous tissue (Fig. Suppl. S3-2). These filaments suggest that these animals shared robust feather attachments ([24]: fig. 13) with some Early Cretaceous birds[11,28] (and probably many feathered non-avian dinosaurs as well). It is probable that other aspects of the modern avian dermal system[16] were already present in basal paravians, but this requires further investigation.

Functional independence between the hind limb and tail of living birds enables them to finely control their respective flight surfaces and is the result of a continuous transition from hip to knee-driven locomotion along the theropod lineage to birds[17,18]. The new hind limb and tail outline results support the absence of a large *M. caudofemoralis* in *Anchiornis*, as predicted by bone morphology[17,18]. This indicates that *Anchiornis* had finer and more independent control of

its hind limb and tail (and the feathers attached to them) compared to more basal theropods[17,18], although the detailed implications of these new hind limb and tail constraints - particularly in comparing the hind limb and tail function of basal paravians with that of modern birds - requires future investigation using quantitative biomechanical modelling. The symmetry of the arm feathers and their regular, non-tract based arrangement suggest that the arms were probably not used in a comparably way to modern birds, despite striking similarities in propatagium shape and camber. This suggests that feathering - particularly its symmetry, size differentiation and spatial arrangement - was highly significant towards how some basal paravians utilized their leg and tail function for aerodynamic benefit. As the new body outline is expected to be similar in asymmetrically feathered basal paravians like *Microraptor* and *Archaeopteryx* based on their skeletal similarities, the new body outline supports their modelled aerodynamic performance[4,6] and promises to reconstruct even greater prowess in the future. This study therefore builds a strong foundation for elucidating the aerodynamic capabilities of *Anchiornis*, if it indeed had any[3,7].

Methods

The body outline in Figure S3-1 and the other figures in the manuscript show the details of nine basal paravian specimens (STM-0-7, 114, 118, 125, 127, 132, 133, 144 and 147) that can all be referred to *Anchiornis*. It has been referred to a basal bird[2], a basal troodontid[3] or a basal deinonychosaur[8] so in the absence of taxonomic consensus it is referred more simply to a basal paravian in this study. Two diagnostic features of *Anchiornis huxleyi* were included in the original description[2] [IVPP V14378]: extreme shortness of the ischium and a sculpturing pattern of numerous small pits on the ventral surface of the coracoid. The ventral position of the latter makes it a difficult feature to observe so it is no surprise that it has yet to be confirmed in other

Anchiornis specimens and in the nine aforementioned specimens. An extremely short ischium is observed in STM-0-7, 118, 127 and 132, but this character is not exposed in the other five specimens figured in the manuscript. Unlike *Xiaotingia*, metacarpal III is thinner than metacarpal II in all of the body outline specimens. Unlike *Eosinopteryx*, STM-0-114, 125 and 132 have more than 23 caudal vertebrae, but this is uncertain in the six other figured specimens. Unlike *Aurornis*, no evidence of an elongate metatarsal I is observed in the body outline specimens, although in STM-0-133 the metatarsals are not well exposed. The overall similarities in the exposed portions of all of the body outline specimens indicate that these individuals can be referred to *Anchiornis* (e.g. a short deltopectoral crest, a straight ulna, etc.); these characters were also used to refer LPM-B00169 to this genus[3].

LSF images were collected using the protocol of Kaye *et al*.[1] so only an abbreviated version of this is given here. *Anchiornis* specimens were imaged with 405nm and 532nm, 500mw lasers. An appropriate long pass blocking filter was used in front of the camera lens to prevent image saturation by the laser. The laser was projected into a vertical line by a Laser Line Optics lens, which was mechanically swept repeatedly over the specimen during the photo's time exposure in a dark room. The images were post processed in Photoshop for sharpness, colour balance and saturation.

The skeletal reconstruction was illustrated in Adobe Photoshop CC 2015. Individual bones were scaled from high-resolution photographs exhibiting minimal parallax using the Photoshop Ruler Tool. The virtual scaling was set according to scale bars photographed in the same plane as the specimens, using Photoshop's Custom Scaling tool (Image -> Analysis -> Set Measurement Scale). Bones were illustrated so that individual measurements end at the edge of the white portion of the bone, as opposed to the middle or outside of the black bounding line.

The skeletal diagram is based primarily on STM-0-118. Missing caudal elements were cross-scaled from STM-0-114. Major elements were illustrated on separate layers to facilitate rotation and transformation into plausible life positions. Presacral vertebrae provided the lengths and representative heights of vertebral elements, but were not preserved with the lateral aspect visible in sufficient quantities to determine the exact curvature of articulation in the neck and back. Articulated and well-exposed presacral series of basal paravians (e.g. *Jinfengopteryx*) were used as supplementary guides for reconstructing vertebral curvature in *Anchiornis*. Forelimb elements were articulated following the left forelimb of STM-0-144, which is preserved with joint angles consistent with contemporary biomechanics work. Hind limb elements of STM-0-118 and STM-0-114 were preserved in articulation, and in good accordance with published interpretations of theropod limb kinematics[17,18], and were the basis for the pose in Figure S3-1.

Examples of soft-tissue preservation were inspected for a lack of continuity and evidence of taphonomic distortion. To reduce discrepancies between specimens of differing size, tissue depth was measured as a percentage of bone width or length. Soft-tissue remains represented by multiple specimens exhibiting similar depth and no signs of distortion were taken at face value and reproduced directly in Figure S3-1, including most distal limb elements. The propatagium depth at the elbow varied in specimens based on the angle of the elbow, a condition also seen in extant birds[24,25], so the depth reconstructed in Figure S3-1 was matched to specimens of similar degrees of elbow flexion. Soft-tissue elements that showed some degree of distortion were used as a qualitative guide for reconstructing the remaining soft-tissue silhouette (represented in black in Fig. S3-1), and other portions were based on dissections of birds and published theropod myology[13,20]. We assigned anatomical terms of soft tissues based on the morphology we

observed, in accordance with traditional morphological interpretations of vertebrate fossils (e.g. bones, scales, feathers, propatagium).

Supplementary Data

SC. 1-1. Supplementary Figures, Supplementary Tables, Supplementary Notes and Supplementary References (PDF 1375 kb)

https://static-content.springer.com/esm/art%3A10.1038%2Fncomms14576/MediaObjects/41467_2017_BFncomms14576_MOESM2137_ESM.pdf

References

1 Kaye, T. G. *et al.* Laser-stimulated fluorescence in paleontology. *PLOS ONE* **10**, e0125923 (2015).

2 Xu, X. *et al.* A new feathered maniraptoran dinosaur fossil that fills a morphological gap in avian origin. *Chinese Science Bulletin* **54**, 430-435 (2009).

3 Hu, D. Y., Hou, L. H., Zhang, L. J. & Xu, X. A pre-Archaeopteryx troodontid theropod from China with long feathers on the metatarsus. *Nature* **461**, 640-643 (2009).

4 Xu, X. *et al.* An integrative approach to understanding bird origins. *Science* **346** (2014).

5 Xu, X. *et al.* Four-winged dinosaurs from China. *Nature* **421**, 335-340 (2003).

6 Palmer, C. The aerodynamics of gliding flight and its application to the arboreal flight of the Chinese feathered dinosaur *Microraptor*. *Biological Journal of the Linnean Society* **113**, 828-835 (2014).

7 Heers, A. M., Dial, K. P. & Tobalske, B. W. From baby birds to feathered dinosaurs: incipient wings and the evolution of flight. *Paleobiology* **40**, 459-476 (2014).

8 Xu, X., You, H. L., Du, K. & Han, F. L. An *Archaeopteryx*-like theropod from China and the origin of Avialae. *Nature* **475**, 465-470 (2011).

9 Foth, C., Tischlinger, H. & Rauhut, O. W. M. New specimen of *Archaeopteryx* provides insights into the evolution of pennaceous feathers. *Nature* **511**, 79-82 (2014).

10 Zheng, X. T. *et al.* On the absence of sternal elements in *Anchiornis* (Paraves) and *Sapeornis* (Aves) and the complex early evolution of the avian sternum. *Proceedings of the National Academy of Sciences* **111**, 13900-13905 (2014).

11 Navalón, G., Marugán-Lobón, J., Chiappe, L. M., Sanz, J. L. & Buscalioni, Á. D. Soft-tissue and dermal arrangement in the wing of an Early Cretaceous bird: Implications for the evolution of avian flight. *Scientific Reports* **5**, 14864 (2015).

12 Zhou, Z. H., Wang, X. L., Zhang, F. C. & Xu, X. Important features of *Caudipteryx* - evidence from two nearly complete new specimens. *Vertebrata PalAsiatica* **38**, 241-254 (2000).

13 Baumel, J. J. Vol. 23 777 (Nuttall Ornithological Club, Cambridge, 1993).

14 Pu, H. Y. *et al.* A new juvenile specimen of *Sapeornis* (Pygostylia: Aves) from the Lower Cretaceous of Northeast China and allometric scaling of this basal bird. *Paleontological Research* **17**, 27-38 (2013).

15 Cuesta, E., Díaz-Martínez, I., Ortega, F. & Sanz, J. L. Did all theropods have chicken-like feet? First evidence of a non-avian dinosaur podotheca. *Cretaceous Research* **56**, 53-59 (2015).

16 Stettenheim, P. R. The integumentary morphology of modern birds - an overview. *American Zoologist* **40**, 461-477 (2000).

17 Hutchinson, J. R. & Allen, V. The evolutionary continuum of limb function from early theropods to birds. *Naturwissenschaften* **96**, 423-448 (2009).

18 Gatesy, S. M. in *Mesozoic birds: above the heads of dinosaurs* (eds L.M. Chiappe & L.M. Witmer) 432-447 (University of Berkeley Press, 2002).

19 Carrano, M. T. & Hutchinson, J. R. Pelvic and hindlimb musculature of *Tyrannosaurus rex* (Dinosauria: Theropoda). *Journal of Morphology* **253**, 207-228 (2002).

20 Hutchinson, J. R., Bates, K. T. & Allen, V. *Tyrannosaurus rex* redux: *Tyrannosaurus* tail portrayals. *Anatomical Record* **294**, 756-758 (2011).

21 Persons, W. S. & Currie, P. J. The tail of *Tyrannosaurus*: reassessing the size and locomotive importance of the *M. caudofemoralis* in non-avian theropods. *The Anatomical Record* **294**, 119-131 (2011).

22 Martin, L. D. & Lim, J. D. Soft body impression of the hand of *Archaeopteryx*. *Current Science* **89**, 1089-1090 (2005).

23 Feduccia, A. & Czerkas, S. A. Testing the neoflightless hypothesis: propatagium reveals flying ancestry of oviraptorosaurs. *Journal of Ornithology* **156**, 1067-1074 (2015).

24 Brown, R. E., Baumel, J. J. & Klemm, R. D. Anatomy of the propatagium - the great horned owl (*Bubo virginanus*). *Journal of Morphology* **219**, 205-224, doi:10.1002/jmor.1052190209 (1994).

25 Brown, R. E. & Cogley, A. C. Contributions of the propatagium to avian flight. *Journal of Experimental Zoology* **276**, 112-124 (1996).

26 McGowan, C. The wing musculature of the Weka (*Gallirallus australis*) a flightless rail endemic to New Zealand. *Journal of Zoology* **210**, 305-346 (1986).

27 Chiappe, L. M. & Lacasa-Ruiz, J. in *Mesozoic birds: above the heads of dinosaurs* (eds L.M. Chiappe & L. Witmer) 230-239 (University of California Press, 2002).

28 Xing, L. D. *et al.* Mummified precocial bird wings in mid-Cretaceous Burmese amber. *Nature Communications* **7**, 12089 (2016).

29 Briggs, D. E. G. & Williams, S. H. The restoration of flattened fossils. *Lethaia* **14**, 157-164 (1981).

Acknowledgments. This study was supported by the Dr. Stephen S.F. Hui Trust Fund (201403173007), the Research Grant Council of Hong Kong's General Research Fund (17103315), The Faculty of Science of the University of Hong Kong and the National Science Foundation of China (41120124002, 41372014 and 41472023). The authors declare no competing interests. The data reported in this paper are detailed in the main text and in the Supplementary Information. Rui Pei is thanked for discussions about Table S1.